NUREG-2195

U.S.NRC
United States Nuclear Regulatory Commission
*Protecting People and the Environment*

# Consequential SGTR Analysis for Westinghouse and Combustion Engineering Plants with Thermally Treated Alloy 600 and 690 Steam Generator Tubes

Office of Nuclear Regulatory Research

# AVAILABILITY OF REFERENCE MATERIALS IN NRC PUBLICATIONS

## NRC Reference Material

As of November 1999, you may electronically access NUREG-series publications and other NRC records at the NRC's Public Electronic Reading Room at http://www.nrc.gov/reading-rm.html. Publicly released records include, to name a few, NUREG-series publications; *Federal Register* notices; applicant, licensee, and vendor documents and correspondence; NRC correspondence and internal memoranda; bulletins and information notices; inspection and investigative reports; licensee event reports; and Commission papers and their attachments.

NRC publications in the NUREG series, NRC regulations, and Title 10, "Energy," in the *Code of Federal Regulations* may also be purchased from one of these two sources.

1. **The Superintendent of Documents**
   U.S. Government Publishing Office
   Washington, DC 20402-0001
   Internet: http://bookstore.gpo.gov
   Telephone: 1-866-512-1800
   Fax: (202) 512-2104

2. **The National Technical Information Service**
   5301 Shawnee Road
   Alexandria, VA 22161-0002
   http://www.ntis.gov
   1-800-553-6847 or, locally, (703) 605-6000

A single copy of each NRC draft report for comment is available free, to the extent of supply, upon written request as follows:

**U.S. Nuclear Regulatory Commission**
Office of Administration
Multimedia, Graphics and Storage & Distribution Branch
Washington, DC 20555-0001
E-mail: distribution.resource@nrc.gov
Facsimile: (301) 415-2289

Some publications in the NUREG series that are posted at the NRC's Web site address http://www.nrc.gov/reading-rm/doc-collections/nuregs are updated periodically and may differ from the last printed version. Although references to material found on a Web site bear the date the material was accessed, the material available on the date cited may subsequently be removed from the site.

## Non-NRC Reference Material

Documents available from public and special technical libraries include all open literature items, such as books, journal articles, transactions, *Federal Register* notices, Federal and State legislation, and congressional reports. Such documents as theses, dissertations, foreign reports and translations, and non-NRC conference proceedings may be purchased from their sponsoring organization.

Copies of industry codes and standards used in a substantive manner in the NRC regulatory process are maintained at—

**The NRC Technical Library**
Two White Flint North
11545 Rockville Pike
Rockville, MD 20852-2738

These standards are available in the library for reference use by the public. Codes and standards are usually copyrighted and may be purchased from the originating organization or, if they are American National Standards, from—

**American National Standards Institute**
11 West 42nd Street
New York, NY 10036-8002
http://www.ansi.org
(212) 642-4900

Legally binding regulatory requirements are stated only in laws; NRC regulations; licenses, including technical specifications; or orders, not in NUREG-series publications. The views expressed in contractor-prepared publications in this series are not necessarily those of the NRC.

The NUREG series comprises (1) technical and administrative reports and books prepared by the staff (NUREG-XXXX) or agency contractors (NUREG/CR-XXXX), (2) proceedings of conferences (NUREG/CP-XXXX), (3) reports resulting from international agreements (NUREG/IA-XXXX), (4) brochures (NUREG/BR-XXXX), and (5) compilations of legal decisions and orders of the Commission and Atomic and Safety Licensing Boards and of Directors' decisions under Section 2.206 of NRC's regulations (NUREG-0750).

NUREG-2195

U.S.NRC
United States Nuclear Regulatory Commission
*Protecting People and the Environment*

# Consequential SGTR Analysis for Westinghouse and Combustion Engineering Plants with Thermally Treated Alloy 600 and 690 Steam Generator Tubes

Manuscript Completed: July 2017
Date Published: May 2018

Prepared by:
S. Sancaktar, M. Salay, R. Iyengar
A. Azarm [1]
S. Majumdar [2]

[1] Innovative Engineering and Safety Solutions, LLC
20817 Spinning Wheel Pl.
Germantown, MD 20874

[2] Argonne National Laboratory
9700 S. Cass Avenue
Argonne, IL 60439

Selim Sancaktar, NRC Project Manager

Office of Nuclear Regulatory Research

# ABSTRACT

This report summarizes severe-accident-induced consequential steam generator (SG) tube rupture (C-SGTR) analyses recently performed by the U.S. Nuclear Regulatory Commission's (NRC's) Office of Nuclear Regulatory Research. C-SGTRs are potentially risk-significant events because thermally induced SG tube failures caused by hot gases from a damaged reactor core can result in a containment bypass event and a large release of fission products to the environment. The current analyses evaluate replacement SGs with thermally treated Alloy 600 and Alloy 690 heat exchange tubes and use the latest tube flaw data available in the 2010 time frame. The methods developed were intended to address the contribution of thermally induced SGTR during severe accidents and pressure-induced SGTR during a number of design-basis accidents. The study developed the methods and the pilot applications so as to establish the framework for performing a more comprehensive probabilistic risk assessment that can address the C-SGTR at a level of detail suitable for other NRC needs. The main conclusion from this work is that the SG geometry and the fluid flow rates in different SG designs can significantly influence the potential likelihood of C-SGTRs. For the cases studied, SG designs with a shallow inlet plenum (resulting in the tubesheet located closer to the hotleg inlet) and a shorter hotleg can result in a greater likelihood of a C-SGTR following a core damage event associated with accident conditions that challenge SG tubes. A shallow inlet plenum design reduces the mixing of hot gases entering the SG, thereby creating a higher thermal load on the tubes. For the specific replacement SG geometries analyzed in this study, the Combustion Engineering plant design had an increased likelihood of a C-SGTR and a higher potential for a large early release, than the Westinghouse plant design.

# CONTENTS

# LIST OF FIGURES

# LIST OF TABLES

# EXECUTIVE SUMMARY

Over the last two decades, the U.S. Nuclear Regulatory Commission (NRC) and the nuclear industry have investigated the safety implications and risk associated with consequential steam generator tube rupture (C-SGTR) events (i.e., events in which steam generator (SG) tubes leak or fail as a consequence of high differential pressures or elevated temperatures during accident sequences). Various probabilistic risk assessments (PRAs) have shown accidents involving SG tube ruptures to be contributors to plant risk because of their potential for causing a release of fission products outside containment (containment bypass sequences).

The analysis methods, tools, and expertise previously developed as a part of the NRC Steam Generator Action Plan (SGAP) were sufficient to resolve the associated technical issues. However, certain limitations restrict its usefulness in supporting future risk assessments. Consequently, the agency identified several areas for additional research and updates. After closure of the SGAP in 2009, and building upon the research conducted to resolve the SGAP, the NRC chartered this study to address the development of a simplified method for assessing the risk associated with consequential tube rupture or leakage in design-basis-accident (DBA) and severe-accident events. This report integrates work done by three disciplines in the NRC Office of Nuclear Regulatory Research—thermal-hydraulic (TH) and computational fluid dynamics analysis, materials, and PRA. The study used updated SG flaw distributions representing the current population of SGs, along with the new TH results from the MELCOR TH code, for an example Combustion Engineering (CE) plant.

This report documents a method for a quantitative risk assessment of C-SGTR during a severe accident (i.e., after the onset of core damage) and during a DBA event (before the onset of core damage). The focus of this study is the estimation of the large early release frequency (LERF) because of C-SGTR and containment bypass. Specifically, the study estimated the probability of containment bypass because of C-SGTR and assessed the fraction of containment bypass that constitutes LERF. It developed simplified LERF calculation methods and applied them to two pressurized-water reactor plants: a Westinghouse (W) and a CE design. In addition, it used the generic stylized models to address C-SGTR related to DBA issues. The scope of this report does not include the development of Level 1 PRA modeling, although the study used full Level 1 PRAs for internal and external events to obtain the frequency of the sequences related to the C-SGTR. The method is illustrated with applications to plants containing replacement SGs with thermally treated Inconel Alloy 600 and Alloy 690 SG tubes.

A key consideration for C-SGTR sequences is the relative timing between the failure of SG tubes and the failure of other locations within the reactor coolant system (RCS). If a thermally induced failure sufficient to depressurize the primary coolant develops in another RCS location either before or shortly after SG tube failure, fission product release through failed SG tubes may be prevented or minimized. In that case, the RCS leakage will preferentially go into the containment, thus significantly reducing or altogether eliminating potential leakages from the RCS into the secondary side of the SG. To properly account for this relative timing, this analysis used the latest available TH analyses for both W and CE plant types, updated flaw statistics pertinent to current reactors, and the latest available models and software for estimating the failure probability and failure timing of SG tubes and other RCS components (i.e., hot leg (HL) and surge line). A software “calculator” was developed in conjunction with this study to simulate multiple flaws in SG tubes and to calculate C-SGTR tube leakage probabilities. Inputs for the calculator include TH parameters of an accident sequence, SG tube flaw distribution, and material properties. This software permits not only numerous “what-if” runs with a minimal effort,

to better understand the progression of an accident, but also pressure and temperature challenges to the tubes.

Several key assumptions were made to support this study:

- The SGs were assumed to have flaw distributions consistent with operating experience obtained in the 2010 time frame. The flaw distributions were based on a statistical analysis of a sample of SG tube inspection results obtained for replacement SGs with an average operating history of 15 years in service.
- Existing models for the high-temperature behavior of RCS components and SG tubes were used to estimate the potential for a C-SGTR event. Chapter 8 discusses the limitations associated with these models.
- An SG "rupture" was defined as a total SG tube leak area equivalent to a guillotine break of one or more tubes.
- A small secondary leak (equivalent to a flow area of 0.5 square inch) is assumed for all accident sequences involving high pressure under primary coolant side and dry SG conditions. This leakage area results in SG depressurization for all dry SG conditions studied.
- A simplified model for HL failure was used for the probabilistic risk analysis portion of the study. However, detailed structural analyses determined that the simplified model consistently predicted later times to HL failure than more detailed modeling, without introducing excessive conservatism. This detailed modeling also indicated that the upper portion of the HL will fail earlier than other RCS regions.
- Mixing coefficients in the SG inlet plenum used in the MELCOR TH analysis were determined based on a detailed computational fluid dynamics analysis, which has been benchmarked using 1/7th scale test data.

The main conclusion from this work is that the SG geometry and the fluid flow rates in different SG designs can significantly influence the potential likelihood of C-SGTRs. For the cases studied, SG designs with a shallow inlet plenum (resulting in the tubesheet located closer to the HL inlet) and a shorter HL can result in a greater likelihood of a C-SGTR after a core damage event associated with high-dry-low conditions. A shallow inlet plenum design reduces the mixing of the hot gases entering the SG, thereby creating a higher thermal load on the tubes. Therefore, for the specific replacement SG geometries analyzed in this study, the CE plant design had an increased likelihood of a C-SGTR, and thus a greater potential for a large early release, than the W plant design.

Moreover, the study has concluded that clearing the RCS cold leg loop seal, which changes the natural circulation flow path within the SG inlet plenum and subjects the SG tubes to hotter gas flow, could cause SG tube failure and be a contributor to C-SGTR for W plants. For CE plants, significant SG tube failures are expected even if the loop seal is not cleared.

The PRA method developed and illustrated in this report, although applied to specific plants and cases, may offer general insights and a process to obtain quantitative measures (e.g., the fraction of C-SGTR given a severe accident) that could be used to support risk-informed regulatory decisionmaking. For example, this work may benefit significance determination process reviews of findings related to SGs, inform NRC reviews for new reactors, or support license renewal reviews for issues related to SG material management.

# ACKNOWLEDGMENTS

In addition to the authors listed on the cover page of this document, many others from the U.S. Nuclear Regulatory Commission (NRC) and outside the NRC contributed to the analyses or documentation of the work. Former NRC employee Charles Harris contributed to Chapter 6 of this report, for the estimation of steam generator tube flaw distributions and related subjects discussed in that chapter. Kevin Coyne's multiple rigorous reviews of this report, his persistence in moving the deliverables forward, and his technical understanding of the overall report also deserve to be mentioned.

In addition, the authors would like to acknowledge the following individuals (listed alphabetically by last name):

From the NRC:

Michelle Gonzalez
Ken Karwoski
Emmett Murphy
Antonios Zoulis

From Information Systems Laboratories and their contractors:

Robert Beaton (currently at the NRC)
Terry Gitnick
Maria Morell Gonzales
Qiming He
Andrew Mlynarczyk
Marcos Ortiz

Many other NRC staff members from different NRC offices contributed to this effort by reviews and meeting support.

# ABBREVIATIONS

| | |
|---|---|
| ac | alternating current |
| ACRS | Advisory Committee on Reactor Safeguards |
| ADAMS | Agencywide Documents Access and Management System |
| AFW | auxiliary feedwater |
| ANL | Argonne National Laboratory |
| ARTIST | Aerosol Trapping in Steam Generator |
| ATWS | anticipated transient(s) without scram |
| | |
| CCDP | conditional core damage probability |
| CCF | common-cause failure |
| CCW | component cooling water |
| CD | core damage |
| CDF | core damage frequency |
| CE | Combustion Engineering |
| CFD | computational fluid dynamics |
| COA | crack-opening angle |
| COD | crack-opening displacement |
| CSGTR (C-SGTR) | consequential steam generator tube rupture |
| CST | condensate storage tank |
| CVCS | chemical volume control system |
| | |
| DBA | design-basis accident |
| dc | direct current |
| DEGB | double-ended guillotine break |
| | |
| EAL | emergency action level |
| EB | emergency boration |
| ECCS | emergency core cooling system |
| EDG | emergency diesel generator |
| EDM | electrostatic discharge machine |
| EDMG | extensive damage mitigation guideline |
| EFPY | effective full power year |
| EOP | emergency operating procedure |
| EPRI | Electric Power Research Institute |
| EQ | equalization |
| | |
| FB | feed and bleed |
| FE, FEM | finite element model |
| FEA | front-end analysis |

| | |
|---|---|
| FP | fission product |
| HDL (H/D/L) | high primary pressure, dry steam generator, and low secondary pressure |
| HL | hot leg |
| HPI | high-pressure injection |
| HPR | high-pressure recirculation |
| HRA | human reliability analysis |
| HTC | heat transfer coefficient |
| ID | inside diameter |
| IE | initiating event |
| INEL | Idaho National Engineering Laboratory |
| IPE | individual plant evaluation |
| IPEEE | individual plant evaluation for external events |
| ISI | inservice inspection |
| L-SSB | large secondary side break |
| LERF | large early release frequency |
| LOCA | loss-of-coolant accident |
| LOOP | loss of offsite power |
| *ltsbo* | long-term SBO (turbine-driven pump fails after battery depletion) |
| MA | mill annealed |
| MDAFW | motor-driven auxiliary feedwater (pump) |
| MFW | main feedwater |
| MSIV | main steam isolation valve |
| MSLB | main steamline break |
| MSSV | main steam safety valve |
| MTC | moderator temperature coefficient (reactivity feedback) |
| NPP | nuclear power plant |
| NRC | U.S. Nuclear Regulatory Commission |
| OD | outside diameter |
| ODSCC | outside-diameter stress-corrosion cracking |
| OTSG | once-through steam generator |
| PDS | plant damage state |
| POD | probability of detection |
| PORV | power-operated relief valve |
| PRA | probabilistic risk assessment |

| | |
|---|---|
| PSA | probabilistic safety assessment |
| PSF | performance-shaping factor |
| PTW | part-through-wall |
| PWR | pressurized-water reactor |
| PWSCC | primary water stress-corrosion cracking |
| PZR | pressurizer |
| | |
| RCP | reactor coolant pump |
| RCS | reactor coolant system |
| RES | Office of Nuclear Regulatory Research |
| RF | release fraction |
| RHR | residual heat removal |
| RPS | reactor protection system |
| RPV | reactor pressure vessel |
| RS | recirculation spray |
| RTD | resistance temperature detector |
| RV | reactor vessel |
| RWST | reactor water storage tank |
| RY | reactor year |
| SAE | site area emergency |
| SAMG | severe-accident management guideline |
| SBO | station blackout |
| SCF | suppress creep failure |
| SG | steam generator |
| SGAP | Steam Generator Action Plan |
| SGT | steam generator tube |
| SGTR | steam generator tube rupture |
| SGTR-INIT | steam generator tube rupture initiator |
| SHR | secondary heat removal |
| SL | surge line |
| SLB | steamline break |
| SLBIC | steamline break inside containment |
| SNL | Sandia National Laboratories |
| SPAR | standardized plant analysis risk |
| SRV | safety relief valve |
| SSB | secondary side break |
| *stsbo* | short-term SBO (AFW pump fails early in SBO) |
| SW | service water |
| | |
| TDAFW | turbine-driven auxiliary feedwater (pump) |
| TH (T&H) | thermal-hydraulic |

| | |
|---|---|
| TT600 (600TT) | thermally treated Inconel 600 |
| TT690 (690TT) | thermally treated Inconel 690 |
| TYPE-I (C-SGTR) | temperature-induced (by creep rupture) C-SGTR |
| TYPE-II (C-SGTR) | pressure-induced C-SGTR |
| UET | unfavorable exposure time |
| Vdc | volts direct current |
| W | Westinghouse |
| ZNPP | Zion Nuclear Power Plant |

# 1 INTRODUCTION

## 1.1 Background

The U.S. Nuclear Regulatory Commission (NRC) and the nuclear industry have expended considerable resources over the last two decades to better understand the safety implications and risk associated with consequential steam generator tube rupture (C-SGTR) events (i.e., events in which steam generator (SG) tubes leak or fail as a consequence of the high differential pressures or elevated temperatures during accident sequences. Various probabilistic risk assessments (PRAs) have shown accidents involving SG tube ruptures to be contributors to plant risk, mainly because of their potential for causing a release outside containment (containment bypass sequences).

The analysis methods, tools, and expertise previously developed as a part of the NRC Steam Generator Action Plan (SGAP) were sufficient to resolve the associated technical issues. However, certain limitations restrict its usefulness in supporting future risk assessments. Several areas were identified for additional research and updates. Building upon the research conducted to resolve the SGAP, the NRC chartered this study to address the development of "a simplified method for assessing the risk associated with consequential tube rupture/leakage in design-basis accident (DBA) and severe accident events." The study used updated SG flaw distributions representing the current population of SGs, along with the new thermal-hydraulic (TH) results from the MELCOR TH code for Combustion Engineering (CE) plants.

The study applied to two sample pressurized-water reactor plants: a Westinghouse (W) and a CE design. The scope of this study is limited to estimating the probability of containment bypass because of C-SGTR and assessing the fraction of containment bypass that constitutes large early release frequency (LERF). It is assumed that a Level 1 PRA is available for both internal and external events such that the frequency of the sequences related to the C-SGTR evaluation can be easily obtained. The method defines the characteristics of the sequences of interest and demonstrates how they can be obtained from the existing PRAs or standardized plant analysis risk models for the two example plants. The scope also includes an assessment of the probability that tube failures (rupture and leaks) can occur before failure of other reactor coolant system (RCS) components. This is shown for two sets of sequences: severe accidents and DBAs. Severe accidents involve all sequences of core damage, where after the onset of core damage, the primary pressure is high (generally at the set point of the primary relief valves), and at least one SGs is dry (no secondary heat removal) with its secondary side depressurized (i.e., near atmospheric pressure). These severe accident sequences are referred to as HDL (or H/D/L), which stands for high primary pressure and dry steam generator(s) with low secondary side pressure. DBAs involve initiating conditions, where the pressure across the tubes is significantly higher than nominal pressure during operation. These sequences include: steamline break, feedwater line break, stuck open SG safety valve or atmospheric dump valve, and anticipated transients without scram.

It is expected that the method described in this report can be applied to a range of PRA applications. The insights from this study can be used to better inform simplified risk approaches by relying on a set of probabilities to screen and categorize emergent issues, such as those identified through inspection findings or operational events. The more detailed methods used in this study could support a more comprehensive risk assessment suitable to support risk-informed decisions and the rulemaking process.

This work has significantly leveraged other ongoing or recently completed NRC activities associated with material characterization and behavior and severe accident analysis. For example, this project relied on updated flaw distributions for reassessment of the conditional probabilities of C-SGTR. The study analyzed flaw data from SG inservice inspections to characterize the flaw parameters and update flaw statistics. It also used TH runs for the example W plant generated by the RELAP code and documented in NUREG/CR-6995, "SCDAP/RELAP5 Thermal-Hydraulic Evaluations of the Potential for Containment Bypass during Extended Station Blackout Severe Accident Sequences in a Westinghouse Four-Loop PWR," issued March 2010 (Ref. 1). New calculations using the MELCOR severe accident code were run for selected sequences for an example CE plant. This information was used as input to C-SGTR software to arrive at the probability of SG tube failure, before failure of the other RCS components. Uncertainties were treated to the extent possible throughout this evaluation. Although this study used the existing Electric Power Research Institute (EPRI) correlations for failure of the hot leg (HL) and surge line (SL), these correlations can be readily updated within the existing C-SGTR software calculator should the improved models become available.

This study represents an important update of the probability values used in prior analyses, which were based on the flaw data from earlier generations of SGs with older TH results, and for W plants only. It compared the updated conditional probability values with values from previous studies and found key areas of disagreement to be attributed to the updated methodology and data.

Past risk studies have commonly considered SGTRs as an initiating event and, in some cases, as the consequential SGTR, such as thermally induced C-SGTR. An example of the latter analyses can be found in NUREG-1570, "Risk Assessment of Severe Accident-Induced Steam Generator Tube Rupture," issued March 1998 (Ref. 2); by EPRI in Technical Report 1006593, "Steam Generator Tube Integrity Risk Assessment," issued 2002 (Ref. 3); and by the Westinghouse Owners Group at a PSA'05 conference, September 11–15, 2005 (Ref. 4). SGTR as an initiating event is a design-basis event for which plants are designed to cope without progressing to a severe accident. Plants have coped with all SGTRs to date. A C-SGTR differs from this sequence in that the severe accident causes the tube rupture.

NUREG/CR-6995 (Ref. 1) and NUREG-1570 (Ref. 2) extensively studied C-SGTR TH behavior for W plants. SCDAP/RELAP performed some work on CE plants but, having predated the final W analysis, it did not incorporate all the modeling improvements made for them. EPRI considered CE plants in its 2002 steam-generator-tube-related risk analysis (Ref. 3).

Because of the capability to predict fission product (FP) releases in addition to TH behavior, the decision was made to switch to the MELCOR code to perform the CE C-SGTR analysis. Lessons learned during the previous W analyses were applied to the CE analysis during the work described in this report. Chapter 3 discusses this topic further.

## 1.2 Objectives

The objective of this report is to document a simplified method for a quantitative assessment of the probability of C-SGTR and LERF associated with C-SGTR during a severe accident after the onset of core damage and during a DBA event before the onset of core damage. Estimating the probabilities of large early releases and containment bypass is the main focus for severe accidents. The report addresses screening probabilities for both core damage and containment bypass for DBA events.

The study used the latest available TH for both W and CE plant designs and the updated flaw statistics pertinent to current reactors. It also used software tools containing the latest available model for estimating the failure probability and timings of SG tubes and other RCS components (i.e., HL and SL). The results from these calculations were distilled into tables that showed the failure probabilities for SG tubes and RCS components. For PRA analysis, the bounding values for the probabilities of equipment failures and human errors were tabulated using of a spectrum of representative accident conditions. These tables could be used in lieu of conducting a detailed plant-specific analysis for performing a simplified C-SGTR LERF evaluation.

Although the methods developed here were intended to address the study objectives (i.e., the screening method), they are meant to establish the framework to perform a more comprehensive PRA that can address the C-SGTR at a level of detail suitable for other needs. Extension of these methods can support the risk-informed decision process and also be used to update the PRA Standards and PRA Procedure Guide.

## 1.3 Scope

The scope of this study is limited to estimating the probability of containment bypass because of C-SGTR and an assessment of the fraction of containment bypass that constitutes LERF. It is assumed that a Level 1 PRA is available for both internal and external events such that the frequency of the sequences related to the C-SGTR evaluation can be easily obtained. The method defines the characteristics of the sequences of interest and demonstrates how they can be obtained from the existing PRAs or standardized plant analysis risk models for the two selected plants. The scope also includes an assessment of the probability that tube failures (rupture and leaks) can occur before failure of other RCS components. This is shown for two sets of sequences: severe accidents and DBAs. Severe accidents involve all sequences of core damage, where the SGs are dry (no secondary heat removal), and the primary pressure is high (generally at the set point of the primary relief valves). DBAs involve initiating conditions, where the pressure across the tubes is significantly higher than nominal pressure during operation. These sequences include: steamline break, feedwater line break, stuck open SG safety valve or atmospheric dump valve, and anticipated transients without scram.

## 1.4 Summary of Differences from Previously Published Work

The study used the latest available THs for both plants, updated flaw statistics pertinent to current reactors, and the latest available models and software for estimating the failure probability and timings of other SG tubes and RCS components (i.e., HL and SL). A C-SGTR software “calculator” was developed in conjunction with this study to simulate multiple flaws in SG tubes and to calculate tube leakage probabilities. Inputs for the calculator include TH parameters of an accident sequence, tube flaws, and material properties. This software allows not only numerous “what-if” runs with minimal effort, to better understand the progression of an accident, but also pressure and temperature challenges to the tubes. Appendix B describes this software.

The other improvements for this study, as compared to previous studies, are the following:

- detailed computational fluid dynamics analysis and MELCOR severe accident modeling for the example CE plant design
- detailed finite element analysis for the RCS HL nozzle to confirm the timing of structural failure

- consideration of more typical replacement SG tube materials, such as thermally treated Alloy 600 and Alloy 690
- comprehensive integration of analyses from different fields, which include TH analyses, study of behavior of "other" RCS components, calculator software that allows study and documentation of many sequences; limited extension into FP release analysis using MELCOR; and, separately, estimation of LERF
- insights obtained about failure behavior of flaws by making a multitude of runs with the calculator

## 1.5 Summary of Research Approach and Organization of Report

The work described in this report uses a PRA approach. However, it includes other work from TH analyses using MELCOR (Chapter 3 of this report) and failure of assessment of "other RCS components" using ABAQUS (Chapter 4). Chapter 5 offers a detailed description and technical bases for predicting the severe accident behavior of SG tubes. In addition, it generates tube flaw distributions for tubes with Alloy 600 and Alloy 690 materials (Chapter 6); the PRA used these distributions.

The PRA sections of this report consist of Chapters 2, 7, and 8. Figure 1-1 outlines the report structure and the flow of information among the work generated by the three different fields; namely, PRA, TH analyses, and materials analyses.

The new TH analyses for the reference CE plant used the MELCOR software. The MELCOR output can be viewed as consisting of two sets of outputs:

- TH profiles (e.g., temperature and pressure as a function of time) in the SG tubes and SG inlet regions (HL and SL) for severe accidents
- fission product release results

The TH results from these analyses (item 1 above) are used in the PRA as input. Further conclusions drawn by the MELCOR analyses for FP release, based on a set of modeling assumptions, are independently generated and are not used by the PRA, which defines and estimates C-SGTR and LERF frequencies, independent of the other types of analyses.

Similarly, PRA used the existing EPRI correlations to estimate failure times for HL and SL, compared to the failure times of the SG tubes. The extra analyses in Chapter 4 by ABAQUS are used for confirmatory purposes.

Chapter 8 summarizes the PRA conclusions. Chapter 9 presents the other overall conclusions for the materials TH and PRA work.

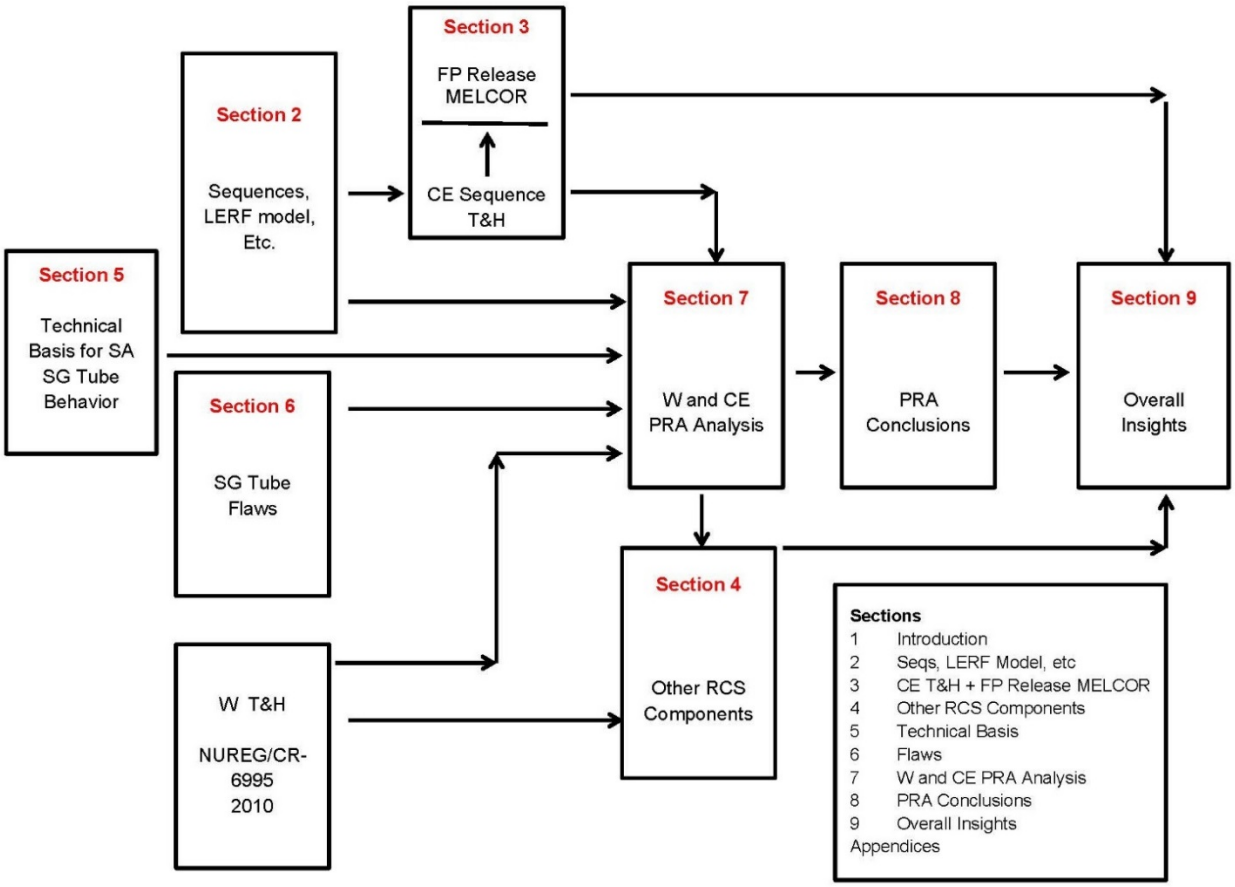


Figure 1-1 Work and report layout

## 1.6 References


1. U.S. Nuclear Regulatory Commission, "SCDAP/RELAP5 Thermal-Hydraulic Evaluations of the Potential for Containment Bypass during Extended Station Blackout Severe Accident Sequences in a Westinghouse Four-Loop PWR," NUREG/CR-6995, March 2010, Agencywide Documents Access and Management System (ADAMS) Accession No. ML101130544.

2. U.S. Nuclear Regulatory Commission, "Risk Assessment of Severe Accident-Induced Steam Generator Tube Rupture," NUREG-1570, March 1998, ADAMS Accession No. ML070570094.

3. Electric Power Research Institute, "Steam Generator Tube Integrity Risk Assessment: Volume 1: General Methodology, Revision 1," Technical Report 1006593, Palo Alto, CA, 2002.

4. Westinghouse Owners Group Simplified Level 2 Modeling Guidelines: Justin Robert Armstrong and Raymond E. Schneider—Westinghouse Electric Company, Westinghouse Owners Group, PSA'05, September 11–15, 2005, San Francisco, CA.

# 2 SEQUENCE DEFINITIONS

This chapter discusses accident sequences that are of interest for consequential steam generator tube rupture (C-SGTR) analysis and that identify limiting (most challenging) sequences for steam generator (SG) types typically used in Westinghouse (W) and Combustion Engineering (CE) plants. The chapter initially describes accident sequence selection for pressure-induced failures of the SG tubes, which are caused by high differential pressure across the SG tubes but do not involve significant thermally induced creep growth of flaws. Next, the chapter describes accident sequences for thermally induced SG tube failures. The focus here is on severe accidents associated with high reactor coolant system (RCS) pressure and dry secondary-side conditions of one or more SGs. The sequences identified are expected to be typical of a pressurized-water reactor (PWR) probabilistic risk assessment (PRA). The remaining sections define the “critical” leak size for defining an SG fault as C-SGTR and provide a model for large early release frequency (LERF).

## 2.1 Pressure-Induced C-SGTR Sequences of Interest

Table 2-1 lists the sequences of interest for pressure-induced SG tube failures, alternatively known as design-basis accident (DBA) events. These sequences could establish a delta pressure across the SG tube walls and, therefore, potentially challenge the integrity of the tubes because of pressure-induced failures. Several PRA sequences are combined and grouped, based on their thermal-hydraulic (TH) behavior, to yield a smaller set of candidate DBA sequences with similar challenges to the SG tubes. Plant-specific design features would determine if a sequence is applicable. For example, sequences involving a total loss of secondary cooling but successful feed and bleed (FB) operation are not applicable to plants that cannot FB (e.g., CE plants with no power-operated relief valves (PORVs)).

Generally, Level 1 PRA sequences can be grouped into one of these selected DBA sequences. The frequency of each of the DBA sequences can then be estimated by summing the individual frequencies of all the PRA sequences. PRAs compile the frequencies of the full accident sequences that result in core damage; however, they do not explicitly provide the frequencies of the partial accident sequences, which have not yet progressed to core damage (CD). The required information for estimating the frequencies of the partial sequences can be easily obtained from the Level 1 PRA for internal and external hazards.

Table 2-1 Selected DBA Sequences Causing Challenges to SG Tubes

| Delta P Across the Tubes | Conditions Causing Delta P Across the Tubes | Accident Sequence | SG Secondary-Side Condition [Pressure, Water Inventory] |
|---|---|---|---|
| ~ 6.9 mega pascals (MPa) (1,000 pounds per square inch (in.) (psi)) | Normal power operation | SGTR event | Not known, will be determined by resulting CD sequences |
| ~ 10.34 MPa (1,500 psi) | FB sequences with medium-head [a] emergency core cooling system (ECCS) pumps | All sequences involving loss of secondary heat removal but success of FB | Low pressure and dry SGs before rupture<br>Low pressure and dry SG condition is expected after CD |
| ~ 10.34 to 11.75 MPa (1,500–1,700 psi) | 1. Unisolable main steamline breaks (MSLB)<br>2. Inadvertent opening of SG relief valves or turbine bypass valves with failure to isolate | All sequences are expected to result in loss of secondary cooling followed by FB cooling. | Low pressure but not dry SGs before rupture<br>Low pressure and possibly dry SG condition after CD |
| ~15.5 MPa (2,250 psi) | FB with high-pressure ECCS pumps | All sequences involving loss of secondary heat removal but success of FB with stuck-open secondary relief valves | Low pressure and dry SGs before rupture<br>Low pressure and dry SG condition after CD |
| ~15.2 MPa (2,200 psi) | Anticipated transient without scram (ATWS) sequences when secondary cooling is not lost and pressure peak is limited to 22.06 MPa (3,200 psi) | ATWS sequences with a favorable moderator temperature coefficient generally result in a pressure peak well below 22.06 MPa (3,200 psi) in the primary. A bounding pressure of 22.06 MPa (3,200 psi) is considered for estimating the delta pressure across the SG tube.[b] | High pressure but not dry; however, failure of SG tube will induce CD.<br>All such CD sequences during ATWS are treated as LERF. |
| 22.06 MPa (~3,200 psi) | ATWS sequences when secondary cooling is lost and pressure peak is limited to <22.06 MPa (<3,200 psi) | ATWS sequences with a favorable moderator temperature coefficient can result in a pressure peak as high as 22.06 MPa (3,200 psi) in the primary. | High pressure and dry; however, failure of SG tube will induce CD. All such CD sequences during ATWS are treated as LERF. |

[a] The ECCS pumps used in U.S. PWRs can have a shutoff head as low as 8.27 MPa (1,200 psi) and as high as 18.27 MPa (2,650 psi).

[b] UET (unfavorable exposure time) is defined as the time during the cycle when the reactivity feedback is not sufficient to prevent RCS pressure from exceeding 22.06 MPa (3,200 psi). Many factors, such as initial power level, time in cycle when transient occurs, reactivity feedback as a function of the cycle life, the number of available primary relief/safety valves, the failure or success of control rod insertion, and auxiliary feedwater (AFW) flow rates, affect UET. The noted pressure below 22.06 MPa (3,200 psi) is used as the bounding primary pressure value for cases when the moderator temperature coefficient is favorable.

### 2.1.1 Core Damage Bridge Event Tree

As discussed in Section 2.1, Table 2-1 characterized DBA events of interest and the types of challenges to the SG tubes. The C-SGTR is characterized by its occurrence probability and the size of its leak area. The study estimated the occurrence probability of C-SGTR using the C-SGTR calculator (see Appendix B) and the latest flaw data, as discussed in Chapter 6. The leak area sizes could be divided into two or more bins (e.g., Small, Medium, and Large) to help in the estimation of time-sensitive human error probability values. A bridge tree was also developed to depict further progression of the accidents from the occurrence of C-SGTR through the onset of core damage. A general assumption used in developing this bridge tree is that the core damage has resulted from the C-SGTR, and it is not the result of the original initiator. It is assumed that the impact of the original initiator (e.g., MSLB or ATWS) would have been mitigated if C-SGTR had not occurred. For example, it is assumed that a proper response would be provided to an MSLB initiator, and the reactor would reach a safe, stable condition if C-SGTR had not occurred. The occurrence of C-SGTR, therefore, results in a transfer of the sequence of interest (entry level sequence) to a bridge tree that would be similar to that of an SGTR initiator (SGTR-INIT) tree in Level 1 PRAs. However, the boundary conditions imposed by the entry level sequence should be preserved by setting proper conditions on the branches of the SGTR-INIT event tree. Plant-specific standardized plant analysis risk trees for SGTR-INIT can be used for this purpose. Figure 2-1 shows the generic CD bridge event tree. The plant-specific event tree can be used if available.

The following headings define the top branches for the event tree in Figure 2-1:

- **SGTR-INIT:** Induced SGTR from DBA events
- **HPI:** High-pressure injection (HPI) systems: both safety injection pumps and charging pumps, if applicable
- **SHR:** Secondary heat removal (SHR) system: main feedwater (MFW) or AFW
- **FB:** FB operation and the supporting relief path
- **EQ:** Operator actions for equalization, which involves control of primary pressure, and depressurization below the pressure set point for the secondary relief valves
- **RWST-MU:** Long-term makeup water to the reactor water storage tank (RWST)
- **HPR:** High-pressure recirculation (HPR) and the associated operator action
- **RHR:** Operator action to cool down to cold shutdown and align the residual heat removal (RHR) system
- **RS:** Recirculation spray (RS) cooling in those plants that do not use RHR heat exchangers as a part of HPR

The end state CD refers to core damage.

With the exception of the ATWS sequence, the effect of other entry sequences will be superimposed on this bridge tree. For example, for sequences involving FB using the high-pressure ECCS, the following conditions will be imposed:

- Top event FB is set to success.
- SHR and EQ are both set to failure.

- Depending on plant-specific design features, HPR may not be possible, since the leakages are through the SGTR ending up to secondary side of the SG rather than in the containment sump.

For ATWS sequences, the C-SGTR is conservatively assumed to result in CD and LERF. This is caused by the difficulty in controlling the boron concentration because of the loss of borated coolant through the ruptured tubes.

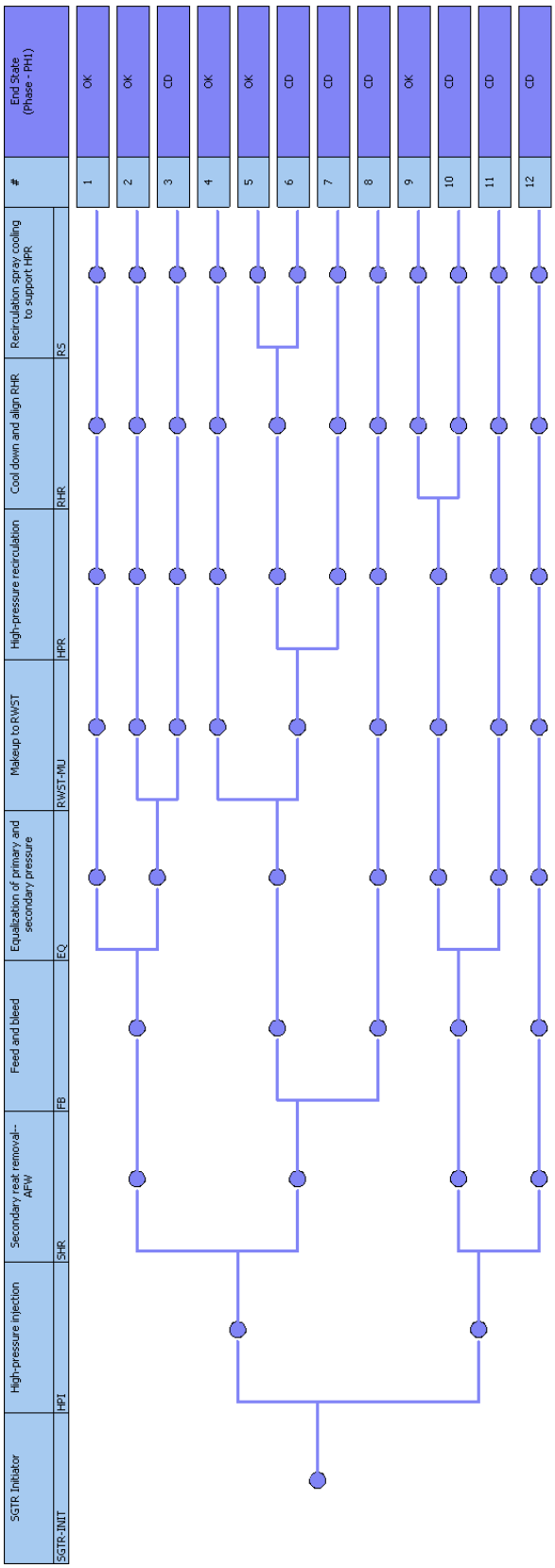


Figure 2-1 Generic CD bridge event tree for DBA induced C-SGTR

### 2.1.2 Level 2 Event Tree: LERF Determination

A detailed Level 2 PRA was considered to be out of scope for this project. A detailed Level 2 PRA model should address the following:

- The availability of primary and secondary components after the occurrence of CD combined with C-SGTR determines the timing and magnitude of releases to the environment. The status of primary (e.g., pressure) and secondary (e.g., flooded or not) are needed to determine different release categories. The status of primary and secondary relief valves (open or close) (i.e., their possible failure modes under the harsh environment of severe accidents) are also needed to determine the release categories associated with C-SGTR.
- Modeling of severe accident management requires an understanding of when these strategies could be effective and how the human reliability methods can address human errors in decisionmaking under limited knowledge and guidance.
- Close coordination among PRA modeling needs, the supporting TH, and severe accident analyses is needed to address adequately the effectiveness of severe accident management guideline (SAMG) activities and their effects on release categories.
- Identifying the time when the emergency actions levels (EALs) are triggered, especially the time when a general emergency is activated in comparison to the time of release, is considered necessary to define the evacuation effectiveness and differentiate between early and late releases.

Instead, a simplified Level 2 model was considered for this study and for the purpose of addressing LERF. The approach heavily relies on two commonly used definitions of LERF:

(1) American Society of Mechanical Engineers PRA Standard (Ref. 1) defines LERF as "The rapid, unmitigated release of airborne fission products from the containment to the environment occurring before the *effective implementation of offsite emergency response and protective actions*."

(2) Pursuant to Regulatory Guide 1.174, "An Approach for Using Probabilistic Risk Assessment in Risk-Informed Decisions on Plant-Specific Changes to the Licensing Basis" (Ref. 2), NRC Manual Chapter 0609, Appendix H, Section 3.2 (Ref. 3) defines LERF as "The frequency of those accidents leading to significant, unmitigated releases from containment in a time frame prior to effective evacuation of the close-in population such that there is a potential for early health effect."

Any large unisolable leakage outside containment through C-SGTR is considered as a site emergency, because it will affect both the reactor coolant and the containment barrier. A general emergency will ensue when potential fuel barrier degradation occurs (at the onset of core uncovery). Therefore, in both cases, there would be a high potential for effective evacuation.

The likelihood of the occurrence of LERF sequences for pressure-induced C-SGTR during DBA sequences is relatively low. The dominant contributor to the risk is the failure to equalize and isolate the faulted SG, followed by the failure to provide makeup water to the RWST. The CD resulting from such sequences typically occurs late enough that evacuation can be credited and LERF be eliminated. Early CD and potential LERF sequences require additional failures, such as failure of the HPI and dry SGs. SGs are generally not expected to be dry unless the

sequence involves failure of both MFW and AFW systems. In such cases, there are two major SAMG actions typically credited for controlling the release and possibly mitigating the accident long before vessel breach. These SAMG actions are as follows:

- to arrest the core melt within the vessel by depressurizing and injecting water into the primary system before any significant fuel melting, core geometry change, or melt relocation has taken place
- to reduce the in-vessel release magnitude by flooding the vessel and scrubbing the releases
- to reduce releases to the environment via ruptured SG tubes by depressurizing the SG and filling it up with an alternate source of water

The vessel can be depressurized by opening all PORVs, thereby allowing coolant injection from the low-pressure ECCS. RCS depressurization could also take place because of a medium or a large LOCA but not generally from a small LOCA. Primary depressurization through secondary cool down using the intact SGs and the pressurizer spray could also be credited for the success of RCS depressurization. However, to provide this credit, the analyst should identify the probability that one or more SGs remain intact (not isolated because of SGTR). Although there could be several possible means for the primary depressurization, all are driven by dependent operator actions.

Primary depressurization could result in the injection of accumulator water into the vessel, which if it occurs at or shortly after the onset of CD, could provide additional time for the operator to align makeup water to the RWST for continued injection into the vessel. Injection to the vessel, if performed early, before significant core melt and debris relocation, could arrest further melting of the core. Therefore, it may significantly limit the amount of in-vessel releases. RCS depressurization or the occurrence of a medium or large LOCA would also create a major path of release to the containment rather than through SGTR. Therefore, if any of these SAMG actions are successful, the release through SGTR is expected to be negligible.

In addition, severe accident analyses are required to examine the effectiveness of such strategies. As an example, early injection into the vessel, when the CD is just initiated and fuel geometry has not significantly changed, could prevent the accident progression to fuel melting. However, a delay in vessel injection, after the fuel is partially melted and a significant change in core geometry has occurred, may not be effective. Failure to inject from the accumulators would significantly reduce the time available for operators to align makeup water to the RWST. It is, therefore, assumed that makeup water to the RWST cannot be successfully performed without the injections from accumulators.

A simplified model was proposed for the current study. This model relies on five factors as defined below:

| | | |
|---|---|---|
| (1) | frequency of DBA sequences with potential for C-SGTR | $f_{AC}$ |
| (2) | C-SGTR probability | $P_{CSGTR}$ |
| (3) | conditional CD probability | $P_{CCD}$ |
| (4) | failure probability of all SAMG actions | $P_{SAMG}$ |
| (5) | probability that early effective evacuation is not successful | $P_{EVAC}$ |

The product of these five factors defines LERF. Conservative estimates were assigned to the above factors for the purpose of the screening study. Chapter 7 contains further discussion.

## 2.2 Thermally Induced C-SGTR Sequences

This section details the sequences of interest for the potential occurrence of C-SGTR after the onset of CD during severe accidents. These sequences generally involve high primary pressure with at least one or more dry SGs and low secondary pressure, known as high-dry-low sequences. One way to identify such sequences is to use the binning information generated for defining plant damage states (PDSs) from Level 2 PRAs. Those PDSs that are binned into a class with a high primary pressure and with at least one or more dry SGs (i.e., loss of both MFW and AFW are required) are candidates for severe accidents with a potential for C-SGTR. Some Level 2 PRAs, however, identify the status of SG (i.e., dry or flooded SG) only for an SGTR-INIT and not for other sequences. Therefore, the determination of the frequencies for the pertinent sequences for thermally induced C-SGTR would require an additional examination of the sequences in Level 1 PRA models. It is strongly suggested that the status of SGs be defined for all sequences as part of the PDS identification in Level 2 PRAs to facilitate their use for C-SGTR evaluation.

Level 1 PRA sequences are to be examined for the sequences that include failure of feedwater (both main and auxiliary) to one or more SGs and where the primary pressure is expected to be high at the time of CD. Sequences involving large, medium, or interfacing system LOCAs could be considered as low primary pressure. Other sequences with low primary pressure could result from stuck-open PORVs or SRVs. Depending on the size of the primary PORVs and SRVs, low-pressure sequences may require the flow through more than one stuck-open valve. A depressurized primary system before CD caused by aggressive secondary cooling may not be considered as a low-pressure sequence, because the pressure is expected to become high at the onset of CD if secondary cooling is lost. For some sequences, SG cooling may not play a role in a CD scenario (such as a small LOCA with failure to inject). A small fraction of the sequence frequency accounting for AFW failure shall then be considered for C-SGTR evaluation.

A selected number of sequences are generically identified to allow a thermally induced C-SGTR screening analysis. This is done to avoid the complexity of identifying the C-SGTR sequences using the above process and for plants without proper Level 2 PRA models. These sequences are identified for the purpose of defining representative TH analyses and determining the time of CD and other information important to C-SGTR. Table 2-2 below shows these sequences. They are selected based on the expected TH behavior and the type of challenges they will have on SG tubes. They are not the same as PRA CD sequences. Several PRA CD sequences from internal and external hazards with similar TH behavior are combined and grouped together under each of these selected sequences. There are five base case sequences, noted as Base Cases 1 through 5. Each base case sequence could be slightly changed to obtain some alternative sequences. The time of the onset of CD from the occurrence of an initiator is specified as early or late in the second column of the table. As will be discussed, “early” generally means less than 8 hours, and “late” generally means greater than 8 hours. The exact timing for “early” and “late” depends on the time when a general emergency is activated. The period of interest is generally between the activation of a general emergency and the onset of CD. It is not associated with the time that the plant initiator occurred.

The extended station blackout (SBO) sequences are the most representative sequences that can cover all the sequences identified in Table 2-2. Some insights for PRA modeling of thermally induced C-SGTR, based on TH results for SBO scenarios of a selected W and a CE plant, are in Sections 2.3 and 2.4, respectively. These analyses did not credit mitigation capabilities provided by FLEX and Extensive Damage Mitigating Guidelines (B.5.b) backup

systems, and post-CD SAMG strategies. The current insights discussed in Sections 2.3 and 2.4 are, therefore, somewhat conservative. Sections 2.5 and 2.6 discuss the critical size for C-SGTR to be considered LERF and the proposed LERF model, respectively.

Table 2-2 Selected Sequences to Evaluate C-SGTR for Severe Accident Sequences (Cont.)

| Core Damage Sequences | Time for the Onset of Core Damage Relative to the Activation of a General Emergency | Availability of DC Power for Primary/Secondary Depressurization and Performing SAMG Activities | Notes |
|---|---|---|---|
| Base Case-1: SBO with failure of TDAFW at time zero, small RCP leakage[a,b] (e.g., 0.001325 m³/s (21 gpm) for some W pumps), and equivalent 0.0127 meters (0.5 inches) of leakage (relief path) from the SG secondary to the environment | Early | Yes | Base case probability of C-SGTR before HL failure |
| Alternate 1: Base Case-1 and 1 PORV or an SRV sticks open | Early | Yes | Lower probability of C-SGTR before HL failure due to lower primary pressure |
| Alternate 2: Base Case-1 except RCP seal leakage greater than 0.01136 m³/s (180 gpm) per pump | Early | Yes | Possibly higher probability of C-SGTR due to possible clearing of the loop seals |
| Alternate 3: Base Case-1 except no leakage or smaller leakages than 0.0127 meters (0.5 in.) from secondary side of SG to the environment | Early | Yes | Lower probability of C-SGTR than nominal since the secondary pressure is maintained and the delta pressure across the tubes is reduced |
| Alternative 4: Base Case-1 except larger leak area through the secondary of SGs (e.g., as a result of a stuck-open SG PORV) | Early | Yes | Higher probability of C-SGTR assumed since, after tube failure, the larger area through SG secondary would depressurize the primary, and therefore, reduce the likelihood of HL failure |
| Base Case-2: SBO with failure to load shed to extend battery life, rendering the failure of TDAFW to continue to run | Early or Late:<br><br>Depending on battery duration, could be considered either late or early | No | Similar C-SGTR probability to Base Case-1 |

Table 2-2 Selected Sequences to Evaluate C-SGTR for Severe Accident Sequences (Cont.)

| Core Damage Sequences | Time for the Onset of Core Damage Relative to the Activation of a General Emergency | Availability of DC Power for Primary/Secondary Depressurization and Performing SAMG Activities | Notes |
|---|---|---|---|
| Base Case-3: SBO with successful load shed to extend battery life. Failure of TDAFW to continue to run after battery depletion | Late | No | Similar C-SGTR probability to Base Case-1 |
| Base Case-4: Non-SBO sequences with total failure of secondary cooling at time zero and failure to do FB operation | Early | Yes | Similar to Base Case-1 probability |
| Base Case-5: Non-SBO sequences [c] with delayed failure of secondary cooling and FB operation (e.g., loss of service water, loss of chilled water due to external hazards] | Late | Yes | Varying probability of C-SGTR, depending on plant-specific features and the details of the sequences. These sequences could also cause RCP seal failures, with varying degrees of leakages. |

[a] RCP leakage for base SBO analyses set at 0.001325 $m^3/s$ (21 gallons per minute) per pump. This is typical of a W plant without SHIELD®[2]. CE plants with Flowserve or similar seals and W plants with SHIELD® mechanical seals or Flowserve pumps or CE plants have very low leakages following SBOs.

[b] Seal LOCAs for CE plants could occur as a result of loss of cooling and failure of the operator to trip the pumps. Seal leakages of 1,703 liters per minute (Lpm) (450 gpm) per pump could result.

[c] Appendix L contains details of a somewhat modified sequence in Base Case-5. These sequences consider that AFW flow is isolated to at least one SG, intentionally by the operator, since the associated secondary relief valve has stuck open.

## 2.3 Representative Sequences for a Westinghouse Plant

The TH analysis and the success criteria used for developing the PRA models for C-SGTR for an example W plant were gleaned from the information reported in NUREG/CR-6995, "SCDAP/RELAP5 Thermal-Hydraulic Evaluations of the Potential for Containment Bypass during Extended Station Blackout Severe Accident Sequences in a Westinghouse Four-Loop PWR," issued March 2010 (Ref. 4). NUREG/CR-6995 documents the TH evaluations performed using the SCDAP/RELAP5 systems analysis code and a model representing a W four-loop PWR (i.e., the Zion Nuclear Power Plant. The plant model benefitted from the following:

- extensive iterative comparisons with evaluations of natural circulation flows and turbulent mixing using a computational fluid dynamics code
- comparison with experimental data for pertinent fluid-mixing behavior

NUREG/CR-6995 also included some sensitivity evaluations and uncertainty analyses of the SBO accident sequences.

The base sequences were modeled assuming a preexisting leakage through the secondary side of each SG, equivalent to a hole of 3.2 square cm ($cm^2$) (0.5 square in. ($in.^2$)). As discussed in Appendix A to Sandia National Laboratories (SNL) JCN Y6486, "Severe Accident Initiated Steam Generator Tube Ruptures Leading to Containment Bypass-Integrated Risk Assessment," issued February 2008 (Ref. 5), this size of leakage is sufficient to ensure that the pressures in the secondary side of the SGs approach the atmospheric pressure after SG dryout. However, the assumed leakage area was shown to be insufficient to maintain a low SG secondary-side pressure after the occurrence of a guillotine break of a single SG tube.

The following points taken from Reference 5 emphasize the expectation that, during a severe accident sequence, the secondary-side depressurization is likely to be present:

- The findings from the TH analyses indicate that secondary leak areas of 3.22 and 6.45 $cm^2$ (0.5 and 1.0 $in.^2$) result in essentially full depressurization of the SG by the time the severe accident-induced temperature ramp occurs.
- ***Leaks directly to atmosphere*.** Given closure of the main steam isolation valves (MSIVs), feedwater isolation valves, and SG blowdown valves, such leaks would need to be in the stems or seals of these valves; the stems or seals of other valves or ports upstream of these valves; or the stems, seals, or seats of the secondary-side PORVs or SRVs. Such leaks would be present during normal operation. Another potential leakage source could occur if a secondary-side PORV or SRV recloses but does not reclose completely (e.g., allows a small amount of leakage).
- ***Leaks into the secondary piping*.** Perhaps more significant is the potential for leakage past the isolation valves into the downstream piping in the secondary system. The long, large runs of piping have a significant volume and so could accept small leakage rates without themselves pressurizing to provide any backpressure. The amount of leakage past the valve seats would be very small relative to the total size of the valve. A 508-cm (20-in.) diameter MSIV would have a total flow area of over 1,935 $cm^2$ (300 $in.^2$). Therefore, an MSIV that is 99.9-percent closed will still not be sufficient to maintain secondary pressure. Not being part of the containment isolation boundary, SG isolation valves are not required to meet containment isolation leak rate requirements. The performance requirements for these valves are based on maintaining pressure in the SGs when full, and so they are not required (nor are they designed, qualified, or tested) for this kind of leak tightness.

The main two sequences modeled were as follows:

(1) SBO with early failure of the TDAFW pump, resulting in CD and a potential for C-SGTR because of creep rupture

(2) SBO with failure of TDAFW after battery depletion

Several sensitivity case studies were also performed. These studies generally addressed different issues, as summarized below:

- A study examined the effect of RCP seal leakage by considering various sizes of RCP seal leakages from 79.5 Lpm (21 gpm) per pump and up. The case runs evaluated the pressure and temperature impact on primary and secondary systems and examined the impact on loop seal clearing potential.
- A study examined the effect of early depressurization on the sequence progression by considering the operator's action to depressurize SGs at 30 minutes, by opening at least one SG atmospheric dump valve or SG PORV per SG. This action drops the primary pressure below 4.83 MPa (700 psi). This actuates the accumulator discharge. Two cases were analyzed, depending on the rate of depressurization (slower and faster rates).
- A study examined the effect of C-SGTR with an equivalent guillotine break of one tube on primary depressurization, thereby preventing or delaying HL failure. This resulted in a slow depressurization of the primary; however, it is not fast enough to prevent HL failure.

Section 7.1 contains a detailed discussion of several other sensitivity case runs, along with their TH behavior, and their effect on PRA results for the example W plant.

## 2.4 Representative Sequences for a Combustion Engineering Plant

The TH analyses used to support the development of the PRA models and success criteria were based on the NRC-sponsored MELCOR evaluation of Calvert Cliffs Nuclear Power Plant for several SBO scenarios. Information contained in the Calvert Cliffs individual plant evaluation and the individual plant evaluation for external events was also used to support the sequence identification and development of the C-SGTR PRA. Chapter 3 details the TH evaluations performed using the MELCOR severe accident analysis code for Calvert Cliffs. MELCOR analyses were performed in two stages. The initial analyses identified additional enhancements to be incorporated into the MELCOR models. All discussion in this document relies on the second stage (enhanced modeling) of MELCOR analyses. Some insights gained from the first-stage sensitivity analyses were used to shape some of the PRA arguments.

The following two representative base sequences used the latest MELCOR analyses. These two sequences modeled a leakage through the secondary side of each SG, equivalent to an area of a 3.22-$cm^2$ (0.5-$in.^2$) hole. The size of this leakage was sufficient to ensure that the pressure in the secondary side of the SGs approached the atmospheric pressure after SGs were dried out. The size of the leakage, however, is not sufficient to maintain low secondary-side pressure if SG tubes have ruptured.

The results from the MELCOR runs were slightly different in format from the SCDAP/RELAP5 results reported in NUREG/CR-6995. The study provides the MELCOR results for each plant loop separately (i.e., RCS loop A with the pressurizer and RCS loop B without the pressurizer). Furthermore, the MELCOR results represent two types of hot tubes: one exposed to the hottest gas temperature and the other exposed to an average hot-gas temperature. This additional information was used in the PRA for CE plants.

(1) This sequence considered an SBO with failure of the TDAFW pumps early in the sequence (i.e., at time zero), followed by an early CD with a potential for C-SGTR because of creep rupture. The sequence also considered an RCP seal

leakage of 79.5 Lpm (21 gpm) per pump. The 79.5-Lpm (21-gpm) pump seal leakage is typical of a W plant without SHIELD®[2]. CE plants with Flowserve or similar seals and W plants with SHIELD® mechanical seals or Flowserve pumps or CE plants have very low leakages following SBOs (generally less than $1.262X10^{-4}$ $m^3/s$ (2 gpm). The 79.5-Lpm (21-gpm) leakage per RCP is assumed for a CE plant just for consistency with the W evaluation. A sensitivity analysis was performed by assuming no RCP seal leakages in the MELCOR model. Section 3.6.6 discusses this. The result of this sensitivity analysis showed that the RCP seal leakage had some impact on early primary depressurization but no impact on long-term primary pressure and temperature response (i.e., after the onset of CD). Therefore, the C-SGTR probability is not expected to be affected by the 79.5-Lpm (21-gpm) seal leakage per each RCP. The base MELCOR results for this SBO scenario (i.e., short SBO) are considered to be representative of several PRA accident sequences with similar behavior (see earlier discussion in this section). A short SBO includes an SBO sequence with simultaneous failures of TDAFW pumps because of common-cause failure to start, or an SBO with an initial availability of TDAFW pumps followed by their failures because of SG overfill in about an hour.

(2) An SBO with delayed failures of TDAFW pumps after battery depletion is considered for this sequence (i.e., long SBO). TDAFW is initially available, but it will fail shortly after the depletion of the battery because of the loss of direct current power. The MELCOR analysis assumes that the TDAFW pumps were operating for a period of 4 hours. A normal RCP seal leakage of 79.5 Lpm (21 gpm) per pump is assumed. Similarly, a sensitivity analysis of RCP seal leakage showed that the impact on the C-SGTR probability is insignificant because of the RCP seal leakage assumption.

Additional sensitivity analyses used the MELCOR evaluation by assuming that there was zero leakage through the secondary system at the start of SBO (instead of the generally assumed leakage area of 3.2 $cm^2$ (0.5 $in.^2$)), such that the secondary relief and safety valves will be demanded early during the accident and before the onset of CD. The MELCOR evaluation for this case further assumes that the secondary relief and safety valves fail to reclose after the first opening.

MELCOR evaluations performed other sensitivity analyses to further examine the effect of various sequences. The following were noted:

- C-SGTR with an equivalent leakage area of the guillotine break of less than one tube will not result in depressurization of the primary.
- An equivalent leakage area of one or more tubes could result in a significant release if one or more of the SG safeties or the relief valves are left open or stick open.
- The primary is initially depressurized and the accumulator discharges when one or more secondary relief valves stick open early in the accident. This will further delay HL/surge line creep rupture failures. The probability of C-SGTR because of creep rupture, however, is not affected as much because the lower secondary-side pressure increases the delta pressure across the tube.

Section 7.2 contains a detailed discussion of these sensitivity case runs, along with their TH behavior and their effect on PRA results for the example CE plant.

## 2.5 Critical Leakage Area for C-SGTR

The leakage area through the failed SG tubes determines the consequence and severity of the C-SGTR accident. It is generally assumed that there is a threshold, or a critical leakage area, beyond which the impact of larger leak areas on the accident severity will be negligible. This section discusses the considerations for determining these critical leakage areas.

The occurrence of pressure-induced C-SGTR during some accident sequences considered for the PRA (e.g., large secondary-side break, ATWS) would require the operator to perform additional actions. These actions are beyond those generally required for the original accident sequence, and they are in response to and to cope with a C-SGTR event. These actions are similar to those operator actions that are generally performed in response to an SGTR initiator. For such events, the size of the leakage determines how fast the operator should attempt to cool down and depressurize the primary to isolate the affected SGs. The most striking PRA effect of larger leakage areas through SG tubes during DBA events is a higher failure probability of the related operator actions.

For thermally induced C-SGTR during a severe accident (i.e., after CD), the size of the leakage area would determine the size of release through the containment bypass. It determines if the end state of a particular containment bypass sequence should be categorized as LERF. For a small leakage, the primary is expected to stay pressurized (generally at the primary relief set point, which is about 15.5 MPa (2,250 psi)), resulting in a failure of other RCS components (e.g., HL) shortly after the failure of the tubes. The failure of the RCS component, therefore, significantly reduces and eliminates any release through the SG tubes. These sequences of containment bypass because of C-SGTR may not be categorized as LERF.

Larger leakages could pressurize the secondary side of the affected SG such that both primary and secondary sides equalize at the pressure set point of the SG relief valves (which are about 8.27 MPa (1,200 psi)). In this case, there is a lower failure probability of the other RCS components (e.g., HL) because of lower primary pressure. This pressure assumes that the SG PORVs and SRVs cycle as many times as needed without any failures. If any of the SG relief valves fail to close (stick open), the primary will be depressurized, and this eliminates any possibility of failure of other RCS components. There could also be a threshold for larger leakage areas through the failed SG tubes such that the countercurrent flow through the HL cannot be maintained. In such cases, the hot steam will flow through the SG tubes, causing a number of tube failures resulting in a large containment bypass. The TH analyses for the example CE and W plants have shown that a guillotine break of at least one SG tube is required to pressurize the SG secondary side such that SG PORVs and SRVs are demanded.

Sections 2.5.1 and 2.5.2 contain detailed discussion of the critical leak areas for DBA and severe accident sequences.

### 2.5.1 Critical Leakage Areas for Design-Basis Accidents

The key mitigating actions, in response to a DBA-induced SGTR (except ATWS sequences), are as follows:

- Establish a secondary heat sink.
- Isolate the affected SGs.
- Depressurize the RCS to avoid cycling the safety valves on the affected SG.

- Refill the RCS.
- Establish long-term cooling.

If the secondary heat sink is lost, FB cooling can be used. When FB cooling is used, long-term actions are needed for cold leg recirculation or for continued makeup to the RWST.

All pressure-induced SGTRs (i.e., burst) during ATWS sequences are conservatively assumed to result in CD and LERF.

The main effect of larger leakage areas from SG tubes during DBAs is the reduction in the amount of time that the operators have to cool down and depressurize the primary system. Because of reduced time, the probability of an operator error causing an SG overfill could significantly increase. This, in turn, could result in flooding the steam lines and possibly causing an SG safety or relief valve to fail to reclose. SG overfill would also cause the failure of the TDAFW because of water carryover. If one were to assume a tube rupture sequence exceeding several tubes failing, it would ensure a stuck-open safety valve. This would lead to a failure to isolate the affected SG with an increased likelihood of CD. Although the timing for the plant response is shortened for some actions as described above, the remaining time available for other key actions in the accident sequence (such as initiation of FB) may not be affected by the size of the C-SGTR leakage areas.

This scoping study considered the following guidelines for the critical leakage areas associated with C-SGTR during DBA sequences.

- For ATWS sequences, tube failures are assumed to directly result in core damage and LERF, regardless of the size of leakage (without further analysis).
- For all other sequences, a leakage area equivalent to a guillotine break of one tube is assumed to have occurred. This size of break requires the operator to follow the emergency operating procedure associated with SGTR initiators. For PRA purposes, such C-SGTR events are transferred to the PRA SGTR event tree for estimating the delta CD frequency and delta LERF.

### 2.5.2 Critical Leakage Areas for Severe Accidents

Earlier studies (such as the SNL study documented in Reference 5) showed that SG tube failures generally occur shortly after the onset of fuel damage for severe accidents. The SNL study performed a rough estimate of a critical SG tube leak area that could release the whole primary volume in 4 hours. This was done because of a lack of detailed severe accident analysis of post-SGTR. The SNL report therefore, determined the following:

- Flow through the cracks is choked (no secondary-to-primary pressure equalization).
- Early containment bypass occurs if the contents of the RCS are released through the cracks in less than 4 hours (no HL failure or failure of other RCS components was considered).

An uncertainty distribution for the required crack opening area was determined by considering the uncertainties in the following:

- the release time for containment bypass
- the temperature of the gas exiting the break
- the specific heat ratio for the gas mixture
- the average molecular weight of the gas mixture

Using this analytical approach, the mean crack opening area for containment bypass is calculated to be 0.52 $cm^2$ (0.081 $in.^2$). The lower and upper 90-percent confidence limits for this value were calculated to be 0.34 $cm^2$ (0.053 $in.^2$) and 0.8 $cm^2$ (0.124 $in.^2$), respectively.

This study considers SNL's estimate to be conservative: for example, this size of leakage is not expected to depressurize the primary fast enough to prevent the failure of the HLs. The likelihood of the failure of an RCS component is expected to be close to 1, if the primary is not significantly depressurized. Furthermore, the analysis does not directly address the overall magnitude of release.

The current study defines critical leak areas by considering the following three SGTR leak areas that could affect the progression of the accident and the amount of releases:

(1) For small C-SGTR leak areas less than a guillotine break of one tube between 4.8–6.4 $cm^2$ (0.75–1 $in.^2$), the primary is not expected to depressurize, and the likelihood of failure of the HL or other RCS components is expected to be quite high. For this leak area size, repeated cycling of primary SRVs, including the possibility that at least one SRV sticks open, is expected to be high. Therefore, most of the in-vessel releases will end up in the containment rather than leaking through the small C-SGTR leak area. The probability that such leakages (i.e., containment bypass) result in LERF is negligible.

(2) There is also a leak area that can pressurize the SG secondary side such that a significant amount of cycling of the SG PORV or SRV is expected (and therefore a release path to the environment). In such cases, the primary and secondary side will equalize at a pressure of around 8.3 MPa (1,200 psi), unless the SG PORV fails to reclose. The results of severe accident analysis (RELAP runs for the example W plant and MELCOR for the example CE plant) indicate that tube leak areas equivalent to a guillotine break of one or more tubes, between 4.8–6.4 $cm^2$ (0.75–1 $in.^2$), generally satisfy this criterion. A typical guillotine break for plants, discussed in Chapter 7, has a maximum total leak area of about 6 $cm^2$(0.9 $in.^2$).

(3) An SG tube leak area could be large enough to collapse the countercurrent flow described in Section 3.1 and transform it to a unidirectional flow regime. It is possible for the counter current flow to be reestablished after some time. However, a large number of tubes are assumed to fail because of exposure to hot gas temperatures. The release is also expected to be large and early, similar to the previous case, without sufficient time available for any recovery actions.

From the discussion provided above, this scoping PRA considered a critical area of containment bypass. Leak areas equivalent to a 4.8–6.4-$cm^2$ (0.75–1-$in.^2$) guillotine break of a tube are considered to have a potential for LERF, if an SG relief valve sticks open. On the contrary, this size of leakage has no LERF potential if the primary relief valve sticks open and none of the SG

relief valves fail. The small secondary hole of 3.2 $cm^2$ (0.5 $in.^2$) that is assumed in the analysis to depressurize a dry SG does not provide a significant contribution to LERF and it is not of sufficient size to depressurize the SG secondary side after C-SGTR occurs.
A leakage area equivalent to the areas of more than three tubes is always considered as LERF because repeated cycling is expected to cause the SG relief valves to fail eventually. The study made similar assumptions for cases where the loop seals are cleared during a severe accident.

For the purpose of this study, using simplified C-SGTR PRA models, a leakage area equivalent to a guillotine break of one or more SG tube if it occurs early, is considered as LERF. This corresponds to assuming a large leakage directly to the environment from the secondary system, equivalent to the area of one SG PORV or SRV. This is consistent with the latest information available from NUREG/CR-7110, "State-of-the-Art Reactor Consequence Analyses Project Volume 2: Surry Integrated Analysis," Volume 2, Revision 1, issued August 2013 (Ref. 6), which indicates that the SG SRVs will fail open within 10 cycles when the gas temperature exceeds 1,000 Kelvin.

## 2.6 A LERF Model

The end state associated with Level 1 event trees generally corresponds to the time when the fuel begins to uncover. For some sequences, there is a large inventory of water in the secondary sides of the SGs at the time when the fuel begins to be uncovered. It could, therefore, take some time (about an hour and a half) for the SG to become dry. The countercurrent flow regime occurs in the HLs after SGs become dry. If the PORV and the direct current power are available or recovered during this period, the operator could open the PORVs and depressurize the primary, thereby avoiding or significantly diminishing the probability of C-SGTR.

If the operators fail to depressurize the primary, and SGTR occurs before HL failure (i.e., C-SGTR), the primary pressure would remain high for small SGTR leak areas. The likelihood of HL failure should then be considered. For larger C-SGTR leaks, however, when the primary is depressurized partially through the ruptured tubes, the likelihood of HL failure is expected to be smaller. Furthermore, after SGs have dried up, it typically takes another 6 to 8 hours for the vessel breach to occur. This provides sufficient time to perform SAMG activities (e.g., early vessel injection to help mitigate further fuel damage and flooding the SG secondary side to scrub any possible releases through the ruptured SG tubes).

The release through C-SGTR will nearly stop when the vessel is flooded and the SG secondary is filled with water. Therefore, the time it takes for SAMG actions to become effective determines the magnitude of the release. This is considered an important step for categorizing the size of releases in terms of the magnitude of the source term.

The release categories are generally binned into several groups, depending on the magnitude of release and the time of release after evacuation. Some past studies (Ref. 7) have suggested the following release bins:

- large-early release (LER)
- large-late release (LLR)
- medium-early release (MER)
- medium-late release (MLR)

- small-early release (SER)
- small-late release (SLR)
- negligible or controlled late releases (CLR)

The open literature has not yet reported the exact definitions of these categories in terms of the timing and the magnitude of the releases. The magnitude is sometimes defined by the fractional releases of iodine (I) and cesium (Cs). For example, large, medium, and small could correspond to a release fraction (RF) of either Cs or I to the environment of greater than 5 percent (RF>5%), between 1 and 5 percent (RF1%≤–≤5%), and less than 1 percent (RF<1%), respectively. The category of no release or negligible release is retained for cases where core damage is arrested within the vessel and all partial releases are scrubbed. The amount of release in the no-release category is generally comparable to that of the fuel gap release plus the radioactivity inventory in the primary coolant (it approximately translates into less than 0.01 percent of I or Cs).

The study bases the definition of early and late on the duration of time between the activation of a general emergency, requiring the start of evacuation, and the time of major radioactivity releases. Early generally reflects a duration of less than 12 hours, and late is defined as a duration greater than 12 hours. Using 12 hours as the threshold is intended to cover the external hazards; therefore, it is considered to be a conservative value for internal event initiators. For most internal event initiators in PRA, a value of 8 hours might be more appropriate.

Figure 2-2 shows an example of an emergency response timeline for the unmitigated long-term SBO (*ltsbo*) sequence (an SBO with failure of TDAFW after batteries are depleted) (Ref. 6). The timing of emergency classification declarations in this figure was based on the EALs contained in the site emergency plan implementing procedure at Surry. Surry was selected as a particular example. Similar timing of EAL classification declarations are also implemented in other PWRs (Ref. 7). Application of this method may be applied to other nuclear stations with proper consideration of possible site-specific issues. Note that this information is intended as an illustration of the general time frames and accident sequence progression. This sequence triggers EAL SS1.1, which specifies that a site area emergency (SAE) is declared if all offsite power and all onsite alternating current power are lost for more than 15 minutes. If the restoration of power seems unlikely within 4 hours, EAL SG1.1 requires that a general emergency be declared. SAE is, therefore, expected to be declared in about 15 minutes, and plant operators would recognize within the first 2 hours that restoration of power within 4 hours is unlikely. A period of 2 hours from the loss of power was selected as a reasonable time for declaration of a general emergency. From the MELCOR analysis, the first fission product gap release occurs 16 hours into the event. This timing diagram basically reveals a high likelihood of an effective evacuation during *ltsbo* sequences.

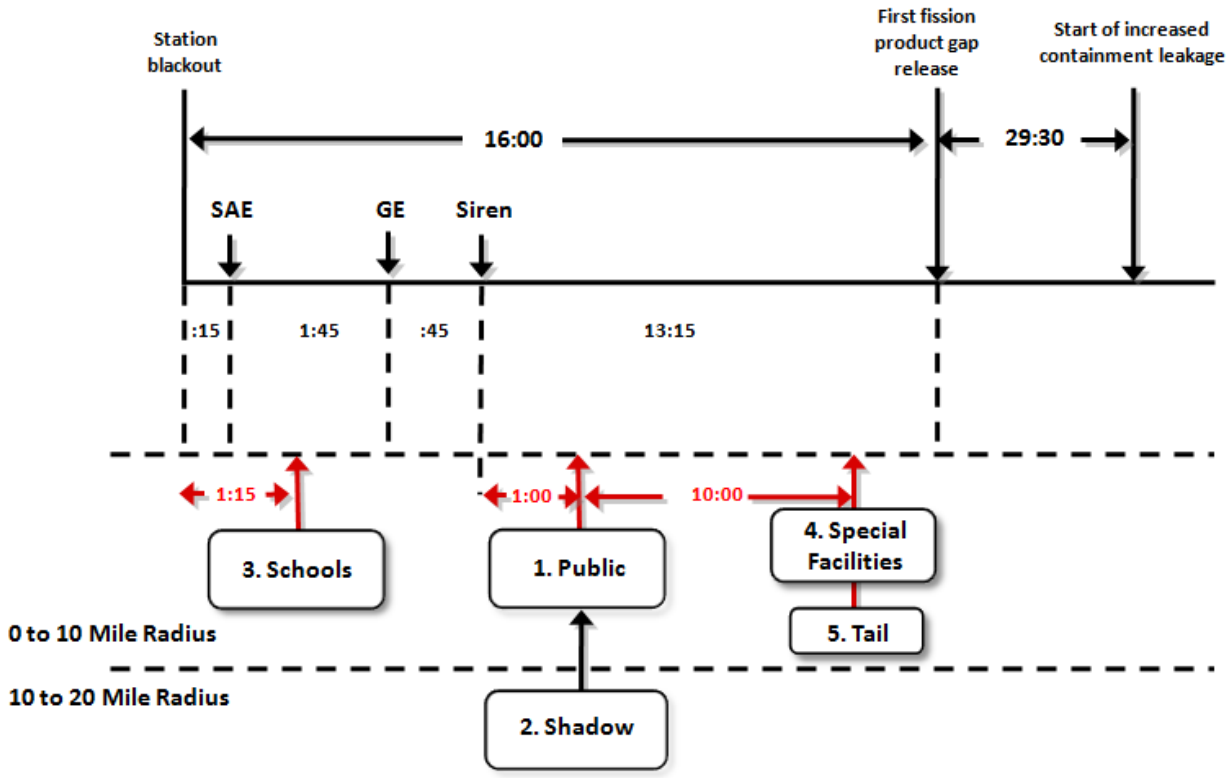


Figure 2-2 Unmitigated ltsbo emergency response timeline

Similarly, Figure 2-3 shows the emergency response timeline for the unmitigated short-term SBO (*stsbo*) sequence (SBO with early failure of TDAFW). For this sequence, SAE is also declared after 15 minutes of SBO, because EAL SS1.1 is triggered. In *stsbo*, the core is expected to be uncovered in less than an hour and a half with the core exit thermocouple reading in excess of 648.89°C (1,200 °F), and with the reactor vessel water level lying below the top of active fuel, prompting the declaration of a general emergency. From the MELCOR analysis, the first fission product gap release occurs about 3 hours into the event, with a significant radioactive release through the containment, if no C-SGTR occurs, in 25.5 hours into the event. This timing diagram basically reveals that there is a high likelihood that an effective and complete public evacuation may not be possible before some radioactive releases.

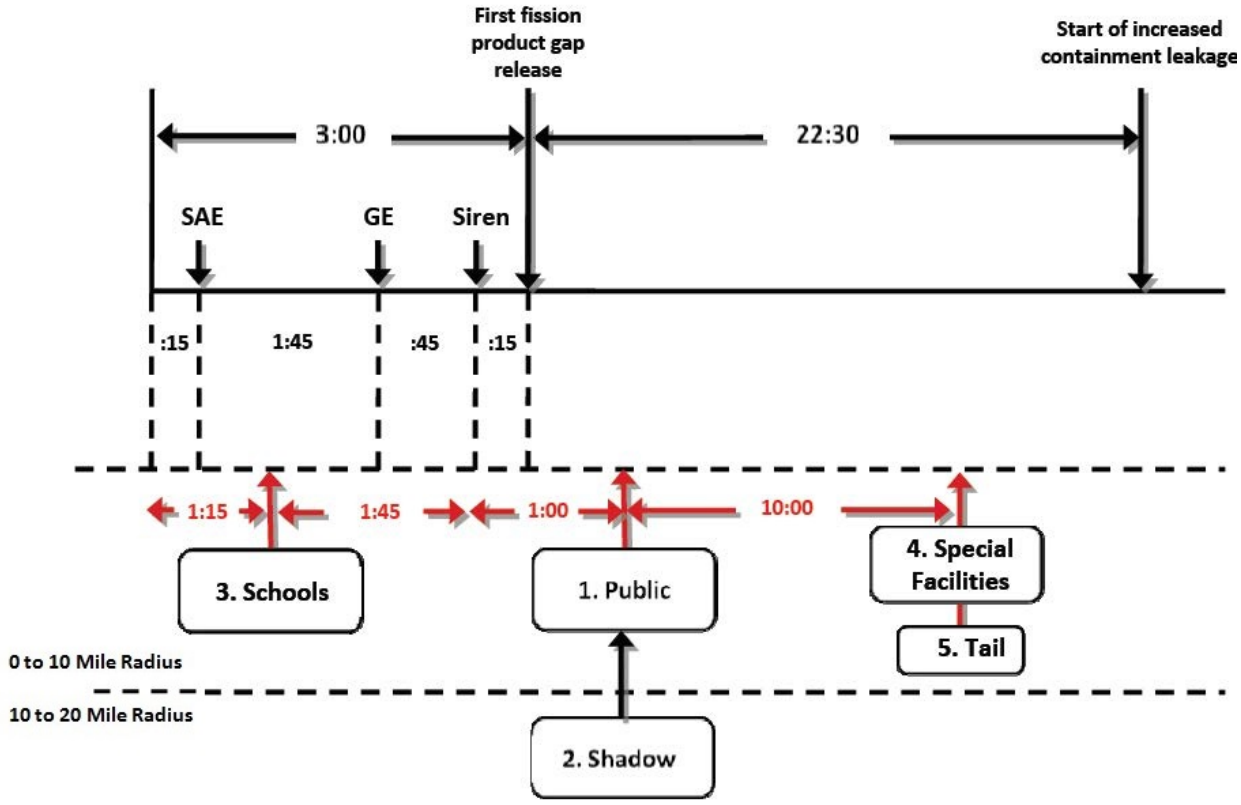


Figure 2-3 Unmitigated stsbo emergency response timeline

A simplified LERF model that relies on five factors, similar to what was defined earlier for C-SGTR because of DBAs, was also defined for C-SGTR because of severe accidents. LERF is estimated by the product of the five factors defined below:

| | | |
|---|---|---|
| (1) | frequency of severe accident sequences with potential for C-SGTR | $f_{AC}$ |
| (2) | C-SGTR probability | $P_{CSGTR}$ |
| (3) | conditional probability that the subsequent failure of RCS, including the stuck-open relief valves, do not occur | $P_{NDEP}$ |
| (4) | failure probability of all SAMG actions | $P_{SAMG}$ |
| (5) | probability that early effective evacuation is not successful | $P_{EVAC}$ |

Chapter 7 uses the above model for the example W and CE plants to make LERF estimates.

## 2.7 References


1. ASME/ANS RA-Sa-2009, “Standard for Level 1/Large Early Release Frequency Probabilistic Risk Assessment for Nuclear Power Plant Applications, Addendum A,” American Society of Mechanical Engineers, March 2009.
2. NRC, RG 1.174, An Approach for Using Probabilistic Risk Assessment in Risk Informed Decisions on Plant-Specific Changes to the Licensing Basis, Revision 2, May 2011, ML100910006.

3. NRC Manual Chapter 0609, Appendix H, “Containment Integrity Significant Determination Process, May 2011.

4. U.S. Nuclear Regulatory Commission, “SCDAP/RELAP5 Thermal-Hydraulic Evaluations of the Potential for Containment Bypass during Extended Station Blackout Severe Accident Sequences in a Westinghouse Four-Loop PWR,” NUREG/CR-6995, March 2010. Agencywide Documents Access and Management System (ADAMS) Accession No. ML101130544.

5. Sandia National Laboratories, “Severe Accident Initiated Steam Generator Tube Ruptures Leading to Containment Bypass-Integrated Risk Assessment,” JCN Y6486, February 2008.

6. U.S. Nuclear Regulatory Commission, “State-of-the-Art Reactor Consequence Analyses Project Volume 2: Surry Integrated Analysis,” NUREG/CR-7110, Vol. 2, Rev. 1, August 2013, ADAMS Accession No. ML13240A242.

7. Azarm, M.A., et al., “Feasibility Study of Risk Informing Emergency Action Levels of Fission Product Barriers Using Level 2 PRA,” PSA 2013, Columbia, SC.

# 3 THERMAL-HYDRAULIC ANALYSES FOR WESTINGHOUSE AND COMBUSTION ENGINEERING PLANTS

Thermal-hydraulic (TH) analyses were performed to study a Combustion Engineering (CE) plant's response to reactor coolant system (RCS) conditions that could lead to consequential steam generator tube rupture (C-SGTR). The results and insights of Chapters 4, 5, and 7 were generated from the TH sequences associated with SCDAP/RELAP runs reported in NUREG/CR-6995, "SCDAP/RELAP5 Thermal-Hydraulic Evaluations of the Potential for Containment Bypass During Extended Station Blackout Severe Accident Sequences in a Westinghouse Four-Loop PWR," issued March 2010 (Ref. 1), for the Westinghouse (W) plant, and the MELCOR runs discussed below for the CE plants.

This chapter summarizes the TH work conducted to study thermally induced C-SGTR for W plants and provides a detailed analysis for CE plants that use replacement steam generators (SGs). The work includes (1) the development of updated CE computation fluid dynamics (CFD) and MELCOR models, (2) the application of these models on select risk-significant sequences to evaluate expected TH behavior, (3) the comparison of results against previous analyses, (4) an uncertainty analysis for the effect of TH parameters, (5) the generation of TH data files in the SGTR probabilistic calculator and finite element (FE) analyses, (6) the generation of release data in updating the risk contribution from these events, and (7) an assessment of the effect of instrument tube failures.

Section 3.1 describes the TH analysis and lists the previous work on the subject. Section 3.2 describes the Sandia National Laboratories (SNL) deck generation and summarizes some of its analyses. Section 3.3 describes the CFD analyses and input used for the SNL and U.S. Nuclear Regulatory Commission (NRC) analyses. Section 3.4 describes two stages of deck modifications made by the NRC, one before the initial set of simulations and one used for the final set of simulations. Section 3.5 describes a conceptual model for loop seal clearing. Section 3.6 summarizes the major simulation results. Section 3.7 describes potential future analyses, and Section 3.9 provides conclusions and recommendations from the TH work.

## 3.1 Introduction

C-SGTR accidents are of interest because of the potential for fission product (FP) releases direct to the environment, bypassing the containment. Reactor designs include containments that reduce releases in the event of an accident. A containment bypass release refers to a situation in which FPs released during core degradation bypass the containment and thus do not benefit from these reductions. Fission products that enter the SG secondary sides are prevented from reaching the environment solely by a series of valves the failure of any of which will result in an open path from the core to the environment.

There are two general types of C-SGTR sequences: one is a thermally induced C-SGTR, in which hot gases emanating from the core during a severe accident cause creep rupture of SG tubes. The second type of C-SGTR is pressure induced, in which a shock from some event, typically a main steamline break, causes tubes to rupture. This section of the report deals exclusively with thermally induced C-SGTR.

In the thermally induced C-SGTR, heat transfer to the tubes by natural circulation results in tube rupture. Figure 3-1 shows the two different forms of severe accident natural circulation flows. The left part of the diagram shows full-loop natural circulation conditions. Hot gases leaving the

core flow through the hot leg (HL) and are cooled as they pass through the SG with the cooled gases returning to the core through the cold legs. The right part of the diagram shows closed-loop-seal natural circulation flow. For this situation, the water in the loop seal blocks the return flow to the core. The cooled gases can only return to the core through SG tubes and the HL. For this situation, a countercurrent flow situation exists where hot gases from the core are flowing to the SGs through the top of the HLs while cooled gases are returning through the bottom of the HL. The volumetric flow rate for countercurrent natural circulation is lower than that for full-loop natural circulation. Thus, closed-loop natural circulation transfers heat less efficiently to the SG tubes, and tube rupture is less likely to occur under these conditions.

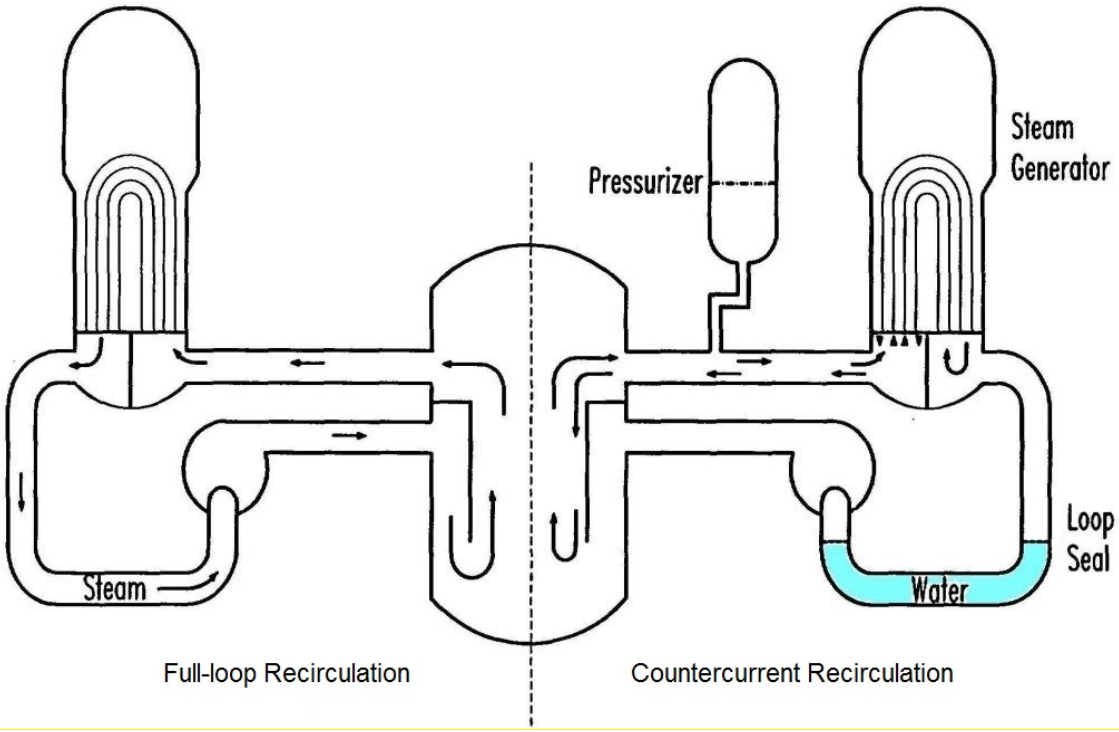


**Figure 3-1 Severe accident natural circulation flows**

The TH work described in this section deals primarily with closed-loop-seal natural circulation behavior, although open-loop natural circulation behavior is also discussed.

Although risk analyses have previously considered SG tube ruptures (SGTRs), they have typically not considered thermally induced C-SGTRs. In the previous analyses, the tube rupture was considered to be the initiating event. This rupture can lead to a severe accident if corrective actions are not taken in time. This type of SGTR is a design-basis event for which plants are designed to cope without progressing to a severe accident. Plants have coped with all SGTRs to date. A C-SGTR differs from this sequence in that the severe accident causes the tube rupture.

NUREG/CR-6995 (Ref. 1) extensively studied C-SGTR TH behavior for W plants. Some work was performed on CE plants (Ref. 2) with SCDAP/RELAP but, having predated the final W analysis, it did not incorporate all the modeling improvements made for the W designs. The Electric Power Research Institute (EPRI) considered CE plants in its 2002 SG-tube-related risk

analysis (Ref. 3), which showed that CE plants were more vulnerable to C-SGTR than are W plants during station blackout (SBO) accidents.

Because of the capability to predict FP releases in addition to TH behavior, the decision was made to switch from SCDAP/RELAP to the MELCOR code to perform the CE C-SGTR analysis, taking advantage of the lessons learned during the previous W analyses.

### 3.1.1 Summary of Results Obtained in NUREG/CR-6995

To put the analysis for CE plants in proper perspective, it is useful to include a summary of the TH results for W plants. The following are some pertinent excerpts from the Executive Summary of NUREG/CR-6995:

> For PWRs [pressurized-water reactors] with U-tube SGs, the natural circulation of superheated steam in the loop piping during specific low probability severe accident conditions could result in sufficient heating of the SG tubes to induce creep-rupture failure under certain scenarios. To support an overall examination of the risk impacts of induced tube failure, thermal-hydraulic analyses have been performed. The analyses used the SCDAP/RELAP5 systems analysis computer code, aided by computational fluid dynamics (CFD) simulations, to examine the pressure and temperature conditions that challenge the integrity of the reactor coolant system pressure boundary and to estimate the timing of specific reactor coolant system component failures.
>
> These evaluations have focused on station blackout (SBO) severe accident scenarios in Westinghouse four-loop PWRs. The scenarios that challenge the tubes primarily involve a counter-current natural circulation flow pattern during conditions referred to as high-dry-low. The high-dry-low scenario refers to a set of conditions that includes a high pressure in the reactor coolant system (RCS), a loss of SG water inventory and a failure to provide a source of feedwater (dry), and a significant leak from the SG secondary side boundary that results in a low pressure on the secondary side of the SG tubes. Another condition posing a challenge to steam generator tubes is associated with full-loop natural circulation flows that are possible if the water in the loop seal is cleared and the reactor vessel downcomer is cleared. Based on our recent SCDAP/RELAP5 analysis, this condition is considered to be much less likely than the condition of counter-current natural circulation flow.
>
> A severe accident-induced failure of an SG tube releases radioactivity from the RCS into the SG secondary coolant system from where it may escape to the environment through the pressure relief valves. An environmental release in this manner is called “containment bypass,” which contrasts with releases into the containment that result from failures of HL piping, pressurizer surge-line piping, or the lower head of the RV [reactor vessel]. The potential for steam generator tube failure by creep rupture and containment bypass under the high-dry-low conditions is effectively eliminated if (1) the RCS pressure is reduced because of operator actions to intentionally depressurize the RCS or primary system leakage (eliminating the high-pressure condition), (2) feedwater flow is maintained (eliminating the dry condition and reducing RCS pressure), or (3) the SG secondary system retains pressure (eliminating the low-pressure condition on the secondary side).

The clearing of a loop seal eliminates the counter-current flow pattern described above and creates a challenging environment for SG tubes. Loop seal clearing (along with a clearing of the fluid in the RV lower downcomer region) results in a direct natural circulation path around the coolant loop (RV, HL, SG, cold leg). Loop seals are more likely to clear when the water in the loop seals is heated and a rapid depressurization occurs. If loop seals are cleared and full loop natural circulation is established, the hot steam from the RV challenges the integrity of the SG tubes.

The timing of the failure of the system components is significant. If a[n] SG tube or tubes are predicted to fail prior to the HL or other RCS components, steam and radioactive FPs (released during core degradation) pass into the SG secondary system and provide a potential for containment bypass. Predictions indicate that a[n] HL or other RCS component will fail shortly after an SG tube fails because the SG tube failures do not immediately depressurize the system. The subsequent failure of the RCS boundary significantly reduces the rate of mass flow from the primary system into the SG secondary system. Alternatively, if a[n] HL or other RCS component of significant size fails prior to an SG tube, the release of contaminated steam would be completely into the containment because the resulting rapid RCS depressurization prevents subsequent failures of SG tubes and the associated containment bypass.

This report documents the current predictions for system behavior during extended SBO scenarios. The objective of this report is to combine the four-loop PWR extended SBO severe accident event sequences that fall into the following three categories:

(1) sequences resulting in containment bypass

(2) sequences providing a potential for containment bypass for which an outcome may be determined by initially comparing the degradation of tube strengths in a prototype SG against the SCDAP/RELAP5-predicted tube-failure margins

(3) sequences not resulting in containment bypass

This categorization of event sequences provides information that—when combined with results from RCS component analyses, probabilistic risk assessments, and environmental release evaluations—will permit an evaluation of risks because of containment bypass for Westinghouse four-loop plants.

A model of a Westinghouse four-loop plant is developed for use with the SCDAP/RELAP5 thermal-hydraulic system code and employed to perform simulations of accident-event sequences pertinent for the containment bypass issue. The SCDAP/RELAP5 code calculates fluid and structure conditions, such as pressures and temperatures, throughout the regions of a plant model. In addition, the code includes models for calculating the progression of core damage behavior during severe accidents and simplified models for creep-rupture behavior of RCS components. In the Westinghouse four-loop plant model, creep-rupture behavior is evaluated with SCDAP/RELAP5 to predict failure times for the HLs, pressurizer surge line, and SG tubes. The creep-rupture model allows one to specify a “stress multiplier.” A multiplier of 1.0 provides a

creep-rupture failure prediction based on no degradation of the structural strength of the material. Multipliers greater than 1.0 represent degraded structural strengths associated with preexisting tube flaws or degradation that may exist. A stress multiplier of 2.0, for example, represents a degraded-strength condition for which the creep-rupture failure of a structure is predicted when the stress applied is only 50 percent of that required to fail the undegraded structure. The term “SG tube failure margin” as used in this report refers to the tube-stress multiplier in the model that results in prediction of SG tube creep-rupture failure coincident with the earliest failure of another RCS pressure boundary component, typically a[n] HL. Therefore, tubes with higher stress multipliers are predicted to be the first RCS pressure-boundary components to fail, in which case containment bypass occurs. Two SG tube failure margins—one for the average tube and another for a tube in the hottest region of the SG—represent the key output from the SCDAP/RELAP5 event sequence simulations.

Event sequences are categorized relative to the potential for containment bypass using the following criteria based on the SCDAP/RELAP5-predicted hottest SG tube failure margin:

- Containment bypass is assumed if the 1.0-stress multiplier (i.e., undegraded) hottest SG tube is predicted to fail prior to the HL, pressurizer surge line, or RV.
- A potential for containment bypass is assumed if the hottest SG tube failure margin is between 1.0 and 3.0. In this case, data for the actual SG tube strengths and their distribution resident in a prototype SG are needed to determine the outcome.
- Containment bypass is not indicated if the hottest SG tube failure margin is 3.0 or higher.

The major findings of the extended SBO event sequence categorization for Westinghouse four-loop PWRs are summarized as follows.

For situations where the operators are assumed to take no action:

- Event sequences that do not involve secondary side depressurization (i.e., leakage from the secondary system of 0.64 $cm^2$/SG [0.1 $in^2$/SG] and smaller) generally do not result in containment bypass. The reduced SG tube stresses resulting from the SG secondary pressures remaining elevated prevent SG tubes from failing prior to the HL, surge line, or RV.
- Event sequences that assume reactor coolant pump (RCP) shaft seal leakage rates lower than 11.36 L/s [180 gpm] per pump generally provide a potential for containment bypass. Event sequences that assume RCP shaft seal leakage rates of 11.36 L/s [180 gpm] per pump and higher generally do not result in containment bypass. A high leak rate leads to lower RCS pressures, and the reduced SG tube stresses prevent SG tubes from failing prior to the HL, surge line, or RV. However, exceptions exist related to the time when RCP shaft seal failures are assumed to occur. For RCP shaft seal failures that occur late in the event sequences,

loop seal clearing and, therefore, containment bypass can occur for leakage rates above 25.23 L/s [400 gpm] per pump.

- Event sequences in which the TDAFW [turbine-driven auxiliary feedwater] system operates and continues operating (or alternate feedwater is available) do not result in containment bypass. The outer surfaces of the SG tubes remain wet, and the RCS heat removal provided prevents system heatup.

For event sequences in which the TDAFW system is assumed to initially operate and later fail, the likelihood of tube rupture is predicted to be very similar to scenarios where the TDAFW does not operate at all because eventually, without other mitigation, the system may reach the high-dry-low condition. However, the timing of potential tube failures is significantly delayed by the initial operation of the TDAFW system. Challenges to continued TDAFW operation are a result of depletion of the station batteries or the depletion of the condensate storage tank inventory. Probabilistically, additional mitigation should be considered as well as the likelihood that auxiliary feedwater may not be maintained.

For situations where the operators take mitigative action:

- An evaluation was performed for a strategy in which operators implement SG feed-and-bleed cooling at 30 minutes into the event sequence (using the TDAFW system and opening the SG PORVs [power-operated relief valves]). The evaluation shows that this strategy is effective in the short term for preventing containment bypass. At a minimum, the onset of the RCS heatup is significantly delayed, thereby providing additional time for other plant recovery opportunities to be considered and implemented. In the long term, the SG PORVs fail closed when the batteries are depleted, and continued success of this strategy requires that a TDAFW water source remains available along with some capability for delivering the water into the SGs. For sequences in which the TDAFW system initially operates but later fails, no large changes in SG tube failure margins (relative to the no-intervention case) were predicted.
- An evaluation was also performed for a post-core damage strategy in which the operators depressurize the RCS by opening one or two pressurizer PORVs after plant instrumentation indicates that core cooling is inadequate. PORVs are opened at the time when the core exit temperature reaches 922 K (1,200 °F) or 12 minutes later. The evaluation shows that opening only one PORV limits the cooling afforded to the RCS, the core fails early (prior to battery depletion), and containment bypass is avoided for both operator action times. The evaluations also show that the greater RCS cooling afforded by opening two PORVs prevents early core damage and also prevents early failure of the HL and SG tube structures. When the PORVs fail closed after battery depletion, the RCS begins repressurizing and reheating, and this subsequently leads to HL and SG tube failures. The SG tube failure margins seen for the operator intervention cases are significantly improved (relative to the no intervention cases), and containment bypass is seen to be avoided for both of the post-core damage operator action times.

### 3.1.2 CE Plant Considerations

The increased vulnerability for CE plants is primarily because of a shorter HL length-to-diameter ratio and to shallower SG inlet plena compared to W SGs. This results in higher temperature gas reaching the SG tubes during closed-loop-seal natural circulation conditions. Consequently, the SG tubes are predicted to reach creep-rupture conditions sooner in CE plants, thus increasing the likelihood of containment bypass.

Several aspects are of interest for the purpose of determining FP releases to the environment: (1) whether an SG tube or some other part of the RCS pressure boundary fails first, (2) whether tube failure results in sufficient and rapid enough RCS depressurization to prevent rupture of some other part of the RCS boundary, and (3) whether the containment pressure is higher than the SG pressure in the long term, thus allowing release of revaporized FPs. This last aspect cannot be addressed in an SCDAP/RELAP analysis but can when using MELCOR. In the W analysis, the presence of a flaw was required for the prediction of tube failure before the failure of other RCS components. This condition leads to the prediction of failure of a single tube and a primary system depressurization rate that is not sufficient to prevent subsequent failure of other RCS components. For CE designs, however, unflawed tubes exposed to the relatively unmixed hot gases that reach the SG tubes can also fail. Moreover, more than one tube could fail, potentially depressurizing the RCS sufficiently to prevent the creep-rupture failure of other components, leaving the containment bypass pathway as the sole release path of FPs from the reactor.

The relatively shallow inlet plenum design of the SG under consideration for the CE plant has an effect on the results of the CFD predictions, as shown in Section 3.3.2 below. The shallow design limits the mixing of the hot gases that enter the SG and creates a higher thermal load on the tubes. The SG considered for the CE plant was a replacement SG. The earlier work on W plants focused on the Zion Nuclear Power Plant, with the associated W Model 51 SGs. To qualify, the applicability of these W predictions for W plants with replacement SGs, the NRC's Office of Nuclear Regulatory Research (RES) has worked with the NRC's Office of Nuclear Reactor Regulation to acquire plant-specific inlet plenum design information from a few plants. Although it was not practical to get design information for as many plants as desired, three sets of drawings were obtained. These included SG drawings from the Donald C. Cook Nuclear Plant, the Diablo Canyon Power Plant, and the Prairie Island Nuclear Generating Plant. The RES staff studied the dimensions for the inlet plenum region and found only small differences between the new designs and the previously studied Model 51 design. No shallow inlet plenum designs were found in the W samples. The expectation is that thermal mixing in the inlet plenums would not be significantly affected by the new SG designs for the sample plants considered.

## 3.2 Initial Deck and Analyses for the CE Plant

SNL developed the MELCOR 1.8.6 initial deck used for the C-SGTR analyses. It exercised the deck on SBO calculations, compared results against those of previous SCDAP/RELAP analyses, and performed an uncertainty analysis to estimate the expected contribution to variability in component failure timing resulting from uncertainty or variability in TH parameters.[1]

[1] See Louie, D.L., et al., "A MELCOR Model of the Calvert Cliffs Two-Loop Pressurized Water Reactor and Containment for the Steam Generator Tube Rupture Scenarios," Sandia National Laboratories, October 2012.

SNL generated the Calvert Cliffs Nuclear Power Plant deck based upon an earlier, less-complex MELCOR 1.8.5 demonstration deck and the 2006 SCDAP/RELAP Calvert Cliffs deck used for prior C-SGTR analyses (Ref. 2). During development, SNL exercised the deck on short-term SBO (*stsbo*) analyses using mixing parameters provided from initial CFD analyses. The SNL deck and analyses did not account for the temperature variability in the hot plume entering the SG tubes, so it cannot be used to test the failure of unflawed hottest tubes. SNL documented the updated deck and the results of the *stsbo* analysis.

SNL compared results from the new deck against those generated using SCDAP/RELAP (Ref. 1). This comparison required some modifications from the base version to more closely match the SCDAP/RELAP deck. They found that both codes predicted a similar sequence behavior and timing, although some later events occurred at somewhat different times. The analysts also found that component failure was not similarly predicted, which is not surprising considering that the MELCOR analysis did not include the hottest tube calculation.

SNL performed an uncertainty analysis to estimate the expected contribution to variability in component failure timing resulting from uncertainty or variability in TH parameters. The RCS-component-to-tube relative failure timing variation because of expected variations in TH parameters approximately followed a normal distribution with about a 600-s standard deviation. Although some aspects of the deck used to generate the failure timing distributions differ somewhat from the final version, the overall system response is not expected to change significantly. The variability in relative failure timing for the hottest tubes is likewise expected to be similar to that of the hot average tubes in the plume.

## 3.3 Computational Fluid Dynamics

CFD is used to study the details of the three-dimensional (3D) mixing behavior in the primary side of a CE SG. The results are used to inform the system-level code of the expected flow rates and mixing parameters in this region of the reactor system during specific severe accident sequences. This work builds upon previous NRC studies. Test data are available from a 1/7th scale facility that provide valuable information on SG inlet plenum mixing and the natural circulation flows during severe accident conditions. These data, however, are limited to a single W-type inlet plenum design, and there are concerns related to the scaling of these data to full-scale conditions. A benchmark study by the NRC staff, documented in NUREG-1781, “CFD Analysis of 1/7th Scale Steam Generator Inlet Plenum Mixing during a PWR Severe Accident,” issued October 2003 (Ref. 4), demonstrate that CFD predictions can adequately predict the inlet plenum mixing observed in the 1/7th scale tests. A set of follow-on analyses, documented in NUREG-1788, “CFD Analysis of Full-Scale Steam Generator Inlet Plenum Mixing during a PWR Severe Accident,” issued May 2004 (Ref. 5), applied the same methods to study full-scale SGs under severe accident conditions. This study extends the experimental results at 1/7th scale to prototypical conditions and provides insights into the effect of the SG inlet plenum geometry and the potential effect of the secondary-side heat transfer conditions. After a review of these predictions, the Advisory Committee on Reactor Safeguards recommended extending the modeling to include a prediction of the full natural circulation flow path between the vessel upper plenum and the SG. A follow-on study, documented in NUREG-1922, “Computational Fluid Dynamics Analysis of Natural Circulation Flows in a Pressurized-Water Reactor Loop under Severe Accident Conditions,” issued October 2010 (Ref. 6), addressed this concern and incorporated other modeling improvements for W-type SGs. The improved modeling approach was then applied to a CE-type SG as a comparison study (Ref. 7).

### 3.3.1 Summary of NUREG-1922 Results for Westinghouse Plants

The analysis in NUREG-1922 used an improved CFD model to determine mixing parameters and coefficients for tuning a system-code model applied to severe accident simulations with 3D natural circulation flows. The CFD model used in this study encompasses a series of lessons learned from several years of analyses, including a benchmark study at 1/7th scale (Ref. 4) and a follow-on study of full-scale SGs (Ref. 5). The updated modeling also addresses the Advisory Committee's comments (Ref. 8).

The natural circulation flows between the reactor vessel upper plenum and the SG were predicted under specific severe accident conditions that were obtained from prior system-code model predictions. A vessel model established the conditions in the upper plenum, which feeds the natural circulation flows in the HL, the pressurizer surge line, and the primary side of an SG. A countercurrent flow pattern is established that carries heat from the upper plenum to the SG tube bundle. An unsteady buoyant plume is predicted in the inlet plenum as the hot-steam-and-hydrogen mixture rises up and into the tube bundle. Time-averaged mass flows and temperatures are obtained throughout the system, and these predictions are used as a numerical experiment to define flow and mixing parameters for use in tuning a system-code model.

A modified mixing formulation is established to account for the HL and inlet plenum mixing, as well as the pressurizer surge-line flows. This updated formulation is considered to be an improvement over earlier models that focused solely on the inlet plenum mixing. In addition, a discharge coefficient is defined that can be used to predict the HL mass flow rates, based on the densities in the vessel upper plenum and the SG inlet plenum. The predictions provide a means of tuning a system code to obtain the mass flows and temperature distribution in the HL, surge line, and SG tube bundle. These predictions can be used to extend the existing experimental data into the specific SG geometry and severe accident conditions studied.

The recommended system-code modeling parameters for a W plant (assumed to have a Model 51 SG) or a plant with similar SG designs are summarized below.

| | |
|---|---|
| f = 0.96 | mixing fraction |
| r = 2.4 | recirculation ratio |
| 41% | hot tube fraction |
| $C_d$ = 0.12 | discharge coefficient |
| $T_m$ = 0.5 | bounding normalized temperature of hottest tube |
| 50 : 50 | hot : cold flow split ratio into side-mounted pressurizer surge line |

Sensitivity studies estimate the variation in these parameters under a variety of conditions and assumptions. In all cases, the discharge coefficient remained relatively constant with maximum variations of less than 8 percent. This demonstrates the benefits of using this approach to establish the HL flows in a system-code model. Similarly, the mixing fraction is found to vary by only a few percent over the range of conditions considered. The recirculation ratio is found to be sensitive to the secondary-side temperature, which affects the tube bundle heat transfer. The tube bundle heat-transfer rate was found to affect the recirculation ratio in previous work (Ref. 5), since the temperatures in the tube bundle affect the buoyancy driving forces. These parameters are found to have the largest effect on the recirculation ratio. The recirculation ratio suggested above, 2.4, is obtained using conditions pulled directly from a realistic system-code prediction of severe accident conditions in a W PWR.

The hot tube fraction is used for sizing the hot and cold SG tube sections in a system-code model. This parameter is difficult to predict with confidence because some of the tubes at the margin (i.e., tubes at the edge of the hot and cold regions) seem to occasionally change direction and the hot tube fraction can change by 10 percent or more in a given analysis. The predictions were not carried out long enough to obtain a consistent long-term average value. One important finding is that the hottest tube region does not appear to be significantly affected by changes in the overall size and shape of the hot tube region. In other words, the core of the hot tube region is somewhat consistent. Changes to the tube flow patterns occur at the edges of the hot tube region where the temperatures are more moderate. The base-case prediction had a long-time average hot tube fraction of 0.41. This value is in the middle of the range of all of the predictions. When the tube bundle flow is significantly increased, the hot tube fraction apparently tends to approach 0.5. At the lowest tube bundle flow rates predicted, the hot tube fraction is found to be as low as 0.26.

The normalized temperature of the hottest tube is a significant parameter because it refers to the portion of the tube bundle where the thermal loading is most severe. Recent NRC studies (Ref. 1) used this parameter to determine whether a tube will fail before the HL or some other RCS component. In the base-case prediction, the mass-averaged normalized temperature entering the hottest tube is found to be 0.43. The data sets were broken down into 40-second intervals, and the study found that the normalized temperature reached 0.5 over some of these intervals. For this reason, a value of 0.5 is recommended as a bounding value for system-code models. The sensitivity of this parameter to changes in the modeling parameters was significant. Average values ranging from 0.36 to 0.47 were obtained. The most significant variation came from changes in the secondary-side temperatures. A separate sensitivity study that moved the surge line to the top of the pipe also showed a significant impact on the hottest tube temperature. The top-mounted surge line removes some of the hottest flow, and the average normalized temperature of the hottest tube drops to 0.34.

The flow (hot:cold) split ratio into the surge-line pipe is predicted for simulations that included a pressurizer surge line. This variable remained generally within 5 percent of a 50:50 split ratio over the range of sensitivity studies, and a 50:50 split ratio is recommended for system-code models with a side-mounted surge line. The temporal variations in this parameter were very large and indicated significant turbulent fluctuations at the surge line-to-HL connection. The 50:50 value represents a long-term average value. The one sensitivity that did significantly affect this result involved moving the surge line to the top of the HL. In this case, approximately 75 percent of the flow into the surge line came from the hot flow in the upper pipe section. The top-mounted surge line, therefore, is subjected to a larger thermal challenge than a side-mounted surge line. This could be important in cases where the surge line is predicted to fail before the HL.

The series of predictions completed with a range of tube leakages from the primary-to-secondary side help to quantify the significance of tube leakage on the overall natural circulation flows. A leakage rate of 1.5 (kilograms (kg)/second (s) resulted in no significant variation. The countercurrent natural circulation between the vessel upper plenum and the SG is maintained for leakage rates up to 6 kg/s but, as the leakage rates increase, the average temperature of the flow entering the tube bundle increases. For a leakage rate of 12 kg/s, the countercurrent flow pattern is essentially broken and the steam temperatures entering the tube bundle begin to approach the HL (hot flow) temperatures.

Some prior qualitative CFD results highlighted the fact that some system-code models will underpredict the convective heat-transfer rates to critical regions of the HL and surge line. In the

regions where the thermal boundary layer is still developing, the fully developed heat-transfer correlations used in system codes underpredict the heat-transfer rates. To account for this underprediction, a set of factors are provided that can be used to adjust the fully developed heat-transfer correlation to account for the local entrance region effect. These factors, or other data, if more appropriate, should be applied in the determination of the HL and surge-line convective heat-transfer rates. In addition to the thermal entrance effects, it is expected that much of the upper HL also will experience mixed convection that would further increase the convective heat transfer to the HL. This topic is suggested for future research if a more detailed analysis of the HL becomes necessary.

### 3.3.2 CFD Results for a CE Plant

A simplified vessel upper plenum and an improved tube bundle are added to the CE SG geometry used in NUREG-1788, as summarized in Reference 7. The CFD model domain includes the upper plenum of the reactor vessel, an HL with the surge-line junction, the SG inlet plenum, and a simplified tube bundle. Symmetry is assumed at the vertical plane of the HL and SG. The tubes are modeled in a manner similar to that used for the W modeling documented in NUREG-1922. Groups of nine tubes are combined into a single tube that maintains the appropriate flow area. Loss coefficients and heat transfer enhancements are added to the tube models to ensure that the tube bundle has the same pressure drop and heat transfer characteristics as a prototypical SG. NUREG-1922 outlines this method for the W SG. The ANSYS/FLUENT v14.5 CFD code is used for the analysis. The predictions qualitatively show all of the flow features observed experimentally in the HL and SG regions. Steady boundary conditions are used that represent a snapshot in time of the severe accident conditions from system-code predictions of representative severe accident sequences. Average mass flows, temperatures, and mixing are predicted throughout the flow domain and used to define key parameters that are used in the 1-dimensional system-level codes to ensure consistency with the 3D CFD predictions.

A discharge coefficient related to a density-based Froude number is used to define the HL flow rates as a function of the densities in the vessel upper plenum and SG inlet plenum. NUREG-1922 outlines this approach. The discharge coefficient is predicted to be in the range from 0.13 to 0.14 for the CE reactor geometry considered.

This study uses the updated inlet plenum mixing model, which includes the HL mixing and entrainment. This approach is consistent with the most recent W CFD predictions. The mixing fraction is found to be within the range from 0.65 to 0.75 and the recirculation ratio is found in the range from 1.05 to 1.1.

Because system-code predictions have shown that the reactor loop with the pressurizer can have the earliest tube failures under some conditions, it is important to consider the effect of the flows into the pressurizer surge line. The mass flow into the surge line is accounted for in the updated mixing model. In addition, the CFD predictions are used to define the mixture of flows that enter the surge line during periods of countercurrent flow. For top-mounted surge lines, the flow entering the surge line enters mainly from the upper (hot) HL flows, and the temperature of the gas entering the surge line is consistent with these hotter temperatures. It is suggested that a top-mounted surge line on the large CE-type HLs would pull all of the incoming flow from the upper HL region.

A key aspect of these predictions is the determination of the tube bundle flows. System-code models typically use a single representative tube for the hot-tube flows, and the temperature is a

mass-averaged value for the entire group of tubes carrying the hot flow. With over 1,000 tubes expected to carry hot flow in a prototypical SG during this sequence, a significant variation in temperature can exist between tubes with the highest and lowest temperatures. A normalized temperature is defined to make the results easy to apply under a variety of conditions. A value of 1.0 represents the temperature of the flow from the vessel upper plenum, and a value of 0.0 represents the temperature of the flow returning to the inlet plenum through the cold-flow tubes. Tube entrance temperatures fall between 0 and 1 on this scale. The average normalized temperature of the hottest tube in the bundle is found to be in the range from 0.95 to 0.99. The total number of tubes that carry the upward hot average flow is found to be in the range from 20 to 25 percent of the total number of tubes. Reference 7 contains the detailed CFD analyses of CE plants. This is discussed later (See Section 3.6.6 for Figure 3-36, which shows the normalized incoming tube temperatures from this work).

### 3.3.3 Conclusions from the CFD Analyses

The ranges of the parameters are not a measure of the true uncertainty because only a modest number of cases are considered. A range gives some idea of the variations observed in the limited number of predictions completed. The table below summarizes the parameters found for W and CE SGs.

**Table 3-1 The governing parameters for W and CE SGs**

| Parameter | Average from NUREG-1922 W SG | Predicted range CE SG |
|---|---|---|
| **Cd**, discharge coefficient | 0.12 | 0.13–0.14 |
| **f**, mixing fraction | 0.96 | 0.65–0.75 |
| **r**, recirculation ratio | 2.4 | 1.05–1.10 |
| hot tube fraction | 41% | 20–25% |
| **Tn**, normalized (hottest tube) | 0.43 | 0.95–0.99 |

These updated predictions build upon previous studies and provide an updated set of parameters for use in 1-dimensional system codes to predict 3D natural circulation flows in PWR loops under severe accident conditions. The results are specific to the geometry and conditions used in this study and in NUREG-1922 and are not considered to be universally applicable. They are used in, and apply to the geometries for, NUREG/CR-6995 (Ref. 1) and in the CE analysis documented in this report.

## 3.4 Deck Modifications and Modeling Assumptions for the CE Analysis

The SNL deck was modified to account for the spatial variation in tube temperatures to more accurately determine tube failure and to apply other lessons learned from the W analyses during the Steam Generator Action Plan work, which included NUREG/CR-6995. The changes include modifications to tubesheet heat transfer, generation of alternate methods to calculate the hottest SG tube temperatures, modifications to the RCS-to-containment heat transfer, a modification to the HL creep-rupture calculation, and modification of the HL natural circulation modeling to match updated CFD-generated mixing parameters. Minor changes were required to merge different versions of the decks.

The primary modification was the determination of the temperature of the hottest tube and the inclusion of a method to calculate this temperature within the MELCOR simulations. To reliably

estimate the time of tube failure, the nonuniformity of tube temperatures must be considered. System codes such as MELCOR only provide an average temperature in the hot plume, not the hottest temperature. Characterizing the effect of the temperature distribution is of particular concern for CE plants with shallow-inlet-plenum replacement SGs, as even unflawed tubes in the hottest section of the SG are susceptible to failure.

Some modifications were made to model heat transfer from flowing gases to RCS components. Because the *relative* failure timing of SG tubes and other RCS components affects the occurrence of containment bypass, accounting for significant heat transfer mechanisms to RCS components improves the prediction of containment bypass. Some of the aspects that should be considered are accounting for radiative heat exchange between the HL wall and the gases flowing through it and ensuring that significant aspects of heat exchange in the RCS are accounted for.

One of the RCS heat transfer modifications was the restructuring of SG tubesheet heat structures. These heat structures were originally generated to be in contact with the secondary side of SGs and with the SG inlet and outlet plena but not with the tubes themselves. Because the SG tubesheets are in contact with far more surface area, and thus have far more heat transfer with the outside of tubes than with the secondary side and inlet plena, these heat structures were modified to be in contact with the SG tube fluid rather than the secondary-side and inlet-plena fluid.

An attempt was made to determine the relative contributions of radiative and convective heat transfer, but it was only partially successful. An alternate radiative heat transfer model was applied to the MELCOR plotfile output to check if it would match that in the output file. The alternate model was used because details of the MELCOR model were not readily available. The heat transfer coefficient (HTC) contribution estimates did not match the output file results very well. The FE analyses used the combined HTC. If the increase relative to fully developed conditions in the HL heat transfer coefficient, because of a thinner boundary layer, affects both the convective and radiative HTCs equally, then the distinction between the two need not be made.

Previous NRC analyses only adjusted the convective HTC for boundary layer effects in the entrance region (Ref. 1), whereas other analyses adjusted both the convective and radiative HTCs. If it cannot be established with sufficient confidence that the boundary-layer entrance effects affect both the radiative and convective HTCs equally, these boundary layer effects (and the separation of radiative and convective HTCs) should be revisited to apply separate factors to the convective and radiative HTCs.

The modeling of thermal radiation exchange between HL surfaces and gas flowing through the HL was reviewed and considered to be acceptable for screening purposes. Because the convective heat transfer modeling in system codes such as MELCOR typically uses correlations applicable for fully developed flow, the enhanced heat transfer in entrance regions where boundary layers are developing, such as at the entrance to the HL—the very location where the HLs are susceptible to failure—are likely underpredicted. It is for this reason that, if RCS and SG tube failure timings are similar, an FE calculation should be used to account for this nonuniform heat transfer.

The original cases did not initially consider a secondary-side relief-valve fail-open model. However, for appreciable FP releases to occur, some secondary-side relief valves must stay open. Otherwise, no pathway (other than potential system leakage) exists for releases to the environment. Failure models were therefore added to the deck. Two modes of main steam

safety valve (MSSV) failure were originally assumed: that valves may stick open when they open fully following heatup and thermal expansion, and that valves may fail open after a fixed amount of cycles. Only the first of the two models was implemented. These failure modes did not result in predictions of MSSVs sticking open.

Two additional MSSV failure modes were added after the initial calculations. One is that MSSVs can fail open after the first opening in the event of a common-cause maintenance failure. The second is not a failure mode but rather accounts for procedures in which the secondary relief valves are intentionally opened to reduce pressure so that water can be pumped in, if available.

The creep-rupture modeling for the HLs was also modified for a sensitivity calculation. The standard creep-rupture model for a single-material tube consists of calculating the stress history in the tube and calculating, from this stress history and the material creep properties, the accumulated damage from creep as a function of time. When this accumulated damage history, referred to as either the creep or damage index, reaches a value of 1, the component is considered to have failed. The HLs are made up of two layers of material, carbon steel and stainless steel. The original deck modeled the creep-rupture failure of the two-layered HLs as follows: determine the stress for both whole HL layers together, as though made of a single substance. The stresses are expected to be somewhat different in both materials. A creep-rupture index was then calculated for each layer, as though the entire wall thickness was made of that material. The maximum of the two creep-rupture indices was then used to calculate HL failure. This model effectively assumes that the entire HL is made up of the weaker HL material. If the thicker layer is not made up of this material, the HL failure would be predicted earlier than it should be. Because HL failure before SG tube rupture prevents the tubes from rupturing, the effective assumption of the entire HL being made of the weaker material (maximum index) could make the difference between containment bypass and no containment bypass. It could be that the decision to use the minimum-creep-strength material was made with the knowledge that the thick layer in the HL was made of this weaker material. Unfortunately, a detailed justification for the use of the maximum was also not described in detail. The potentially nonconservative model was therefore changed instead to use the minimum of the two materials' creep-rupture indices to assess the potential impact. This change results in an effective assumption that the entire HL is made of the stronger material. While this is not ideal, it avoids a potential major nonconservatism in containment bypass calculations. This change delayed the HL failure time by nearly 2 1/2 hours. It would be preferable to find or develop a model that accounts for the different stresses in the materials, perhaps even accounting for the different thermal expansions of the materials; find a justification for omitting the thin-layered material; or use FE analyses.

A choice had to be made for the number of unflawed tubes that fail, because the creep failure model does not predict this and a model has not been developed to estimate this parameter. The failure of a flawed tube is assumed to result in the failure of the single tube. Multiple tubes can fail almost simultaneously, however, if unflawed tubes reach failure conditions. The number of tubes that fail depends on the shape of the spatial temperature distribution in the hottest part of the SG tube, the variability in strength because of manufacturing flaws, and the depressurization of the system that occurs as the initial tubes start failing. Expert elicitation of NRC staff members previously involved in the issue resulted in a range from 10 to 100 tubes failing. For the MELCOR simulations, a value of 20 unflawed tubes were assumed to fail upon prediction of creep rupture. A single tube failure was assumed for the average hot (flawed) tube. The PRA analysis in Chapter 7 does not use the MELCOR analysis assumptions and conclusions regarding tube failure.

The number of tubes that fail does not directly affect RCS component failure beyond the point at which depressurization time becomes much shorter than the tube-to-other-RCS-component creep-rupture time for a situation where SG tubes fail first. Although this number was not identified, it can vary, depending on conditions; the failure of 20 tubes is generally sufficient under the conditions modeled.

It should be noted that this is a simplified model that does not account for the factors considered by the PRA analysis described in Chapter 7. The PRA analysis does not use the MELCOR conclusions regarding tube failure. Chapter 7 only uses the TH (pressure and temperature profiles as a function of time) in the progression of an accident sequence studied in MELCOR. Section 7.2.1 further discusses the use of TH for failure modeling in the PRA.

These modifications, which were originally made to an earlier version of the SNL Calvert Cliffs MELCOR deck, were later merged with the final version of the SNL deck.

An early set of runs was made using these selected TH results for use as initial and boundary conditions for the FE and SG-calculator calculations of RCS component failure. Chapter 4 discusses these calculations.

Other changes to the plant model were made after further review of the results. These changes consist of modifications to HL natural circulation modeling during the reconciliation of differences in RCS flows between MELCOR and the previous SCDAP/RELAP simulations. The changes consist of modifications to HL natural circulation modeling, to be consistent with the CFD results, and further changes to the MSSV fail-open model.

Two separate modifications were made to HL natural circulation models—one that consisted of stabilizing an existing active control method and a second, new, method that consists of reformulating the Froude-based relationship to a standard friction form and determining an effective loss coefficient that represents countercurrent flow losses. Both methods produced stable velocities consistent with those determined from the CFD and Froude-based velocities and those of the previous SCDAP/RELAP runs. After testing, the new friction-based formulation was chosen for continued use.

## 3.5 Loop Seal Clearing

One of the issues not fully addressed in the analyses is loop seal clearing. Although limitations in the deck did not allow this topic to be addressed within the simulation, a conceptual model was developed to aid in understanding the phenomena. It is based on a consideration of the loop seal bubble behavior to determine the loop seal clearing behavior.

Loop seal clearing was covered during the work for NUREG/CR-6995 (Ref. 1). The issue had also been covered previously.

Loop seal clearing can result in significant consequences compared to those of closed-loop-seal natural circulation. Loop seal clearing results in the development of full-loop natural circulation. This reduces the mixing of hot gases before it enters the tubesheet. For sequences where closed-loop-seal natural circulation would already result in tube failure, a cleared-loop-seal condition would advance the predicted tube failure time. For sequences in which tubes would not be predicted to rupture under closed-loop-seal natural circulation conditions, clearing of a loop seal may result in SG tube rupture. Previous analyses have concluded that unflawed, and therefore multiple, tubes are susceptible to rupture under open-loop-seal natural circulation.

Figure 3-2 depicts the conceptual model for loop seal clearing. The system is considered as two different-sized manometers at different elevations, coupled on both ends. The bubble regions are considered to consist of vapor and potentially noncondensables. A heat source at one end represents the reactor core. The bubble at the other end represents the gas in the SG outlet plenum. The core bubble and SG bubble are considered to be connected. The center bubble between the two manometers represents the cold-leg bubble. Some limited flow area between the core region and the center cold-leg bubble represents core bypass leakage. Heat transfer is considered to be possible from the core to the cold-leg bubble across the downcomer. Heat losses are also considered from the cold leg to the environment. The term *HT* in the figure refers to heat transfer with net heat flow either *into* or *out of* the cold-leg bubble.

The term “loop seal” in this section without a further description describes the SG-to-cold-leg loop seal.

The loop seal behavior is considered by focusing on the behavior of the lower (cold-leg) bubble between the two loop seals. The primary considered mechanism of clearing occurs when this bubble size decreases to the point that the loop seal water level rises to the bottom of the cold leg. At this point, the cold leg behaves like a siphon, even if only partially liquid filled, allowing water to flow from the loop seal to the downcomer until gases can pass the loop seal. At this point, the loop seal is considered to be cleared. If the net bubble growth rate is negative, the water level will eventually rise to the point that it crosses over the HL to the downcomer if the downcomer seal does not somehow clear first.

Side-to-side liquid motion or bubble compression and expansion that can occur during perturbations, such as PORV openings, are considered to affect the clearing timing somewhat, but overall loop seal clearing behavior, including whether the seal clears or not, should be largely determined by the net bubble growth behavior.

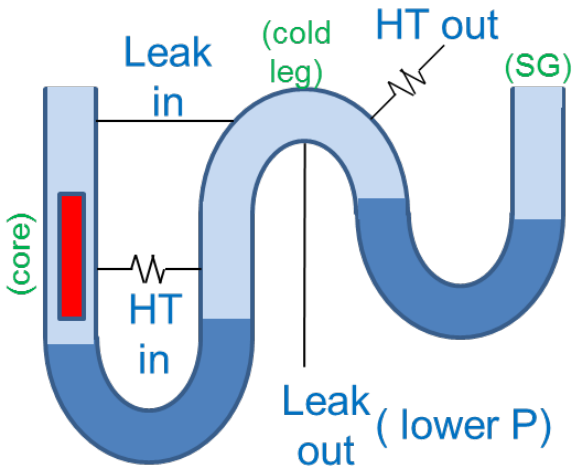


Figure 3-2 Conceptual model of loop seal clearing

The following bubble mass sources and sinks are considered to contribute to the bubble growth rate and thus the loop seal clearing behavior:

- leakage from the system through pump seal leaks
- leakage into the system by core bypass leakage
- condensation of bubble vapors by heat transfer to the containment through RCS piping
- evaporation of downcomer-to-core loop seal water by heat transfer from the hot core barrel

An equation that describes the bubble growth rate is:

$$Dm\_bubble/dt = leak\ in - leak\ out + evaporation\ rate - condensation\ rate$$

Figure 3-3 shows the relevant mass flow rates that affect loop seal clearing. This figure shows the cumulative downcomer-to-upper-vessel flows, each of the pump seal flows, and the net mass flow rate of the two combined. The remainder (i.e., the difference of the plotted net from 0) is expected to be made up of phase change in the bubble region, rate of change of bubble size, flow across cleared upper (standard) or lower (downcomer-to-core) loop seals, or some combination of the three.

In the absence of bypass leakage, a nonheated vapor bubble would collapse because of heat transfer through the RCS to the containment. Heat transfer from the core barrel to the downcomer may result in evaporation countering bubble collapse.

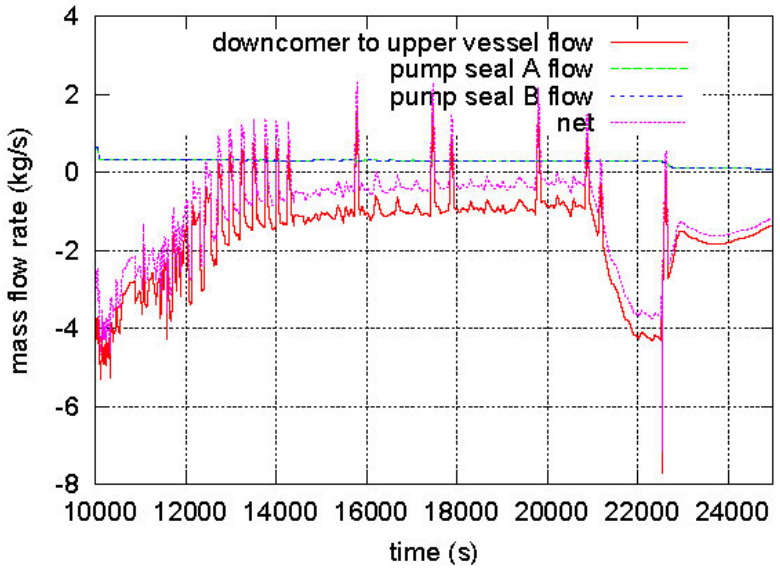


Figure 3-3 Pertinent flows for loop seal clearing

A downcomer-to-core seal clearing event involves a sufficient level change that the seal is expected to allow gases to bubble through the downcomer-to-core loop seal before the water level rises to the cold leg. These gases transferring from the core region can replenish the loop seal bubble. This would be a transient and not a permanent clearing. Gas reaching the loop seal

bubble through the downcomer could possibly result in a drop of the downcomer water level and could reseal the downcomer-to-core loop seal.

Such transient clearing, if the loop seal water inventory is insufficient to rise to the cold leg without gases passing through, can also occur for the loop seal, depending on geometry. If sufficient leakage exists between both manometer bubbles (i.e., bypass leakage in the reactor) vapor can flow through the leak path to preserve the loop seal bubble or create a loop seal bubble if it does not already exist.

Loop seal water level changes alter the pressure drop between the two gas regions. If the pressure drop is less than the head of water required to reach the cold leg, the water level will not reach the cold leg, it will stabilize at a lower level, and the loop seal will not clear.

Previous SCDAP/RELAP results show significant cooling of the loop seal water after about 8,000 seconds into the transient. Because of this, it is likely that, instead of forming a bubble, the steam will rapidly collapse and heat the water in the cold leg. Noncondensables could get trapped in the void region if this occurs before the seal is cleared. Despite the fact that the loop seal liquid appears to be cooling, the liquid level in the loop seal continues to decrease.

To summarize, in the absence of noncondensables and leaks, the bubble is expected to do the following:

- collapse (clear loop seal) if heat transfer out is greater than heat transfer in
- not collapse if heat transfer out is less than heat transfer in

Other expected behavior includes the following:

- Bubble will not collapse without net out leakage if sufficient noncondensables present.
- Leak out (pump seal leakage) accelerates bubble collapse.
- Leak in from upper vessel through core bypass counters bubble collapse.
- If the bubble shrinks (i.e., $dm/dt < 0$), then one of the following three things will happen depending on system geometry and liquid inventory in both loop seals:
  - The cold leg loop seal will clear.
  - The core-to-downcomer loop seal will clear.
  - The pressure difference will sufficiently change parameters (leaks and evaporation) such that a steady state is reached (i.e., $dm/dt = 0$).

Both loop seals shown in Figure 3-2 for an individual RCS loop must clear for open-loop-seal natural circulation to occur.

If the lower downcomer-to-core loop seal is cleared, perturbations such as PORV openings are not expected to be sufficient to clear the loop seal, as similar pressure drops will occur on both sides of the loop seal.

If the loop seal clears first, the downcomer-to-core loop seal may subsequently clear by a reduction in water level through evaporation.

## 3.6 Analysis Results

### 3.6.1 Discussion of MELCOR Analyses

Two sets of simulations were conducted, one in October 2012 and another in 2013. The 2013 set of simulations was run because HL flow rates in MELCOR under natural circulation for the October runs were found to be higher than those of the FLUENT and SCDAP/RELAP simulations. Higher HL velocities prefer tube over HL failure. To properly characterize component failure timing, it is essential that the HL flow rates be representative. Additional review indicated that the HL natural circulation modeling in the MELCOR deck needed to be modified to match updated FLUENT results.

The 2013 runs used the updated HL natural circulation modeling. The primary difference between the 2013 and 2012 runs is this modeling change. A second difference is that no secondary SG leakage to containment was assumed for most of the 2013 runs. Instead, updated MSSV stick-open modeling, the third difference, was relied upon to establish secondary-side pressure. The change to no-secondary-leakage and updated MSSV stick-open modeling was made because of the finding that assuming even 20 tubes to rupture at low pressure was not sufficient to fully open the MSSVs, which was the original simulated criterion for sticking to occur. Some of the MSSVs did partially open.

Section 3.6.3 provides plots and tabulations of select results.

Although a single case was desired, other cases had to be run to address behavior that had not previously been considered. A notable parameter that led to the requirement of more runs was the effect of sticking assumptions for secondary-side relief valves. Assumptions about secondary-side relief valves failing open, which was not a parameter originally focused on, was found to be a major parameter in system behavior. This was because previous analyses did not model secondary relief valve behavior but assumed that a bypass would occur if SG tubes failed or some fraction of the time that the tubes failed. It was found that, if valve failure was not explicitly modeled as an assumption, no appreciable releases would occur even if SG tubes had ruptured. The simulations had to be run repeatedly to come up with relief valve behavior that resulted in releases to the environment:

- assuming failure upon full valve opening following a tube rupture did not change releases, as the valves did not fully open and thus did not stick
- assuming a stick-open-failure upon full valve opening at any time also did not result in appreciable releases because, even for those cases, the valves did not stick open
- assuming that secondary-side relief valves stick as far as they have opened or assuming that they are opened by operators did result in releases

It appears that the secondary-side valves are not as pressure stressed when the tubes rupture several hours into the accident, so they do not leak. They may be thermally stressed, which is not considered for the valve-opening model.

The valve failure criteria were varied, not based on failure data, but rather to evaluate the failure criteria that would possibly result in FP releases to the environment. During the analyses for the Steam Generator Action Plan, tube failure was the criterion used to consider that containment had been bypassed. The initial CE simulations indicated that, if tubes failed while the SG secondary side was depressurized, the secondary-side relief valves opened for a short period

before closing (if they opened at all), resulting in a small amount of FP releases to the environment. This behavior may be scenario dependent.

The base sequence consisted of a long-term SBO (*ltsbo*) with the TDAFW system and batteries assumed to be operating for 4 hours. The initial cases assumed a secondary-side-to-containment leakage to ensure that the SG secondary sides were at low pressure. This approach for reducing SG secondary pressure has not been universally accepted. Cases with no SG-secondary-to-containment leakage were run using an MSSV stick-open model in which the valves were assumed to stick to the extent they had been predicted to open by the code. A situation was also simulated in which operators open the secondary-side relief valves soon after the accident to reduce SG secondary pressure to allow water to be pumped in.

Case run times were set based on the primary need to evaluate the TH system behavior. Because of this, some of the cases terminated before parts of the release occurred. Therefore, the release fractions listed in this table do not represent the total release fraction but the release fraction at the time of problem termination. On the other hand, the SG secondary-side decontamination determined from the Aerosol Trapping in Steam Generator (ARTIST) project was not included, which would reduce predicted releases. This decontamination would be expected to reduce release potentially by about a factor of 5. This decontamination factor cannot be directly applied to the result because the decontamination is particle-size dependent and because the decontamination would replace and not add to the SG decontamination already calculated by MELCOR during the run.

Two of the 2013 cases are considered representative, although the results are very different. Both cases use the updated natural circulation modeling. The difference between the -a case is otherwise identical to the base case. For the -as case, the secondary-side-to-containment leakage shut off and the MSSVs are assumed to stick open as far as they have been predicted to open by the code.

Whether the MSSV was assumed to stick open and whether SG secondary was assumed to leak to containment resulted in very different behavior. MELCOR predicted HL failure first and no environmental releases for the case with SG secondary-to-containment leakage and no-MSSV-sticking model. For the case with the SG secondary-to-containment leakage and no-MSSV-sticking model, the tubes were predicted to fail first with calculations predicting FP releases to the environment.

The ltsbo case with no secondary-side-to-containment leakage and sticking MSSVs had a Cs release of about 5 percent at the time the run terminated. This was, by far, the highest release of all run cases. For this sequence, FPs were being released at a significant rate at the end of the simulation so the actual predicted release fraction (RF) will be higher if the simulation is extended. To obtain the code-calculated RFs for the cases in question, the simulations would have to be run until the RFs reached their asymptotic values or at least beyond the time when risk analyses estimated that mitigative actions would occur.

Some of the sequences stopped upon reflood when a smaller time step would be required for stability. Because the primary purpose of the runs was to obtain the TH histories, the cases were not rerun if sufficient data were output to characterize TH behavior.

Other cases were run as needed to characterize unexpected behavior. These included cases to establish a suitable secondary-side relief-valve failure model, to assess the importance of

parameters, and for somewhat different sequences, to address additional issues that were raised.

One of these was the high-dry-high sequence (high primary pressure, dry secondary side, high secondary pressure). This involved no SG-secondary-to containment leakage. Although an MSSV stick-open model was used that would predict sticking if valves fully opened, they did not do so. Even for HL flows that were higher than the CFD calculated, little damage occurred to tubes by the time the HLs failed.

This report added Appendix I to discuss melting temperatures and steel oxidation.

Appendix J discusses loop seal clearing considerations, both from a MELCOR modeling and from a PRA modeling point of view.

### 3.6.2 Summary of Accident Sequences Studied and Nomenclature

This section summarizes the accident sequences modeled and analyzed by MELCOR. It also provides the nomenclature that is later used in the Section 7.2 PRA. The TH results from selected cases provide input for the PRA analysis.

Table 3-4 gives an inventory of CE MELCOR runs considered for the PRA, which considered 12 cases. The base sequence being modeled (*stsbo*) is a high-pressure SBO with the following conditions:

- All emergency core cooling systems fail.
- TDAFW fails.
- Accumulators are operable.
- Dc power functions for 4 hours.
- There is a 3.23-$cm^2$ (0.5-$in.^2$) leak in the SG secondary side.
- There is a 0.085-$cm^2$ (0.013-$in.^2$) leak in loop seals through RCP seals (results in a ~79.5 liters per minute (~21 gallons per minute) leak of water at high SRV-setpoint).
- Creep failure of AvgHot tube, which represents failure of a single flawed tube, is assumed to result in the opening of a flow area equal to a double-ended guillotine break (DEGB) of 1 tube (i.e., 2 tube flow areas).
- Creep failure of the hottest tube, which represents failure of unflawed tubes, results in the opening of a flow area equal to a DEGB of 20 tubes (40 tube flow areas).

For the equivalent *ltsbo* case, the TDAFW system functions for 4 hours.

Figure 3-4 shows the cases that were run. They are separated into two groups: the top group represents the original October 2012 cases, and the bottom group represents the July 2013 cases that included modifications to the HL natural circulation modeling.[2] The arrows from each

[2] The *stsbo-mssvstick* model was run in 2013 and incorporated the alternate natural circulation modeling with a low effective counter-current-flow loss coefficient (which then results in a higher flow rate during closed-loop-seal natural circulation.)

deck point to its derivative decks. The smaller text indicates the deck files that were altered from the source deck.

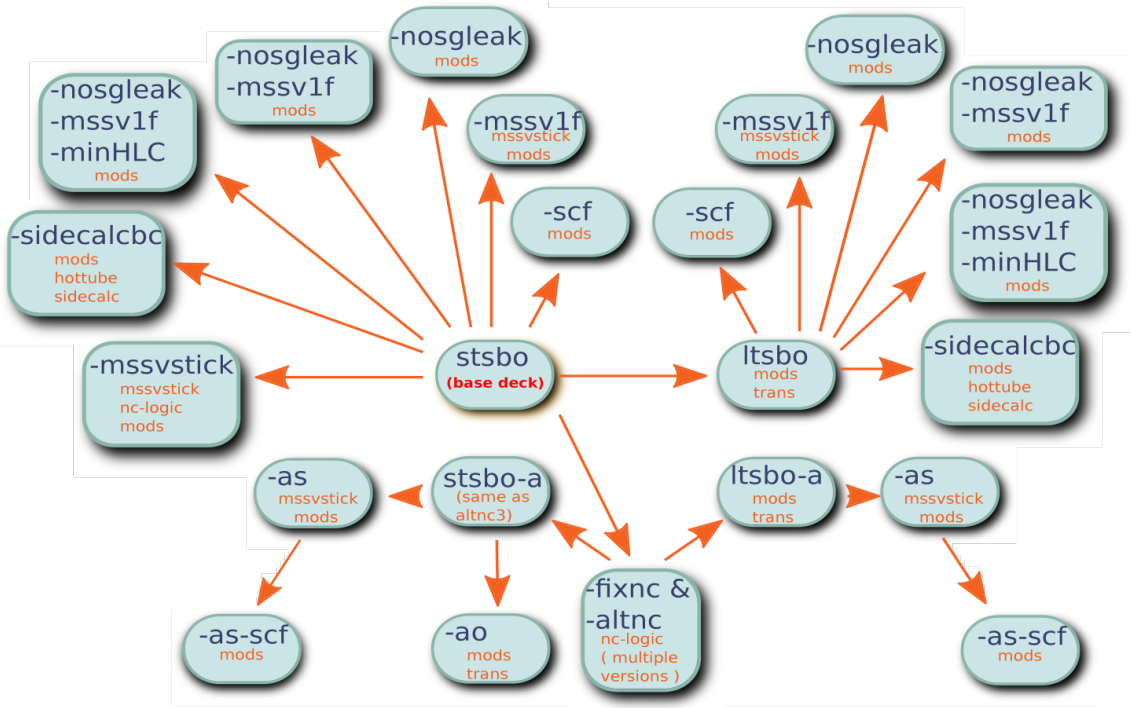


Figure 3-4 Organization of C-SGTR decks

The following are the October 2012 cases:

- ***stsbo*** base deck
- ***ltsbo*** the *stsbo* deck with TDAFW functioning for 4 hours and a longer run time
- modified versions of the *stsbo* and *ltsbo* cases:
  - **-SCF** runs have creep failure suppressed.
  - **-MSSV1F** runs modify the corresponding case with failure of MSSV assumed if they open fully following an SGTR event.
  - **-noSGleak** runs modify the corresponding case by removing secondary leakage. This modification provides the high-dry-high scenario (high secondary pressure in addition to high primary pressure and dry secondary), if secondary-side relief valves are assumed to not stick open.
  - **-noSGleak-MSSV1F** runs modify the corresponding case by applying both no-secondary-side leakage and stick-open valve after full opening of secondary valve.
  - **-noSGleak-MSSV1F-minHLC** same as -noSGleak-MSSV1F but uses the minimum rather than the maximum of the two HL creep-rupture indices to predict failure. No *ltsbo* case was run.
  - **-sidecalcbc** Original hottest tube calculation method. This method was replaced and this document does not include results for it.

The second set of cases in 2013 consisted of additional modifications to the original input decks:

- **-fixnc** Multiple *stsbo* decks used in modified natural circulation modeling method.
- **-altnc** Multiple *stsbo* decks used an alternate natural circulation model. The only difference between the different versions of this deck is that the effective counter-current loss coefficient is being numerically solved for. Versions 1–9 represent different stages in the iteration.
- **-MSSVstick** An MSSV sticking model was added, for which valves open, along with a low-resistance counter-current-flow loss coefficient using the alternative HL natural circulation modeling. No *ltsbo* case was run.
- **-a** This is the base deck with altered HL natural circulation modeling. It is the -altnc deck, which uses the "converged" counter-current-flow loss coefficient model so that the HL flow matches that predicted by the FLUENT CFD code (-altnc3).
- **-as** This is the -a alternate natural circulation deck with the secondary-to-containment leakage area closed and MSSVs sticking open as far as the code has predicted that they open. This MSSV sticking model can represent either a common-mode maintenance failure where the valves stick or operator action to open the valves.
- **-ao** This is the -a alternate natural circulation deck with the secondary-to-containment leakage area closed and full opening of secondary PORVs and MSSVs soon after the SBO. This simulates operator action to reduce secondary pressure. No *ltsbo* case was run.
- **-as-SCF** This is the -as case with component failure suppressed.

An additional **–a-SCF** (the –a case with component failure suppressed) was run upon request following the other analyses solely for the purpose of providing input for the C-SGTR calculator. The results for this case were not processed other than to provide data for the calculator.

### 3.6.3 Select CE Sequence Results

Code results have been plotted for select cases. The output parameters presented include system pressures, structure temperatures, select RCS component creep-rupture indices, liquid levels, and gas concentrations. Select events are listed. Creep-rupture indices for the average tubes were also plotted for each case for stress multipliers ranging from 1 to 2.5.

Table 3-2 shows the timings of some of the major events for select sequences. The cases are ordered by time of initial gap release. Major features of the accident progression are discussed below.

Table 3-2 Timing of Selected Events

| | Time (h) | | | | | | |
|---|---|---|---|---|---|---|---|
| **Event** | ***stsbo-as*** | ***stsbo-ao*** | ***stsbo-a*** | ***stsbo*** | ***ltsbo-a*** | ***ltsbo*** | ***ltsbo-as*** |
| Station Blackout | 0.0 | 0.0 | 0.0 | 0.0 | 0.0 | 0.0 | 0.0 |
| Loss of TDAFW | 0.0 | 0.0 | 0.0 | 0.0 | 4.0 | 4.0 | 4.0 |
| ST Rupture Disk | 1.8 | 1.6 | 2.1 | 2.1 | 9.1 | 9.0 | 14.1 |
| Initial Gap Release | 4.1 | 4.3 | 5.1 | 6.0 | 12.7 | 13.6 | 19.4 |
| SG Tube Rupture | 4.4 | 4.7 | - | 6.3 | - | 13.7 | 19.8 |
| HL Rupture | - | - | 5.9 | 7.2 | 13.2 | 14.7 | - |
| Accumulator injection | 4.7 | 0.1 | 5.9 | 7.3 | 13.2 | 14.7 | 1.7 |

The original *stsbo* base case will be used as the reference case, since all subsequent runs were compared to it. Some notable differences in other cases are also shown. The figures are listed first, as the chronological walkthrough below covers all cases simultaneously.

Several figures for the base case are provided: Figure 3-5 shows the main system pressures for the *stsbo* calculation. These pressures include primary system pressure, SG A and SG B secondary-side pressures, and containment pressure. Figure 3-6 shows the SG secondary collapsed liquid level for the *stsbo* calculation. Figure 3-7 shows the main structure temperatures for the *stsbo* calculation. Figure 3-8 shows the creep-rupture indices for the *stsbo* calculation. Failures calculated with these components affected the accident sequence and subsequent TH behavior. Figure 3-9 shows the creep-rupture indices for various stress multipliers on the hot-average tubes for the *stsbo* calculation. These indices were only evaluated to obtain an indication of the flaw size that would be necessary to cause a failure and did not otherwise affect results (i.e., these failure predictions did not influence subsequent TH behavior). Figure 3-10 shows the hydrogen concentrations in different locations in the SG A tubes for the *stsbo* calculation. Figure 3-11 shows the volatile FP release fractions for the *stsbo* calculation.

A smaller set of figures are provided for the original *ltsbo* case. This set of figures includes pressures, SG water levels, and structure temperatures, along with direct comparisons of these pressures and structure temperatures to those of the *stsbo* calculation. These calculations demonstrate that the *ltsbo* calculation can be reasonably approximated by a time-shifted *stsbo* calculation.

Figure 3-12 shows the main pressures for the *ltsbo* calculation. Figure 3-13 shows the SG secondary collapsed liquid level for the *ltsbo* calculation. Figure 3-14 shows the main structure temperatures for the *ltsbo* calculation. Figure 3-15 compares the main pressures in the *ltsbo* calculation to those of the *stsbo* calculation. Figure 3-16 compares the *ltsbo* calculation SG secondary-side collapsed liquid levels to those of the *stsbo* calculation. Figure 3-17 compares the *ltsbo* calculation loop A structure temperatures to those of the *stsbo* calculation. Figure 3-18 compares the *ltsbo* calculation loop B structure temperatures to those of the *stsbo* calculation.

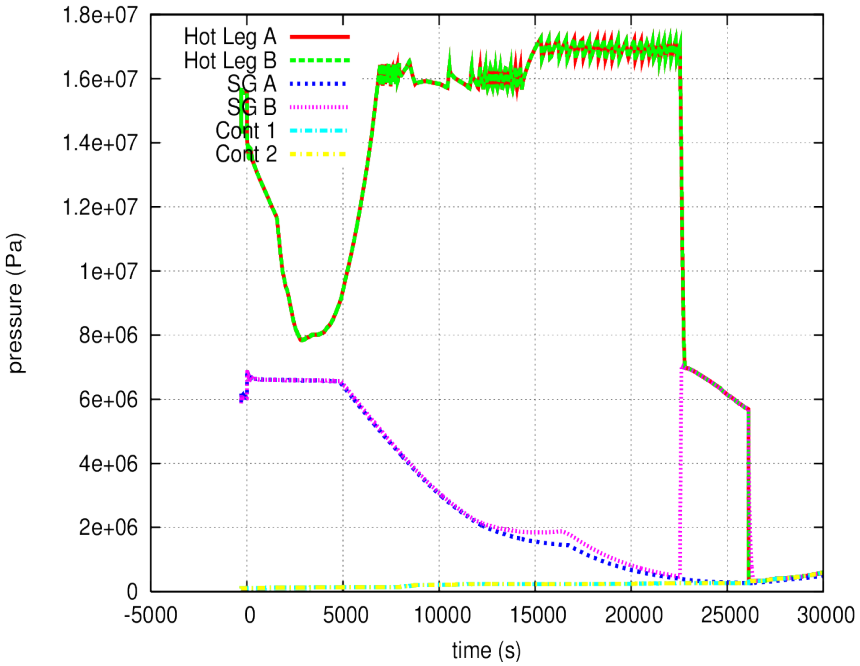


Figure 3-5 Main pressures for the stsbo calculation

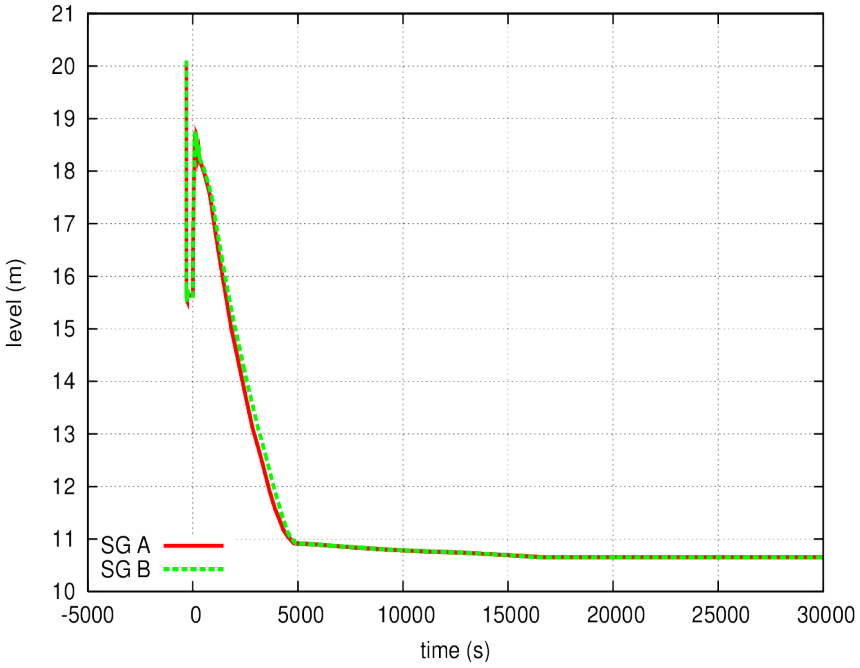


Figure 3-6 SG secondary collapsed liquid level for the stsbo calculation

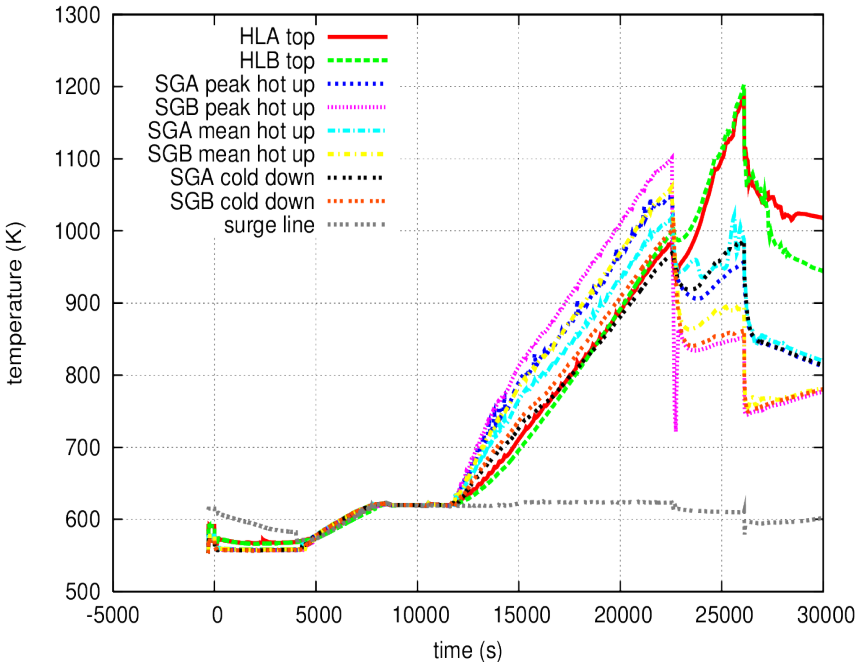


Figure 3-7 Main structure temperatures for the stsbo calculation

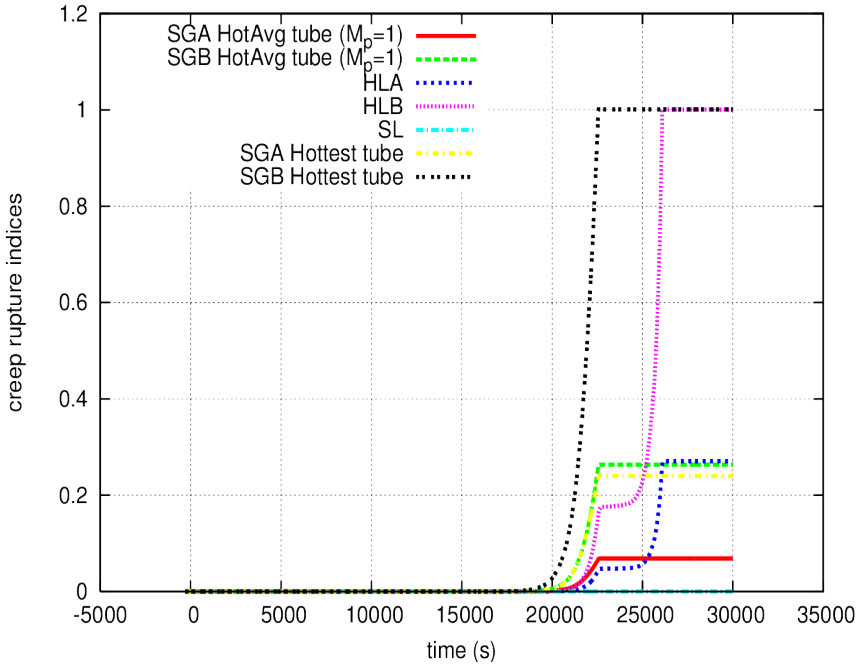


Figure 3-8 Creep-rupture indices for the stsbo calculation

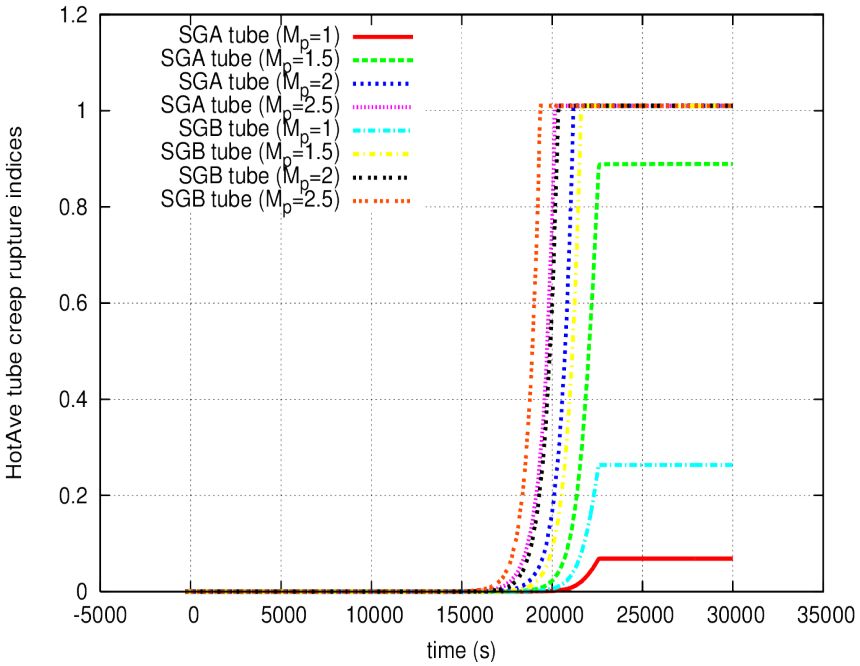


Figure 3-9 HotAve tube creep-rupture indices for the stsbo calculation

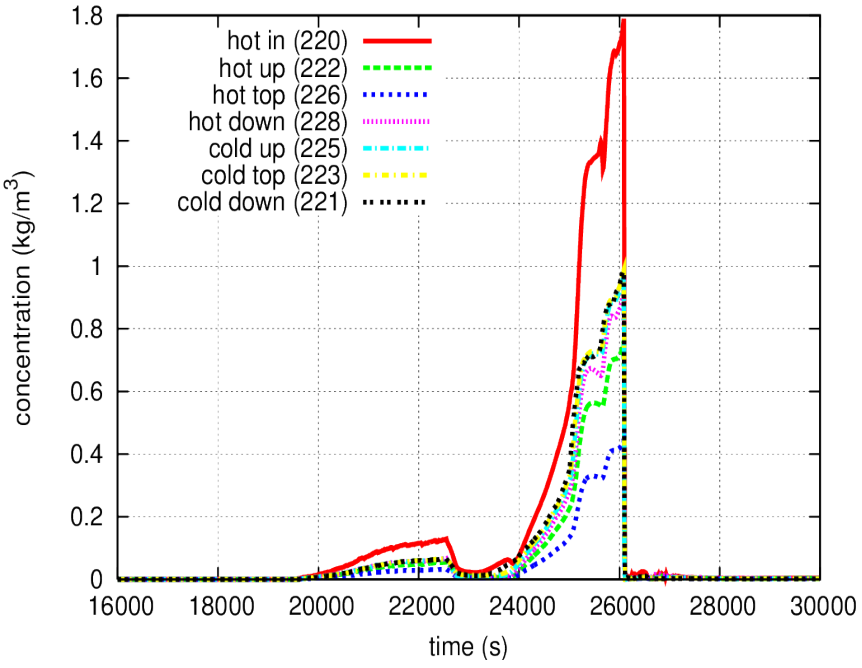


Figure 3-10 Hydrogen concentrations in SG A tubes for the stsbo calculation

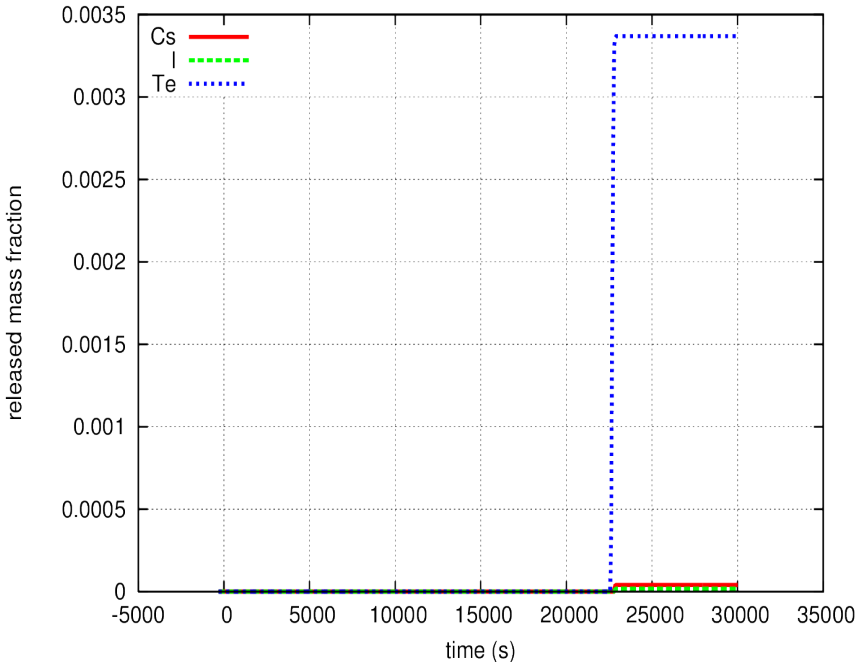


Figure 3-A Volatile FP release fractions for the stsbo calculation

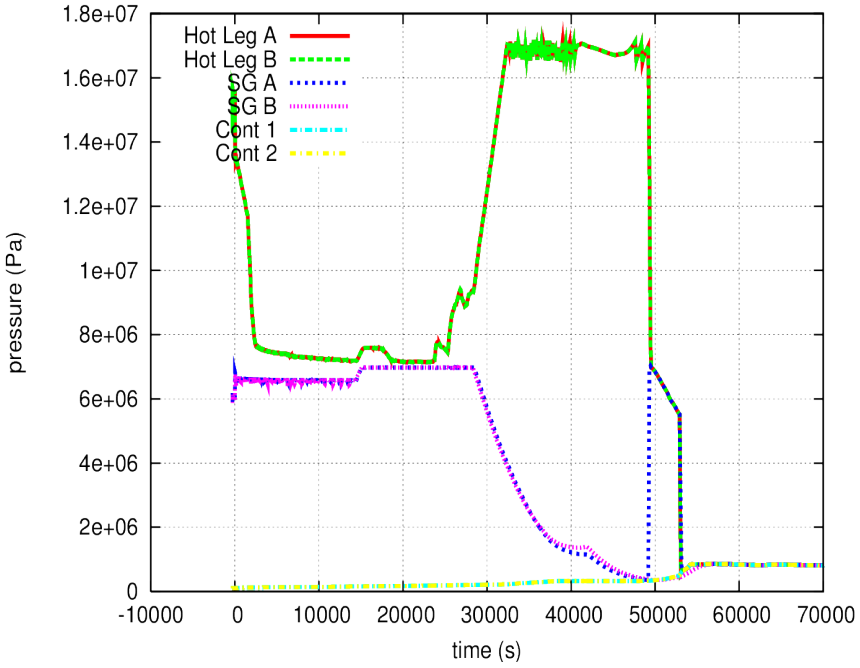


Figure 3-B Main pressures for the ltsbo calculation

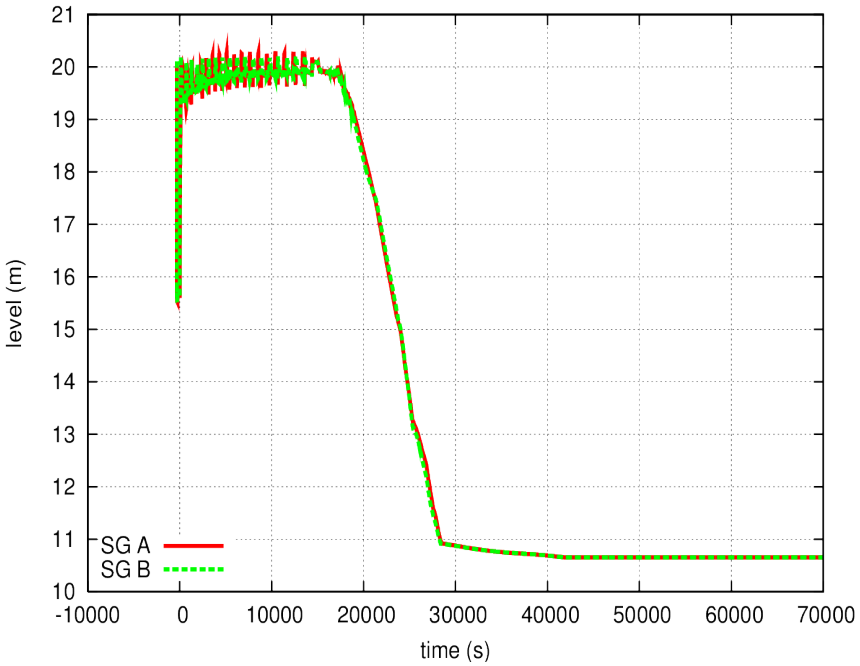


Figure 3-13 SG secondary collapsed liquid level for the ltsbo calculation

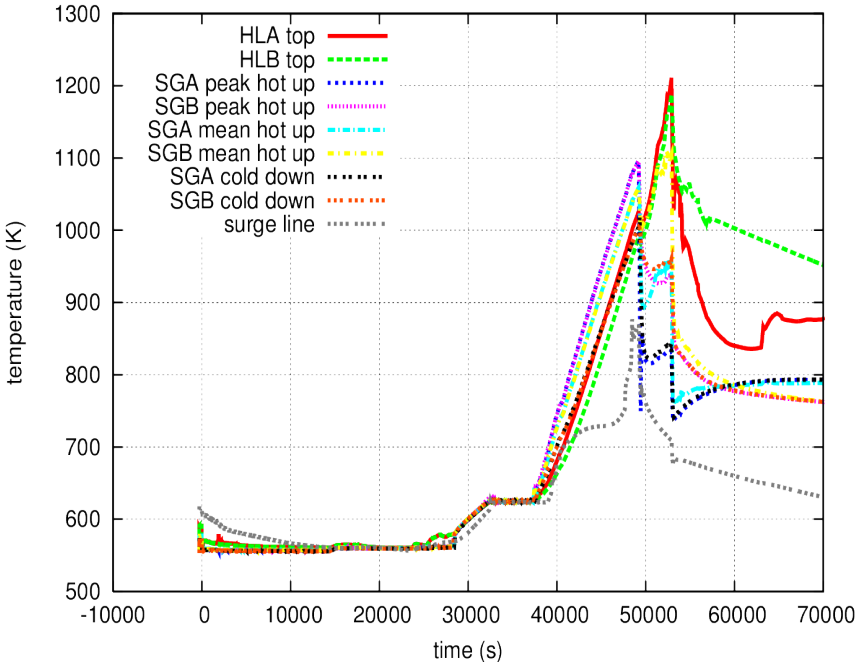


Figure 3-14 Main structure temperatures for the ltsbo calculation

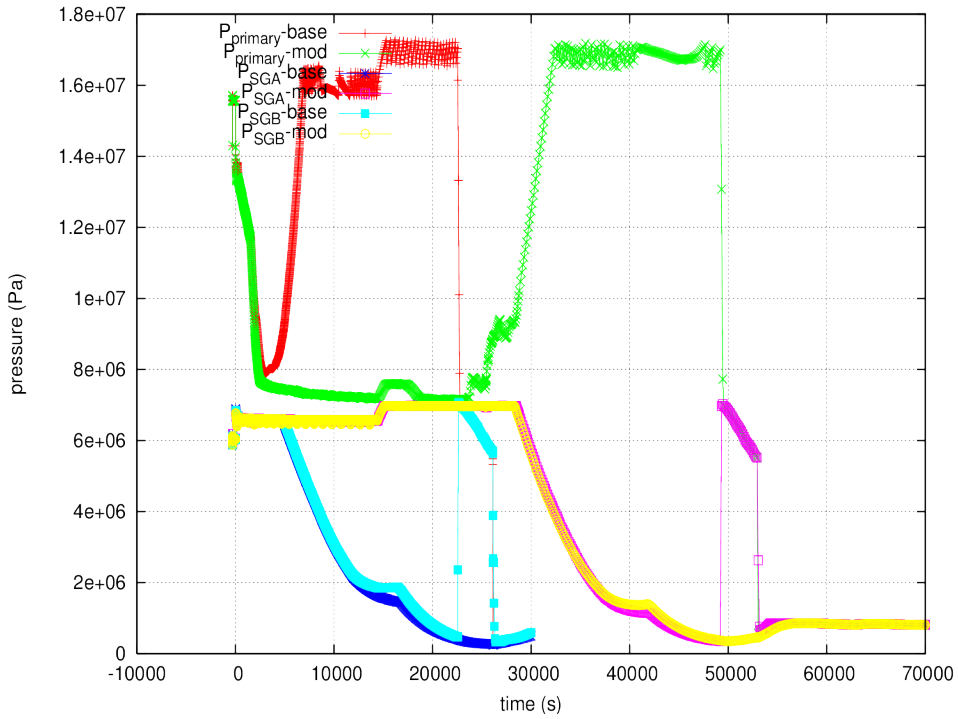


Figure 3-15 Comparison of ltsbo pressures to those of stsbo

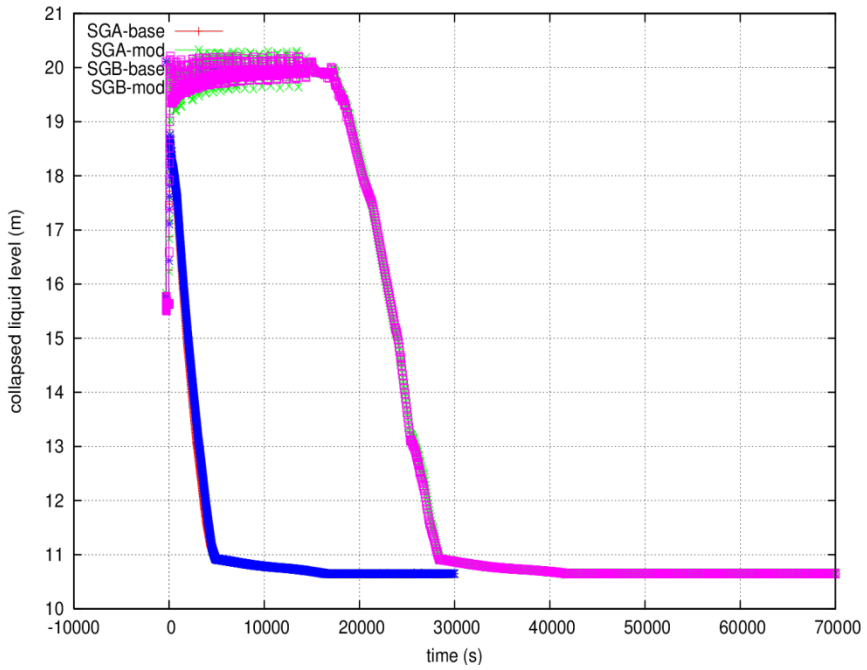


Figure 3-16 Comparison of ltsbo SG boiler collapsed liquid levels to those of stsbo

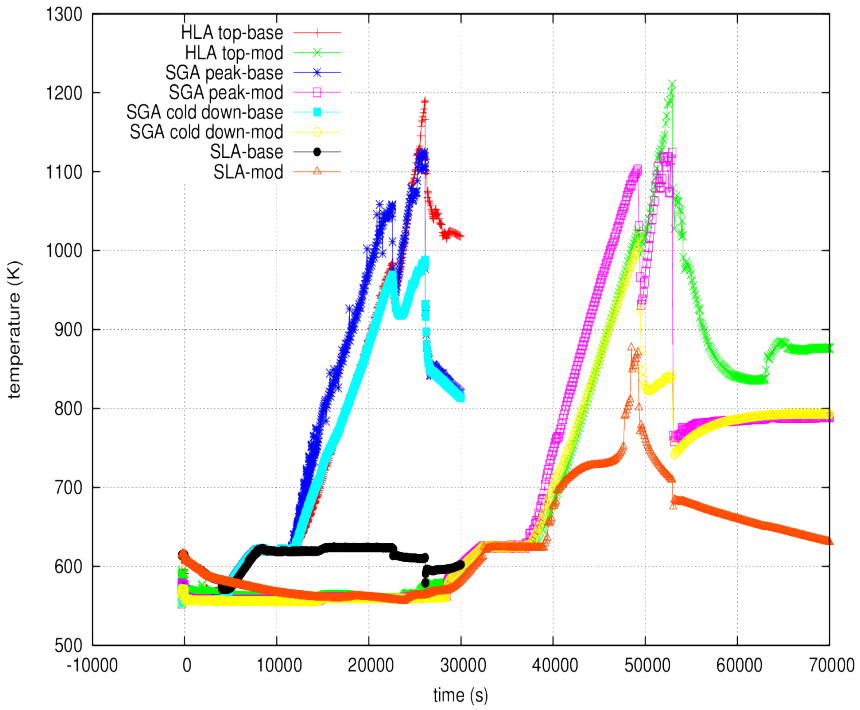


Figure 3-17 Comparison of ltsbo loop A structure temperatures to those of stsbo

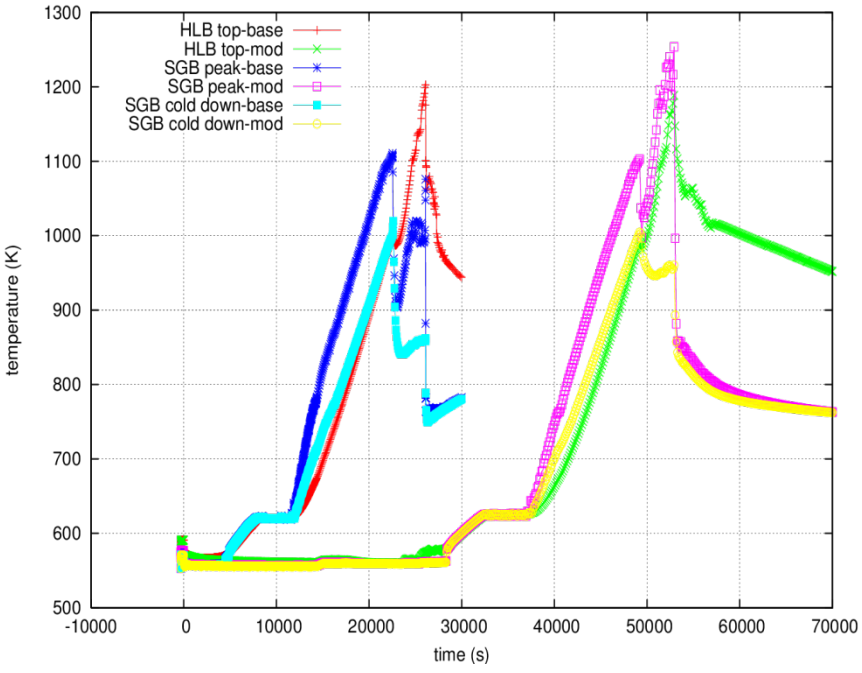


Figure 3-18 Comparison of ltsbo loop B structure temperatures to those of stsbo

A full set of figures is provided for the *ltsbo-a* case because this is the case that experienced the highest releases before the calculation terminated. Figure 3-19 shows the main system pressures for the *ltsbo-a* calculation. Figure 3-20 shows the SG secondary collapsed liquid level for the *ltsbo-a* calculation. Figure 3-21 shows the main structure temperatures for the *ltsbo-a*

calculation. Figure 3-22 shows the creep-rupture indices for the *ltsbo-a* calculation. Figure 3-23 shows the creep-rupture indices for various stress multipliers on the hot-average tubes for the *ltsbo-a* calculation. These were only evaluated to obtain an indication of the flaw size that would be necessary to cause a failure (i.e., these failure predictions were not made to influence subsequent TH behavior). Figure 3-24 shows the hydrogen concentrations in different location in the SG A tubes for the *ltsbo-a* calculation. Figure 3-25 shows the volatile FP release fractions for the *ltsbo-a* calculation.

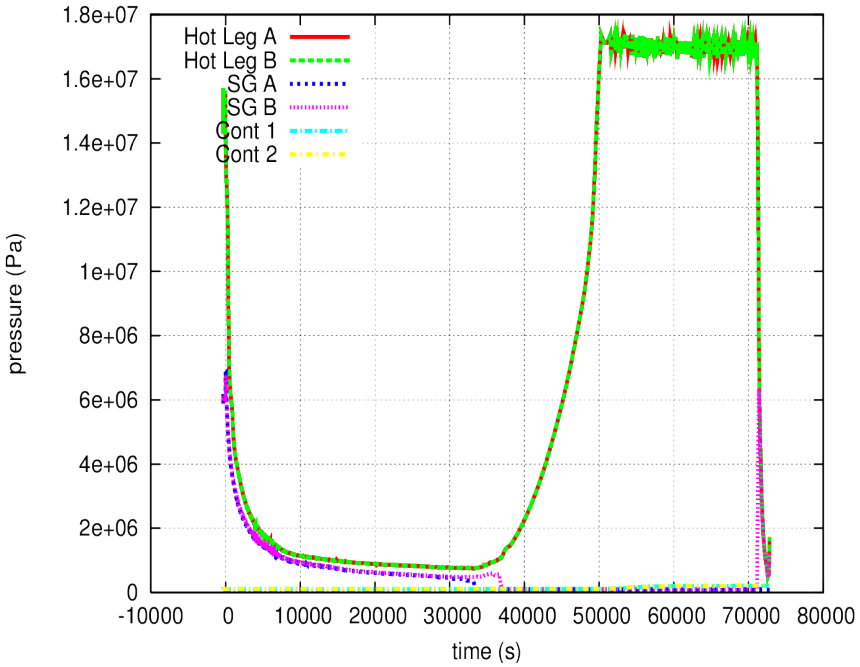


**Figure 3-19 Main pressures for the ltsbo-as calculation**

For other cases in the newer set of calculations, only the system pressures and volatile FP releases are provided. Figure 3-26 shows the main pressures for the *stsbo-a* calculation. Figure 3-27 shows the volatile FP release fractions for the *stsbo-a* calculation. Figure 3-28 shows the main pressures for the *ltsbo-a* calculation. Figure 3-29 shows the volatile FP release fractions for the l*tsbo-a* calculation. Figure 3-30 shows the main pressures for the *stsbo-as* calculation. Figure 3-31 shows the volatile FP release fractions for the *stsbo-as* calculation. Figure 3-32 shows the main pressures for the *stsbo-ao* calculation. Figure 3-33 shows the volatile FP release fractions for the *stsbo-ao* calculation.

This set of figures provides a fairly complete indication of results for the second set of simulations when considering the similarities in system behavior from case to case.

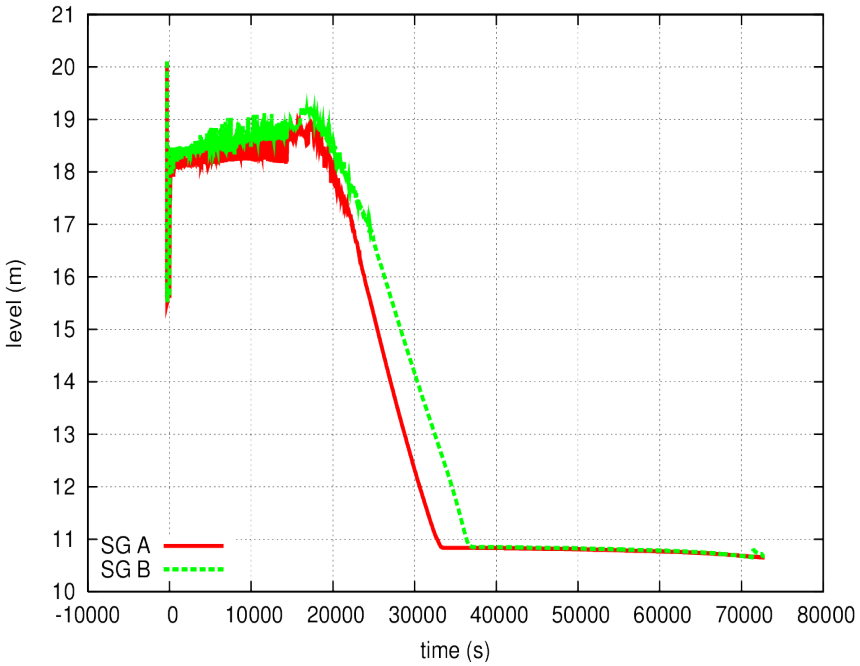


Figure 3-20 SG secondary collapsed liquid level for the ltsbo-as calculation

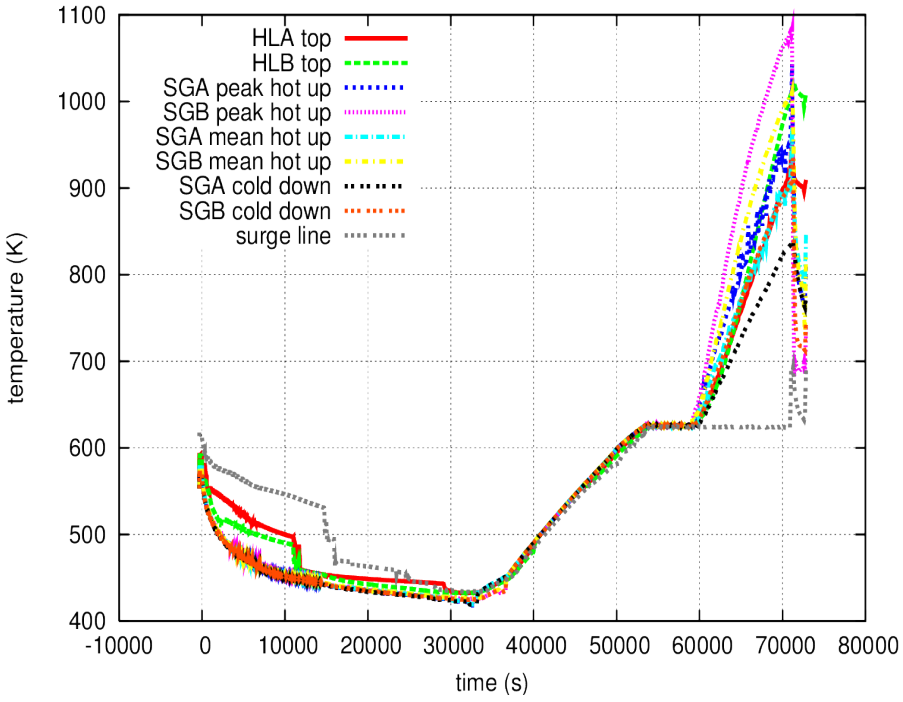


Figure 3-21 Main structure temperatures for the ltsbo-as calculation

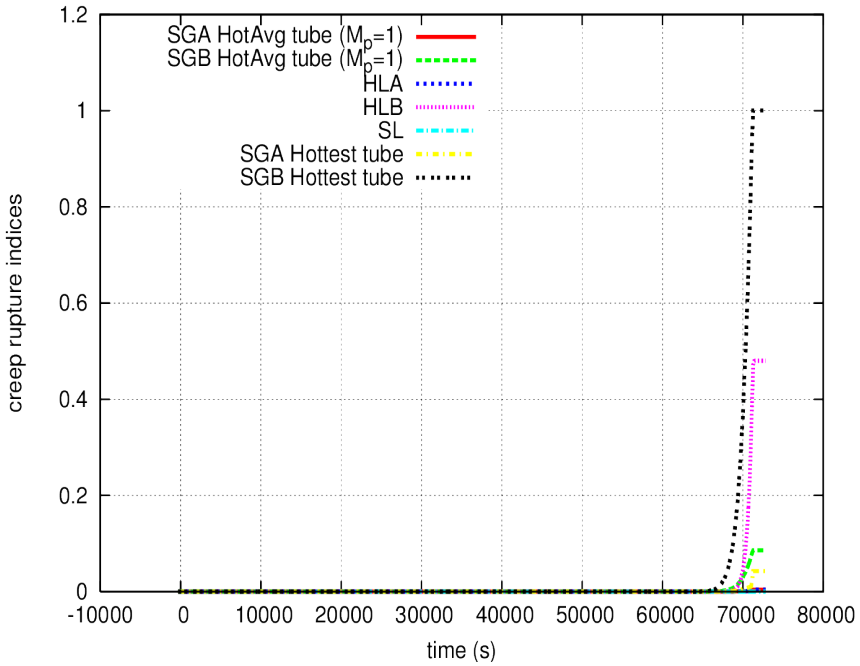


Figure 3-22 Creep-rupture indices for the ltsbo-as calculation

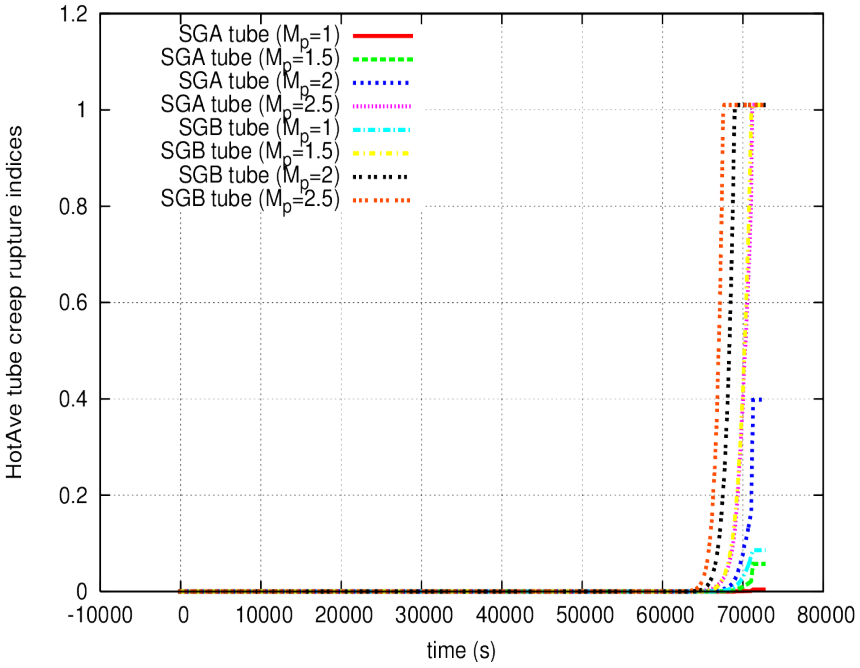


Figure 3-23 HotAve tube creep-rupture indices for the ltsbo-as calculation

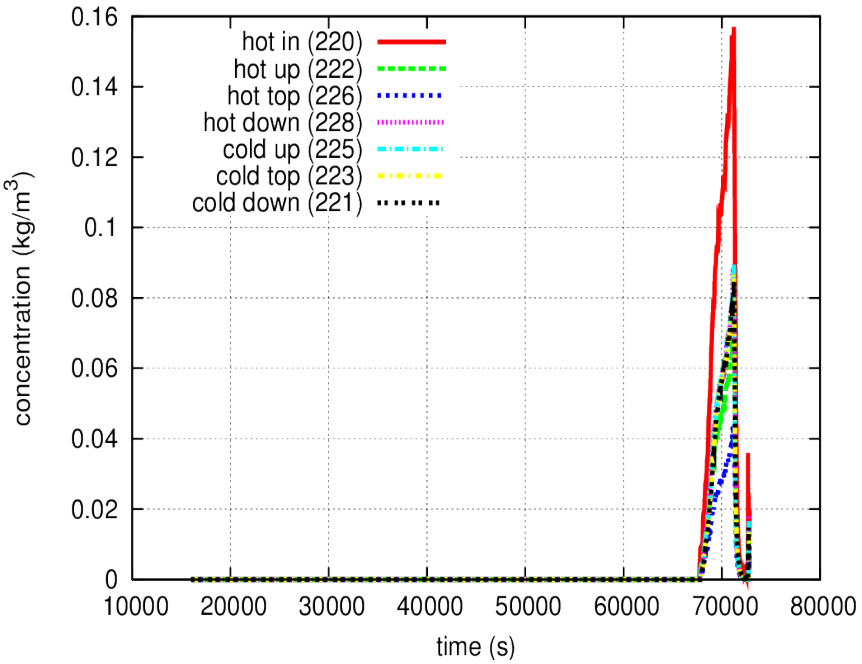


Figure 3-24 Hydrogen concentrations in SG A tubes for the ltsbo-as calculation

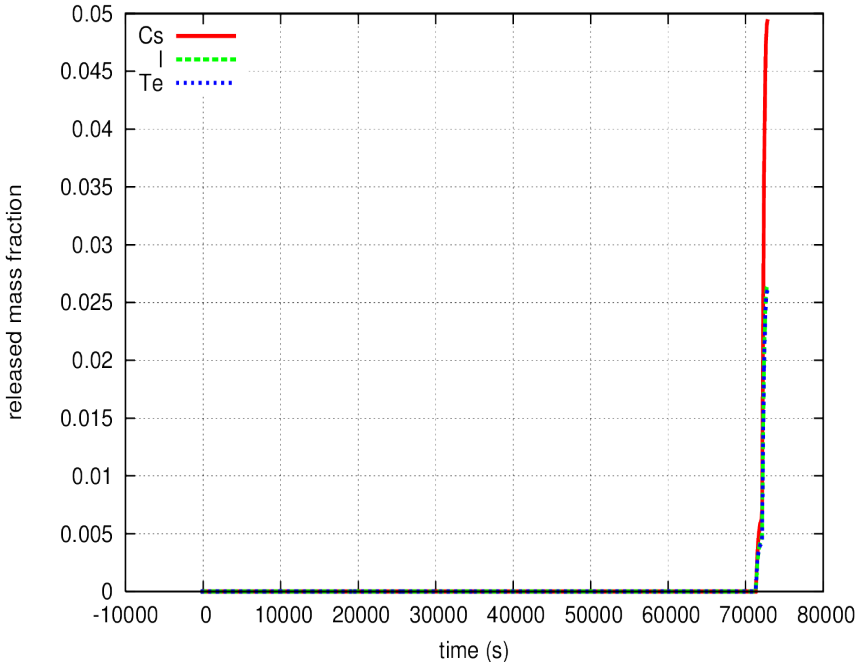


Figure 3-25 Volatile FP release fractions for the ltsbo-as calculation

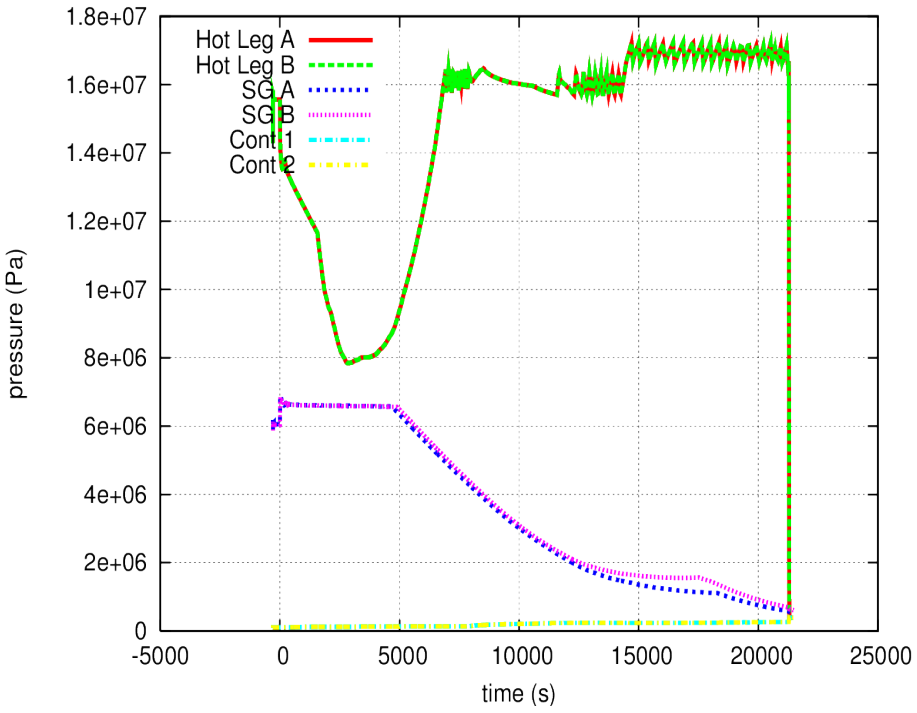


Figure 3-26 Main pressures for the stsbo-a calculation

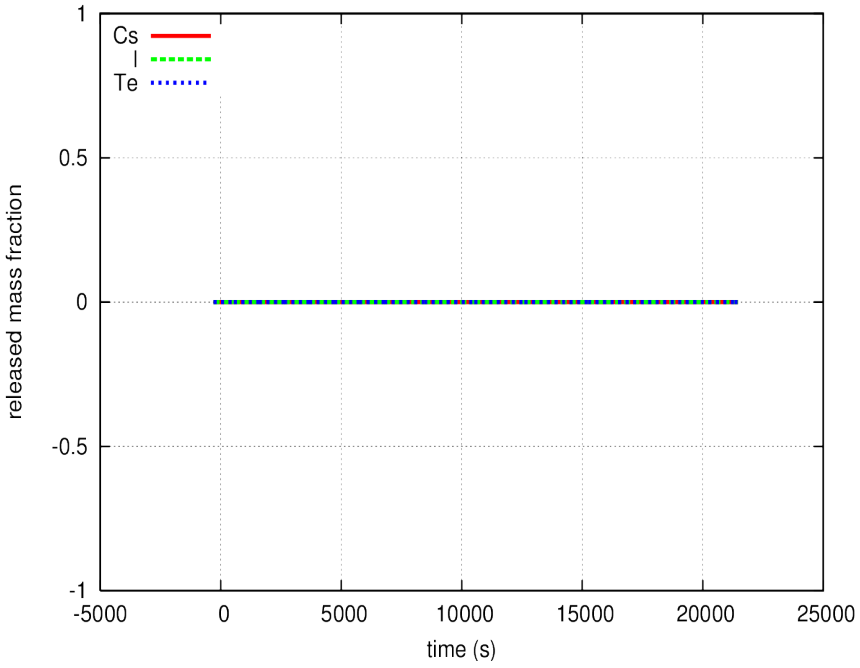


Figure 3-27 Volatile FP release fractions for the stsbo-a calculation

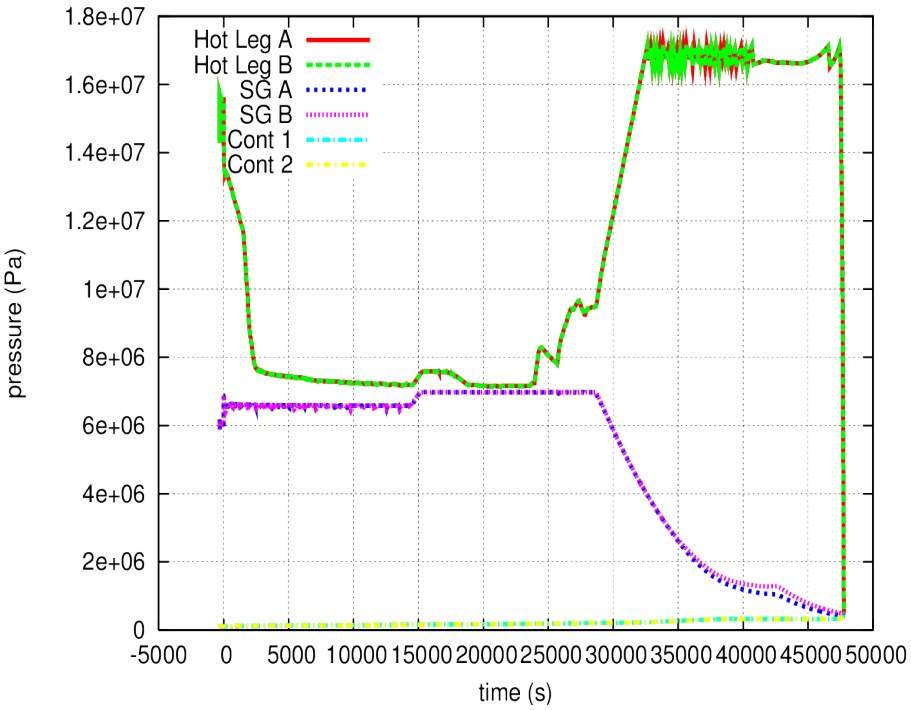


Figure 3-28 Main pressures for the ltsbo-a calculation

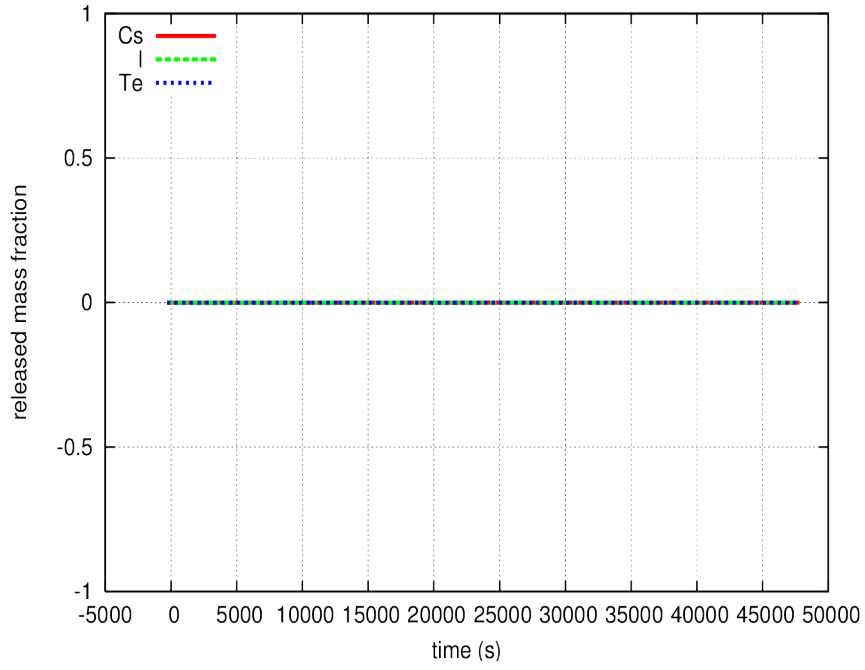


Figure 3-29 Volatile FP release fractions for the ltsbo-a calculation

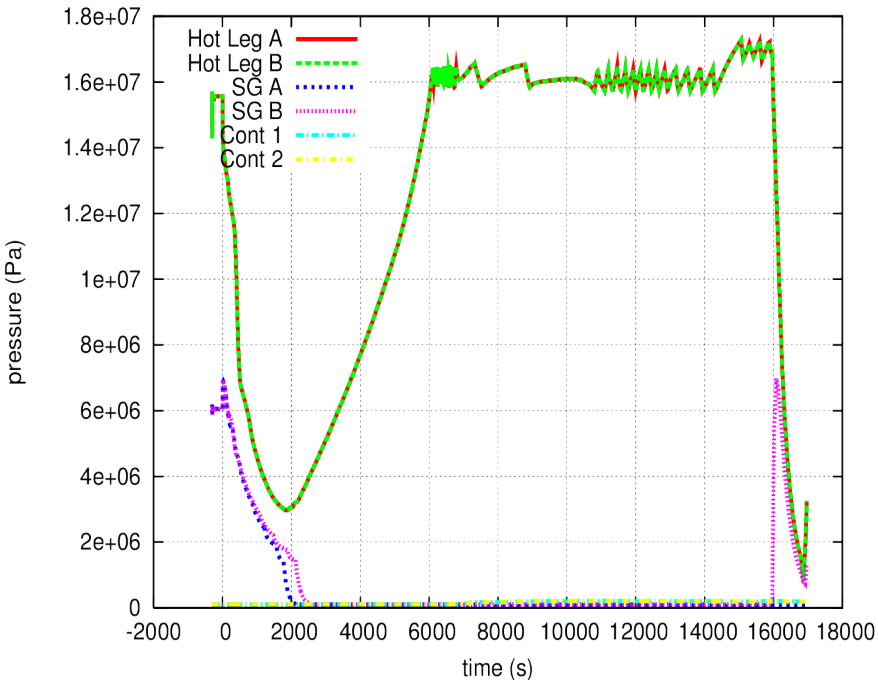


Figure 3-30 Main pressures for the stsbo-as calculation

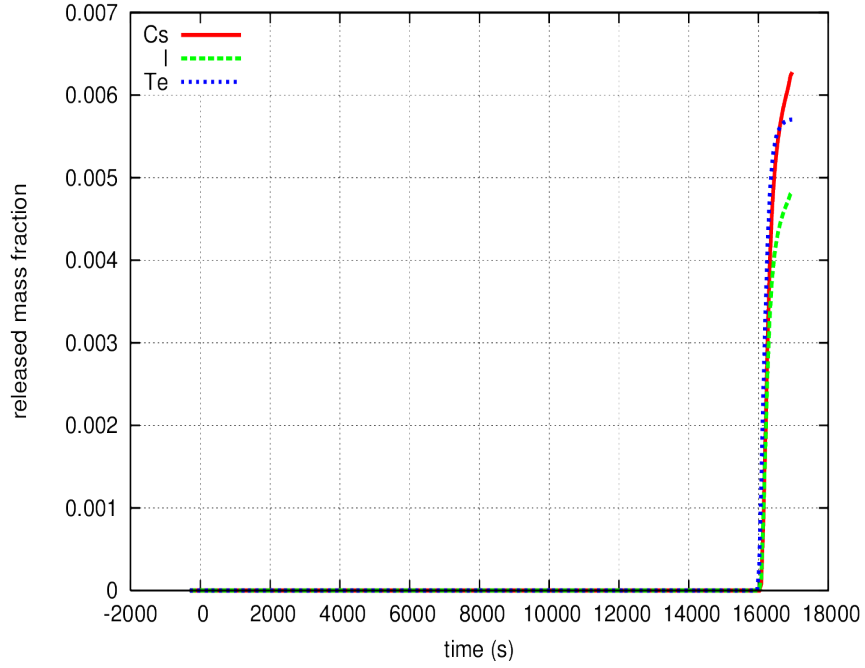


Figure 3-31 Volatile FP release fractions for the stsbo-as calculation

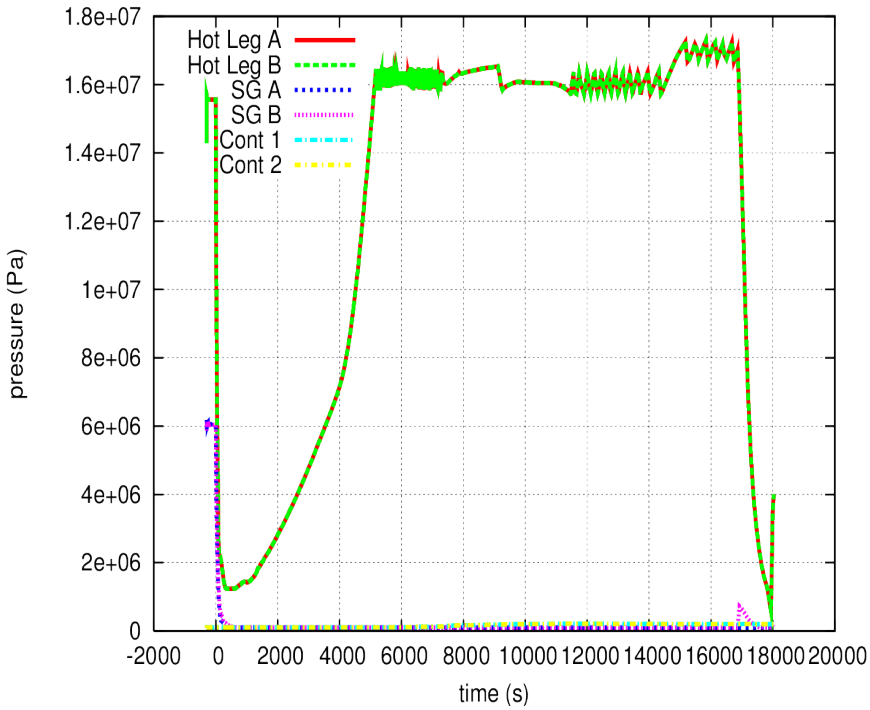


Figure 3-32 Main pressures for the stsbo-ao calculation

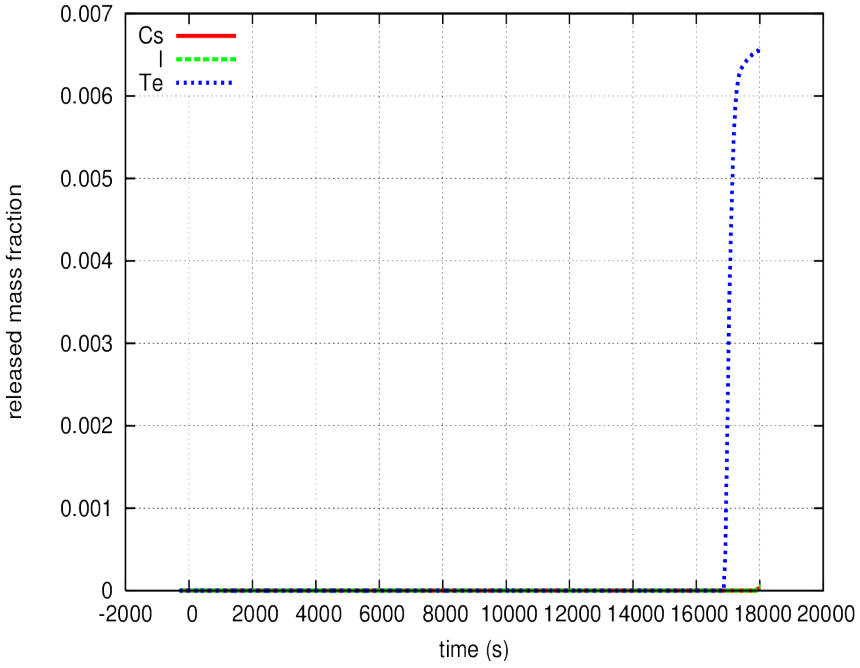


Figure 3-33 Volatile FP release fractions for the stsbo-ao calculation

All simulated accident sequences start with an SBO, which includes a loss of offsite power and a failure of emergency generators to start. The reactor and equipment are assumed to successfully trip. Valves, including main steam isolation valves (MSIVs), are assumed to close as planned. For some scenarios, the TDAFW pump was assumed to fail to start. Batteries are assumed to deplete at 4 hours. For others, the TDAFW pump was assumed to continue operating until assumed battery depletion at 4 hours. Scenarios for which the TDAFW pump was assumed to fail to start are referred to as short-term station blackout (*stsbo*). Scenarios for which the TDAFW pump was assumed to remain functional until batteries are depleted are referred to as long-term station blackout (*ltsbo*).

The loss of reactor power coupled with the continued removal of heat by the SG cools the system, which results in the condensation of steam and a reduction in system pressure. This can be seen in any of the main pressure figures (e.g., Figure 3-5).

As long as substantial water remains in the SG, secondary-side pressure is governed by the setpoint of the governing safety valves. This pressure is governed at first by the secondary PORVs (e.g., Figure 3-5), unless, for some reason, valves open at this time either by sticking or by operator action.

If secondary relief valves are open, this not only reduces the secondary pressures and temperatures down but it also reduces primary pressures. This occurs for both sticking (-as cases) (e.g., Figure 3-19) and by valve opening by operator action (-ao case), Figure 3-32. MELCOR predicted the pressure drop to be sufficient to drop pressures below the accumulator activation setpoint.

If the TDAFW pump remains operational (*ltsbo* cases), water remains in the secondary side when the batteries deplete and TDAFW pump fails. In this case, the secondary-side pressure is governed by the MSSVs. This can be seen as a jump in secondary pressure at 4 hours (14,400 s) for the *ltsbo* cases in which secondary valves are not open early on (i.e., *ltsbo* and *ltsbo-a*) (e.g., Figure 3-12 and Figure 3-28, respectively).

When the TDAFW pump stops replenishing water to the SGs, water in the SG secondary sides boils off. The boil-off begins soon after accident initiation for *stsbo* cases (e.g., Figure 3-6) and after the batteries deplete for *ltsbo* cases (e.g., Figure 3-13). Except for some RCS-to-containment heat losses, nearly all core decay power contributes to this boil-off as long as sufficient water is available in the SG secondary sides to reject the decay heat.

The SG water eventually boils off to a level at which the SGs can no longer remove all the decay heat. The primary pressure then begins to rise until the governing primary relief valve setpoint is reached. Before battery depletion, the PORVs govern the primary pressure. The SRVs govern the primary pressure following battery depletion.

During this time decay, heat boils off the primary inventory. When the core is liquid covered, temperatures stay at saturation. The saturation temperature can be seen to increase with increased primary pressure (e.g., Figure 3-7). Eventually the core uncovers and structure temperatures begin to rise. This rise is nearly linear in time.

This temperature rise occurs a little slower for the *ltsbo* cases because of the lower decay heat. This can be seen in Figure 3-17. Other than this minor effect, the *ltsbo* behavior is very similar to that for the equivalent *stsbo* case (Figures 3-15 through 3-17).

What differentiates one case from another is the timing of boil-off of both secondary and primary inventories and of the time those temperatures start to rise. Otherwise, scenario progression is rather similar. Cases where secondary valves are open lose heat sink faster than those that do not. If the valve opening cools the system and drops the primary system pressure below to the accumulator setpoint pressure, this additional water inventory delays the heatup time.

When the core is uncovered, the hot gases coming from the core establish a closed-loop-seal natural convection pattern, as described above. These hot gases heat up RCS structures, including the HLs and the SG tubes. The calculations predict the surge line to remain relatively cool from the presence of liquid water.

As mentioned earlier, a failure of an RCS component releases FPs to the containment, whereas the failure of tubes could result in FPs bypassing the containment and being released to the environment. The failure of another RCS component before SG tubes is preferred because the containment is not bypassed.

The SG tubes more closely track the adjacent gas temperature because they are thin and therefore have a short thermal response time. Thicker structures such as HLs respond more slowly to the adjacent gas temperature. The gas temperature adjacent to the tubes is somewhat cooler because of mixing with cooler gases between the HLs and the tubes.

When the structure temperatures increase sufficiently, the pressure differential across them can result in creep. The accumulated damage for vulnerable structures is tracked using creep-rupture indices. When a given creep-rupture index reaches a value of 1, that structure is considered to have failed. The creep-rupture indices, assuming no flaws in structures, are used to predict thermal and hydraulic system response (e.g., Figure 3-8).

For some scenarios the hottest SG tubes in loop B, the loop without the pressurizer, failed first, but the pressure remained high enough for other RCS components (i.e., HL) to subsequently fail (e.g., *stsbo*, *ltsbo*). For other cases, RCS components other than the SG tubes failed first, thereby depressurizing the primary system and preventing tube failure (e.g., *stsbo-a*, *ltsbo-a*). For still others cases, the hottest SG tubes failed first but depressurized the system sufficiently to prevent the failure of other RCS components (e.g., *stsbo-as*, *ltsbo-as*, *stsbo-ao*).

Although they did not otherwise influence the calculation, creep-rupture indices for hot average tubes for stress multipliers ranging from 1 to 2.5 were evaluated to give an indication of the tube failure timing for different sized flaws (e.g., Figure 3-9).

Components fail near the time of rapid zirconium (Zr) oxidation. A sharp rise in hydrogen concentrations provides an indication of when this occurs (e.g., Figure 3-10).

In cases where the HLs fail first, no bypass releases to the environment occur.

For scenarios that included SG secondary leakage to containment and no assumed valve failure or operator opening of these valves, either minimal release occurred because one of two things happened: (1) the secondary relief valves opened very briefly before FPs were leaked to the containment through the assumed leakage (*stsbo*, Figure 3-11, and *ltsbo*) or (2) the leakage kept the SG secondary pressure low enough that the secondary relief valves remained seated and no bypass FPs were released at all (e.g., *stsbo-a*, Figure 3-27, and *ltsbo-a*, Figure 3-29).

Cases that involved intentional opening or failed open secondary relief valves resulted in releases to the environment (*stsbo-as* (Figure 3-31), *ltsbo-as* (Figure 3-25), and *stsbo-ao* (Figure 3-33)). Note that releases are not terminated for these cases. These cases were run to evaluate the TH behavior. They would have to be rerun to fully evaluate FP bypass releases.

Table 3-3 shows the RCS failure times and RFs to the environment. Because the primary purpose of the runs was to obtain the TH histories, cases were not rerun if sufficient data were output to characterize TH behavior. Because of this, some of the cases terminated before some of the release occurred. Therefore, the RFs listed in this table do not represent the total RF but the RF at the time of problem termination. It instead represents the releases when the more stringent time step restrictions upon material relocation or reflood caused the calculation to terminate. On the other hand, the SG secondary-side decontamination determined from the ARTIST project, which was not included, would reduce predicted releases. This decontamination would be expected to reduce the release potentially by about a factor of 5. This decontamination factor cannot be directly applied to the result because the decontamination is particle-size dependent and because the decontamination would replace and not add to the SG decontamination already calculated by MELCOR during the run.

### Table 3-3 Failure Times and Release Fractions to Environment

| | ***stsbo*** | | | ***ltsbo*** | | |
|---|---|---|---|---|---|---|
| | **Fail t(h)** | | **RF**** | **Fail t(h)** | | **RF**** |
| | **SG** | **HL** | | **SG** | **HL** | |
| **-a** | - | 5.9 | - | - | 13.2 | - |
| **-as** | 4.4 | - | *0.006 | 19.8 | - | *0.048 |
| **-as-SCF** | 4.4 | 4.9 | N/A | 19.8 | 19.9 | N/A |
| **"base"** | 6.3 | 7.2 | 0.003 | 13.7 | 14.7 | 0.001 |
| **-SCF** | 6.3 | 6.5 | N/A | 13.7 | 13.9 | N/A |
| **-ao** | 4.7 | - | *0.007 | N/A | N/A | N/A |
| **-MSSVstick** | 4.5 | - | *0.009 | N/A | N/A | N/A |
| **-noSGleak** | - | 8.1 | - | - | 16.1 | - |
| **-MSSV1F** | 6.3 | 7.2 | 0.003 | 13.7 | 14.5 | - |
| **-noSGleak -MSSV1F** | - | 8.1 | - | - | 16.1 | - |
| **-noSGleak -MSSV1F -minHLC** | N/A*** | | | - | 18.5 | - |

* RF at the time of calculation termination. Releases are ongoing.

** Maximum of volatile (Cs, I, and Te) release fractions.

*** Case did not run to failure time.

### 3.6.4 Data Output Fields Provided for Use by External Failure Calculator and FE Analyses

Data files are transmitted to perform independent assessments of component failure. The data channels in these files are generally labeled by parameter (e.g., P for pressure, T for temperature), location, and material.

The main datafile for each loop provides the following data channels. Loop A labels are shown here. Data in items 1 through 7 are used as the TH input for the C-SGTR calculator in the Section 7.2 PRA analysis.

| | | |
|---|---|---|
| (1) | Time | |
| (2) | Pp | Primary system pressure |
| (3) | TSL−s | Inside surface temperature of the surge line |
| (4) | TH LAt−s | Inside surface temperature of the top of the HL 1 |
| (5) | TSGAhu−s | Inside surface temperature of the hot-up 2 SG tubes |
| (6) | TSGAcd−s | Inside surface temperature of the cold-down SG tubes |
| (7) | PsA | Secondary-side pressure for SG |
| (8) | TH LAt−g | Gas temperature in the top of the HL |
| (9) | TH LAb−s | Inside surface temperature in the bottom of the HL |
| (10) | TH LAb−g | Gas temperature in the bottom of the HL |
| (11) | TSGAhu−g | Gas temperature in the hot-up SG tubes |
| (12) | TSGAhd−g | Gas temperature in the hot-down SG tubes |
| (13) | TSGAhd−s | Inside surface temperature of the hot-down SG tubes |
| (14) | TSGAcd−g | Gas temperature of the cold-down SG tubes |
| (15) | TSL−g | Gas temperature in the Surge Line |
| (16) | hH LAt | Heat transfer coefficient for the top of the HL |
| (17) | hH Lab | Heat transfer coefficient for the bottom of the HL |
| (18) | hSGAhu−in | Heat transfer coefficient on the inside of the hot-up SG tubes |
| (19) | hSGAhu−out | Heat transfer coefficient on the outside of the hot-up SG tubes |
| (20) | ThA | Thot used to scale the CFD hottest tube results. This is the gas temperature entering the SG inlet plenum from the HL |
| (21) | TSGA−boil | Gas temperature in the SG secondary side |
| (22) | Pc1 | Containment pressure |
| (23) | TSGAhot−s | The hottest tube temperature calculated with the side calculation |
| (24) | TH LAt−smid | HL temperature at middle |
| (25) | TH LAt−sout | HL outer surface temperature |

Notes:

(1) HL temperatures are provided for the control volumes and heat structures that are adjacent to the reactor vessel. Tube temperatures are provided for the control volumes and heat structures adjacent to the tubesheet. Surge-line temperatures are provided for the control volumes and heat structures adjacent to the HL.

(2) Up and down refer to the direction of flow during closed-loop-seal natural circulation. For example, hot up and cold down both represent tube sections adjacent to the SG inlet plenum. The surge-line temperatures were also provided in the data for loop B to preserve the data channel numbering.

(3) The SG-tube HTCs were used to estimate the hottest tube temperature using the CFD and the AvgHot tube results, which are provided in the datafiles.

The supplemental datafile provides the hottest SG tube gas and surface temperatures calculated from the output data, along with the parameters used to determine these values.

The supplemental datafile (-addl) for each loop provides the following data channels.

| | | |
|---|---|---|
| (1) | Time | |
| (2) | TSGA−g−peak | Hottest tube inlet gas temperature calculated using the CFD normalized temperature (see Figure 3-36), Thot, and Tcold. |
| (3) | ThA | Thot used to scale the CFD hottest tube results. This is the same data as ThA in the main datafile. |
| (4) | TcA | Tcold used to scale the CFD hottest tube results. This is the same as the cold-down SG gas temperature in the main datafile. |
| (5) | TSGA−g−mean | Hot-up tube gas temperature to compare to the calculated gas temperature |
| (6) | TSGA−s−peak | Hottest tube temperature determined by a heat transfer calculation using secondary and calculated hottest-tube-primary gas temperatures along with the inside and outside heat transfer coefficients |
| (7) | TSGA−s−mean | Hot-up tube surface temperature to compare to the calculated tube temperature. This is the same curve as in the hot-up SG tube temperature in the main datafile. |
| (8) | TSGA−boil | SG secondary-side gas temperature. This is the same curve as in the main datafile. |

### 3.6.5 MELCOR Cases to Support the C-SGTR Calculator

Section 7.2 summarizes the use of the temperature and pressure profiles of the selected accident sequences for the C-SGTR calculator. These profiles are used as input files to the C-SGTR calculator to study the SG tube leak generation and HL and surge-line failure for given flaws and materials.

Other examples of T&H files created from MELCOR output files as input files for the C-SGTR calculator can be found in the Appendices; Appendix D gives such an example.

Table 3-4 MELCOR Cases to Support C-SGTR Calculator

| | | AFW Fails at T=0 | AFW Fails at T=4 h | RCS Loop A (with PRZR) | RCS Loop B | Secondary-Side Leak at 0.5 $in^2$ | Secondary-Side Relief Valve Sticks Open | Creep Rupture Suppressed |
|---|---|---|---|---|---|---|---|---|
| 1 | *stsbo-a-SCF-a* | √ | | √ | | √ | | Yes |
| 2 | *stsbo-a-SCF-b* | √ | | | √ | √ | | Yes |
| 3 | *ltsbo-a-SCF-a* | | √ | √ | | √ | | Yes |
| 4 | *ltsbo-a-SCF-b* | | √ | | √ | √ | | Yes |
| | | | | | | | | |
| | *stsbo-as-SCF-a* | √ | | √ | | | √ | Yes |
| | *stsbo-as-SCF-b* | √ | | | √ | | √ | Yes |
| | *ltsbo-as-SCF-a* | | √ | √ | | | √ | Yes |
| | *ltsbo-as-SCF-b* | | √ | | √ | | √ | Yes |
| | | | | | | | | |
| | *stsbo-a-a* | √ | | √ | | √ | | No |
| | *stsbo-a-b* | √ | | | √ | √ | | No |
| | *ltsbo-a-a* | | √ | √ | | √ | | No |
| | *ltsbo-a-b* | | √ | | √ | √ | | No |

Cases 1 through 4 are used in the base case analyses in Section 7.2.

### 3.6.6 MELCOR Cases to Support RCP Seal Leakage Sensitivity Evaluation

A TH sensitivity case was run to study the impact of RCP seal leakage on primary pressure, while failure timings of C-SGTR addressed the much smaller RCP seal leakages of a CE plant. The previous MELCOR runs considered an assumed 79.5 Lpm (21 gpm) RCP seal leakage for each RCP seal for the CE plant to be consistent with the W calculations. The question arose regarding the impact of this seal leakage on primary system pressure during auxiliary feedwater operation and how much it would change if CE seals leaked far less. To look at this issue, the base case was run with RCP seal leakage disabled (i.e., zero seal leakage flow).

Figure 3-34 compares the pressures predicted for the base case and for the no-seal-leakage case. Figure 3-35 shows structure temperatures, the ones that provide most stress for loop B, the loop that fails first. Preventing RCP seal leakage results in substantially less reduction in primary system pressure. Preventing RCP seal leakage also preserves inventory in the primary system, thereby delaying the temperature rise and thus component failure by nearly 10 minutes.

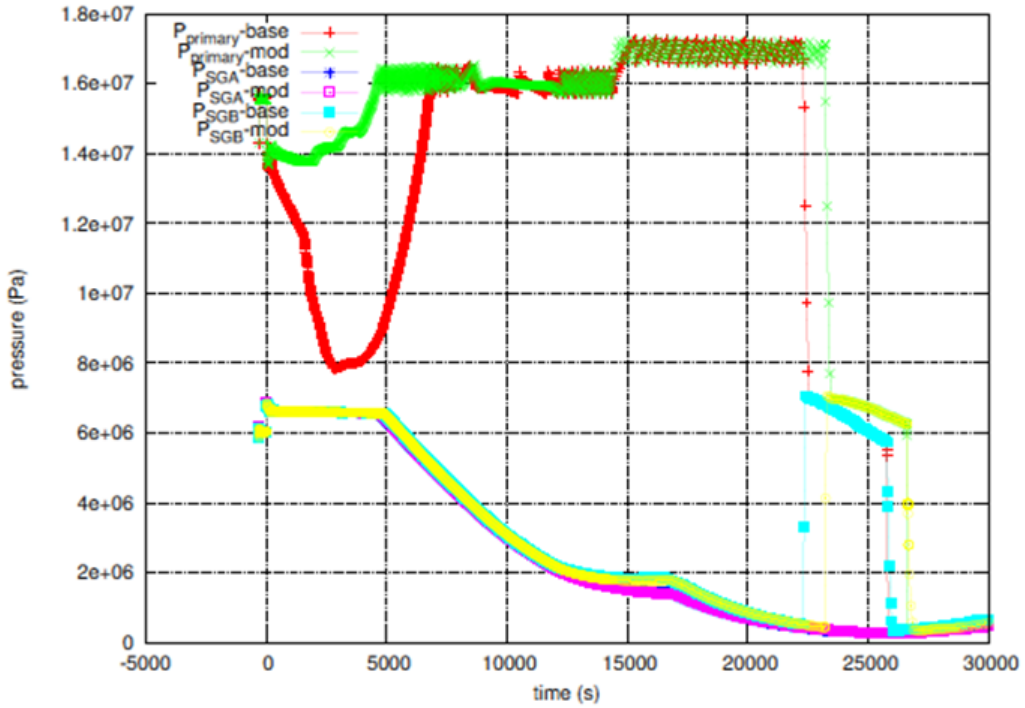


Figure 3-34 Primary pressure and secondary pressure for SG A and B for base case of short SBO with and without RCP seal leakage

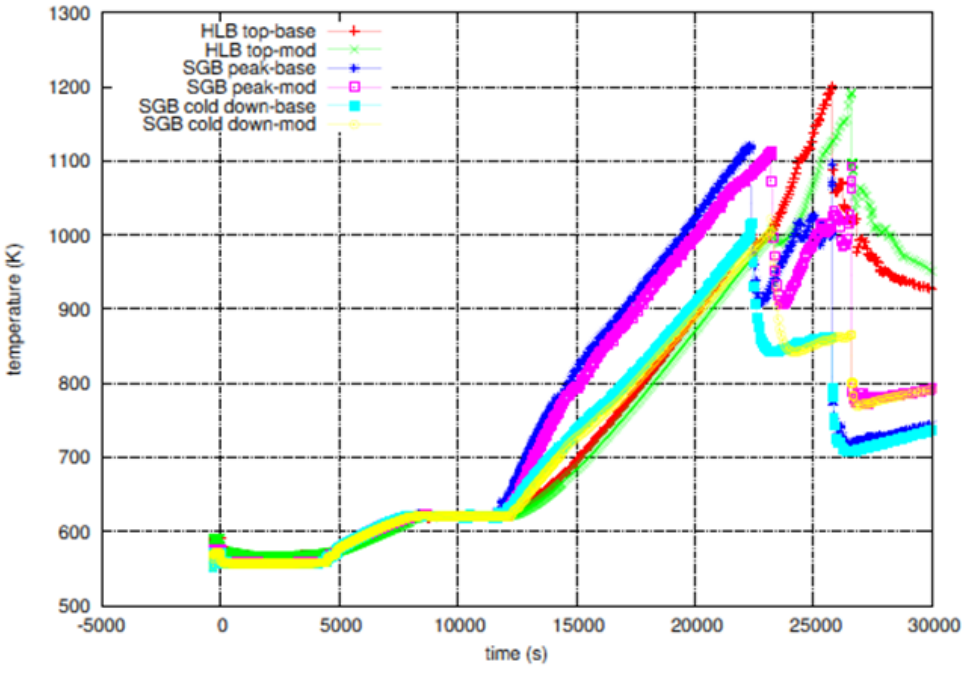


Figure 3-35 The HL structure and peak SG tube temperature for loop B for base case of short SBO with and without RCP seal leakage

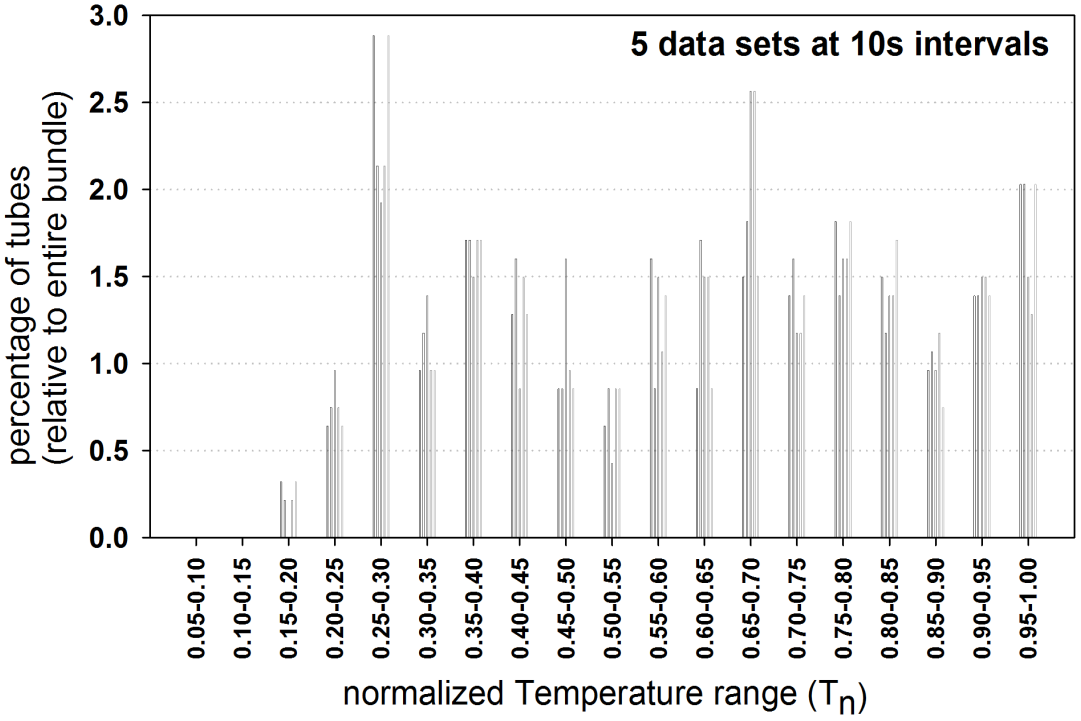


**Figure 3-36 Normalized temperature distribution at the SG tube sheet inlet for a CE plant**

## 3.7 Potential Future Analyses

Several aspects of the modeling and analyses were not pursued at this time in the interest of reducing the number of cases run and the level of effort involved with the idea of finding a representative "limiting" analysis. Additional analyses can be performed to explore pertinent aspects of system behavior and regions of the event tree and to look into different sensitivities in more detail.

Additional modeling may include the following:

- updating the deck to handle loop seal clearing, which involves switching SG tube natural circulation modeling from an active control to a friction-based method and a renodalization of the SG tubes and cold legs
- review of surge-line draining behavior and reconciliation of modeling
- performing a detailed review of HL creep-rupture modeling and materials
- updating some nodalization connectivity issues; double checking parameters found to significantly affect system behavior
- application of ARTIST SG decontamination factors in calculating environmental FP releases
- accounting for the likelihood of specific flaws coinciding with sections of SG tubes at specific locations in the SG tube spatial temperature distribution

It is also possible to eliminate the artificial natural-circulation-related pipe-switching logic, as the coupling between the upper and lower HL volumes should be applicable throughout the entire accident sequence.

Additional analyses may include the following:

- performing a detailed analysis of loop seal clearing
- reconciling surge-line discrepancies with previous analyses
- comparing and reconciling results with those of previous industry analyses
- studying HL creep-rupture behavior in more detail
- performing detailed sensitivities to better characterize the effect of parameters
- analyzing additional relevant sequences in the event tree or similar sequences for somewhat different designs

Use of already-developed multiparameter variable-input scripts allow multiple input parameters to be varied so that the different sequences can easily be run with the same MELCOR input deck. For example, these scripts can be used to perform MELCOR analyses for all relevant permutations of the C-SGTR event tree with probabilistic sampling of nondiscretely defined events or other parameters if needed.

The text below provides additional information on a few of these items.

A change that could have the most significant effect on predicted consequences is updating the deck to address loop seal clearing. Should the loop seals clear for any of these cases, the enhanced heat transfer to the tubes would greatly accelerate tube failure thus increasing the potential for FP releases. The deck was not generated with the specific intent to resolve loop seal clearing. The active SG natural circulation control may significantly affect loop seal clearing behavior. Furthermore, some inconsistencies exist between the flow-path and control-volume nodalization for the cold legs in that they do not represent quite the same diameter.

As mentioned above, the SG decontamination factors determined from the ARTIST project, which were not included in the determination of FP releases to the environment, would be expected to reduce FP releases potentially by about a factor of 5.[3] This was not updated.

The accuracy of the SG tube failure calculation can be improved by linking the SG temperature and flaw distributions to determine the likelihood of a flaw occurring at a hot location on a tube. Judging by the TH results, this improvement would result in a more accurate prediction of tube failure timing and would likely alter the expected tube failure time by several minutes. The flaw and temperature distributions within the SG can be combined to improve these estimates. This improvement is only worth implementing if the improved results would be used in the risk determination.

Significant conclusions were drawn about plant behavior that relate to the operation of the secondary-side relief valves. It would be prudent to check and document a comparison of relief

[3] For example, NUREG/CR-7110, "State-of-the-Art Reactor Consequence Analyses Project, Volume 2: Surry Integrated Analysis," issued August 2013, provides an estimate for SG aerosol decontamination between 4.7 and 9.

valve opening criteria with that described in plant documentation. Doing so is critical if safety decisions will be made from the analysis conclusions. If the modeled relief valve behavior is different than that for the plant, incorrect conclusions will be drawn.

**Recommendations**

Given the inherent uncertainties that cannot be reduced and the level of effort involved, it may not be worth the effort to further pursue some of the potential future work. However, several of the potential deck modifications should be made eventually, as they will likely affect other non-C-SGTR analyses. These include the following:

- addressing differences between current pressurizer draining behavior and that of previous analyses
- switching from active control to a friction-based method to model SG natural circulation, along with preforming the associated renodalization
- analyzing loop seal clearing in more detail

The results release fraction calculation should be checked once against methods by running it on a problem for which releases have been extracted. A match in RFs for a simple case would confirm proper functionality.

## 3.8 Conclusions

### 3.8.1 Analysis-Based Conclusions

This study developed CE CFD and MELCOR models. These models were exercised on selected risk-significant sequences to evaluate expected TH behavior. Datafiles were generated from the system-code output and provided to RES analysts for use as initial and boundary conditions in their detailed component failure analysis. FP release data were generated from these analyses for use in updating the risk contribution from these events.

The initial planned single bounding case did not result in releases. Because of this, additional cases had to be run to address behavior that had not previously been considered.

Most of the additional run requirements resulted from analyzing the different aspects of the problem together, unlike in previous analyses. The coupling of phenomena was explicitly modeled rather than assumed or modeled separately, as in previous analyses. Unlike in previous analyses, RCS ruptures were modeled to alter TH behavior and affect subsequent failures.

The initial approach did not sufficiently capture the interactions between the different aspects of the sequence.

Unlike in previous TH analyses, FP releases were calculated in addition to the TH feedback. As part of this analysis, secondary-side relief valve behavior was explicitly modeled.

Accounting for these coupled phenomena led to feedback that had not been considered. To obtain reasonable results, further analyses had to be performed. A notable parameter that led to the requirement of additional runs was the effect of sticking assumptions for secondary-side

relief valves. Addressing the valve behavior was not a consideration in the initial project planning but proved to have a major impact. This is apparent only upon an analysis of results.

The assumption of MSSVs failing open, which was not originally focused on, was found to significantly affect system behavior. This was the case because previous analyses did not model secondary relief valve behavior but assumed that a bypass would occur if SG tubes failed some time before other RCS components. It was found that, with the whole system being modeled, if valve failure was not explicitly modeled, no appreciable releases would result, *even if a substantial number of SG tubes had ruptured*. The simulations had to be run repeatedly to establish relief valve behavior that resulted in releases to the environment. Assuming failure upon full valve opening following a tube rupture did not change releases, as the valves did not fully open and thus did not stick. Assuming a stick-open-failure upon full valve opening at any time also did not result in appreciable releases because, even for those cases, the valves did not stick open. Assuming that secondary-side relief valves stick as far as they have opened or assuming that they are opened by operators did result in releases. It seems that the secondary-side valves are not as pressure stressed when the tubes rupture several hours into the accident so they do not leak. They may be thermally stressed, which is not considered for the valve-opening model.

Note that if an SG-secondary-to-containment leakage is assumed, as in the original model, and secondary-side valves are open, this constitutes a leak path from the containment to the environment. Perhaps it would be more appropriate, when assuming leakage, to assume that it occurs through secondary-side isolation valves.

The analyses results indicate the following:

- Even if an SGTR occurs first, without an assumption of secondary relief valves stick-open-failure or opening by operator action, no or minimal releases will occur.
- For a high-pressure secondary side (high-dry-high) situation, an HL will fail before an unflawed tube, thus preventing tube rupture in the absence of tube flaws.

The prediction of minimal releases without an assumption of secondary-side relief valve failure is rather insensitive to uncertainties in component failure timing. The amount of FPs released in a temporary partial valve opening immediately following tube rupture may be somewhat dependent on the assumption of the number of SG tubes that rupture. Twenty tubes are assumed to fail if unflawed tubes fail. Rupture of a flawed tube is considered to result in the full rupture of a single tube.

For the high-dry-high situation, by the time the HL was predicted to fail (damage index = 1), the tube damage index was very low, indicating a significant flaw would be required for tubes to fail first for this condition. Previous analyses, and earlier single-tube-failure analyses within this project, have shown that a single tube failure will not reduce pressure at a sufficient rate to prevent HL failure that limits the amount of FPs that can be released.

Considerable uncertainties exist in component failure timing.

An SNL uncertainty analysis using an earlier version of the Calvert Cliffs Nuclear Power Plant deck indicated that the RCS-component-to-tube relative failure timing variation because of expected variations in TH parameters approximately followed a normal distribution with about a 600-s standard deviation.

A change of a few percent in the HL countercurrent flow rate alone was found in analyses to make the difference between HLs or SG tubes failing first. The SNL uncertainty analysis addressed this parameter w by varying the discharge coefficient and factored the parameter into the relative-failure-timing uncertainty distribution.

Results from a sensitivity analysis indicate that the impact of creep-rupture-related material properties not considered in the uncertainty analysis can also greatly affect HL failure timing.

The difference in the prediction of HL failure timing was found to vary greatly, simply by the assumption of material (stainless or carbon steel)—approximately 2.5 hours. Because the SG calculator and FE calculations are providing more precise estimates of component failure timing, the results from the calculator software was used for the PRA analysis. Therefore, updating the HL creep modeling within MELCOR was not prioritized over other modeling aspects that provide information not available from other sources.

Although this difference in failure timing is not directly applicable as an additional uncertainty in failure timing for this analysis, it does underscore the importance of using the correct creep-rupture-related material properties. It indicates that this material property can make the difference in whether an SG tube or an HL fails first.

The highest volatile-FP release was 5 percent at the time the run terminated for the *ltsbo* case with no secondary-side-to-containment leakage and sticking MSSVs. This was the highest release of all cases considered.

These RFs should be taken with caution. Some of the RFs reflect the releases at the time the problem terminated, not the overall release. For this sequence, FPs were being released at a significant rate at the end of the simulation, so the actual predicted RF will be higher if the simulation is extended. To obtain the code-calculated RFs for the cases in question, the simulations would have to be run until the RFs reached their asymptotic values or at least beyond the time when risk analyses estimated that mitigative actions would occur. If precise output RFs are needed, this can be done.

### 3.8.2 Deck-Generation-Based Conclusions

Because the heat transfer and flow models are based on accepted practice and because natural circulation flow was set based on CFD analyses of a sequence for which the code has been validated, the MELCOR results are considered suitable for screening for component failure timing under closed-loop-seal natural circulation. The CFD modeling approach was validated against experiments representing somewhat different SG geometry.

MELCOR can therefore be used as a screening tool to establish which cases need further scrutiny by more detailed component failure calculation methods conducted using the SG tube failure calculator and FE analyses.

Primarily because of active SG natural circulation control, which can alter closed loop flows, loop seal clearing likely cannot be accurately predicted with the current deck. Even if this were updated, large uncertainties would remain in the prediction of loop seal clearing. Because natural circulation flows are consistent with those provided by CFD, active control is not expected to significantly affect tube failure timing.

A potential change that could have the most significant effect on predicted consequences is updating the deck to address loop seal clearing. Should the loop seals clear for any of these cases, the enhanced heat transfer to the tubes would greatly accelerate tube failure, thus increasing the potential for FP releases.

A conceptual model of loop seal clearing behavior was developed. It is based on considering the loop seal bubble behavior to determine what happens with the loop seal.

Another potential modification that may have a significant effect is resolving the difference in pressurizer draining time between current and previous analyses. The matter should be looked into further.

An attempt was made to determine the relative contributions of radiative and convective heat transfer, as only the combined heat transfer coefficient was available in the plot file to provide phenomena-specific HTCs for use in the FE calculation. It was not completely successful. The impact of this change should be assessed.

Previous NRC analyses only adjusted the convective HTC for developing-boundary-layer effects, whereas other analyses have adjusted both the convective and radiative HTCs. Because the two HTCs could not be distinguished in the MELCOR plotfile, both HTCs were adjusted for developing-boundary-layer effects for the FE analyses. This change would tend toward accelerating the prediction of HL failure.

The accuracy of the SG tube failure calculation can be improved by linking the SG temperature and flaw distributions to determine the likelihood of a flaw occurring at a hot location on a tube. This improvement would result in a more accurate screening-level prediction of tube failure timing and would likely alter the expected tube failure time by several minutes. This statement applies to predictions using MELCOR analyses; it does not apply to the PRA analyses in Chapter 7 of this report.

## 3.9 References


1. U.S. Nuclear Regulatory Commission, “SCDAP/RELAP5 Thermal-Hydraulic Evaluations of the Potential for Containment Bypass During Extended Station Blackout Severe Accident Sequences in a Westinghouse Four-Loop PWR,” NUREG/CR-6995, March 2010, Agencywide Documents Access and Management System (ADAMS) Accession No. ML101130544.
2. Fletcher, C.D. and R.M. Beaton, “SCDAP/RELAP5 Station Blackout Analyses for the Calvert Cliffs Plant,” Information System Laboratories, May 2006.
3. Fuller, E.L., et al., “Steam Generator Tube Integrity Risk Assessment: Volume 1: General Methodology, Revision 1,” Electric Power Research Institute (EPRI) Technical Report 1006593, Palo Alto, CA, 2002.
4. U.S. Nuclear Regulatory Commission, “CFD Analysis of 1/7th Scale Steam Generator Inlet Plenum Mixing during a PWR Severe Accident,” NUREG-1781, October 2003, ADAMS Accession No. ML033140399.
5. U.S. Nuclear Regulatory Commission, “CFD Analysis of Full Scale Steam Generator Inlet Plenum Mixing during a PWR Severe Accident,” NUREG-1788, May 2004, ADAMS Accession No. ML041380224.

6. U.S. Nuclear Regulatory Commission, “Computational Fluid Dynamics Analysis of Natural Circulation Flows in a Pressurized-Water Reactor Loop under Severe Accident Conditions,” NUREG-1922, October 2010, ADAMS Accession No. ML110110152.

7. Boyd, C., “CFD Prediction of Severe Accident Natural Circulation Flows in a Combustion Engineering Pressurized-Water Reactor Loop,” ADAMS Accession No. ML16068A170, International Topical Meeting on Advances in Thermal Hydraulics 2016, New Orleans, LA, June 2016.

8. U.S. Nuclear Regulatory Commission, Advisory Committee on Reactor Safeguards, letter to Travers, William D., May 21, 2004, ADAMS Accession No. ML041420237.

# 4 BEHAVIOR OF REACTOR COOLANT SYSTEM COMPONENTS OTHER THAN STEAM GENERATOR TUBES

## 4.1 Introduction

During postulated pressurized-water reactor severe accidents, there is a concern that degraded core effluents could be allowed to bypass the containment if the steam generator tubes (SGTs) experience structural failures. However, if other components of the reactor coolant system (RCS) (i.e., non-SGTs) fail before the SGTs, containment bypass could be averted if those failures prevent fission product (FP) releases outside of containment. Prediction of RCS component failure will help determine the related RCS thermal-hydraulic response and the relative sequence of the RCS failure, the risk importance, and the associated uncertainties.

The probabilistic risk assessment used the calculator software to predict the time-dependent failure probability for SGTs and for hot legs (HLs) and surge lines. The correlation used for estimating the failure probability for SGTs is based on previous NRC studies, mostly performed by Argonne National Laboratory (ANL). The calculator software also used empirical models to predict HL and SL failures, as documented in Information Systems Laboratories, ISL-NSAD-TR-10-13, “Technical Basis and Software User Guide for SGTR Probability,” issued December 2014, based on previous correlations by the Electric Power Research Institute.

Chapter 4 documents detailed structural analyses for the Zion Nuclear Power Plant (ZNPP), which were conducted to verify the adequacy of the RCS time-dependent failure times predicted by the simplified model in the calculator software. The results showed that the simplified models consistently predicted later times to HL failure than more detailed modeling. This detailed modeling also indicated that the upper portion of the HL will fail earlier than other RCS regions.

Chapter 5 documents the technical basis and the empirical model for predicting ligament rupture pressure, crack opening area, and unstable burst pressure of SGTs with flaws under severe-accident transients. The calculator software uses these same models.

## 4.2 Analyses of RCS Components for a Typical Westinghouse Plant

RCS drawings from ZNPP were studied (except drawings of the reactor vessel (RV), the SG, and the pressurizer (PZR) internals). It was determined that the following components qualify as potential failure sites:

- HL and surge line
- primary manway in the SG
- PZR power-operated relief valve (PORV), and safety valve (PSV)
- three resistance temperature detectors (RTDs) that penetrate the HL to monitor reactor coolant temperature
- socket weld connection of the instrument lines to the RTD flanges
- a small-diameter drain line that is attached to the bottom of the HL-pipe elbow at the HL connection to the SG

- a small-diameter sample line that is connected to the HL to monitor reactor coolant water chemistry before the coolant enters the SG

Failure or excessive creep deformation of the SG primary manway cover bolts, together with gasket creep, could lead to significant leakage of primary coolant and depressurization of the primary side. Of the two safety valves, the PORV is challenged more because it cycles more often than the PSV during a severe accident and is therefore hotter. Of the other remaining three items listed above, the welds, which join the RTD at the top of the HL to the HL, are the most vulnerable and have the highest potential to depressurize the primary side because they are located on the hot side of the HL during the severe-accident transient; also, their failure would create the largest diameter hole in the HL. Therefore, this particular RTD to the HL junction was analyzed in detail. Failure of the socket weld that attaches the instrument line to the RTD flange could open up a 25-millimeter (mm) (0.98-inch (in.)) diameter channel through which steam from the HL can vent and potentially reduce the primary-side pressure significantly. Because this instrument line is of the same diameter as the sample line and the drain line, but will be at a higher temperature, its weld connection to the RTD flange was analyzed in detail.

### 4.2.1 Hot Leg and Surge Line

The Type 316 stainless steel HL has a straight 0.86-meter (m) (34-in.) outside diameter (OD) with a 6.4-centimeter (cm) (2.5-in.) wall thickness that extends 2.64 m (8 ft. $7^{30}/_{32}$ in.) from the end of the reactor vessel (RV) nozzle (A 508 Class 2) to the end of the loop isolation valve, which is a massive 11,364-kilogram (kg) (25,000-pound (lb)) dry weight motor-operated gate valve with a projected horizontal length of 1.68 m (5 ft., 6 in.). At the other end of the loop isolation valve is a 1.2-m (47.5-in.) mean radius, 50 degrees reducing elbow (CF8M A351) whose inner diameter increases from 0.74 m (29 in.) to 0.79 m (31 in.) at the SG nozzle (SA 216 WCC) end over a projected horizontal length of 1.05 m (3 ft., 5⅜ in.). The RV and SG nozzles support the full weight of the HL and the loop isolation valve. The surge line intersects the HL at a distance of 2.19 m (7 ft., $2^{1}/_{32}$ in.) from the end of the RV nozzle. The 36-cm (14-in.) OD, 3.6-cm (1.4-in.) wall thickness surge line is a long, sinuous Type 316 stainless steel pipe whose center line coordinates were obtained from Reference 1. The HL and surge line are insulated with Type 304 stainless steel.

The RV support system permits the reactor to expand radially but resists translational and rotational movements. It was assumed that the reactor end of the RV nozzle was fixed against translations and rotations but was free to expand radially during a severe-accident transient. The HL in the model extended from the reactor end of the RV nozzle to the lower head of the SG (including the inlet nozzle) and the supports for the SG. The surge-line model extended from the junction with HL to the junction of the PZR nozzle and the PZR, which was assumed to be fixed against translations and rotations but to be free to expand radially during the severe-accident transient. Nine surge line supports are present: three flailing restraints, one variable-support spring hanger, one threaded-rod support, one constant-support hanger, one sway-strut assembly, and two hydraulic-snubber restraints. The model included all of the surge-line supports except the hydraulic snubbers, which are not expected to be active during a slow severe-accident transient.

In addition to pressure-induced stresses, significant thermal membrane and bending stresses are expected to occur in the HL and surge line because of external constraints. Therefore, failure can occur either by creep rupture or, if the stresses are not relaxed rapidly enough by creep, by tensile rupture.

### 4.2.2 Steam Generator Primary Manway

Each ZNPP SG contains two primary manways; the one that is in the inlet plenum was selected because it is hotter. This manway is on the lower head, in an area where, during a severe accident, the relatively cool recirculating steam flows down through the SGTs on its way to the HL and back to the RV. The manway consists of a 67.9-cm (26.73-in.) OD, 10.2-cm (4-in.) thick cover plate made of SA 533 Grade A Class I, a 52-cm (20.5-in.) OD, 13-mm (0.5-in.) thick insert made of SA 240 Type 304 stainless steel, and a 40.8-cm (16.06-in.) inside diameter (ID), 45.9-cm (18.06-in.) OD, 4.4-mm (0.17-in.) thick spiral-wound gasket made of Inconel with asbestos filler. These components are secured to the lower head by 16 4.8-cm (1.88-in.) diameter, 19-cm (7.5-in.) long threaded bolts made of SA 193 Grade B7 on a 58.4-cm (23-in.) diameter bolt circle. The opening diameter of the manway is 40.6 cm (16 in.). The bolts are tightened in a crisscross pattern by using three torque passes with an initial torque of 540±20 newton meters (N-m) (400±15 foot pounds (ft-lb)), an intermediate torque of 1,490±54 N-m (1,100±40 ft-lb), and a final torque of 2,170±80 N-m (1,600±60 ft-lb). The final nominal bolt stress is 207 megapascals (MPa) (30,000 pounds per square inch (psi)). During high-temperature exposure, the bolts will lose most of their prestress, after which the cover plate will lift off from the mating flange of the lower head. Depending on the gasket springback (which may be minimal at high temperature because of creep), the liftoff could lead to significant leakage of steam and reduction of primary pressure.

### 4.2.3 Resistance Temperature Detector

Three RTDs, 120 degrees apart, penetrate the HL and monitor the coolant temperature during normal operation. The 7-cm (2.75-in.) OD, 30-cm ($11^{13}/_{16}$-in.) long RTDs are made of forged A-182 F316 stainless steel and project 19.5-cm ($7^{11}/_{16}$-in.) into the interior of the HL. The RTD scoops are welded to the HL elbow by full-penetration welds with A308 filler material. Failure of the welds at high temperature could potentially blow the RTD scoop out of the HL and open a 7-cm (2.75-in.) diameter hole in it, leading to rapid depressurization of the primary side. Because of the postulated recirculating flow of the hot steam during a severe accident (assuming maintenance of the loop seal), the RTD at the top of the HL is the most vulnerable of the three that are present, because it is exposed to the hottest steam temperature.

### 4.2.4 Socket Weld Connection of Instrument Line to the RTD Flange

Failure of the socket weld that attaches the 25-mm (1-in.) diameter instrument line to the RTD flange could reduce the primary side pressure significantly. During a severe accident, hot steam flowing through the internal drilled channel of the RTD scoop, RTD flange, and then to the instrument line through the socket weld connection could heat the socket weld to high temperatures. The pressure forces acting on the instrument line could create shear stresses that are sufficiently high to cause creep failure of the socket weld and the possible expulsion of the instrument line, an event that could open up a 25-mm (1-in.) diameter channel through which steam could escape and depressurize the primary side, or at least reduce the system pressure significantly.

The dimensions of the socket weld of the ZNPP plant were not available. For the 25-mm (1-in.) ID and 34-mm (1.33-in.) OD instrument line, the minimum socket weld dimensions were obtained from Figure NB-4427-1 of the American Society of Mechanical Engineers (ASME) Boiler and Pressure Vessel Code (ASME Code), Section III (Ref. 2), which stipulates that the minimum dimension of the socket weld is 1.09 times the nominal pipe wall thickness, which, for the current case reduces to 4.5 mm (0.18 in.). In this analysis, the socket weld dimension of

5 mm (0.2 in.) was used as a reference, to analyze the effect of a larger weld size on the failure as part of the sensitivity analysis.

### 4.2.5 Power-Operated Relief Valve

Drawings of a typical PORV were obtained from a valve manufacturer. The PORV contains a 50-mm (2-in.) diameter plug that is connected by a stem to the actuator that drives the plug up and down inside the cage. During normal operation, a 45.7-cm (18-in.) long AISI 6150 low alloy steel spring (spring constant = 814 N/mm (4,700 pound-force (lbf)/in.) holds the plug pressed against the cage with a force of 43 kilonewton (kN) (9,760 lbf). The contact surfaces between the plug and the cage are both tapered, with slightly different (2.5-degree) taper angles. Hence, when the valve is closed, the plug makes a line contact with the cage. A solenoid valve controls the air pressure (maximum 0.7 MPa (105 psi)) across a diaphragm that drives the actuator. When activated, the air pressure is sufficient to overcome the closing force of the spring and opens the passage for the subcooled water to flow through. When closed, the diaphragm chamber is vented, and the spring forces the plug against the cage. The valve manufacturer has estimated the impact velocity to be 32 mm/second (s) (1.25 in./s). The plug material is Type 316 stainless steel with a Stellite overlay, and the cage material is ASME SA 564 (17-4 PH steel). The plug and cage are contained inside the valve body, which is sealed off at the top by a bonnet. The bonnet is secured to the valve body by a bolted joint.

The PZR PORV, which is subjected to many opening and closing cycles during a severe-accident transient, can fail by several complex mechanisms. The frequent discharge of subcooled water through the PORV during the initial phase of a severe accident can lead to cavitation/erosion damage of the PORV internals by flashing of water to steam and subsequent two-phase flow. Chattering, which is also a potential problem during this phase of the accident, can lead to high-cycle fatigue failure caused by repeated plug-to-cage impact. PORVs are susceptible to surface galling of the valve stem, mainly because of differential thermal growth during a severe-accident transient. The cage material of PORVs (17-4 PH steel, condition H1100) is heat treated and tempered at 593 degrees Celsius (C) (1,100 degrees Fahrenheit (F)). Therefore, if the temperature of the cage exceeds 593 degrees C (1,100 degrees F), the cage will lose all of the mechanical properties that were obtained from heat treating. The high temperature, combined with the loss of some of the mechanical properties, can increase the galling potential between the plug and cage. Should galling occur, the valve would not be operational. Thermal binding of the plug and the cage is also possible. The body-to-bonnet gasket joint is held by SA 193 (B7) bolts, which are rated in the ASME Code to permit their use to less than or equal to 427 degrees C (800 degrees F) and which are susceptible to loss of prestress (with consequent leakage) and creep rupture at higher temperatures. The PORV actuator diaphragm is made of buna-N rubber, which could be damaged at temperatures that exceed 93 degrees C (200 degrees F). Although the diaphragm stays relatively cool during normal operation, repeated cycling of the PORV during severe accidents could increase its temperature by heat conduction to greater than 93 degrees C (200 degrees F). The proper functioning of the diaphragm is necessary to open the valve but is not necessary for the PORV to go to the fail-safe position, which is closed. However, the spring that keeps the PORV closed under normal operation may lose strength and stiffness at high temperatures, and the steam pressure may overcome the spring closing force and make the PORV behave like a PSV.

Each of the above failure mechanisms is a complex problem in its own right, and the development of methods for predicting its failure would require analyses as well as extensive test programs. As a starting point, the problem of plug-to-cage impact was considered because it is amenable to front-end analysis (FEA), the results from which could be used to evaluate the

potential for fatigue damage of the plug or the cage contact areas. Because the impacts occur over very short time intervals, tensile properties are sufficient to carry out the stress analyses, and creep properties are not needed.

## 4.3 Thermal-Mechanical Analyses of Selected RCS Components

All of the thermal conduction and stress analyses were conducted with the commercially available finite-element program ABAQUS®. ABAQUS® is used widely in the nuclear and aerospace industry for conducting high-temperature nonlinear analyses and has been validated with a number of solutions for which analytical solutions are available. The thermal-hydraulic analysis results from the SCDAP/RELAP5 code were used as the starting point for all analyses under the current program. The thermal mechanical analyses were performed in two steps. First, a thermal transient analysis was conducted to obtain the temperature distribution throughout the model, based on the heat transfer analysis by the SCDAP/RELAP5 code. Second, the nodal-temperature data, together with the pressure and structural-support and boundary condition data, were entered into the structural-analysis model. The following sections present the analyses for the selected RCS components, other than HL and surge line. Detailed analyses of HL and surge-line failure will be described later in this chapter.

### 4.3.1 SG Primary Manway

Figure 4-1 shows the various parts (SG lower head, insert, cover plate, gasket, and bolts) of the structure that were analyzed.

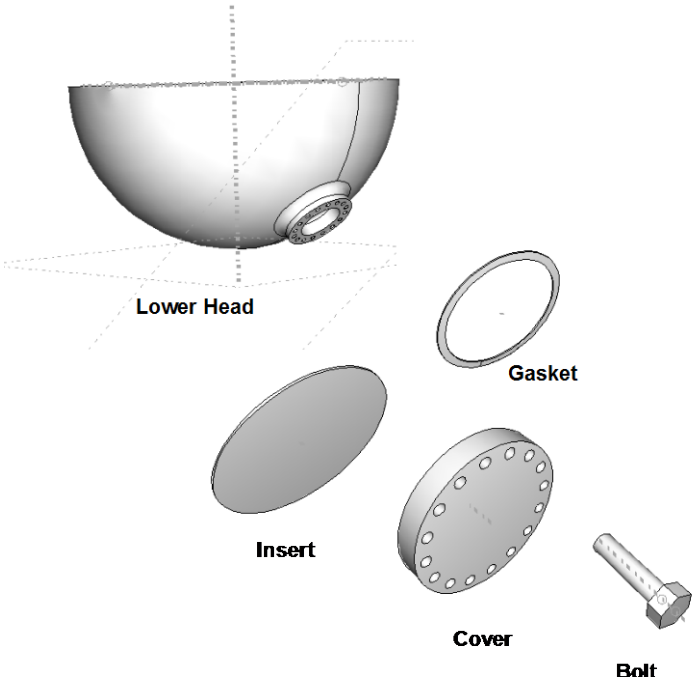


Figure 4-1 Parts for the ZNPP HL primary manway

The gasket was not included in the structural model, because high-temperature properties for it were not available. Because the stiffness of the gasket is small relative to the other parts, the stresses should not be affected significantly by its neglect. Once bolt preloads are relaxed by thermal creep, the area available for leakage will depend on the gasket springback, which is

expected to be small because of gasket creep. However, gasket creep data at high temperatures are not available.

Figure 4-2 shows the finite-element model (FEM) of the full assembly, which uses a total of 45,383 elements and 67,809 nodes. The manway assembly was structurally supported vertically at the top edge, which was allowed to deform radially in an unconstrained manner. A uniform and constant pressure of 16 MPa (2.35 kilopound per square inch [ksi]) was applied during the full transient.

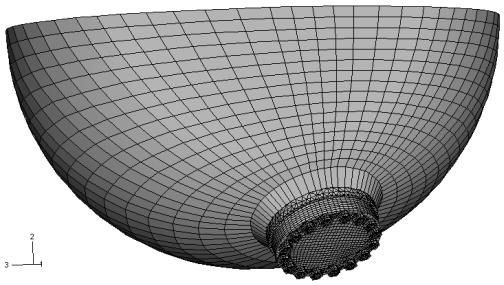

Figure 4-2 Finite-element model of manway assembly

The RELAP5 analysis did not report the temperature of the manway because the model did not include a cell at the location of the primary manway. The lower head region at the inlet plenum contained only three cells. The temperature of Cell 105 represented the hot inlet plenum wall and Cell 106 represented the mixed mean temperature of the inlet plenum wall (Figure 4-3a). Because the primary manway was at the bottom of the SGTs that contained the cooler steam of the return flow, the temperature history reported for Cell 106 should be closer to that of the manway than to the history reported for Cell 105. A more detailed computational fluid dynamics (CFD) calculation of the inlet plenum region has shown that the steam adjacent to the manway is even cooler than the mixed mean plenum steam temperature (Figure 4-3b). However, the heat transfer coefficients or the surface heat fluxes that correspond to the CFD calculations were not available. Using the surface heat flux history from RELAP5 on the ID surface of the lower head plenum wall and on the interior surface of the insert, and assuming zero resistance to heat flow across all the interfaces, a transient heat conduction analysis of the manway was performed. The analysis gave an OD temperature for the lower head of 885 degrees C away from the manway and 760 degrees C near the manway, both much higher than that calculated by RELAP5. Because of the uncertainties in the heat transfer coefficients or surface heat fluxes and thermal resistances across various interfaces in the manway, results from transient thermal conduction analysis were not used in the stress analysis. Instead, a transient thermal conduction analysis was carried out, using the transient temperature history at the outside surface of the plenum wall as calculated by RELAP5 (Figure 4-3a) as boundary conditions, and considered it the reference case. It was decided to address the temperature effects on stress and deformation of the manway components by temperature uncertainty analyses.

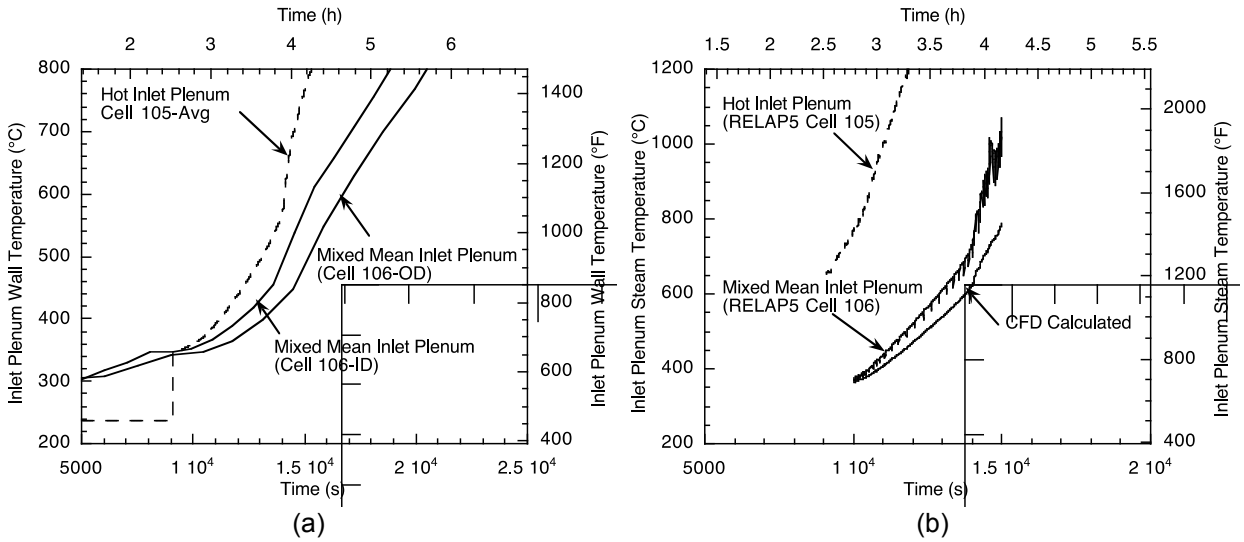


**Figure 4-3 Time-temperature histories of inlet plenum**

***(a) time-temperature histories of the inlet plenum wall for RELAP5 Cells 105 and 106***

***(b) RELAP5 and CFD-calculated steam temperatures near manway in inlet plenum***

A critical input in the structural analysis of the manway is the initial bolt stress or prestress. Westinghouse (W) specifications for the ZNPP plant call for the torque on the SG primary manway bolts during the final pass to be 2,170±80 N-m (1,600±60 ft-lb) and their design manual assumes a nominal value for the initial bolt stress as 207 MPa (30,000 psi). The relationship between the applied torque and the resultant tensile stress in the bolts is highly complex. J. Shigley[4] has reported the following simple relationship between the torque and the bolt preload:

$$T = KFd \tag{4.1}$$

where T is torque, K is the torque coefficient, F is the bolt preload, and d is the fastener diameter. For typical values of friction coefficients (μ = 0.15), K = 0.2, which is found to be relatively insensitive to changes in the bolt diameter and the thread characteristics. For the ZNPP manway bolts, application of Equation 4.1 gives F = 225 kN (51,200 lbf), which corresponds to a bolt stress of 130 MPa (18,540 psi). A bolt prestress of 207 MPa (30,000 psi) was used as recommended in the W manual.

The structural analysis was carried out in three steps:

(1) Apply bolt preload at room temperature (elastic analysis).

(2) Increase temperature of manway assembly uniformly from room temperature to 350 degrees C and apply coolant pressure (elastic analysis).

(3) Apply severe-accident-transient temperature history (elastic-creep analysis).

The bolt preloads were applied simultaneously to all 16 bolts with the bolt preload feature of ABAQUS. The bolts were stressed to a nominal tensile stress of 207 MPa (30 ksi).

[4] See J. Shigley, "Mechanical Engineering Design," McGraw Hill, New York, NY, 1963.

### *Elastic-Creep Analysis*

When creep deformation is taken into account, the bolt loads are relaxed rapidly, as shown in Figure 4-4a. Note that the bolt axial loads reach a lower plateau at 14,346 s, which corresponds to a temperature of 450 degrees C. A residual axial load is maintained in all of the bolts to balance the force because of the pressure loading on the insert. The exact relaxation history is dependent on the creep properties (both primary and secondary creep) of the material, which, as mentioned earlier, were not available for this material at the time the analysis was carried out. Figure 4-4b shows the variation of the maximum and minimum principal stresses, as well as the section average stresses across Bolt 1, indicating that the bolts are subjected to significant bending. The stresses are below yield at the relevant temperatures.

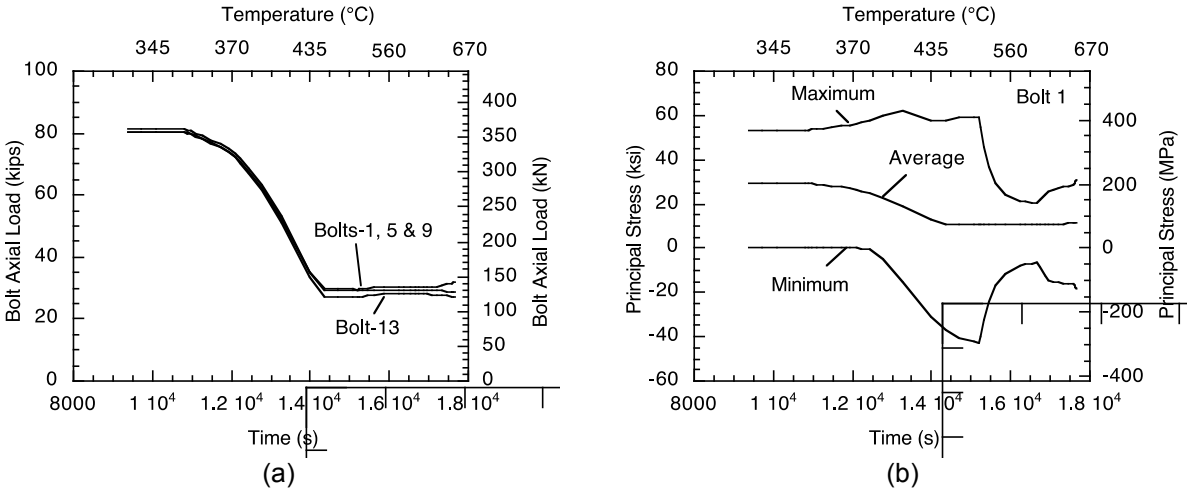


**Figure 4-4 Elastic-creep analysis of manway bolts**

***(a) relaxation of preloads with time and temperature because of creep in Bolts 1, 5, 9, and 13***

***(b) changes in maximum and minimum principal stresses and average stress in Bolt 1 with time and temperature***

Figure 4-5a shows the distribution of the maximum principal creep strains in Bolt 1 at 650 degrees C (1,202 degrees F) at 17,650 s; comparison with Figure 4-5b suggests a rapidly accumulating creep strain with time and temperature. A plot of the variation of maximum creep strain with time in Figure 4-5b confirms that, by the time the temperature reaches 670 degrees C (1,238 degrees F) at 18,000 s, the maximum creep strain reaches 35 percent. If failure at 20-percent maximum creep strain is postulated, the failure time for the bolt is 17,770 s (Tests conducted subsequently by ANL have shown that this material has a tensile total elongation of 80 percent and creep ductility of 60–90 percent at 650 degrees C (1,202 degrees F)). However, the failure time does not appear to be strongly dependent on creep ductility.

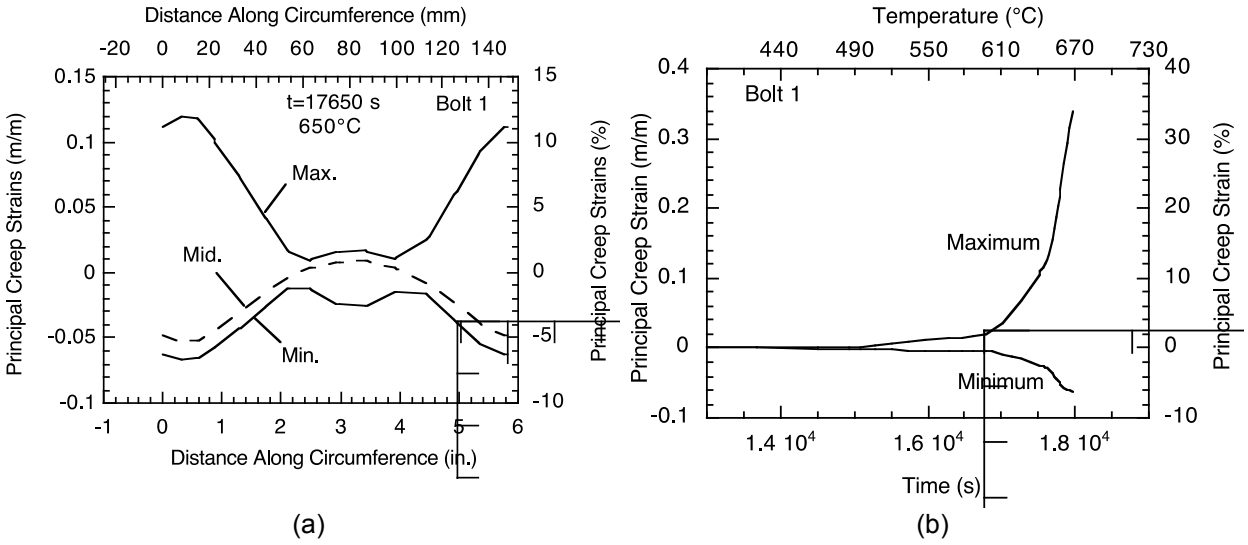


**Figure 4-5 Principal creep strain**

***(a) distribution of principal creep strain around circumference of bolt 1 at 650 degrees C***

***(b) variation of principal creep strains in bolt 1 with time and temperature***

An important objective of the present analysis is to quantify the lifting of the cover plate from the flange, thus creating a leakage flow path for the steam during the accident. Figure 4-6a shows the variation of the maximum contact pressure around the outer periphery of the insert with temperature. It is evident that the contact pressures are reduced to zero by 450 degrees C (14,346 s). Beyond 450 degrees C, the contact between the insert/cover plate and the lower head flange is lost all around, the cover plate begins to lift off from the lower head flange, and leakage of steam becomes possible. Figure 4-6b shows the variation of the total opening area with time and temperature because of the cover plate lifting. It is evident that, even when 8 of the 16 bolts are preloaded to 85 percent of the design preload, the opening characteristics are the same as in the reference case. An area of 19 square centimeters ($cm^2$) (3 square inches [$in.^2$]), which is approximately equivalent to a 50-mm (2-in.) diameter hole, is created by 600 degrees C (1,112 degrees F) (16,726 s). The actual flow area will be less than 19 $cm^2$ (3 $in.^2$) because of gasket spring-back, which should be minimal at these temperatures because of thermal creep. However, gasket creep data at high temperature are not currently available.

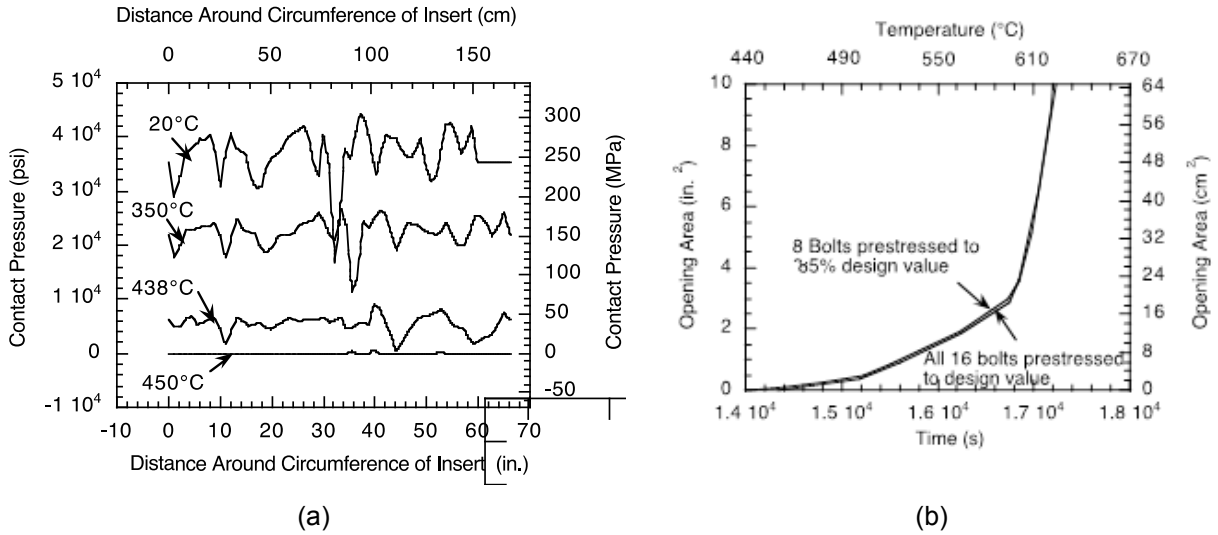


(a) (b)

**Figure 4-6 Crack mouth pressure and opening area variations**
***(a) Distribution of contact pressure between outer periphery of insert and lower head flange as function of temperature and position***
***(b) Variation of opening area with time and temperature***

To determine the effect of temperature on the opening area, an analysis was conducted with the temperature history of Cell 105 (average) (Figure 4-3a), which is considerably hotter than the reference case (Cell 106, OD). Figure 4-7a shows the variations of the opening area as a function of time and Figure 4-7b shows the same as a function of temperature for the two temperature loadings. Although the opening area histories differ widely when viewed as a function of time, they are much closer when viewed as a function of temperature, indicating that temperature is the predominant driving force for this problem.

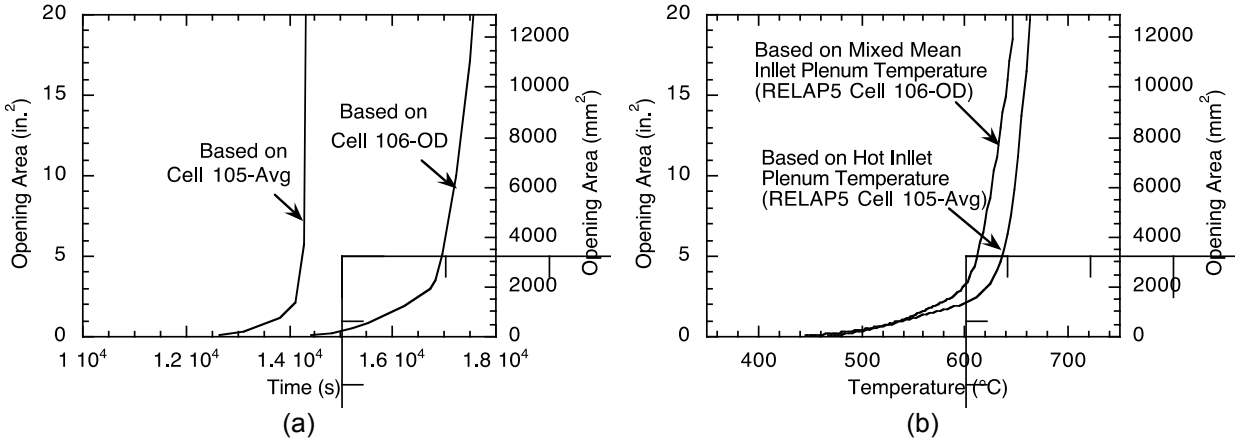


(a) (b)

**Figure 4-7 Variation of opening area with (a) time and (b) temperature for two temperature histories**

Another situation where temperature variation may have an important effect on the opening area arises after lift-off of the cover plate from the lower head flange when leakage of hot steam through the opening area will cause local heating of the bolts. The coupled structural/thermal-hydraulic analysis of this problem is complex and was not attempted.

Instead, after lift-off of the cover plate, the temperature of the bolts was manually increased to that of the inlet plenum mixed mean steam temperature (Figure 4-3b), which is 200–500 degrees C (392–932 degrees F) hotter than the RELAP5 OD temperature for Cell 106. This should be considered as an upper-bound effect and the result, plotted in Figure 4-8, indicates that a 19-$cm^2$ (3-$in.^2$) opening area could be created in 15,200 s instead of the reference 16,726 s, a reduction in time of 1,500 s. In reality, the bolt temperatures will rise much less rapidly, particularly when the area of the opening is small. If a few hundred seconds in time can make a difference in the outcome of the accident, leakage must be considered in a more rigorous manner.

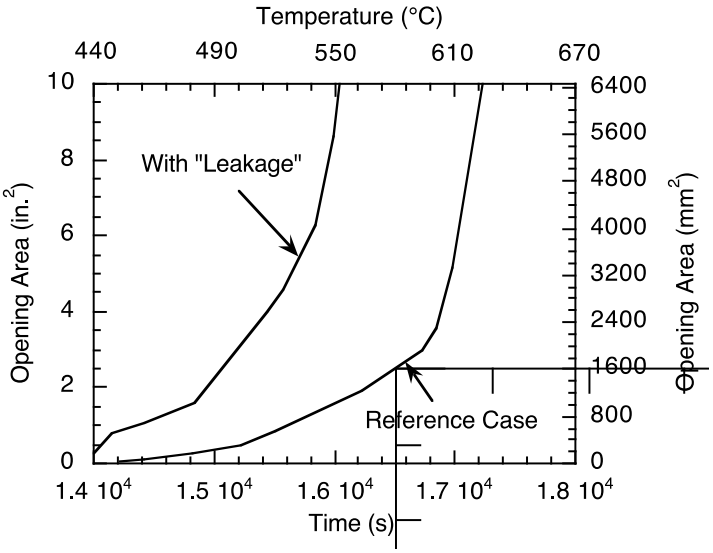


Figure 4-8 Effect of steam leakage on opening area

### *Discussion of Results*

The results presented here are based on creep curves for SA 193-B7 bolts that were estimated from available creep data for AISI 4140 steel. Appendix A presents more recent data on SA 193-B7 bolt material, based on tests conducted at ANL. The test data indicated that the creep equations used in this analysis overestimated the creep strains observed in the tests by a factor of 5-10, as shown in Figures 4-9a and 4-9b. Therefore, the calculated creep results for the bolts presented here overestimate the actual creep strains significantly, which would imply that the stresses in the bolts should relax significantly less rapidly during the severe accident than calculated here.

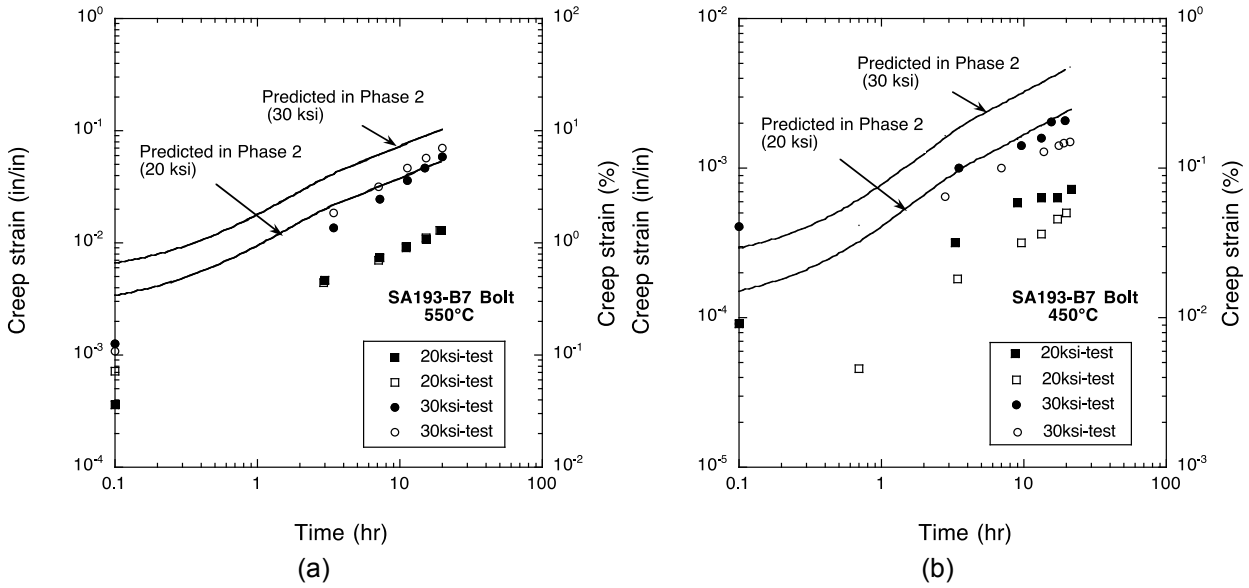


**Figure 4-9 Predicted vs. observed creep curves of SA 193-B7 for duplicate tests at 20 and 30 ksi at (a) 550 degrees C and (b) 450 degrees C**

### 4.3.2 Resistance Temperature Detector Welds

Three RTD scoops are located 120 degrees apart in the elbow of the HL; they are used to monitor the primary-side temperature during normal operation. The analysis was done for the one at the top, which is the hottest of the three RTDs because of the counter flow coolant circuit postulated to occur during a severe-accident transient. Because creep failure of the welds that connect the RTD to the HL is of primary concern, it was assumed that the RTD was attached to a straight section of the HL, ignoring the curvature of the elbow.

The geometry information for the SG RTD scoop was assembled from the drawings obtained from ZNPP. The RTD is attached to the HL by full–penetration welds, as shown in Figure 4-10. Failure of the A 308 welds could potentially lead to the expulsion of the RTD scoop and the creation of a 7-cm (2.75-in.) diameter hole in the HL.

Figure 4-11 shows the finite element meshes used to analyze a 30-cm (12-in.) long section of the HL, the RTD, and the welds. A total of 5,144 elements were used to model the HL; 1,110 elements to model the ID weld; 1,377 elements to model the OD weld; and 1,488 elements to model the RTD. The total number of nodes was 6,329. The FEM included the drilled channel inside the RTD.

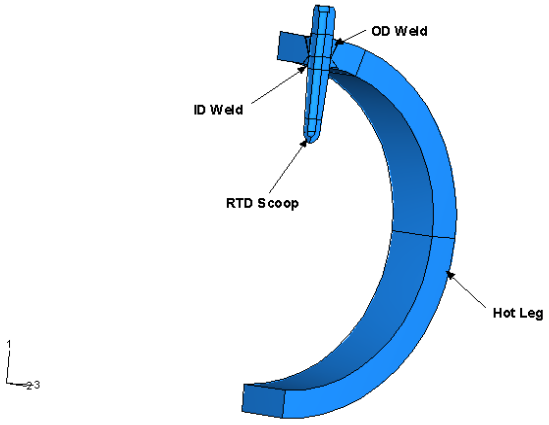


Figure 4-10 RTD scoop and welds connecting it to HL

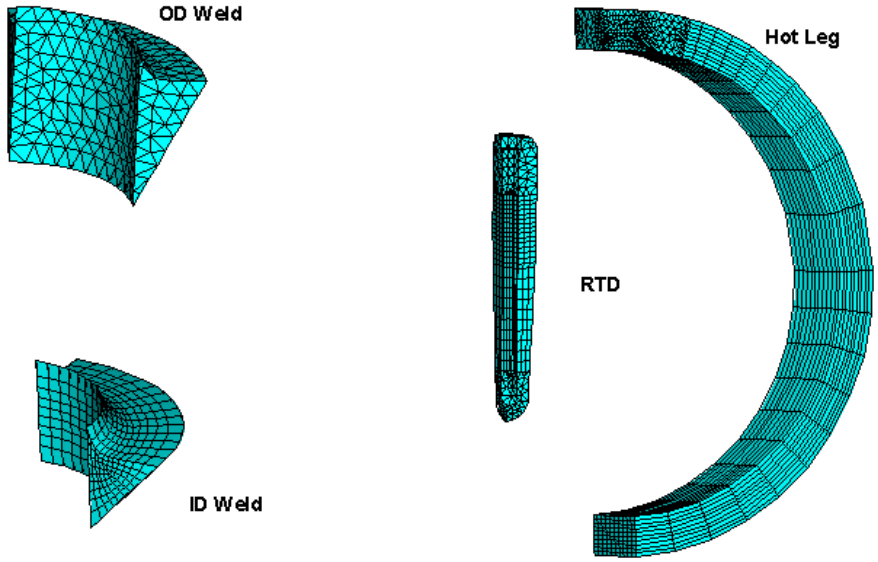


Figure 4-11 Meshes used to analyze RTD scoop, welds, and HL

The heat transfer coefficients for the top half (hot side) and bottom half (cool side) of the HL and the respective steam temperatures were obtained from the RELAP5 analysis. Figure 4-12 shows the steam temperatures as functions of time. The hot-side heat transfer coefficient and steam temperature were also applied to the outside surface of the portion of the RTD that projected into the HL. The heat transfer coefficients of the RTD should most likely be higher because the RTD is situated transverse to the flow direction. Heat should also flow into the RTD from the interior surface of the annular area through which the steam flows into the instrument line. However, because of the uncertainties in the heat transfer coefficients, in the reference case, heat transfer coefficients were applied only to the outside surface of the RTD.

The potentially higher heat fluxes on the RTD outside surface, as well as heat fluxes on its internal surface, were treated as part of the sensitivity analyses.

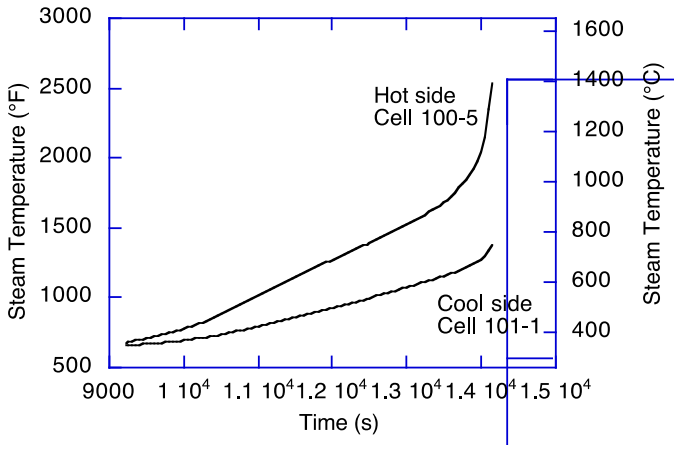


**Figure 4-12 Steam temperature histories for the hot side and the cool side of the RTD**

A constant pressure of 16 MPa (2.35 ksi) was applied on all the pressure boundaries. No axial constraint was applied on the HL. Although the HL has significant axial stress, the behavior of the welds (which are of primary focus here) should be relatively insensitive to this stress. The stress analysis was conducted in two steps. First, the pressure loading was applied at 343 degrees C (650 degrees F); then, the severe-accident transient temperatures computed by the thermal conduction analysis were applied and the stress analysis was conducted by elastic-creep analysis.

Figure 4-13 shows the temperature distribution in the RTD, HL, and the welds at time t = 14,400 s. Note that the lower half of the HL is significantly cooler than the upper half, as expected. Also, because of its smaller mass, the RTD heats up much more rapidly than the HL. The maximum temperature in the RTD is 1,254 degrees C (2,289 degrees F). The RTD temperature approaches that of the HL at the junction with the HL. Figure 4-14 shows the average temperatures in the ID and OD welds at their junctions with the RTD. The average ID weld temperature is 50–80 degrees C (122–176 degrees F) hotter than the average OD weld temperature.

Figure 4-15 plots the distribution of von Mises effective stress at the ID weld/RTD interface at time t = 14,148 s; Figure 4-16 plots the same for the OD weld/RTD interface. Figure 4-17a plots the variations of the average von Mises effective stresses at these interfaces with time. The time at the maximum and minimum points in this figure coincide with the time at which there is a step increase in temperature ramp rate (see Figure 4-3a). Although, initially, the average stress is higher at the ID weld interface than at the OD weld interface, because of the higher temperature at the ID than at the OD, the average stress at the ID weld interface is reduced and that in the OD weld interface is increased with time. Creep effects begin to dominate and stresses are relaxed rapidly at 14,000 s, when the average temperature reaches 800 and 880 degrees C in the OD and ID weld interfaces, respectively. Some localized high-stress areas are present that would undergo plastic yielding and accumulate plastic strain (i.e., high strain rate creep), which the current analysis ignores. However, plastic yielding effects were considered as part of the sensitivity analysis.

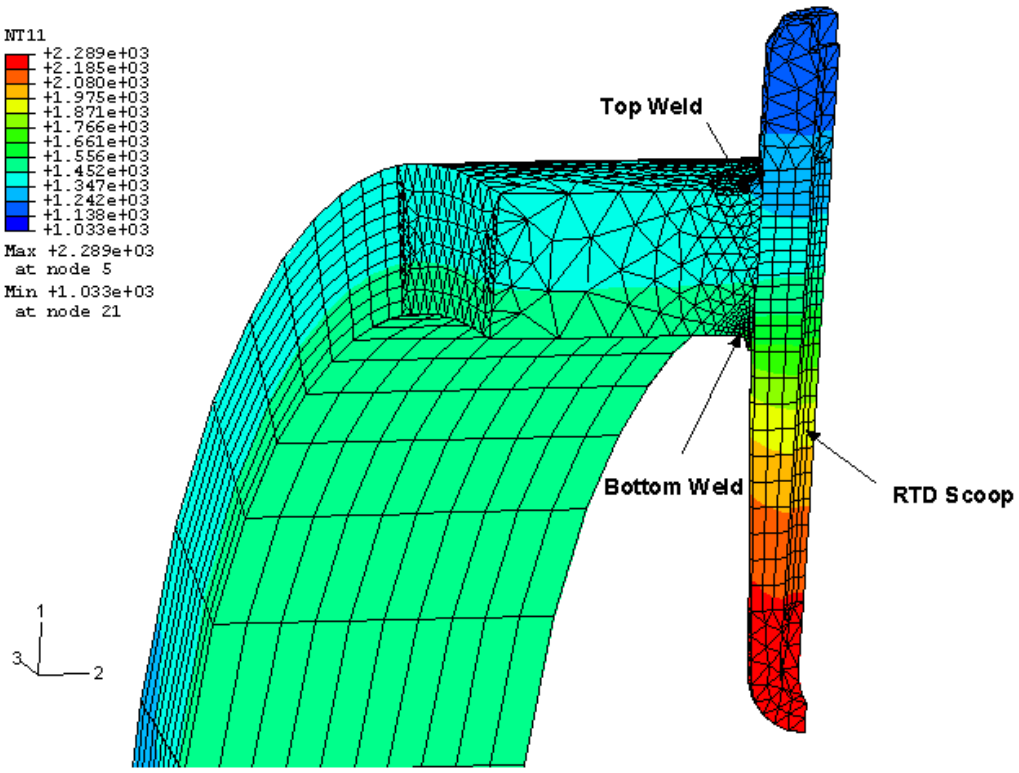


Figure 4-13 Closeup view of temperature (in °F) in HL RTD scoop at 14,400 s
***To convert from degrees F to degrees C, subtract 32 and divide by 1.8.***

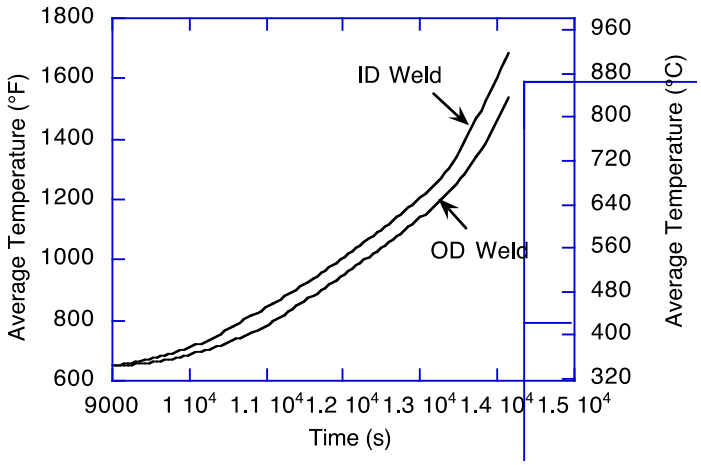


Figure 4-14 Variation of average temperature in ID and OD welds with time

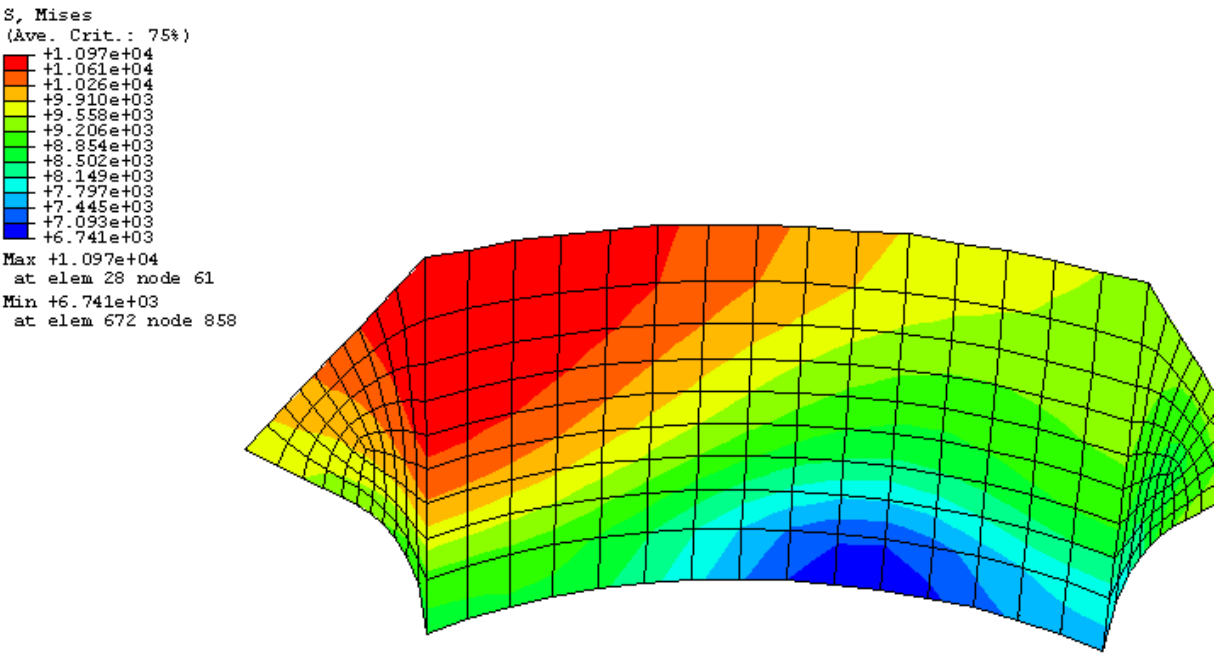


**Figure 4-15 Von Mises effective stress (in psi) distribution at ID weld RTD interface at 14,148 s**
***Note 1,000 psi = 6.895 MPa.***

Figure 4-17b plots the time evolution of the average effective creep strain in the ID and OD weld interfaces. Although the average stress in the ID weld interface is lower than in the OD weld interface, because of its higher temperature, the average creep strain in the ID weld is close to (actually slightly higher than) that in the OD weld interface. An average equivalent creep strain of 20 percent is reached in 13,890 and 14,000 s in the ID weld/RTD and OD weld/RTD interfaces, respectively.

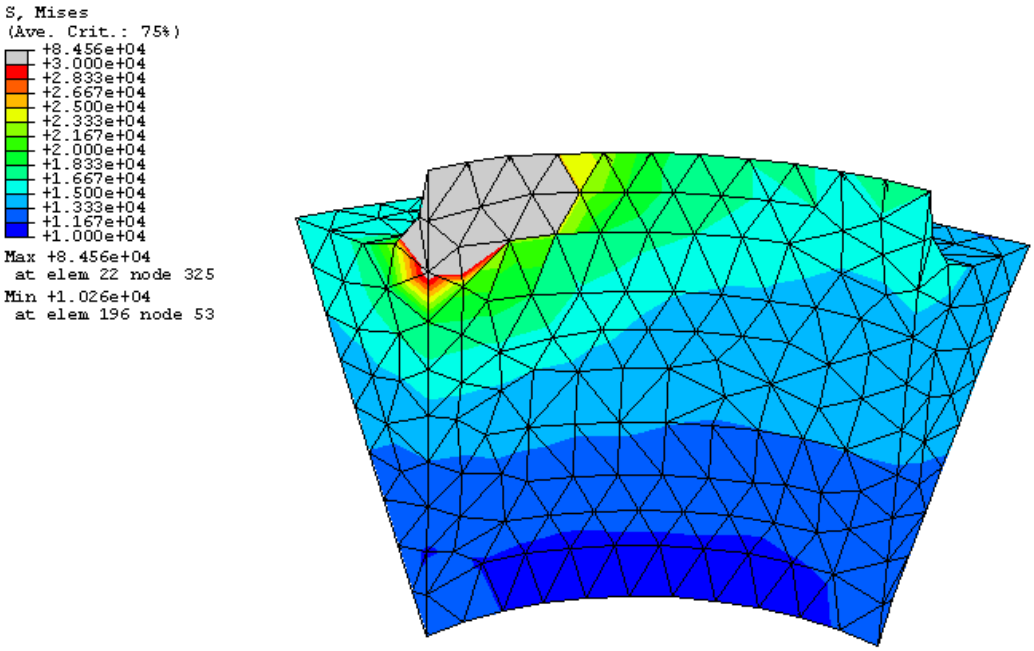


**Figure 4-16 Von Mises effective stress (in psi) distribution at OD weld RTD interface at 14,148 s**
***Note 1,000 psi = 6.895 MPa.***

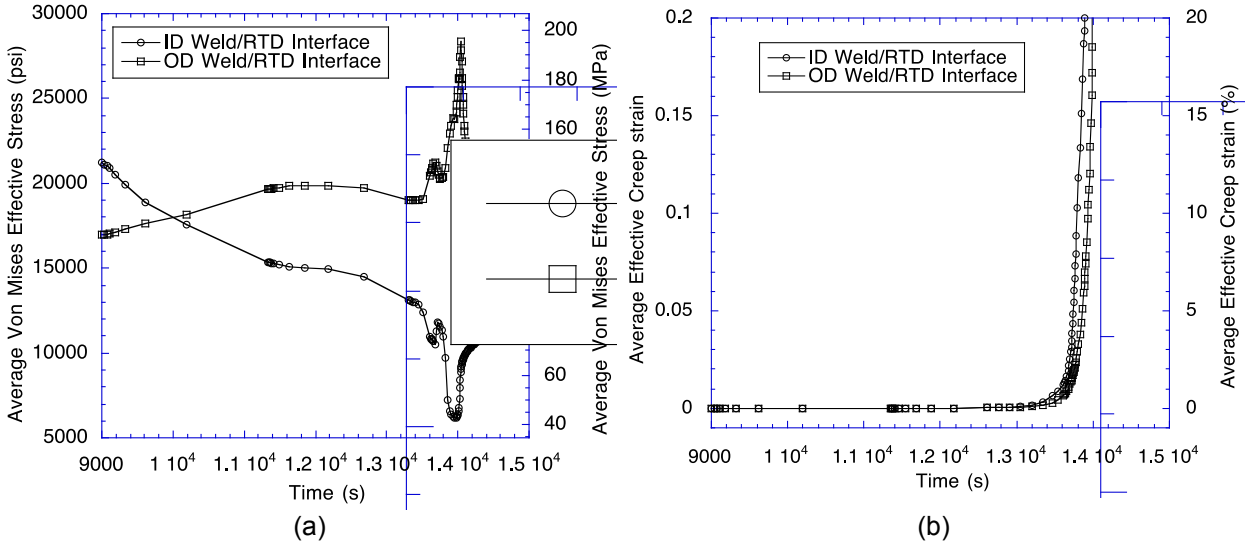


**Figure 4-17 Time evolution of (a) average von Mises effective stress and (b) average effective creep strain at interfaces of ID and OD welds with RTD**

***Results from Sensitivity Analyses***

Sensitivity analyses addressed the uncertainty in the current analysis arising from uncertainties in the temperatures, creep rates of the weld material, and possible creep-plasticity-interaction effects.

Sensitivity analyses showed that, when the outside heat transfer coefficients on the RTD are increased by a factor of 2 from the reference values, still ignoring the internal surface heating on the RTD, an average equivalent creep strain of 20 percent is reached in, respectively, 13,706 and 13,725 s in the ID weld/RTD interface and OD weld/RTD interface, a reduction of 184 and 275 s, respectively, from the reference times to reach 20-percent creep strain. If the reference heat transfer coefficients are applied equally to both the outside and inside surfaces of the RTD, an average equivalent creep strain of 20 percent is reached in 13,790 and 13,890 s in the ID weld/RTD interface and OD weld/RTD interface, a reduction of 100 and 110 s, respectively, from the reference times. Creep rate has a significant effect on the failure time. A factor of 10 increase in creep rate reduces the time to accumulate 20-percent creep strain by 180 s in the ID weld interface and 90 s in the OD weld interface, when compared with the reference times.

Inclusion of both creep and plasticity effects in the analysis showed that the time to accumulate 20-percent creep strain is increased by 176 s (tr =14,066 s) in the ID weld/RTD interface and 104 s (tr =14,104 s) in the OD weld/RTD interface, when compared with the reference case. The times to accumulate 20-percent total inelastic strain (plastic plus creep) in the two weld interfaces are virtually the same as the times to accumulate 20-percent creep strain. If a 2-percent average effective plastic strain failure criterion is adopted for the welds, the failure times are 14,123 s and 13,930 s for the ID and OD weld interfaces, which are, respectively, 57 s greater than and 74 s less than the corresponding times to accumulate 20-percent effective creep strains. Thus, the inclusion of plasticity effects does not change the estimates of the failure times significantly.

### 4.3.3 Socket Weld that Connects Instrument Line to RTD Flange

The possible failure of the socket weld that attaches the 25-mm (1-in.) diameter instrument line to the RTD flange is considered. During a severe accident, pressure forces could create sufficiently high stresses to cause creep failure of the weld and the possible expulsion of the instrument line from the RTD flange. The resultant opening of a 25-mm (1-in.) diameter channel could potentially reduce the primary-side pressure significantly.

Figure 4-18 shows a simplified axisymmetric model for the instrument line connection to the RTD flange. There is no direct tie connection between the RTD flange and the instrument line, although contact elements were used to prevent penetration of the instrument line into the RTD flange. Restraint of the instrument line to vertical movement is provided by the weld, which is tied to both the RTD flange and the instrument line. The lower end of the RTD flange is supported in the vertical direction.

A constant internal pressure of 16 MPa (2.35 ksi) was applied to all of the pressure-retaining surfaces. The axial component of the internal pressure loading on the instrument line was applied as an axial pressure loading at the top end of the instrument line.

Internal heating of the RTD increases the temperature of the RTD at the top, near the connection with the instrument line. Therefore, a uniform temperature field was applied to the entire model (Figure 4-19).

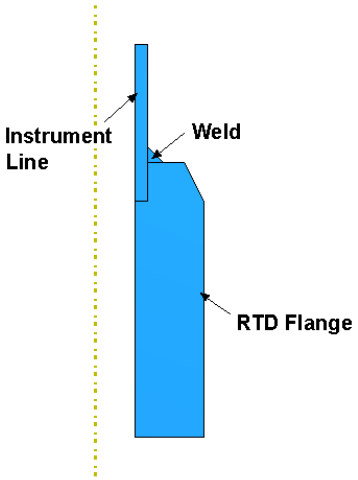


Figure 4-18 Simplified axisymmetric model for connection of instrument-line-to-RTD-flange weld

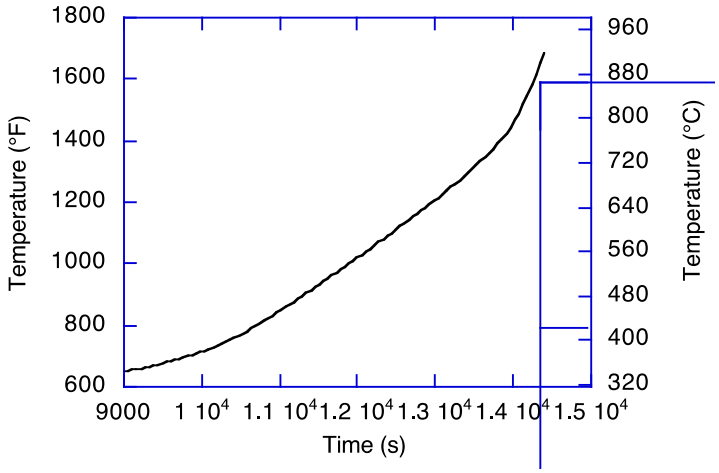


Figure 4-19 Temperature loading applied as uniform temperature to model of connection of instrument-line-to-RTD flange weld

A combined creep-plasticity analysis was conducted. Figures 4-20a and 4-20b plot the time evolution of the average von Mises effective stress and the effective creep strains in the weld interfaces with the instrument line and the RTD flange. Although, initially, (at low temperatures) the average stress at the weld/RTD flange interface is lower than that at the weld/instrument line interface, the two stresses tend to converge with time (at high temperatures). Therefore, creep strain was accumulated at both interfaces at the same rate. The average effective creep strain at the interfaces reaches 20 percent at time t = 14,230 s, which is about 440 s later than the failure of the RTD/HL ID weld, discussed in the previous section.

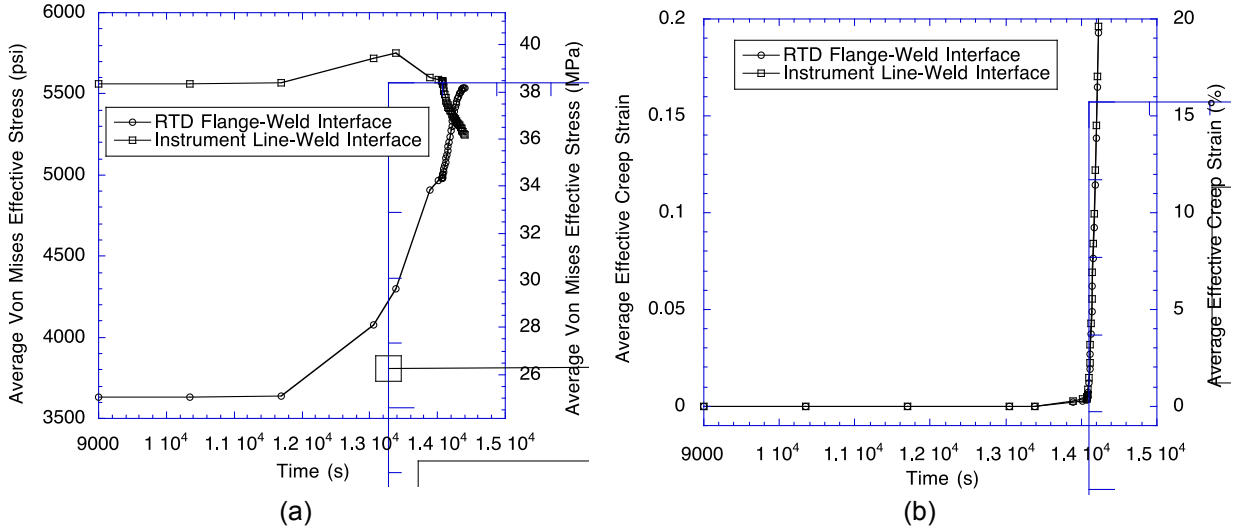


**Figure 4-20 Time evolution of (a) average von Mises effective stress and (b) average effective creep strain at interfaces of weld with instrument line and RTD**

Much larger creep strains than those in the weld are predicted to occur in the instrument line (assumed to be made of stainless steel) close to the weld, as shown in Figure 4-21. This is not surprising because the pressure-induced membrane stress in the instrument line is about 65 MPa (9.5 ksi), which is larger than the maximum stress in the weld. Figure 4-22 shows that the average effective creep strain in the instrument line away from the weld reaches 20 percent at 14,150 s, which is about 80 s before the failure time of the instrument line/RTD flange weld.

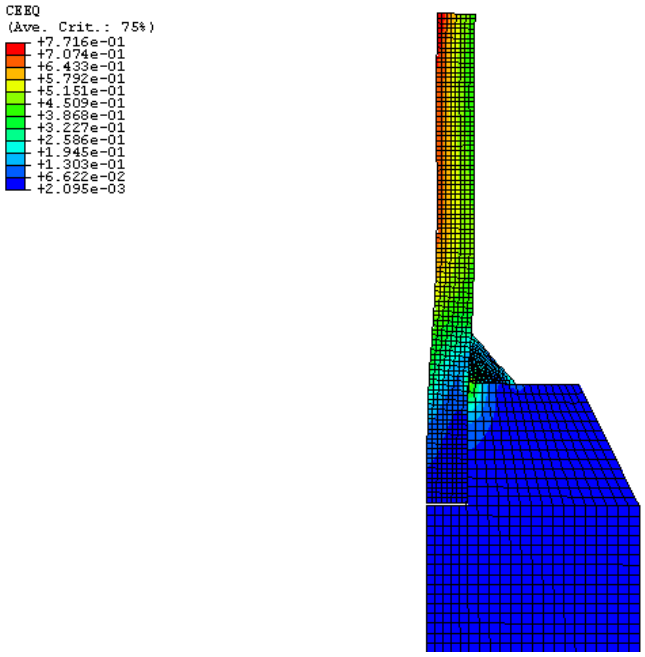


**Figure 4-21 Effective creep strain distribution in instrument line at time t=14,230 s**

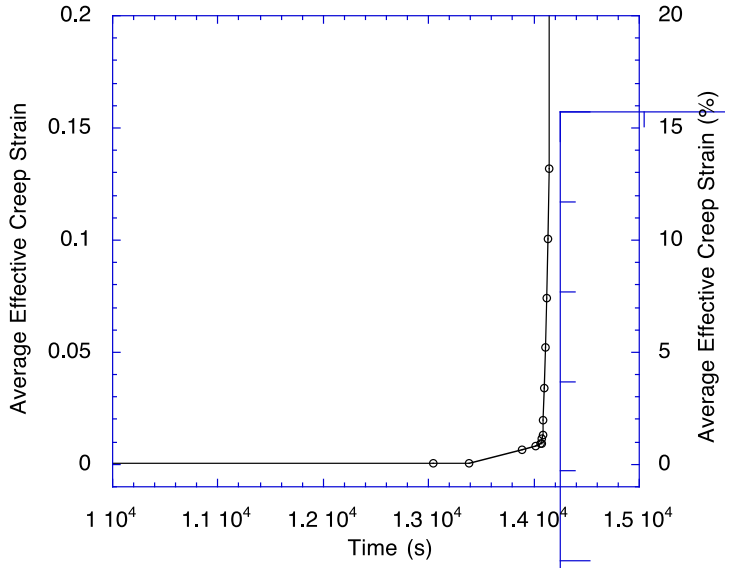


**Figure 4-22 Time evolution of average effective creep strain in instrument line away from welds**

Sensitivity analysis showed that the average stresses are reduced significantly by doubling the weld dimensions. However, in contrast to the reference case, the average stress in the weld/RTD interface remains less than that in the weld/instrument line at all times. Therefore, the creep strain accumulates faster in the weld/instrument line interface than in the weld/RTD flange interface. The time to accumulate an average creep strain of 20 percent in the weld/instrument line interface is 14,330 s, which represents a 100-s delay in failure time, compared to the reference case.

Increasing the creep rate by a factor of 10 compared to the reference case causes the stresses at the weld/RTD flange interface, which are initially lower than those at the weld/instrument line interface, to increase more rapidly than the stresses in the reference case. With time (at high temperatures), these stresses converge with those at the weld/instrument line interface. The average effective creep strain at the interfaces reaches 20 percent at time t = 14,110 s, which is about 120 s earlier than the reference case. The instrument line itself fails at 14,090 s, which is about 20 s before the failure time of the weld.

### 4.3.4 PORV Plug-to-Seat Impact Analysis

The PZR PORV, which is subjected to many opening and closing cycles during a severe-accident transient, can fail by several complex mechanisms. The frequent discharge of subcooled water through the PORV during the initial phase of a severe accident can lead to cavitation and erosion damage of the PORV internals by flashing of water to steam and subsequent two-phase flow. Chattering, which is also a potential problem during this phase of the accident, can lead to high-cycle fatigue failure caused by repeated plug-to-cage impact. PORVs are susceptible to surface galling of the valve stem, mainly because of differential thermal growth during a severe-accident transient. The cage material of PORVs (17-4 PH steel, condition H1100) is heat treated and tempered at 593 degrees C (1,100 degrees F). Therefore, if the temperature of the cage exceeds 593 degrees C (1,100 degrees F), the cage will lose all of the mechanical properties that were obtained from heat treating. The high temperature, combined with the loss of some of the mechanical properties, can increase the galling potential

between the plug and cage. Should galling occur, the valve would not be operational. Thermal binding of the plug and the cage is also possible. The body-to-bonnet gasket joint is held by SA 193 (B7) bolts, which are rated in the ASME Code to permit their use to less than or equal to 427 degrees C (800 degrees F) and which are susceptible to loss of prestress (with consequent leakage) and creep rupture at higher temperatures. The PORV actuator diaphragm is made of buna-N rubber, which could be damaged at temperatures that exceed 93 degrees C (200 degrees F). Although the diaphragm stays relatively cool during normal operation, repeated cycling of the PORV during severe accidents could increase its temperature by heat conduction to greater than 93 degrees C (200 degrees F). The proper functioning of the diaphragm is necessary to open the valve but is not necessary for the PORV to go to the fail-safe position, which is closed. However, the spring that keeps the PORV closed under normal operation may lose strength and stiffness at high temperatures, and the steam pressure may overcome the spring closing force and make the PORV behave like a PSV.

Each of the above failure mechanisms is a complex problem in its own right, and the development of methods for predicting its failure would require analyses as well as extensive test programs. As a starting point, the problem of plug-to-cage impact was considered because it is amenable to FEA, the results from which could be used to evaluate the potential for fatigue damage of the plug or the cage contact areas. Because the impacts occur over very short time intervals, tensile properties are sufficient to carry out the stress analyses, and creep properties are not needed.

A literature search carried out on impact wear models and mechanisms collected the following recent publications:

- R.W. Fricke and C. Allen, “Repetitive impact wear of steels,” Wear, Vol. 162–164, pp. 837–847, 1993

- Y. Yang, H. Fang, Y. Zheng, Z. Wang, and Z. Jiang, “The failure models induced by white layers during impact wear,” Wear, Vol. 185, pp. 17–22, 1995

- A.A. Voevodin, R. Bantle, A. Matthews, “Dynamic impact wear of TiCxNy and Ti–DLC composite coatings,” Wear, Vol. 185, pp. 151–157, 1995

- B. Zhang, Y. Liu, W. Shen, Y. Wang, X. Tang, and X. Wang, “A study on the behavior of adiabatic shear bands in impact wear,” Wear, Vol. 198, pp. 287–292, 1996

- B. Zhang, W. Shen, Y. Liu, X. Tang, and Y. Wang, “Microstructures of surface white layer and internal white adiabatic shear band,” Wear, Vol. 211, pp. 164–168, 1997

- B. Zhang, W. Shen, and Y. Liu, “Adiabatic shear bands in impact wear,” J. Mater. Sci. Lett., Vol. 17, pp. 765–767, 1998

- G.Sheng, W. Hua, and J. Zhang, “Head-disk impact stresses in dynamic loading process and the extrapolation of parameters for sliding rounding and interface durability,” J. Information Storage and Processing Systems, Vol. 3, pp. 203–206, 2001

Most of the above publications deal with very high-speed, near-normal repetitive impact, where adiabatic shear bands form in steels at room temperature and, hence, are not directly relevant to the impact wear of PORVs during severe accidents. Only the first publication is somewhat

relevant. It reports a study to determine the material, microstructural, design, and operating parameters of importance in minimizing the impact wear of valves operating in hydro-powered stopping mining equipment in South Africa. Tests were conducted to simulate the repetitive impact wear experienced by poppet valves. Wear damage occurred at the point of contact between the reciprocating valves and their seats. The tests were conducted with line-contact (which is also characteristic of PORV) specimens on various heat-treated alloys and stainless steels at frequencies between 5 and 50 hertz (Hz), impact velocities from 4 to 10 m/s, and impact energies from 2 to 5 joule (J). The line contact during the tests was achieved by using a flat-ended 8-mm diameter cylindrical striker repetitively striking a conical seat (made of the same material as the striker) with a 30-degree taper. All of the tests were conducted in a room-temperature water environment. The wear rates followed an empirical power law for tests carried out on AISI 431 steel:

$$W = KNEn \tag{4.2}$$

where W = wear loss, N = number of impacts, E = impact energy, and K and n are empirical constants.

Under lubricated conditions, two wear mechanisms were observed—pitting and surface traction. Surface traction, which is a result of partial slip (i.e., slip occurs at the exit edge but not at the leading edge), was caused by metal-to-metal adhesion and produced most of the wear.

Initially, during impact testing with line contact, greater deformation occurred in the striker than in the seat. With each successive impact, the contact stresses were reduced. The greatest amount of deformation occurred during the first impact, and, in the absence of wear, the contact stresses were reduced with each successive impact until a steady state was reached when the material could support the impact load. An incubation period was observed preceding wear loss, a finding that indicated that wear proceeds only after surface material has been strained to capacity and stresses cycled a sufficient number of times for crack initiation and propagation to occur under the predominantly compressive stress conditions. Debris in the form of flakes or thin platelets was produced in this way. Following the incubation period, the wear rate was high and decreased toward zero as the contact area increased and the impact stress decreased. It was concluded that the rate of wear was a function of impact energy, material properties, contact areas, and wear mechanisms.

Although of much interest, the results from this study are not directly applicable to the impact wear of PORV during severe accidents for the following reasons:

The impact velocity of the plug in the PORV during closure is on the order of 0.5 cm/s (1.25 in./s), which is much smaller than the impact velocities used in the tests (4–10 m/s).

Tests were conducted at room temperature in a water environment, whereas the PORV will operate at high temperature, first in subcooled water and then in a superheated steam environment during severe accidents.

The plug in the PORV is Type 316 stainless steel with a hard Stellite overlay and the cage is heat-treated and tempered steel. The tests were conducted with the striker and the seat made of the same material without any overlay.

Although line contact was used in the tests, the angle between the two contacting surfaces was 30 degrees, which is much greater than the 2.5 degrees for the PORV. Therefore, the PORV

plug has a much greater parallel velocity component relative to the normal component than the tests. The frequency of impact in the tests was much greater than expected in the PORV during severe accidents.

Although the results from the tests are not directly applicable to the PORV during severe accidents, similar mechanisms should be operative, and crack initiation and propagation will play important roles in the wear rates and failure of the plug and cage.

The stress-strain field created by the repeated impact of the plug on the cage because of PORV cycling was analyzed. Figure 4-23 shows the various parts selected for impact analysis.

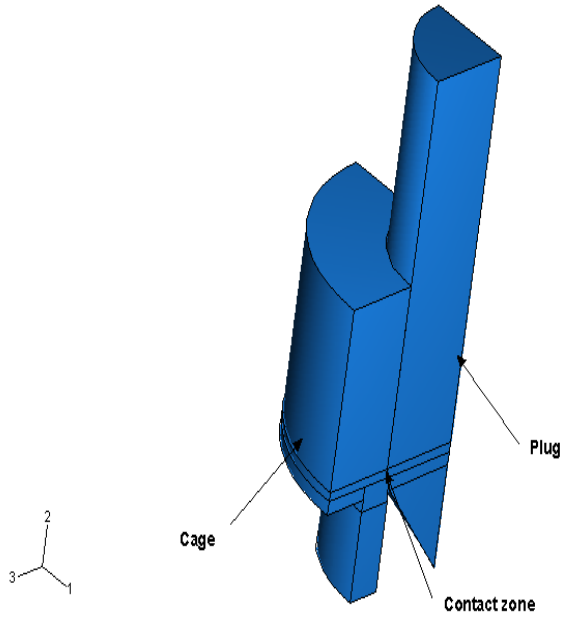


**Figure 4-23 Various parts included in the plug to cage impact analysis**

The taper of the contacting surfaces of the plug and the cage differs slightly (2.5°). Consequently, the initial contact between the plug and the cage is almost tangential in the axial direction and along a line in the circumferential direction. For simplicity, the FEA was axisymmetric. The reference case analysis did not include the Stellite overlay but the sensitivity analysis did include it. During normal operation, a 46-cm (18-in.) long AISI 6150 low-alloy steel spring (spring constant = 814 N/mm [4,700 lb/in.]) holds the plug pressed against the cage with a force of 43 kN (9,760 lb). The FEM included the spring as a linear-spring element. The cage was supported in the vertical direction at the shoulder region. In view of the large relative contact displacement between the plug and the cage, and to handle the dynamics of the problem, a full nonlinear (finite deformation) analysis was implemented with ABAQUS-explicit.

The entire model was assumed to be at a uniform and constant temperature during the impact. Because of the high strain rate involved during the impact, the analysis was carried out with an

elastic-plastic constitutive relationship for both the plug (Type 316 stainless steel) and the cage (17-4 PH steel H1100). A rate effect on the constitutive relationship was not included in the analysis. The strength properties were obtained from the ASME Code, Section II, and Figure 4-24 shows the bilinear stress-strain curves that the analysis used. Note the much higher strength of the cage when compared with that of the plug. At temperatures greater than 593 degrees C (1,100 degrees F), the cage material will lose strength rapidly. However, because of lack of data, analyses were conducted for 288 and 538 degrees C (550 and 1,000 degrees F) only.

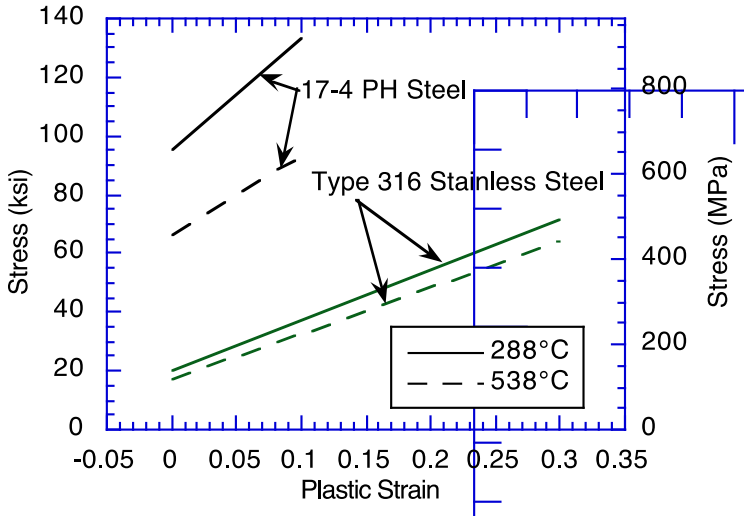


**Figure 4-24 Stress plastic strain curves at 288 and 538 degrees C (550 and 1,000 degrees F) used in analysis**

In the reference case, the initial velocity of the plug was set at 32 mm/s (1.25 in./s), as recommended by the manufacturer, starting from a position just in contact with the cage. The analysis was continued until the elastic waves travelling back and forth were significantly reduced. The variation of the spring force with time for a single impact, plotted in Figure 4-25, shows that the time taken by the plug to come to a complete rest is 0.01 s. After the first impact, the plug was retracted rapidly to the same position it occupied before the first impact and was held in place for 0.005 s. It was then given the same initial velocity as in the first impact, and the analysis continued as before. Finally, the plug was retracted and a third impact was analyzed.

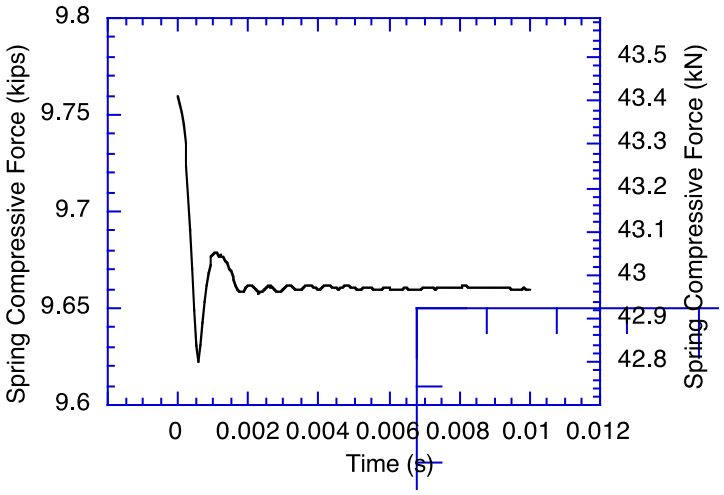


**Figure 4-25 Variation of spring force with time during single impact**

Figures 4-26a and 4-26b show the variations of the maximum equivalent plastic strain with von Mises effective stress and time, respectively. The additional stress cycles in Figure 4-26a are because of elastic wave propagation in the plug. Note that the maximum effective plastic strain increases with each impact, although at a diminishing rate. After three impacts, residual effective plastic strains of 8.4 and 9.4 percent are created at 288 and 538 degrees C (550 and 1,000 degrees F), respectively. Although plastic strain ratcheting occurred with each loading cycle, Figure 4-26a shows no open hysteresis loop in the stress-plastic strain plot, which indicates that low-cycle fatigue should not be a problem for this type of cycling. In contrast to the plug, the cage does not experience any plastic strain at these temperatures because the maximum stresses are too low.

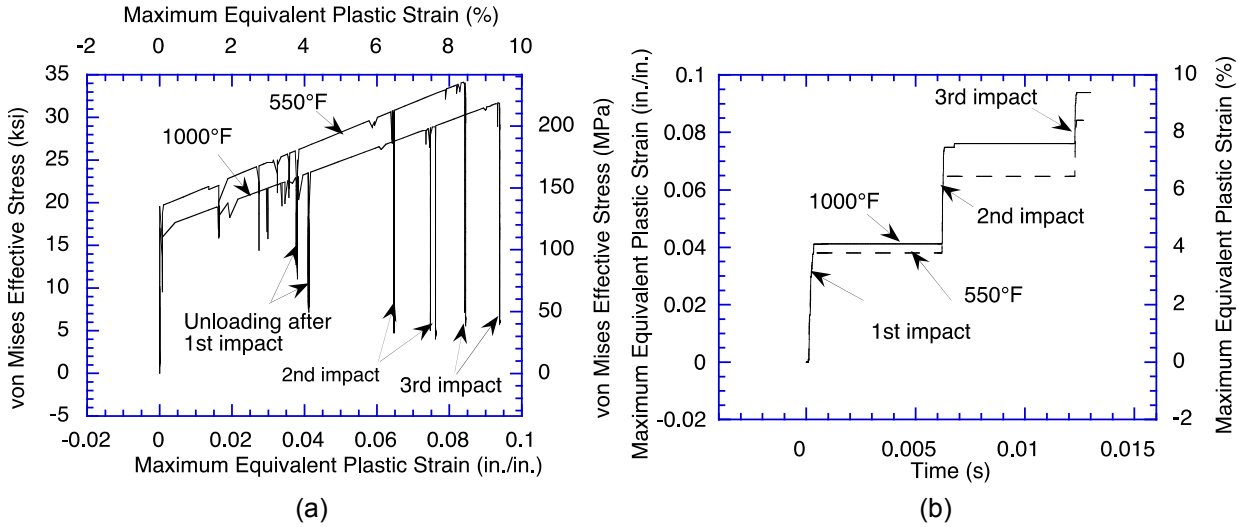


**Figure 4-26 Variation of equivalent plastic strain with (a) von Mises effective stress and (b) time for most highly strained element in plug at 288 and 538 degrees C (550 and 1,000 degrees F)**

***Stellite Overlay Effect***

In practice, a hard Stellite overlay is present on the soft plug material; it will have a major influence on the stress-strain distribution in the plug. For the purpose of investigating the effect of the overlay, a simplified model of the plug-to-cage impact was adopted (Figure 4-27a). The impact analysis of the plug with a 2-mm (0.08-in.) thick Stellite overlay was conducted at 538 degrees C (1,000 degrees F) with the stress-plastic strain curves shown in Figure 4-27b. At 538 degrees C, the Stellite coating is stronger than the 17-4 PH steel and considerably harder than stainless steel. The FEA showed that no plastic strain was generated in the overlay, the plug, or the cage during the impact. A plot of the distribution of the von Mises effective stress, shown in Figure 4-28, shows that the maximum stresses in the overlay, the plug, and the cage are less than their respective yield stresses. The Stellite overlay effectively shields the underlying stainless steel plug from developing high contact stress and plastic strain.

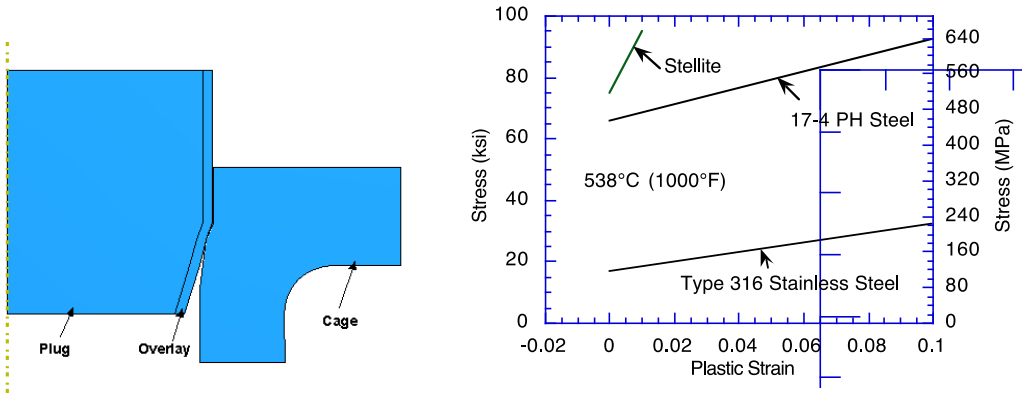


(a) (b)

Figure 4-27 Stress-plastic strain on 2-mm thick plug

***(a) Simplified axisymmetric model of plug-to-cage impact, where satellite overlay on plug is 2-mmthick***

***(b) stress-plastic strain curves used in impact analysis of plug with 2-mm-thick satellite overlay***

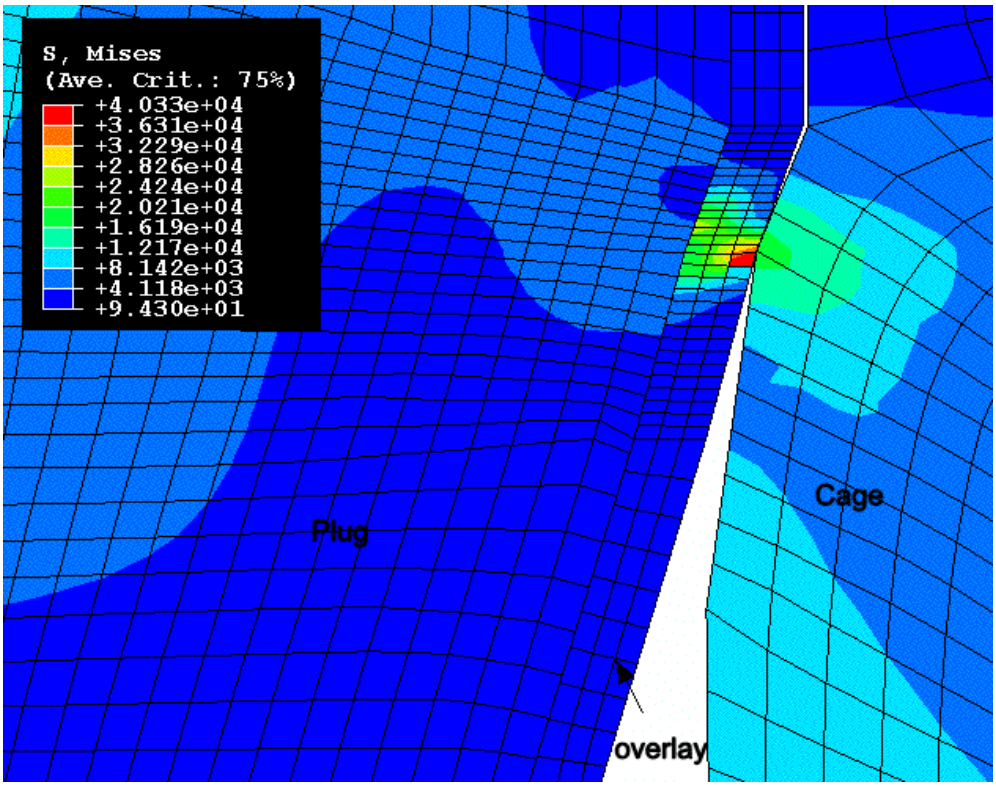


**Figure 4-28 Distribution of von Mises effective stress (in psi) near contact zone of cage and plug with 2-mm Stellite overlay**
***Note 1,000 psi = 6.895 MPa.***

## 4.4 Thermal-Mechanical Analyses of the HL and Surge Line

The thermal mechanical analyses were performed in two steps. First, a thermal transient analysis obtained the temperature distribution throughout the model. Second, the nodal-temperature data, together with the pressure and structural-support and boundary condition data, were entered into the structural-analysis model. The basic nodal configuration and numbering of both models were the same.

### 4.4.1 FEM for Thermal Analysis and Boundary Conditions

Two slightly different versions of the same basic FEM were used in two analyses in sequence. The first version was used to analyze the thermal model, which included all the components shown in Figure 4-29. The second version of the FEM was used to analyze the structural model, which, in addition to the components shown in Figure 4-29, included the supports and flailing restraints. The supports and flailing restraints were not included in the thermal FEM because they do not affect the thermal analysis of the HL or the surge line and were not of interest from a thermal standpoint. All of the components of the thermal model were modeled with second-order (8 nodes) thick quadrilateral shell elements with five integration points across the thickness.

The finite element mesh, shown in Figure 4-30, for the thermal analysis was highly refined in areas suspected of damage, namely the elbow, HL, and nozzles. The number of finite elements is close to 4,000, with close to 63,000 degrees of freedom.

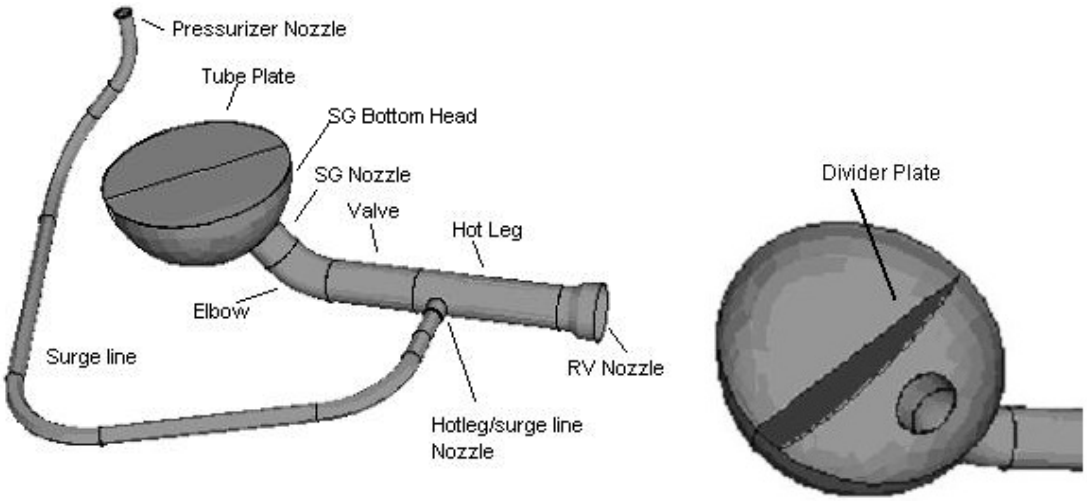


Figure 4-29 Components of first version of FEM for thermal conduction analysis

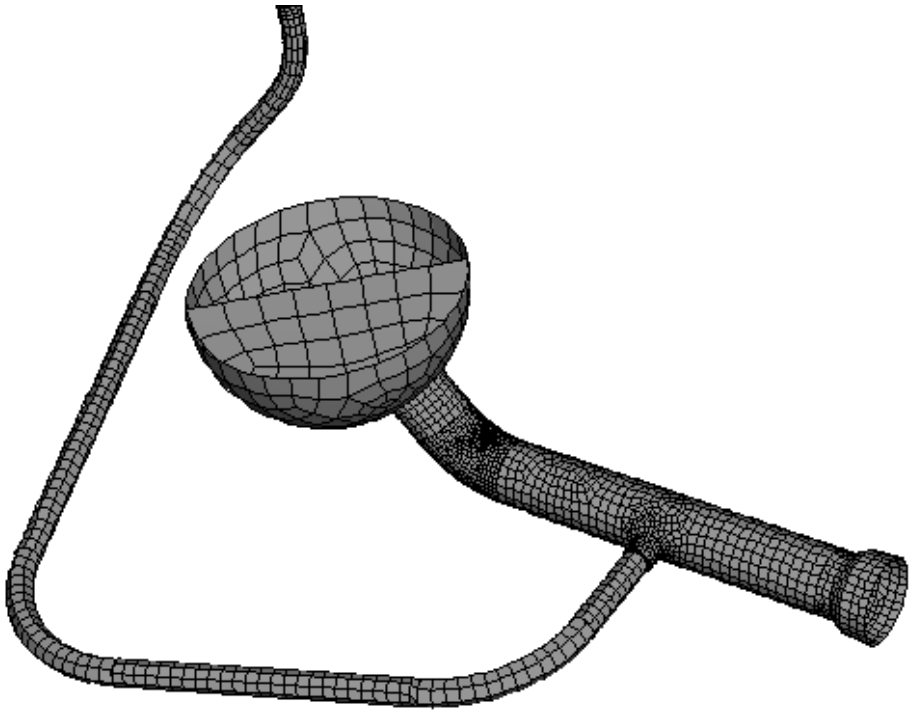

Figure 4-30 FEM for thermal analysis

The initial temperature was assumed to be the operating temperature of 300 degrees C (572 degrees F). The outer surfaces of the system, including the tube support plate, were assumed perfectly insulated. The ends of the RV and PZR nozzles were assumed insulated as well. The system was brought to steady-state conditions, with a heat flux value that was equal to that given at time zero. After the system reached steady state, a transient thermal solution ensued, driven by the heat flux profiles. Although the profiles extend to 32,000 s, the thermal simulations were terminated when the component temperatures exceeded 1,600 K (2,421 degrees F), because the structural models reveal significant damage at temperatures

well below 1,600 K. In fact, the structural data do not support temperatures higher than 1,400 K. Although the tensile and creep-rupture properties of the materials used in these simulations are restricted to temperatures below 1,400 K, it is expected that these materials significantly soften and will experience rapid high-temperature damage at temperatures above 1,400 K. Section 4.5.5 discusses the implications of this.

### 4.4.2 FEM for Structural Analysis and Boundary Conditions

The second version of the FEM, which is used to conduct the structural analysis, is identical to that of the thermal model (Figure 4-31), except that the supports and flailing restraints were included in the structural model, as shown in Figure 4-31. The temperature history obtained from the thermal analysis was entered directly into the structural model for stress and damage analysis. Because the severe-accident transient occurs at a relatively slow rate, the hydraulic snubbers were not included in the structural model. The surge line contains four supports and three flailing restraints. The flailing restraints were included in the structural model because preliminary results indicated that the surge line was experiencing significant rigid body displacements that exceeded the 12.5-cm (5-in.) radial gaps in the flailing supports. Only the bottom head of the SG was modeled with sufficient detail to capture the damage around the SG nozzle. Because the SG weight and center of mass were significant factors, their effect was included by modeling the remainder of the SG (above the tube support plate) by a rigid body (coupled with the bottom head) with an SG effective center of mass at an elevation of 187.3 m (614.5 ft.).

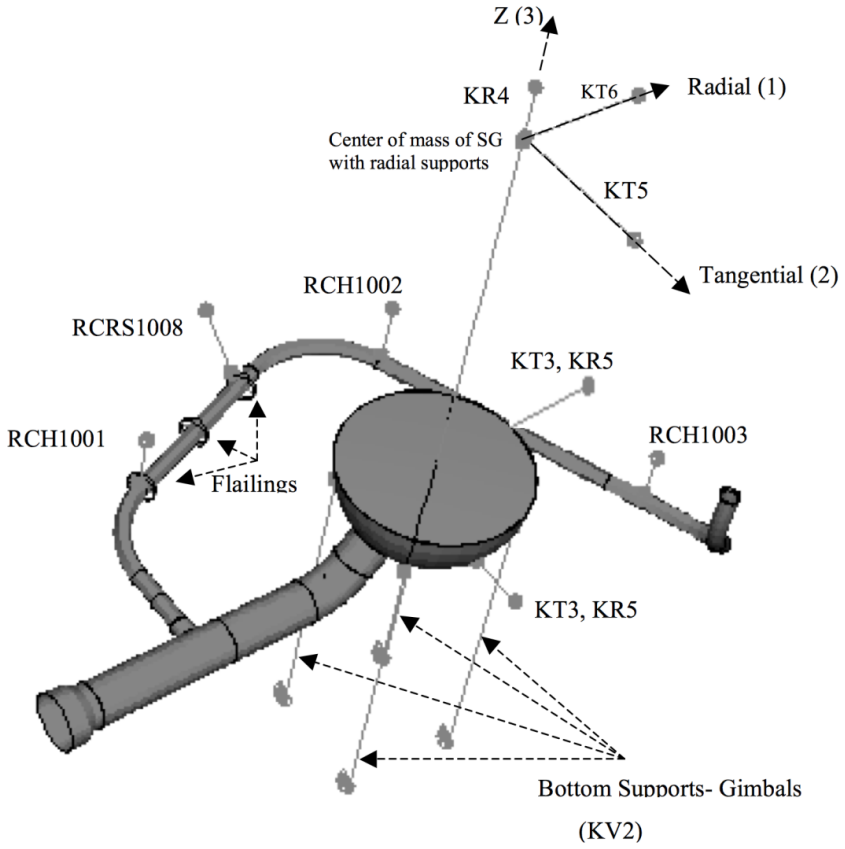


**Figure 4-31 Components of second version of FEM for structural analysis with supports, flailing restraints, and hangers**

### *Reactor Vessel Nozzle*

The HL/surge line model extends to the junction of the RV and the RV nozzle. It is assumed that the RV provides full restraint against all rigid-body translations and rotations of the RV nozzle end but allows free growth in the radial direction.

### *Steam Generator*

The support arrangement of the SG allows it to move as a rigid body, radially away from the RV, as the temperature of the system is increased from room to operating temperature. The gaps and shims are designed so the SG bears against the top and bottom bumpers at full power. During a severe-accident transient, when the HL temperature increases, the supporting structures restrain the SG from moving any further than allowed by the elastic deformation of the supports. These supports were modeled as nonlinear springs that can carry compressive but not tensile loads. Thus, the snubbers at the upper lateral support allow the SG to tip away from vertical toward the RV during a relatively slow severe-accident transient. The SG dead weight in such a scenario could potentially apply significant bending and twisting moments on the SG inlet nozzle.

The SG required six elastic supports in the direction of the six global rigid degrees of freedom; namely, three translations and three rotations. These supports were developed and are described according to the local coordinate system shown in Figure 4-31 and labeled as Radial, Tangential, Z, or 1, 2, 3. The SG rests on four gimbals that are modeled as simple beam members that provide axial elastic support in the vertical direction (Z) with an axial stiffness of KV2. Both ends of the beam members are pinned end boundaries.

The rotational stiffness of the SG in the Z direction is referred to as KR4. In the tangential direction, both axial and rotational elastic supports (KT3 and KR5) are at the bottom head, and the arrangement in the Radial direction along the HL (KT4 and KR5) is similar. Two elastic axial supports are at the top of the SG (close to the center of mass). The one in the tangential direction is KT5. The radial one (KT6) provides a nonlinear elastic support; if the top of the SG leans toward the HL, this support provides resistance only after a displacement of 210 mm (8.3 in.). If the top moves backward, away from the HL, the support resists at a different rate, as shown in Table 4-1.

Table 4-1 Spring Rates of Steam Generator Supports

| Support Name | Spring Rate | | Note |
|---|---|---|---|
| | lb/ft | N/mm | |
| KT3 | 1.63E+08 | 2.38E+06 | Linear |
| KT4 | 1.39E+08 | 2.03E+06 | Linear |
| KT5 | 5.52E+08 | 8.06E+06 | Linear |
| KT6 | 1.92E+08 | 2.80E+06 | Moving toward HL after 210-mm (8.3-in.) displacement |
| KT6 | 1.24E+08 | 1.81E+06 | Moving away from HL |
| KV2 | 2.24E+08 | 3.27E+06 | Linear |
| KR4 | 1.51E+10* | 2.05E+13** | Linear |
| KR5 | 4.30E+09* | 5.83E+12** | Linear |

* lb-ft/rad ** N-mm/rad

***Surge Line Supports***

The FEM for structural analysis contains nine surge-line supports: three flailing restraints, one variable support spring hanger, one threaded-rod support, one constant-support hanger, one sway strut assembly, and two hydraulic snubber restraints. The stiffness values for the various supports came from Reference 1.

The flailing restraints provide vertical and horizontal supports but a gap allows for thermal movement of up to 0.127 meters (5 in). Therefore, effectively, these supports do not provide any restraint until the surge line moves significantly. The vertical stiffness is $1.38X10^6$ kN/m ($9.475X10^7$ lb/ft) and the horizontal stiffness is $3.60X10^7$ kN/m ($2.47X10^9$ lb/ft) in compression and $4.13X10^6$ kN/m ($2.83X10^8$ lb/ft) in tension.

The stiffness of the hanger of the variable-support spring 189.14 kN/m (12,960 lb/ft) is much smaller than the stiffness of the other restraints. The threaded support spring hanger exhibits a stiffness of $3.58X10^4$ kN/m ($2.45X10^6$ lb/ft), and carries a vertical dead weight of 37,245 N (8,373 lb) during normal operation. The constant-support hanger supports a constant vertical dead weight of 30,248 N (6,800 lb). The stiffness of the sway strut assembly, which provides support in both the horizontal and vertical directions, is $1.36X10^6$ kN/m ($9.3X10^6$ lb/ft).

The FEM included all of the supports except the snubbers. Figure 4-31 describes the four supports (excluding the flailing restraints) that are modeled for the surge line, and Table 4-2 lists their types. Three of the supports provide elastic support with a specified spring rate, while the fourth (RCH1003) provides a constant load. The other three supports are oriented as shown in Figure 4-32.

Table 4-2 Surge-Line Supports in FEM for Structural Analysis

| Support Reference Name | Type | Stiffness | Load |
|---|---|---|---|
| **RCH1001** | hanger | 69,869 N/mm (4.89E6 lb/ft) | - |
| **RCH1002** | hanger | 69,869 N/mm (4.89E6 lb/ft) | - |
| **RCH1003** | constant load | - | 30E3 N (6800 lbf) |
| **RCRS1008** | solid lateral & vertical support | 69,869 N/mm (4.89E6 lb/ft) | - |

***Pressurizer Nozzle***

The HL/surge-line model extends to the junction of the PZR shell and the PZR nozzle. The PZR is rigidly supported by the upper and lower lateral supports, which prevent translational and torsional movements but allow free radial and vertical thermal growth. The vertical load is carried by four columns, attached rigidly to the ring beam of the lower lateral support. Therefore, it was assumed that the PZR provides full restraint against all rigid-body translations and rotations of the PZR nozzle end but allows free radial growth.

### 4.4.3 Mechanical and Surface Heat Flux Loading

#### *4.4.3.1 Gravity and Pressure Loading*

The whole system was subjected to gravitational loading. The weight of the SG was applied at its center of mass. The weight of the HL valve was distributed throughout its volume. The surge

line and the HL gravity loads were applied as body forces. Table 4-3 lists the weights and/or the mass densities used for gravity loading; it also shows that steam pressure used throughout the systems is 16.2 MPa (2,350 psi).

**Table 4-3 Weights and Pressure Loading and Mass Densities Used in Thermal-Mechanical Analysis of the HL and Surge Line**

| | Metric | English |
|---|---|---|
| **Valve weight** | 111 KN | 25,000 lb |
| **SG weight** | 3,720 KN | 836,476 lb |
| **Surge-line mass density** | 7,500 kg/m$^3$ | 0.28 lb/in$^3$ |
| **HL mass density** | 7,500 kg/m3 | 0.28 lb/in3 |
| **Steam pressure** | 16.2 MPa | 2,350 psi |

*4.4.3.2 Surface Heat Flux (Heat Transfer Coefficients)*

The thermal model was driven by heat flux profiles as functions of time. Fourteen such profiles are assigned to 14 regions, as shown in Figure 4-32 and labeled according to heat flux information obtained from RELAP5 calculations.

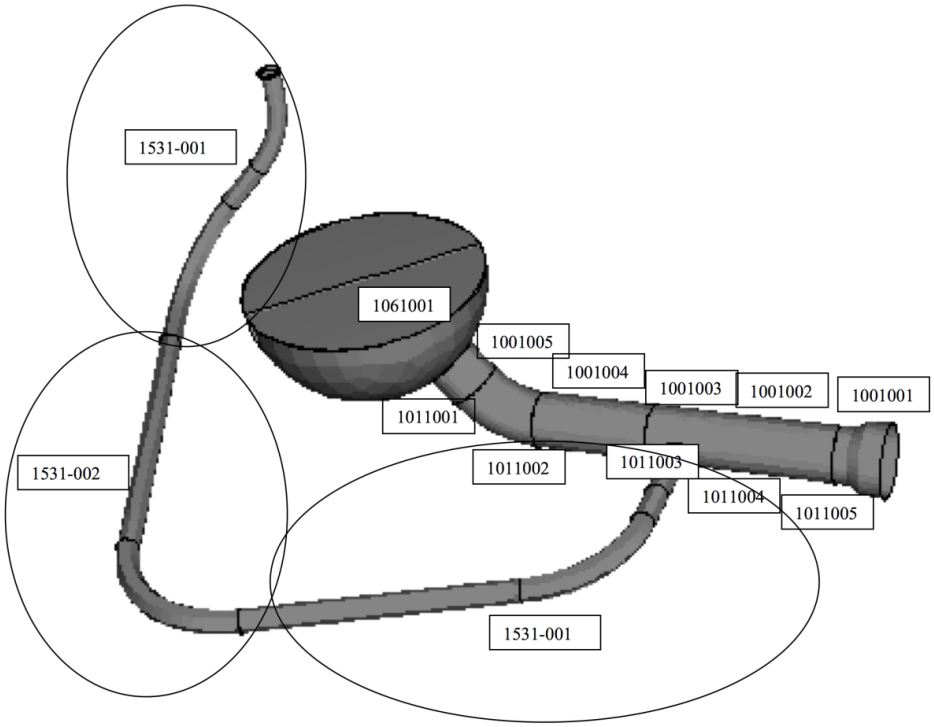


**Figure 4-32 Control volumes for thermal-hydraulic analysis of the HL and surge line by RELAP5**

RELAP5 divided the HL into two noninteracting independent halves. The top half carries the hot steam from the reactor to the SG and the bottom half returns the cool steam from the SG to the reactor. The top half of the HL was divided into five cells (1001001 through 1001005), each with constant heat flux. The bottom half of the HL was also divided into five cells (1011001 through 1011005), each with constant heat flux. The outer surfaces of the HL and surge line were

assumed to be perfectly insulated. The highest heat fluxes in the top and bottom halves are in cells 1001001 and 1011005, respectively. The lower head of the SG was assigned the SG inlet plenum heat flux. The surge line was divided into three cells, with the closest cell to the HL designated as 1531003. For the present analysis, the heat transfer coefficient from the RELAP5 results was spatially adjusted in the HL and surge line, based on the developing curve provided in NUREG-1922, "Computational Fluid Dynamics Analysis of Natural Circulation Flows in a Pressurized-Water Reactor Loop under Severe Accident Conditions," issued March 2010 (Ref. 3).

### 4.4.4 Results of Thermal-Mechanical Analysis of HL and Surge Line

The basic reference case used the thermal properties along with heat flux profiles discussed in the previous sections. The thermal transient analysis, after reaching the steady state, started at time = 9,222 s and terminated at ≈19,330 s. After completion of the thermal solution, the temperature time histories were input into the structural portion of the model. The components were assumed to respond to the structural, gravity, and thermal loads by an additive combination of elastic, rate-dependent plastic, and creep (visco-plastic) material behaviors. The material model consisted of using a simple thermal plasticity combined with a secondary creep law. Figure 4-33 shows the stress versus plastic strain curve used for the Type 316 stainless steel. Reference 1 was the source for the properties used for the A508 carbon steel and the Alloy 182 weld metal, and Appendix A contains the properties for the Type 316 stainless steel. Because material data were not available for temperatures higher than 1,373 K, these same properties were used at higher temperatures. However, as will be seen, failure is predicted before the temperatures get much higher than this.

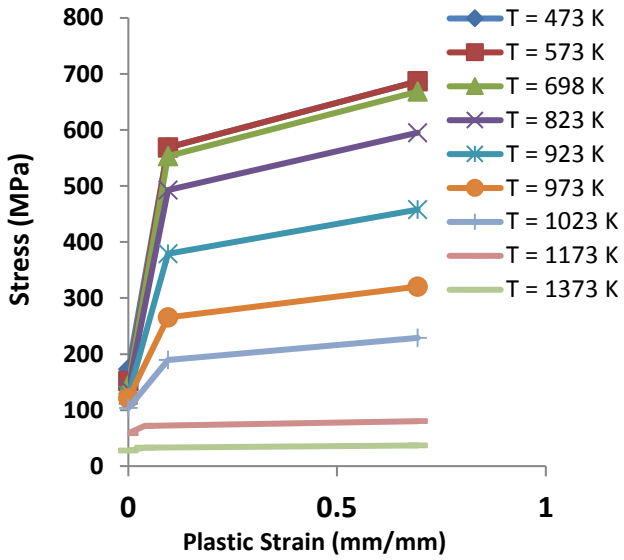


**Figure 4-33 Temperature-dependent stress strain curves for 316 stainless steel (Appendix A)**

An ABAQUS power-law model is chosen to model creep behavior, given by:

$$\dot{\varepsilon}^{cr} = A\tilde{q}^{n}t^{m} \tag{4.3}$$

where $\dot{\varepsilon}^{cr}$ is the uniaxial equivalent creep strain rate, $\tilde{q}$ is the uniaxial equivalent deviatoric stress, and t is the total analysis time, and A, n are temperature dependent constants and m=0. The analysis uses the creep properties given in Appendix A.

Figures 4-34 and 4-35 show representative temperature contours of the whole system, captured at 9,222 s and 13,555 s, respectively. The model was based on metric units, with temperature expressed in Kelvin. The steady-state temperature of 623 K is reached at 9,222 s in the entire region of consideration, as shown in Figure 4-34. The upper half of the HL experiences much higher temperatures during the transient, as shown in Figure 4-35.

Figures 4-36 and 4-37 show the contours of effective creep strain and plastic strains, respectively. Both the figures indicate that the upper half of the HL experiences higher creep and plastic strains. The plastic strains and creep strains are predicted to reach above 30 percent and 7 percent in the upper half of the HL. These levels of strains are quite high and indicate potential failure in the regions of interest.

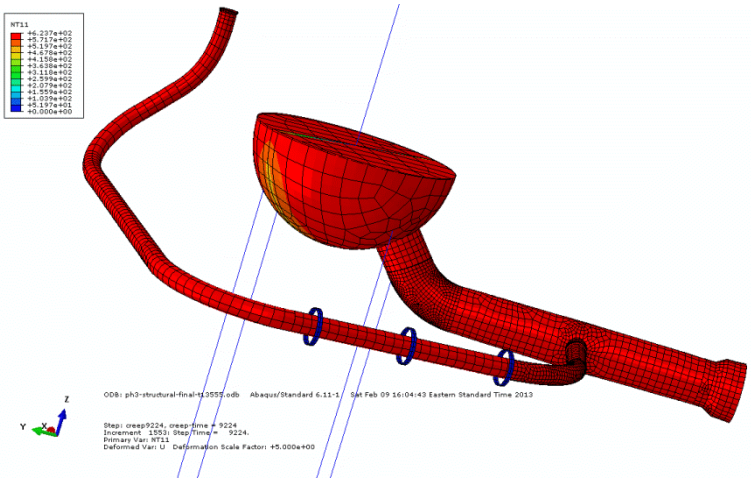

**Figure 4-34 Temperature contours at inner surface at 9,222 s indicate the steady-state condition of 623 K in the entire region of consideration**

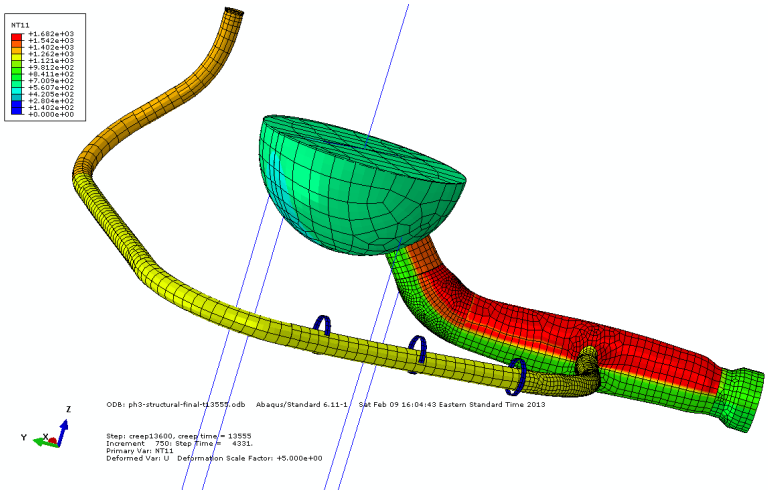

**Figure 4-35 Temperature contours at inner surface at 13,555 s indicate the higher temperature in the upper half of the HL region**

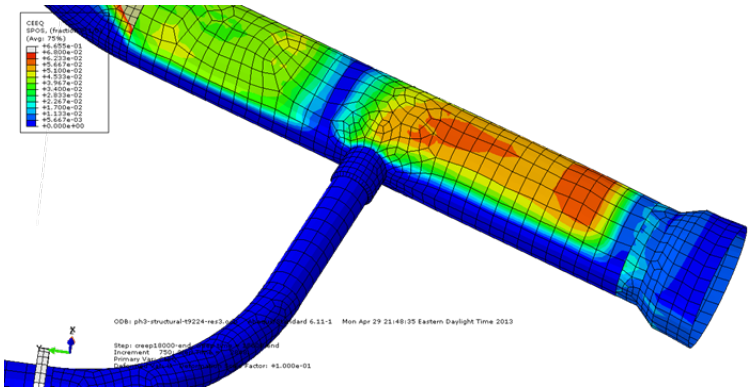

**Figure 4-36 Contours of accumulated creep strain at inner surface at 12,300 s indicate the significant creep strains in the upper half of the HL region**

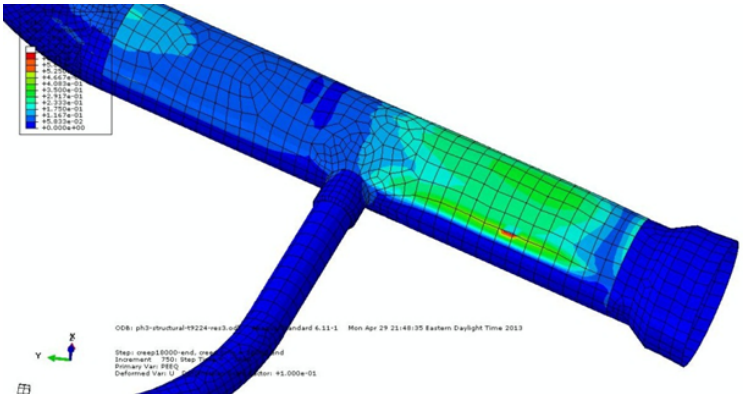

**Figure 4-37 Contours of plastic strain at inner surface at 12,300 s indicate the concentration of plastic strains in the upper half of the HL region**

### 4.4.5 Evaluation of Structural Damage

Creep failure can be predicted either by exhaustion of material creep ductility or by accumulation of creep damage. Failure by exhaustion of creep ductility occurs when

$$\text{Effective Creep Strain} = \varepsilon = \varepsilon_c = \text{Creep Ductility} \tag{4.4}$$

Because creep ductility data for the materials used in the analyses are available for the entire temperature range of interest, the linear time fraction damage rule was used to calculate the creep damage as follows:

$$\text{Creep Damage} = \sum \frac{\Delta t}{t_r(T,\sigma)} \tag{4.5}$$

where $\Delta t$ is the time interval at temperature T, $\sigma$ is von Mises effective stress, and $t_r$ is the time to creep rupture at temperature T. Failure is predicted to occur when the creep damage is equal to 1.

Given the state of stress and temperature, the Larson Miller parameter was used to evaluate the time to rupture, $t_r$:

$$t_r = 10^{\left(\frac{PLM}{T} - C\right)} \tag{4.6}$$

where T is the absolute temperature in Kelvin, PLM is the Larson Miller parameter, which can be obtained approximately as a function of effective stress σ as follows:

$$PLM = A*Log_{10}(\sigma) + B \tag{4.7}$$

and A, B, and C are material parameters given in Appendix A.

Creep damage was considered only if the in-plane principal stress was tensile, because compressive in-plane stress does not initiate cracking.

At elevated temperatures, creep deformation tends to relax the stresses and keep them below the yield strength of the material. However, in the presence of a time-dependent driving force, such as thermal expansion, creep deformation may not be fast enough to relax the stresses to below the yield stress. In such cases, failure by tensile rupture is a possibility.

Uniaxial tension tests conducted at high temperatures indicate that stainless steels and the ferritic steels experience a uniform elongation of the order of few percent (2–5 percent), beyond which necking and plastic strain localization occurs and any additional plastic displacement is negligible. Based on this, it is possible to determine failure time and location when a material point reaches a through-thickness plastic strain of 2 percent. Because this failure criterion is quite arbitrary, this study did not adopt it. Nonetheless, it should be pointed out that the plastic strains reach values of above 10 percent in the upper half of the HL before the failure is predicted using the Larsen-Miller parameter approach described above.

Figures 4-38 and 4-39 show the creep damage, calculated using Equation 4.5, in the section of HL experiencing higher creep and plastic strains. The through-thickness damage shown in Figure 4-38 indicates that the maximum damage of 1 (indicated by red color) occurs on the upper half of the HL away from the nozzle. The corresponding damage in the outer and inner surfaces shown in Figures 4-39a and 4-39b indicates that it is rather uniform through the thickness, although the maximum damage occurs in the inner surface earlier. This indicates that failure through the thickness is quite rapid, perhaps because of the steep increase in the temperature transient.

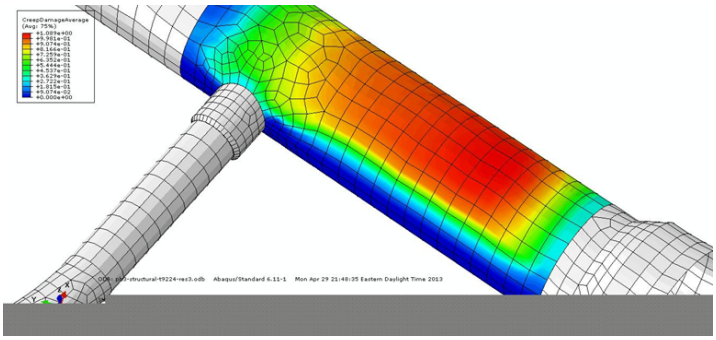

**Figure 4-38 Contours of through-thickness damage at 12,300 s shown in the section of HL experiencing higher strains**
***The red-colored regions reach the creep damage of unity.***

The structural analysis of the system model considered here posed convergence issues beyond 14,000 s. Although maximum damage is predicted much earlier, this model is not conducive to conducting additional analyses to examine the effect of weld-overlay and the effects of varying material response. In addition, the system model took considerable computer processing hours to perform the needed calculations. Because the failure occurs in the HL region, further analyses used a finite element model of the HL region.

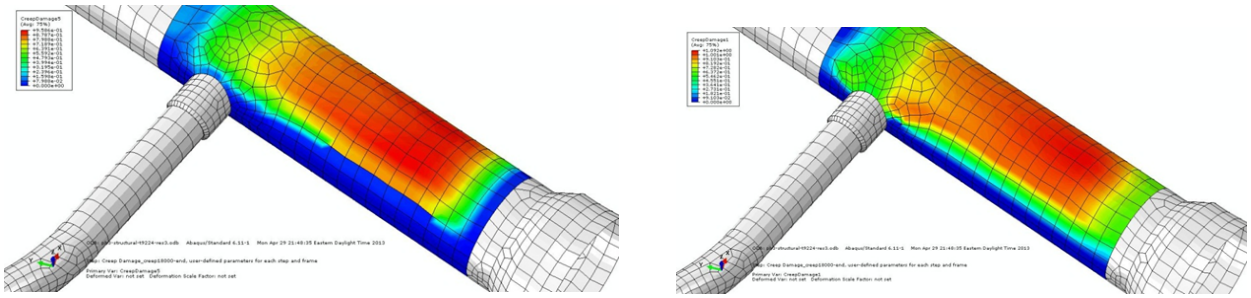

(a) Outer surface (b) Inner surface

**Figure 4-39 Contours of creep damage at 12,300 s shown in the (a) outer surface and (b) inner surface of HL experiencing higher strains**
***The red-colored regions reach the creep damage of unity.***

### 4.4.6 HL Model

The thermal mechanical analysis using the smaller HL model employed the same procedure described for the system model. Figures 4-40 and 4-41 show the contours of effective creep strain and plastic strains, respectively, at time equals 12,430 s. The strain distributions in the upper half of the HL are similar to those shown in Figures 4-36 and 4-37 for the system model. Figures 4-40 and 4-41 indicate that the upper half of the HL experiences higher creep and plastic strains. The plastic strains and creep strains are predicted to reach above 40 percent and 6 percent in the upper half of the HL. These levels of strains are similar to those predicted using the system model. Thus, the smaller HL model yields similar results to the larger system model. Because of slightly lower levels of strains predicted using the smaller HL model, the failure time may be longer. However, because of the steep transient, the failure time using the HL model, shown in Figure 4-42, was only 126 s longer than the time predicted using the system model.

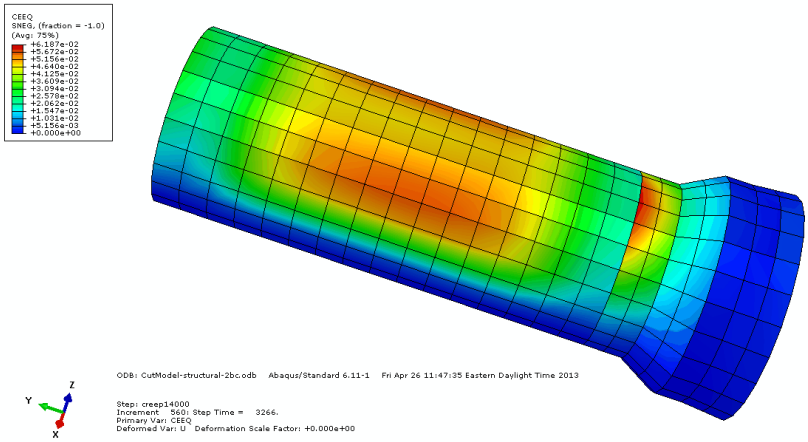


Figure 4-40 Contours of accumulated creep strain at inner surface at 12,430 s indicate the significant creep strains in the upper half of the HL region
***The strain distribution and maximum strain level are similar but not identical to the system model.***

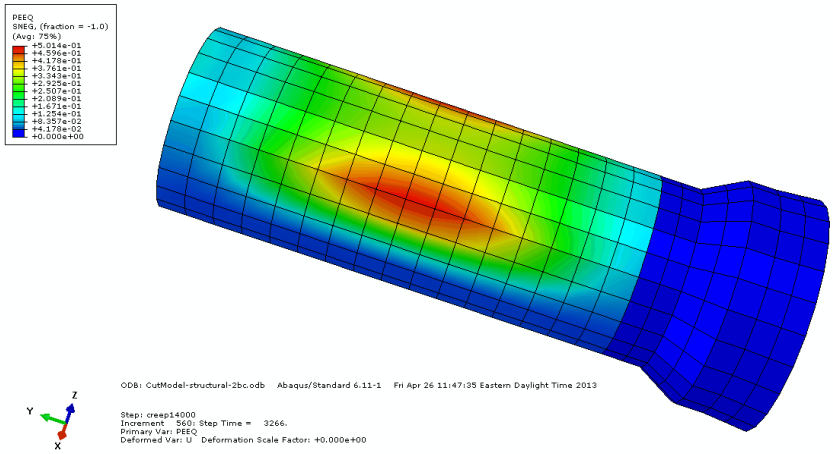


Figure 4-41 Contours of accumulated plastic strain at inner surface at 12,430 s indicate the significant creep strains in the upper half of the HL region
***The strain distribution and maximum strain level are similar but not identical to the system model.***

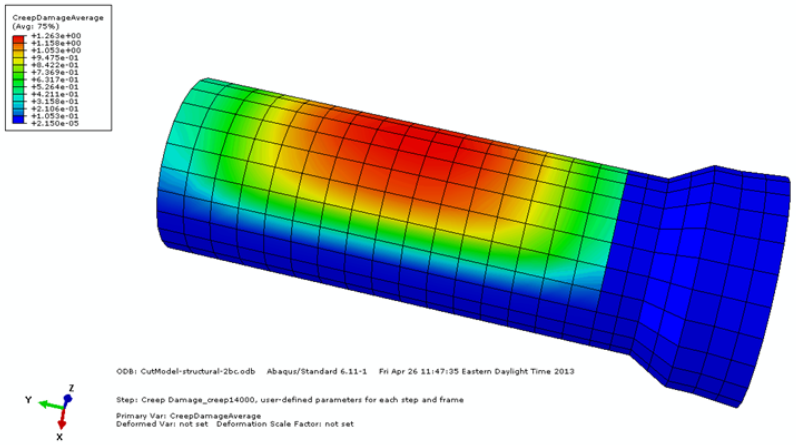

**Figure 4-42 Contours of through-thickness damage at 12,430 s shown in the section of HL experiencing higher strains**
***The red-colored regions reach the creep damage of unity.***

### *Sensitivity Analyses*

Several additional analyses examined the effects of material response and the effect of not spatially adjusting the heat transfer coefficients obtained from RELAP results. To examine the effect of material behavior, the analyses assumed only creep or plastic response. The earlier results were obtained using combined plasticity and creep response. Assuming only creep behavior accelerates the failure time to 12,140 s (Figure 4-43a), while assuming plasticity only delays the failure time to 13,205 s (Figure 4-43b). Assuming only plasticity behavior at the severe-accident temperatures is not realistic. Additionally, the damage is predicted using creep-rupture data. These two considerations, coupled with the observation that the effective plastic strain in the HL region reaches values beyond 400 percent, invalidate the use of the plasticity-only model.

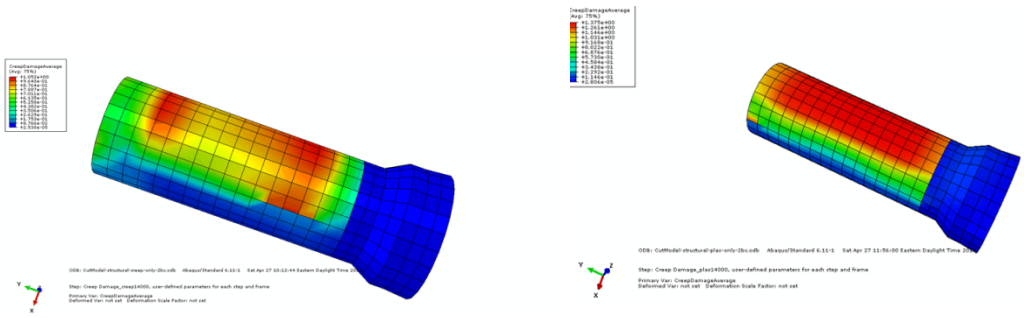

(a) Creep Response (b) Plasticity Response

**Figure 4-43 Contours of through-thickness damage assuming (a) creep-only behavior at 12,140 s and (b) plasticity-only behavior at 13,025 s**

The red-colored regions reach the creep damage of unity. Note that damage is predicted in different sections of the upper half of the HL.

The earlier analyses accounted for the spatial adjustment of the heat transfer coefficient obtained from RELAP, based on the developing curve given in NUREG-1922 (Ref. 3).

The spatial adjustment increases the surface temperature inside the HL, which may accelerate failure. Thus, one would expect the failure time to be longer without the spatial adjustment. Figure 4-44 shows contours of through-thickness damage assuming no spatial adjustment of e heat transfer coefficient obtained from RELAP. Failure is predicted at 12,610 s, which is 180 s longer than the result predicted with the spatial adjustment of heat transfer.

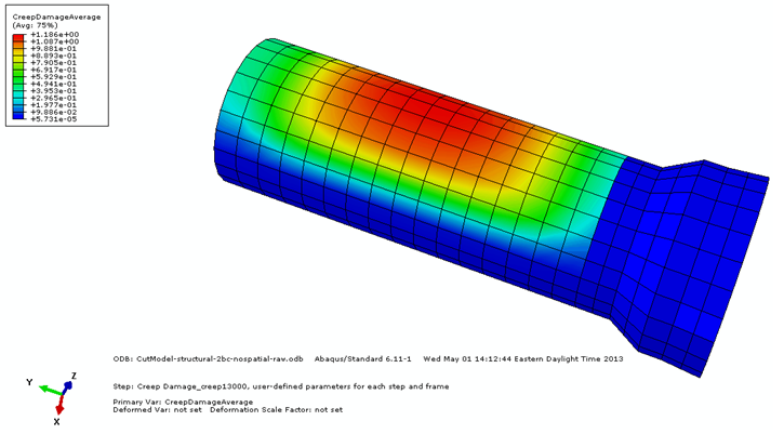


**Figure 4-44 Contours of through-thickness damage assuming no spatial adjustment of heat transfer coefficient obtained from RELAP**
***The red-colored regions reach the creep damage of unity.***

### *Effect of Weld Overlay*

The welded region between the HL nozzle and pipe could be prone to primary water stress-corrosion cracking. One of the preventive methods to mitigate potential failure of the pipe during normal operation involves applying a weld overlay, where additional material is welded over the pipe. This results in increasing thickness of pipe over the welded region. To examine the effect of the weld overlay in increasing the failure time during the severe-accident sequence considered in the previous analyses, an HL model with an overlay was analyzed. The boundary conditions and thermal transient were identical to the previous analyses. Contours of through-thickness damage for the HL pipe with weld overlay, shown in Figure 4-45, indicate failure at 12,500 s. Note that the failure location is similar, and the failure time is increased by 72 s relative to the pipe with no weld overlay.

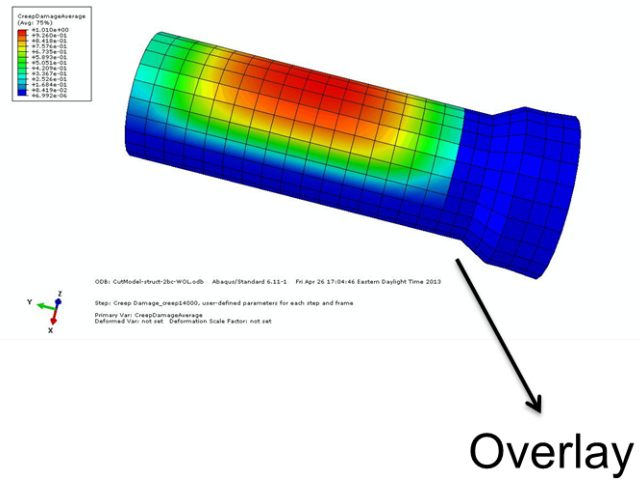


**Figure 4-45 Contours of through-thickness damage for the HL pipe with weld overlay at 12.500 s**

Note that the failure location is similar to the pipe without a weld overlay. The failure time increases by 70 s relative to the pipe with no weld overlay.

## 4.5 Conclusions

### 4.5.1 SG Primary Manway

The bolt loads are fully relaxed by thermal creep, and the contact pressure in the joint was reduced to zero by the time the bolt temperature reached 450 degrees C (842 degrees F), which corresponds to 14,346 s. If 8 of the 16 bolts were initially loose (85-percent design preload), their loads would be relaxed out at 440 degrees C, or 824 degrees F (14,156 s). If the bolts were uniformly preloaded but if the creep rate were 10 times greater than the assumed reference creep rate, bolt loads would be relaxed out by 430 degrees C, or 806 degrees F (13,975 s). These calculations are based on estimated creep rate data of alloys similar to SA 193 (B7).

Rather than bolt rupture, a more likely sequence for the depressurization of the primary side is the lifting off of the cover plate after the bolt loads have relaxed out and created a leakage path for the steam. Considering a 5-cm (2-in.) diameter hole with an area 20 $cm^2$ (3 $in.^2$) to be sufficient to rapidly depressurize the primary side, a leakage area equivalent to such a hole is created in the reference case by 600 degrees C, or 1,112 degrees F (16,726 s). The actual flow area will be less because of gasket springback, which should be minimal at these temperatures because of thermal creep. However, gasket creep data at high temperature are needed to verify this.

Sensitivity analyses showed that the time to open a sufficiently large leakage area is virtually unchanged, even if 8 of the 16 bolts were initially tightened to only 85 percent of the design preload. The opening time was also found to be strongly dependent on the bolt temperature. A simplified model of the effect of steam leakage on local heating of the bolts showed that the opening time could be reduced by more than 1,500 s relative to the reference case, which does not account for leakage effects. A more rigorous treatment of this problem must be obtained by a coupled thermal-hydraulics and stress analysis in the future.

Finally, subsequent creep tests on SA 193-B7 have shown that the creep strains in the analysis were overestimated by a factor of 5 to 10. This would imply that the bolt load relaxation should be significantly less rapid than calculated here and the failure times calculated may be highly conservative (i.e., overestimated).

### 4.5.2 RTD Welds

A heat conduction FEA of the RTD, the ID and OD attachment welds to the HL, and an axial segment of the HL showed that the average ID weld temperature is 50–80 degrees C (122–176 degrees F) hotter than the average OD weld temperature. The tip of the RTD scoop also is heated very rapidly to a high temperature.

Stress analysis showed that significant load is transferred between the ID and the OD welds because of creep effects. Inclusion of both creep and plasticity effects in the analysis showed that the initiation of tensile rupture failure is predicted to occur at the OD weld/RTD interface at 13,930 s. On the other hand, if plastic yielding is suppressed, initiation of creep failure is predicted to occur at the ID weld/RTD interface at 13,890 s. Thus, regardless of which failure criterion is applied, the failure time is close to 13,900 s.

The sensitivity analysis showed that, when the outside heat transfer coefficients on the RTD are increased by a factor of 2 from the reference values, ignoring the internal surface heating on the RTD, failure time is reduced by 184 s from the reference failure time. If the reference heat transfer coefficients are applied equally to both the outside and inside surfaces of the RTD, failure time is reduced by 100 s from the reference failure time. A factor of 10 increase in creep rate reduces the creep failure time by 180 s when compared with the reference failure time.

### 4.5.3 Instrument Line

The stress analysis showed that stresses at the weld interfaces with the instrument line and the RTD flange are at all times less than the yield strength. The reference creep failure time at both interfaces of the weld is 14,230 s. Because the maximum stress in the instrument line away from the weld is greater than the maximum stress in the weld, the instrument line itself fails at 14,150 s, which is 80 s earlier than failure at the interfaces.

The sensitivity analysis showed that, by doubling the weld dimensions, the average stresses are reduced significantly and the creep failure time is increased to 14,330 s. Increasing the creep rate by a factor of 10, when compared with the reference case, reduces the failure times of the instrument line and the instrument line weld to 14,090 and 14,110 s, respectively.

### 4.5.4 PORV Plug-to-Cage Impact

An analysis of multiple impacts with 32-mm/s (1.25-in./s) impact velocity at 288 degrees C (550 degrees F) showed that, in the absence of the Stellite overlay on the plug, the maximum effective plastic strain in the plug increased from 3.8 percent, in the first impact, to 6.4 percent in the second impact, and to 8.4 percent in the third impact. At 538 degrees C (1,000 degrees F), the corresponding plastic strains were 4.1, 7.6, and 9.4 percent, respectively. The stress-plastic strain response showed no open hysteresis loop. The cage did not experience any plastic yielding. The plastic strains did not change if the plug impact velocity was doubled.

Inclusion of a 2-mm thick hard Stellite overlay on the plug suppressed plastic strain in the plug and in the overlay at 538 degrees C (1,000 degrees F). The cage also did not suffer any plastic strain.

Plastic strains will develop during impacts at higher temperatures because both the cage material (17-4 PH steel) and the Stellite overlay will lose strength at temperatures greater than 593 degrees C (1,100 degrees F). Stress-strain properties of the cage material and the Stellite overlay are needed at higher temperature so similar impact analyses may be conducted.

### 4.5.5 HL and Surge Line

The analyses presented in Section 4.4 indicate that the upper half of the HL will fail much earlier than the other RCS regions. Table 4-4 summarizes the failure times predicted by the various analyses considered in Section 4.4. The predicted failure times for all the cases considered are below the 5th percentile failure time of 12,800 s estimated by the C-SGTR calculator, assuming one HL. In addition, the 5th percentile failure time predicted by the C-SGTR calculator, assuming four HLs and a surge line, is 12,700 s. It is important to examine these results in the context of the assumptions. Firstly, the predicted values indicate the relative influence of various assumptions with respect to material behavior, such as creep and plasticity, spatial adjustment of heat-transfer coefficient, and weld overlay. Secondly, the predicted values fall within a narrow band of 500 s of predicted failure time. This is not surprising because, after an initial slow rise, the temperatures rise sharply beyond 12,000 s, imparting significant damage to the HL portion closer to the reactor pressure vessel nozzle. Hence, the various assumptions do not yield significantly different predicted failure times. It was pointed out earlier that the materials properties used in these simulations were restricted to temperatures below 1,400 K (1,126 degrees C or 2,060 degrees F), and that these materials will experience rapid high-temperature damage at temperatures above 1,400 K. This consideration implies that the actual failure times could be less than the predicted failure times. Nonetheless, this difference is not likely to be large because of the sharp rise in temperatures beyond 12,000 s.

Table 4-4 Summary of Predicted HL Failure Times for the Various Analyses

| Finite Element Model | Features | Weld Overlay | Failure Time (seconds) |
|---|---|---|---|
| System | Creep and Plasticity: Spatially Adjustment of HTC | No | 12300 |
| | | | |
| Hot Leg Model | Creep and Plasticity: Spatially Adjustment of HTC | No | 12430 |
| | | | |
| | Creep and Plasticity: Spatially Adjustment of HTC | Yes | 12500 |
| | | | |
| | Creep only: Spatially Adjustment of HTC | No | 12140 |
| | | | |
| | Creep and Plasticity: HTC not adjusted spatially | No | 12560 |

## 4.6 References


1. Brust, F.W., et al., “Summary of Weld Residual Stress Analyses for Dissimilar Metal Weld Nozzles,” Proceedings of ASME PVP conference, July 2010, paper PVP2010-26106.

2. ASME BPVC-III, 2015 ASME Boiler and Pressure Vessel Code, Section III: Rules for Construction of Nuclear Facility Components, General Requirements for Division 1 and Division 2.

3. U.S. Nuclear Regulatory Commission, “Computational Fluid Dynamics Analysis of Natural Circulation Flows in a Pressurized-Water Reactor Loop under Severe Accident Conditions,” NUREG-1922, March 2010, Agencywide Documents Access and Management System (ADAMS) Accession No. ML110110152.

# 5 TECHNICAL BASIS FOR PREDICTING BEHAVIOR OF FLAWED STEAM GENERATOR TUBES IN SEVERE ACCIDENTS

## 5.1 Introduction

This report summarizes the technical basis for predicting ligament-rupture pressure, crack-opening area, and unstable burst pressure of steam generator (SG) tubes with flaws under severe-accident transients. The content of this report is based on research carried out by the Nuclear Engineering Division of Argonne National Laboratory (ANL), under U.S. Nuclear Regulatory Commission (NRC) sponsorship and the results reported in NUREG/CR-6575, "Failure Behavior of Internally Pressurized Flawed and Unflawed Steam Generator Tubing at High Temperatures—Experiments and Comparison with Model Predictions," issued 1998 (Ref. 1), and NUREG/CR-6756, "Analysis of Potential for Jet-Impingement Erosion from Leaking Steam Generator Tubes during Severe Accidents," issued May 2002 (Ref. 2).

To develop an understanding of the risks associated with SG tube rupture, the NRC contracted with ANL in 1995 to develop rupture pressure and leak rate correlations for tubes with flaws and validate them by subjecting them to pressures and temperatures associated with severe-accident transients. The NRC subsequently published the results from the ANL study in NUREG/CR-6575 and NUREG/CR-6756.

Operating experience with pressurized-water reactor SGs in both the United States and abroad has shown that cracks of various morphologies can and do occur in SG tubes, starting early in life. These may be single cracks that are axial or circumferential, inside diameter (ID) or outside diameter (OD) initiated, and part-through-wall or through-wall, or multiple cracks that are parallel or form a network. Tests have shown that, depending on the location and morphology of these cracks, the SG tubes can be weakened to various extents.

Under normal operating conditions, the temperature in an SG is about 300 degrees Celsius (C) (572 degrees Fahrenheit (F)), and the pressure across the tube wall, $\Delta p_{no}$, is about 9 megapascals (MPa) (1,300 pounds per square inch (psi)). Under design-basis accidents, such as a main steamline break (MSLB) in which the secondary side has dropped to atmospheric pressure, the pressure across the tube wall, $\Delta p_{MSLB}$, is 18 MPa (2,560 psi) and the temperature of the SG tubing is less than 350 degrees C (662 degrees F). In this temperature range, creep effects are negligible in Alloy 600. Degraded tubes must actually be capable of withstanding $3 \cdot \Delta p_{no} \approx 27$ MPa (3,900 psi) and $1.4 \cdot \Delta p_{MSLB} \approx 25$ MPa (3,660 psi) to meet requirements for continued operation. For typical unflawed SG tubes made of Alloy 600, the failure pressure, $p_b$, at these temperatures is about 65 MPa (9,400 psi).

Severe accidents involving significant core damage are unlikely events in nuclear reactors. Even in the unlikely event that such an accident should occur, in most cases any potential risk to the public is mitigated by the presence of a robust containment. The behavior of SG tubing during such severe accidents is of particular interest, since failure of the SG tubes could lead to bypass of the containment. The accident sequences that appear to produce the greatest risk of SG tube failure are those in which the reactor pressure vessel fails to depressurize, but depressurization does occur on the secondary side. The NRC is pursuing studies to better understand the progression of such sequences, the temperature of the SG tubes during such accidents, and the behavior of SG tubes at the high temperatures associated with such accidents. At these high temperatures, plastic deformation is likely to be much more extensive than at normal reactor operating temperatures, and creep effects may no longer be negligible.

The development and validation of models to describe the failure of flawed SG tubes at high temperatures was a major objective of the ANL study. The tests conducted and the models developed do not attempt to accurately simulate any particular severe-accident scenario; rather they are intended to provide tools that can be used to determine failure under a broad range of pressure and temperature histories.

## 5.2 Ligament-Rupture Pressure

### 5.2.1 Analytical Failure Models

There is substantial literature on the development and validation of analytical models to describe the behavior of flawed tubes at normal reactor operating temperatures 288–320 degrees C (550–608 degrees F). These models and data can be used to analyze the potential for failure during design-basis accidents, during which the temperature of the SG tubing is less than 350 degrees C (662 degrees F). In this temperature range, creep effects are negligible in Alloy 600. However, in postulated severe accidents, much higher temperatures are possible. At these higher temperatures, plastic deformation is likely to be much more extensive than at normal reactor operating temperatures, and creep effects can no longer be neglected. Until recently, there were no test data or validated models to predict the failure of flawed tubes at temperatures associated with postulated severe accidents.

*5.2.1.1 Axial Cracks*

*5.2.1.1.1 Flow-Stress Model*

ANL developed two analytical models for predicting ligament-rupture pressure of tubes with axial part-through-wall flaws at elevated temperatures. The first one, based on flow-stress theory, was obtained by slightly modifying an empirical stress magnification factor $m_p$ (Ref. 3), which depends only on the geometry of the flaw and the tube but is independent of the flow stress of the tube material. The modified form of the $m_p$ factor developed by ANL is as follows:

$$m_p = \frac{1 - \alpha \frac{a}{mh}}{1 - \frac{a}{h}} \tag{5.1}$$

where

$$\alpha = 1 + \left(\frac{a}{h}\right)^2 \left(1 - \frac{1}{m}\right)$$

a = crack depth

h = tube wall thickness

m = bulging factor used for predicting unstable burst pressure of tubes with through-wall axial cracks and is given by

$$m = 0.614 + 0.481\lambda + 0.386\exp(-1.25\lambda)$$

where

$$\lambda = \left[12(1-\nu^2)\right]^{\frac{1}{4}} \frac{c}{\sqrt{R_m h}} = \frac{1.82c}{\sqrt{R_m h}}$$

2c = axial crack length

$R_m$ = mean radius of the tube

$\nu$ = Poisson's ratio

The ligament rupture ($p_{sc}$) and unstable burst ($p_{cr}$) pressures are obtained by reducing the unstable burst pressure ($p_b$) of the unflawed tube by dividing it by $m_p$ and m, respectively; i.e.,

$$p_{sc} = \frac{\bar{\sigma} h}{m_p R_m} = \frac{p_b}{m_p} \text{ and} \qquad (5.2a)$$

$$p_{cr} = \frac{\bar{\sigma} h}{m R_m} = \frac{p_b}{m} \qquad (5.2b)$$

where $\bar{\sigma}$, the flow stress of the material, is defined as an average of the yield and ultimate tensile strengths ($\sigma_y+\sigma_u$)/2 and the unstable burst pressure of the unflawed tube is given by

$$P_b = \frac{\bar{\sigma} h}{R_m} \qquad (5.2c)$$

Tests conducted at ANL validated Equations 5.2a and 5.2b at low temperatures on Alloy 600 tubes with axial EDM notches (Figures 5-1a and 5-1b). (An EDM notch is a mechanically simulated defect, which is made by removal of material with an electrostatic discharge machine (EDM).)

The generalized flow-stress model assumes that, for any arbitrary history of hoop stress $\sigma(t)$ and temperature T(t), failure occurs at a temperature T and hoop stress $\sigma$ whenever the following failure equation is satisfied, independent of stress-temperature history:

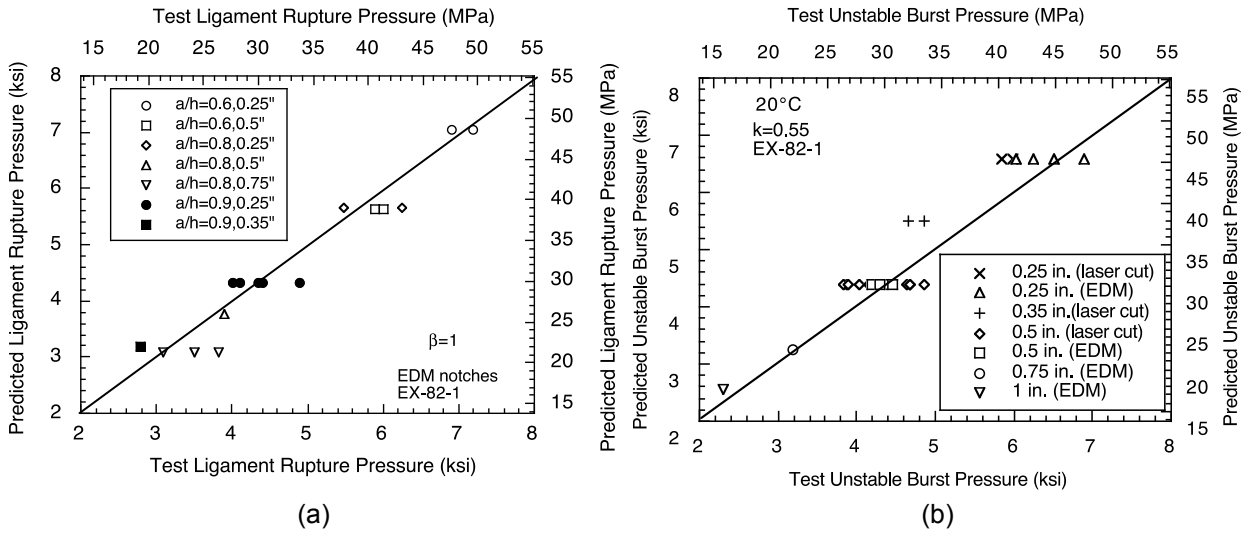


**Figure 5-1 Predicted vs. observed (a) ligament-rupture pressures and (b) unstable burst pressures of Alloy 600 tubes with axial notches at room temperature**

$$\sigma = \frac{\overline{\sigma(T)}}{m_p} \tag{5.3}$$

where $\overline{\sigma(T)}$ is the flow stress at temperature T and $m_p$ is the stress-magnification factor.

Figure 5-2 plots flow stresses for Alloy 600 computed from the above data, together with others from various sources. Most of these tests were conducted under stroke-control at a nominal strain rate of 34 percent/minute (min). Figure 5-2 also shows data from room-temperature tensile tests on the tubing being tested at ANL. The flow stress decreases markedly with temperature above 600 degrees C (1,112 degrees F). Note that, although there may be a wide variation in the flow stress at low temperatures, the heat-to-heat and product form variations in the flow stress diminish rapidly with increasing temperature. The Idaho National Engineering Laboratory (INEL) flow-stress curve, which covers the widest range of temperature, is used for failure predictions.

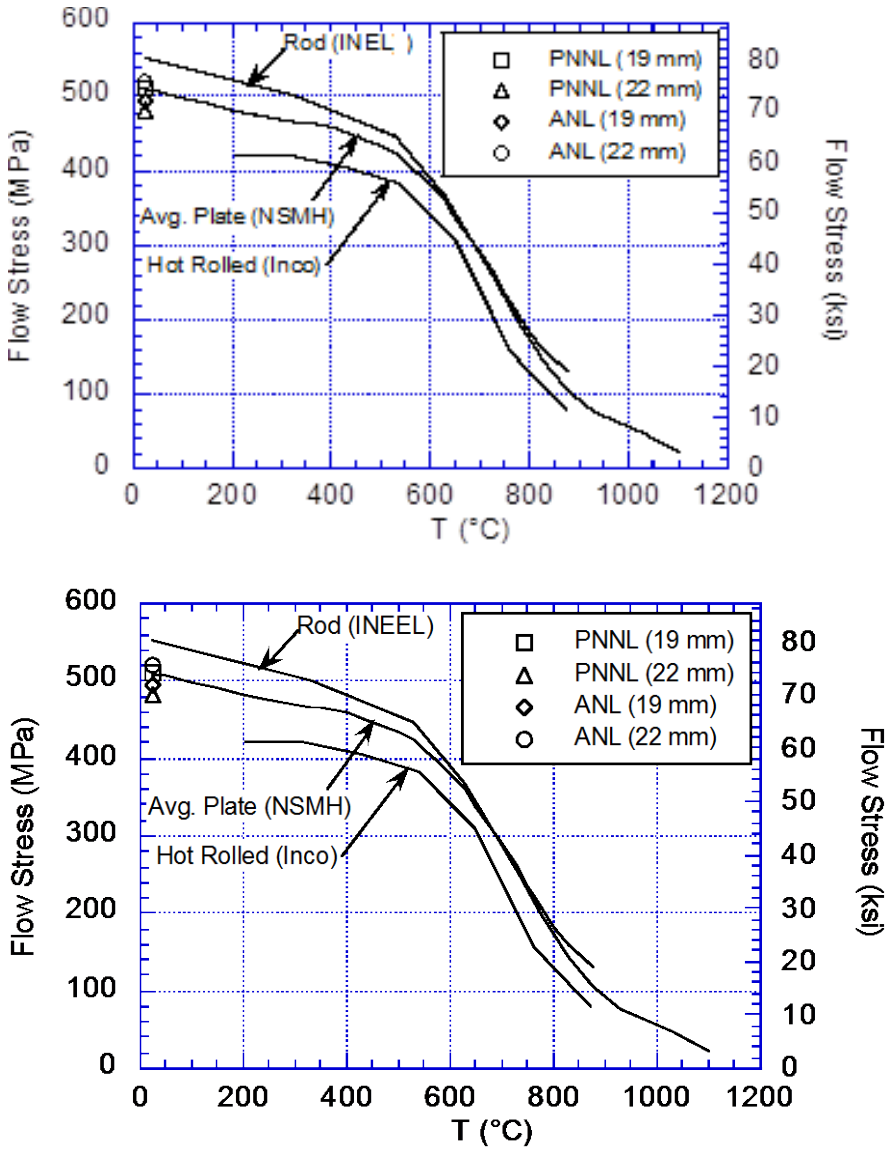


**Figure 5-2 Flow-stress curves for various product forms of Alloy 600**

*5.2.1.1.2 Creep-Rupture Model*

In the creep-rupture model, creep failure of an unflawed tube under a varying stress and temperature history can be predicted by a relatively straightforward analysis (Ref. 4), based on a linear time-fraction damage rule, such as used in the American Society of Mechanical Engineers (ASME) Boiler and Pressure Vessel Code, Section III, Subsection NH, as follows:

$$\int_0^{t_f} \frac{dt}{t_R(T,\sigma)} = 1 \qquad (4a)$$

where $t_R$ is the time to creep rupture for a uniaxial specimen under a stress $\sigma$ and temperature T, both of which may be functions of time, and $t_f$ is the time to failure of the tube. In the

creep-rupture model for flawed tubes, it was assumed that failure can be predicted by the following equation:

$$\int_0^{t_f} \frac{dt}{t_R(T, m_p\sigma)} = 1 \qquad (4b)$$

The available literature data on the creep-rupture properties of Alloy 600 were reviewed. Figure 5-3 shows a least-squares best fit, along with the estimated ±95 percent confidence limits.

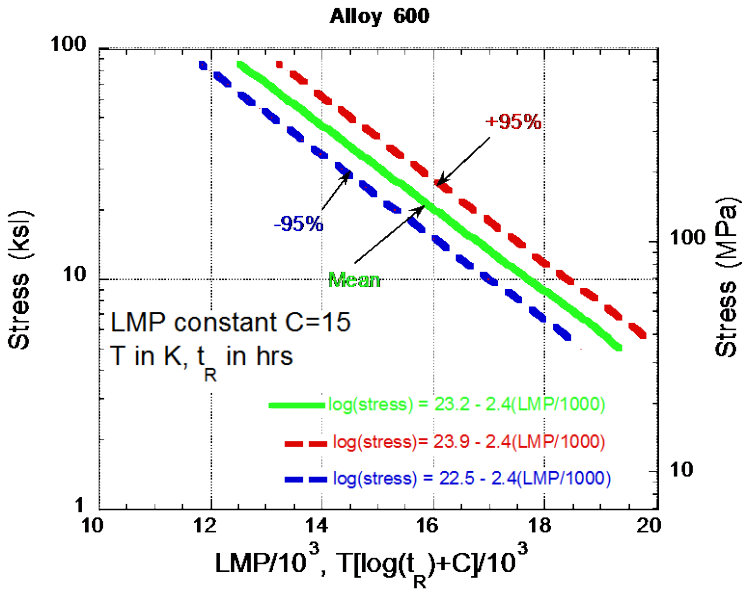


**Figure 5-3 Larson-Miller plot for Alloy 600 tubes**

In equation form, the Larson-Miller parameter is given by

$$\text{LMP} = (23.2 \pm 0.7 - 2.4 \ln\sigma) \times 103 \text{ for } \sigma > 5.7 \text{ ksi} \qquad (5.4)$$

where the time to rupture $t_R$ is then given by

$$t_R = 10^{\frac{10^{-3} LMP}{T} - 15} \qquad (5.5)$$

with $t_R$ in h and T in K.

*5.2.1.2 Circumferential Cracks*

*5.2.1.2.1 Through-Wall Circumferential Cracks*

Failure loads of tubes with a single circumferential crack critically depend on the bending constraint imposed externally on the tubes. The two extreme cases are the free-bending case

and the fully constrained case. In reality, SG tubes are partially constrained against bending by tube support plates.

**Free-Bending Case**

For an unconstrained (free-to-bend) tube with a through-wall crack of angular length $2\theta$, where $\theta$ is the circumferential angle of the tube cross-section, and no applied primary bending stress, the critical failure pressure is (Ref. 5):

$$p_{cr} = \frac{2\bar{\sigma}h}{R_m}\left(1 - \frac{\theta}{\pi} - \frac{2\beta}{\pi}\right) \tag{7a}$$

where the angular location of the neutral axis is given by

$$\beta = \sin^{-1}\left(\frac{\sin\theta}{2}\right) \tag{7b}$$

**Fully Constrained Case**

Equation 7a is applicable to one extreme case, where the tube is completely free to bend. In the opposite extreme case of total constraint against bending, a criterion based on maximum shear stress in the net section (Ref. 1) can be used to calculate the instability limit pressure:

$$p_{cr} = \frac{2(\gamma^2 - 1)(\pi - \theta)\bar{\sigma}}{2\pi + (\pi - \theta)(\gamma^2 - 1)} \tag{8a}$$

where

$$\gamma = \frac{R_o}{R_i} \tag{8b}$$

The following thin-shell, uniaxial approximation to Equation 8a is often used to predict the failure of SG tubes that are fully constrained against bending:

$$p_{cr} = \frac{2\bar{\sigma}h}{R_m}\left(1 - \frac{\theta}{\pi}\right) \tag{8c}$$

In reality, the tube support plates offer significant but not total restraint against bending, a circumstance that tends to increase the failure pressure to somewhere between the pressure of those predicted by Equations 7a and 8a (or 8c).

*5.2.1.2.2 Part-Through-Wall Circumferential Cracks*

Consider a tube with mean radius $R_m$ and wall thickness h, that contains either two symmetrical part-through circumferential cracks (SC) (Figure 5-4a) or a single part-through circumferential crack (Figure 5-4b) of angular length $2\theta$ and depth a. At low temperatures, where creep effects

are negligible, the ligament-failure pressure ($p_{sc}$) is generally expressed in terms of a stress-magnification factor ($m_p$) by equating the magnified axial stress in the ligament to the flow stress,

$$p_{sc} = \frac{2\bar{\sigma}h}{R_m m_p} \tag{5.6}$$

Failure pressure for circumferentially cracked tubes (i.e., the value of the stress-magnification factor $m_p$), depends strongly on the degree of restraint the tubes are subjected to against bending. The two extreme cases (i.e., the free-bending case and the completely constrained case) are relatively easy to analyze. Generally, SG tubes are sufficiently constrained laterally that the failure loads are expected to be much closer to the completely constrained case than the free-bending case. The discussion here assumes that the tubes are either completely constrained or are completely free to bend.

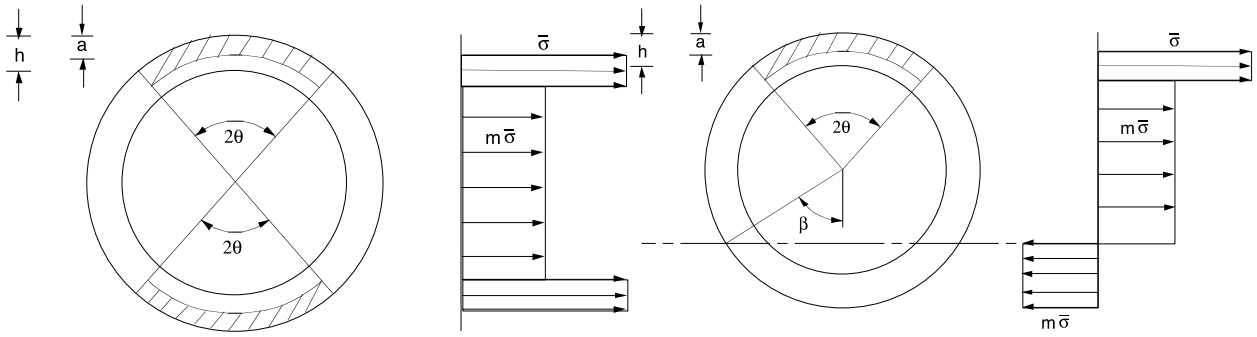


(a) (b)

**Figure 5-4 Stress distributions through section at failure of tubes with (a) two symmetrically located part-through circumferential cracks and (b) single part-through circumferential crack**

### Fully Constrained Case

The fully constrained case would also include the case for an unrestrained tube that contains two symmetrical cracks (Figure 5-4a). In this case, the whole section that contains the crack (or cracks) is subjected to axial tensile stress, with the ligament (or ligaments) being subjected to stress intensification. If the average stress in the ligament (or ligaments) is expressed as 1/m times the average stress in the rest of the section that contains the crack (or cracks), the average ligament axial stress ($\sigma_{lig}$) can be calculated from a simple equilibrium of axial forces,

$$\sigma_{lig} = \frac{pR_m}{2h} \frac{1}{\left[m + \left(\frac{n\theta}{\pi}\right)\left(1 - \frac{a}{h} - m\right)\right]} \tag{10a}$$

where

n = 1 for a single crack
n = 2 for 2 symmetrical cracks.

Defining mp as the ratio of the average ligament axial stress and the average axial stress in the unflawed tube, $m_p$ is given by

$$m_p = \frac{1}{\left[m + \left(\frac{n\theta}{\pi}\right)\left(1 - \frac{a}{h} - m\right)\right]} \tag{10b}$$

Originally, the following empirically obtained expression was used (Ref. 6).

$$m = 1 - \left(\frac{a}{h}\right)^{\kappa}\left(\frac{n\theta}{\pi}\right)^{\mu} \tag{11}$$

with n = 1.

Although Kurihara recommended values of $\kappa = 2$ and $\mu = 0.2$ for the exponents, the results are almost indistinguishable from those obtained by using $\kappa = 3$ and $\mu = 0.3$. Because the behavior of Equation 11 is not correct (i.e., m does not tend to 0) when a/h tends to 1 for all $\theta$, it was modified to have the same form as in the case of axial cracks; that is,

$$m = \frac{1 - \frac{a}{h}}{1 - \frac{a}{Nh}} \tag{12a}$$

where

$$N = 1 + \lambda\left(\frac{n\theta}{\pi}\right)^{\gamma} \tag{12b}$$

and $\lambda$ and $\gamma$ are fitting parameters.

Both the failure modes and moments of the original set of test data from four-point bending failure tests on pressurized part-through circumferentially cracked Type 304 stainless steel pipes at room temperature (used by Kurihara) can be predicted somewhat better by the current model with $\lambda = 0.2$ and $\gamma = 0.2$ and by defining the flow stress as $0.55[\sigma_y + \sigma_u]$, (see Figures 5-5a and 5-5b for two possible empirical models).

Unsymmetrical part-through circumferentially cracked 165.2-mm diameter (11-mm wall thickness) pipe specimens were subjected to a four-point bend test with a constant internal pressure of 6.9 MPa (1,000 psi) at room temperature). Dashed lines denote predicted failure bending moments for through-wall cracks, open symbols denote tests that failed by leakage, and filled symbols denote those that failed by breaking into two pieces.

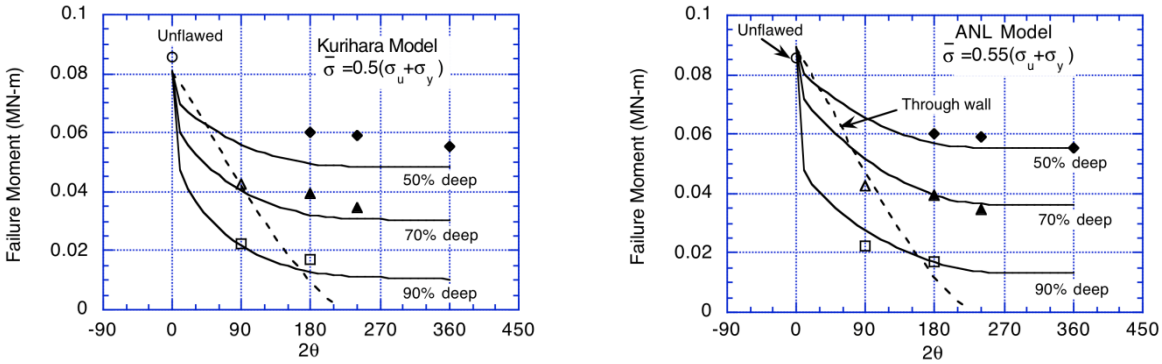


**Figure 5-5 Variations of experimental failure bending moments with crack angle and those predicted by (a) Kurihara model and (b) ANL model**

### Free-Bending Case

Figure 5-4b shows that, in the free-bending case, part of the section that contains the crack will, in general, be subjected to compressive stress. As a result, Equation 10a must be replaced by

$$\sigma_{lig} = \frac{pR_m}{2h}\frac{1}{\left[m\left(1-\frac{2\beta}{\pi}\right)+\left(\frac{n\theta}{\pi}\right)\left(1-\frac{a}{h}-m\right)\right]} \tag{13a}$$

where the angle $\beta$ that defines the location of the neutral axis is given by

$$\beta = \sin^{-1}\left\{\frac{\sin\theta}{2}\left[1-\frac{1}{m}\left(1-\frac{a}{h}\right)\right]\right\} \text{ for } \beta \le \pi - \theta \tag{13b}$$

and Equation 10b has to be replaced by

$$m_p = \frac{1}{\left[m\left(1-\frac{2\beta}{\pi}\right)+\left(\frac{n\theta}{\pi}\right)\left(1-\frac{a}{h}-m\right)\right]} \tag{13c}$$

with m and N defined by Equations 12a and 12b, respectively.

## 5.2.2 Validation Tests for Ligament Rupture

### *5.2.2.1 Validation Tests for Axial Notches*

Seventy-three tests designed to validate the ANL creep-rupture model were carried out in the high-temperature test facility using three types of loading histories. The tests were conducted on 19.1-mm ($^3/_4$-in.) and 22.2-mm ($^7/_8$-in.) diameter Alloy 600 tubes that contained a variety of EDM flaws. Such flaws are typically 0.0203-centimeter (cm) (0.008-inch [in.]) wide and are not as sharp as real cracks, but previous tests at lower temperatures have shown that the failure pressures of specimens with corrosion cracks are at most about 10 percent less than those predicted by failure correlations developed from specimens with machined flaws (Ref. 7). At higher temperatures, because of crack tip blunting, the effect of the initial crack tip geometry would be expected to be of even less significance.

**Measurement of Axial Flaw Depth**

The flaw depth and length are critical parameters in calculating the expected failure pressures of the tubes, and these dimensions must be determined as precisely as possible. The accurate determination of the flaw depths, in particular, poses some difficulties. Four methods were developed to measure the depths of the machined flaws. Two of these methods are applicable to the specimens before testing, one is performed after testing, and the fourth method is destructive and thereby prevents subsequent pressure testing of the specimen.

The first technique used to measure flaw depth was posttest fractography. In this method, the fracture surfaces of the failed specimen are photographed at a known magnification after the test, and the contrast between the machined portion of the fracture surface and the region of subsequent ductile fracture in the photograph permits a reasonably accurate determination of flaw depth.

The second technique used to measure flaw depth was replication of the premachined flaws. In this technique, a plastic replica was made of the flawed region of the specimen before testing, and the height of this replica, which corresponds to the depth of the flaw, was then determined by optical microscopy.

A third technique is to directly measure the flaw depth before testing with a traveling optical microscope that gives a digital readout of the x, y, and z positions of the objective lens. The flaw depth can be measured by focusing first on the outer surface of the specimen and then on the bottom of the machined flaw. The flaw depth corresponds to the movement of the microscope objective between these two steps; readings accurate to within about ±2,500 micrometer (μm) (±0.1 mil) are possible.

A fourth technique for determining flaw depth is destructive metallography of the flawed tube. The tube is simply sectioned through the flaw, and the depth at that position is determined from a microphotograph.

The ANL program used all four of these techniques, and NUREG/CR-6575 (Ref. 1) lists the results in a table. Aside from one invalid measurement, the agreement among the various techniques for these flaws was quite good. The largest variation in measured flaw depth was 0.02 mm (0.9 mils), or about a 6-percent variation between the values measured by pretest optical microscopy and posttest metallography. In general, the flaw depth values obtained by replication are slightly greater than those obtained by posttest fractography; the pretest

microscopy determinations agree reasonably well with the values obtained by replication. Because the posttest fractography values represent the only consistent set of values for all of the specimens, the analysis and modeling of the tests used these flaw-depth values.

*5.2.2.1.1 Constant Temperature/Pressure Rupture Tests*

Unflawed tubes, tubes with shallow notches (55–65-percent deep, 2.54 cm (1 in.) long) and tubes with deep notches (90-percent deep and 0.635–5.08 cm (0.25–2 in.) long) were tested under constant pressure and constant temperature conditions until failure. The unflawed tubes were tested at 700–800 degrees C (1,292–1,472 degrees F) and 12.4–31.0 MPa (1.8–4.5 kilopound per square inch [ksi]). The shallow notches were tested at 667–800 degrees C (1,233–1,472 degrees F) and 9.6–31 MPa (1.4–4.5 ksi) pressure, and the deep notches were tested at 800 degrees C (1,292 degrees F) and 2.1–3.1 MPa (0.30–0.45 ksi). The unflawed tubes and the tubes with shallow notches burst in an unstable manner with large crack opening and notch tip tearing. The predicted ligament-rupture pressures of the tubes with shallow notches were greater than the burst pressure of the 100-percent through-wall notches with the same length, thus precipitating burst immediately after ligament rupture. There was enough strain energy stored in these specimens to drive them to burst, even though the pump could not maintain the pressure after ligament rupture. The deep flaws failed by ligament rupture with very little crack opening and stored energy. Figure 5-6 shows a plot of the predicted (creep-rupture model) vs. observed failure pressures of the specimens. In all cases, the failure pressures are predicted to within ±95 percent prediction limits. It should be noted that the flow-stress model is incapable of predicting time to failure for tests of this type and, in fact, would predict that none of the tubes should have failed.

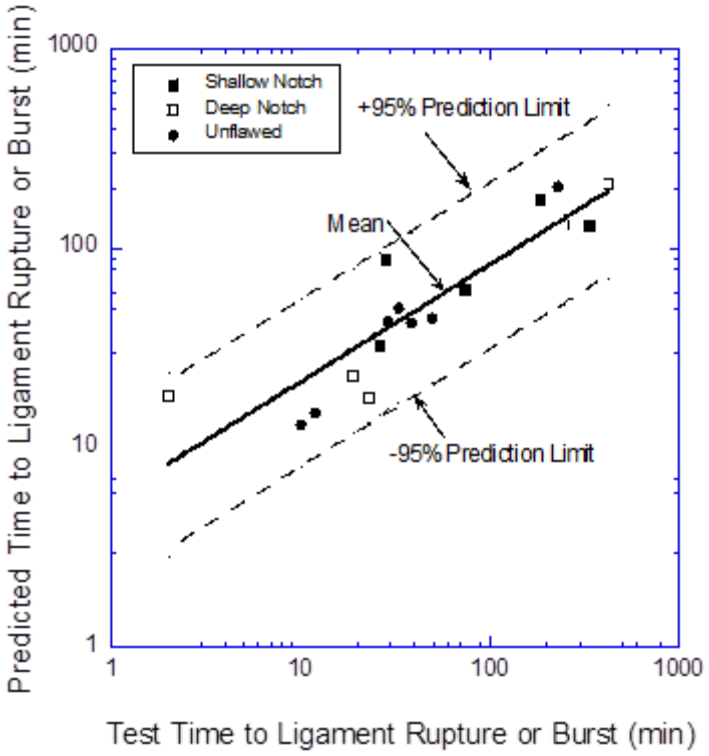


**Figure 5-6 Predicted vs. observed time to failure of flawed and unflawed tubes under constant temperature and pressure condition**

*5.2.2.1.2 Pressure and Temperature Ramp Tests*

To evaluate the importance of loading rates on the failure conditions and compare the predictive capabilities of the creep-rupture model and the flow-stress model, two additional types of tests were conducted. In the first type, the specimens were heated to a temperature and then pressurized isothermally at a constant pressure ramp until failure. In the second type, the specimens were first pressurized at low temperature and then, with the pressure held constant, were subjected to a constant temperature ramp until failure.

*5.2.2.1.3 Pressure Ramp Tests*

Eleven pressure ramp tests were conducted on notched and unnotched specimens. Most of the tests were conducted at a pressure ramp of 16 MPa/min (2.3 ksi/min) while the specimens were held at a constant temperature. The test temperature varied between 700 and 840 degrees C (1,292 and 1544 degrees F). Two tests were conducted at 1.6 MPa/min (0.23 ksi/min) on unnotched specimens. Figures 5-7a and 5-7b show plots of the observed failure pressures vs. failure pressures predicted by the creep-rupture model and the flow-stress model, respectively. For both ramp rates, the creep-rupture model gives more consistent and accurate predicted failure pressures than the flow-stress model.

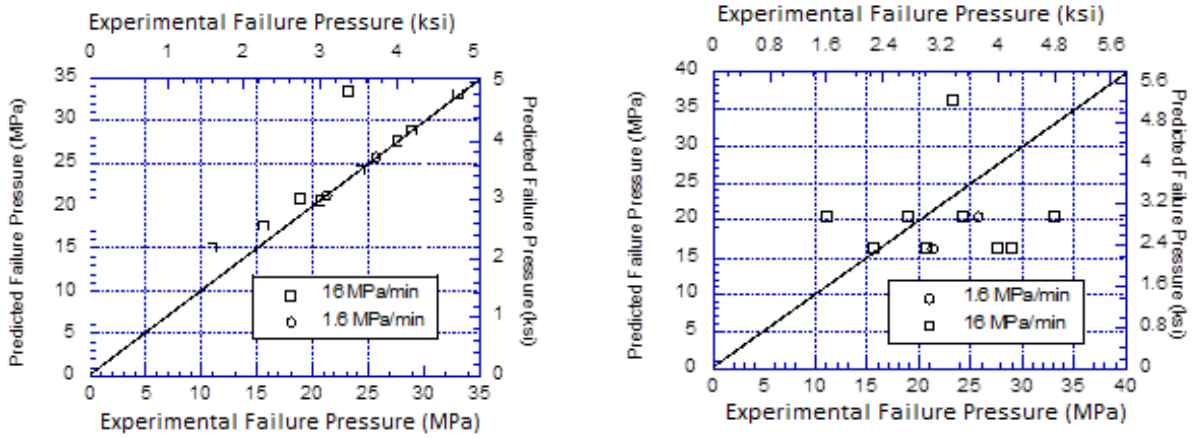


**Figure 5-7 Predicted vs. observed failure pressures for isothermal (700–840 degrees C) pressure ramp tests on unflawed and flawed tubes 0.25–1 in. long and 65–80 percent deep by (a) creep rupture model and (b) flow-stress model**

Figure 5-8 shows a plot of the same set of data but plotted as effective flow stress (i.e., $m_p$ x $\sigma_h$ at failure) vs. test temperature. Figure 5-8 also includes a flow stress vs. temperature plot (solid line) obtained from conventional tensile tests. Note that the experimentally derived effective flow stress increases with the ramp rate and the flow-stress model using the flow-stress curve (from tensile tests) would underpredict the failure pressures significantly. Figure 5-8 clearly demonstrates that, for the flow-stress model to be able to predict the failure pressures correctly, the flow-stress curve has to be a function of the ramp rate. On the other hand, the creep-rupture model automatically takes the rate effect into account.

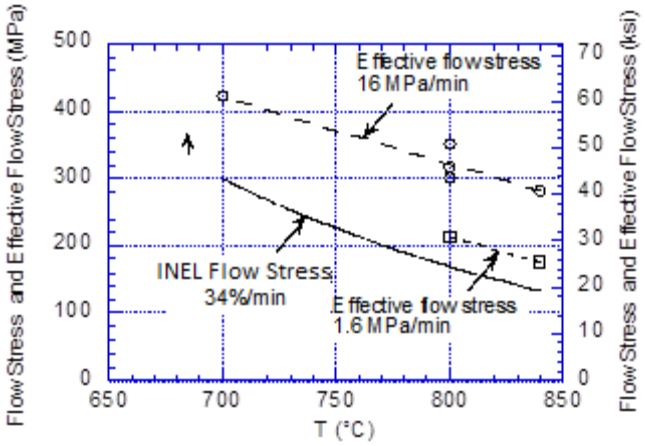


**Figure 5-8 Effective flow-stress curves (dashed lines) computed from the pressure ramp tests (symbols) vs. temperature of test**
***Also shown is the standard flow-stress curve of Alloy 600 (solid curve).***

*5.2.2.1.4 Temperature Ramp Tests*

Thirteen flawed and unflawed specimens were tested at various temperature ramp rates. The flaw lengths in the tests varied from 0.64–5.1 cm (0.25–2 in.) and the flaw depths varied from 65–93 percent. Three temperature ramp rates were chosen, 0.2, 2, and 20 degrees C/min. During the tests, the specimens were held at constant pressures ranging from 1.38–16.20 MPa (0.22–2.35 ksi). Figures 5-9a and 5-9b compares the observed failure temperatures with those predicted by the creep-rupture and flow-stress models, respectively. It is evident that the creep-rupture model predicts the failure temperatures much more accurately than the flow-stress model.

Two notched tests were specifically designed such that the product of $m_p$ and the nominal hoop stresses were approximately equal. Thus, the predicted failure temperatures for both geometries fall approximately on a single line for either the creep-rupture or flow-stress models, as shown in Figure 5-10. The experimental results are in much better agreement with the predictions of the creep-rupture model and confirm that the effect of flaws on failure can be characterized by the $m_p$ approach. Therefore, the creep-rupture model can be expected to predict failure under varying temperature and pressure histories during severe accidents more reliably than a simple rate-independent flow-stress model.

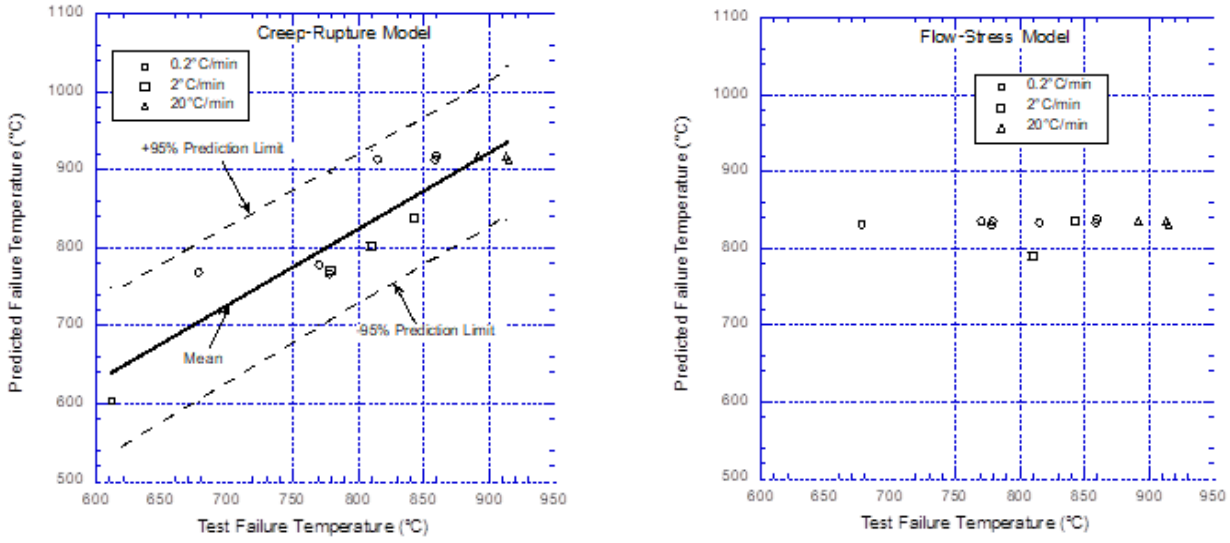


(a) (b)

**Figure 5-9 Comparison of observed failure temperatures with those predicted by (a) creep rupture model and (b) flow-stress model for temperature ramp tests**

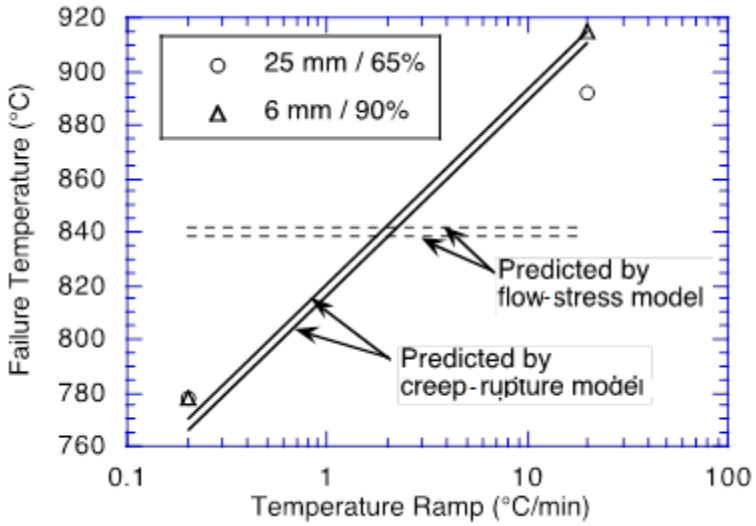


**Figure 5-10 Comparison of predicted failure temperatures by the creep rupture and flow stress models for flawed specimens as a function of temperature ramp rate**

*5.2.2.1.5 Tests under Simulated Severe Accident Time-Temperature Histories*

Finally, ANL performed tests to determine the behavior of flawed tubes under time/temperature histories similar to those projected to occur under severe-accident conditions. The purpose of the tests was to further validate the creep-rupture model to support its use in determining the time to failure of flawed tubes under projected time/temperature histories that could reach temperatures as high as 850 degrees C (1,562 degrees F).

In all the tests, the internal pressure was held constant at 16.2 Mpa (2,350 psi). Tests were conducted on both 19.1-mm (3/4-in.) and 22.2-mm (7/8-in.) diameter tubes with wall thicknesses of 1 mm (0.043 in.) and 1.3 mm (0.050 in.), respectively. Four different nominal flaw geometries with axial lengths of 6 mm (0.25 in.), 25 mm (1 in.), and 50 mm (2 in.), and depths varying from 20 percent to 65 percent of thickness were tested. Duplicate tests were run for all the 22.2-mm (7/8-in.) diameter tube tests. Rupture tests were also run on unnotched virgin samples.

The tests considered two time/temperature histories. Both were based on preliminary analyses of an accident sequence involving total station blackout (SBO) with a stuck-open SG secondary-side atmospheric dump valve, resulting in loss of feed water and secondary-side depressurization. One, which is referred to as the "INEL ramp," was based on a preliminary analysis by INEL and the other, referred to as the "EPRI ramp," was based on a preliminary analysis reported by the Electric Power Research Institute (EPRI). Figures 5-11a and 5-11b show the time-temperature scenarios calculated by INEL [5] and EPRI [6] for some postulated severe-accident sequences, respectively, which also show the time-temperature histories used in the ANL tests. In both series of tests, the specimens were first heated rapidly to 300 degrees C (572 degrees F), equilibrated at 300 degrees C (572 degrees F), and then subjected to the test ramps. Both analyses also predict depressurization of the system because of the failure of the surge line. Because the primary purpose of the tests was to help develop a failure model, the tests have ignored the predicted depressurization. The EPRI analysis also predicts a reduction in temperature following a short 5-min hold at 667 degrees C (1,232 degrees F). To increase the contribution of creep damage in the tests, the EPRI temperature history was arbitrarily modified to include a 2-hour holdtime at 667 degrees C (1,232 degrees F) and ignored the predicted reduction of temperature after the hold. If the specimen did not fail in 2 hours of constant temperature hold, it was subjected to a temperature ramp of 2 degrees C/min until failure. Neither ramp chosen for the tests was intended to be an accurate representation of a particular sequence, but together they can represent a range of histories for which a failure model would be needed. Thus, although the INEL and EPRI analyses predict that failure of the surge-line nozzle and consequent depressurization of the system will occur before the failure of the SG tubes, with or without flaws, ANL continued the tests at full pressure until failure occurred.

Figures 5-12a and 5-12b compare the observed vs. predicted failure temperatures (calculated by the flow-stress and creep-rupture models). The creep-rupture model gives a uniformly more accurate prediction of the failure temperatures than the flow-stress-model. Again, the difference in prediction between the two models arises because the creep-rupture model includes rate effects, which are ignored by the flow-stress model.

---

[5] See P. G. Ellison, et. al, "The Risk Significance of Induced Steam Generator Tube Rupture," INEL-95/0641, Rev. 1 (Draft), Lockheed Martin Idaho Technologies, Inc., Idaho National Engineering Laboratory (now Idaho National Engineering and Environmental Laboratory (INEEL)), December 15, 1995.

[6] See E. L. Fuller, et. al, "Risks from Severe Accidents Involving Steam Generator Tube Leaks or Ruptures," EPRI TR--106194, Electric Power Research Institute, Palo Alto, CA (to be published).

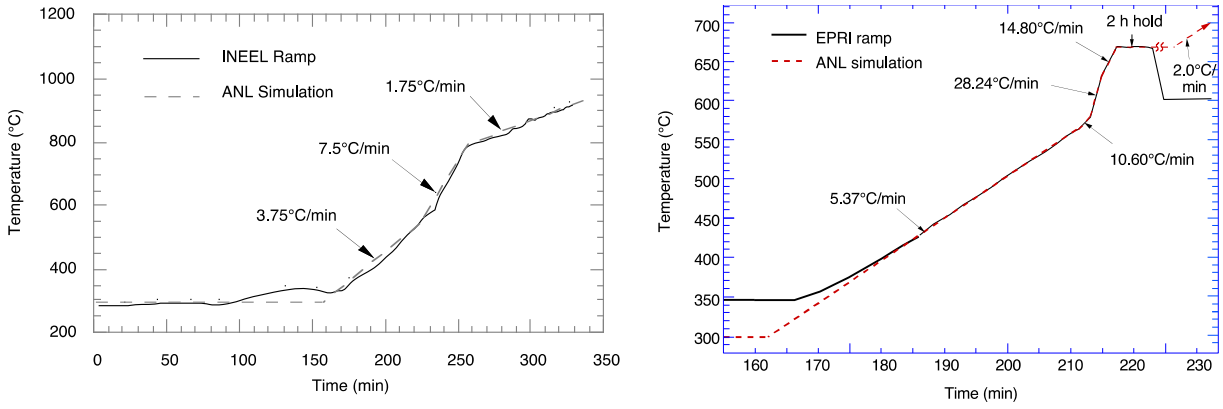


(a) (b)

**Figure 5-11 Calculated and ANL simulation of (a) INEL ramp and (b) EPRI ramp for high temperature tests**

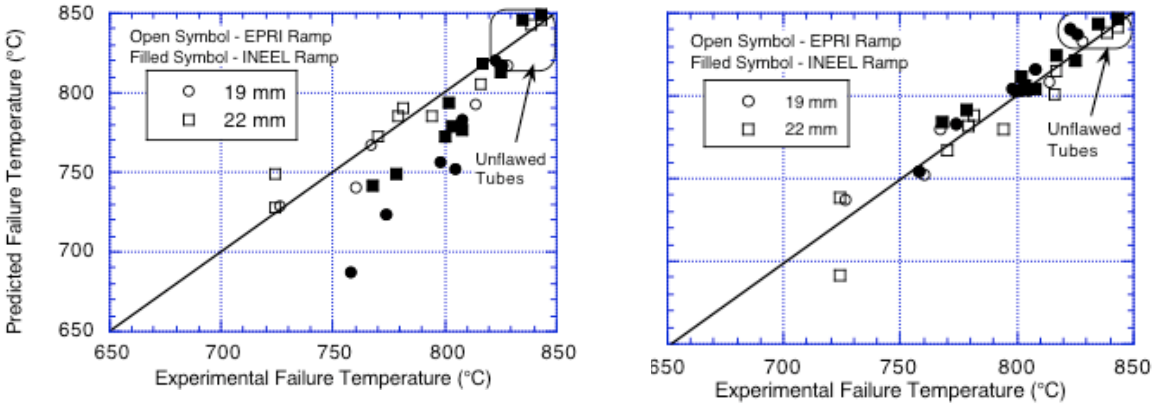


(a) (b)

**Figure 5-12 Observed vs. predicted failure temperatures by (a) creep-rupture model and (b) flow-stress model for tests simulating severe-accident transients**
***Tests were conducted on 19-mm (0.75-in.) as well as 22-mm (0.875-in.) diameter Alloy 600 tubes.***

### *5.2.2.2 Validation Tests for Circumferential Notches*

In contrast to axial cracks, only 15 failure tests with part-through circumferential cracks were conducted. These tests had a single loading history that consisted of a constant internal pressure of 16.2 MPa (2,350 psi) and a temperature ramp of 10 degrees C/min from 300–600 degrees C, followed by a temperature ramp of 2 degrees C/min to ligament failure. As in the case of axial cracks, all specimens were depressurized immediately after ligament failure.

Constraint to bending was simulated by testing specimens with two symmetrically located cracks (Figure 5-4a). Tests were also conducted on unconstrained tubes with a single circumferential crack. In all but one case, the crack opening at failure was significantly smaller than the openings observed for axial cracks. The only exception was a single tube with a 360-degree crack; this tube broke into two pieces. Most tests failed by developing pinhole leaks

in the ligament. A single tube with a 240-degree crack failed by ligament failure across the whole front of the flaw.

As expected, all of the tubes with symmetrical flaws failed without significant bending. Tubes with deep flaws showed little or no bulging of the section that contained the flaws; those with shallower flaws showed some bulging. In contrast, all of the specimens with a single crack showed significant bending at failure (Ref. 8).

*5.2.2.2.1 Tubes with Two Symmetrical Circumferential Flaws*

Specimens with cracks of angular length $2\theta$ = 90 degrees, 120 degrees, 150 degrees, and 180 degrees (which is a full 360-degree crack) were tested. To keep the effects of crack length separate from the effects of crack depth, the depth to thickness ratio a/h was kept approximately constant at 0.77 for most of the test specimens.

Figure 5-13 plots the failure temperatures against the flaw length of $2\theta$ in. Because of the variability of the crack depth around the circumference, the specimens with 360-degree ($2\theta$ = 180 degrees) cracks showed the largest scatter. However, the specimens with the highest failure temperature contained the shallowest cracks. The failure temperatures increased significantly when the crack depth was reduced at any angular crack length.

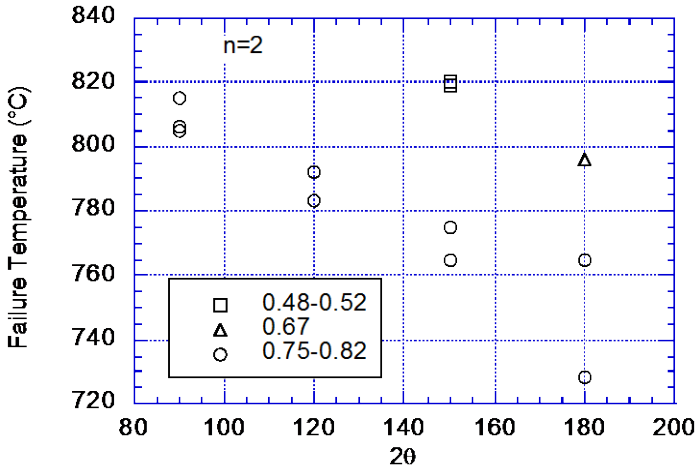


**Figure 5-13 Variation of failure temperatures with crack angle for specimens with two symmetrical cracks of various depths**

The failure temperatures for the tests were predicted by Equations 4b and 10b for mp. The $m_p$ values were calculated with both the Kurihara model (Equation 11) and the ANL model (Equations 12a and 12b). Figure 5-14 presents the predicted failure temperatures with the experimentally observed failure temperatures. On average, the ANL model gives a closer prediction of the failure temperatures than the Kurihara model. The maximum error in predicted failure temperature for the ANL model is 43 degrees C (109 degrees F).

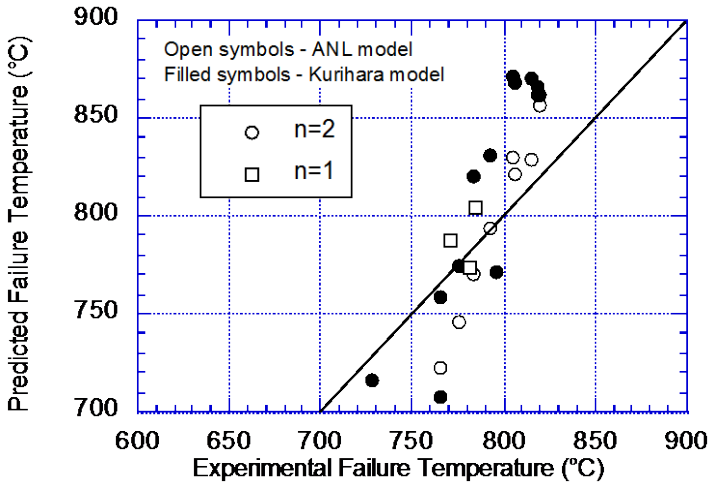


**Figure 5-14 Experimental failure temperatures and failure temperatures predicted by the Kurihara and ANL models for two symmetrical part-through circumferential cracks of various semiangular length θ**

*5.2.2.2.2 Tubes with a Single Circumferential Flaw*

Three failure tests were conducted on free-to-bend specimens with a single circumferential flaw (Ref. 8). Specimens with cracks of angular length $2\theta$ = 90 degrees, 180 degrees, and 240 degrees were tested.

The failure temperatures for the tests were predicted by Equation 16b, with $m_p$ given by Equation 13c. The $m_p$ values were calculated with the ANL model (Equations 12a and 12b). The predicted failure temperatures were close to the experimentally observed failure temperatures in all cases (Ref. 8).

*5.2.2.2.3 Comparison of Failure of Tubes with a Single Flaw and with Two Flaws*

The failure of tubes with two symmetrical cracks was usually initiated on the crack with the greater depth. However, very little overall bending of the specimen occurred. Conversely, significant bending occurred in the specimens with a single crack. The longer the crack, the more bending the specimen sustained.

All but one specimen with a 360-degree crack failed by ligament failure. A single specimen out of three with 360-degree cracks broke into two pieces. In most cases, ligament failure occurred locally, leading to a pinhole leak. One specimen with a single 240-degree crack failed by full ligament failure (accompanied by a loud noise). However, because of rapid depressurization of the specimen, the resulting through-wall crack did not propagate unstably to give rise to a guillotine break.

To demonstrate the influence of bending on failure pressure, Figure 5-15 plots the test results from both types of specimens against the total angular crack length (n = $2\theta$). Note that the specimens with 360-degree cracks may be considered either as specimens with a single 360-degree crack (n = 1) or two 180-degree cracks (n = 2). Thus, the failure temperatures for both types of cracked specimens coincide at n = $2\theta$ = 360 degrees. However, at smaller angles,

the free-to-bend specimens failed at lower temperatures than the specimens with two symmetrical cracks, as expected.

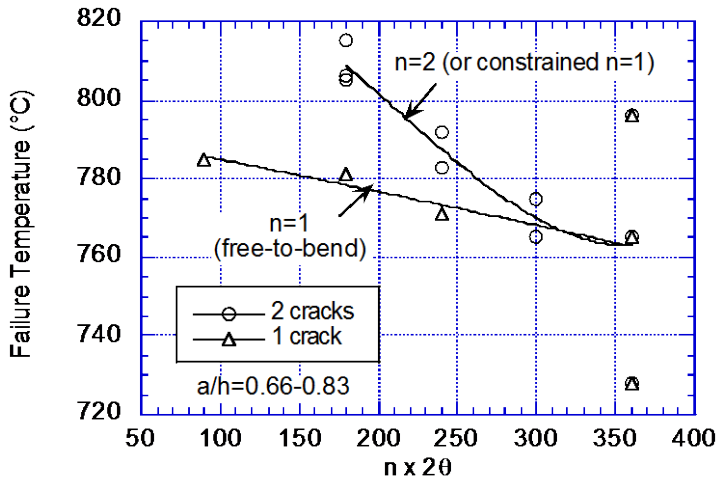


**Figure 5-15 Failure temperatures for specimens with one (n = 1) and two (n = 2) circumferential cracks**

## 5.3 Crack-Opening Rate at High Temperature

To determine the leak rate after through-wall penetration of axial cracks during severe accidents, it is necessary to estimate the crack opening area as a function of time. A simple model was developed to calculate the crack-opening area as a function of time and temperature during severe accidents. It is derived by analogy from a model that is applicable to cracks in a rectangular plate. The model was used to analyze crack-opening areas in flawed tubes subjected to severe-accident transients.

Consider a through-wall central crack of length 2c in a rectangular plate of width 2b (b>>c) subjected to a remotely applied axial load P. For a material with stress-plastic strain law

$$\frac{\varepsilon}{\varepsilon_0} = \alpha\left(\frac{\sigma}{\sigma_0}\right)^{m'} \tag{14}$$

the crack-opening displacement (COD) at the middle of the crack, ignoring elastic displacement, is given by:

$$\delta = \alpha\varepsilon_0 c h_2(c/b, m')\left(\frac{P}{P_0}\right)^{m'} \tag{15}$$

In Equation 15, $P_0$ = plastic collapse load and the function $h_2$ is tabulated in EPRI-NP-1931 (Ref. 9). Equation 15 was applied to the case of an axial crack in a relatively long SG tube by

replacing the remote stress with the nominal hoop stress $\sigma = \frac{\Delta pR}{h}$ (R and h are the mean radius and thickness of the tube and $\Delta p$ is the pressure differential), the collapse stress with $\sigma_0/m$ (m is the bulging factor) and by putting c/b = 0; i.e.,

$$\delta = ch_2(0,m')\frac{\alpha\varepsilon_0}{(\sigma_0)^{m'}}(m\sigma)^{m'} \tag{16}$$

Equation 16 is expected to give reasonable estimates of CODs as long as the pressure is small compared to the unstable burst pressure.

Equation 16 can be generalized for the high-temperature creep case as follows. If the material obeys a power law creep-rate equation; i.e.,

$$\dot{\varepsilon} = A\sigma^n \tag{17}$$

then the crack-opening rate is given by analogy with Equations 14 and 16 as follows:

$$\dot{\delta} = Ach_2(0,n)(m\sigma)^n \tag{18}$$

### 5.3.1 Creep-Rate Equation for Alloy 600

Figure 5-16 plots the creep-rate data obtained by INEL. The data at three temperatures can be collapsed onto a bilinear plot (log-log basis) by using activation energy of 65 kilocalorie (kcal)/mole and plotting the stress normalized by the Young's modulus at temperature, as shown in Figure 5-16.

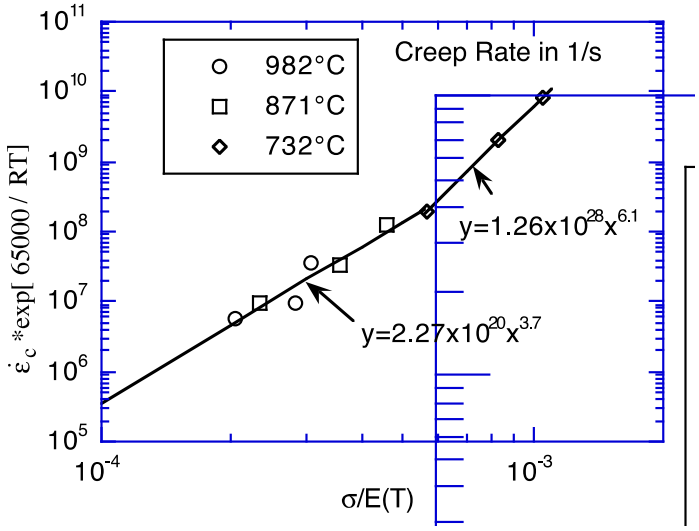


**Figure 5-16 INEL creep rate on Alloy 600 vs. stress data plotted using activation energy of 65 kcal/mole and stress normalized by Young's modulus at temperature**

### 5.3.2 Crack-Opening Area for Axial Cracks

Figure 5-17a plots the function $h_2$ (c/b, n) as a function of c/b for three values of n in. Since our interest is in the value of $h_2(0,n)$, the graphs were extrapolated to c/b = 0 by polynomial fits and the results plotted as a function of n in Figure 5-17b.

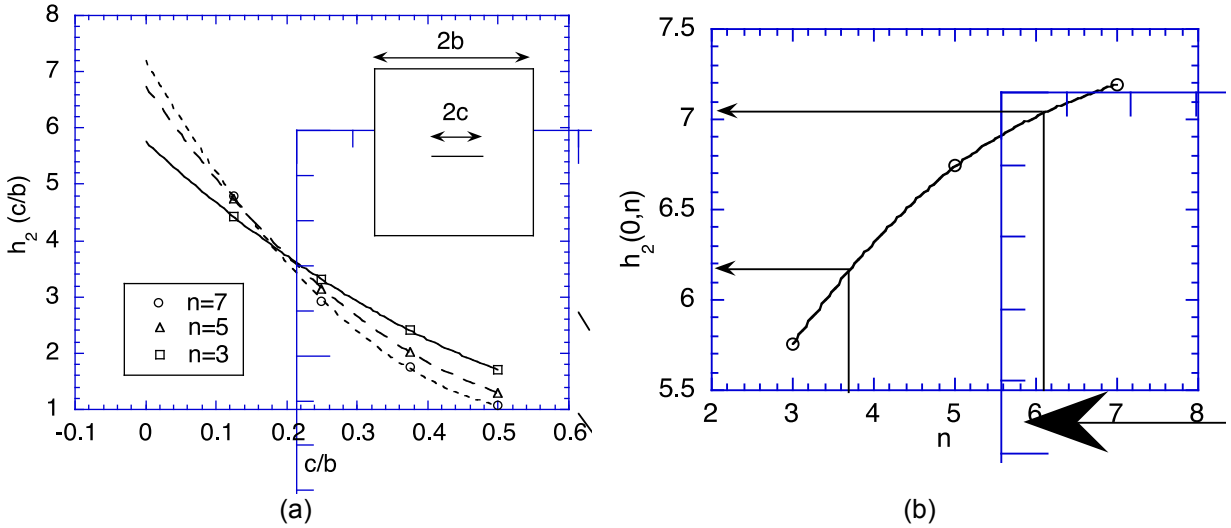


**Figure 5-17 Variations of Crack Opening Parameters**
**(a) Variation of $h_2$ (c/b,n) with c/b for various values of n**
**(b) Variation of $h_2$ (0,n) with n; Values of $h_2$ (0,n) are 7.03 and 6.16 for n = 6.1 and 3.7, respectively.**

### 5.3.3 Tests on Specimens with Circumferential Notches at High Temperature

Because in a tube under internal pressure, the crack-opening area for a given crack length is much greater for an axial crack than it is for a circumferential crack, the primary interest is in axial cracks. It is, however, extremely difficult to carry out creep tests on tubular specimens with through-wall axial notches subjected to internal pressure. The validation tests were conducted instead on axially loaded tube specimens with two symmetrical through-wall circumferential EDM notches (Figure 5-18a). The symmetrical notches minimize bending and ensure a pure tensile loading on the notches similar to that experienced by axial cracks in an internally pressurized tube. By keeping the notch lengths small, the effects of tube curvature can be minimized. The small interaction between the two notches can be taken into account by using equations applicable to cracks in rectangular plates of finite width (Figure 5-18b).

As mentioned earlier, the periodicity of the circumferential crack geometry requires that the corresponding rectangular plate be of finite width (Figure 5-18b). Equation 16 gives the COD of cracks in plates of finite width. For the current geometry, the remotely applied axial load $P = 2\pi Rh\sigma$ and the plastic collapse load $P_0 = 2(\pi-2\theta)Rh\sigma_0$, and Equation 16 reduces to the following:

$$\delta = c h_2\left(\frac{c}{b}, m'\right)\frac{\alpha\varepsilon_0}{(\sigma_0)^{m'}}\left(\frac{\pi}{\pi-2\theta}\sigma\right)^{m'} \qquad (19)$$

where $\sigma$ is the remotely applied axial stress, $2\theta$ is the angular length of each circumferential crack, R and h are the mean radius and thickness of the tube, and

$$\frac{c}{b} = \frac{2\theta}{\pi} \text{ (c/b=0.25 for 45° cracks)} \quad (20)$$

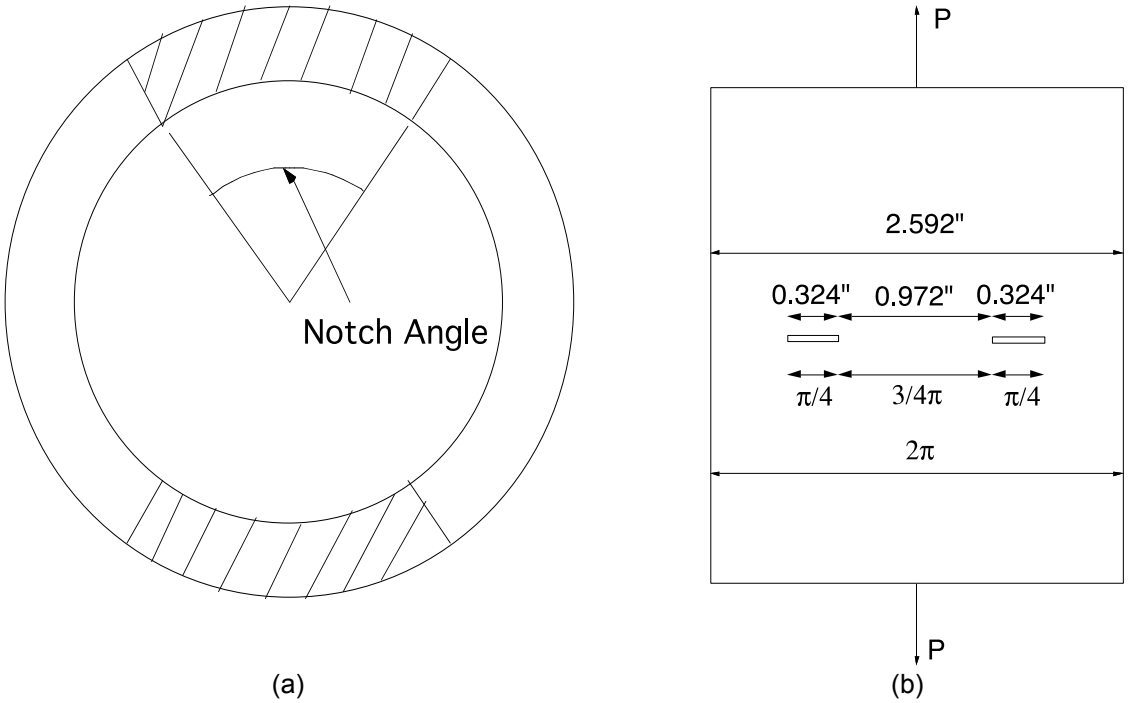


**Figure 5-18 Illustration of circumferential cracks**
**(a) Tube with two symmetrical through-wall circumferential notches**
**(b) Axial loading on a tube with two symmetrical 45-degree notches plotted after making an axial cut and unfolding the tube circumference into a plane**

As before, under creep conditions, Equation 19 by analogy gives an expression for the displacement rate,

$$\dot{\delta} = A c h_2\left(\frac{c}{b}, n\right)\left(\frac{\pi}{\pi - 2\theta}\sigma\right)^n \quad (21)$$

The variation of the function $h_2$ (c/b, n) with c/b is shown in Figure 5-19 for two values of n applicable to Alloy 600. Note that, in contrast to axial cracks that were considered earlier, c/b ≠ 0 for the circumferential notches.

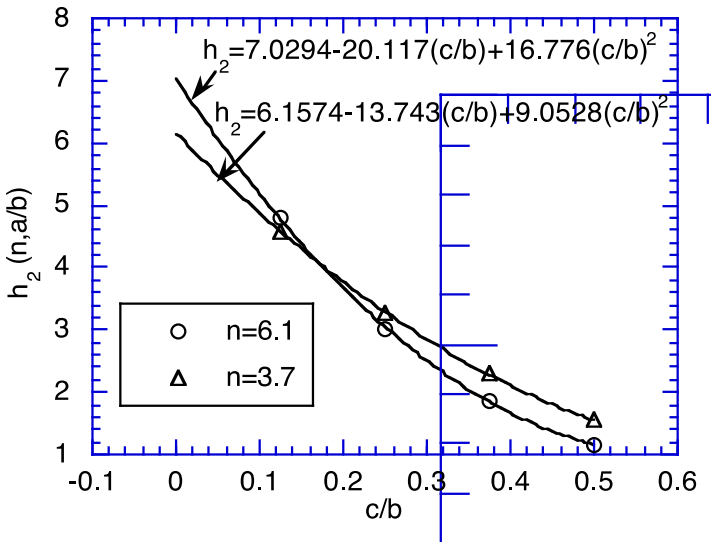


**Figure 5-19 Variation of $h_2$ with c/b for creep-rate exponents n = 3.7 and 6.1**

*5.3.3.1 Validation Test Results*

Six isothermal and nonisothermal tests were conducted to validate the approach. Two tests with 45-degree circumferential EDM notches were first conducted. The predicted notch opening with time for two symmetrical 45-degree circumferential cracks at two applied axial loads is compared with the experimentally observed notch opening in Figures 5-20a and 5-20b. The test under an axial load of 1,106.8 kilogram force (kgf) (2,440 lbs) (Figure 5-20a) was started initially at 695 degrees C (1,283 degrees F), but changed to 685 degrees C (1,265 degrees F) after 1 hour. The test under an applied axial load of 1,224.7 kgf (2,700 lb) (Figure 5-20b) was conducted at 665 degrees C (1,229 degrees F) with less variation in temperature. The agreement between experimentally measured notch openings and predicted values is reasonably good.

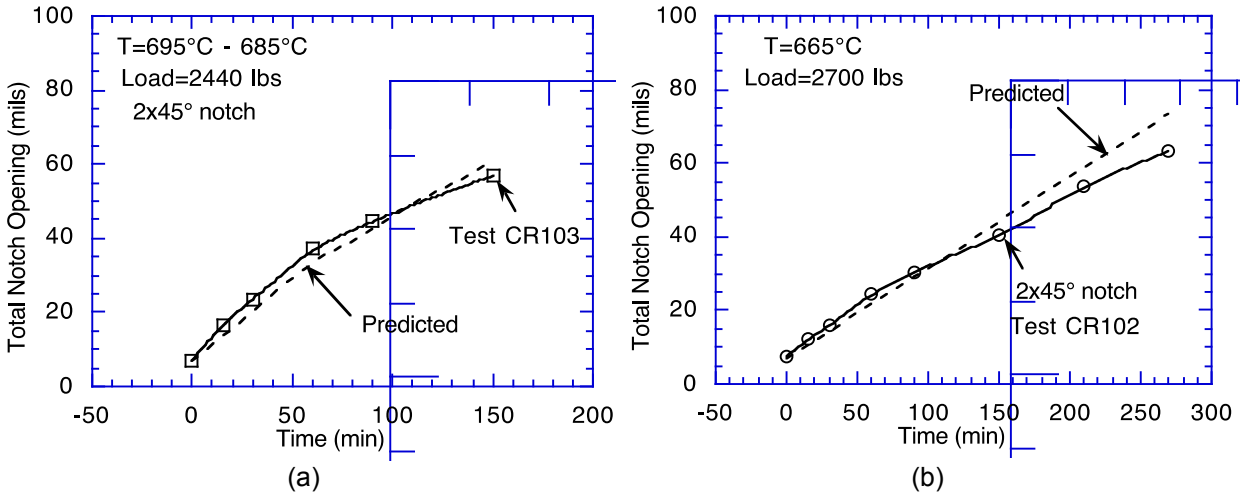


**Figure 5-20 Experimentally measured and predicted variation of total notch opening with time for specimens with two 45-degree circumferential notches loaded at (a) 1,106.8 kgf (2,440 lb) and (b) 1,224.7 kgf (2,700 lb)**

The temperature control of the specimen was improved subsequently. The next series of tests involved 2 x 0.635 cm (0.25 in.) and 2 x 0.508 cm (0.20 in.) circumferential notches subjected to an axial load of 1,089 kg (2,400 lb) at a constant temperature of 700 degrees C (1,292 degrees F). Figures 5-21a and 5-21b show a comparison between measured and predicted notch openings with time for specimens with two symmetrical circumferential notches of length 0.635 cm (0.25 in.) and 0.508 cm (0.20 in.), respectively, each subjected to an applied axial load of 1,106.8 kgf (2,400 lbs.). As before, the predicted openings are close to the measured values.

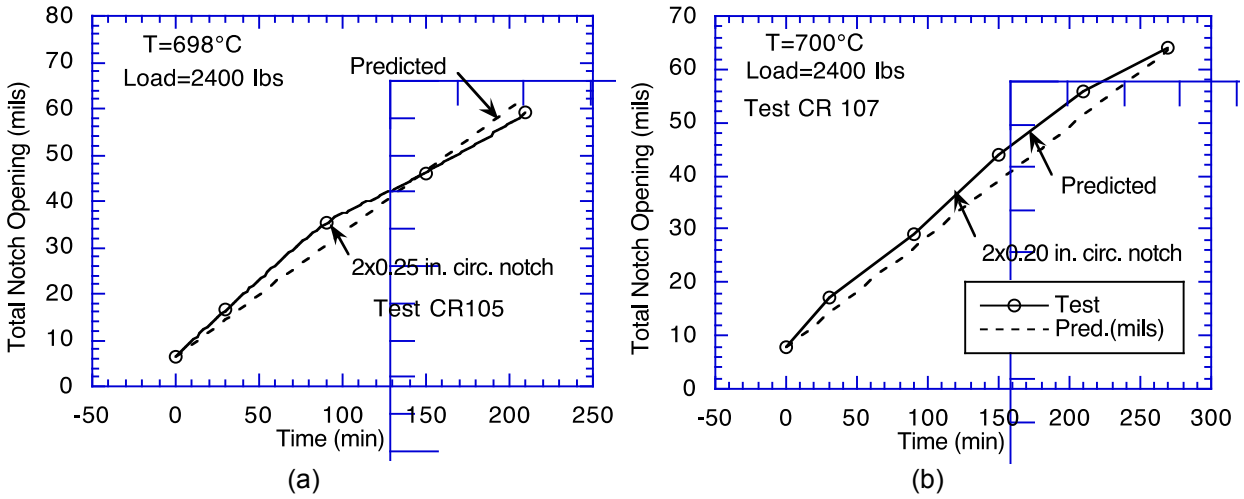


**Figure 5-21 Experimentally measured and predicted variation of total notch opening with time for specimens with two symmetrical circumferential notches loaded at 1,108 kg (2,400 lb) for notch lengths (a) 6.35 mm (0.25 in.) and (b) 5.1 mm (0.20 in.)**

All the tests reported so far were conducted isothermally. To validate the model for nonisothermal loading, two tests were conducted in which the temperature was ramped following the Case 6RU transient (Figure 5-22). In the nonisothermal tests, the displacements could only be measured at the end of the test. Both nonisothermal tests had a constant axial load of 1,362 kg (3,000 lb). Test CR 106 had 2 x 6.35 mm (0.25 in.) circumferential notches and Test CR 108 had 2 x 5.1 mm (0.20 in.) circumferential notches. Figures 5-23a and 5-23b give the predicted notch-opening displacement vs. temperature plots for the two tests, which also include the measured notch-opening displacements at the end of the tests. One of the predicted notch openings is close to the measured value, and the other one is off by 20 percent.

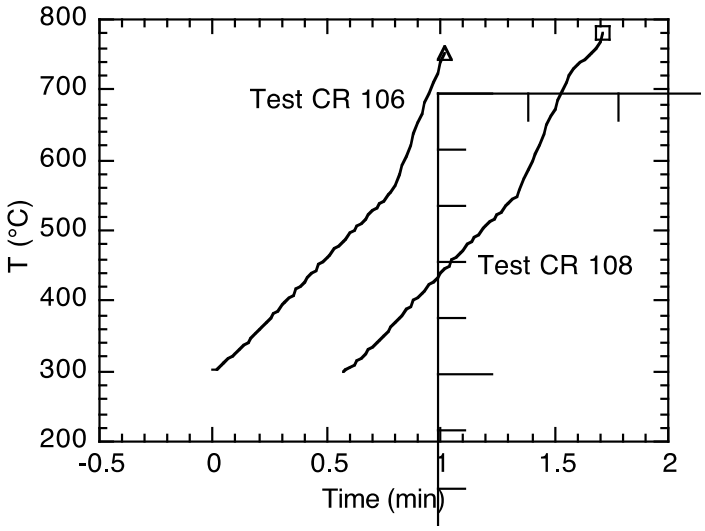


**Figure 5-22 Time vs. temperature plot for tests CR 106 and CR 108**
***The curve for CR 108 has been displaced in the horizontal direction for clarity.***

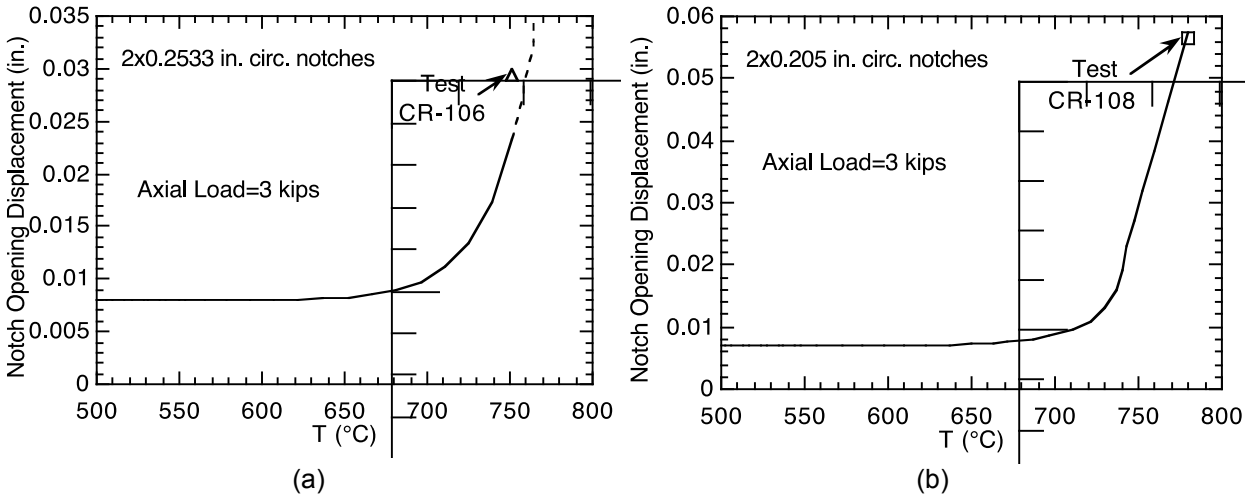


**Figure 5-23 Comparison of predicted (solid line) and experimentally measured (symbols) notch-opening displacements for (a) Test CR 106 and (b) Test CR 108**

### 5.3.4 Predicted Axial Crack-Opening Rate at High Temperature

Figure 5-24a shows the variation in the crack-opening rate with the crack length calculated using Equation 18 for SG tubes at 700 degrees C (1,292 degrees F) subjected to an internal pressure of 16.2 MPa (2,350 psi). Note that the crack-opening rate increases very rapidly for crack lengths greater than 10 mm (0.4 in.).

Figure 5-24b shows the crack-opening area at temperatures of 700 and 750 degrees C (1,292 and 1,382 degrees F) as a function of crack length for an SG tube subjected to a thermal transient characteristic of an SBO “high-dry” accident (Case 6RU in Reference 10). Note that, for temperatures greater than or equal to 750 degrees C (1,382 degrees F), cracks greater than 15-mm (0.6-in.) long will have crack-opening areas that are greater than the tube

cross-sectional flow area (303 square millimeters (0.47 square inch) for a 22.2-mm [0.875-in.] diameter tube).

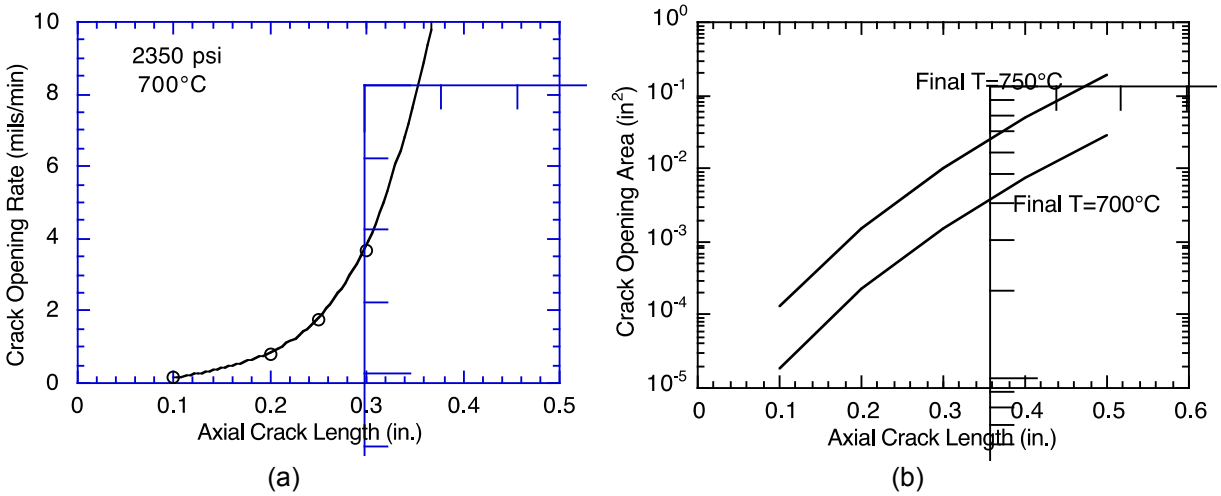


**Figure 5-24 Variations of (a) COD rate with through-wall axial crack length for a tube subjected to internal pressure of 2,350 psi at 700 degrees C and (b) crack-opening area with crack length at final temperatures 700 and 750 degrees C for a tube subjected to severe-accident transient**

## 5.4 Stability of Flaws after Ligament Rupture

To address the question of stability of part-through cracks after ligament failure, two specimens were fabricated with 12.7-mm (0.5-in.) through-wall cracks and with inside metallic liners to act as patches to prevent leakage of the pressurizing gas. It was hoped that the metallic liner would transmit the pressure to the tube wall by creep. In the first specimen, a 0.25-mm (0.01-in.)-thick pure nickel liner was used. It was first heated to 850 degrees C (1,562 degrees F) and then pressurized at a rate of 7 MPa/min (1,000 psi/min). The nickel liner developed a pinhole under the crack at a pressure of 10.3 MPa (1,500 psi), just as the cracked section of the tube started to bulge. The predicted instability pressure for the tube was 16 MPa (2,300 psi). A second specimen, also with a 12.7-mm (0.5-in.) through-wall crack but with a 0.2-mm (0.008-in.)-thick Type 304 stainless steel liner was heated to 750 degrees C, (1,382 degrees F), pressurized to 16.2 MPa (2,350 psi) and then held. This specimen also developed a leak because of failure of the stainless steel liner after about 1 min of temperature and pressure hold. The measured crack opening after the test was 1.1 mm (0.043 in.). Subtracting the initial flaw width of 0.2 mm (0.008 in.), the crack-opening rate in this specimen because of creep was 0.89 mm/min (0.035 in./min). No other tests with through-wall cracks were performed.

Although none of the part-through flawed specimens failed in an unstable manner after ligament failure, some of the specimens with shallower initial flaws and higher failure pressure showed tearing at the crack tip. The tearing may indicate that these specimens were probably close to instability when the ligaments failed. At failure, the crack-opening angles (COAs) of these specimens were 40–50 degrees. To get an estimate of the time it would take for a through-wall crack to open to a COA of 45 degrees, the calculations based on C* analysis, Equation 19 and Figure 5-18, were performed, although admittedly a more rigorous analysis would require that the effects of finite deformation at the crack tip be taken into account. The calculations showed that the crack-opening rate for a pressure of 16.2 MPa (2,350 psi) is as plotted in Figure 5-25a.

For a 6-mm (0.25-in.) crack, the times to open to 0.25 mm (0.010 in.) are about 2 minutes at 732 degrees C (1,350 degrees F) and a few seconds at 871 degrees C (1,600 degrees F). Considering the measured COD result reported earlier for a 12.7-mm (0.5-in)-long through-wall crack with stainless steel liner, the calculated COD because of creep at 732 degrees C (1,350 degrees F), after correcting for hoop stress because of the stainless steel liner, is 1.0 mm/min (0.04 in./min), which agrees reasonably well with the measured value of 0.89 mm/min (0.035 in./min).

Figure 5-25b shows the times to open an initially closed through-wall crack of various lengths to a COA of 45 degrees at 732 degrees C (1,350 degrees F) and at 871 degrees C (1,600 degrees F) under an internal pressure of 16.2 MPa (2,350 psi). Note that the time varies from greater than 40 min for a 6.4-mm (0.250-in.)-long crack, to 3 min for a 12.7-mm (0.5-in.)-long crack, and to 10 s for a 25.4-mm (1-in)-long crack at 732 degrees C (1,350 degrees F). The corresponding times at 871 degrees C (1,600 degrees F) are 4 min, 50 s, and 5 s, respectively. Because most of the failure temperatures for tests were in the range of 750 degrees C (1,382 degrees F) to 850 degrees C (1,562 degrees F), the times to open the cracks to a COA of 45 degrees are relatively short unless the cracks are less than 5 mm (0.2 in.).

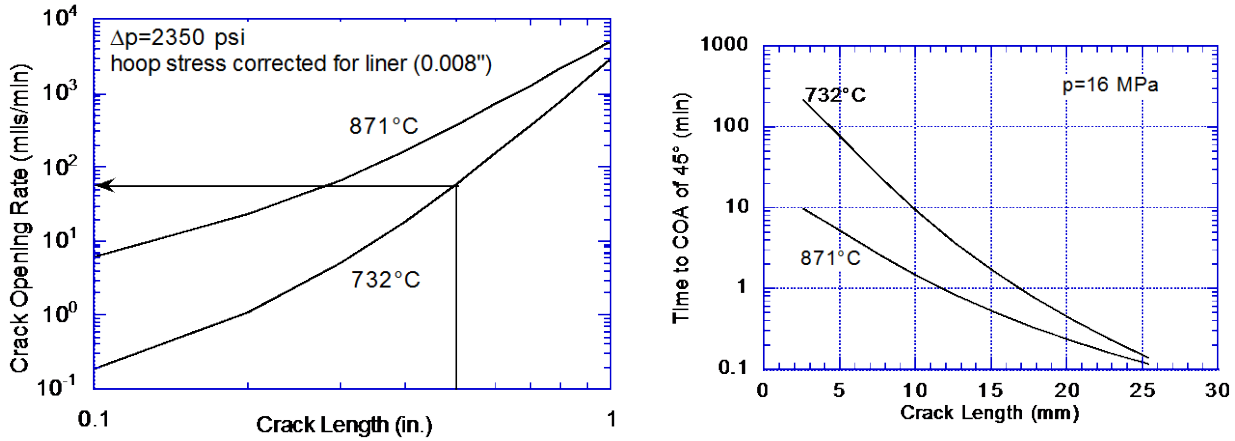


**Figure 5-25 Crack opening rate and time to reach COA of 45 degrees**
**(a) Crack-opening rate in mm/min versus crack length at 732 degrees C and 871 degrees C**
**(b) Time to open initially closed through-wall cracks to a COA of 45 degrees for a 22.3-mm (7/8-in.) diameter SG tube at 732 degrees C (1,350 degrees F) and 871 degrees C (1,600 degrees F) under a constant internal pressure of 16 MPa (2,350 psi)**

### 5.4.1 Failure Modes of Specimens Tested at High Temperature

Depending on the absence or presence of flaws in the specimens and on the pressure and temperature at failure (independent of the details of the loading history), a variety of failure modes was observed.

#### *5.4.1.1 Unflawed specimens*

Typically, most of the unflawed specimens failed in an unstable manner. However, a single unflawed specimen subjected to 12.4 MPa (1,800 psi) at 800 degrees C (1,472 degrees F) showed a completely different failure mode that is more typical of creep failure of internally pressurized tubes. It failed in 4 hours by developing a pinhole leak and after accumulating a significant amount of creep deformation (ballooning). This was the only specimen that was tested at a pressure less than 14 MPa (2,000 psi). All the other unflawed specimens were tested at greater pressures and failed in an unstable manner, independent of the temperature history.

#### *5.4.1.2 Flawed Specimens*

None of the flawed specimens failed in an unstable manner with fishmouth opening. Test specimens with initial flaws that were 50-mm (2-in.) long/20 percent deep, 25-mm (1-in.) long/60 percent deep, and 6-mm (0.25-in.) long/90 percent deep, were depressurized immediately on ligament failure. At a given failure pressure and temperature, the longer and shallower the initial flaw, the greater was the crack opening at failure. The 50- and 25-mm (2- and 1-in.)-long cracks showed evidence of a slight tear at the crack tips.

The CODs in all the failed specimens with axial cracks were measured. Flaws that had a measurable crack opening are classified as “fishmouth,” and flaws that had no measurable COD are classified as leakers. Figures 5-26a and 5-26b plots the CODs and COAs against the initial flaw depths (a/h), respectively, where a trend of increased COD and COA with decreasing initial flaw depth is clearly evident. Intuitively, this is to be expected, because the shallower flaws require proportionately larger pressures or higher temperatures or longer times to cause failure of the ligament than the deeper flaws of the same length. The specimens with the 1-in. (2.54-cm) and 2-in. (5.1-cm) cracks, which showed the largest COA at failure, also had slight tears at the crack tips.

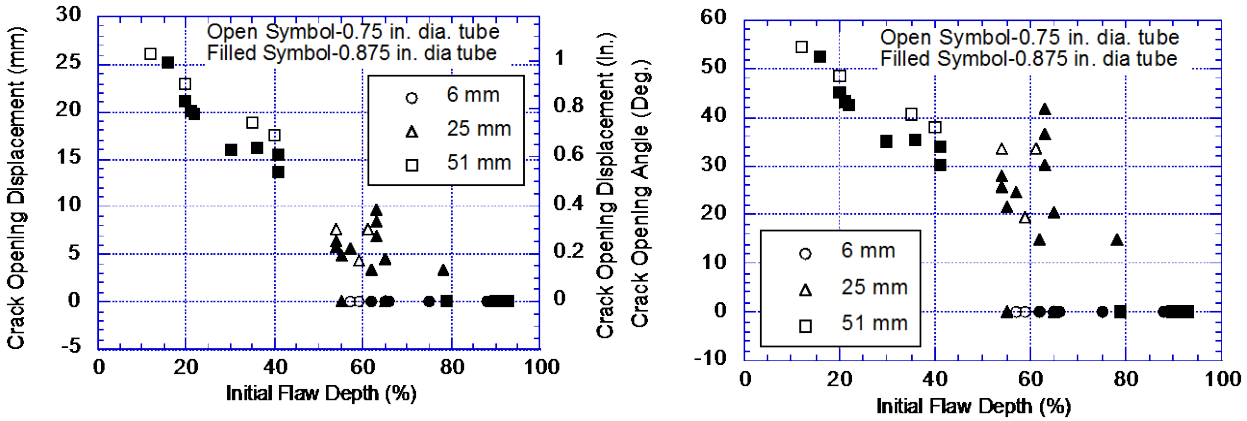


**Figure 5-26 Measured (a) CODs and (b) COAs in failed high-temperature test specimens as a function of initial axial flaw depth and initial flaw length**

At low temperatures, stability of a part-through crack after ligament failure can be determined from the following conditions:

$$\text{If } p_{cr} > p_{sc} \text{ then the crack is stable} \quad (22a)$$
$$\text{If } p_{cr} < p_{sc} \text{ then the crack is unstable} \quad (22b)$$

where $p_{cr}$ and $p_{sc}$ are the unstable burst pressures of through-wall cracks and ligament-rupture pressures of part-through-wall cracks, respectively. In other words, the stability boundary on a plot with crack length (2c) and crack depth (a/h) as axes is given by

$$m = m_p \quad (23)$$

which is independent of the flow stress or loading and depends only on the crack length and the crack depth. Figure 5-27a plots the curve corresponding to Equation 23, together with all the high-temperature test data. Although the curve $m = m_p$ appears to separate the specimens that leaked from those that fishmouthed remarkably well, a closer examination of the data for 25 mm (1 in.) crack length shows that the correlation does not work for all constant pressure tests. Figure 5-27b plots constant pressure data (both isothermal and T-ramp tests) for specimens with a 25-mm (1-in.) crack. Contrary to what would be expected from the correlation, all the specimens below the $m = m_p$ line did not fishmouth. Figure 5-28 shows a better correlation that distinguishes specimens that fishmouthed from those that leaked for specimens with a 25-mm (1-in.) flaw in a plot of failure pressure versus temperature at failure.

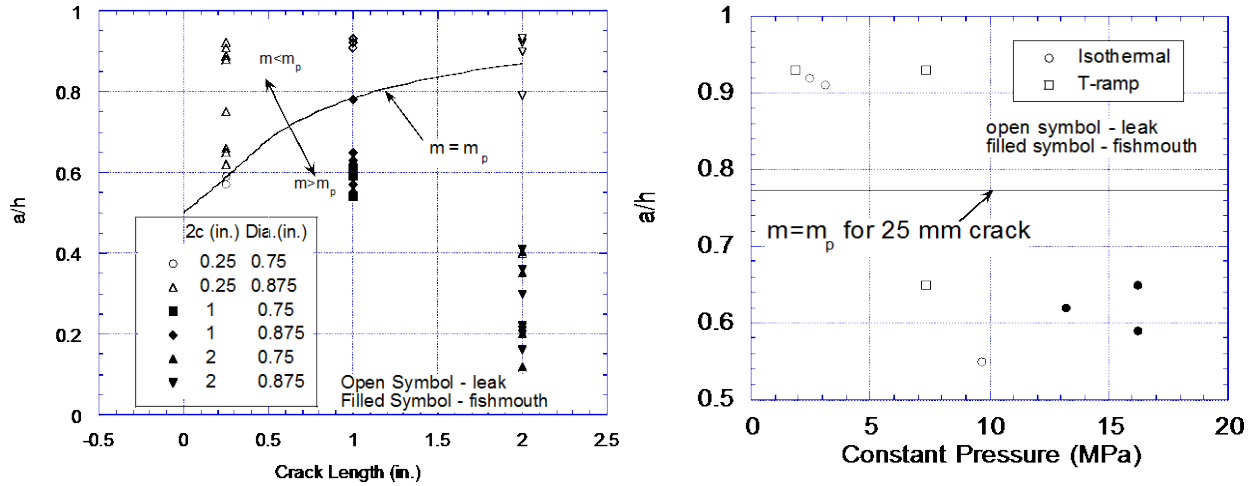


**Figure 5-27 Test results for unstable burst pressure**
**(a) Initial flaw depth (a/h) versus axial crack length plot for specimens tested at high temperature**
**(b) Flaw depth (a/h) versus pressure plot for constant-pressure tests on specimens with 25-mm (1-in.) part-through axial crack conducted isothermally or under a temperature ramp**

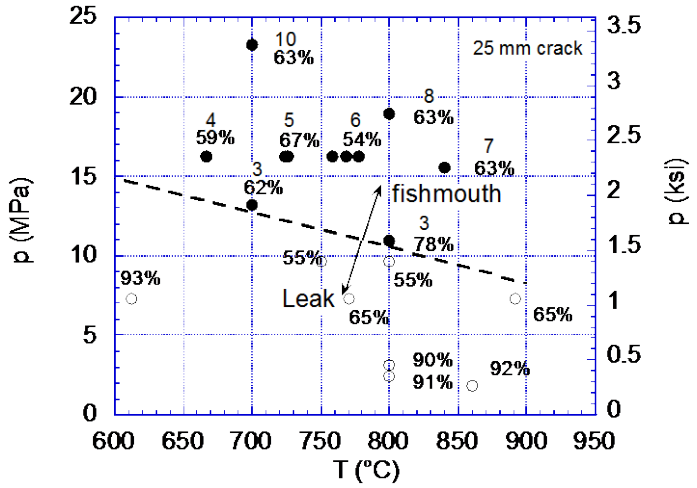


**Figure 5-28 Variation of failure pressure with failure temperature for tests conducted on specimens with a 25 mm (1 in.)-long crack**
***Open symbols denote specimens that leaked (no measurable COD) and filled symbols denote specimens whose cracks opened (fishmouthed). The numbers denote COD (in mm) at failure for the specimens that fishmouthed.***

### 5.4.2 Lower Bound Flow Stress for Computing Unstable Burst at High Temperature

A lower bound to the flow stress for computing the unstable failure of tubes with through-wall cracks can be obtained by ignoring the time it takes for a crack to open to a critical COA after ligament failure and calculate effective flow stresses from the dashed line in Figure 5-28 by using Equation 2b. Such calculated flow stresses are plotted together with flow stresses obtained from tensile tests in Figure 5-29. Note that the calculated flow-stress curve lies considerably above those obtained from tensile tests at high temperatures but approaches the latter at lower temperatures. This is to be expected, because the tensile tests are normally conducted at about $10^{-3}$/s, whereas the maximum flow stresses at instability correspond to much higher strain rates. Although more data would be desirable, the instability pressures calculated from the flow-stress curve in Figure 5-29 and indicated by solid lines in Figures 5-30a and 5-30b are consistent with the failure modes of the test specimens with 0.6-cm (0.25-in.) and 2-in. (5.1-cm) cracks. It is proposed that the higher flow-stress curve of Figure 5-29 can be used to determine the stability of a through-wall crack conservatively, using only the pressure and temperature at the moment of ligament failure and ignoring the pressure and temperature histories before ligament failure.

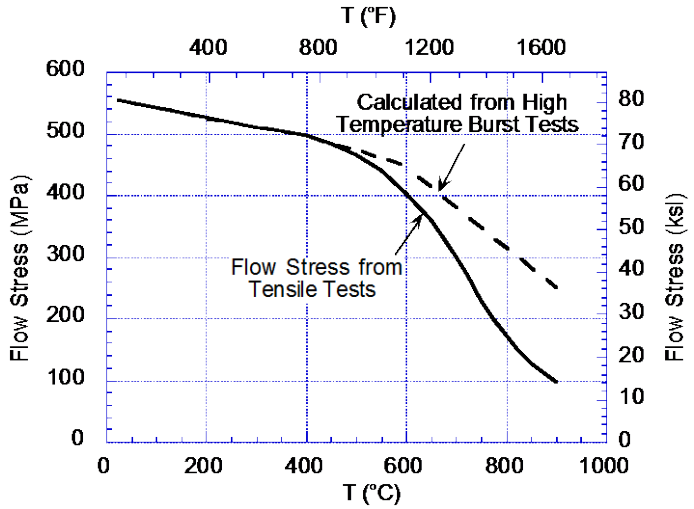


Figure 5-29 Temperature variation of flow stress (using k=0.5) of Alloy 600 specimens derived from tensile test data as reported in the literature
***Dashed line indicates a lower bound to flow stress (calculated from dashed line in Figure 5-28 using Equation 2b) for calculating instability pressures of tube specimens with through-wall cracks.***

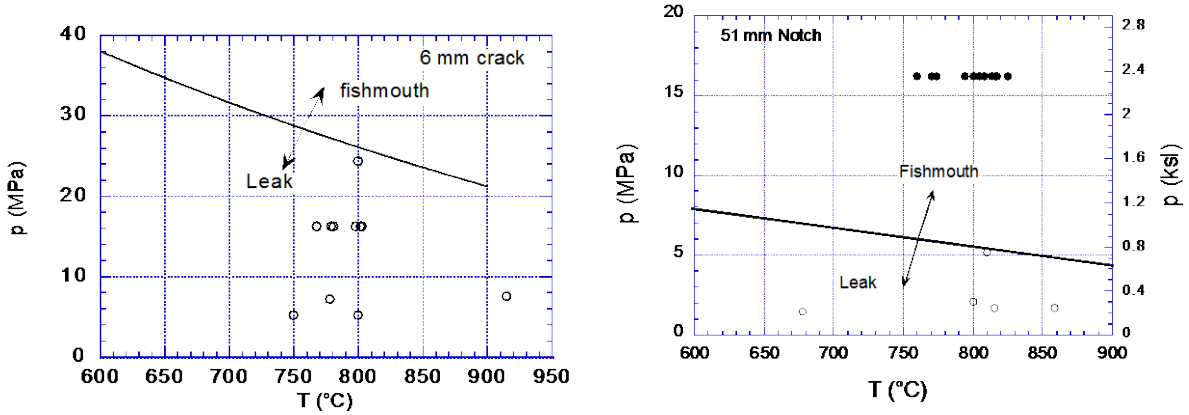


Figure 5-30 Pressure at failure as a function of temperature at failure for all specimens with a (a) 6 mm (0.25 in.)-long axial crack and (b) 51 mm (2 in.)-long axial crack
***The solid lines are predicted from the higher flow-stress curve of Figure 5.2-32.***

Figure 5-31 shows the critical crack length for a 22.2-mm (7/8-in.) diameter tube as a function of temperature at a pressure of 16.2 MPa (2,350 psi). For typical severe-accident temperatures (600–900 degrees C, or 1,112–1,652 degrees F) at a pressure of 16.2 MPa (2,350 psi), the critical crack length varies from 23 mm (0.9 in.) at 600 degrees C (1,112 degrees F) to 10 mm (0.4 in.) at 900 degrees C (1,652 degrees F). These represent minimum lengths of part-through cracks that will become unstable immediately after ligament rupture. However, at high temperatures, shorter cracks can grow in a stable manner by creep mechanisms before becoming unstable.

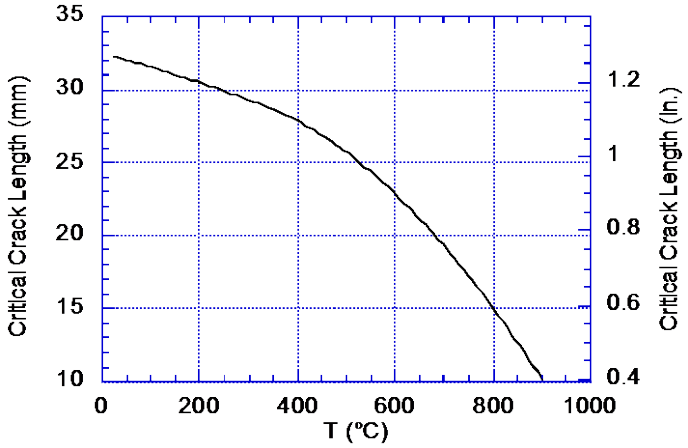


**Figure 5-31 Critical crack length as a function of temperature for a 22.3 mm (7/8 in.)-diameter Alloy 600 tube at an internal pressure of 16 MPa (2,350 psi)**

## 5.5 References


1. Cochet, B., J. Engstrom, and B. Flesch, "PWR Steam generator tube and tube support plate plugging criteria," Paper 4.1, *Steam Generator Tubes Mechanical, LBRB, and Probabilistic Studies*, Electricité de France, France, 1990.

2. Flesch, B., and B. Cochet, "Crack stability criteria in steam generator tubes," *International Conference on Pressure Vessel Technology*, Beijing, China, September 1988.

3. Kiefner, J.F., et al., "Failure stress levels of flaws in pressurized cylinders," *Progress in Flaw Growth and Fracture Toughness Testing*, Kaufman, J.G., National Symposium on Fracture Mechanics (6th: 1972: Philadelphia), American Society for Testing and Materials, Committee E–24 on Fracture Testing of Metals, American Society for Testing and Materials, ASTM Special Technical Publication 536, Philadelphia, PA, 1973.

4. Finnie, I. and W.R. Heller, "Creep of Engineering Materials," New York, NY, McGraw-Hill, 1959.

5. Ranganath, S., and H.S. Mehta, "Engineering Methods for the Assessment of Ductile Fracture Margin in Nuclear Power Plant Piping," *Elastic Plastic Fracture Second Symposium*, Vol. 2, Fracture Resistance Curves and Engineering Applications, American Society for Testing and Materials, ASTM Special Technical Publication 803, Philadelphia, PA, 1973.

6. Kurihara, R., S. Ueda, and D. Sturm, "Estimation of the ductile unstable fracture of pipe with a circumferential surface crack subjected to bending," *Nuclear Engineering and Design*, Vol. 106, 1988.

7. Alzheimer, J.M., et al., "Steam Generator Tube Integrity Program Phase I Report," NUREG/CR–0718, PNL-2937, Richland, WA, September 1979.

7. U.S. Nuclear Regulatory Commission, Rempe, J.L., et al., “Light Water Reactor Lower Head Failure Analysis,” NUREG/CR-5642, EGG-2618, Idaho National Engineering Laboratory, Idaho Falls, ID, October 1993.

8. Majumdar, S., et al., “Failure Behavior of Internally Pressurized Flawed and Unflawed Steam Generator Tubing at High Temperatures – Experiments and Comparison with Model Predictions,” NUREG/CR-6575, Argonne National Laboratory, 1998.

9. Kumar, V., M.D. German, and C.F. Shih, “An Engineering Approach for Elastic-Plastic Fracture Analysis,” EPRI NP-1931, Electric Power Research Institute, 1981.

10. U.S. Nuclear Regulatory Commission, SGTR Severe Accident Working Group, “Risk Assessment of Severe Accident-Induced Steam Generator Tube Rupture,” NUREG-1750, 1998, Agencywide Documents Access and Management System (ADAMS) Accession No. ML070570094.

# 6 ESTIMATION OF STEAM GENERATOR TUBE FLAW DISTRIBUTIONS

## 6.1 Introduction

This chapter presents the recent estimates for steam generator (SG) tube flaw distributions, based on selected inservice inspection (ISI) reports available to the U.S. Nuclear Regulatory Commission (NRC) for U-tube SGs (for Westinghouse (W) and Combustion Engineering (CE) nuclear power plants (NPPs).

Section 6.4 also includes the discussion for once-through SG axial loads on tubes during severe accidents.

The SG flaw distributions are used as input in estimating consequential SG tube rupture (C-SGTR) probabilities during severe accidents after core damage occurs, as well as for initiating events during power operation where sudden large pressure differences between the primary and the secondary sides can occur. Such probability estimates were done in support of the NRC's Steam Generator Action Plan during the early 2000s but were not formally documented. In that work, the estimated flaw distributions available at that time were used in supporting probabilistic risk assessment (PRA) reports, such as Reference 1. Those flaw distributions were based on data for SGs that have been replaced since then. Reference 2 provides the most recent SG flaw distributions, applicable to both the W and CE plants.

Table 2 in NUREG/CR-6521, "Estimating Probable Flaw Distributions in PWR Steam Generator Tubes," issued 1996 (Ref. 3), summarizes the flaw distributions. This table, which is reproduced below as Figure 6-1, comes with the following clarification concerning primary water stress-corrosion cracking (PWSCC) and outer diameter stress-corrosion cracking (ODSCC):

> The examples in Appendix C do not cover axial PWSCC at roll transitions, nor do they cover circumferential ODSCC at TTS…. (This quote is taken from page 17 of the reference and applies to the table below.)

Table 6 of Section 3 of Reference 2 summarizes the new SG tube flaw distribution estimates. This table is reproduced as Table 6-2 for the convenience of the reader.

*Table 2. Flaw Distributions for Hypothetical Example Cases* NUREG/CR-6521

**Plant Characteristics**

| | |
|---|---|
| No. of Steam Generators: | 3 |
| No. of Tubes = 3*3388 = | 10164 |
| Tube Material | LTMA 600 |
| Expansion Method: | Wextex |
| Hot Leg Temperature, °F: | 605 |
| BOC EFPY: | 14 |
| EOC EFPY: | 15.2 |

| | | Moderately Affected Plant | Severely Affected Plant | Lightly Affected Plant |
|---|---|---|---|---|
| **1. Circumferential SCC at TTS (Mostly PWSCC)** | | | | |
| Number of tubes with Circ. SCC at TTS at 15.2 EFPY (Note 1) = | | 7.0 | 46.3 | 1.4 |
| Gamma distribution parameters for crack arc length; arc length in degrees (Note 2):* | $\alpha$ = | 2.84 | 2.84 | 2.84 |
| | $\beta$ = | 28.1 | 28.1 | 28.1 |
| *For macrocracks. Macrocracks consist of series of 0.3 " thru-wall cracks separated by 0.05" long ligaments. | | | | |
| **2. Circumferential ODSCC at Dents at TSPs** | | | | |
| Number of tubes with cracks at15.2 EFPY Note 1) = | | 4.2 | 40.1 | 0.32 |
| Gamma distribution parameters for crack arc length; arc length in degrees (Note 2):* | $\alpha$ = | 34.4 | 34.4 | 34.4 |
| | $\beta$ = | 3.23 | 3.23 | 3.23 |
| *For individual macrocracks. There are typically two near thru-wall diametrically opposed macrocracks per cracked location. See Figures C-6 and 7 for distribution of combined crack lengths. | | | | |
| **3. Free Span ODSCC** | | | | |
| Number of tubes with cracks at 15.2 EFPY (Note 1) = | | 5.2 | 60.2 | 1.7 |
| Gamma distribution parameters for length, in. (Note 2):* | $\alpha$ = | 0.17 | 0.17 | 0.17 |
| | $\beta$ = | 0.88 | 0.88 | 0.88 |
| Gamma distribution parameters for depth, % wall (Note 2):* | $\alpha$ = | 17.0 | 17.0 | 17.0 |
| | $\beta$ = | 3.80 | 3.80 | 3.80 |
| * Crack length and depth distributions are assumed to be independent. | | | | |
| **4. IGA/SCC in Hot Leg Sludge Pile** | | | | |
| Number of tubes with cracks at 15.2 EFPY (Note 1) = | | 39.6 | 60.2 | 18.9 |
| Gamma distribution parameters for length, in. (Note 2):* | $\alpha$ = | 0.17 | 0.17 | 0.17 |
| | $\beta$ = | 0.88 | 0.88 | 0.88 |
| Gamma distribution parameters for depth, % wall (Note 2):* | $\alpha$ = | 17.0 | 17.0 | 17.0 |
| | $\beta$ = | 3.80 | 3.80 | 3.80 |
| * Crack length and depth distributions are assumed to be independent. | | | | |
| **5. Axial ODSCC at TSPs** | | | | |
| Number of tubes with ODSCC (0.85 volt level) at 15.2 EFPY (note 1) = | | 569.7 | 6024.6 | 131.1 |
| Gamma distribution parameters for depth of 0.75" long cracks; depth in % of wall: | $\alpha$ = | 0.770 | 0.770 | 0.770 |
| | $\beta$ = | 4.480 | 4.480 | 4.480 |
| **6. Flaws Due to Loose Parts** | | | | |
| Number of tubes with flaws at 15.2 EFPY = | | 0.7 | 0.7 | 0.7 |
| Gamma distribution parameters for length, in.:* | $\alpha$ = | 1.900 | 1.900 | 1.900 |
| | $\beta$ = | 0.458 | 0.458 | 0.458 |
| Gamma distribution parameters for depth, % wall:* | $\alpha$ = | 2.275 | 2.275 | 2.275 |
| | $\beta$ = | 17.235 | 17.235 | 17.235 |
| * Flaw length and depth distributions are assumed to be independent. | | | | |

Notes
1. Numbers of tubes are totals that reflect adjustment for detection efficiencies.
2. Gamma distributions are for "actual" flaws, i.e., after adjustment for measurement error and POD.

Figure 6-1 Table 2 reproduced from NUREG/CR 6521

## 6.2 Data Selection

To aid the PRA of SG tube rupture events, a series of plant SG tube inspection reports were chosen to represent the flaw distributions in SG tubes for current U.S. NPPs. The following paragraphs explain the rationale for the selection of specific reports.

Pressurized water reactor (PWR) plants in the United States were divided into three main categories: CE-designed plants, W designs, and plants with once-through SG (OTSG) designs. For the W and the CE designs, specific power plants were selected. Raw data from the SG tube inspection reports for those plants were provided as input for estimating probable flaw distributions, as were primary coolant leakage estimates for various accident scenarios.

Regarding C-SGTR in OTSGs, Argonne National Laboratory (ANL) investigated an issue of axial loads on SG tubes during design-basis accidents. Other analyses have shown that the once-through design is not susceptible to the problems of steam backflow, and the associated much higher temperatures, which could occur during severe accidents in SGs with recirculating designs. Therefore, this study does not include ISI reports for OTSG plants.

Because most U.S. plants have replaced their original SGs, this study only includes ISI data for currently operating SGs. It considered only SG tubes made of either thermally treated (TT) nickel Alloy 600 or nickel Alloy 690, because those are the main tube materials in use in the United States. (There are some mill-annealed Alloy 600 tubes in service in the United States, but they are rare exceptions.)

NUREG-1771, “U.S. Operating Experience with Thermally Treated Alloy 600 Steam Generator Tubes,” issued April 2003 (Ref.4), and NUREG-1841, “U.S. Operating Experience with Thermally Treated Alloy 690 Steam Generator Tubes,” issued August 2007 (Ref.5), contained historical summaries of SG operating experience. Those documents were reviewed for a select group of plants that would be considered representative of the current NPPs with regard to the distributions of SG flaws.

The study collected and reviewed sets of consecutive inspection reports dating from the most recent inspection back through approximately 10 or 12 years, and even as far back as 20 years. The number of reports varied, of course, depending on the SG date of replacement.

It could be suggested that SGs in service for longer times would experience more tube degradation. However, that is not always the case, depending upon such factors as operating temperatures, water chemistry, contaminants, and others. So, to properly characterize the current fleet, it was decided to include plants that had a lot of degradation and those that had little degradation, regardless of the number of effective full-power years (EFPYs) of operation. In this way, the flaw distributions for C-SGTR would be bounded by best and worst cases. Indeed, it was found that some of the longest operating SGs have fewer flaws, while some of the newly replaced SGs have more flaws.

Two main categories are used here to characterize SG tube flaw types in the ISI reports: cracks and wear scars. Cracks are generally tight, sharp-tipped, irregularly shaped (jagged) defects, which can be described as a “tearing of the material.” Wear scars are usually of a more smooth and broader (not tight) shape. Wear scars are essentially a removal of surface material at areas where the tube comes in contact with another surface, such as a support plate, antivibration bar, loose part, or another tube. Wear defects have been found in all SGs, regardless of the materials used to manufacture the tubes. Cracks, however, have not yet been found in any Alloy

690 SG tubes in the United States despite some being in operation for over 20 years. So, the ISI data used herein for flaw distribution estimates include cracks and wear defects for thermally treated Alloy 600TT SGs, but only wear flaws for SGs constructed with Alloy 690 material. It should be noted that the flaw data did not include any ISI data for mill-annealed tubes.

For CE plant designs, all of the replacement SGs have been constructed with tubes made of Alloy 690 material with the exception of Palisades. The following plants were selected:

- Millstone 2 was the first CE plant to employ Alloy 690. Reviewing the longer history of Millstone 2 could provide insights into the progression of flaw growth and incidence of new flaw initiation over time.

- Calvert Cliffs had several ISI reports that included extra dimensional data describing tube defects, beyond the minimum information required. For example, one report lists the length, depth, and width of defects, while only the depth (or through-wall percentage) is required to be reported.

- St. Lucie 1, with relatively newer SG replacements, showed some more flaw defects, compared to some of the older, similar SGs in service at CE plants.

W-design power plants in the United States use some SGs made with Alloy 600TT tubes, and some SGs made with Alloy 690 tubes. Therefore, ISI reports from both of these categories of W SGs were collected to characterize the current SGs used at W-design power plants.

Following a similar rationale as explained above for CE-design plants, ISI reports for certain power plants were selected to represent the current state of flaw distributions in the W NPPs. For the two major categories of tube materials (Alloy 690TT and Alloy 600TT), four plants were chosen to characterize the flaws in the SGs currently used at W plants.

To characterize Alloy 690TT SG tubes at W plants, the study compiled four sets of ISI reports from four different power plants (two lightly degraded plants and two of the more degraded plants): Donald C. Cook Unit 2, McGuire Unit 1, Prairie Island Unit 1, and Sequoyah Unit 1.

Likewise, for the W-design power plants with Alloy 600TT SG tubes, the following plants were chosen: Byron Unit 2, Seabrook Unit 1, Surry Unit 2, and Vogtle Unit 1.

Table 6-1 summarizes all the plants selected to have their ISI reports reviewed and compiled for the purpose of characterizing the state of flaw distributions in the current fleet, to be used in C-SGTR risk assessments.

In Table 6-1, the “current model” designations in the table refer to the SG manufacturers and the size or geometry of the SG. The basic design of all these SGs, at both CE and W plants, is a recirculating design with inverted U-bend-shaped tubes. However, different manufacturers have different designs as to the exact dimensions and the number of tubes. The symbols for the current manufacturers are explained as follows:

- BWC = Babcock and Wilcox Canada
- Fr = Framatome (now called AREVA)
- ABB/Doosan = ABB/Doosan
- all others are W (W/51 F, D5, F, and W/54F)

Table 6-1 SG Properties for Flaw Distribution Estimates for C-SGTR Studies

| CE Plant Designs | | | |
|---|---|---|---|
| **Plant** | **Current Model** | **Material** | **Replace Date** |
| Calvert Cliffs 1 | BWC—7811 | 690TT | Jun-02 |
| Millstone 2 | BWC | 690TT | Jan-93 |
| St. Lucie 1 | BWC | 690TT | Jan-98 |

| W—Alloy 600TT SG Tubes | | | |
|---|---|---|---|
| **Plant** | **Current Model** | **Material** | **Replace Date** |
| Byron 2 | D5 | 600TT | Not Applicable (NA) |
| Seabrook 1 | F | 600TT | NA |
| Surry 2 | W/51 F | 600TT | Sep-80 |
| Vogtle 1 | F | 600TT | NA |

| W—Alloy 690TT SG Tubes | | | |
|---|---|---|---|
| **Plant** | **Current Model** | **Material** | **Replace Date** |
| Donald C. Cook 2 | W/54F | 690TT | Mar-89 |
| McGuire 1 | BWC | 690TT | May-97 |
| Prairie Island 1 | Fr 56/19 | 690TT | Nov-04 |
| Sequoyah 1 | ABB/Doosan | 690TT | Jun-03 |

This report reviewed and summarized all the raw data from the plants selected above, for the currently operating SGs. The data were used for statistical estimations of flaw distributions, with respect to size and number of flaws. Finally, the flaw numbers and sizes may be used as input for the overall estimation of the large early release consequences of an SG tube rupture caused by a severe accident.

## 6.3 Estimation of SG Tube Flaw Distributions in Replacement SGs

### 6.3.1 Summary

The data in previous work estimating SG tube flaw distributions for SGs existed before 1995. These (U-tube) SGs were replaced with those having new SG tube materials. Recent work has estimated a new set of flaw distributions for U-tube SGs (used by domestic W and CE NPPs) (Ref. 2). For this purpose, selected data from ISI reports available to the NRC were used, as discussed in Section 6.2. Reference 2 discusses this work and contains the analysis of the ISI reports, the creation of the database, and the estimation of flaw rate and other flaw characteristics. Because of the limitations of the detailed information available for the flaw characteristics, the data have been consolidated into Inconel 600 material applicable to all SGs (W and CE) as a function of EFPY (parameter K in the equations of Table 6-2), and similarly for Inconel 690. Thus, the equations are not distinguished by the SG-type but provide flaw distributions as a function of time (EFPYs).

The number of flaws generated in the last operating cycle K can be estimated by calculating the number of flaws at $K^{th}$ and $(K-1)^{th}$ cycles and subtracting the two. This allows an estimation of the large (deep) cracks (e.g., greater than 30-percent deep) that may be present during an accident sequence in the $K^{th}$ cycle. It can be assumed that flaws with 40 percent or more depth observed before the $K^{th}$ cycle are removed by plugging the associated tubes.

Table 6-2 summarizes the new SG tube flaw distributions that can be used for NPPs with replacement SGs. These distributions are applicable to both W and CE replacement SGs with thermally treated Inconel 600 and 690 materials.

Appendix K contains a further discussion of input flaw data (empirical distribution) and shifted flaw distribution as used for PRA purposes. Section 7.1.3 of this report introduces the shifted flaw distribution.

### Table 6-2 SG Tube Flaw Distributions Taken from Reference 2

| Flaw Characteristics | Thermally Treated Inconel 600 | Thermally Treated Inconel 690 |
|---|---|---|
| Volumetric/Wear Flaw Rates | $h(k) = 6.4166 \cdot 10^{-5}\ K + 1.3236 \cdot 10^{-3}$<br>$\mu = 6.4166 \cdot 10^{-5}$, $\Omega = 1.3236 \cdot 10^{-3}$ | $h(k) = 5.5826 \cdot 10^{-5}\ K + 6.8627 \cdot 10^{-4}$<br>$\mu = 5.5826 \cdot 10^{-5}$, $\Omega = 6.8627 \cdot 10^{-4}$ |
| Axial Crack Flaw Rates | K<15, h(k) = Negligible<br>$\mu = 0.0$, $\Omega = 0.0$<br>K>15, $h(k) = 2.0 \cdot 10^{-4}$<br>$\mu = 0.0$, $\Omega = 2.0 \cdot 10^{-4}$ | h(k) = Negligible<br>$\mu = 0.0$, $\Omega = 0.0$ |
| Circumferential Crack Flaw Rates | K<15, h(k) = Negligible<br>$\mu = 0.0$, $\Omega = 0.0$<br>K>15, $h(k) = 1.0 \cdot 10^{-3}$<br>$\mu = 0.0$, $\Omega = 1.0 \cdot 10^{-3}$ | h(k) = Negligible<br>$\mu = 0.0$, $\Omega = 0.0$ |
| | | |
| Axial Flaw Length: Axial Cracks, Wear Marks, or Volumetric Flaws | Gamma($\alpha$ =2.33318781, $\beta$= 2.0847) | |
| Circumferential Crack Angle | 0.58 Gamma($\alpha$=28.6565, $\beta$=0.4187) + (1-0.58)·Gamma($\alpha$=9.5638, $\beta$=0.0670) | |
| Flaw Depth: Cracks, Wear, Volumetric Flaws | Gamma($\alpha$ =2.0658, $\beta$=16.3274) | |

Note: If the gamma function in EXCEL is to be used to evaluate values with the above parameters, the “beta” to be placed in the EXCEL gamma function is actually 1/ β of Table 6.3-1.

### 6.3.2 An Example Calculation

Table 6-2 provides a linear hazard rate for the SG tube flaws as a function of EFPY. This hazard rate is defined by:

$$h(k) = \mu * k + \Omega$$

where k is EFPY, and both coefficients μ and Ω are positive.

Given the above hazard rate, the cumulative flaw probability can be expressed by:

$$P(f) = 1 - \exp[-\{(1/2) * \mu * k^2 + \Omega * k\}] \quad (6.1)$$

A four-loop W plant (four SGs) with thermally treated Inconel 600 SG tubes is considered. Each SG is assumed to have 3,300 tubes, and the plant has accumulated 15.6 EFPYs of operation.

The expected number of flaws (NFlaws-Avg) that will be identified at the end of the current cycle is estimated from the cumulative probability distribution using the following equation:

$$\text{NFlaws-Avg} = (3{,}300 * 4) * [1.0 - \exp[-\{(1/2) * \mu * k2 + \Omega * k\}]] \quad (6.2)$$

The values μ and Ω can be found in Table 6-2. For the case discussed above, it is expected that 370 wear/volumetric flaws would be present in all the SGs (13,200 tubes). Thirty-one out of these 370 flaws will be generated in this cycle. This is estimated directly by setting k=15.6 in the equation for hazard rate

$$(h(k) = 6.4166 \cdot 10^{-5} K + 1.3236 \cdot 10^{-3})$$

It also implies that the larger flaws could only be found in the last cycle (the estimated 31 flaws), since large flaws found earlier in a previous cycle were all subjected to plugging and other repair practices per inspection procedure.

The current statistical analysis and this illustrative example are based on flaws that are detected. They do not account for the hidden flaws that are not detected during ISIs. The number or fraction of the hidden flaws is generally estimated by using a probability of detection (POD). The POD delivers the realistic, statistical assessment of the reliability for a nondestructive testing method. The POD curves (typically S shaped) are developed as a function of flaw size and type. The larger and deeper the flaw, the higher the POD will be. The POD value also depends on the flaw type. For example, the POD value is larger for a crack with sharp edges than for a wear with smooth surface (see NUREG/CR-6791, “Eddy Current Reliability Results from the Steam Generator Mock-up Analysis Round-Robin,” Revision 1, issued October 2009 (Ref. 6). For more detailed analysis, the flaws in the last cycle should be adjusted for not considering the POD, using the information in NUREG/CR-6791. The impact of such adjustments for large flaws is expected to be around 10 percent.

Figure 6-2 shows the NFlaws-Avg, which includes both wear and cracks for 13,200 tubes, as a function of EFPY for both 600 and 690 thermally treated tubes.

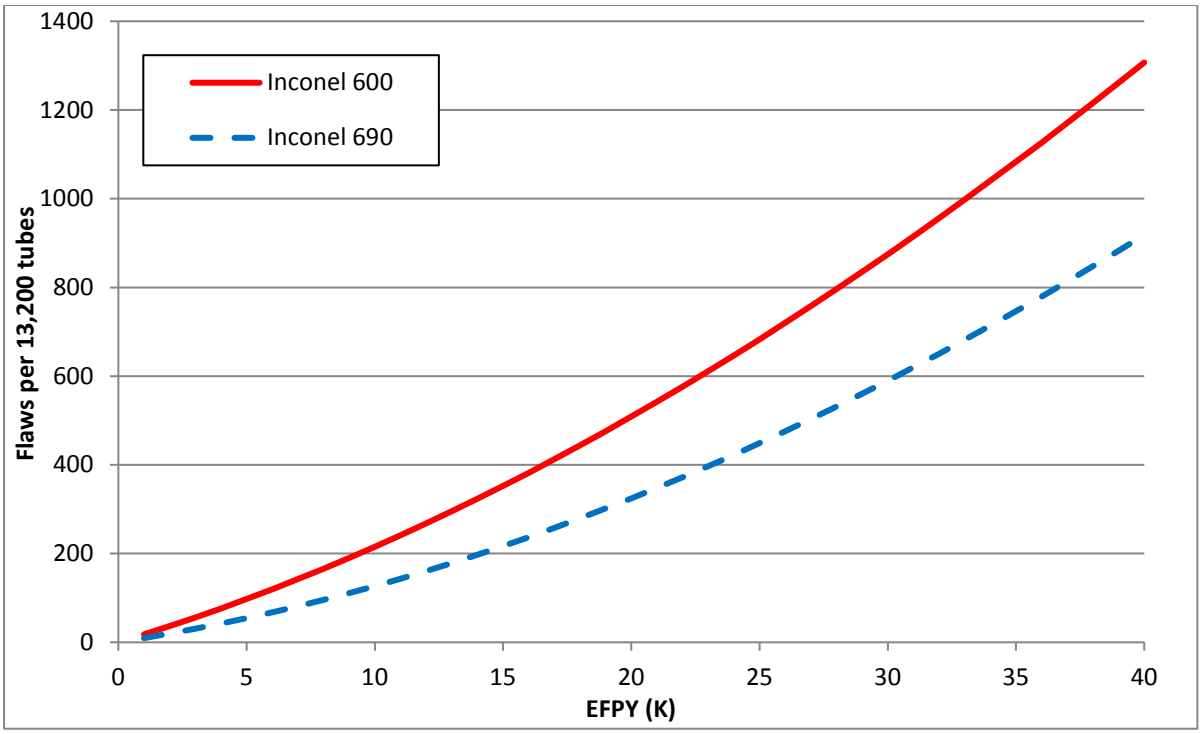


Figure 6-2 Average number of flaws as a function of EFPY for four SGs

### 6.3.3 Example Flaw Samples

To illustrate the flaws that may be present during the 15th EFPY, 10 flaw samples were generated for one SG with 3,588 600TT tubes. It is assumed that the tubes with 40-percent deep and deeper flaws are plugged when revealed by tests. Analysts created 775 total flaws in 10 samples, with an average of 78 flaws per sample per SG. The average length of the 775 flaws is 1.1 centimeters (0.43 inch); the average depth is 18 percent. All flaws are of the "wear" type.

Histograms in Figures 6-3 and 6-4 show the distribution of the 775 flaws by length and depth. Note that all flaws of a depth of 40 percent or deeper are removed at or before the last outage; thus, such large flaws have been generated since the last refueling outage or were not detected (i.e., POD less than 1).

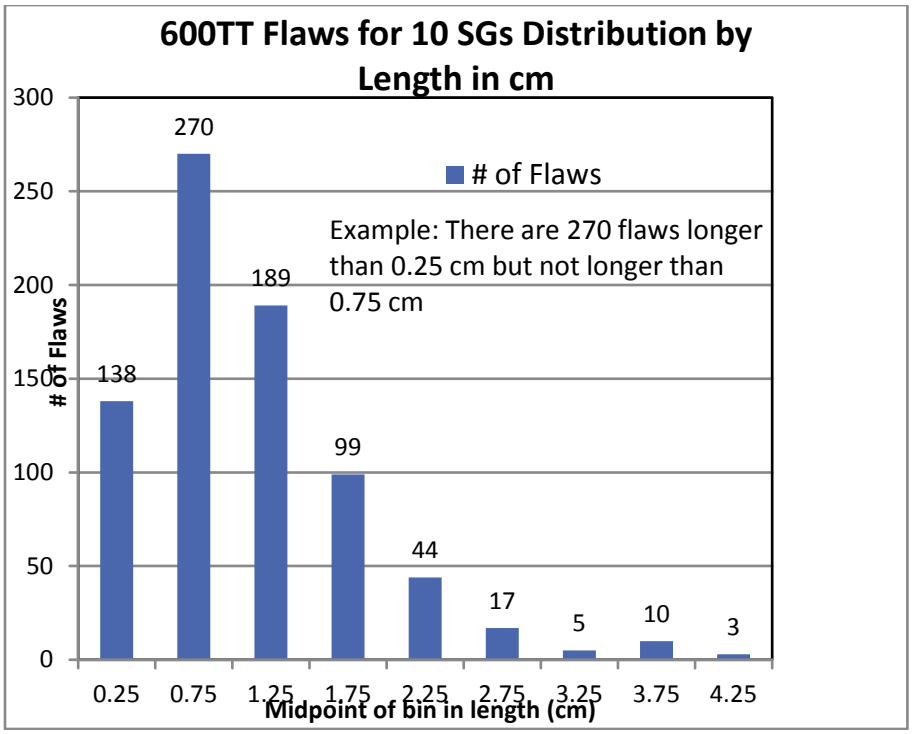


Figure 6-3 600TT flaws for 10 SGs—distribution by length

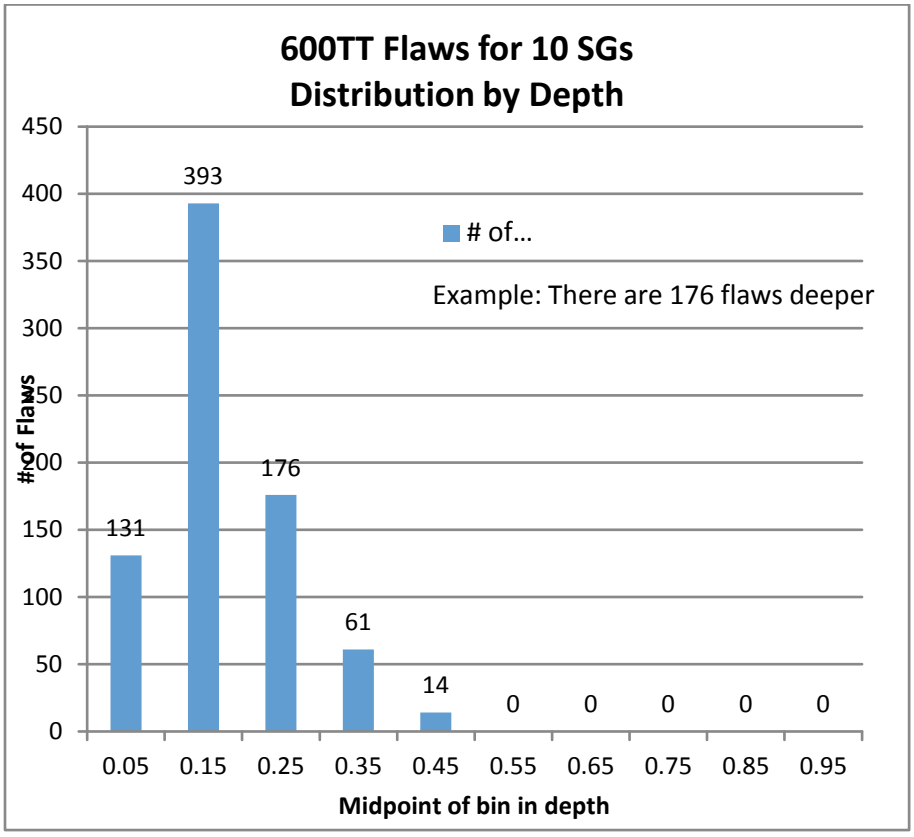


Figure 6-4 600TT flaws for 10 SGs—distribution by depth

## 6.4 OTSG Axial Loads on Tubes during Severe Accidents

ANL has completed a study for NRC's Office of Nuclear Regulatory Research (RES), "Stability of Circumferential Flaws in Once-Through Steam Generator Tubes under Loading during LOCA, MSLB, and FWLB," now being reviewed, on the assessment for potential elevated axial tube loads because of thermal expansion between the SG shell and tubes during severe-accident conditions in OTSGs. Also, OTSG designs are not susceptible to a severe-accident effect of a backflow of steam, which may cause much higher local temperatures in recirculating SGs. Based on the preliminary results of the ANL work, and the backflow characteristics, RES's current assessment is that the phenomenon investigated does not contribute significantly to C-SGTR for severe-accident conditions.

## 6.5 References


1. Sandia National Laboratories, "Severe Accident Initiated Steam Generator Tube Ruptures Leading to Containment Bypass—Integrated Risk Assessment," JCN Y6486, February 2008, Agencywide Documents Access and Management System Accession No. ML15054A514.

2. Azarm, M.A., et al., "A Letter Report on Flaw Database and C-SGTR Calculator Flaw Input," Information Systems Laboratories, December 2014.

3. Gorman, J.A., et al., "Estimating Probable Flaw Distributions in PWR Steam Generator Tubes," U.S. Nuclear Regulatory Commission, NUREG/CR-6521 (ANL-96/20), 1996.

4. U.S. Nuclear Regulatory Commission, "U.S. Operating Experience With Thermally Treated Alloy 600 Steam Generator Tubes," NUREG-1771, April 2003.

5. U.S. Nuclear Regulatory Commission, "U.S. Operating Experience With Thermally Treated Alloy 690 Steam Generator Tubes," NUREG-1841, April 2003. Agencywide Documents Access and Management System Accession No. ML072330588.

6. Kupperman, D.S., et al., "Eddy Current Reliability Results from the Steam Generator Mock-up Analysis Round-Robin," U.S. Nuclear Regulatory Commission, NUREG/CR-6791, Revision 1, October 2009.

# 7 CONSEQUENTIAL STEAM GENERATOR TUBE RUPTURE PROBABILISTIC RISK ASSESSMENT FOR THE EXAMPLE COMBUSTION ENGINEERING AND WESTINGHOUSE PLANTS

This chapter considers example Westinghouse (W) and Combustion Engineering (CE) plant designs to estimate both the consequential steam generator tube rupture (C-SGTR) probabilities and corresponding large early release frequency (LERF) fractions.

Section 7.1 discusses probabilistic risk assessment (PRA) for the example W plant; Section 7.2 discusses PRA for the example CE plant.

## 7.1 Example Westinghouse Plant

The information reported in NUREG/CR-6995, "SCDAP/RELAP5 Thermal-Hydraulic Evaluations of the Potential for Containment Bypass During Extended Station Blackout Severe Accident Sequences in a Westinghouse Four-Loop PWR," issued March 2010 (Ref. 1), provided the thermal-hydraulic (TH) analysis and the success criteria used for developing the PRA models for C-SGTR for the example W plant. NUREG/CR-6995 documents the TH evaluations performed using the SCDAP/RELAP5 systems analysis code and a model representing a W four-loop pressurized-water reactor (PWR) (i.e., Zion Nuclear Power Plant (ZNPP), Unit 1). The plant model for TH evaluation benefitted from the following:

- extensive iterative comparisons with evaluations of natural circulation flows and turbulent mixing using a computational fluid dynamics code
- comparison with experimental data for pertinent fluid-mixing behavior

NUREG/CR-6995 also included some sensitivity evaluations and uncertainty analyses for the station blackout (SBO) accident sequences. ZNPP was the example W plant for the C-SGTR PRA evaluation, and the available documents on its PRA provided the other required input information for the C-SGTR PRA evaluation.

### 7.1.1 Description of the Selected TH Sequences for C-SGTR PRA for the Example Westinghouse Plant

The following representative scenarios from NUREG/CR-6995 (Ref. 1) were examined for potential use in evaluating C-SGTR. These scenarios modeled leakage through the secondary side of each steam generator (SG), equivalent to a hole of 3.2 square centimeters ($cm^2$) (0.5 square inch ($in.^2$)). This size of leakage is sufficient to ensure that the pressure in the secondary side of the SGs approaches the atmospheric pressure after SG dryout. However, this assumed leakage area is not sufficient to maintain a low SG secondary-side pressure after the occurrence of a guillotine break of a single SG tube.

(1) **Station Blackout with Early Failure of the Turbine-Driven Auxiliary Feedwater (TDAFW) Pump Resulting in Core Damage and a Potential for C-SGTR Caused by Creep Rupture:** This scenario models the normal reactor coolant pump (RCP) seal leakage of 79.4 liters per minute (Lpm) (21 gallons per minute (gpm)) per pump. Core damage is expected in less than 2 hours. The potential for C-SGTR is considered after the onset of core damage.

This scenario is referred to as the "Wnewbase" case. Figure 7-1a shows the primary and secondary-side pressure in pounds per square inch (psi) and the hot-leg (HL) temperature in degrees Celsius (C). Figure 7-1b shows the difference between the HL temperature and the hottest tube temperature, the average hot tube temperature, and the average cold tube temperature.

(2 & 3) **Station Blackout with Failure of TDAFW Pump after Battery Depletion:** The TDAFW pump is initially considered available, but it fails after loss of direct current (dc) as the batteries deplete. The model uses the normal RCP seal leakage of 79.4 Lpm (21 gpm) per pump. The operator's action to depressurize SGs at 30 minutes, by opening at least one SG atmospheric dump valve or SG power-operated relief valve (PORV) per SG, drops the primary pressure below 4.82 megapascal (MPa) (700 psi). This actuates the accumulator discharge. The study analyzed two cases, referred to as Cases 153 and 153A, depending on the rate of depressurization (slower and faster rate). Case 153A results in sequence timing, including the CD that is delayed by at most 1.3 hours compared to Case 153, because of depressurization of the SGs to the lower pressure (120 psi absolute (psia), rather than 280 psia for Case 153). Greater depressurization of the RCS resulted in more accumulator injection.

(4) **Station Blackout with Early Failure of the TDAFW Pump and Guillotine Break of One SG Tube after Core Damage:** The model assumes the normal RCP seal leakage of 79.4 Lpm (21 gpm). Early core damage is expected in less than 2 hours because of a total loss of feedwater at the onset of the transient. At approximately 12,926 seconds, one of the flawed tubes with a stress magnification factor of 2 ($m_p$ = 2) ruptures. The resulting modeled leak area is equivalent to the area associated with a guillotine break of one tube. This will result in a slow depressurization of the primary; however, it is not fast enough to prevent HL failure. The HL fails shortly thereafter (13,630 seconds, approximately 11 minutes), terminating the containment bypass. Figure 7-2 shows the results of this scenario, referred to as Case F2.

**Similar to Case F2 Except that the Failed Flawed Tube Has a Stress Magnification Factor of 3 ($m_p$ = 3):** The flawed tube fails at 12,930 seconds. The model excluded the HL failure. Therefore, this case run captured the prolonged depressurization of the primary as a function of time because of the guillotine break of one SG tube. Figure 7-3 shows the results of this scenario, referred to as Case F3.

**Similar to "Wnewbase" Case Except with Different Sizes of Reactor Coolant System Seal Leakages:** Initial leakage is 79.4 Lpm (21 gpm) per RCP. At 13 minutes, leakage is increased to 226.8 Lpm (60 gpm) per RCP. Finally, when fluid in the RCPs becomes saturated, leakage is increased to 1,703 Lpm (450 gpm) per RCP. This case, called Case Run C21-60-450, resulted in a clearance of the loop seal.

The observations below result from the TH analyses used in developing the PRA models and the associated sensitivity runs.

As noted in Figures 7-1a and 7-1b, the HL temperature is significantly higher than the average hot tube and the hottest tube temperatures by as high as 400 degrees C (752 degrees Fahrenheit (F)). Figure 7-1b shows the differences between the HL temperature and the hottest tube temperature, average hot tube temperature, or average cold tube temperature. A higher HL temperature is the driving factor for HL failure before the failure of the

SG tubes. This would also explain the lower estimate of the risk associated with the C-SGTR for the example W plant.

For those cases where the TDAFW pump is operating, the time to core uncovery depends on the scheme used for primary depressurization. In both cases analyzed by SCDAP/RELAP5 models, Cases 153 and 153A, aggressive cooling and depressurization using the secondary system resulted in dropping the primary pressure below the accumulator discharge setpoint. The accumulator discharge resulted in a significant delay in core uncovery (about 11 hours for Case 153 and 13 hours for Case 153A). No case runs were performed for when the operator fails to depressurize the primary via rapid secondary cooldown. In such cases, it is assumed that the TH response will be similar to the Wnewbase case but shifted by at least 4 hours, corresponding to the battery duration.

As shown in Figure 7-3, the guillotine break of one tube will not depressurize the primary such that it prevents subsequent HL failure. Therefore, the PRA event trees and resulting estimated probabilities should differentiate between single tube failures and multiple tube failures.

As seen in Figure 7-3, the failure of SG tubes with a leak area equivalent to the guillotine break of one tube will result in the pressurization of the SG secondary side. For the purpose of severe-accident management guideline (SAMG) activities related to flooding the SG, the SG secondary side has to be fully depressurized. This requires opening the secondary-side PORVs or safety relief valves (SRVs). The opening of PORVs or SRVs occurs under the harsh environment caused by the core melt accident.

The TH runs showed that the loop seal is cleared when the RCP leakage is about 1,703 Lpm (450 gpm) per pump. The TH runs also indicate that the time of RCP seal failure, and its relation to the time when the cold leg becomes saturated, affects loop seal clearing.

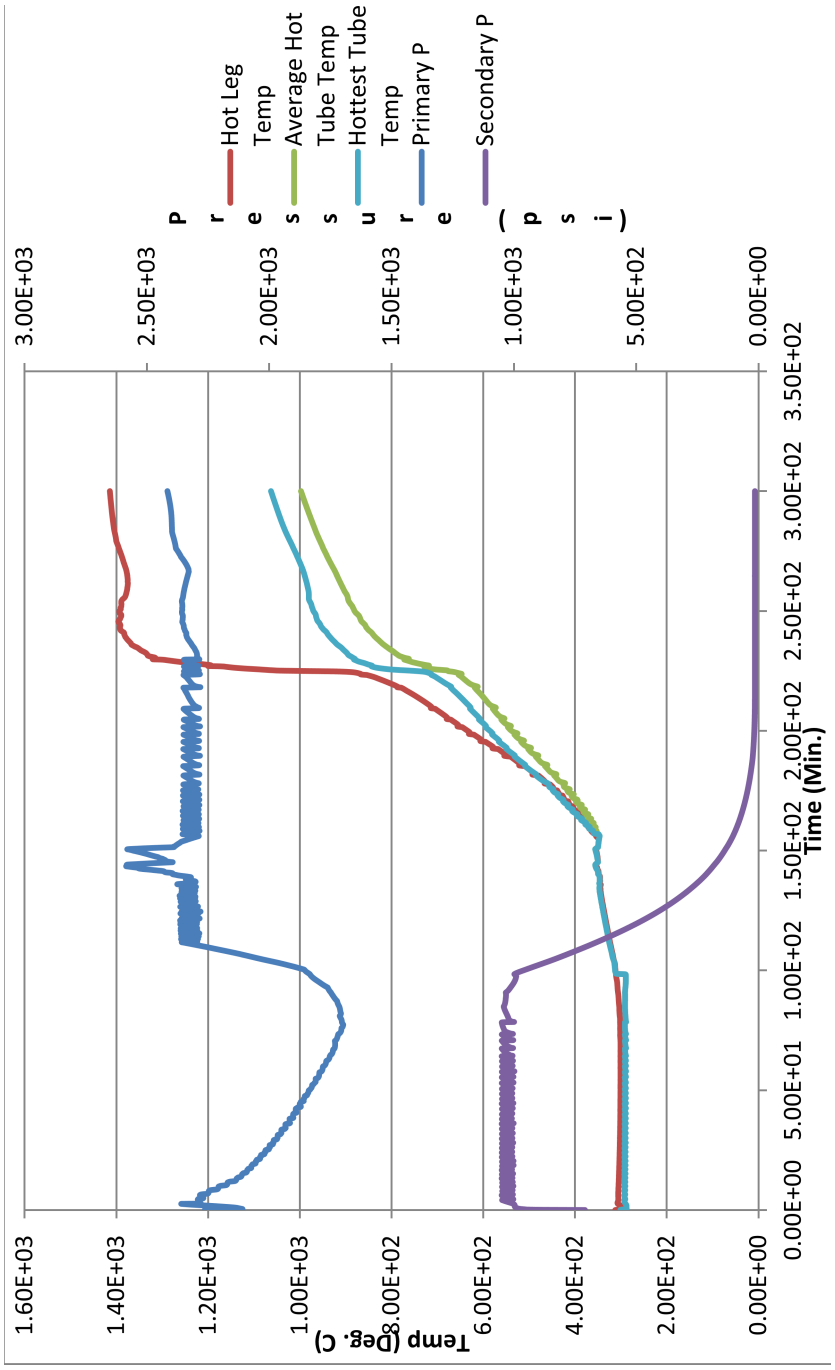


Figure 7-1(a) TH results for Wnewbase

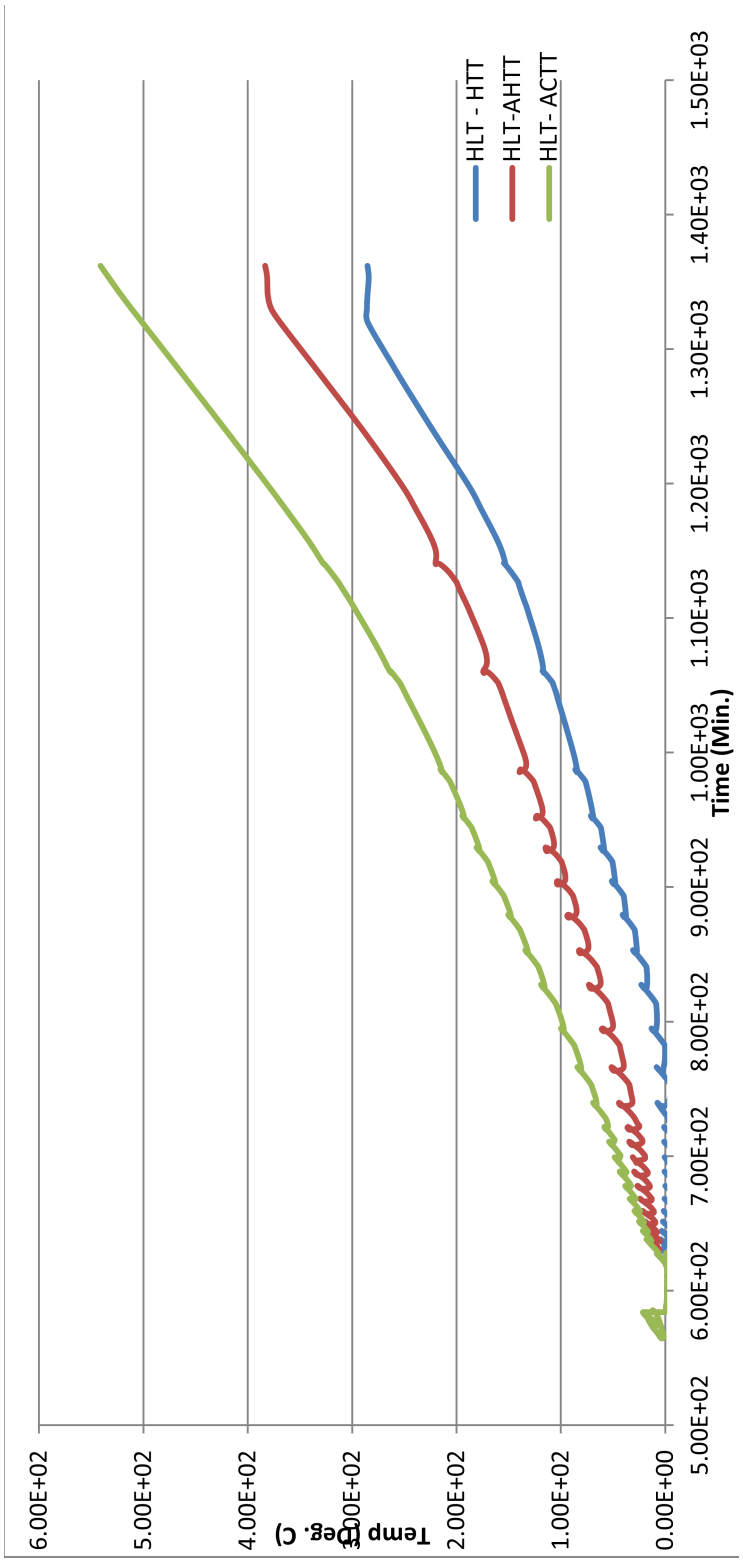


**Figure 7-1(b) Difference between the HL temperature and the temperatures of the hottest tube (HTT) and the average hot tube (AHTT) and cold tube (ACTT) for Wnewbase**

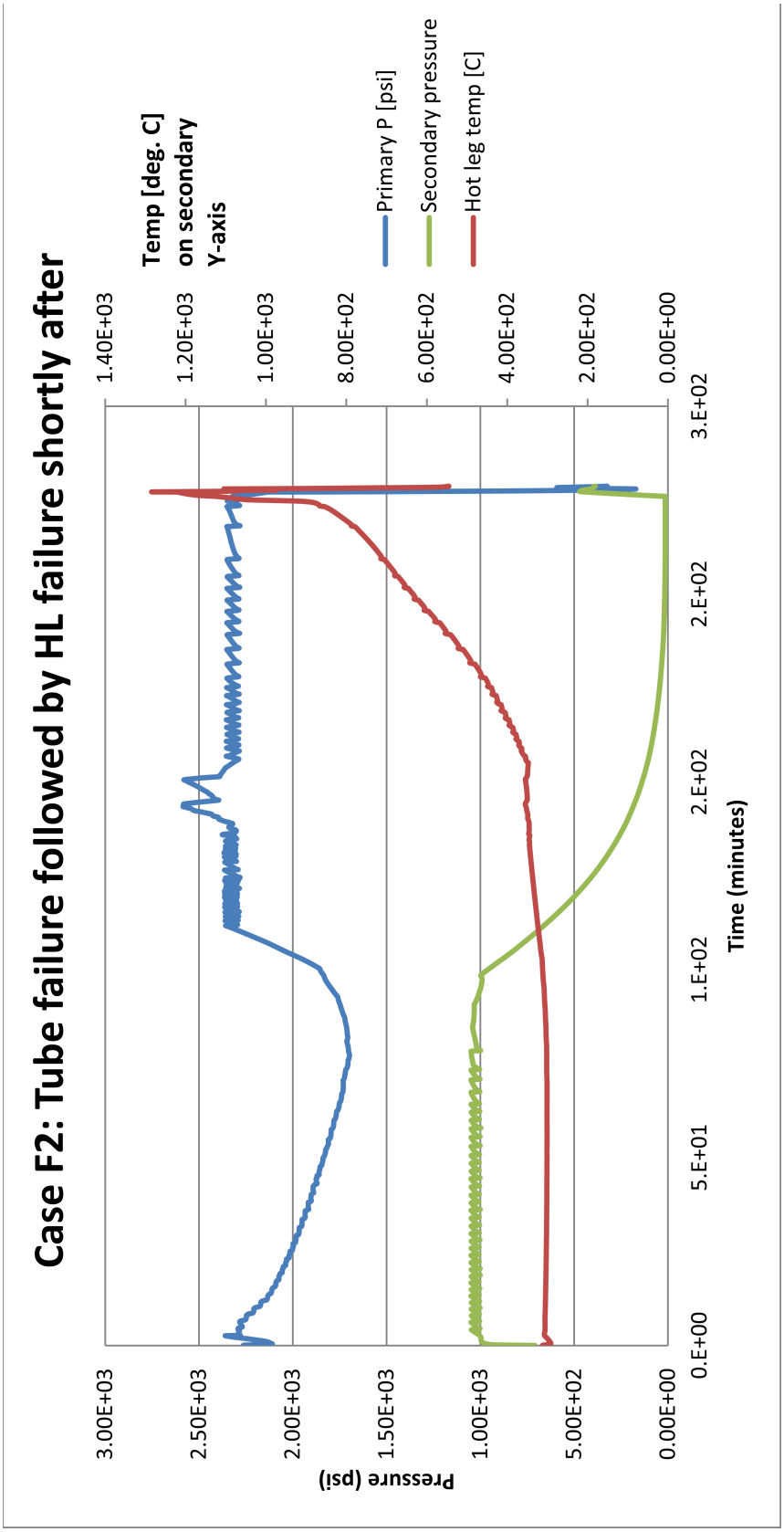


Figure 7-2 TH results for Case F2

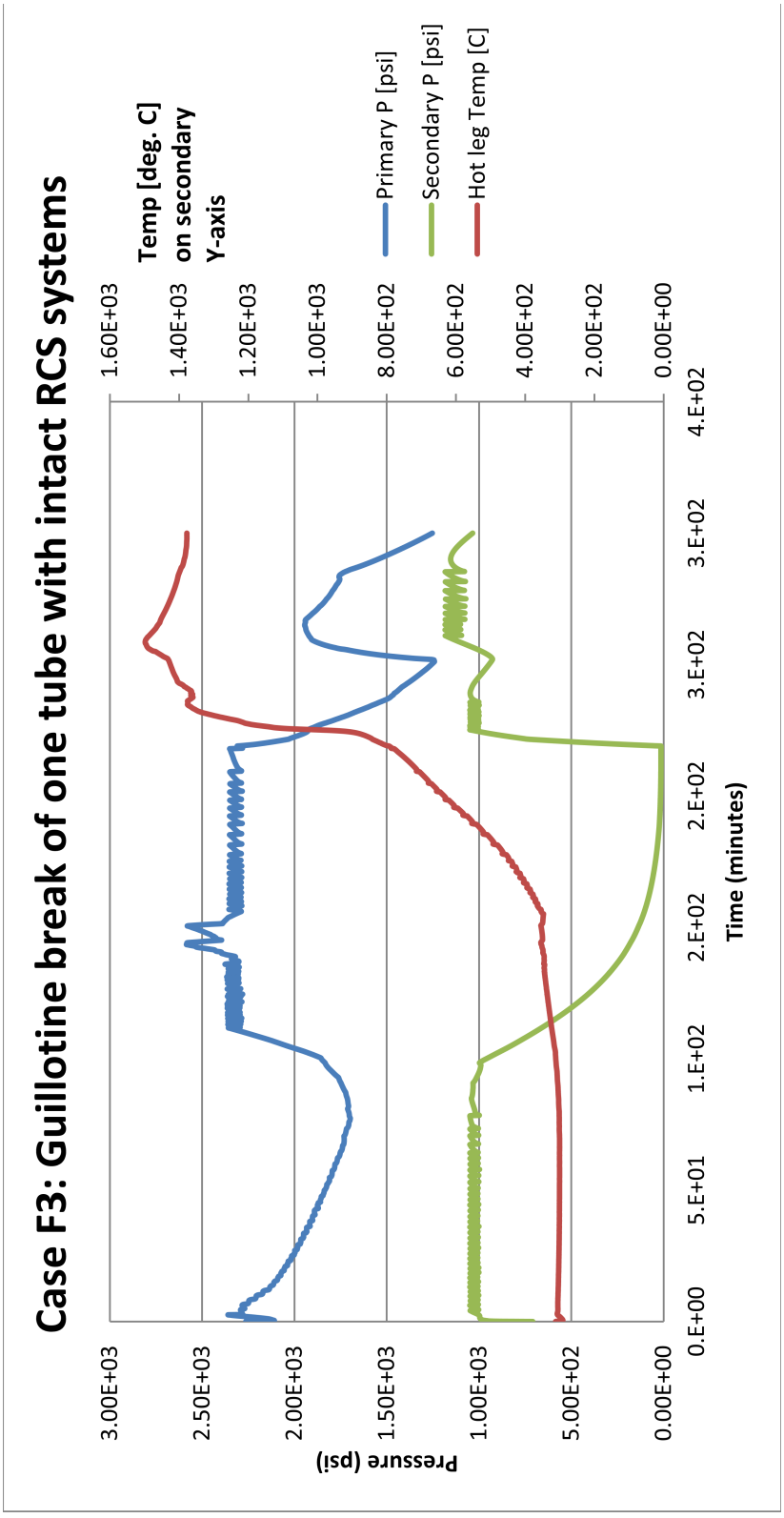


Figure 7-3 TH results for Case F3

### 7.1.2 Estimating the Entry Frequency from Level 1 PRA for C-SGTR

ZNPP was selected for developing C-SGTR PRA models to ensure consistency with the TH analyses results. No current PRA or standardized plant analysis risk (SPAR) models are available for ZNPP, and ZNPP units are no longer in operation. The accident frequency for the entry point to the C-SGTR PRA was, therefore, estimated based on the plant design features and information from vintage ZNPP PRA documents. Appendix G provides a detailed discussion of various core damage frequency (CDF) contributors from SBO scenarios to overall CDF from both internal and external events. The technical discussion in Appendix G (Section G.1) supports the quantitative values used in this section.

Because of a long-term SBO (*ltsbo*) (beyond battery depletion) that can be used as the entry point for a Level 2 PRA, the CDF estimate is around $1.2X10^{-5}$ per reactor year (RY). This is consistent with the estimate of the *ltsbo* scenarios reported in NUREG-1935, "State-of-the-Art Reactor Consequence Analyses (SOARCA) Report," issued November 2012 (Ref. 2) (between $1.0X10^{-5}$ and $2.0X10^{-5}$ per RY). Table 7-1 shows the contributions from both internal and external hazards.

Table 7-1 Contributions of Various Events to Long-Term SBO Scenarios

| Initiating Event | Long Term SBO CDF | Percent Contribution | Source |
|---|---|---|---|
| Internal events, including internal floods | 5.2E-6 | 25.5% | NUREG-4551 |
| Seismic | 5.6E-6 | 27.5% | NUREG/CR-3300 |
| Fire | 9.5E-6 | 47.0% | Appendix G |
| Total | 2.03E-5 | 100.0% | |

The uncertainties associated with these frequencies are not presently estimated because of the lack of detailed models and data. Surrogate uncertainties from similar plants, such as Indian Point Unit 3, could be considered if needed.

Table 7-2 shows the main plant features of ZNPP that are pertinent to this study.

Table 7-2 Related Information from Zion Nuclear Stations for This Study

| Systems | System Features |
|---|---|
| Number of SGs and number of tubes per SG | 4 SGs each with 3,300 tubes |
| Emergency Power System | a. Each unit consists of 3 4160-VAC class 1E buses, each feeding 1 480-VAC class 1E bus and a motor control center.<br>b. For the 2 units, there are 5 diesel generators, with one being a swing diesel generator shared by both units.<br>c. 3 trains of dc power are supplied from the inverters and 3 unit batteries. It has a battery life of 6 hours. |
| Auxiliary Feedwater (AFW) System | a. Two 50-percent motor-driven pumps and one 100-percent turbine-driven pump.<br>b. Pumps take suction from their own unit condensate storage tank (CST) but can be manually cross-tied to the other unit's CST. |
| Service Water (SW) | a. Shared system between both units<br>b. Consists of 6 pumps and 2 supply headers<br>c. Cools component cooling heat exchangers, containment fan coolers, diesel generator coolers, AFW pumps<br>d. 2 out of 6 pumps can supply sufficient flow. |
| Component Cooling Water (CCW) | a. Shared system between both units<br>b. Consists of 5 pumps, 3 heat exchangers, and 2 surge tanks<br>c. Cools RHR heat exchangers, RCP motors and thermal barriers, RHR pumps, SI pumps, and charging pumps<br>d. One of 5 pumps can provide sufficient flow. |
| Secondary Relief | a. Steam dump valves<br>b. Atmospheric dump valves (one per SG)<br>c. SRVs |
| Primary Relief | a. 2 PORVs<br>b. 3 SRVs |
| Containment | a. Large, dry, prestressed concrete<br>b. 2.6 million cubic foot volume<br>c. 49 psig design pressure |

Reproduced from NUREG/CR-3300 (Ref. 3), NUREG/CR-4550 (Ref. 4), and NUREG/CR-4551 (Ref. 5).

### 7.1.3 Conditional Probability of C-SGTR at Each Flaw Bin

In this section, the flaw distributions obtained in Chapter 6, and the Wnewbase sequence TH input discussed earlier in Section 7.1, serve to gain an understanding of various SG tube leaks and their relation to HL failure time for different individual flaw sizes; an analysis of the effect of multiple flaws appears later in this section.

A series of calculations used the C-SGTR calculator, which was developed to support the work in this report. The calculator is used to estimate the failure times and leak sizes of SG tubes with different types of flaws. The software also has built-in models for HL and surge-line failures caused by the creep-rupture failure mechanism, and it estimates the failure times and probabilities of the HL and surge line. The scope of the models currently includes new SG tube materials and the associated property data for thermally-treated Inconel 600 and 690 (600TT and 690TT). The C-SGTR calculator is designed to support the PRAs that address the risk associated with steam generator tube rupture (SGTR) scenarios—as an initiator, as a consequence of plant transients (design-basis accident (DBA) scenarios), and as a result of core damage sequences (C-SGTR). The calculator software uses plant-specific design information, material properties, plant-specific SG tube flaw data, and scenario-specific TH results as input to generate an estimate of the

C-SGTR probability. Appendix B discusses examples of calculator runs, as well as input files and runs.

Flaw bins were developed to represent different sizes of flaws. Using Wnewbase as the TH input file, and the flaw length and depth representing the midpoint of each flaw bin, a series of case runs were performed, using the C-SGTR calculator. Each case run estimated the probability of an SGTR with an area of at least 1 $cm^2$ (0.16 $in.^2$) before HL or surge-line failure. The 1 $cm^2$ (0.16 $in.^2$) threshold leak area was conservatively selected as the criterion for potential gross tube failure.

All case runs for the W plant in Section 7.1.4 assumed that a flawed tube can be exposed to either an average hot tube temperature or an average cold tube temperature. The fraction of tubes exposed to the average hot temperature and average cold temperature used in the analysis were 0.45 and 0.55, respectively. The contribution from the hottest tubes was not included in these analyses and was judged to be insignificant. The hottest tube temperature deviates significantly from the average hot tube temperature for temperatures exceeding 850 degrees C (1,562 degrees F) (e.g., see Figure 7-1a, around 225 minutes). HL will be exposed to a very high elevated temperature, and HL failure is generally expected to occur before this deviation takes place. Therefore, the effect of the hottest tube temperature could be enveloped with the average hot tube temperature for flawed tubes.

Table 7-3 presents the results from these case runs for each flaw bin for Inconel 600 and Table 7-4 presents them for Inconel 690. The results reaffirm that, for the wear flaws, the bounding probability of tube failure is only a function of the flaw depth. These results show that a significant contribution to C-SGTR probability for the selected W plant comes only from flaws with a depth greater than 60 percent. For all smaller flaw sizes, the probability that the SG tubes fail before the HL fails is estimated to be negligible (i.e., zero).

**Table 7-3 Probability that a Flaw that Belongs to a Bin Defined by Depth and Length Range Fails [a] before the HL Failure for Inconel 600 Tubes for "Wnewbase" TH File for the Selected W Plant**

| Depth/ Length | 1 cm | 2 cm | 3 cm | 4 cm | 5 cm | 6 cm | Average Across Length |
|---|---|---|---|---|---|---|---|
| 0.0 to 0.1 | ~ 0 | ~ 0 | ~ 0 | ~ 0 | ~ 0 | ~ 0 | ~ 0 |
| 0.1 to 0.2 | ~ 0 | ~ 0 | ~ 0 | ~ 0 | ~ 0 | ~ 0 | ~ 0 |
| 0.2 to 0.3 | ~ 0 | ~ 0 | ~ 0 | ~ 0 | ~ 0 | ~ 0 | ~ 0 |
| 0.3 to 0.4 | ~ 0 | ~ 0 | ~ 0 | ~ 0 | ~ 0 | ~ 0 | ~ 0 |
| 0.4 to 0.5 | ~ 0 | ~ 0 | ~ 0 | ~ 0 | ~ 0 | ~ 0 | ~ 0 |
| 0.5 to 0.6 | ~ 0 | ~ 0 | ~ 0 | ~ 0 | ~ 0 | ~ 0 | ~ 0 |
| 0.6 to 0.7 | ~ 0.05 | ~ 0.05 | ~ 0.05 | ~ 0.05 | ~ 0.05 | ~ 0.05 | ~ 0.05 |
| 0.7 to 0.8 | ~ 0.8 | ~ 0.8 | ~ 0.8 | ~ 0.8 | ~ 0.8 | ~ 0.8 | ~ 0.8 |
| 0.8 to 0.9 | ~ 1 | ~ 1 | ~ 1 | ~ 1 | ~ 1 | ~ 1 | ~ 1 |
| 0.9 to 1.0 | ~ 1 | ~ 1 | ~ 1 | ~ 1 | ~ 1 | ~ 1 | ~ 1 |

[a] For Tables 7-6 and 7-7, a conservative screening criterion of a flaw leak area greater than 1 square cm is used to determine failure.

Table 7-4 Probability that a Flaw that Belongs to a Bin Defined by Depth and Length Range Fails before the HL Failure for Inconel 690 Tubes for "Wnewbase" TH File for the Selected W Plant

| Depth/ Length | 1 cm | 2 cm | 3 cm | 4 cm | 5 cm | 6 cm | Average Across Length |
|---|---|---|---|---|---|---|---|
| 0.1 | ~ 0 | ~ 0 | ~ 0 | ~ 0 | ~ 0 | ~ 0 | ~ 0 |
| 0.2 | ~ 0 | ~ 0 | ~ 0 | ~ 0 | ~ 0 | ~ 0 | ~ 0 |
| 0.3 | ~ 0 | ~ 0 | ~ 0 | ~ 0 | ~ 0 | ~ 0 | ~ 0 |
| 0.4 | ~ 0 | ~ 0 | ~ 0 | ~ 0 | ~ 0 | ~ 0 | ~ 0 |
| 0.5 | ~ 0 | ~ 0 | ~ 0 | ~ 0 | ~ 0 | ~ 0 | ~ 0 |
| 0.6 | ~ 0.05 | ~ 0.05 | ~ 0.05 | ~ 0.05 | ~ 0.05 | ~ 0.05 | ~ 0.05 |
| 0.78 | ~ 0.75 | ~ 0.75 | ~ 0.75 | ~ 0.75 | ~ 0.75 | ~ 0.75 | ~ 0.75 |
| 0.8 | ~ 1 | ~ 1 | ~ 1 | ~ 1 | ~ 1 | ~ 1 | ~ 1 |
| 0.9 | ~ 1 | ~ 1 | ~ 1 | ~ 1 | ~ 1 | ~ 1 | ~ 1 |

Tables 7-3 and 7-4 show the probability of a C-SGTR with leakage areas greater than 1 $cm^2$ (0.16 $in.^2$), from a single flawed tube as a function of the flaw depth. These probabilities could be viewed as relative indications of the effect of flaw depth on the C-SGTR probability for the W plant. Two observations are based on these results:

(1) The contribution to C-SGTR probability from flaws with a depth less than 60 percent is expected to be small.

(2) Inconel 600TT and 690TT tube materials have comparable performance when considering the overall C-SGTR probability.

The first observation signifies that flawed tubes should be plugged at a threshold depth significantly less than 60 percent, so that the possibility of a flaw growing to a depth greater than 60 percent in the next cycle is minimized. It also signifies that a more accurate estimate of the rate of flaw generation with large depths is necessary for risk assessment of C-SGTR scenarios. The second observation emphasizes that a lower flaw rate generation in Inconel 690 is offset with a slightly higher creep-rupture resistance of the Inconel 600.

Current W plants use SGs with Inconel 600TT and 690TT. The number of flaws per cycle for 600TT and 690TT SG tubes is significantly lower than the older SG tubes made of mill-annealed Inconel 600. As Chapter 6 discusses, the available surveillance data were the basis for the size distributions of flaws in terms of flaw length and depth. Because of the limited number of plants and inspection cycles in the surveillance data, the estimated flaw rates and flaw characteristics are significantly dependent on the degree to which the surveillance data represent the U.S. plants. Any potential anomalies in the data of even one plant would significantly affect the estimates because of the small number of plant samples.

Lack of surveillance data from a larger population of plants limits the range of the applicability of the estimates, and it causes uncertainties in the estimated parameters for characterizing the flaws. As an example, a large number of unreliable small-depth measurements; less than 10 percent, from one of the plants in the surveillance data, significantly skewed the depth distribution toward the shallow flaws. This issue was compounded because surveillance records had a large number of missing depth measurements. The depth distribution generated from the

data, therefore, is expected to be skewed toward the lower depth values. Some adjustments were made to the original estimated distributions of flaw depth and length to compensate for the potential shift of flaw size distributions toward the shallower and smaller flaws. This was done by shifting the depth distribution by 7 percent deeper and the length distribution by 0.8 cm (0.31 in.) longer to ensure that the numbers of large flaws (i.e., flaws that are plugged) have been maintained. The raw data for plugging are readily available in the flaw database. The flaw data show that, out of 2,440 flaws, 233 were plugged (about 9.5 percent). Furthermore, a plugged tube is expected to have a flaw with an average length of 1.3 cm (0.5 in.), and a depth greater than 30 percent. The size distributions are shifted such that the probability of an occurrence of a flaw below these sizes accounts for 90 percent (it is approximately equal to 100 percent minus the 9.5 percent of tubes that were plugged) of the total number of flaws. Figures 7-4 and 7-5 show the shifted distribution for flaw depth and flaw length. These distributions apply to both CE and W SGs and to both Inconel 600TT and 690TT.

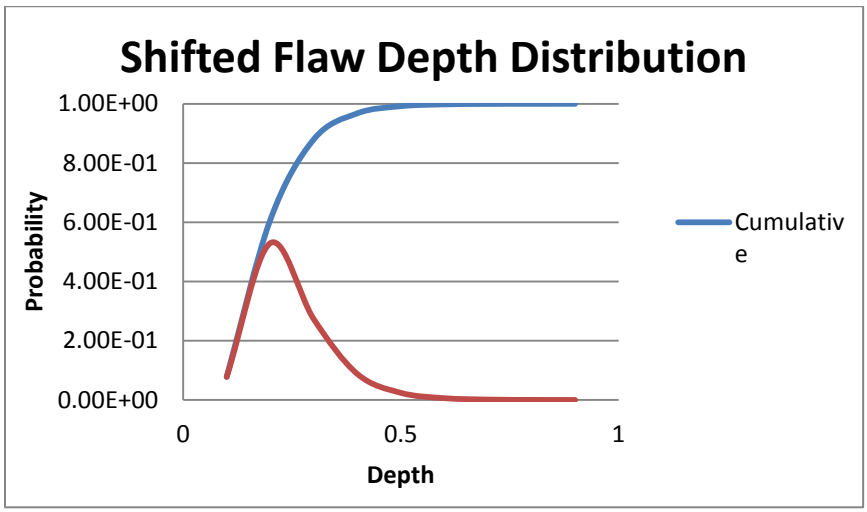


Figure 7-4 Shifted distribution for flaw depth

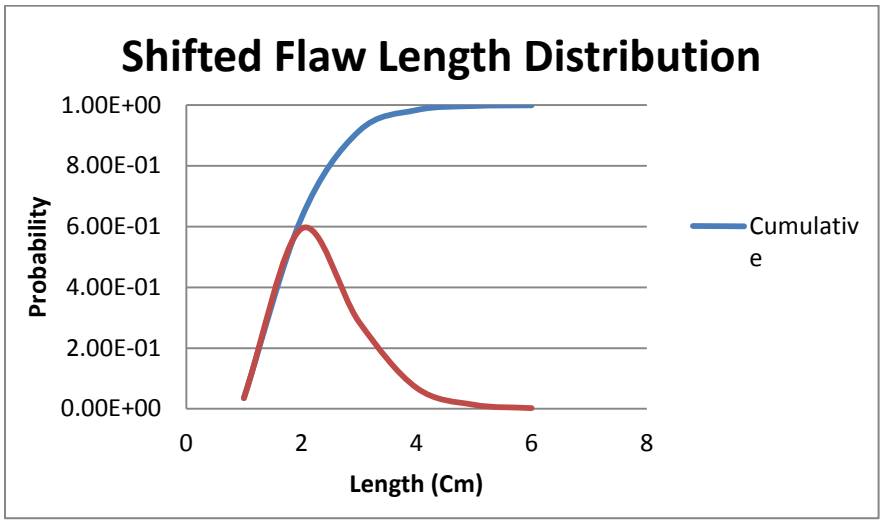


Figure 7-5 Shifted distribution for flaw length

ZNPP had four SGs, each with about 3,300 tubes that this study assumes could be made of either Inconel 600 or Inconel 690. There are, therefore, 13,200 unplugged tubes for a unit of ZNPP. The average number of flaws generated for the first 14 effective full-power years (EFPYs) of operation using the Inconel 600TT flaw generation rate equation, is about 323 flaws per one unit of ZNPP. (Section 6.3.2 includes a sample calculation.) At the end of the 14 EFPYs, the study assumed that there was a periodic SG inspection; therefore, all the large flaws out of 322 flaws per unit are expected to be plugged (approximately 30 plugged tubes for four SGs). An additional 31 flaws will be generated during the 15 EFPYs of operation. Therefore, 323 flawed tubes were expected for all four SGs during the operating period at 15 EFPYs, with an average of about 2 to 3 large flaws that may need plugging at the end of the 15 EFPYs.

Flaw lengths and depths are sorted into a set of bins. Table 7-5 shows the probability that a flaw resides in one of the bins at a time of 15 EFPYs for ZNPP SG tubes made of either Inconel 600 or 690. The length and depth distributions shown in Figures 7-4 and 7-5 form the basis for these estimated probabilities, apply to both Inconel 600TT and 690TT, and do not differentiate between the W and CE plants. These probabilities are multiplied by the number of flaws estimated earlier to determine the average numbers of flaws for each flaw bin. The estimates for bins consisting of large flaws consider the expected number of flaws only in the last cycle. All flaws deeper than approximately 0.3 (bin with a depth between 0.3 and 0.4) discovered in the previous cycles are assumed to have been plugged. The total number of flaws used for calculating the expected number of flaws for each bin, therefore, follows the following rules:

- For flaw bins with a depth of less than 0.3 (30 percent of the wall thickness), the total number of flaws used to estimate the expected number of flaws was the summation of all flaws in previous cycles plus the number of flaws in the last cycle. For Inconel 600, this value is 354 flaws (322 flaws in previous cycle plus 31 flaws in the last cycle). For Inconel 690, this value is 218 flaws (198 flaws in previous cycle plus 20 flaws in the last cycle).

- For flaw bins with a depth greater than 0.3 (30 percent of the wall thickness), the total number of flaws is based on the flaws generated in the last cycle (cycle 15). The values for Inconel 600 and 690 are 31 and 20, respectively.

Tables 7-6 and 7-7 show the average number of flaws for Inconel 600 and 690, respectively. The values shown in these tables represent the expected number of flaws in each bin, rounded to the nearest integer. Therefore, a value of zero for the expected numbers of flaws in a bin should not be construed as having a zero probability of occurrence. To find the probability that a flaw is realized in each flaw bin, consult Table 7-5.

Table 7-5 Probability that a Detected Flaw Belongs to a Bin Size at 15 EFPYs

| | | Flaw Length | | | | | | Total |
|---|---|---|---|---|---|---|---|---|
| | | 0 cm to 1 cm | 1 cm to 2 cm | 2 cm to 3 cm | 3 cm to 4 cm | 4 cm to 5 cm | 5 cm to 6 cm | |
| Flaw Depth%/100 | 0 to 0.1 | 2.74E-3 | 4.62E-2 | 2.23E-2 | 5.38E-3 | 1.04E-3 | 1.80E-4 | 7.78E-2 |
| | 0.1 to 0.2 | 1.86E-2 | 3.14E-1 | 1.52E-1 | 3.66E-2 | 7.08E-3 | 1.23E-3 | 5.29E-1 |
| | 0.2 to 0.3 | 9.59E-3 | 1.62E-1 | 7.81E-2 | 1.89E-2 | 3.64E-3 | 6.31E-4 | 2.73E-1 |
| | 0.3 to 0.4 | 3.09E-3 | 5.21E-2 | 2.52E-2 | 6.07E-3 | 1.17E-3 | 2.03E-4 | 8.78E-2 |
| | 0.4 to 0.5 | 8.47E-4 | 1.43E-2 | 6.90E-3 | 1.66E-3 | 3.22E-4 | 5.57E-5 | 2.41E-2 |
| | 0.5 to 0.6 | 2.14E-4 | 3.61E-3 | 1.74E-3 | 4.21E-4 | 8.13E-5 | 1.41E-5 | 6.08E-3 |
| | 0.6 to 0.7 | 5.14E-5 | 8.67E-4 | 4.19E-4 | 1.01E-4 | 1.95E-5 | 3.38E-6 | 1.46E-3 |
| | 0.7 to 0.8 | 1.19E-5 | 2.01E-4 | 9.73E-5 | 2.35E-5 | 4.54E-6 | 7.86E-7 | 3.39E-4 |
| | 0.8 to 0.9 | 2.71E-6 | 4.57E-5 | 2.21E-5 | 5.32E-6 | 1.03E-6 | 1.78E-7 | 7.70E-5 |
| | 0.9 to 1.0 | small | | | | | | |
| | **Total** | 3.51E-2 | 5.93E-1 | 2.87E-1 | 6.92E-2 | 1.34E-2 | 2.32E-3 | 1.00E+00 |

Table 7-6 Expected Number of Flaws that Belong to a Flaw Bin Defined by Depth and Length Range for Zion SGs with Tubes Made of Inconel 600

| Depth/ Length | 0 cm to 1 cm | 1 cm to 2 cm | 2 cm to 3 cm | 3 cm to 4 cm | 4 cm to 5 cm | 5 cm to 6 cm | Total |
|---|---|---|---|---|---|---|---|
| 0 to 0.1 | 1 | 16 | 8 | 2 | 0 | 0 | 27 |
| 0.1 to 0.2 | 7 | 111 | 54 | 13 | 3 | 0 | 188 |
| 0.2 to 0.3 | 3 | 57 | 28 | 7 | 1 | 0 | 96 |
| 0.3 to 0.4 | 1 | 2 | 1 | 0 | 0 | 0 | 4 |
| 0.4 to 0.5 | 0 | 0 | 0 | 0 | 0 | 0 | 0 |
| 0.5 to 0.6 | 0 | 0 | 0 | 0 | 0 | 0 | 0 |
| 0.6 to 0.7 | 0 | 0 | 0 | 0 | 0 | 0 | 0 |
| 0.7 to 0.8 | 0 | 0 | 0 | 0 | 0 | 0 | 0 |
| 0.8 to 0.9 | 0 | 0 | 0 | 0 | 0 | 0 | 0 |
| **Total** | 12 | 186 | 91 | 22 | 4 | 0 | 315 |

The expected values of flaws in each bin illustrate the expected size distribution of flaws. The values shown in the tables also account for the flaws detected in previous cycles that were so large that the affected tubes were plugged. The approximation used in these calculations, plus the effect of rounding off the expected number of flaws per bin, has generally resulted in slightly fewer flaws than expected. As an example, for Inconel 600, Table 7-6 indicated an expected number of 315 flaws, rather than the 323 flawed tubes estimated earlier.

Table 7-7 Expected Number of Flaws that Belong to a Flaw Bin Defined by Depth and Length Range for Zion SGs with Tubes Made of Inconel 690

| Depth/ Length | 0 cm to 1 cm | 1 cm to 2 cm | 2 cm to 3 cm | 3 cm to 4 cm | 4 cm to 5 cm | 5 cm to 6 cm | Total |
|---|---|---|---|---|---|---|---|
| 0 to 0.1 | 1 | 10 | 5 | 1 | 0 | 0 | 17 |
| 0.1 to 0.2 | 4 | 68 | 33 | 8 | 2 | 0 | 115 |
| 0.2 to 0.3 | 2 | 35 | 17 | 4 | 1 | 0 | 59 |
| 0.3 to 0.4 | 1 | 1 | 1 | 0 | 0 | 0 | 3 |
| 0.4 to 0.5 | 0 | 0 | 0 | 0 | 0 | 0 | 0 |
| 0.5 to 0.6 | 0 | 0 | 0 | 0 | 0 | 0 | 0 |
| 0.6 to 0.7 | 0 | 0 | 0 | 0 | 0 | 0 | 0 |
| 0.7 to 0.8 | 0 | 0 | 0 | 0 | 0 | 0 | 0 |
| 0.8 to 0.9 | 0 | 0 | 0 | 0 | 0 | 0 | 0 |
| **Total** | 8 | 114 | 56 | 13 | 3 | 0 | 194 |

The information generated in Tables 7-5 through 7-7 can be used to obtain an initial estimate of the C-SGTR probability.

### 7.1.4 Estimating C-SGTR Probability

This section estimates the C-SGTR probability. The analyses are performed in a progressive manner, starting with the least rigorous method for estimating the C-SGTR probability using the individual flaw depth, assuming that the flaw length is sufficiently large that it can create substantial C-SGTR leakage. Next, the section considers information on flaw lengths and the impact of multiple tube failures, rather than the failure of a single tube. Finally, the section discusses a rigorous method for aggregating over all flawed tubes with various depths and lengths.

#### *7.1.4.1 C-SGTR Probability Based on a Single Flaw with Large Lengths and Varying Depths*

The following discussion is a simple and quick estimate of C-SGTR probability using information obtained in the previous section. This approach assumes that only large flaws generated during the last operating cycle significantly contribute to C-SGTR. The analysis can be used for risk-informed screening purposes or for evaluating inspection findings in which the surveillance data are only available for flaw depth. This assumes that all flaws with greater than 30-percent depth were plugged during the last inspection outage. The analysis does not use information on flaw length to estimate the C-SGTR leakage area, and it includes all leakage areas of 1 $cm^2$ (0.16 $in.^2$) or larger.

The approach consists of the following steps:

(1) Estimate the number of flaws generated during the last operating cycle using distributions in Chapter 6.

(2) Using Table 7-5, estimate the expected number of flaws in each depth bin, based on the total number of flaws generated during the cycle.

(3) Determine the probability of one or more flaws failing during a high/dry/low accident sequence by multiplying the expected number of flaws in each depth bin by the conditional probability of the flaw leak area exceeding 1 $cm^2$ (0.16 $in.^2$) during a representative C-SGTR accident sequence (obtained from Table 7-3 for Alloy 600TT and Table 7-4 for Alloy 690TT tubes) and summing across all depth bins.

As discussed in Section 7.1.3, assume that 31 flaws were generated during the last cycle for SG tubes made of Inconel 600TT. The probability that at least one flaw out of these flaws belongs to the three large bins that contribute to C-SGTR (depths of 0.6, 0.7, and 0.8) is estimated by multiplying the cell probabilities in Table 7-3 by 31 flaws. The C-SGTR probability for each flaw bin is then estimated by multiplying the resulting number by the conditional C-SGTR probability for that bin from Table 7-6. The overall C-SGTR probability is then estimated by summing over the bins. This is shown below:

Table 7-8 C SGTR probability summed over the flaw bins for Inconel 600/690 (W)

| Depth Bin | Probability of Flaw Belonging to Depth Bin (Table 7-3) | Expected Number of Flaws in Depth Bin | Probability of C-SGTR from a Single Flaw in Depth Bin (Table 7-6) | Conditional Probability of C-SGTR for Accident Sequence |
|---|---|---|---|---|
| 0.6 – 0.7 | 1.46E-3 | 0.0453 | 0.05 | 0.00226 |
| 0.7 – 0.8 | 3.39E-4 | 0.0105 | 0.80 | 0.00841 |
| 0.8 – 0.9 | 7.70E-5 | 0.0024 | 1.00 | 0.00239 |
| 0.9 – 1.0 | small | small | 1.00 | small |
| Total | | | | 0.01310 |

A similar example using Alloy 690TT tubes with 20 flaws generated during the last operating cycle yields an estimate of $8.1X10^{-3}$ for the conditional probability of C-SGTR for the representative accident sequence.

Although this approach provides a relatively straightforward method for estimating the potential for an SG flaw to lead to C-SGTR, it does not consider the potential for the failure of multiple flaws, and it assumes that deep flaws have large lengths. The next section includes multiple flaws. The length assumption is also relaxed by only including the flaw lengths greater than 2 cm (0.78 in.) in the analysis. The criteria for gross tube failure was increased from a 1-$cm^2$ (0.16-$in.^2$) leak area to 2 $cm^2$ (0.32 $in.^2$), to reduce the conservatism in the C-SGTR estimates. The fractions of the C-SGTR probability caused by failure of multiple tubes (i.e., two or three tubes) are estimated. This analysis is more rigorous and involves additional calculations to estimate the C-SGTR probability.

### *7.1.4.2 Approach Based on Flaw Depth and Length; Addressing Failures of Multiple Flawed Tubes*

Appendix H describes in detail a refined method that accounts for the distributions of both flaw lengths and depths. This approach focuses on large flaws generated in the last cycle and neglects all smaller flaws that have no potential for C-SGTR. Large flaws are characterized as flaws that, if detected, would require the associated tube to be plugged. It is believed that the data associated with flaw sizes of large flaws, which are subject to tube plugging, are more precise and less susceptible to measurement errors. This approach evaluated both single and multiple tube failures with flaw sizes capable of creating leakage areas to be considered C-SGTR. The results showed that the contribution from single tube failure is comparable to the estimates obtained from the previous method. The results also showed that, for Inconel 600, the single tube failure contribution to C-SGTR is about $1.31X10^{-2}$ from both this and previous methods. Similarly, for Inconel 690, the single tube failure contribution to C-SGTR is $8.1X10^{-3}$ and $8.9X10^{-3}$ from the previous and this method, respectively. The estimated contribution of multiple tube failures causing C-SGTR was $8.2X10^{-5}$ and $3.8X10^{-5}$ for Inconel 600 and 690. The results in Table 7-9 generally show that the contribution of multiple tube failures to C-SGTR is negligible compared to single large tube failure in the example W plant.

**Table 7-9 Probability of Single and Multitube Failure in C SGTR for Inconel 600/690 (W)**
***(Sequences with early failure of TDAFW pump)***

| Tube Materials | C-SGTR: One Tube Failure | C-SGTR: Two Tube Failures | C-SGTR: More Than Two Tube Failures |
|---|---|---|---|
| Inconel 600 | 1.31E-2 | 8.24E-5 | Negligible |
| Inconel 690 | 8.90E-3 | 3.85E-5 | Negligible |

### *7.1.4.3 C-SGTR Probability Estimation Using Integrated Flaw Samples*

This approach estimates and aggregates the leak rate over all flawed tubes and assumes that the flaw lengths and depths are available for all tubes in each SG, based on the SG periodic inspection data. This approach could also be used with simulated flaw data for SG tubes, generated by statistical sampling of flaw generation rate, depth, and size distribution. In this manner, the approach accounts for the distributions of flaw depth, flaw length, and number of flawed tubes. The approach demonstrated in this study for W SGs simulated a set of flaws that included at least one large flaw (a set of expected flaws plus one large flaw). This method accounted for single and multiple tube failures and the likelihood that the leak area exceeds the critical leak area discussed in Section 2.5 (i.e., 6 $cm^2$ (0.93 $in.^2$)). This is the most flexible approach for a state-of-the-art PRA. It has wide applicability to various regulatory evaluations, including cases where the actual data from SG periodic surveillance are available.

As an example, assume that an expected flaw sample consists of 315 flaws shown earlier in Table 7-6. A case run was performed with the C-SGTR calculator to estimate the conditional probability of C-SGTR for these 315 expected flaws in the four SGs. Each flaw was modeled using the mid-point of its associated flaw bin. For example, a flaw cell with a length ranging from 2 to 3 cm (0.79 to 1.18 in.), and a depth ranging from 0.2 to 0.3 cm (0.08 to 0.12 in.) was represented by a flaw with a length of 2.5 cm (0.98 in.) and a depth of 0.25 (25 percent of wall thickness). There would be 28 flaws for this flaw bin; therefore, the same flaw size is repeated 28 times in the flaw file. A C-SGTR software case run then used this flaw file and the TH case run of Wnewbase. The results from this case run were used to estimate the failure probability

(or survival probability) of the reactor coolant system (RCS) and C-SGTR as a function of accident time.

The survival probability of the RCS at a given time is defined by the probability that the surge line has not failed and that none of the four HLs has experienced any failures. An easy way to combine these probabilities is to estimate the individual hazard rates (h(t)) of each of the RCS components (four HLs and one surge line) as a function of time. This is done for the individual RCS components using the following equation.

$$h(t) = \left[\frac{\frac{d(F(t))}{dt}}{1-F(t)}\right] = ([F_{i+1} - F_i]/[T_i - T_{i+1}])/(1 - F_i) \quad (7.1)$$

where F(t) is the cumulative failure probability.

The failure rate for the RCS ($\lambda_{RCS}$) can then be estimated by the sum of the hazard rates for the four HLs and the one surge line. $\lambda_{RCS}$ is used to estimate the survival function of RCS, shown in Figure 7-6. The probability that the RCS has not failed at a given time can be read from the curve. The graph shows a very rapid drop of the survival probability as a function of time. This indicates that the survival distribution has a small variance. RCS failure probability can be estimated by the complement of the survival probability (1-Survival probability).

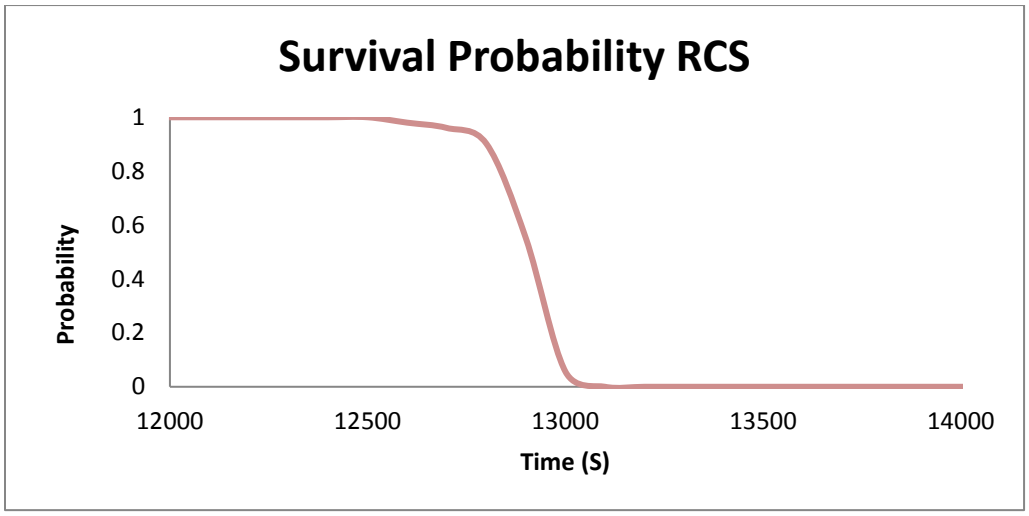


**Figure 7-6 RCS survival probability as a function of accident time for Wnewbase**

The failure probability for SG tubes was estimated by examining the percentiles of the leak area at the critical leak area (6 $cm^2$ (0.93 $in^2$) for this case study) as generated by the C-SGTR software. The survival probability then was estimated by one minus the failure probability. Figure 7-7 shows the percentiles of leak rate area for this case run.

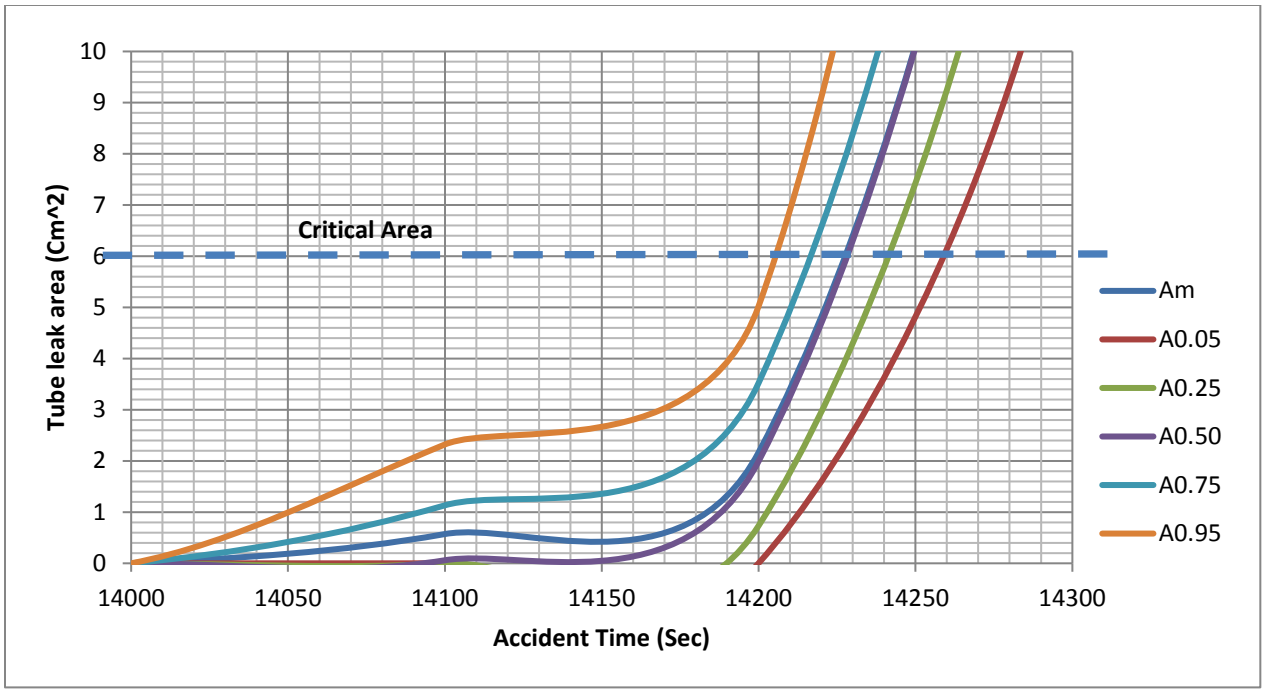


**Figure 7-7 Percentiles of the SG leak area distribution as a function of accident time**

The study used the percentile of the leak area probability at the critical area of 6 $cm^2$ (0.93 $in.^2$) to generate the probability distribution for critical failure time and used this distribution to calculate the SG survival probability. Figure 7-8 shows the resulting survival probabilities for RCS components and the survival and failure probabilities for SG tubes (with a leak area less than the critical area).

The probability of C-SGTR between t to (t + dt), was estimated by the product of the probabilities that RCS has survived up to time (t) and the SG failure with critical area has occurred between t and (t + dt).

$$Prob(CSGTR) = \int Prob\,(RCS\ survive\ at\ t) * Prob(CSGTR\ occurs\ between\ t\ and\ (t + dt) * dt \qquad (7.2)$$

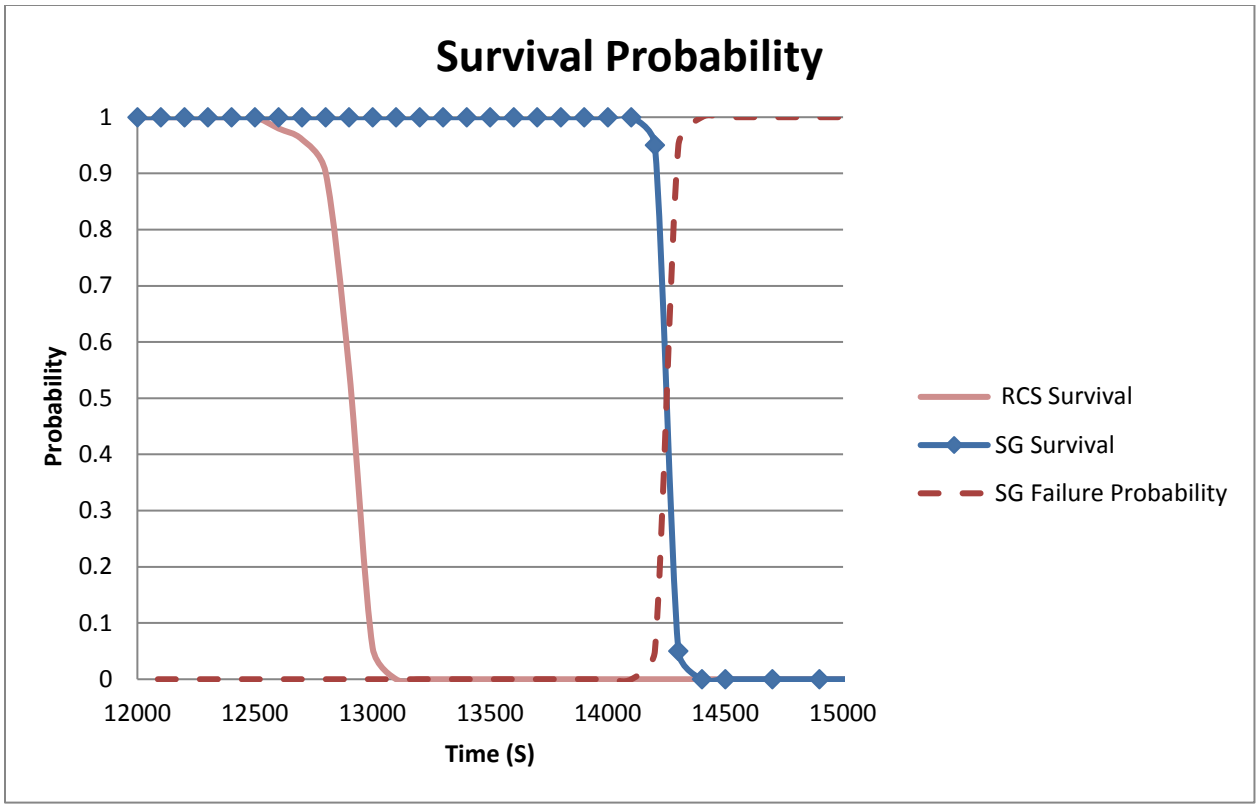


**Figure 7-8 Survival functions for RCS and SG tube failures with critical leak rate**

Figure 7-8 shows no overlap between the SG failure probability and RCS survival function, thereby indicating a negligible probability of the occurrence of C-SGTR for this set of flaws (i.e., SGTR failure with an area greater than the critical area can occur before RCS fails). Simple numerical integration, using spreadsheet calculations, shows that this probability is practically zero because of the very small variances of the two random variables depicted by the survival graphs (less than $1.0X10^{-10}$).

Although the above conclusion is valid for the expected flaw sample set, it may not hold when a flaw sample deviates from the expected set. Past experiences have shown that, even with a low probability, there is some possibility of detecting one or two large flaws at the end of an operating cycle. This is the main reason why the previous sections calculated much higher SGTR probabilities. To examine this hypothesis and its effect on C-SGTR probability, further case runs used the earlier expected flaw sample and added a large flaw. The earlier results showed that the additional large flaw needs to be larger than 60 percent of the nominal depth to effectively change the C-SGTR probability.

A new case run, therefore, used the expected flaw set and an added flaw with a length of 3.5 cm (1.4 in.) and a depth of 65 percent. Figure 7-9 shows the percentiles of leak rate area for this case run.

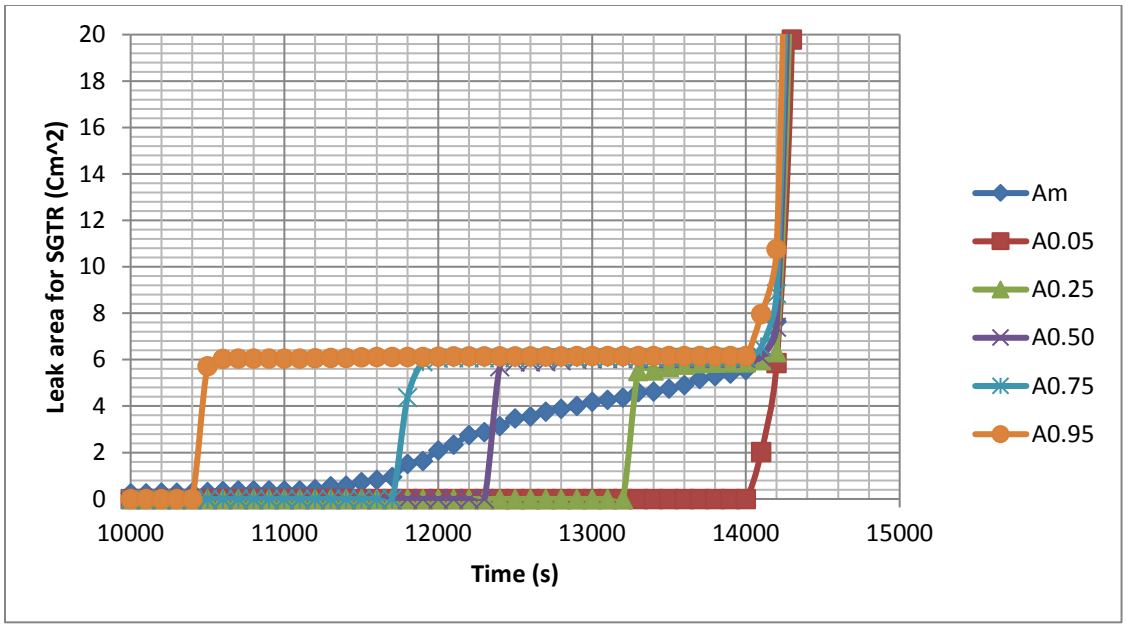


**Figure 7-9 Percentiles of the SG leak area distribution as a function of accident time**

Using the percentile of the leak area probability at the critical area of 6 $cm^2$ (0.93 $in.^2$), the probability distribution for critical failure time was generated. This distribution was used to calculate the SG survival probability. Figure 7-10 shows the resulting survival probabilities for RCS components and SGs for this case.

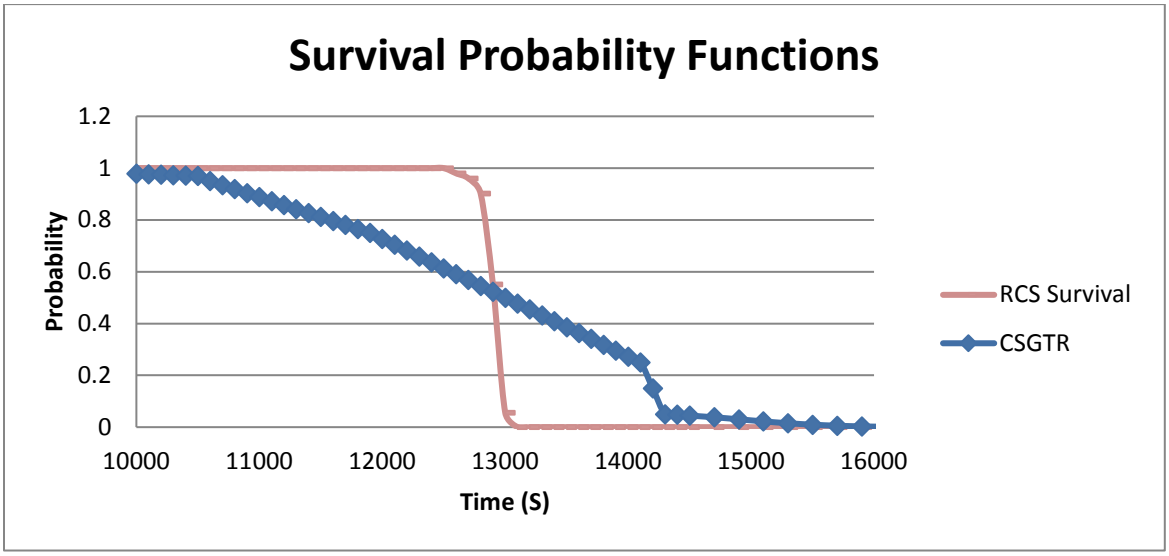


**Figure 7-10 Survival probability functions for RCS and flawed tubes**

This graph shows a significant overlap between the two survival probabilities. When the RCS survival probability is very close to one (around 12,900 seconds), the probability of C-SGTR is as high as 40 percent (i.e., 1 – 0.6). Therefore, the probability that C-SGTR could occur before HL failure is expected to be greater than 40 percent. In fact, simple numerical integrations, using spreadsheet calculations, show that the conditional C-SGTR probability, given the specified

65-percent depth flaw and accident sequence, is about 0.47. A better estimate of the C-SGTR probability can be obtained by estimating the C-SGTR probabilities for a large number of flaw samples and averaging them over the flaw samples. The C-SGTR probability is expected to be negligible for the majority of flaw samples except for a few of them that include at least one large flaw. The C-SGTR probability from such an analysis is expected to be about $1.0X10^{-2}$.

*7.1.4.4 Summary of the Results of C-CSGTR Calculations*

Sections 7.1.4.1 to 7.1.4.3 calculated the C-SGTR probability for the W-type SGs by three methods, each with different assumptions and complexity. This is so that the calculator does not directly assess the C-SGTR probability but only calculates the progression of the total leak area resulting from a set of input flaws. Other calculations must be made to get a probability of C-SGTR for a specified critical leak area. Therefore, it would be difficult to use the calculator to determine the distribution of C-SGTR probability, which accounts for variations among the plants and the performance of their SGs, as reflected by a large number of flaw sets. A set of flaws, which are determined, or sampled, external to the calculator, are placed as an input for the calculator. Thus, the three methods discussed in this section are designed to provide quantitative insights to the expected probability of C-SGTR without performing large numbers of simulations.

Table 7-10 summarizes the results of each of the methods, along with the assumptions used. The following briefly discusses the benefits and limitations of each approach:

- Integrated Analysis: The method in Section 7.1.4.3 uses a single flaw set to determine the expected probability of C-SGTR among all similar W plants. This flaw set reflects the flaws and the flaw sizes expected (i.e., averaged over all similar plants) in cycle 15 of their operations. Using the average flaw set as input, the calculator is expected to estimate the probability of C-SGTR in an average plant. There could be plants with higher or lower C-SGTR probability, as reflected by their plant-specific flaw sets. The method in Section 7.1.4.3 is the most rigorous, and it can be used for plant-specific analysis when plant-specific flaw data are available. It involves calculations that are in the spirit of this project. The results from this method indicated that the C-SGTR probability is generally negligible unless the flaw set includes one or more large flaws. The estimated probability that a plant experienced such a flaw set is about 0.01 per year. The result, described as “negligible” in Table 7-10, showed that the analysis used an average flaw set that did not include any large flaws. C-SGTR probability for W plants with no large flaw is expected to be negligible.

- Refined Screening Approach: The calculation in Section 7.1.4.2 uses an expected plugging rate (average over all plants) at cycle 15 of operation. The number of tubes that will be plugged at the end of cycle 15, therefore, follows a binomial distribution with the specified rate. The flaw sizes associated with these plugged tubes (i.e., the flaw bins) are estimated based on the tails of the flaw size distributions. This can be done for W plants because only large flaw sizes will contribute to the probability of C-SGTR. This method estimates the contribution to C-SGTR from failures of single and double large flaws. It shows that the contribution of failures of multiple flaws to C-SGTR probability is much smaller than the contribution of the failure of a single flaw. However, the probability of C-SGTR or its contribution from each flaw bin estimated by this method is not as rigorous as the method in Section 7.1.4.3. The contribution to the probability of C-SGTR, as a result of the failure of a flaw in a bin, is estimated approximately by the probability that a relatively large C-SGTR leakage occurs before the time of HL failure. The time of

HL failure is defined when the HL failure probability reaches 0.5. Relative large leakage should be defined here as a leakage area below the critical C-SGTR leakage area (guillotine break of one tube), since each flaw is examined individually as its potential contribution to C-SGTR. This method used a value of 2 $cm^2$ (0.32 $in.^2$) as the minimum leakage area.

- Screening Approach: The calculation in Section 7.1.4.1 is very similar to the calculation in Section 7.1.4.2, with the following differences:

  – No specific rate for plugged tubes was used and the expected number of flaws in a large flaw bin was estimated based on the distributions of flaw depth and length. Possible variations of the number of flaws within a flaw bin of large flaws is not considered (i.e., no binomial distribution was applied).

  – A value of 1 $cm^2$ (0.16 $in.^2$) rather than 2 $cm^2$ (0.32 $in.^2$) was used for the minimum leakage area.

  Although this method is the least rigorous of the three methods, it generated similar quantitative results for the probability of C-SGTR and offered a quick method to estimate the C-SGTR probability using the "lookup tables" calculated from the results of the calculator for a set of runs. This method is, therefore, quite easy to use and provides reasonable estimates for many PRA applications for similar W PWR plants.

**Table 7-10 Summary of 3 Types of C-SGTR Failure Probability Estimates Discussed in Sections 7.1.4.2, 7.1.4.3, and 7.1.4.4**

| I. Considering Deep Flaws Only (7.1.4.2) > = 60% Deep<br><br>Screening Approach | II. Considering Deep Flaws with Size Distribution Only (7.1.4.3) >= 50% Deep<br>Refined Screening Approach | III. Considering a Sample of Flaws (7.1.4.4) of All Sizes and Depths<br>Integrated Analysis |
|---|---|---|
| EFPY = 15 | EFPY = 15 | EFPY = 15 |
| 31 flaws generated in the last cycle—with earlier deep flaws plugged | 1 to 3 deep flaws generated in the last cycle (binomial probability with a fixed rate)—with earlier deep flaws plugged | 315 flaws in 4 SGs (statistical sample) |
| Critical area for declaring SGTR is >= 1 $cm^2$ | Critical area for declaring SGTR is >= 2 $cm^2$ | Critical area for declaring SGTR is >= 6 $cm^2$ (equivalent to a guillotine break of one tube) |
| **C-SGTR Probability** | | |
| Alloy 600 1.3E-2 | Alloy 600 1.3E-2 1 tube (*) | Negligible (**)<br>Estimated for a flaw set that did not include any large flaws |
| Alloy 690 8.1E-3 | Alloy 690 8.1E-3 1 tube | |
| | | |
| | Alloy 600 8.2E-5 2 tubes (**) | |
| | Alloy 690 3.9E-5 2 tubes | |
| | | |
| | Greater than 2 tubes—negligible | |

Notes:
* This uses the probability that one large flaw is created in the 15th cycle.
** This is based on C-SGTR runs with a limited sample of flaws that did not include any large flaw with a depth of 50% or more. For these cases, the margin between HL failure time and SG tube failure time (for the critical leak area to be reached) is large and the overlap in uncertainty is insignificant.

The two screening approaches are applicable only if the major contribution to C-SGTR is from a few large flaws. The screening approaches cannot be used if the TH run for an accident scenario, used as an input to the calculator, indicates that small flaws will also contribute to the probability of C-SGTR. For these cases, only the integrated analysis method should be used for either generic industrywide analysis or plant-specific analysis. This is the case for the TH results of the SBO scenarios for the selected CE plant. Therefore, the CE plant analysis, which follows in Section 7.2, will not discuss these two screening approaches.

### 7.1.5 Estimating Containment Bypass Frequency

Table 7-10 of Section 7.1.4.4 estimates the probabilities of C-SGTR for Inconel 600/690 for a core damage sequence with behavior similar to those initiated by SBO and with an early failure of the TDAFW pump. The occurrence of such C-SGTR would lead to a containment bypass scenario. All the containment bypass scenarios have a potential to become a LERF, if the release is large; it starts early, before an effective evacuation; and it is not terminated by successful SAMG actions.

In section 7.1.4, the preliminary estimate of the annual frequency of containment bypass because of consequential failures of one or more tubes was discussed. The earlier estimates did not include two additional contributors to containment bypass caused by C-SGTR:

(1) Operators are expected to start the RCPs (bump the pumps) and transfer the accumulated water in the loop seal into the vessel, thereby clearing the loop seal. This is only applicable if offsite power is recovered after the onset of core damage. A cleared loop seal can cause the failure of additional SG tubes only if the operator fails to restore the secondary cooling first. Unlike CE and Babcock & Wilcox (B&W) plants, the W SAMG does not explicitly require the operator to bump the pumps. It is, therefore, unlikely that the operators at a W plant would inadvertently perform such errors of commission.

(2) Operators are expected to introduce secondary cooling to an SG that has dried out, after alternating current (ac) power is recovered. This action is expected to be performed slowly, and the operator should maintain certain cooling/flow limits. The SG tubes are considered ductile and, for recirculating (U-tube) SGs, the tubes can expand axially. Both the SAMG and the emergency operating procedure (EOP) provide some guidance on limiting the cooling rate/secondary flow, which appears to be intended to limit the added strain caused by thermal shock and the resulting steep temperature gradient across the tube wall. For the purpose of PRA analysis, it is assumed that a significant deviation from the recommended limits for introducing the cold feedwater into a hot SG could result in tube failures. Introduction of cold water into a dry SG could also take place before the onset of core damage. Therefore, it has a specific procedure under EOPs. Operators are fully aware of the limits associated with this action. Should tubes rupture as a result of the introduction of cold water into a dry SG, the radioactive releases are expected to be significantly less than a C-SGTR accident with a dry SG secondary side. The presence of subcooled water in the secondary side of the SG is expected to provide a scrubbing action of the radioactive releases and to significantly reduce the offsite consequences. The contribution from this mechanism to the LERF, therefore, is expected to be significantly lower than other mechanisms for multiple tube failures.

A simplified SBO event tree in Figure 7-11 depicts the three types of SBO core damage sequence most likely to dominate the C-SGTR risk:

(1) Sequences with early failure of AFW: For these sequences, the containment bypass fraction is defined as Q1. The value of Q1 is approximately set to 0.01 for both Inconel 600 and 690 (see Table 7-9 in Section 7.1.4.2).

(2) Sequences with loop seal clearance are assigned to the containment bypass fraction Q2: the value of Q2 is equal to 1.0. *Note that TH runs indicated that the probability that the loop seal is cleared is almost certain if the RCP leakage is about 1,703 Lpm (450 gpm) per pump. For RCP seal leakage of 1,135 Lpm (300 gpm), the TH analysis predicted no possibility that the loop seal would be cleared. For the purpose of a bounding analysis, the probability of loop seal clearing is considered to be 0.1 when the proceduralized operator action of rapid depressurization fails (seal leakage range of 1,135–1,817 Lpm (300–480 gpm) per pump exists); 0.0025 when this operator action is successful (only 1,817 Lpm (480 gpm) per pump seal leakage scenario is postulated).*

(3) Sequences with the failure of the TDAFW pump in the intermediate timeframe (approximately 4 hours):[7] although the C-SGTR probability and the fraction of containment bypass could vary, depending on the depressurization scheme, it is bounded by twice the values estimated for the SBO sequences with an early failure of the TDAFW pump. The containment bypass fraction Q3 is assigned to these sequences. The estimate for this fraction is currently considered to be twice the value for the sequences with early failure of the TDAFW pump, namely 2Q1.[8]

These containment bypass (Cont.-BP) fractions are to be used with individual core damage sequences. Figure 7-12 gives an example of using these containment bypass fractions in a sequence from an internal event SBO sequence. The probabilities used are deemed to be representative of the event tree nodes typically used in PRA models.

For other SBO events, such as those induced during seismic, external flooding, and high-wind-related events, the ac power recovery could be drastically different from the internal events. Figure 7-13 presents an example of an external-event-driven SBO event tree for quantification of containment bypass probability due to C-SGTR.

One can also define an additional containment bypass fraction that could be used with an SBO CDF (instead of being used with an individual SBO sequence). Figures 7-12 and 7-13 calculate this frequency as the ratio of the total C-SGTR frequency to the total CDF frequency. The values estimated in these two figures are 0.02 and 0.018, respectively.

---

[7] PRAs sometimes consider a longer timeframe for ac recovery. They are related to the recovery of ac for crediting SAMG actions and other recovery actions for controlling the radioactive releases

[8] Both in W and CE plants, TH input files exhibit the following property when the SG tube temperatures reach the creep-rupture range, namely 600–700 degrees C (1,112–1,292 degrees F): the temperature difference between the HL and the average tube temperature is larger for the scenarios where the TDAFW pump fails at T = 0, compared to when the AFW fails at T = battery depletion. This results in a slightly higher likelihood for HL failure in the case with earlier AFW failure. Thus, the C-SGTR probability is slightly higher for the sequences with "late" failure of AFW. The event trees in Figures 7.12 and 7.13 use an approximate value of 0.01 for C-SGTR probability for *stsbos* and 0.02 for *ltsbos*. It should be noted that the C-SGTR, if it occurs, occurs much later in the sequences with late AFW failure, compared to sequences where AFW fails at T = 0, so it is not generally considered as a large early release.

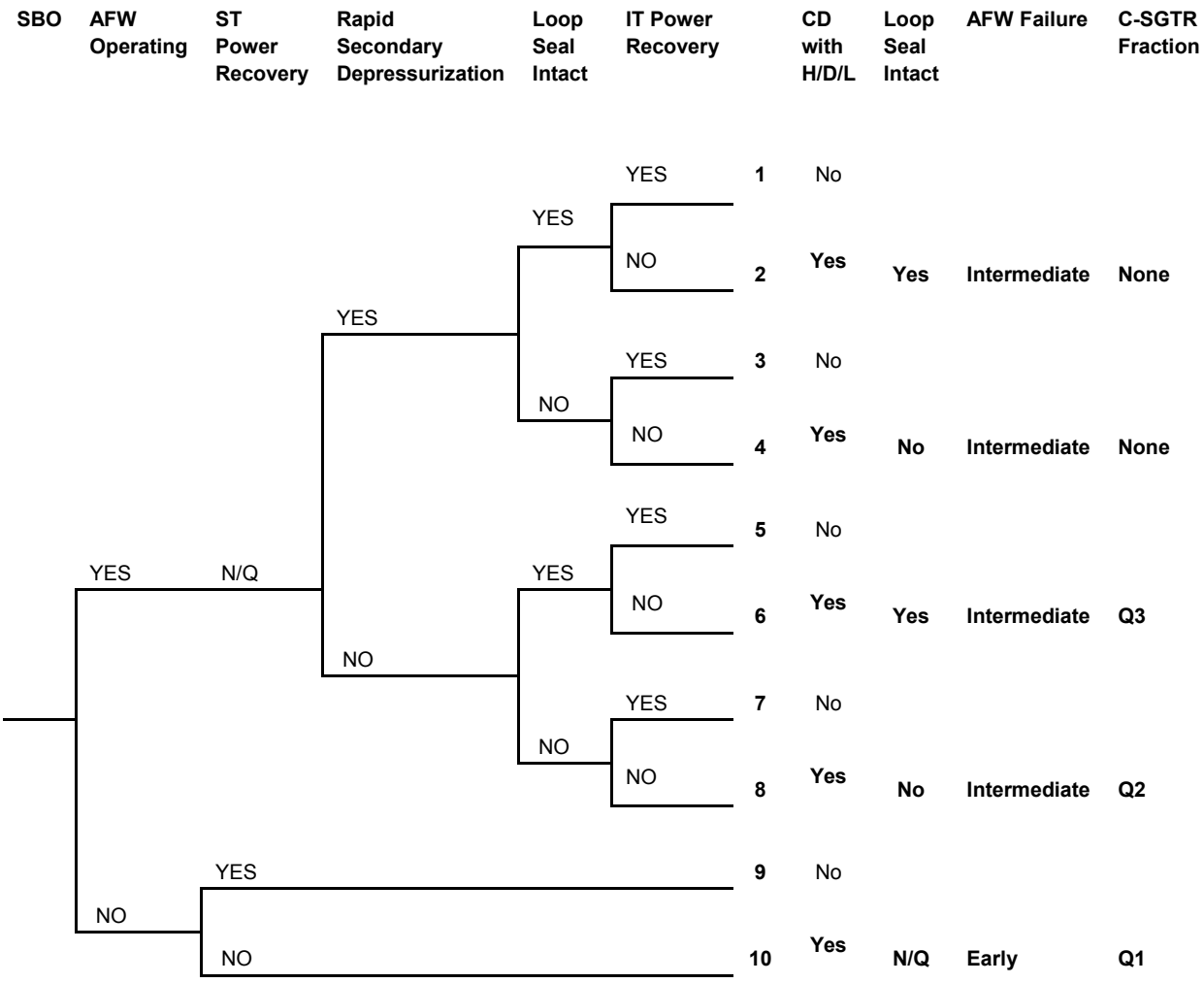


Figure 7-11 Definition of bounding SBO sequences with high/dry/low (H/D/L) conditions

General Notes:

a. N/Q = Not Questioned
b. ST (short term ac power recovery) refers to 1–2 hours following failure of TDAFW Pump (fails to start)
c. IT (intermediate term ac power recovery) refers to 4–6 hours following later failure of TDAFW Pump (fails to run, battery depletion)
d. The ac power can also be recovered later than the IT window. This can be credited for release frequency calculations: it is not used in the current estimates.
e. SBO refers to occurrence of a loss of offsite power event coupled with a loss of emergency ac power.
f. Power recovery refers to reestablishment of either offsite or onsite emergency power to at least one of the safety-related ac buses.
g. Loop seal is intact if 1,817 Lpm (480 gpm) per pump and 1,135 Lpm (300 gpm) per pump RCP seal loss-of-coolant accident (LOCA) does not occur.
h. If rapid secondary depressurization is successful, the primary is depressurized similar to SCDAP/RELAP case runs 153 and 153A. The core damage and C-SGTR is occurring late due to accumulator discharge.
i. If rapid secondary depressurization is not successful, then the sequence is assumed to be the same as an SBO with early failure of the TDAFW pump with the time line shifted by 4 hours.

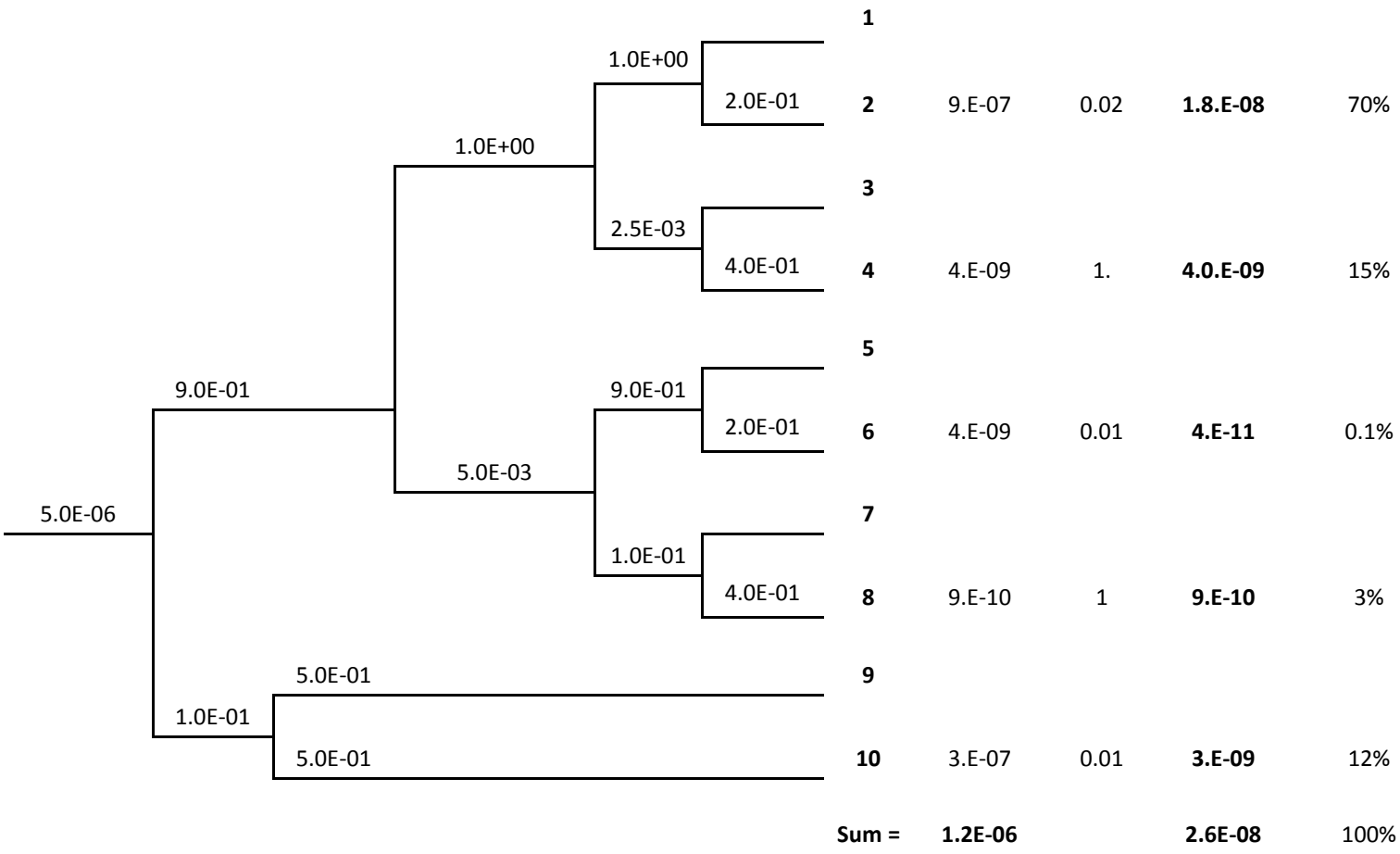


Figure 7-12 An estimate of bounding SBO sequence frequencies leading to C-SGTR and containment bypass

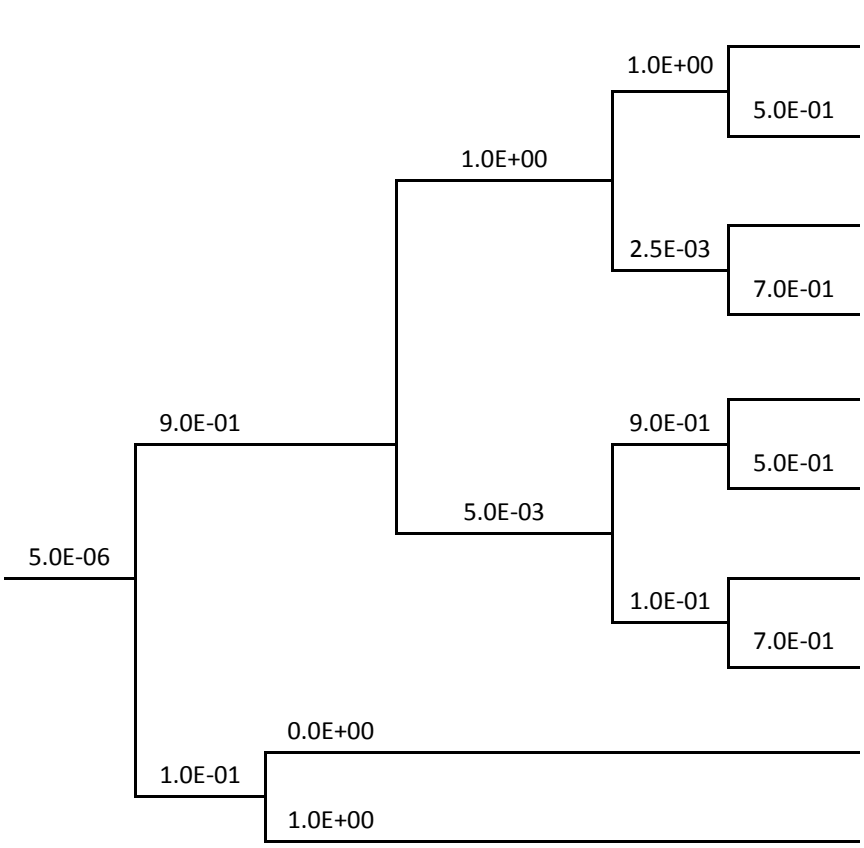


| | Sequence Frequency | C-SGTR Fraction | Cont. BP Frequency | % Contribution to Cont. BP |
|---|---|---|---|---|
| **1** | | | | |
| **2** | 2.E-06 | 0.02 | **4.E-08** | 72.7% |
| **3** | | | | |
| **4** | 8.E-09 | 1 | **8.E-09** | 14.5% |
| **5** | | | | |
| **6** | 1.E-08 | 0.01 | **1.E-10** | 0.2% |
| **7** | | | | |
| **8** | 2.E-09 | 1 | **2.E-09** | 3.6% |
| **9** | | | | |
| **10** | 5.E-07 | 0.01 | **5.E-09** | 9.0% |
| **Sum =** | **3.E-06** | | **5.5E-08** | 100% |

Figure 7-13 Another estimate of bounding SBO sequence frequencies leading to C SGTR and containment bypass

This section showed earlier that the total frequency of SBO core damage sequences for internal events only, and for all hazard categories, were $5.2X10^{-6}$/year and $2.0X10^{-5}$/year, respectively. The estimate for the containment bypass frequency caused by C-SGTR for these two cases will use a containment bypass fraction of 0.02. Note that this fraction is consistent with the two corresponding values estimated in Figures 7-12 and 7-13.

For internal event SBOs:

**Cont.BP**$_{C\text{-}SGTR}$ = CDF * 0.02 = $5.2X10^{-6}$ * 0.02 = $10^{-7}$/year

For SBOs from all hazard categories:

**Cont.BP**$_{C\text{-}SGTR}$ = CDF * 0.02 = $2.0X10^{-5}$ * 0.02 = $4X10^{-7}$/year

Table 7-13 further summarizes the estimates from this section.

### 7.1.6 Level 2 Analysis of C-SGTR for ZNPP

This section expands on the discussion provided in Section 2.6 on a simplified Level 2 analysis. An SBO event is considered as an entry level for the Level 2 analysis. The TDAFW pump is demanded right after SBO. The time required for SG dryout is about an hour and a half based on the TH analysis shown in Figure 7-1 for the Wnewbase case. The vessel breach is not expected until at least 8 hours after core uncovery. The recovery of offsite power in less than 8 hours is needed to credit the SAMG activities. Table 7-11 shows the timing for the major events corresponding to the accident progression of a scenario of an SBO and early failure of TDAFW pumps. A combination of RELAP results and sensitivity case runs with C-SGTR software generates these timings.

Based on an examination of the information shown on this table, three observations can be made:

(1) For cases where the primary pressure is maintained at the primary relief set point (approximately 15.2 MPa, or 2,200 psi), the HL is expected to fail before the occurrence of SGTR unless there are one or more large flaws with a depth of at least 60 percent in one of the SGs. This is generally consistent with the deterministic results obtained from RELAP runs.

(2) For cases where there is at least one large flaw in one of the SGs, such that C-SGTR occurs early and shortly after core uncovery, the HL is expected to fail in less than 15 minutes after C-SGTR, as long as the primary is not significantly depressurized. Therefore, the releases through containment bypass are expected to be small and be of short duration. This statement is valid even if the primary is somewhat depressurized, as long as it stays above the accumulator setpoint (4.82 MPa, or 700 psi).

(3) For cases where primary pressure is reduced below 4.82 MPa (700 psi), such that the accumulators are discharged, HL failure is not expected to occur until the core is uncovered and repressurization of the primary system takes place. In such cases, the releases are expected to be late and possibly diverted into the containment rather than through the ruptured SG tubes.

Based on the above discussion, a large early release (LER) can mainly occur if secondary relief valves are open (either intentionally or by stick-open failures) post-C-SGTR, such that the primary system remains depressurized and the probability of HL failure is significantly reduced.

**Table 7-11 Timing of Major Events during an SBO with Early Failures of TDAFW Pumps (Wnewbase with Inconel 600TT SG)**

| Time | Events for Extended SBO with Early Failure of TDAFWs |
|---|---|
| 0 | SBO started |
| ~ 14 minutes | ECCS signal actuated |
| ~ 2 hours, 30 minutes | Onset of core uncovery, corresponding to 648.69°C (1,200 °F) |
| ~3 hours, 30 minutes | 50% probability of HL failure if the primary pressure remains around 15.17 MPa (2,200 psi) after onset of core uncovery (as estimated by C-SGTR software) |
| ~3 hours, 30 minutes | Cladding damage and start of gap release |
| Around 3 hours, 30 minutes to 3 hours, 45 minutes | Some likelihood of SGTR with varying leak rates if there is at least one flaw larger than 60% of nominal depth |
| Around 3 hours, 45 minutes | HL failure if the primary pressure reduced to around 4.826 MPa (700 psi) but above accumulator discharge pressure) at the time of core uncovery due to the opening of a PORV or a single PORV and SRV [b] stuck open |
| ~ 4 hours | DC assumed depleted [a] |
| Between 7 and 8 hours | Core structure failures, fuel melting and quenching; start of in-vessel releases |
| ~ 8 hours | HL failure if the primary system is fully depressurized at the onset of core uncovery [b] |

[a] Although RELAP models assume dc is depleted in 4 hours for both early and late failure of TDAFW pumps, PRA considers dc to be available for a longer duration for the case when TDAFW pumps were not available at time zero. The availability of dc will facilitate SAMG activities such as primary and secondary depressurization.
[b] These values were supported by sensitivity runs performed using C-SGTR software.

For those cases where TDAFW pumps are operating, the time to core uncovery depends on the scheme used for primary depressurization. RELAP models analyzed two cases: Cases 153 and 153A. In both cases, aggressive cooling and depressurization using the secondary system resulted in the dropping of primary pressure below the accumulator discharge setpoint. The discharge of accumulator resulted in core uncovery being delayed significantly (about 11 hours for Case 153 and 13 hours for Case 153A). The C-SGTR and HL failure occurs shortly after the onset of core uncovery. If the operators do not take any action to depressurize and perform aggressive cooling, although they are instructed by the EOPs to do so, the scenario is expected to be similar to that of SBO with early failures of TDAFW pumps but after the secondary cooling is lost. The time associated with the sequence of events in this case is similar to the Wnewbase case, but they are shifted by about 4 hours. As an example, in this case, the onset of core uncovery is expected to occur in 6 hours and 33 minutes, with the core damage starting at around 8 hours. There is currently no SCDAP/RELAP case run available for this case.

Table 7-12 shows the timing for the major events corresponding to the accident progression of a scenario of an SBO and the failure of TDAFW pumps after battery depletion for a normal depressurization scheme (RELAP Case 153). A combination of SCDAP/RELAP results and sensitivity case runs with C-SGTR generates these timings.

Table 7-12 Timing of Major Events during an SBO with Failures of TDAFW Pumps after Battery Depletion (SCDAP/RELAP Case 153 with Inconel 600TT SG)

| Time | Events for Extended SBO with Early Failure of TDAFWs |
|---|---|
| 0 | SBO started |
| ~ 4 hours | Dc assumed depleted |
| ~ 11 hours, 30 minutes | Onset of core uncovery, corresponding to 1,200 °F |
| ~12 hours, 30 minutes to 12 hours, 45 minutes | Some likelihood of SGTR with varying leak rates if there is at least one flaw bigger than 50% depth |
| ~12 hours, 45 minutes | HL failure |
| ~13 hours, 30 minutes | Cladding damage and start of gap release |

Section 7.1.4 contained a detailed estimate of the frequency of containment bypass because of C-SGTR. The fractions of containment bypass scenarios that can lead to an LER depend on the following three factors:

(1) For an LER to occur after C-SGTR, a large release path must lead directly to the environment through the open secondary side, such as an open path caused by one or more SG PORVS/RVs failing in the open position (stuck open).

(2) For an LER to occur, the radioactive releases from C-SGTR should occur early (i.e., before commencement of an effective evacuation).

(3) For an LER to occur, both of the following SAMG actions should fail:

– Flood the vessel by depressurization and injection of water. This action should preferably take place early enough after core damage but before significant fuel melt and changes in core configuration.

– Flood the SG secondary side by depressurizing the SG and filling it up with an alternate water source, to significantly reduce the magnitude of radioactive releases by scrubbing.

This study assumes that a large leakage path always exists on the SG secondary side. The cycling of SG PORVs/SRVs during the harsh environment after core damage is not reliable and could result in one or more valves sticking open. Furthermore, these valves could be opened intentionally as a part of SAMG actions.

This study also assumes that the releases from all C-SGTR scenarios associated with short-term SBO (*stsbo)* will be early and before commencement of an effective evacuation. The study, however, acknowledges that the diverse and flexible mitigation capabilities (FLEX) equipment, including the extended dc, could delay the core damage and the occurrence of C-SGTR. The authors decided, however, that a quantitative analysis of FLEX strategies within the PRA is not currently a state of practice, and it cannot be performed unless better knowledge is gained about the timing and the effectiveness of these strategies.

The authors reviewed the SAMG actions, as discussed in the W SAMGs but decided that a quantitative analysis is not currently within the scope of this project. The paragraphs below discuss some aspects of the SAMGs.

The vessel can be depressurized by opening all PORVs (both PORVs are required to open, based on the success criteria identified in TH case runs for post-core damage in ZNPP). Dc power is required for PORV operations after core damage occurs. This is possible if ac power is restored or the availability of dc power is ensured by load shedding or through other means. Relieving the primary pressure would allow injection from either the high-pressure or low-pressure emergency core cooling system (ECCS). RCS depressurization could also take place because of a medium or large LOCA but not because of post-core damage from a small LOCA.

Primary depressurization for SBO scenarios with early failure of TDAFW pumps could result in discharge of the accumulator water into the vessel, which could provide more time for the operator to align the makeup water sources to the reactor water storage tank (RWST) for later injection into the vessel. Injection into the vessel, if occurring early, could arrest core melt and reduce in-vessel releases. In both cases analyzed in NUREG/CR-6995 (Ref. 1) (Cases 153 and 153A), aggressive cooling and depressurization using the secondary system dropped primary pressure below the accumulator discharge setpoint. The discharge of accumulators resulted in core uncovery being delayed significantly (about 11 hours for Case 153 and 13 hours for Case 153A). These cases were not considered to be contributors to LERF, since the radioactive releases would be late and be expected to occur after the initiation of effective evacuation.

RCS depressurization through the PORVs or the occurrence of a medium or large LOCA would also create a major path of release into the containment rather than through the ruptured SG tubes. A lower release magnitude would, therefore, be expected. These cases were also not considered to be contributors to LERF.

SAMG also recommends both depressurizing the SG using the available relief paths when an SG tube ruptures and filling the SG secondary side using motor-driven AFW trains after power is recovered. If power is not recovered, injection from low-pressure alternate water sources, such as fire water, could be used. As guided by TH analysis, operation of the atmospheric dump valve (one per SG) or opening of main steam isolation valves (MSIVs) and bypass valves, will be required if an alternate source of water is used. SG depressurization would require dc power as well as instrument air. In addition, local manual operation would be possible and might not require dc power. However, the possibility of a high-radiation environment should also be considered.

Section 2.6 discussed the emergency response timeline and the process for effective evacuation of the SBO scenario with early and late failure of TDAFW pumps (e.g., after batteries are depleted). The conclusion was that the evacuation is most likely effective for C-SGTR containment bypass events during SBO scenarios with late failures of TDAFW pumps and not effective for SBO scenarios with early failure of TDAFW pumps. The only exception to this general rule is the C-SGTR containment bypass scenarios of SBO with late failure of TDAFW pumps and the failure of operators to rapidly depressurize the primary through secondary systems. As discussed earlier, in such scenarios, the time available for effective evacuation could be reduced to less than 10 hours for some plants, such that assuming probability of 1 for successful and effective evacuation during some external events may not be conservative. Site- and plant-specific analysis may be needed to address the probability of effective evacuation for such cases.

### 7.1.7 Quantification of Level 2 Models

Section 2.6 discussed a simplified LERF model that relies on five factors:

(1) frequency of severe accident sequences with potential for C-SGTR ($f_{AC}$), as discussed in Section 7.1.2

(2) C-SGTR probability ($P_{CSGTR}$) (see discussion for estimating containment bypass probability in Section 7.1.5)

(3) conditional probability that the subsequent failure of RCS, including the stuck-open relief valves, does not occur ($P_{NDEP}$)

(4) failure probability of all SAMG actions ($P_{SAMG}$)

(5) probability that early and effective evacuation is not successful ($P_{EVAC}$)

The issues considered for estimating $P_{NDEP}$, $P_{SAMG}$, and $P_{EVAC}$ are qualitatively discussed below. Some values are suggested for each of these three parameters for estimating the bounding values of LERF.

$P_{NDEP}$: Failure of the HL shortly after C-SGTR or stick-open failures of at least two primary relief valves (SRVs/PORVs) will divert most of the releases into the containment, thereby significantly reducing the conditional LER probability, given a containment bypass caused by C-SGTR. For cases where only one relief valve fails to reclose (sticks open), the HL failure would be delayed because of primary depressurization. The conditional LER probability, given containment bypass, will therefore increase. Note that the above discussion is not applicable when the TDAFW pump is initially available and the primary is further depressurized by rapid secondary cooling. In such cases, the primary pressure is expected to be initially reduced below 4.82 MPa (700 psi) because of rapid primary depressurization through the secondary and through the stick-open primary relief valve. Accumulators are then discharged, core melt is delayed, and C-SGTR and HL failure are not expected to occur before the restart of core melt. The release through containment bypass is expected to be relatively small (a portion of the release will be diverted into the containment through stick-open relief valves) and the release would be late. It is, therefore, not considered as an LER. Generally, the conditional probability that C-SGTR is not followed shortly (e.g., less than 30 minutes) by a large primary opening (i.e., $P_{NDEP}$) is expected to be small (much less than 1). As discussed, the only possible way for a containment bypass because of C-SGTR to result in an LER is when only one of the primary relief valves (SRVs or PORVs) sticks open after core uncovery. However, the performance of these relief valves after onset of core damage is not well understood. The probability that the relief valves stick because of limited clearance in some parts, under the harsh environment after core damage in severe accident scenarios, is not known. These components are demanded under a severe accident condition, although they are generally qualified for DBAs. For these reasons and for the purpose of a bounding evaluation, a value of 1.0 is assigned to $P_{NDEP}$.

$P_{SAMG}$: A bounding value of 1.0 is proposed for $P_{SAMG}$ to obtain a bounding estimate for LERF. This crude approach is implemented because the state of knowledge is limited for both equipment operation and operator performance for performing SAMG activities after core damage. SAMG's actions are not procedure based; they are directed by emergency directors, coordinated by emergency coordinators, and executed by emergency responders and operators. For the SAMG, there is no scripted compliance. The appropriate actions must be

defined “on the fly,” based on understanding the plant conditions and the pros and cons of carrying out a particular set of actions versus an alternative set of actions or no action at all (see Reference 8). This is considered as a human decisionmaking process that would be influenced by the complexity of the situation, training, and other personal attributes of the operator. The human reliability model for these actions, under severe accident conditions, is expected to be different than those governed by EOPs. Finally, the effectiveness of SAMG activities under different accident conditions is not known.

$P_{EVAC}$: The timing diagrams discussed in Section 2.5 indicate that there is a high likelihood that effective evacuation can be completed for all SBO scenarios with an initial availability of TDAFW pumps and a successful aggressive depressurization through secondary cooling. Therefore, for all these scenarios, the value estimated for $P_{EVAC}$ is considered to be zero. For SBO scenarios with initial availability of TDAFW pumps but failure of aggressive depressurization through secondary cooling, releases can occur at an earlier time but only after at least 8 hours. The timing of the release will depend on the battery capacity and the duration of dc power availability, including potential load shedding. Furthermore, the failure probability for aggressive depressurization is expected to be small, about $1.0 \times 10^{-3}$ per demand. Therefore, for all SBO scenarios with an initial availability of TDAFW pumps, $P_{EVAC}$ was assigned a value of zero.

The same timing diagrams revealed that there is a high likelihood that effective evacuation cannot be completed in time for all SBO scenarios with early failure of TDAFW pumps. Therefore, $P_{EVAC}$ is assigned a failure value of 1.0 to all SBO scenarios with an early failure of TDAFW pumps.

Table 7-13 summarizes the conditional LERF probabilities because of C-SGTR for SBOs with early or late failures of TDAFW pumps.

**Table 7-13 Conditional LERF Probabilities for an SBO with Early and Late Failures of TDAFW Pump for the W Plant**

| Factors | Applicability | LERF Factors [a] |
|---|---|---|
| $P_{CSGTR}$ | Because of one or more tube breaks in an SBO CD sequence | 1.3E-2 |
| | — Due to single tube breaks only | 1.3E-2 |
| | — Due to multiple tube breaks | 8.2E-5 |
| | In an SBO, CD sequence with loop seal clearing | 1.0 |
| $P_{NDEP}$ | In an SBO, CD sequence with loop seal clearing or multiple tube breaks | 1.0 |
| | In an SBO, CD sequence with one tube breaks | 1.0 [b] |
| $P_{SAMG}$ | In an SBO, CD sequence with loop clearing or multiple tube breaks | 1.0 |
| | In an SBO, CD sequence with one tube breaks | 1.0 [b] |
| $P_{EVAC}$ | In an SBO, CD sequence with early failure of TDAFW | 1.0 |
| | In an SBO, CD sequence with late failure of TDAFW (at least with 4 hours battery capacity) | 0 |

[a] LERF factors are applicable to SBO scenarios with both early and late failure of TDAFW pumps unless this is specifically identified.
[b] This value is believed to be conservative, and it is used for screening purposes only.

A crude estimate of the conditional probability of containment bypass for all the prolonged SBO scenarios is about 0.02 when considering scenarios involving loop seal clearing. The CDF from SBO sequences, considering all hazard categories, is about $2.0X10^{-5}$/year from Table 7-1. This CDF multiplied by the conditional probability of containment bypass (0.02) gives a bounding containment bypass frequency estimate of $4X10^{-7}$/yr for all hazard categories. Please note that the LERF estimate is negligible (approximately 0), since only the containment bypass resulting from the SBO scenarios with early failure of TDAFW pumps have a potential for an LER.

A bounding estimate of the conditional LERF probability, given an SBO with early failure of TDAFW pumps, is about 0.02. The all-hazard CDF, multiplied by the early failure probability of TDAFW pumps (approximately 0.1) and the LERF fraction of 0.02, gives a bounding LERF estimate of $4X10^{-8}$/yr for all hazard categories. Considering SBO CDF for internal events only is $5.2X10^{-6}$/yr, the LERF estimate due to C-SGTR for the W plant is about $1.0X10^{-8}$/yr for internal events.

### 7.1.8 Concluding Remarks

The TH results obtained from various case studies significantly influenced the occurrence of C-SGTR, containment bypass probability, and LERF. These TH results reflect the specific design, configuration, and geometry of the plant systems, specifically the SG design and primary connections, such as HL and surge line. They should not be interpreted as generic results for W plants. The following are the eight more important plant features that can affect the results:

(1) mixing in the SG inlet plenum (deep or shallow SG inlet plenum)

(2) mixing in HL (physical characteristics such as length and diameter of HL)

(3) pressure drop in HL and SG tubes (i.e., an integral effect)

(4) heat transfer and heat losses from the HL walls (e.g., heat up inertia, including condition of the insulation on the HL)

(5) performance of primary and secondary relief valves before or after onset of core damage

(6) duration of dc availability, including load shedding capabilities

(7) effectiveness and success of SAMG activities

(8) success of other severe accident mitigation measures that are provided by extensive damage mitigation guidelines (EDMGs) and FLEX, including extended diversified power sources, black start, and extended operation of TDAFW pumps without dc.

This study makes the following conclusions of this study, based on the case studies performed for the example W plant, as described in this chapter:

- The contribution of C-SGTR to LERF is expected to be about $4.0X10^{-8}$ when all hazard categories applicable to the site are included.

- The contribution of C-SGTR to LERF is expected to be about $1.0X10^{-8}$ when only internal event SBO core damage sequences are considered.

- Based on the existing PRAs, C-SGTR appears not to be a major contributor to LERF for these types of plant design.

- It is generally concluded that, in plants with designs similar to the example W plant, the C-SGTR and the associated LERF do not make a significant contribution, unless large and deep flaws exist in one or more SGs.

## 7.2 Example Combustion Engineering Plant

MELCOR analyses were performed in two stages over a given time period to study Calvert Cliffs Nuclear Power Plant (CCNPP) as an example of a CE plant's response to RCS conditions that could lead to C-SGTR. The first stage analyses were completed in October 2012. These analyses were initially used in the PRA evaluation of C-SGTR probability. The second stage of MELCOR analyses were completed in August 2013. The updated PRA evaluation discussed in this section used these updated MELCOR analyses and results.

The second stage TH analyses are mainly used in support of the development of the PRA models.

Therefore, the C-SGTR PRA used CCNPP as an example CE plant. The documents for the CCNPP individual plant evaluation (IPE) and individual plant evaluation for external events (IPEEE) provided the other required information for C-SGTR PRA evaluation. Chapter 3 contains a detailed discussion of the MELCOR model and the results of the MELCOR evaluation for CCNPP.

### 7.2.1 Description of the Selected TH Sequences for C-SGTR PRA for the Example CE Plant

A specific naming scheme is used in defining main features of various scenarios evaluated in this section. The general format for the naming scheme is "SBO type," "Secondary side relief mode," "Creep-rupture failure progression," and "plant loop." These are further defined below:

(1) SBO type (*stsbo* or *ltsbo*)

- *stsbo*: SBO scenario with failure of TDAFW pump at time zero
- *ltsbo*: SBO scenario with failure of TDAFW pump after batteries are depleted (i.e., after 4 hours of operation)

(2) Secondary side relief mode (a/as)

- a: no stick-open failure of either primary PORVs or SRVs, or secondary PORVs or main steam safety valves (MSSVs); an assumed preexisting leakage area of 3.22 $cm^2$ (0.5 $in.^2$) on the secondary side
- as: no stick-open primary PORVs or SRVs but failure of MSSVs to reclose when first demanded (before onset of core damage); no other preexisting leakage assumed

(3) Creep-rupture failure progression (SCF)

– Suppress creep failure (SCF) nomenclature is used when creep-rupture failure is suppressed. In such cases, the scenario will proceed without any failure of RCS components or SG tubes caused by creep rupture.

(4) Plant loop (a/b)

– a: refers to the plant loop equipped with the pressurizer
– b: refers to the plant loop without pressurizer

The MELCOR predicts the temperature profile for the average hot tube where the gas flows from the hot side of the SG to the cold side and the average temperature of cold tubes where the gas flow is reversed. The average hot tube is divided into two sections: the section where the gas flows upward and the section where the gas flows downward. The average temperature of the upward flow section is higher than the downward flow section. The average hot tube temperature in the following graphs refers to the section of the hot tubes where the hot gas flows upwards. The average section where the gas flows downward has a temperature profile similar to that of the cold tubes, and they are averaged with the temperature of cold tubes to obtain an average cold tube temperature for the purpose of estimating the C-SGTR probability using the C-SGTR software. The fraction of tubes considered to be exposed to the average hot temperature, where the gas flow is upward, is estimated to be around 0.25 for the base case analysis. This same fraction was also used as the probability that a flaw in an SG will be exposed to the average hot tube temperature for all base-case evaluation. The sensitivity analysis used a fraction of 0.125 instead of 0.25 and estimated its impact on the final C-SGTR probability, as discussed in Section 7.3.2.

The number of tubes exposed to the hottest temperature is approximated by the number of tubes exposed to a normalized temperature of 0.9 to 0.99 for a CE plant. Multiple unflawed tubes generally could fail because of creep rupture before HL failures with a varying leakage area. Expert elicitation of staff members of the Nuclear Regulatory Commission previously involved in the issue resulted in a range from 10 to 100 tubes failing (see Section 3.4). The PRA study, therefore, considered a small number of tubes; it assumed about 100 tubes in each SG would be exposed to hotter gas temperatures.

These tubes are referred to as the hottest tube and presented by a single average hottest temperature. Considering 8,247 tubes per SG, the fraction of the hottest tubes is estimated to be around 0.01.

The evaluation of the following two representative base scenarios used the second stage of the MELCOR evaluation in estimating the base probability of C-SGTR. These two scenarios modeled a leakage through the secondary side of each SG, equivalent to a hole with an area of 3.2-$cm^2$ (0.5-$in^2$). This size of leakage was sufficient to ensure that the pressure in the secondary side of the SGs approached the atmospheric pressure after SGs have been dried out. This size of leakage, however, is not sufficient to maintain low secondary-side pressure if SG tubes have ruptured.

- The first scenario considers an SBO with failure of the TDAFW pumps early in the sequence (i.e., at time zero), followed by early core damage with a potential for C-SGTR because of creep rupture. This scenario also considered an RCP seal leakage of 79 Lpm (21 gpm) per pump. The MELCOR results for these case runs are applicable to

several PRA accident sequences with similar behavior (see the discussion in Chapter 2). For SBO sequences, this includes an SBO scenario with simultaneous failures of TDAFW pumps (i.e., two pumps for CCNPP) because of common-cause failure (CCF) to start, and an SBO with an initial availability of TDAFW pumps followed by their failures because of SG overfill in an hour. For this case run, the onset of core damage is expected to occur in less than 2 hours. The scenario considers the potential for the occurrence of C-SGTR after the onset of core damage. Figure 7-14 shows the temperature at the inner surface of the top section of the HL in degrees Celsius, the average temperature of the hot SG tubes, the average temperature of the cold SG tubes, and the temperature of the hottest SG tube for loop A, which is equipped with a pressurizer. Figure 7-15 shows similar results for the loop without the pressurizer (loop B). Figures 7-16 and 7-17a show the differences between the HL temperature and the average tube and the hottest tube temperature for loops A and B, respectively. These graphs show that the temperature response for HL heatup after core damage is slower than the SG tube temperature response. Therefore, the HL is expected to be initially at a lower temperature than the average hot and the hottest tube after the onset of core damage. This would increase the probability of C-SGTR. Figure 7-17b shows the pressure in the primary and the secondary sides of SGs. This graph shows that 3.2 $cm^2$ (0.5 $in.^2$) of assumed leakage will cause the secondary side to depressurize. The primary side pressure is maintained at the set point of primary SRVs.

- The second scenario considers an SBO with delayed failures of TDAFW pumps after battery depletion. The TDAFW pump is initially available, but it will fail shortly after the depletion of the batteries. The scenario considers a normal RCP seal leakage of 79 Lpm (21 gpm) per pump. The MELCOR analysis assumes that the TDAFW pumps were operating for a period of 4 hours. Figure 7-18 shows the temperature at the inner surface of the top section of the HL in degrees Celsius, the surge-line temperature, the average temperature of the hot SG tubes, the average temperature of the cold SG tubes, and the temperature of the hottest SG tube for loop A. Figure 7-19 shows similar results for loop B. Figures 7-20 and 7-21a show the differences between the HL temperature and the temperature of the different SG tubes for Loops A and B, respectively. These graphs show that the temperature response for HL heat up after core damage is much slower than the SG tube temperature response. Therefore, the HL is initially expected to be at a lower temperature than the average hot and the hottest tube after the onset of core damage. This results in a higher probability of failure of SG tubes caused by creep rupture, before creep-rupture failure of the HL. Figure 7-21b shows the pressure in the primary and the secondary sides of SGs. This graph shows that the secondary side will be depressurized due to 3.2 $cm^2$ (0.5 $in.^2$) of assumed leakage. The primary side pressure is maintained at the set point of primary SRVs.

As discussed in Section 2.5, for C-SGTR during a severe accident, the size of the leak area would determine the size of the release through containment bypass (i.e., it determines if the containment bypass should be categorized as an LER). For a small leak, the primary is expected to stay pressurized (generally at primary relief set point approximately 15.5 MPa (2,250 psi)), resulting in the failure of other RCS components (e.g., HL) shortly after the failure of the tubes. This significantly reduces and eliminates any release through the SGs. Larger leaks could pressurize the secondary side of the affected SG such that both the primary and secondary sides equalize at the pressure set point of the SG relief valves. In this case, there is a lower probability of the failure of other RCS components (e.g., HL) because of a lower primary pressure (approximately 8.3 MPa (1,200 psi)). This pressure assumes that the SG PORVs and MSSVs cycle as many times as needed without any failures. If any of the SG relief valves fails

open (sticks open) early during an accident, the primary will be depressurized, and it will practically eliminate any possibility of the HL failure (or other RCS components). The SG relief valves could also be opened and potentially stick open, in *stsbo* scenarios by the operators following the onset of core damage per SAMG. In SBO scenarios where the TDAFW pump is initially operating, the probability that the operator opens any of the secondary relief valves after the onset of core damage is small, since the batteries are assumed to have been depleted, and the recovery of dc power in the short period of time after the onset of core damage and before C-SGTR, is less likely. There could also be a threshold for larger leak areas through the failed SG tubes, such that the countercurrent flow through the HL can no longer be maintained. In such cases, the hot steam will flow through the SG tubes, causing failures of a number of tubes, resulting in a large containment bypass.

A sensitivity analysis using the MELCOR evaluation assumed that there is zero leakage through the secondary system at the start of SBO (instead of the generally assumed leakage area of 3.2 $cm^2$ (0.5 $in.^2$)), such that the secondary relief and safety valves will be demanded early during the accident and before the onset of core damage. The MELCOR evaluation for this case further assumes that the secondary relief and safety valves fail to reclose after the first opening. The result of this sensitivity case run shows an increase in C-SGTR probability and discusses it in Section 7.3 as part of the sensitivity case studies.

Additional sensitivity analyses were performed by Stage 1 and 2 MELCOR evaluations to further examine the impact of various scenarios. The following were noted:

- C-SGTR with an equivalent leakage area of the guillotine break of less than one tube will not result in depressurization of the primary.

- An equivalent leakage area of one or more tubes could result in a significant release if one or more of the SG safeties, or the relief valves, are open intentionally or stick open.

- The primary is initially depressurized and accumulator discharges when one or more secondary relief valves stick open early in the accident. This will further delay HL/surge-line creep-rupture failures. The probability of C-SGTR caused by creep rupture, however, is not affected as much, since the lower secondary-side pressure increases the delta pressure across the tube.

For PRA quantifications and in PRA models (event trees and probability estimations), the analyst should, therefore, differentiate between C-SGTR equivalent leakage areas less than or greater than the guillotine break of a single tube. PRA models also should consider the probability that manual secondary-side depressurization is performed to facilitate the performance of SAMG activities for flooding the SG secondary side. MELCOR runs were not performed for such scenarios. In addition, MELCOR runs did not provide any information about the conditions for loop seal clearing or the large C-SGTR leakages that could possibly reverse the direction of the cold gas flow, eliminating the countercurrent flow regime in the HL.

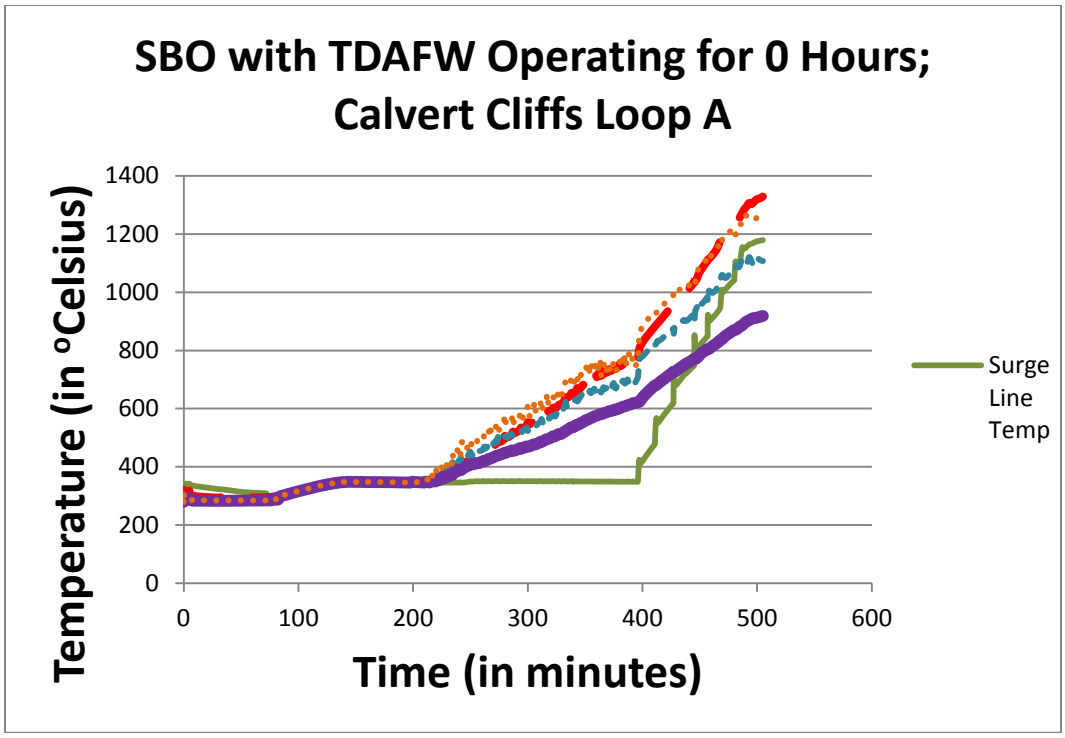


Figure 7-14 Loop A temperature profiles of the HL and SG tubes for the SBO with an early failure of TDAFW pumps

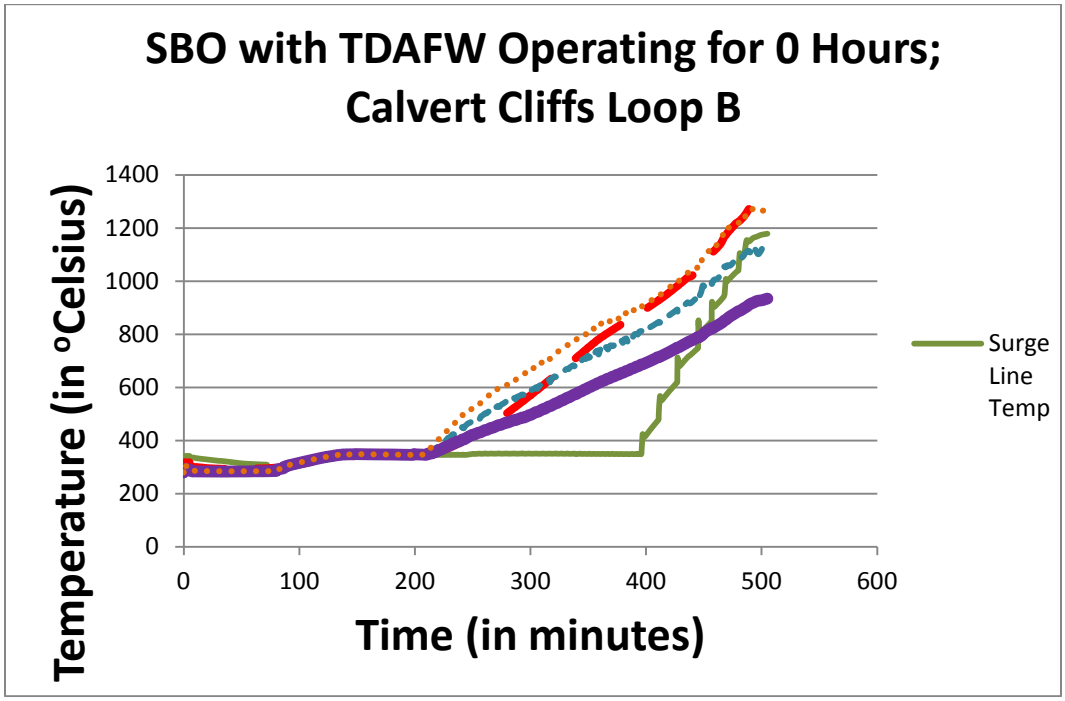


Figure 7-15 Loop B temperature profiles of the HL and SG tubes for the SBO with an early failure of TDAFW pumps [surge-line temperature of loop A is shown to facilitate comparison of loop A and B temperature trends]

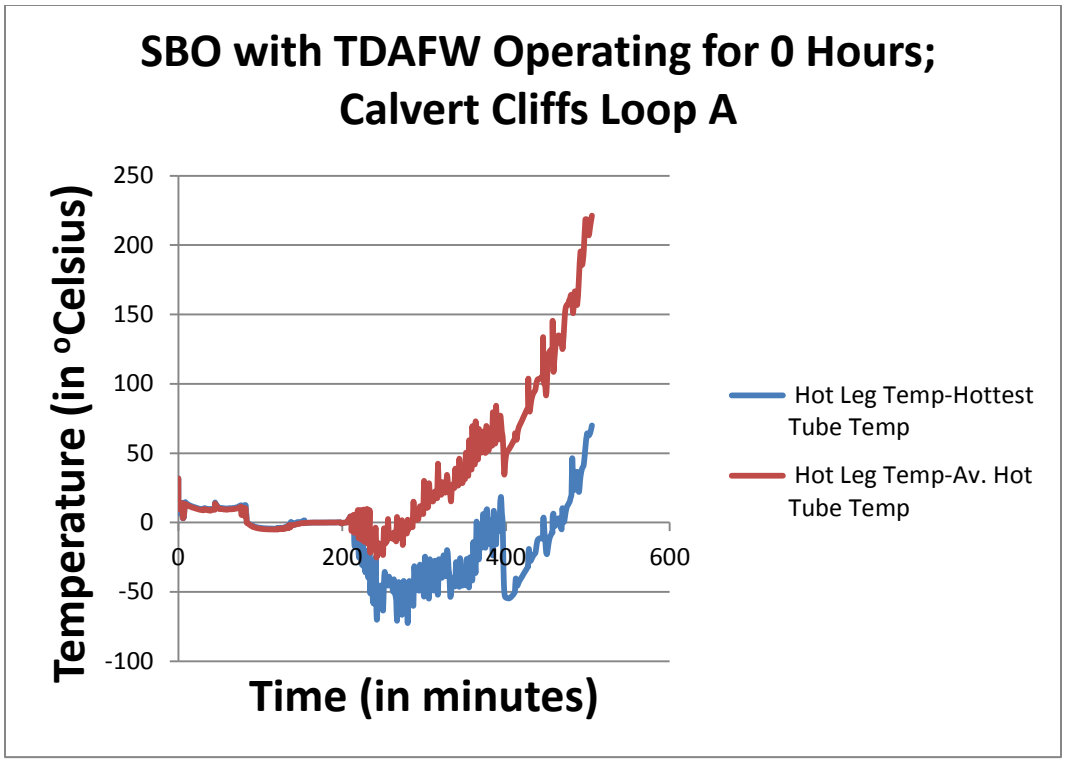


Figure 7-16 Difference in loop A temperature of the HL and SG tubes for the SBO with an early failure of TDAFW pumps

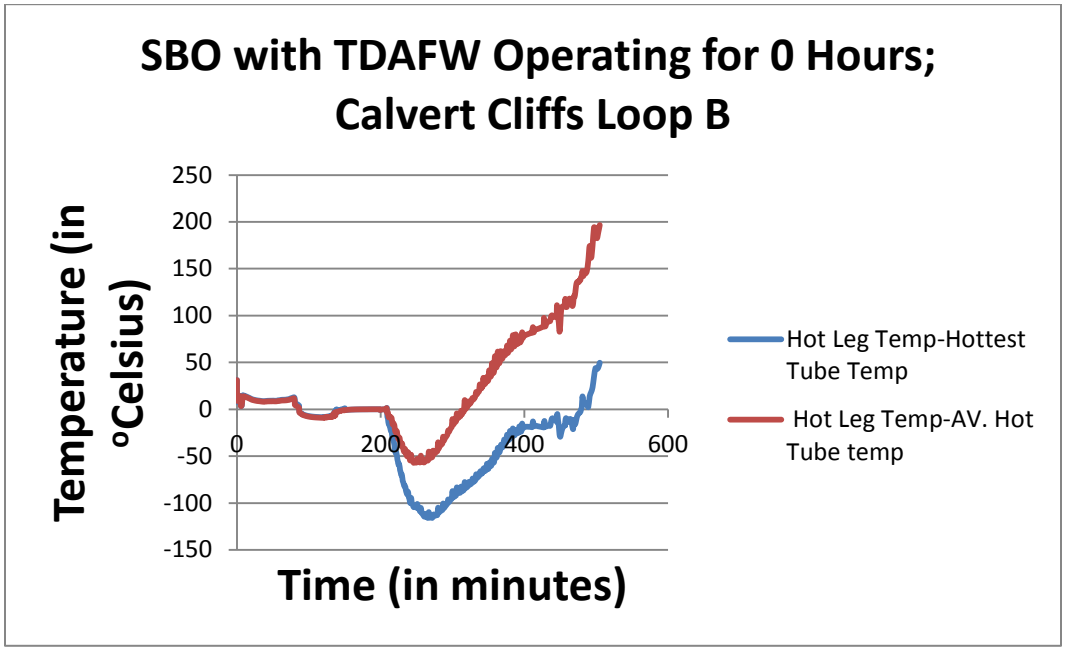


Figure 7-17(a) Difference in loop B temperature of the HL and SG tubes for the SBO with an early failure of TDAFW pumps

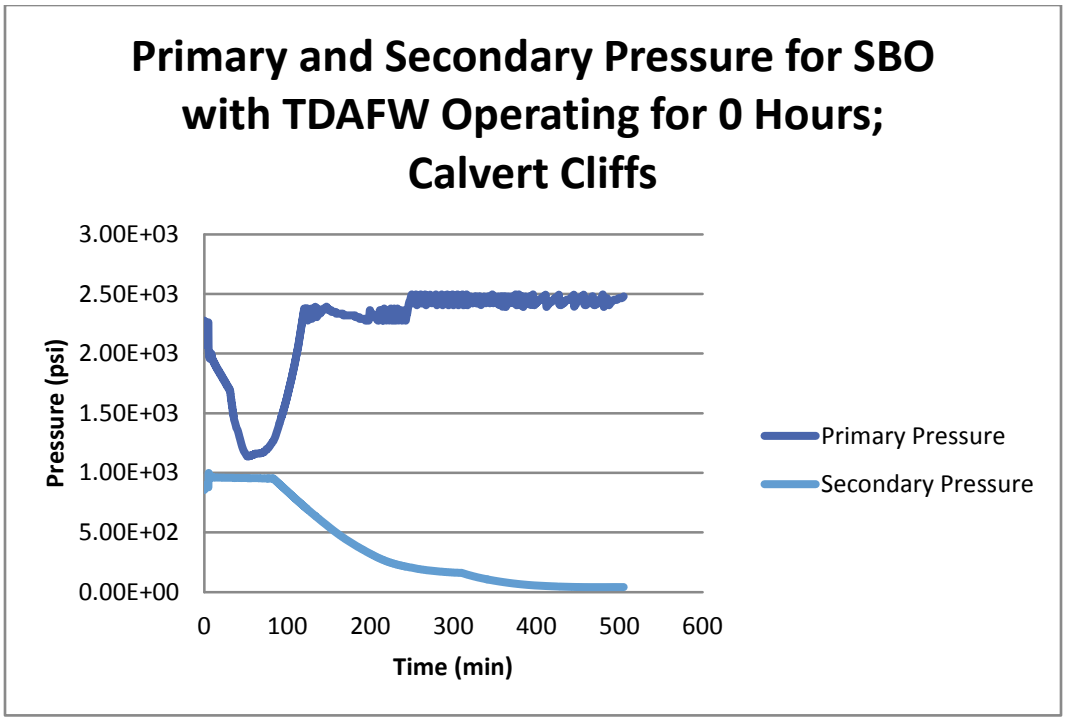


Figure 7-17(b) Primary and secondary pressure for the SBO with an early failure of TDAFW pumps

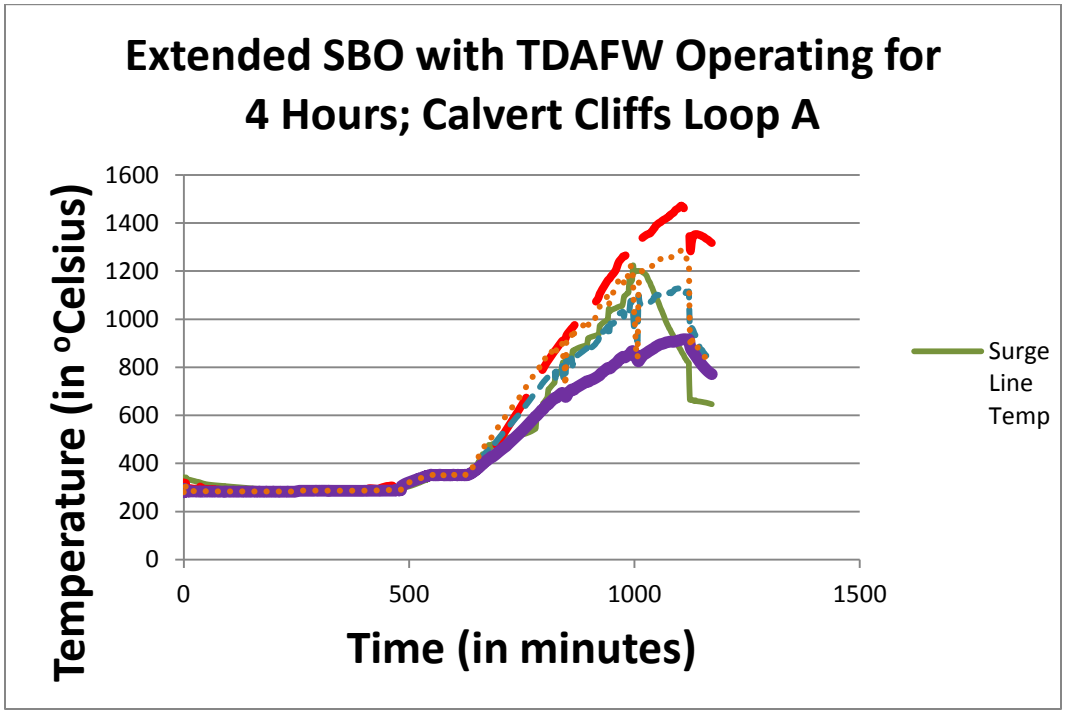


Figure 7-18 Loop A temperature profiles of the HL and SG tubes for the SBO with a delayed failure of TDAFW pumps

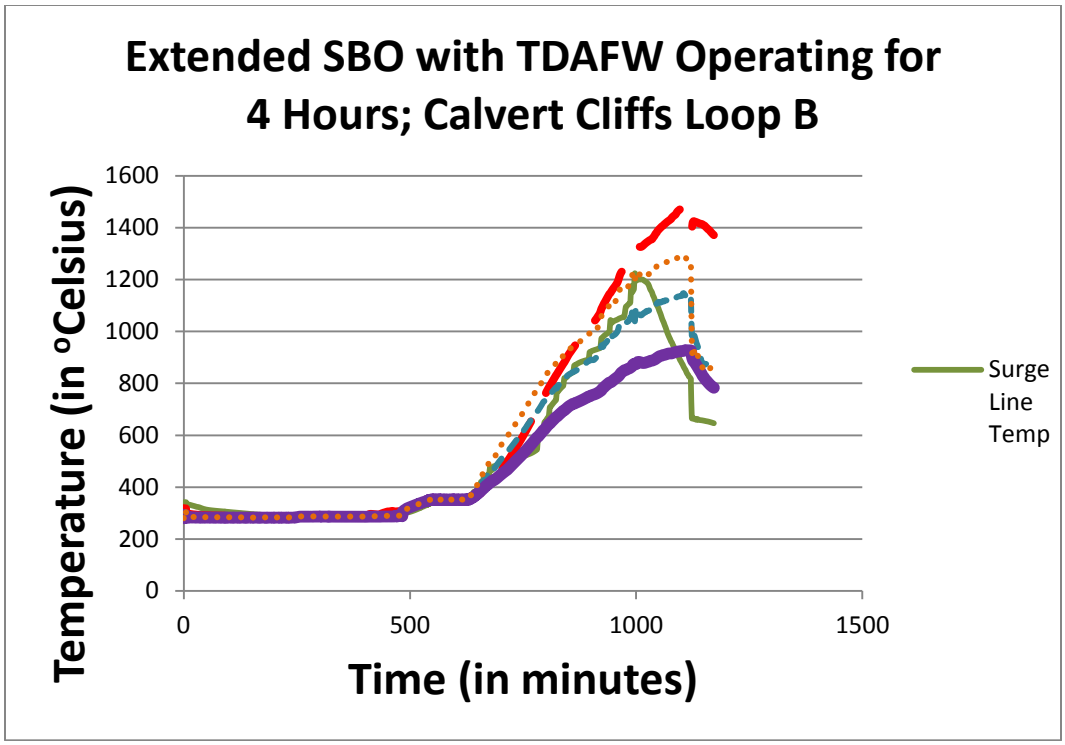


Figure 7-19 Loop B temperature profiles of the HL and SG tubes for the SBO with a delayed failure of TDAFW pumps (surge-line temperature of loop A is shown to facilitate comparison of loop A and B temperature trends)

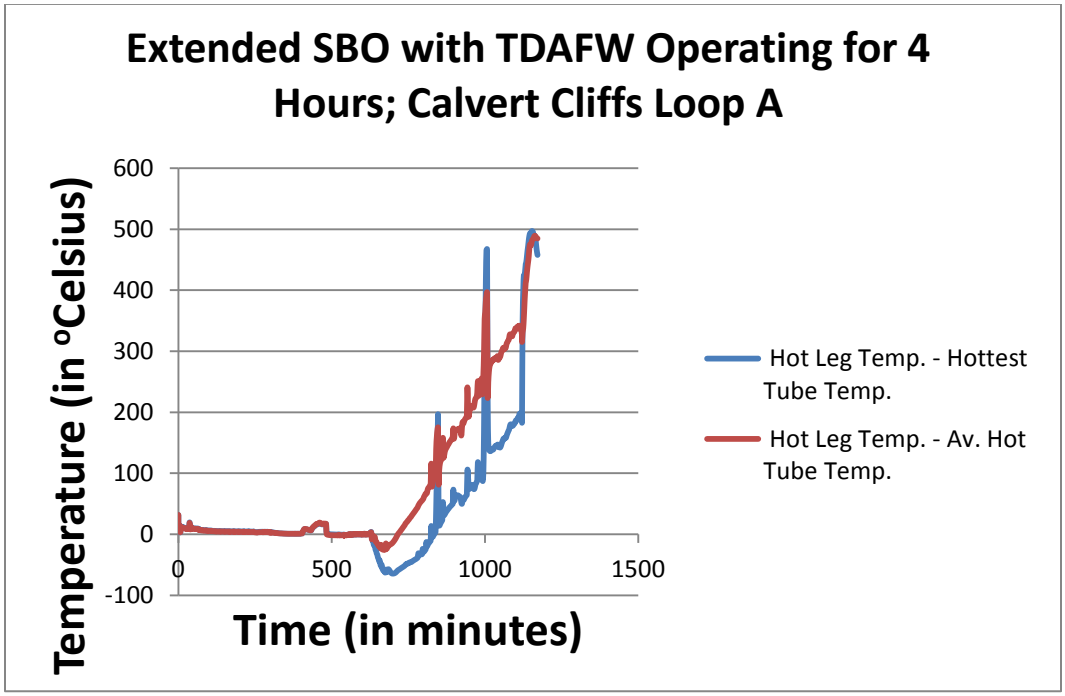


Figure 7-20 Difference in loop A temperature of the HL and SG tubes for the SBO with a delayed failure of TDAFW pumps

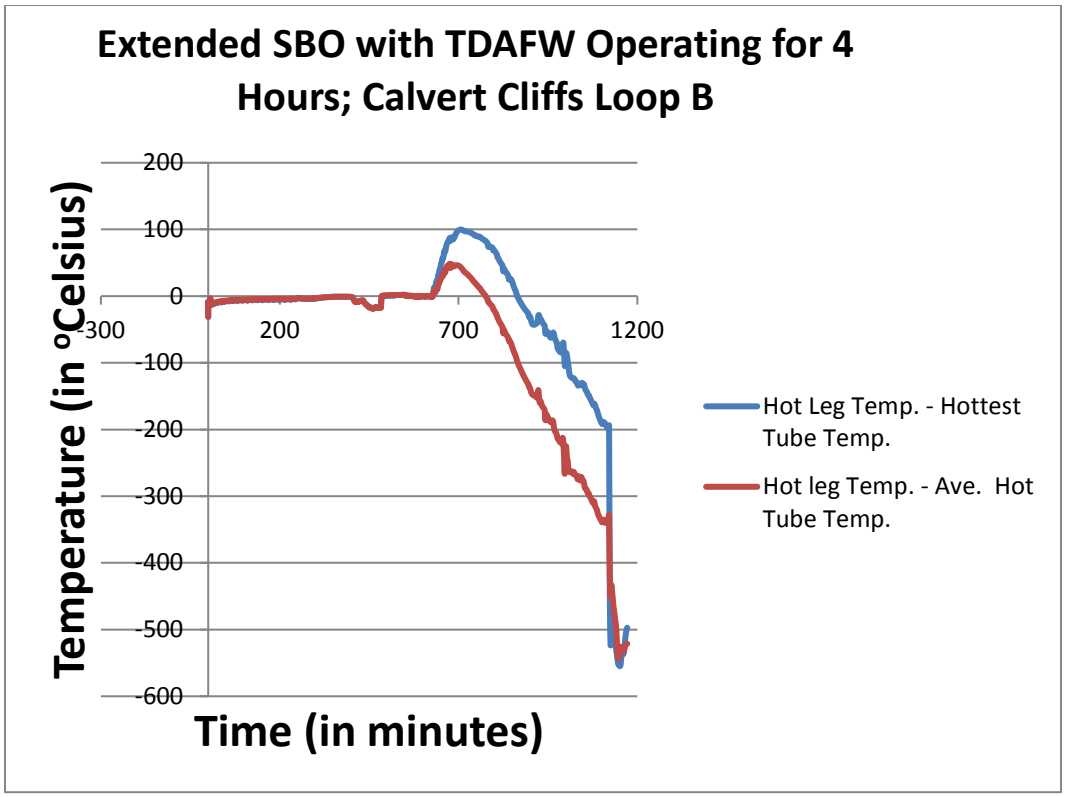


**Figure 7-21(a) Difference in loop B temperature of the HL and SG tubes for the SBO with a delayed failure of TDAFW pumps**

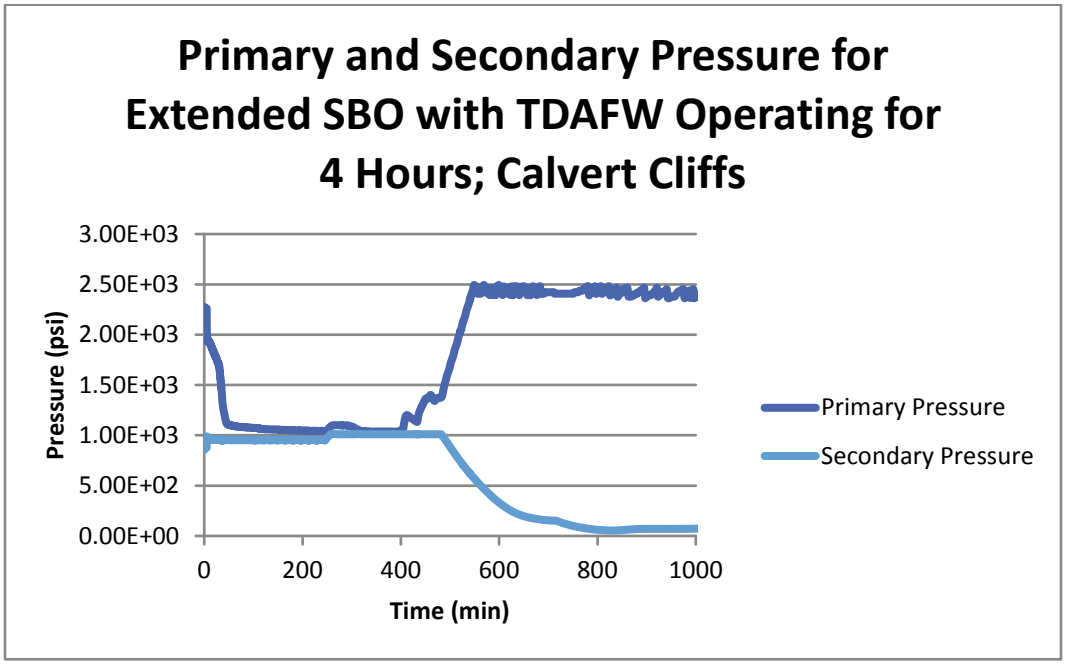


**Figure 7-21(b) Primary and secondary pressure for the SBO with a delayed failure of TDAFW pumps**

### 7.2.2 Estimating the Entry Frequency from Level 1 PRA for C-SGTR PRA Analysis

This study also selected CCNPP as the reference plant for developing the PRA models, to ensure consistency with the TH analyses results. The estimates for a prolonged SBO condition, as the entry point for C-SGTR PRA, were based on the plant design features and the information obtained from SPAR models for the internal events, and from the vintage CCNPP IPE/IPEEE[9] documents for external and other internal hazards. This section discusses the process to develop the Level 2 PRA entry condition for containment bypass resulting from C-SGTR for CCNPP Unit 1. Appendix G (Section G.2) provides a detailed discussion of various CDF contributors from SBO scenarios to overall CDF from both internal and external events. The technical discussion in Appendix G supports the quantitative values used in this section. All potential conditions from the internal and external hazards resulting in a prolonged SBO are considered.

Table 7-14 provides relevant plant information for CCNPP Units 1 and 2. Each CCNPP unit is equipped with two TDAFW pumps, and the duration to battery depletion is nominally 2 hours, although they are expected to last for 4 hours. TH runs in MELCOR also used a value of 4 hours for battery depletion.

The frequency of SBO with either early failures of AFW or failure of AFW after battery depletion, which is used as the entry point for a Level 2 PRA, is estimated based on the discussion provided for each internal and external hazard for the single and dual unit core damage. Table 7-15 shows the contributions from both the internal and external hazards, broken down for the two scenarios of the SBO with early and delayed failures of AFW, for single and dual unit CDF.

The CDF contributions of SBO scenarios from internal and external initiating events, for both units of CCNPP, are partitioned into two bins as follows:

(1) The frequency of those SBO core damage scenarios affects only one unit (i.e., only one unit experiences SBO). For example, a single unit loses offsite power with failure of its emergency power system (e.g., diesel generators).

(2) The frequency of those SBO core damage scenarios affects both units (e.g., a dual unit loss of offsite power (LOOP) followed by failure of emergency power systems in both units (e.g., CCF of all emergency diesel generators (EDGs))).

[9] See IPE Summary Report, "Calvert Cliffs Nuclear Power Plant December 1993," IPEEE Summary Report, Vol. 1, Calvert Cliffs Nuclear Power Plant, August 1997.

Table 7-14 Related Information from the Reference CE Plant

| Systems | System Features |
|---|---|
| Emergency Power System | • Currently there are 5 EDGs for the 2 units. One of these 5 EDGs is the SBO EDG, which can power any safety-related 4-kV bus at either unit. The operation of 1 EDG with success of 1 TDAFW pump per unit is adequate for long-term SG heat removal. The SBO EDG requires operator action to align it to a safety bus and is credited as a recovery action in the PRA models.<br>• At the time when plant IPE/IPEEE was performed, each unit had a dedicated EDG with a shared EDG for both units. Therefore, the information contained in IPE/IPEEE should be used as a guide, and they are not directly applicable.<br>• Each unit has 3 4,160-VAC Class 1E buses, each feeding 1 480-VAC Class 1E bus and motor control center.<br>• 3 trains of dc power are supplied from the inverters and 3 unit batteries. The battery duration is 2 hours, but it is expected to last 4 hours during most scenarios. |
| Auxiliary Feedwater System | Each unit is equipped with 2 TDAFW pumps and 1 motor-driven (MDAFW) pump. There is a cross-connection to the other unit's MDAFW discharge line. |
| Salt Water System (SW) | There are 2 cross-tied trains, each with 1 pump and 1 heat exchanger. A third pump could also supply either train, if needed. |
| Service Water (SRW) | There are 2 trains, each with a salt-water pump, a CCW HX, an SRW HX, and ECCS pump room air cooler. A third pump could be aligned to each train if needed. |
| Component Cooling Water (CCW) | The CCW pumps do not restart automatically after a LOOP. The operators manually reestablish RCP seal cooling after a LOOP. |
| Secondary Relief | • 4 Turbine Bypass Valves—TBVs (2 SG)<br>• Atmospheric dump valve (1 per SG)<br>• MSSRV (8 per SG) |
| Primary Relief | • 2 reverse-seated PORVs 16.547 Mpa (2,400 psi):<br>1. The PORVs do not require dc power for once-through cooling (feed and bleed).<br>2. 2 block valves are powered from the opposite 480 VAC with respect to their PORVs.<br>• 2 spring-loaded SRVs (P>17.237 MPa) or (P>2,500 psig) |
| Containment | Large, dry |

The SBO frequency for single and double units is then further evaluated to arrive at the CDF for *stsbo* and *ltsbo* contributions of single and double units. The overall frequency of the SBO scenarios can be categorized in the following six bins:

(1) the CDF for *stsbo* scenarios affecting Unit 1 only
(2) the CDF for *ltsbo* scenarios affecting Unit 1 only
(3) the CDF for *stsbo* scenarios affecting Unit 2 only
(4) the CDF for *ltsbo* scenarios affecting Unit 2 only
(5) the CDF for *stsbo* scenarios affecting both units
(6) the CDF for *ltsbo* scenarios affecting both units

The results shown in Table 7-15 indicate that the risk of the SBO scenarios is dominated by the SBO scenarios with the failure of TDAFW trains, after the depletion of the battery. A similar conclusion is reached for the dual unit SBO scenarios. The uncertainties associated with these frequencies are not presently estimated, because of the lack of detailed models and data. Surrogate uncertainties from similar plants could be considered, if needed.

**Table 7-15 Contributions of Various Events to the Long-Term SBO Scenarios for Single and Dual Unit Core Damage**

| Initiating Event | SBO with Early Failure of AFW | | SBO with Failure of AFW after Battery Depletion | | Unit CDF from SBO Scenarios with | |
|---|---|---|---|---|---|---|
| | Single Unit * | Dual Unit | Single Unit * | Dual Unit | Early Failure of AFW | Failure of AFW after Battery Depletion |
| Internal events | 1.9E-8 | 5.5E-9 | 4.5E-8 | 1.2E-7 | 2.5E-8 (~13%) | 1.7E-7 (~87%) |
| Seismic | 5.0E-8 | 1.4E-8 | ε + | 2.0E-7 | 6.4E-8 (24%) | 2.0E-7 (~76%) |
| Fire | ε | 2.4E-6 | 2.2E-5 | 2.2E-6 | 2.4E-6 (~9%) | 2.4E-5 (~91%) |
| Flood | ε | ε | 1.6E-6 | ε | ε | 1.6E-6 (~100%) |
| High wind | ε | 4.7E-8 | ε | 4.3E-6 | 4.7E-8 (~1%) | 4.3E-6 (~99%) |
| Total | 6.9E-8 | 2.5E-6 | 2.4E-5 | 6.8E-6 | 2.6E-6 (~8%) | 3.1E-5 (~92%) |

* The unit with the largest CDF contribution is used.
+ For the details of the quantitative values, consult Appendix G (G-2). "ε" generally indicates a value less than 1.0E-8 per year that could not be easily quantified by the results of plant-specific PRA.

### 7.2.3 Flaw Bins to Calculate C-SGTR Probability

CE plants use SGs with Inconel 690TT. Similar to the discussion in the previous chapter, the number of flaws per cycle for these SG tubes is significantly lower than the older SG tubes made of mill-annealed Inconel 600. For Inconel 690TT, the estimated probability that a flaw length and depth belong to a certain range (or bin) uses the adjusted flaw distributions (see Section 7.1.3). Note that the flaw distribution equations derived earlier apply to any SGs (W and CE), as long as the same tube material is used.

Each CCNPP unit has two SGs with 8,471 Inconel 690TT tubes. There are, therefore, 16,942 tubes for each unit and 33,884 tubes for both units. The average number of flaws generated for the first 14 EFPYs of operation using the Inconel 690 flaw-generation rate equation (first row, second column of Table 6-2) is about 127 flaws per SG, or 253 flaws per unit. It is further assumed that the last periodic SG inspection occurred at the end of the 14 EFPYs. All the large flaws, therefore, are assumed to have been plugged (approximately 12 plugged tubes per SG) before EFPY 15 begins. An additional 13 flaws are expected to be generated for each SG during EFPY 15. Therefore, about 128 flawed tubes per SG (or 256 flaws per unit—two SGs) were expected during EFPY 15, with an average of two large

flaws that could need to be plugged at the end of EFPY 15. The expected number of flaws (the expected flaw sample) is estimated to be about 125 flawed tubes per each SG (about 253 per each unit and 505 tubes for both units—all four SGs). The number of flaws is rounded off to avoid fractional tubes. Tables 7-16 and 7-17 show the expected sample flaw for one SG and one unit, respectively.

**Table 7-16 Expected Number of Flaws per Each SG that Belong to a Flaw Bin Defined by Depth and Length Range**

| Depth / Length | 1 cm | 2 cm | 3 cm | 4 cm | 5 cm | 6 cm | Total |
|---|---|---|---|---|---|---|---|
| 0.1 | 0 | 6 | 3 | 1 | 0 | 0 | **10** |
| 0.2 | 3 | 44 | 21 | 5 | 1 | 0 | **74** |
| 0.3 | 1 | 23 | 11 | 3 | 1 | 0 | **39** |
| 0.4 | 0 | 2 | 0 | 0 | 0 | 0 | **2** |
| 0.5 | 0 | 0 | 0 | 0 | 0 | 0 | **0** |
| 0.6 | 0 | 0 | 0 | 0 | 0 | 0 | **0** |
| 0.7 | 0 | 0 | 0 | 0 | 0 | 0 | **0** |
| 0.8 | 0 | 0 | 0 | 0 | 0 | 0 | **0** |
| 0.9 | 0 | 0 | 0 | 0 | 0 | 0 | **0** |
| **Total** | **4** | **75** | **35** | **9** | **2** | **0** | **125** |

**Table 7-17 Expected Number of Flaws per Loop A and Loop B (One Unit; Two SGs) that Belong to a Flaw Bin Defined by Depth and Length Range**

| Depth / Length | 1 cm | 2 cm | 3 cm | 4 cm | 5 cm | 6 cm | Total |
|---|---|---|---|---|---|---|---|
| 0.1 | 1 | 13 | 7 | 2 | 0 | 0 | **22** |
| 0.2 | 6 | 88 | 43 | 11 | 2 | 1 | **151** |
| 0.3 | 3 | 45 | 22 | 5 | 1 | 0 | **76** |
| 0.4 | 1 | 1 | 1 | 0 | 0 | 0 | **3** |
| 0.5 | 0 | 1 | 0 | 0 | 0 | 0 | **1** |
| 0.6 | 0 | 0 | 0 | 0 | 0 | 0 | **0** |
| 0.7 | 0 | 0 | 0 | 0 | 0 | 0 | **0** |
| 0.8 | 0 | 0 | 0 | 0 | 0 | 0 | **0** |
| 0.9 | 0 | 0 | 0 | 0 | 0 | 0 | **0** |
| **Total** | **10** | **148** | **73** | **18** | **3** | **1** | **253** |

The expected values of flaws in each bin illustrate the expected size distribution of flaws. The values shown in the tables also account for the flaws detected in previous cycles that were large enough to require the affected tubes to be plugged. The approximation used in these calculations, plus the effect of rounding off the expected number of flaws per bin, generally resulted in slightly fewer flaws than expected. As an example, Table 7-16 shows an expected set of 125 flaws per each SG, rather than the 128 flawed tubes (127 flaws in previous cycles, plus 13 flaws in the last cycle, and minus approximately 12 plugged tubes) estimated earlier.

For CE plants, TH results are different for the loop with a pressurizer (loop A) and the loop without a pressurizer (loop B). Therefore, the probability of C-SGTR is calculated for each loop separately. Table 7-17 shows the expected number of flaws for the whole plants (i.e., two loops and two SGs). However, the analysis does not use this flaw set, and it is only presented for consistency with W plant and as an illustrative example of a unit flaw set.

### 7.2.4 SGTR Probability Estimation Using Integrated Flaw Samples

An integrated plant wide analysis would involve generating a large number of flaw samples for the hottest tube, hot tubes, and cold tubes for both loops A and B, and performing integrated C-SGTR calculator case runs to establish sufficient statistics to estimate C-SGTR probability and its uncertainty distribution. Because the C-SGTR software is not designed to accept different TH files for different loops and treat temperature distributions for the tubes (e.g., average hot, hottest, and cold), such an integrated analysis is impractical.

Short of performing an integrated analysis, the study took the following steps to obtain an estimate for C-SGTR using a sample of flaws:

(1) The 125 expected flaws per each SG, as shown in Table 7-16, was considered for performing C-SGTR case runs.

(2) A C-SGTR case run was performed with the 125 expected flaws. A 0.25 probability was used for a flaw to be exposed to the average hot tube temperature. A probability of 0.75 was used to indicate that a flawed tube is exposed to the average cold tube temperature.

(3) Step 2 was repeated for the hottest tubes with the 125 expected flaws. A probability of 0.01 was assigned for a flawed tube (any of the 125 flaws) to be exposed to the hottest tube temperature.

(4) The distribution percentiles (5 percent to 95 percent) of SGTR cumulative leak areas estimated by the C-SGTR code for each time step was transformed to the probability of a leak size at each time step for the average hot and the hottest tube for loop A. These leak area distributions were then added probabilistically (i.e., by convolution of leak distributions) at each time step to obtain the cumulative C-SGTR leak area distribution for loop A, from both the average and the hottest tubes.

(5) The probability of RCS failure (i.e., HL or surge-line failure) was also estimated for each time step for loop A.

(6) Steps 2 through 5 were repeated for loop B. The probability of HL failure was used as the probability of RCS failure for loop B.

(7) The integrated C-SGTR leak areas from loop A and loop B were then probabilistically added (i.e., the two distributions were convolved at each time step). Similarly, the probability of RCS failure was estimated by aggregating the probabilities of RCS failure of loop A with loop B.

(8) For a critical SG leak area (i.e., 6 $cm^2$ (0.93 $in.^2$)), the probability of RCS survival was multiplied with the probability that the SG leak area distribution exceeds the critical C-SGTR leak area for each time step. The resulting probability value is then integrated

over all time steps to obtain the C-SGTR probability. This is shown in the equation below:

$$Prob(CSGTR) = \int Prob\ (RCS\ survive\ at\ t) * Prob\big(CSGTR\ occurs\ between\ t\ and\ (t + dt)\big) * dt \qquad (7.3)$$

Figures 7-22 and 7-23 show examples of the graphical results generated from Steps 2 and 3 for the *stsbo* scenario for the average hot and the hottest tubes. These graphs show the probability of RCS survival and the distributional percentiles of the SGTR leak areas as a function of time. The graphs also show that there is significantly more spread for leak area distribution associated with the hottest tube. For a leak area of 3 cm$^2$ (0.46 in.$^2$), the graphs show that the survival probability of RCS could vary from 0.03–0.17 for the average hot tube and from 0–0.43 for the hottest tubes.

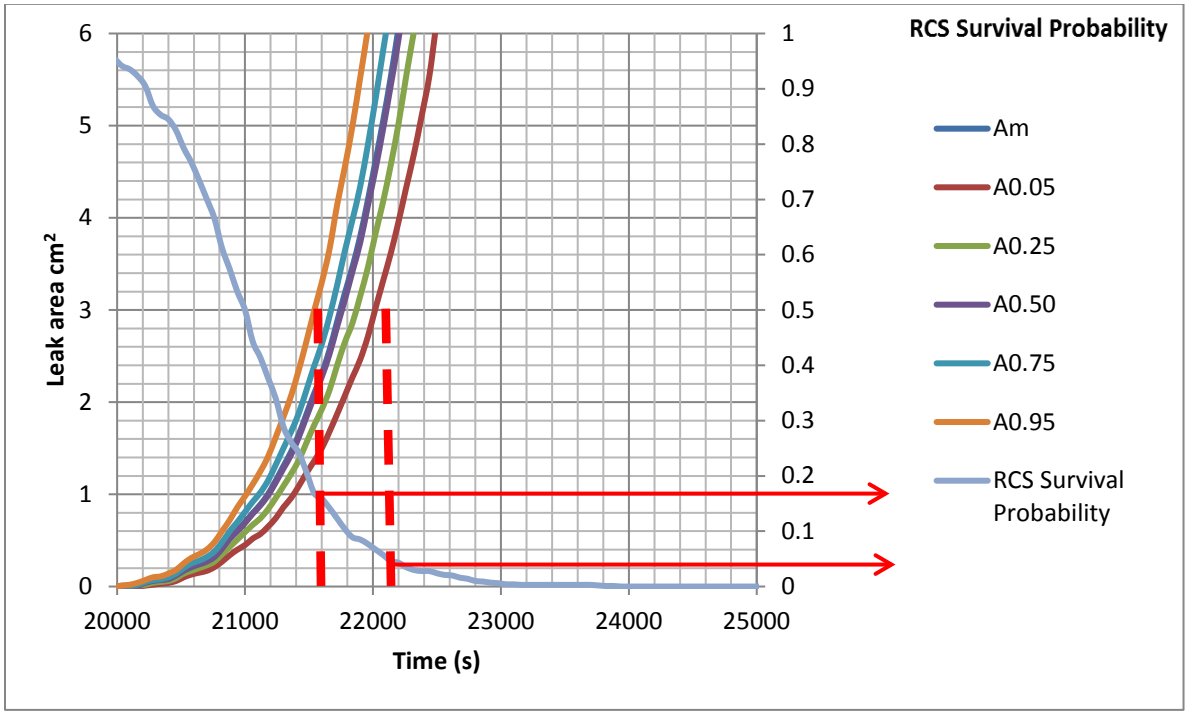


**Figure 7-22 The RCS survival probability and percentiles of SGTR leak areas for *stsbo-a-average* hot tubes**

Figures 7-24 and 7-25 present the graphical results from Steps 4 and 5 for loop B and loop A, respectively. Figure 7-24 shows that, at about 2,000 seconds, the probability of RCS survival is 0.5 and the probability that the SGTR leak exceeds 3 cm$^2$ (0.46 in.$^2$) is approximately 0.4 (1 – 0.6). Similarly, at 2,080 seconds, the probability that RCS has survived is 0.6 and the probability that SGTR leak exceeds 3 cm$^2$ (0.46 in.$^2$) is approximately 0.02 (1 – 0.98). The current method can generate similar graphs for any size of SGTR leak areas. Figure 7-26 contains an example showing the leak probability curves for both a 3 and 6 cm$^2$ (0.46 and 0.93 in.$^2$) SGTR leak area for the *stsbo-a-b-scf* sequence.

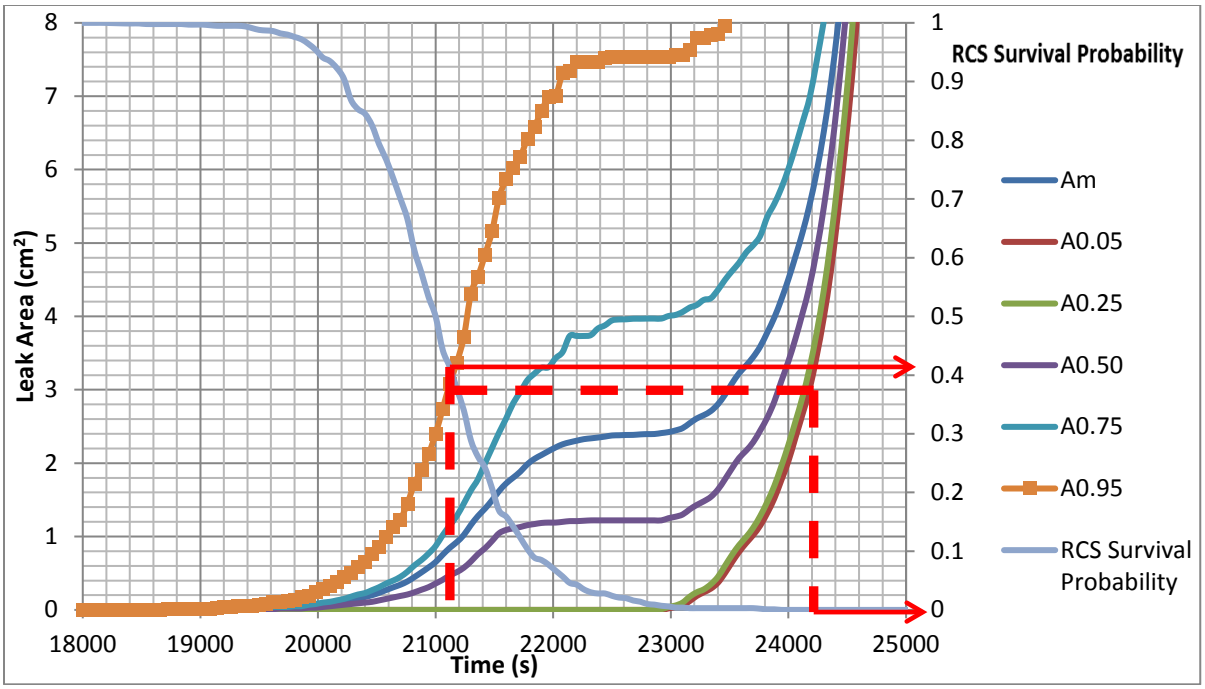


**Figure 7-23 The RCS survival probability and percentiles of SGTR leak areas for *stsbo-a-hottest* tubes**

Figure 7-27 shows the graphical results from Step 7 of the approach. It shows the probability of RCS integrity and the time-dependent probability that the SGTR leak area from both SGs is less than a predefined critical leak area criterion (i.e., 6 $cm^2$ (0.93 $in.^2$)).

A C-SGTR probability of about 0.2 was estimated for the *stsbo-a* sequence based on the procedure given in Step 8 of the approach.

Table 7-18 shows the results for the probability of SGTR exceeding 6 $cm^2$ (0.93 $in.^2$) for loop B before the failure of its HL. This result could also represent a bounding estimate for the plant C-SGTR, which is the equivalent of assuming that both loops (A and B) experience the TH behavior of loop B (i.e., worse condition for C-SGTR), and both loops fail dependently. The next paragraphs discuss more detailed calculations that differentiate between the TH behaviors of the two loops. These calculations showed that the probability of C-SGTR for the selected CE plant is about 0.2 for SBO scenarios where the TDAFW pump(s) failed initially and about 0.3 when the TDAFW pump(s) operated for at least 4 hours. These results show that, if the TH behavior of loop B is only used for a simplified PRA analysis, the resulting C-SGTR probability will not be significantly overestimated (less than 10 percent overestimation). For these analyses, primary or secondary relief valves are assumed to reclose after opening and no failure to stick open is considered. Section 7.3.2 discusses the sensitivity results for cases where one or more of the secondary relief valves may fail open (i.e., stick open). Figure 7-28 shows an example of calculations for loop B resulting from Step 6 of the approach to compare with Figure 7-26. Table 7-18 shows the comparative results for the probability of SGTR exceeding 3 or 6 $cm^2$ (0.46 or 0.93 $in.^2$) for loop B before the failure of HL.

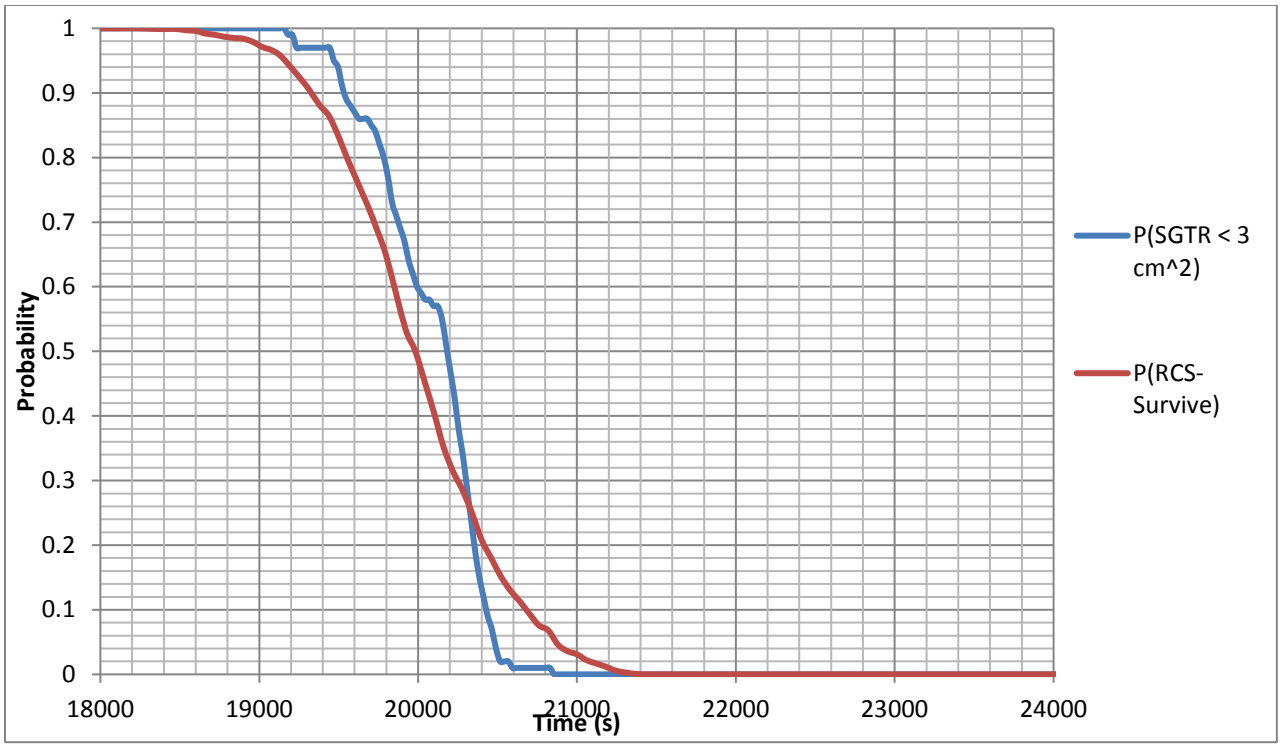


Figure 7-24 The RCS survival probability and the probability of SGTR with a leak area less than 3 $cm^2$ for ***stsbo-a-b***, aggregated over average hot and hottest tubes

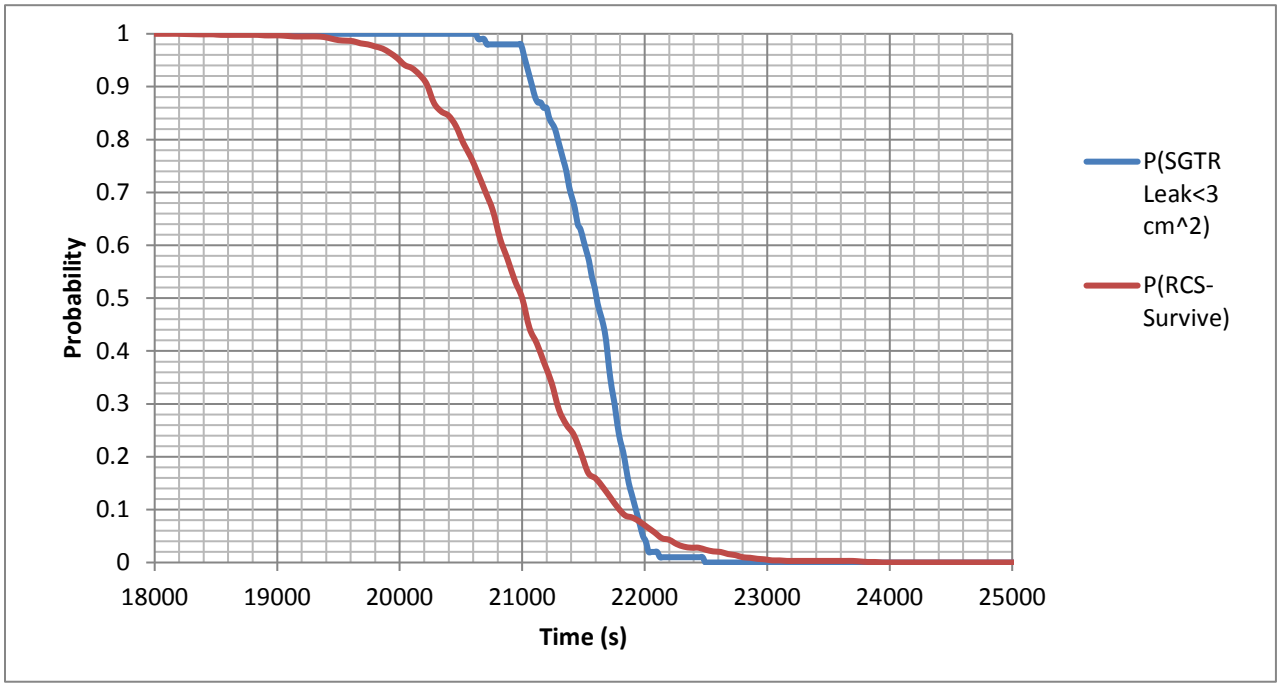


Figure 7-25 The RCS survival probability and the probability of SGTR with a leak area less than 3 $cm^2$ for ***stsbo-a-a***, aggregated over average hot and hottest tubes

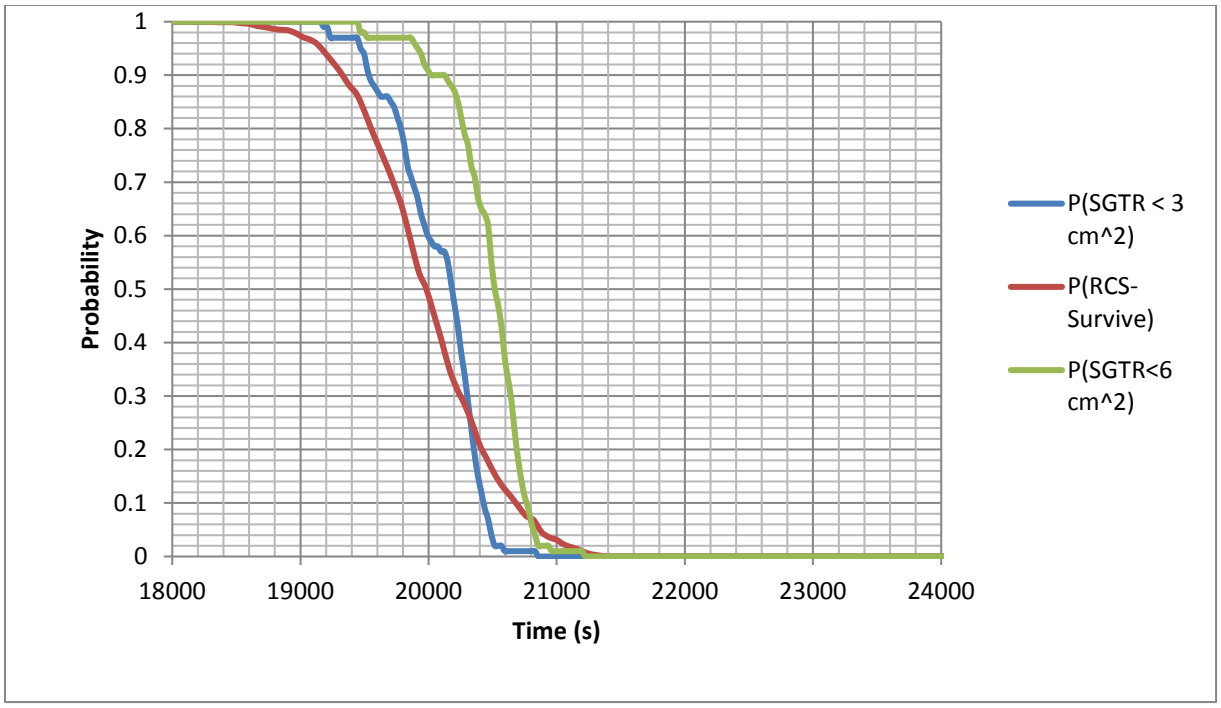


**Figure 7-26 The RCS survival probability and the probability of SGTR with a leak area less than 3 and 6 cm$^2$ for *stsbo-a-b-scf***

The probability of C-SGTR for the selected CE plant is, therefore, 0.2 for SBO scenarios where the TDAFW pump(s) failed initially and 0.3 when TDAFW pump(s) operated for at least 4 hours. Similar observations were noted for the W case studies. The following discusses the main reasons behind the higher probability of C-SGTR for *ltsbo* compared to *stsbo*.

For both the CE and W cases, the conditional C-SGTR probability is higher for the severe accident sequences with late failure of AFW than those sequences with early failure of AFW. Both W and CE TH input files exhibit a slower temperature ramp in *ltsbo* than *stsbo* after the SG tube temperatures reach the creep-rupture range; namely, 600–700 degrees C (1,112–1,292 degrees F). However, the difference between the HL and SG tube temperatures remains approximately the same for long and short SBOs. The notion that the probability of containment bypass is governed by the difference in HL and SG tube temperatures should be tempered by the effect of the absolute temperature and the rate of temperature ramp. The equations for creep-rupture failures of HL and SG tubes depend on the absolute temperature and the time temperature integral. The probability of containment bypass, therefore, is governed not only by the difference in HL and SG tube temperatures but also by the absolute temperature and the rate of the temperature ramp in severe accidents. Figures 7-15 and 7-16 illustrate this phenomenon for early AFW failure and Figures 7-18 and 7-19 for late AFW failure. It should be noted that the C-SGTR, if it occurs, occurs much later in the sequences with late AFW failure (*ltsbos*) and carries significantly less public consequence (i.e., not considered an LER), compared to the sequences where AFW fails at T=0 (*stsbos*).

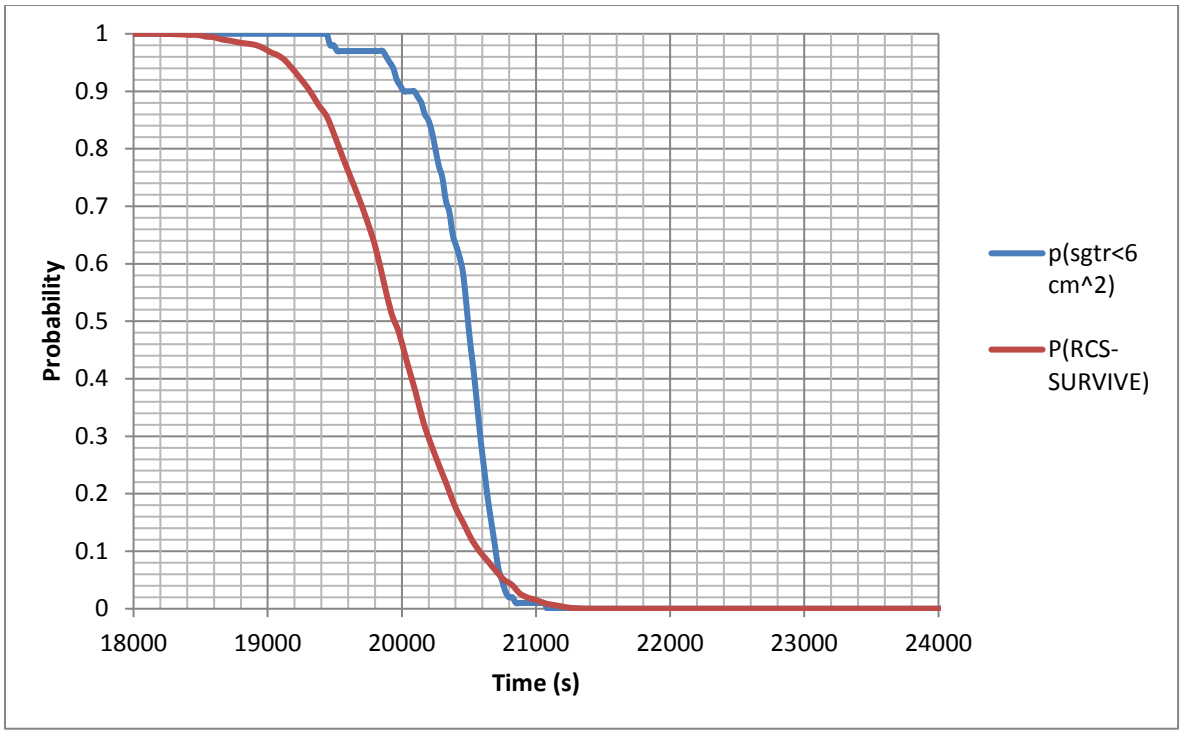


Figure 7-27 The RCS survival probability and the probability of SGTR with a leak area less than 6 $cm^2$ for the whole plant for an SBO scenario with failure of TDAFW pump at time zero and no stuck-open secondary relief valves (***stsbo-a-scf***)

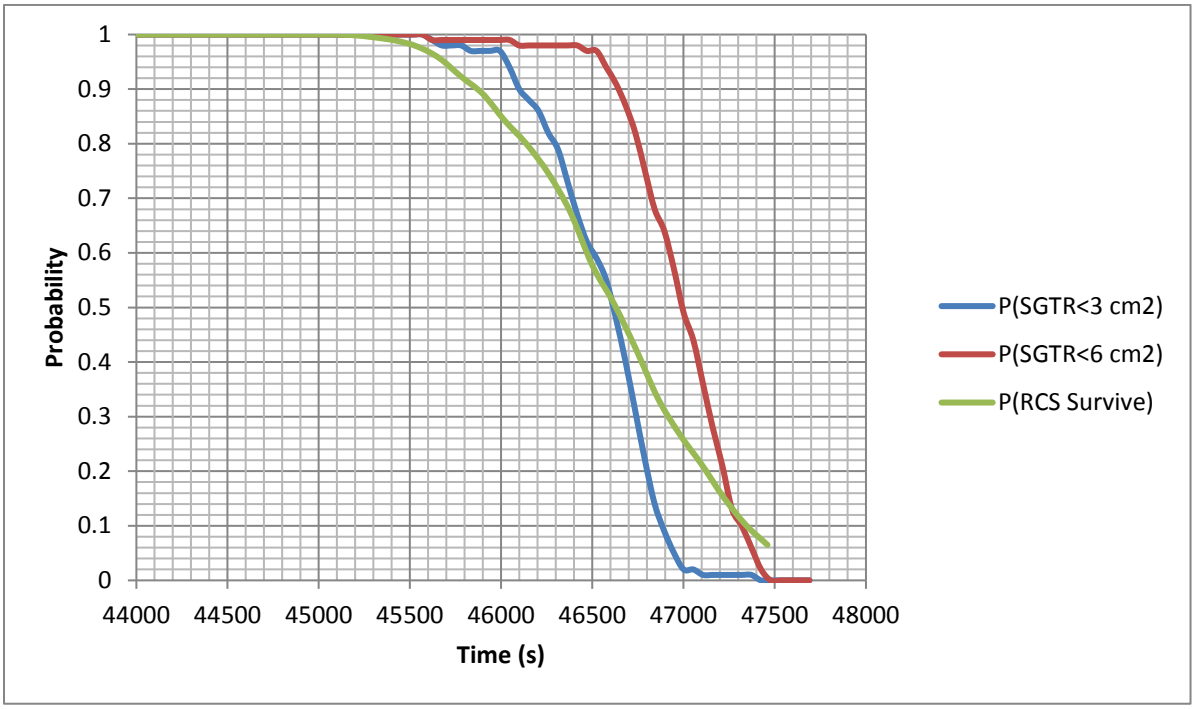


Figure 7-28 The RCS survival probability and the probability of SGTR with leak areas less than 3 and 6 $cm^2$ for ***ltsbo-a-b-scf***

Table 7-18 Comparison of C SGTR Probability for SBO

| Case Run (Sequence) | P(C-SGTR>6 $cm^2$) using TH of loop B for both loops |
|---|---|
| Short-Term SBO | 0.22 |
| Long-Term SBO | 0.31 |

### 7.2.5 Level 2 Models for Containment Bypass Evaluation

Table 7-19 shows the timing for the major events corresponding to the accident progression of a scenario of an SBO and early failure of TDAFW pumps. A combination of MELCOR results and sensitivity case runs with C-SGTR software generates these timings.

Table 7-19 Timing of Major Events during an SBO with Early Failures of TDAFW Pumps

| Time | Events for SBO with Early Failure of TDAFWs |
|---|---|
| 0 | SBO started |
| ~ 14 minutes | ECCS signal actuated |
| ~ 4 hours | Dc assumed depleted [a] |
| ~ 5 hours | Onset of core uncovery, corresponding to 648.89 °C (1,200 °F) |
| Between 5 hours and 30 minutes and 5 hours and 45 minutes [b] | SGTR expected with varying leak rates [c] |
| Between 5 hours and 21 minutes and before 5 hours and 50 minutes | HL failure if the primary pressure remains around 15.17 MPa (2,200 psi) as estimated by C-SGTR software |
| Between 5 hours and 8 minutes and 5 hours and 30 minutes | Gap release from rod groups 1 through 5 |
| Around 5 hours and 54 minutes | HL failure if the primary pressure remains around 8.27 MPa (1,200 psi) [b] (SG relief set point) after 65 hours, 30 minutes |
| Around 6 hours | HL failure if the primary pressure is reduced around 4.83 MPa (700 psi) |
| Between 7 and 8 hours | Core structure failures, multiple melting and quenching; start of in-vessel releases |
| ~ 11 hours | Vessel breach, HL failure not expected if primary is fully depressurized |

[a] Although MELCOR assumes dc is depleted in 4 hours for both early and late failure of TDAFW pumps, PRA considers dc would be available for a longer time for the case when TDAFW pumps were not available at time zero. The availability of dc will facilitate SAMG activities such as depressurization of primary and secondary.
[b] The ranges are defined based on 10 and 90 percentiles of the associated failure distribution.
[c] These values were supported by sensitivity runs performed using C-SGTR software.

An examination of the information shown in this table leads to the following six observations:

(1) For cases when C-SGTR occurs before HL failure but the primary pressure is maintained at the primary relief set point (approximately 15.2 MPa (2,200 psi)), the HL is expected to fail shortly after the occurrence of SGTR. The size of the SGTR leak for such cases is approximately equivalent to the area of a guillotine break of one tube.

MELCOR runs show that this amount of SGTR leakage may not demand any cycling of the secondary relief valves. In general, no depressurization of the primary system is expected. The releases are therefore limited to a fraction of the fuel gap release plus the radioactivity source term contained in the primary reactor system. These are categorized under negligible releases. Larger releases are possible only if the secondary-side relief valves sticks open during or before C-SGTR.

(2) For cases where the primary pressure equalizes with the secondary pressure and the pressure remains at the secondary relief set point (approximately 8.3 MPa (1,200 psi)) after the occurrence of C SGTR, the HL failure would be delayed but it occurs before the vessel breach. The status of SG relief valves (stuck open or not) would determine the magnitude of release. It is expected that the larger the C-SGTR leak area, the larger the release magnitude would be. The releases are generally not categorized as LERs if no secondary relief valve sticks open.

(3) If the primary system is somewhat depressurized to an intermediate pressure of about 4.83 MPa (700 psi); for example, caused by the failure of one primary relief valve in a partially open position, the failure of HL will be delayed and, if one or more secondary relief paths have stuck open, there is a potential for some early releases. The releases, however, will be limited, since the stuck-open primary relief valve will cause some fraction of releases to end up in the containment.

(4) For cases where the secondary relief valves stick open early in the accidents, the primary is expected to depressurize below the accumulator discharge set point. This will delay the failure of HL and the occurrence of SGTR. Higher delta P on the tubes is expected, however, because of lower secondary-side pressure, which can increase the probability of SGTR. For these cases, the probability of C-SGTR is expected to increase, and the releases are considered to be LERs because of a large containment bypass area provided by the stuck-open secondary relief valves. Section 7.3.2 discusses the specific set of MELCOR runs for this case in more detail.

(5) For cases where the primary and secondary are equalized and both are depressurized completely, the HL may not fail until vessel breach (approximately 11 hours) occurs. All in-vessel releases should then be considered as a part of the source term. This situation could occur if the operator has depressurized the primary system for SAMG actions but failed to flood the secondary side of the SG or the primary system. The primary depressurization could also take place by failures of multiple primary relief valves (stuck open) under the harsh environment associated with post-core melt.

(6) The occurrence of a very large C-SGTR leak area (because of loop seal clearing, or the failure of three or more tubes) is conservatively categorized as an LER. Such cases can demand secondary-side relief, and multiple secondary-side relief paths could fail open. However, the release could be significantly reduced if the secondary side of SG is filled with fire water as a part of SAMG actions.

Table 7-20 shows the timing for the progression of accidents for a scenario of an SBO and failures of TDAFW pumps after 4 hours. A combination of MELCOR results and sensitivity case runs with C-SGTR software similarly generates these timings. They follow very similar trends as those for the first scenario when TDAFW failed early. There are two differences between the accident progressions of an SBO with failures of TDAFW pumps after battery depletion and an

SBO with the early failure of TDAFW pumps. These differences are important for developing and quantifying the Level 2 models for C-SGTR:

(1) Dc is expected to be depleted by 4 hours, so no operation of active components from the control room can be credited unless the power is recovered. If the offsite power is recovered, credits for successful SAMG actions can be provided.

(2) Extended dc could be provided through portable generators and other means. This could also facilitate the long-term availability of dc for SAMG actions or to maintain the operation of the TDAFW pumps. The success probability for such actions could be increased if they are initiated early after the occurrence of an SBO. This is a plant-specific PRA issue that cannot be addressed generically at this time.

**Table 7-20 Timing of Major Events during an SBO with Failures of TDAFW Pumps after Battery Depletion**

| Time | Events for SBO with Early Failure of TDAFWs |
|---|---|
| 0 | SBO started |
| ~ 14 minutes | ECCS signal actuated |
| ~ 4 hours | Dc assumed depleted |
| ~ 12 hours and 05 minutes | Onset of core uncovery, corresponding to 648.89 °C (1,200 °F) |
| Between 12 hours and 45 minutes and 13 hours and 05 minutes | SGTR expected with varying leak rates |
| Between 12 hours and 30 minutes and 13 hours and 15 minutes (average 12 hours and 55 minutes) | HL failure if the primary pressure remains around 15.17 MPa (2,200 psi) as estimated by C-SGTR software |
| Between 12 hours and 40 minutes and 13 hours and 15 minutes | Gap release from rod groups 1 through 5 |
| Between 13 hour and 20 minutes | HL failure if the primary pressure remains around 8.27 MPa (1200 psi) (SG relief set point) after the onset of core damage |
| Around 17 hours | Core structure failures, multiple melting and quenching; start of in-vessel releases |
| ~ 18 hours | Vessel breach, if primary fully depressurized |

Similar to the discussion of the W plant in the previous section, a five-factor formula was used to estimate the frequency of containment bypass and LERF because of C-SGTR. The fractions of containment bypass scenarios that can lead to LERs depend on the success probabilities of SAMG actions and effective evacuation. The SAMG actions for the CE plant are similar and comparable to those of the W plant, as discussed previously.

Section 2.5 discussed the emergency response timeline and the process for effective evacuation of the SBO scenario with the early and late failure of TDAFW pumps (e.g., after batteries are depleted). That discussion applies to both the W and CE plants. It is assumed that, for the CE plants similar to the W plant, the evacuation is most likely effective for C-SGTR containment bypass events during SBO scenarios with late failures of TDAFW pumps and not effective for SBO scenarios with early failure of TDAFW pumps. This assumption is valid despite

the fact that the estimated time to core damage for the CE plant was somewhat longer than for the W plant.

### 7.2.6 Quantification of Probability of Containment Bypass due to C-SGTR

A simplified five-factor formula for LERF, as discussed in Section 2.5, was used. The five factors are as follows:

(1) frequency of severe accident sequences with potential for C-SGTR ($f_{AC}$), as discussed in Section 7.2.2

(2) C-SGTR probability ($P_{CSGTR}$); see the discussion for estimating C-SGTR and containment bypass probability in Section 7.2.4

(3) conditional probability that the subsequent failures of RCS components, including the stuck-open primary relief valves, do not occur ($P_{NDEP}$)

(4) failure probability of all SAMG actions ($P_{SAMG}$)

(5) probability that early effective evacuation is not successful ($P_{EVAC}$)

The qualitative discussion provided in the previous section for estimating the parameters—$P_{NDEP}$, $P_{SAMG}$, and $P_{EVAC}$—are considered to be applicable here. Bounding values for each of these three parameters, similar to what was suggested in Section 7.1, were also used. Table 7-21 shows the values for SBOs, with early or late failures of TDAFW pumps.

**Table 7-21 Conditional LERF Probabilities for an SBO with Early and Late Failures of TDAFW Pumps for the Example CE Plant**

| Factors | Applicability | LERF Factors (early, late)[a] [b] |
|---|---|---|
| $P_{CSGTR}$ | Sequences with no stick-open primary or secondary relief valves | (0.2, 0.3) |
| | Sequence with loop seal clearing | (1.0,1.0) |
| $P_{NDEP}$ | Sequence without loop seal clearing | (1.0, 1.0) |
| | Sequence with loop seal clearing | (1.0, 1.0) |
| $P_{SAMG}$ | Sequence without loop seal clearing | (1.0, 1.0) |
| | Sequence with loop seal clearing | (1.0, 1.0) |
| $P_{EVAC}$ | For all sequences | (1.0, 0.0) |

[a] The two numbers in parenthesis are for SBO scenarios with early and late failure of TDAFW pumps.
[b] This value is considered to be conservative, and it is used for screening purposes only.

Table 7-15 showed earlier that more than 92 percent of the total SBO scenarios; from both internal and external events, resulted from the SBO scenarios with the failure of TDAFW pumps after battery depletion for the selected plant (last row last column of Table 7-15). Moreover, the results for internal event models also showed that 87 percent of the total SBO scenarios resulted from the SBO scenarios with the failure of both TDAFW pumps after battery depletion for the selected plant (last column, first row after headings). The CDF from SBO sequences, considering all hazard categories, is about $3.3X10^{-5}$/year, and for the internal event, is about 1.9

$X10^{-7}$/year (obtained from Table 7-15). This CDF, multiplied by the conditional probability of containment bypass (0.2), gives a bounding containment bypass frequency estimate of ~$6.8X10^{-6}$/year for all hazard categories, and ~$4.0X10^{-8}$/year for internal events only. The overall LERF estimate from each unit is about $5.1X10^{-7}$, since only the containment bypass resulting from the SBO scenarios with early failure of both TDAFW pumps (i.e., about 8 percent of the total CDF) has a potential for an LER.

The relatively small values for LERF for the selected CE plant (i.e., CCNPP) are the result of the unique design feature of its AFW system. CCNPP is equipped with two TDAFW pumps that significantly reduce the CDF resulting from the SBO scenarios with the early failure of TDAFW pumps. This design feature is not generally shared by other CE plants. However, all current U.S. plants are equipped with additional SBO diesel generators and will have a set of new FLEX equipment to significantly reduce the probability of core damage during all SBO scenarios.

This study does not currently use detailed quantification of Level 2 PRA models, considering the complexity of human reliability analysis for SAMG actions and the survivability of equipment after core melt. It is expected that plant-specific features will play important roles in the detailed quantification of containment bypass probability.

### 7.2.7 Concluding Remarks

The TH results obtained from various case studies significantly influence C-SGTR, containment bypass probability, and LERF. These TH results reflect the specific design, configuration, and geometry of the plant systems (specifically the SG design), and primary connections such as HL and surge line. They should not be interpreted as generic results for CE plants. The more important plant features that can affect the results are as follows:

- SG flaws (i.e., number, type, depth, and size of the flaws)
- mixing in SG inlet plenum (e.g., deep or shallow SG inlet plenum and the angle of HL entry)
- mixing and heat transfer in HL (e.g., HL diameter and length)
- reliability of primary and secondary relief valves pre/post onset of core damage
- operational procedures regarding the depressurization of the secondary side of SGs
- duration of dc availability, including load shedding capabilities
- effectiveness and success of SAMG activities
- success of FLEX and EDMG

The paragraphs below discuss the conclusions of this study, based on the case studies performed for the selected CE plant described in this chapter.

- The contribution of C-SGTR to LERF is expected to be about $5.1X10^{-7}$/yr when all hazard categories applicable to the site are included.

The contribution of C-SGTR to LERF is expected to be about $5.0X10^{-9}$/yr when only internal event SBO core damage sequences are considered. This value is lower than the expected value for other CE plants, since the selected CE plant is equipped with two TDAFW trains; however, current plants are equipped with additional SBO diesel generators and a set of new FLEX equipment.

- All the hazard models for the SBO scenarios considered for this study showed that the large fraction of core damage scenarios will involve both units (approximately 86 percent). This issue may be considered further as a part of the integrated site PRA.

- There is a significantly higher probability for C-SGTR for the CE plant compared to the W plant—this conclusion focuses too heavily on the unique PRA aspects of the reference plant—particularly that relatively shallow flaws can provide a significant contribution to C-SGTR probability in the CE plant.

- The CE plant has unique safety features that may not be representative of the PWRs using similar SGs. (For example, the two TDAFW pumps, as mentioned above, are deemed to be an asset, since it would make the failure of the TDAFW pumps less likely than at a typical plant with only one TDAFW pump.)

The following observations consider the frequency of containment bypass, which may or may not result in an LER:

- For the selected CE plant, the contribution of C-SGTR to containment bypass could be as high as $6.8X10^{-6}$, considering contributions from all hazard categories. If only internal events are considered, this contribution is expected to be about $4.0X10^{-8}$.

- Based on the existing PRAs, C-SGTR appears to be the highest contributor to containment bypass scenarios.

- The containment bypass contribution occurs mainly from the scenarios where the TDAFW pump initially worked but was later rendered inoperable after the depletion of batteries. This is mainly because the CDF contribution from the scenarios with failure of TDAFW pump(s) after battery depletion is much larger than the CDF from the SBO scenarios with the early failure of TDAFW pump(s). However, these scenarios are not considered to contribute to LERF, since evacuation is expected to be effective.

- Extending the battery life and operation of TDAFW pumps can reduce the frequency of containment bypass, by reducing the frequency of the core damage sequences that challenge the SG tubes. This also facilitates the use of additional equipment, such as the existing EDMG or the future equipment in response to the FLEX program.

## 7.3 Sensitivity Analyses for C-SGTR in Different SG Types

This section examines the robustness of the results and conclusions discussed earlier in Sections 7.1 and 7.2 under varying sets of assumptions. These sensitivity analyses are also designed to support the development of Level 2 PRA models. Appendix D provides a detailed discussion on the approach, assumptions, case runs, and results of the analysis for both the selected W and the CE plants.

Section 7.3.1 is devoted to the example W plant and summarizes the results and insights from a series of sensitivity analyses that Appendix D discusses in detail. Section 7.3.2 similarly summarizes the results and insights from different sets of sensitivity analyses for the example CE plants. In some cases, the results of sensitivity analysis performed for one example plant could be applicable and provide insights for the other plant.

### 7.3.1 Summary of Sensitivity Analyses for the Westinghouse Plant

The following sensitivity analyses were performed for the W plant. The measure of comparison used for these sensitivity analyses was based on the difference between the time when HL failure is imminent and the time when C-SGTR is expected. The ratio of this time margin over the base time margin is used as a means of qualitatively ranking the impact of sensitivity results.

#### *7.3.1.1 Uncertainty in Predicting the HL and SG Tube Temperatures*

This sensitivity analysis studied the effect of uncertainties of TH prediction in terms of the delta temperature between the HL and the average hot tube. It is generally expected that, if the difference between the HL temperature and the SG tube temperature decreases, the probability of C-SGTR would increase. This assumes that the delta-T between the HL and hot tube is only 50 percent as large as the base case. The results of the sensitivity analysis for the example W plant showed that the time margin measure is reduced by 4 minutes. This is considered to be a low impact.

#### *7.3.1.2 Sensitivity of HL Thickness*

The HL materials and thickness are clearly defined plant-specific parameters. There could, however, be some variations across similar plants because of the differences in the thickness of the weld overlay. In this sensitivity case, the effect of an increase in HL thickness caused by a weld overlay is examined to gain insights on the potential variability across plants. For this purpose, the HL thickness of 6.35 cm (2.5 in.) in the base case is increased by 50 percent, to 9.5 cm (3.74 in.). This sensitivity analysis showed a reduction of 2 minutes in the time margin, and it is, therefore, categorized as low impact.

#### *7.3.1.3 Secondary Side Not Depressurized*

In this sensitivity study, it is assumed that the secondary side will not be depressurized, either as a result of preexisting leakage or because of intentional opening or stick-open failure of one or more secondary relief valve before and after the onset of core damage. The results of sensitivity analysis show that the time margin actually increases, since HL failure time is not affected, but the tube flaw failure time is considerably delayed. This sensitivity analysis shows no adverse impact on C-SGTR probability.

#### *7.3.1.4 Early Secondary-Side Depressurization*

In this sensitivity analysis, the operator depressurizes SGs at 30 minutes by opening at least one atmospheric dump valve or PORV for each SG, thereby dropping the primary pressure below 4.82 MPa (700 psi). This actuates the accumulator discharge. The TDAFW pump will fail after the batteries are depleted. The results of this sensitivity analysis show that the time margin is increased by about 4 minutes, and, furthermore, the onset of core damage is delayed significantly. This sensitivity analysis, therefore, shows no adverse impact on C-SGTR probability.

#### *7.3.1.5 Tube Material; Comparison of Alloy 600TT and 690TT Tubes*

This sensitivity analysis compared the W SG types with 600TT and 690TT tube material. The results showed that the margin for 690TT is reduced by about 10 minutes, indicating that 690TT material with a "large" flaw will leak earlier than SG tubes with 600TT material with the same "large" flaw. However, the number of flaws and the flaw sizes for 690TT are expected to be smaller than those of 600TT. Therefore, the performance of 690TT is expected to be similar to 600TT as far as C-SGTR is concerned. However, large flaws, if detected in 690TT, could be more prone to C-SGTR than similar flaws in 600TT.

### 7.3.2 Summary of Sensitivity Analyses for Combustion Engineering Plant

The following sensitivity analyses were performed for the example CE plant. The measure of comparison used for these sensitivity analyses was based on the reevaluation of C-SGTR probability for short SBO sequences where LERF is of concern. In some cases; the C-SGTR probability was only reevaluated for one loop, rather than for the reactor unit (i.e., two loops: loop A and loop B). When the reevaluation for sensitivity analysis was limited to one loop, loop B was selected because of its higher contribution to C-SGTR. The difference between the revised C-SGTR probability and the base C-SGTR probability was used to prioritize the effect of the sensitivity results. A change of less than 25 percent is assigned as low, 25 to 50 percent as moderate, 50 to 100 percent as high, and any increases above 200 percent as significant.

#### *7.3.2.1 Stick-Open Failure of Secondary Relief Valves before SG Dryout*

In SBO scenarios, before SG dryout, the secondary-side relief valves (SG PORVs or MSSVs) could be demanded and fail to reclose. This could happen in either or both SGs. Stuck-open relief valves initially depressurize and cool the primary below the accumulator discharge setpoint. However, the primary will repressurize and the onset of core damage will be reached, although slightly delayed. A bounding analysis of this scenario was evaluated using the MELCOR package. This scenario is referred to as *stsbo-as* or *ltsbo-as* in Chapter 3. The overall C-SGTR was reevaluated for this scenario. The results show that the failure of secondary-side relief valves early during the sequence can have a significant impact on the LERF contribution due to C-SGTR. Table 7-22 below shows the results of this reevaluation.

**Table 7-22 Sensitivity Results for Early Stick-Open Failures of the Secondary Relief Valves**

| Case Runs | Loop b C-SGTR>3 $cm^2$ | Loop a C-SGTR>3 $cm^2$ | C-SGTR> 6 $cm^2$ |
|---|---|---|---|
| Short-Term SBO—Base | 0.45 | 0.227 | 0.20 |
| Short-Term SBO [Stuck-open secondary relief valve] | 0.999 | 0.997 | 0.990 |

#### *7.3.2.2 Opening of Secondary Relief Valves after SG Dryout*

The operators are guided to depressurize the SGs by opening the secondary relief valves in anticipation of using an alternate source of water to refill the SGs as a part of SAMGs. This sensitivity analysis examines the effect of an intentional opening of the secondary relief valve after the onset of core damage when the operators fail to refill the SGs. This sensitivity analysis sets the secondary-side pressure to $1.0X10^5$ Pa (1 bar or 14.5 psi) after the hot gas temperature reaches about 640 degrees C (1,184 degrees F). The effects on primary pressure or temperature are not expected to be significant. The results show that the opening of

secondary-side relief valves after SG dry out and the onset of core damage can increase the LERF contribution from C-SGTR by about 65 percent (from 0.2 to 0.33) for *stsbo-a* scenarios. Failures of one or more secondary relief valves to reclose are therefore considered to have a moderate impact on C-SGTR probability. However, the additional benefit of SAMG could outweigh this higher probability of C-SGTR. Table 7-23 below shows the results of this reevaluation.

**Table 7-23 Sensitivity Results for Opening the Secondary Relief Valves after SG Dryout**

| Case Runs | Loop b C-SGTR > 3 $cm^2$ | Loop a C-SGTR > 3 $cm^2$ | C-SGTR > 6 $cm^2$ |
|---|---|---|---|
| Short-Term SBO—Base (*stsbo-a*) | 0.450 | 0.217 | 0.20 |
| Short-Term SBO [Stuck-open secondary relief valve—after SG dryout] (*stsbo-a*) | 0.591 | 0.262 | 0.33 |

### *7.3.2.3 Critical C-SGTR Leak Area*

The critical area equivalent to a guillotine break of one tube (approximately 6 $cm^2$ (0.93 $in.^2$])) was chosen as a sufficient leakage area that can be considered to be an LER if the secondary-side relief valves are open. Some MELCOR analyses showed that this size of leakage may not be sufficient to depressurize the primary or pressurize the secondary, such that SG relief valves are demanded. These analyses, however, assumed that there is a preexisting secondary leakage area of 3.2 $cm^2$ (0.5 $in.^2$) for each SG from the starting point of the sequence. To ensure that the secondary relief valves are demanded and the primary can be depressurized, a larger critical C-SGTR leak area needs to be considered. A critical C-SGTR leak area of 12 $cm^2$ (1.86 $in.^2$) instead of 6 $cm^2$ (0.93 $in.^2$) reduces the probability of C-SGTR from 0.2 to 0.06. The effect is, therefore, considered to be high for reducing C-SGTR probability. Figure 7-29 shows the results for the *stsbo-a* sequence. Similar graphs can be generated for any size of critical leak area, and they generally follow the trend shown in Figure 7-29.

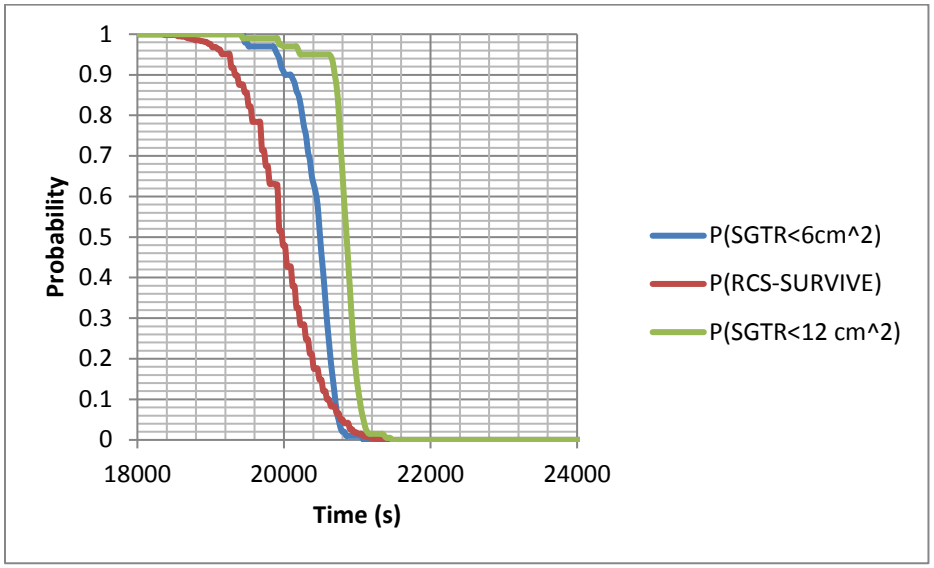


**Figure 7-29 The sensitivity results for (*stsbo-a*) for C-SGTR leak areas of 12 $cm^2$ and 6 $cm^2$**

## 7.4 Case Studies for Pressure-Induced C-SGTR Scenarios

Section 2.1 summarized the sequences of interest for DBA events that could establish a delta pressure across the SG tube walls, and therefore, potentially challenge the integrity of the tubes because of pressure-induced failures. A limited effort was devoted to evaluating the bounding contribution of C-SGTR to CDF and LERF as a result of these sequences.

These evaluations considered two bounding scenarios represented by stylized TH inputs for the C-SGTR software. This eliminated the need for performing specific MELCOR or RELAP runs for these case studies. Furthermore, these bounding analyses apply to both W and CE plants.

The section below summarizes the two TH scenarios and the corresponding accident conditions, including the bounding estimates in terms of the increase in CDF and LERF. Appendices C and F contain additional supporting analyses.

### 7.4.1 C-SGTR during Anticipated Transients without Scram

This bounding scenario selected for evaluation the loss of a main feedwater anticipated transients without scram (ATWS) event. The termination of feedwater flow to the SGs results in a large imbalance in the heat source/sink relationship. This heat buildup in the primary system also raises the RCS temperature and pressure. In general, the availability of main feedwater for ATWS events results in a less severe power mismatch between the heat source and the heat sink; therefore, the peak pressure attained in the primary system will not be as severe as the case with loss of feedwater.

The ATWS event considered here is for the case when the moderator temperature coefficient (MTC) is considered favorable. UET (unfavorable exposure time) is defined as the time during the cycle when the reactivity feedback is not sufficient to prevent RCS pressure from exceeding 22.1 MPa (3,200 psig). Many factors, such as initial power level, time in cycle when transient occurs, reactivity feedback as a function of the cycle life, number of available primary relief or safety valves, failure or success of control rod insertion, and AFW flow rates affect UET. The primary pressure during favorable MTC is below about 22.1 Mpa (3,200 psi). For bounding evaluation, a primary pressure of about 22.1 Mpa (3,200 psi) is used for cases when the MTC is favorable. For unfavorable MTC when the pressure exceeds about 22.1 Mpa (3,200 psi), rupture of one or more components in the primary system and the occurrence of core damage are assumed. C-SGTR is not considered for LERF analysis, since most releases will be into the containment through failed primary components.

If the failure of the reactor protection system (RPS) is not caused by the failure to insert sufficient rods (i.e., mechanical rod failures), manual actions to trip the reactor and the backup to the reactor trip system provided by the ATWS Mitigation System Actuation Circuitry can be credited to eventually scram the reactors. However, such actions are not fast enough to prevent the formation of an early primary pressure peak, which can induce a C-SGTR. If C-SGTR occurs and the reactor scram is subsequently successful, the event would behave like that of SGTR with the failure of the main feedwater (MFW) system. However, if C-SGTR occurs in ATWS scenarios because of the mechanical failure of the rods, or in the unlikely event that the backup manual scram actions are not successful, the accident progression may differ from the traditional SGTR scenario. In most PRAs, such scenarios are considered as eventual core damage because of the following issues:

- A C-SGTR following an ATWS could result in an uncontrolled cooldown of the primary system unless the faulted SGs are isolated. Such cooldown and its reactivity feedback could render emergency boration (EB) ineffective.

- A C-SGTR following an ATWS could reduce the boron concentration in the primary system through primary-to-secondary leakage.

The effect of C-SGTR on the reactivity feedback and the effectiveness of EB would depend on the size of the primary-to-secondary leakage. This study considers the leakages greater than an equivalent guillotine break of one tube to be of a sufficient size to influence the effectiveness of EB.

ATWS scenarios will expose all SGs to a higher pressure; therefore, C-SGTR can occur at any of the SGs. Appendix F used the probability that a flaw belongs to a flaw bin and multiplied that by the probability that the flawed tube fails under induced pressure to arrive at the probability of C-SGTR during ATWS. The analysis in Appendix F conservatively concludes that a single failed tube should have a flaw length of about 3 cm (1.2 in.) or more to be a consequential source of SGTR leakage for ATWS conditions. When considering the number of flawed tubes, this translated to a C-SGTR probability of 0.01 for the example W plant with four SGs, and $8.0X10^{-3}$ for the example CE plant with two SGs, for the 15th cycle of operation.

Simplified PRA calculations used a PWR SPAR model (Shearon Harris plant) for the two ATWS scenarios of concern, discussed below.

#### *7.4.1.1 ATWS with Successful Manual Scram but Occurrence of C-SGTR*

For all ATWS scenarios, where the failure of RPS is not caused by the inability to insert a sufficient number of rods and subsequent manual/backup scram through the ATWS Mitigation System Actuation Circuitry are successful, the C-SGTR accident progression will proceed as if the SGTR were the initiator. The probability of ATWS because of electrical RPS failure is generally set at about $1.5X10^{-5}$ per demand, assuming that there is about 1 transient per year demanding the RPS. Table 7-24 lists the main contributors.

**Table 7-24 Contributors to Electrical RPS Failures that Do Not Impact Manual Scram**

| Basic Event Name | Failure Probability | Description |
|---|---|---|
| RPS-UVL-CF-UVDAB | 1.040E-5 | CCF UV DRIVERS TRAINS A AND B (2 OF 2) |
| RPS-TXX-CF-6OF8 | 2.700E-6 | CCF 6 BISTABLES IN 3 OF 4 CHANNELS |
| RPS-CCX-CF-6OF8 | 1.830E-6 | CCF 6 ANALOG PROCESS LOGIC MODULES IN 3 OF 4 CHANNELS |
| RPS-BME-CF-RTBAB | 1.610E-6 | CCF OF RTB-A AND RTB-B (MECHANICAL) |

The probability of electrical ATWS and C-SGTR is about $1.5X10^{-7}$ per year. This scenario has a frequency that is about 4 orders of magnitude smaller than the frequency of the SGTR initiator, which is about $2.0X10^{-3}$ per year. The C-SGTR initiator and these scenarios will progress similarly if the manual scram is successful.

#### *7.4.1.2 Nonrecoverable ATWS Followed by C-SGTR*

The probability of ATWS because of mechanical failures to insert a sufficient number of rods is estimated to be about $1.2X10^{-6}$, if one transient per year is assumed. The main contributor for this event as reported by SPAR model is specified below.

| Basic Event Name | Failure Probability | Description |
|---|---|---|
| RPS-ROD-CF-RCCAS | 1.2E-6 | CCF 10 OR MORE RCCAS FAIL TO DROP |

The probability of mechanical ATWS and C-SGTR is about $1.2X10^{-8}$ per year.

### 7.4.2 C-SGTR during Steamline Break Scenarios

Several sequences identified earlier in Table 2-1 can be bounded by an unisolable main steamline break (MSLB). These sequences could also include spurious opening of one or more SG relief valves in addition to MSLVs. The TH behavior of these scenarios can be bounded by high primary pressure at about 15.5 MPa (2,250 psi) and a low atmospheric secondary pressure. The resulting delta pressure across the SG tubes is expected to be between 10.34 and 11.72 MPa (1,500 and 1,700 psi), since the secondary leakages tend to cool and depressurize the RCS. The use of 15.51 MPa (2,250 psi), therefore, is considered to be conservative and bounding. The primary temperature is generally expected to be subcooled. A temperature of 300 degrees C (572 degrees F) is used, since the saturated primary temperature at 15.5 MPa (2,250 psi) is about 345 degrees C (653 degrees F). Atmospheric pressure is also considered for the secondary-side pressure at the faulted SG. The scenario considered that the MSIV on all unaffected SGs will close, thereby blowing the steam out of only one SG and eliminating the potential for pressurized thermal shock sequences because of excessive overcooling. This was considered as the bounding TH behavior for these sequences when evaluating the potential pressure-induced C-SGTR. In such a scenario, tubes in all SGs will be initially exposed to high delta pressure with a potential for C-SGTR. However, after the MSIV closure, only one faulted SG would remain unisolated. The C-SGTR probability of the faulted SG is used for the PRA evaluation, since the CDF and LERF contributions result mainly from the unisolated SG.

Appendix F used the probability that a flaw belongs to a flaw bin and multiplied that by the probability that the flawed tube fails because of induced delta pressure caused by a steamline break (SLB) to arrive at the probability of C-SGTR. The analysis in Appendix F conservatively concludes that a single failed tube should have a flaw length of about 3 cm (1.2 in.) or more to cause enough leakage for it to be consequential under SLB conditions. When considering the number of flawed tubes, this translated to a C-SGTR probability of about $2.5X10^{-3}$ for the example W plant and a probability of about $4.0X10^{-3}$ for the example CE plant for the 15th cycle of the operation.

The initiating event (IE) frequency for the different types of SLB accidents could vary amongst the plants. The information provided in NUREG-1570, “Risk Assessment of Severe Accident-Induced Steam Generator Tube Rupture,” issued March 1998 (Ref. 6), is mainly used for establishing the IE frequency for bounding analysis. NUREG/CR-6928, “Industry-Average Performance for Components and Initiating Events at U.S. Commercial Nuclear Power Plants,” issued February 2007 (Ref. 7), was used when more recent updates were reported. The following summarizes the impact on accident progression for each of these initiating events, when a C-SGTR occurs.

### *7.4.2.1 SLB Inside Containment*

SLB inside containment (SLBIC) has an approximate IE frequency of $1.0X10^{-3}$ per reactor year as reported in NUREG-1570. If this initiating event induces a C-SGTR, all releases will remain inside the containment; therefore, they will not contribute to LERF caused by containment bypass. However, they will contribute to CDF. It is also assumed that the MSIV on all unaffected SGs will close, thereby eliminating the potential for pressurized thermal shock sequences because of excessive overcooling.

When SLBIC is followed by C-SGTR, the PRA models should be integrated by transferring the SLBIC event tree branch that includes C-SGTR, to the SGTR event tree discussed in Chapter 2 and shown in Figure 2-1. However, some of the C-SGTR branches will be affected through this transfer, as summarized below:

- It would be more difficult to diagnose the SGTR at the faulted SG because the operator should mainly rely on high secondary-side activity (high-radiation alarm), rather than on a high uncontrollable level in the affected SG. The operator may terminate the high pressure injection in response to SLBIC, if he/she is not able to diagnose C-SGTR in the early stages. However, the operator could reestablish the high head injection after a short period due to a low pressurizer level. The failure rate for high head injection should be increased to account for the potential of operator failure to diagnose the occurrence of C-SGTR in time.

- It will not be possible to isolate the faulted SG because of SLBIC, although the feedwater to the faulted SG will be isolated. The conditional core damage probability for C-SGTR should be reevaluated without any credit for isolation.

The release of radioactivity because of a potential core damage scenario involving SLBIC and induced C-SGTR is mainly to the containment; therefore, it is not considered to be a LERF contributor. The SLBIC IE is also an order of magnitude lower than an SLB outside containment (SLBOC) IE. The SLBIC scenarios are not considered any further, since they are not expected to contribute to LERF.

### *7.4.2.2 Spurious Opening of SG-PORVs or Stuck-Open MSSVs (SGR)*

This IE includes the spurious opening of an SG-PORV during a fire event or other events, and the potential for one or more MSSVs to stick open after a demand. The spurious opening of an SG PORV could be mitigated by isolating the path, whereas the spurious opening of MSSVs cannot be recovered. The frequency of the IE for spurious openings (and subsequently to stick/remain open) of one or more SG relief valves is taken to be $3.0X10^{-3}$ per reactor year from NUREG/CR-6928, which was an update to NUREG-1570. This value in NUREG/CR-6928 is generically applicable to safety/relief valves both for primary and secondary systems. It should be noted that the failure of one MSSV can cause a severe overcooling transient with primary depressurization if feeding to the SG is maintained (not a C-SGTR concern). The scenario of interest for C-SGTR, however, assumes that the operator will terminate feedwater to the affected SG and thereby let the SG go dry and depressurized. This scenario is only applicable to one specific SG and does not affect others. Therefore, the appropriate estimated C-SGTR probability of one SG is to be used for the PRA estimations (i.e., a C-SGTR probability of $2.5X10^{-3}$ for the example W and $4.0X10^{-3}$ for the example CE plant).

When a spurious opening of one or more SG relief valves is followed by a C-SGTR, the accident progression will be similar to SLBIC with C-SGTR. However, the latter could result in containment bypass and an LER, since the releases will be made outside the containment.

#### *7.4.2.3 SLB Outside Containment*

SLBOC has an approximate IE frequency of $1.0X10^{-2}$ per reactor year. This initiating event can expose the tubes in all SGs to a higher delta pressure, therefore, with some possibility that C-SGTR occurs. Sequences where only one MSIV fails to fully close were considered, thereby eliminating the potential for pressurized thermal shock sequences caused by excessive overcooling in this scenario. The estimated probability that one out of the four MSIVs will fail to close is about $4.0X10^{-3}$ per demand. This estimate uses the MSIV failure probability of $9.51\ X10^{-4}$ per demand from the Shearon Harris SPAR event MSS-AOV-00-SGMSIV (i.e., $4X9.51X10^{-4}$ about $4.0\ X10^{-3}$). The IE frequency of an unisolable SLBOC is, therefore, estimated at about $4.0\ X10^{-5}$ per year.

When an unisolable SLBOC is followed by C-SGTR, the impact on SGTR branches will be the same as when the SLBIC is followed by C-SGTR. The core damage that results when an unisolable SLBOC is followed by C-SGTR will also bypass containment and should be considered as an LER.

### 7.4.3 C-SGTR during High-Pressure Feed-and-Bleed Operation

Some of the U.S. PWRs have high-pressure ECCS pumps supporting feed-and-bleed operations with shutoff pressure above the primary pressure relief set points. For all initiating events that involve the loss of the MFW system followed by the failure of the AFW system, there could be a possibility of C-SGTR. For these scenarios, the secondary sides of SGs are assumed to be dry and depressurized. Small leaks of less than 3.2 $cm^2$ (0.5 $in.^2$) are sufficient to depressurize the SGs during the feed-and-bleed operation. The occurrence of C-SGTR during such events is not expected to increase the CDF because high-pressure injection (HPI) is assumed to be injecting makeup flow because of the success of the initial phase of feed and bleed operation. All core damage sequences where a feed and bleed operation is initially successful but is followed by C-SGTR are considered a containment bypass with the potential of contributing to LERF.

The Shearon Harris SPAR model was the basis for estimating the IE frequency that can put the plant in a condition where a feed-and-bleed operation is initiated. This estimate added the frequency of transients where MFW is lost i.e., IE-LOCHS, IE-LOIA, IE-LOMFW, and IE-LONSW). A bounding value of 0.2 per year was assigned to the IE frequency. This initiating event frequency must then be multiplied by the probability that the AFW system is not available. The base nominal failure probability of AFW is $2.0X10^{-5}$ per SPAR model. However, the specific value of AFW failure probability would be different for different initiators. A bounding value of $1.0X10^{-4}$ for generic AFW failure probability was used. The bounding IE frequency for this category of pressure-induced C-SGTR sequences is, therefore, estimated to be about $2.0X10^{-5}$ per reactor year. There could be an additional contribution in some plants from possible fire scenarios causing spurious ECCS actuations. The LERF contribution from these scenarios is not expected to be significant.

All SGs will be exposed to an environment conducive to C-SGTR during a high-pressure feed and bleed operation. The C-SGTR probability is, therefore, bounded by 0.01 for the example W plant and $8.0X10^{-3}$ for the example CE plant at the 15th cycle of operation.

### 7.4.4 LERF and Core Damage Contribution of Pressure-Induced C-SGTR

The contribution of pressure-induced C-SGTR to CDF and LERF is estimated by the following equations:

$$P(CDF) = f(IE) * P(CSGTR|IE) * P(CD|IE, CSGTR) \quad (7.4)$$

$$P(LERF) = f(IE) * P(CSGTR|IE) * P(CD|IE, CSGTR) * P(LERF|IE, CSGTR, CD) \quad (7.5)$$

The estimates for f (IE), P (C-SGTR|IE), and P (LERF|IE, C-SGTR, CD) were discussed for each sequence separately (see Appendix C). P (CD|IE, C-SGTR) is estimated using the SPAR model for the Shearon Harris PRA. This conditional probability is estimated by modifying the probability of the appropriate event tree branches to reflect the impact of the sequence. As an example, for ATWS scenarios, the branch heading associated with EB is set to true.

For SLB sequences, two other branches should be modified. The HPI branch should reflect that there is a possibility for the operator to terminate the HPI in response to SLB, not knowing that C-SGTR has occurred. Operators should also fail to recognize the need to reestablish HPI flow even after pressurizer low level is indicated. The event tree branch for isolating the faulted SG should also be set to true.

The probability that the operator fails to diagnose the occurrence of C-SGTR after an SLB scenario was estimated, using the SPAR-H worksheet, to be around $2.5X10^{-2}$. Four adjustments were made to the nominal values of the SPAR-H worksheet for diagnosis:

(1) Available time: The radiation alarms in the secondary side and the low pressurizer level indication will alert the operator of the possibility of C-SGTR at least an hour before the onset of core damage. Extra time is, therefore, assigned with a performance-shaping factor of 0.1.

(2) An extreme stress condition is expected to be present in SLB combined with C-SGTR scenarios, since such events are uncommon and the changes in plant parameters will be rapid. A performance-shaping factor of 5 is assigned.

(3) Procedures are available for SLB and SLB with C-SGTR. However, the transition between the two procedures and the required monitoring would be difficult. A performance-shaping factor of 5 is assigned.

(4) All other PSF values were considered to be nominal.

The conditional core damage probability for high-pressure feed-and-bleed scenarios were estimated by using the MFW event tree and setting the failure of both the initiator and the failure of AFW to true.

The conditional core damage probabilities were then estimated using the SPAR model for Shearon Harris PRA and the proposed changes. Tables 7-25 and 7-26 summarize the results of these analyses for the example W and CE plants, respectively.

Table 7-17 Changes in Core Damage Frequency and LERF as a Result of Pressure Induced C-SGTR for the Example W Plant

| IE | f(IE) per year | P(CSGTR\|IE) | P(CD\|IE,CSGTR) | P(LERF\|IE,CSGTR,CD) | Δ-CDF per year | Δ-LERF per year |
|---|---|---|---|---|---|---|
| ATWS-Electrical | 1.5E-5 | 0.01 | 1.6E-4 | 1 | <1.0E-9 | <1.0E-9 |
| ATWS-Failure of Rods | 1.2E-6 | 0.01 | 1 | 1 | 1.2E-8 | 1.2E-8 |
| SLBIC | 1.0E-3 | 2.50E-3 | 3.2E-2 | 0 | 8.0E-8 | 0 |
| Spurious Opening of SG Relief Valves | 3.0E-3 | 2.50E-3 | 3.2E-2 | 1 | 2.4E-7 | 2.4E-7 |
| SLBOC | 4.0E-5 | 2.50E-3 | 3.2E-2 | 1 | 3.2E-9 | 3.2E-9 |
| High-Pressure Feed-and-Bleed Scenarios | 2.0E-5 | 0.01 | 2.5E-2 | 1 | 5.0E-9 | 5.0E-9 |
| All IEs—Total Contribution | | | | | 3.4E-7 | 2.6E-7 |

These bounding values are deemed to be acceptable. Maintaining a low probability for a large flaw to develop during operation via an adequate periodic surveillance program will help to control this risk contributor. For example, for a PWR with a total CDF of $2X10^{-5}$ per year and LERF of $1.0X10^{-6}$, the additional CDF and LERF of $5.3X10^{-7}$ and $4.0X10^{-7}$ would add less than 3 percent to CDF and 40 percent to LERF. The LERF contribution is expected to be an order of magnitude lower if SAMGs are considered as a part of the PRA analysis. The results indicate that the CDF and LERF contribution of pressure-induced C-SGTR cannot be considered negligible, although they are within the acceptable ranges, based on these bounding estimations for a generic U.S. PWR.

Table 7-18 Changes in Core Damage Frequency and LERF as a Result of Pressure Induced C-SGTR for the Example CE Plant

| IE | f(IE) per year | P(CSGTR\|IE) | P(CD\|IE,CSGTR) | P(LERF\|IE,CSGTR,CD) | Δ-CDF per year | Δ-LERF per year |
|---|---|---|---|---|---|---|
| ATWS-Electrical | 1.5E-5 | 8.0E-3 | 1.6E-4 | 1 | <1.0E-9 | <1.0E-9 |
| ATWS-Failure of Rods | 1.2E-6 | 8.0E-3 | 1 | 1 | 9.6E-9 | 9.6E-9 |
| SLBIC | 1.0E-3 | 4.0E-3 | 3.2E-2 | 0 | 1.3E-7 | 0 |
| Spurious Opening of SG Relief Valves | 3.0E-3 | 4.0E-3 | 3.2E-2 | 1 | 3.8E-7 | 3.8E-7 |
| SLBOC | 4.0E-5 | 4.0E-3 | 3.2E-2 | 1 | 5.1E-9 | 5.1E-9 |
| High-Pressure Feed-and-Bleed Scenarios | 2.0E-5 | 8.0E-3 | 2.5E-2 | 1 | 4.0E-9 | 4.0E-9 |
| All IEs—Total Contribution | | | | | 5.3E-7 | 4.0E-7 |

## 7.5 References


1. U.S. Nuclear Regulatory Commission, “SCDAP/RELAP5 Thermal-Hydraulic Evaluations of the Potential for Containment Bypass During Extended Station Blackout Severe Accident Sequences in a Westinghouse Four-Loop PWR,” NUREG/CR-6995, March 2010, Agencywide Documents Access and Management System (ADAMS) Accession No. ML101130544.

2. U.S. Nuclear Regulatory Commission, “State-of-the-Art Reactor Consequence Analyses (SOARCA), Final Report,” NUREG-1935, November 2012, ADAMS Accession No. ML12332A057.

3. U.S. Nuclear Regulatory Commission, “Review and Evaluation of the Zion Probabilistic Safety Study: Plant Analysis,” NUREG/CR-3300, May 1984, ADAMS Accession No. ML091540533.

4. U.S. Nuclear Regulatory Commission, “Analysis of Core Damage Frequency: Internal Events Methodology,” Vol. 1, Rev. 1, NUREG/CR-4550, SAND86-2084, January 1990.

5. U.S. Nuclear Regulatory Commission, “Evaluation of Severe Accident Risks: Methodology for the Containment, Source Term, Consequence, and Risk Integrations Analyses,” NUREG/CR-4551, December 1993, ADAMS Accession No. ML072710062.

6. U.S. Nuclear Regulatory Commission, “Risk Assessment of Severe Accident-Induced Steam Generator Tube Rupture,” NUREG-1570, March 1998, ADAMS Accession Number ML070570094.

7. U.S. Nuclear Regulatory Commission, “Industry-Average Performance for Components and Initiating Events at U.S. Commercial Nuclear Power Plants,” NUREG/CR-6928, February 2007, ADAMS Accession No. ML070650650.

8. Lutz, Robert and Melissa Lucci, “Modeling Post-Core Damage Operator Actions in the PRA,” ANS PSA 2008 Topical Meeting, Knoxville, TN, September 7–11, 2008.

# 8 PROBABILISTIC RISK ASSESSMENT CONCLUSIONS AND RECOMMENDATIONS

The conclusions in this chapter are based on the probabilistic risk assessment (PRA) analysis in Chapter 7. Chapter 9 summarizes the insights from additional analyses for fission product release, discussed in Chapter 3, for the failure of other reactor coolant system (RCS) components, discussed in Chapter 4.

This report documents a method for a quantitative risk assessment of consequential steam generator (SG) tube rupture (C-SGTR) during a severe accident, after the onset of core damage, and during a design-basis-accident event, before the onset of core damage. The method is illustrated with applications to two plants containing replacement SGs with thermally treated Inconel Alloy 600 and 690 tubes. Appendix L summarized additional examples of C-SGTR risk assessment, using an existing internal-event PRA model.

The focus of this study is on estimating the probability of large early release (LER) because of C-SGTR and containment bypass. It applies the simplified methods to two selected pressurized-water reactor (PWR) plants: a Westinghouse (W) and a Combustion Engineering (CE) design. In addition, the generic stylized models addressed C-SGTR related to pressure-induced C-SGTRs, as discussed in Section 7.4.3 and Appendix C. Section 8.1 provided the insights and observations obtained for these applications.

The study used the latest available thermal hydraulics (TH) for both plants, updated flaw statistics pertinent to current reactors, and the latest available models and software for estimating the failure probability and timings of other SG tubes, as well as RCS components (i.e., hot leg (HL) and surge line).

The scope of this study is limited to estimating the probability of containment bypass because of C-SGTR and to a bounding assessment of the fraction of containment bypass that constitutes LER frequency (LERF). The scope does not include the development of a Level 1 PRA, although the study used full Level 1 PRAs for internal and external events to obtain the frequency of the sequences related to the C-SGTR.

This study used the existing results from other related research as input. It made no attempt to conduct additional research or develop new models. The study is, therefore, limited by the available supporting analyses and models. These are referred to as limitations of supporting analyses for PRA models, as discussed in Section 8.2.

## 8.1 Insights and Observations

This study concluded that the overall contribution of C-SGTR scenarios to containment bypass is about a factor of 10 larger for the selected CE plant than for the W plant. This conclusion is valid because, although the station blackout (SBO) contributions to core damage frequency (CDF) are comparable between the two plants, conditional C-SGTR is an order of magnitude higher. It further demonstrated that the contribution of C-SGTR to containment bypass is negligible for the selected W plant. The study also considered that the size of C-SGTR leaks that contribute to LERF is equivalent to the area of at least the guillotine breaks of one tube. Moreover, the study concluded that the cleared loop seal, which causes the failure of multiple tubes, could be a contributor to C-SGTR for the selected W plant. For the CE plant, multiple

tube failures could occur even if the loop seal is not cleared; therefore, loop seal clearing will not have significant impact on C-SGTR probability.

This study generally found that the flaw sizes that do not meet the integrity performance criteria (e.g., safety factor of 3)[10] have a low probability of survival during the severe accident scenarios discussed in this report. Table 7-7 showed that the C-SGTR probability for the W plant for large flaws with a through-wall depth greater than 0.7 is about 80 percent. Similar tables for the CE plant (not included in the report) show a probability close to 1.0.

The estimated frequency of containment bypass was further adjusted to estimate the fraction of all containment bypass scenarios that can contribute to LERF. This was done by examining the timing of the accident progression for each type of accident scenario to determine if the effective evacuation can be credited. The LERF did not include those containment bypass scenarios where the releases were expected to occur after an effective evacuation (i.e., late releases). The report also identified and discussed the severe accident management guideline (SAMG) activities that could mitigate core damage or reduce the release magnitude, although they were not credited in further reducing the LERF.

Table 8-1 summarized the high-level quantitative conclusions of the study for both containment bypass and LERF. The paragraphs below, based on Sections 7.1.8 and 7.2.6, further discuss these results.

Note that the estimates for the frequency of the containment bypass because of C-SGTR and LERF, as shown in Tables 8-1a and 8-1b, are for all-hazards CDF sequences, which include both the internal events and all external event CDF sequences leading to C-SGTR. Although the all-hazards sequence CDF estimates might not be as robust as those for internal events, consideration of all-hazards CDF as a measure for comparisons could provide further insights for the following reasons:

- Accident sequences for hazard categories other than internal events may have a higher contribution to multiunit SBOs on sites with multiple units.

- The evacuation times for accident sequences for other hazard categories could be considerably longer than those for internal events.

- Some important recovery actions credited in internal-event sequences may not be feasible or may be seriously delayed for other hazard categories.

Section 7.1 discussed and quantified the LERF scenarios for the example W plant. The study estimated the conditional C-SGTR (i.e., containment bypass) probability for SBOs with early or late failures of turbine-driven auxiliary feedwater (TDAFW) pumps at approximately 0.02, excluding the scenarios involving the clearing of the loop seals. This conditional containment bypass probability, when multiplied by the CDF of SBO with an early or late failure of TDAFW pumps, results in a frequency of $1.5\times10^{-07}$ per reactor year for both SBO scenarios. Table 8-1 shows the more precise estimates of the containment bypass frequency. These estimates include the contributions of the scenarios in which the loop seals have been cleared. Table 8-1 shows that the containment bypass frequency estimates are $2.3X10^{-7}$ for Inconel 600 and $1.6 X10^{-7}$for Inconel 690, considering the internal-event initiators.

[10] See the letter transmitting TSTF-449, Revision 4, "Steam Generator Tube Integrity," dated April 14, 2005 (Agencywide Documents Access and Management System Accession No. ML051090200).

Table 8-1 Summary of the Frequency Estimates for Containment Bypass and LERF

| SG Type | Tube Material | #of SGs | EFPY | Hazard Cate-gory | SBO CDF Frequency (per RY) | Cont.-Bypass Frequency per Year | LERF Fraction (%) | LERF (per RY) |
|---|---|---|---|---|---|---|---|---|
| CE | 690 | 2 | 15 | All [a] | 3.3E-5 | [b] 1.0E-5 | [b] 5.6% | [b] 5.7E-7 |
| CE | 690 | 2 | 15 | Internal | 1.9E-7 | 5.7E-8 | 9.5% | 5.4E-9 |
| W | 600 | 4 | 15 | All | 2.0E-5 | [c] 8.8E-7 | 3.7% | 3.2E-8 |
| W | 600 | 4 | 15 | Internal | 5.2E-6 | 2.3E-7 | 3.6% | 8.4E-9 |
| W | 690 | 4 | 15 | All | 2.0E-5 | 6.3E-7 | 3.5% | 2.2E-8 |
| W | 690 | 4 | 15 | Internal | 5.2E-6 | 1.6E-7 | 3.5% | 5.8E-9 |

[a] "All" refers to the contribution of CDF from internal events, internal flood, fire, and seismic PRA.
[b] From Table 7.2-2, the CDF for short-term SBO (*stsbo*) and long-term SBO (*ltsbo*) from all-hazards models are ~2.6E-6/RY and 3.1E-5/RY, respectively. The total containment bypass (Cont.-Bypass) probability is estimated by [(2.6E-6*.22+3.1E-5*.31) = [5.72E-7+9.61E-5] =1.02E-5. The LERF contribution is from the *stsbo*. It is estimated at 5.7E-7 or about 5.6%.
[c] Per the discussion in Section 7.1.5, the probability of C-SGTR is about 1.3E-2 for *stsbo* with Inconel 600 materials and 8.9E-3 for Inconel 690. The probability of C-SGTR caused by a cleared loop seal due to reactor coolant pump seal failures was also estimated at 2.5E-03. The overall probability of C-SGTR is estimated to be about 1.6E-2 and 1.1E-2 for *stsbo* and for Inconel 600 and 690, and 2.85E-2 and 2.0E-2 for *ltsbo* and for Inconel 600 and 690.

Table 8-2 summarizes the conditional probability of C-SGTR calculated for the base cases studied.

Table 8-2 Summary Table for Conditional Probability of C-SGTR Studied as Base Cases

| | Conditional Probability of C-SGTR | | |
|---|---|---|---|
| SG Type | SBO with TDAFW Pump Failure at Time = 0 | SBO with AFW Failure at Battery Depletion | Inconel Material |
| CE | 2.2E-1 | 3.1E-01 | 690 |
| W | 1.3E-2 | (*) | 600 |
| W | 8.9E-3 | (*) | 690 |

* This sequence is not studied as a base case.

Section 7.1 discussed and quantified the LERF scenarios for the example W plant and made the following observations:

- For the W plant, the contribution of C-SGTR to containment bypass could be as high as $9\times10^{-07}$ per year, considering all hazard categories. If only internal events are considered, this value would be $2\times10^{-07}$ per year or lower.

- Based on the existing PRAs, C-SGTR does not appear to be a major contributor to LERF for the example W plant.

- The containment bypass contribution is mainly from the scenarios where the TDAFW pump initially worked but was later rendered inoperable after the depletion of batteries. Such scenarios are not generally considered as contributors to LERF.

- It is generally concluded that, for the selected W plant, the C-SGTR and the associated LERF do not make any significant contribution, unless large and deep flaws exist in one or more SGs.

This study focused on a four-loop W plant and used the design parameters and measurement of original W Model 51 SGs. Many of the current operating W plants are equipped with replacement SGs with different design features and measurements. The conclusions and results noted above, therefore, should be tempered with the specific design of SGs.

Section 7.2 discussed and quantified the LERF scenarios for the example CE plant. The conditional containment bypass probabilities from C-SGTR for SBOs with early or late failures of TDAFW pumps were about 0.22 and 0.31, respectively. These conditional probabilities of containment bypass, when multiplied by the frequency of the entry conditions (i.e., SBO with early or late failure of TDAFW pumps (Table 7-14)), resulted in a frequency of approximately $1.1\times10^{-05}$ per reactor year for both SBO scenarios (i.e., $9.5\times10^{-06}$ for SBO scenarios with failures of TDAFW pumps after battery depletion and $5.7\times10^{-07}$ for SBO scenarios with early failure of TDAFW pumps). The LERF contribution is from those scenarios where early failures of TDAFW pumps occurred.

The study made the following observations for the CE plant:

- For the selected CE plant, the contribution of C-SGTR to containment bypass could be as high as $1.0\times10^{-05}$, considering contributions from all hazard categories. If only internal events are considered, this contribution is expected to be about $5.65\times10^{-08}$.

- Based on the existing PRAs, C-SGTR appears to be the highest contributor to LERF for all hazard models.

- The containment bypass contribution mainly results from the scenarios where the TDAFW pumps initially worked but were later rendered inoperable after the depletion of batteries. Such scenarios are not generally considered as contributors to LERF.

- Extending the battery life and operation of TDAFW pumps can reduce the frequency of containment bypass. This also facilitates the SAMG operation and use of additional equipment, such as the existing extensive damage mitigation guidelines or the future equipment supplied in response to the FLEX program.

## 8.2 Limitation of Supporting Analyses for PRA Models

This PRA study relied on the following existing models and analyses:

- representing variations in tube temperatures by average hot tube and the hottest tube
- TH evaluation of accident sequences
- severe accident analysis
- creep-rupture and fracture-mechanic models for failure of flawed and pristine tubes
- leak-area models for failed tubes
- creep-rupture models and data for HL and surge line
- surveillance data from SG periodic inspections
- material properties at high temperature

The sections below summarize the status of each of the above elements and their limitations.

### 8.2.1 Variations in Tube Temperatures by Average Hot Tube and the Hottest Tube

The tube temperature varies across the tubes and within a tube (along the tube length). This temperature profile is varying in a continuous manner. It may be represented with a set of temperature bins to capture temperature variations among the tubes and within a tube. The larger the number of bins or the higher the bin resolutions, the more calculations and increased code capabilities are required. This study currently uses two temperature bins, reflecting the average hot tube temperature and the hottest tube temperature. Small uncertainties (approximately 0.3 percent) are built into the code to capture slight temperature variations within a bin.

### 8.2.2 TH Evaluation of Accident Sequences

TH analyses used RELAP code for W plants and MELCOR for CE plants. Consistent use of either MELCOR or RELAP for both CE and W plants will provide a better basis for comparing the results and will help to better characterize the uncertainties.

### 8.2.3 Severe-Accident Analysis

A limited number of MELCOR analyses of severe accidents were available for CE plants to address such Level 2 PRA issues as the magnitude of releases. These are in addition to and independent of the simple LERF model used in the PRA analysis. Additional MELCOR runs informed by PRA assumptions will be needed to develop the Level 2 PRA for C-SGTR for both CE and W plants.

### 8.2.4 Creep-Rupture and Fracture-Mechanic Models

The creep-rupture and pressure-induced fracture-mechanic models for tube failures are only available for tubes with a crack flaw. Wear flaws are the dominant flaw mechanisms for replaced SGs. The models for crack flaws do not necessarily apply to wear flaws. This study used a tube thinning model to approximate the failure probability of a tube with a wear flaw. Fracture mechanics and creep-rupture models for wear flaws, when available, can improve the results of this study. For the pristine tubes, fracture-mechanic models are available to predict the tube failures but not the resulting leak rates. The study estimated the tube leak rates for wear flaws using the equations for the crack flaws with the equivalent flaw sizes.

### 8.2.5 Leak-Area Models for Failed Tubes

The models to predict the resulting leak area from a failed tube are available for a tube with a crack flaw. Leak models, however, are not available for failed pristine tubes. The leak areas estimated for crack flaws from these models have relatively large uncertainties. The models used to predict failures from wear flaws have not yet been studied at the same level as the failure models for the cracked flaws. This could result in additional uncertainties. Enhanced models to estimate leak areas for a wear flaw can reduce the uncertainties associated with the quantitative results.

### 8.2.6 Creep-Rupture Models and Data for HL and Surge Line

The study used Electric Power Research Institute (EPRI) models to predict the failures of HLs and surge lines caused by creep rupture in the PRA analysis. Failures were assumed to be catastrophic, resulting in a very large leak area. This study neither performed, nor found any reference to confirm the EPRI correlations. However, the more detailed analyses performed for HL failures, as discussed in Chapter 4, showed consistent results.

### 8.2.7 Surveillance Data from SG Periodic Inspection

This study used the most recent data from periodic surveillance inspections to better represent the flaw generation rate and characteristics. However, the number of plants with available data was quite limited, and the data on flaw size may not be representative. Updating flaw characteristics on a periodic basis will not only help the PRA quantification process but will also help the U.S. Nuclear Regulatory Commission's oversight program on SGs.

### 8.2.8 Material Properties at High Temperature

The primary circuits, including the SG tubes, are expected to be exposed to high temperatures because of severe accidents (after core damage). The study obtained the material properties of interest from various sources. Additional work for the same materials for nuclear application could improve the prediction of fracture-mechanic models.

# 9 OVERALL SUMMARY

The work documented in this report, performed over multiple years by different disciplines, has evolved into its current scope and form during those years because of technical and project-related constraints. The main thrust of the report is on estimating the potential consequential steam generator tube rupture (C-SGTR) risk in different types of steam generators (SGs), using quantitative probabilistic risk assessment (PRA) methods. In parallel with this PRA work, the report includes two other types of analyses: thermal-hydraulic (TH) analyses and structural analyses. Thus, these three types of independent analyses make up the report's contents.

The objective of this chapter is to summarize the nature and conclusions of the three types of analyses mentioned above. The following chapters contain these:

- Chapter 7 and 8 for PRA
- Chapter 3 for TH using MELCOR for a Combustion Engineering (CE) plant
- Chapter 4 for structural analyses of other reactor coolant system (RCS) components

The conclusions of these three analyses appear at the end of this section, following a discussion of some of the modeling aspects.

Chapter 2 defines three basic modeling pieces to define and focus the scope of PRA work:

- accident sequences to be modeled
- "critical tube-leak size" for PRA purposes
- a large early release frequency (LERF) model for PRA purposes

In Chapter 3, MELCOR software is used to model key accident sequences for a CE plant. This work, carried out specifically for this project, can be viewed in terms of two parts:

(4) generation of accident sequence TH parameters (e.g., pressure and temperature as a function of time)

(5) estimation of fission product (FP) release characteristics for these sequences

The results of the first part serve as input into the PRA model, which Chapter 7 documents. Additionally, MELCOR is used for calculating FP release characteristics. This information is not used in PRA models for the following reasons:

- the PRA model uses a more advanced flawed tube model, whereas MELCOR modeled tube flaws using stress multiplication factors

- definition of what constitutes a C-SGTR (critical size, failure of other RCS components)

- definition of a LERF model in PRA as a surrogate to model FP release

The PRA analysis takes the accident sequence TH parameters for the example Westinghouse (W) plant from NUREG/CR-6995 (Ref. 1), "SCDAP/RELAP5 Thermal-Hydraulic Evaluations of the Potential for Containment Bypass During Extended Station Blackout Severe Accident Sequences in a Westinghouse Four-Loop PWR," issued March 2010, which used

SCDAP/RELAP5 for analysis. Chapter 3 contains the accident sequence TH parameters for the example CE plant, generated by MELCOR.

Conclusions about FP release characteristics for a CE plant, as discussed in Chapter 3, versus those in Chapters 7 and 8, should be viewed in light of the independent modeling assumptions for MELCOR analyses and PRA models.

The PRA model includes credit for the failure of another RCS component before the failure of SG tubes, thus resulting in a lesser release consequence. The PRA model uses an existing hot-leg (HL)/surge-line failure model developed by the Electric Power Research Institute. Chapter 4 contains later confirmatory work in structural analysis using more state-of-the art modeling on W sequences. It should be noted that the PRA calculations did not include the confirmatory work models and their results discussed in Chapter 4.

Although the PRA models focused on the "temperature-induced" C-SGTR sequences (after occurrence of core damage) caused by creep rupture, the report models two types of tube failure correlations:

(1) a high-pressure, low-temperature (e.g., below creep-rupture range) correlation
(2) a high-temperature correlation for temperatures in the creep-rupture range

The second correlation was not deemed suitable at lower temperatures with high pressure. Section 7.4 discusses the risk estimates for potential pressure-induced C-SGTR sequences (such as anticipated transients without scram and large steamline breaks). Such sequences might contribute to additional core damage frequency, as opposed to temperature-induced C-SGTR sequences, which are initiated by already identified core damage sequences. It requires very large pressure differences across the SG tubes at lower temperatures to cause the failure of flawed tubes, and the contribution of pressure-induced sequences to plant core damage frequency is not expected to be significant, since the probability that a tube with a deep flaw (e.g., more than 70-percent deep) exists in at least one SG is quite low.

Another new analysis, in Chapter 6, is the generation of tube-flaw distributions for thermally treated Alloy 600 and 690 material used in replacement SGs of the current fleet of plants. These distributions are generated from a limited set of SG inspection reports submitted to the U.S. Nuclear Regulatory Commission. The analysis resulted in the following observations on these tube materials:

- There were mostly "wear-type" flaws (volumetric, as opposed to the circumferential and axial cracks found in the previous generation of SG tubes).

- Some cracks (i.e., crack flaws) started to appear around the 15th effective full-power year of operation in thermally treated 600 Inconel tubes.

The PRA model uses the 15-year flaw distribution as the base criterion to make estimates and comparisons. SG tubes with fewer years of operation will have more favorable estimates and vice versa.

Software referred to as the C-SGTR calculator was developed to support the work in this report. The calculator is used to estimate failure times and leak sizes of SG tubes with different types of flaws. The software also has built-in models for HL and surge-line failure because of the creep-rupture failure mechanism, and it estimates HL and surge-line failure times and

probabilities. The scope of the models currently includes new SG tube materials and the associated property data for both thermally treated Inconel 600 and 690. Appendix B briefly discusses this calculator.

## 9.1 PRA Conclusion Insights

The main PRA conclusion is that the conditional probability of creep rupture of C-SGTR in core damage scenarios with high primary pressure, dry SGs, and low secondary pressure (HDL) is about a factor of 10 larger for plants with shallow inlet SG plenum (e.g., the selected CE plant) than the plants with deep inlet SG plenum (e.g., the example W plant). The contribution of HDL scenarios to core damage and subsequently to LERF, from creep-rupture failure of SG tubes, is driven by the plant-specific design and operational features (e.g., availability of two trains of TDAFW pumps).

Previous conclusions on the effect of “loop seal clearing” are not changed; for any of the SG geometries, if loop seal clearing occurs in an accident sequence (such as the one caused by a large reactor coolant pump (RCP) seal leak), the tube failures are expected to happen early. The TH analysis reported in NUREG/CR-6995 indicated that the probability that the loop seal is cleared is almost certain if the RCP leakage is about 1,700 liters per minute (Lpm) (450 gpm). For RCP seal leakage of 1,135 Lpm (300 gpm), the TH analysis predicted no possibility that the loop seal is cleared.

## 9.2 Conclusion on Other RCS Components (from Chapter 4)

The analyses in Section 4.4 indicated that the upper half of the HL will fail much earlier than the other RCS regions. Table 4.4 summarized the failure times predicted by the various analyses considered in Section 4.4. The predicted failure times for all the cases considered are below the median failure time of 12,600 seconds estimated by the C-SGTR calculator, but not excessively so. Therefore, the C-SGTR calculator provides a reasonable estimation of HL failure.

## 9.3 MELCOR Conclusions for CE Plant

CE plants with replacement SGs receive additional scrutiny because their geometry is more susceptible to C-SGTR than the W designs. The short HL length-to-diameter ratio and relatively shallow SG inlet plena in some replacement SGs results in high-temperature gas reaching the SG tubes during closed-loop-seal natural circulation conditions. Hotter gases reaching the SG tube reduce the time before tube failure, which increases the likelihood of containment bypass. A station blackout (SBO) is the situation in which thermally induced C-SGTR is expected to occur. A few aspects of the scenario are of interest in determining FP releases to the environment: (1) whether an SG tube or some other part of the RCS pressure boundary fails first, and (2) whether tube failure results in sufficient and rapid enough RCS depressurization to prevent rupture of some other part of the RCS boundary. In the W analysis, the presence of a flaw is required for the prediction of tube failure before other RCS component failures. For a W plant, failure of a single tube does not depressurize the primary at a rate sufficient to prevent the subsequent failure of other RCS components. However, the possibility of multiple tube failures exists in CE plants, which could result in primary depressurization. Unlike the W example, the unflawed tubes exposed to the relatively unmixed hot gases that reach the SG tubes in CE designs with shallow-inlet-plenum replacement SGs can also fail multiple tubes, which can depressurize the RCS sufficiently to prevent the creep-rupture failure of other components, thus leaving the containment bypass pathway as the sole release path of FPs from the reactor.

The MELCOR analyses were performed somewhat independently from the PRA, with their own set of assumptions and conclusions. These are summarized below.

The relatively shallow inlet plenum design of the replacement SG under consideration for the CE plant has an impact on the results of the computational fluid dynamic predictions. The shallow design limits the mixing of the hot gases that enter the SG, which creates a higher thermal load on the tubes.

The study reached the following conclusions:

- Even if an SGTR occurs before HL failure, as long as no failure or intentional opening of relief valves follows, the magnitude of release through the repeated cycling of relief valves is expected to be small, as indicated by the MELCOR runs. This conclusion differs from the PRA, which conservatively assumes all releases will be significant enough to be considered as LERF (i.e., the relief valves are assumed to stick open rather than continue cycling).

- For a high-pressure secondary-side (high-dry-high situation) scenario, an HL will fail before an unflawed tube fails, thus preventing multiple unflawed tube failures. This conclusion is consistent with PRA calculations.

## 9.4 References

1. U.S. Nuclear Regulatory Commission, “SCDAP/RELAP5 Thermal-Hydraulic Evaluations of the Potential for Containment Bypass During Extended Station Blackout Severe Accident Sequences in a Westinghouse Four-Loop PWR,” NUREG/CR-6995, March 2010, Agencywide Documents Access and Management System (ADAMS) Accession No. ML101130544.

# APPENDIX A

# HIGH-TEMPERATURE DEFORMATION AND DAMAGE OF REACTOR COOLANT SYSTEM MATERIALS

## A.1 Material Properties Used in Chapter 4

Section A-2 gives the results of a literature search conducted for high-temperature material properties data that are needed to carry out the analyses. Table A-1 lists the various components in the Zion Nuclear Power Plant (ZNPP) that were analyzed, the materials used, and the range of temperatures for which high-temperature tensile and creep properties were initially collected. The table identifies gaps in the required database, which Argonne National Laboratory (ANL) partially filled by conducting a materials testing program during the follow-on program funded by the U.S. Nuclear Regulatory Commission (NRC) to obtain high-temperature tensile and creep properties of materials identified in Table A-1. Section A.2 contains the details of the test results. The base materials tested were as follows:

- SA 516 Grade 70 carbon steel
- SA 240 Grade 316 stainless steel
- SA 351 Grade CF8M cast stainless steel
- SA 193 B7 bolt material

In addition, the program tested the following weldments:

- stainless (SA 240 Grade 316) steel plate to carbon steel (SA 516 Grade 70) plate weldment

- wrought stainless (SA 240 Grade 316) plate to cast stainless steel (SA 351 Grade CF8M) plate weldment

- stainless (SA 240 Grade 316) steel plate to stainless (SA 240 Grade 316) steel plate weldment

Table A-2 gives the temperature range for the various tests.

**Table A-1 Range of Temperatures (°C) for which High-Temperature Material Properties Data Are/Are Not Available**

| RCS Component | Material | Tensile Properties | | Creep Properties | |
|---|---|---|---|---|---|
| | | Stress–Strain Curves | Tensile Strengths | Creep Rate | Rupture Time |
| Piping, RTD Body PORV plug | SA 240 Grade Type 316 SS | 400–982 | 400–1093 | 538–816 | 427–1093 |
| HL Elbow | SA 351 Grade CF8M | | 400–871 | 538–649 | 454–1000 |
| Surge Line to HL Nozzle | SA 182 F316 | Not found | 400–538 | Not found | 549–699 |
| Weld | 308 SS | 565 | 482–593 | 593 | 454–704 |
| RV Nozzle | A–508 Class 2 | Not found | 400–727 | 627–752 | 627–95 |
| SG and PZR Nozzles | SA 216 WCC | Not found | 400–538 | Not found | Not found |
| Manway Cover | SA 533 A1 (SA 533 B1) | Not found (649–1200) | 400–538 (400–1200) | Not found (400–1100) | Not found (400–1100) |
| Manway Insert | Type 304 SS | 700–1100 | 400–1100 | 427–1077 | 538–1077 |
| Manway Bolts | A 193 (B7) | Not found | Not found | Not found | Not found |
| PORV Cage | SA 564 (17–4PH) H1100 | Not found | 400–538 | Not found | Not found |

**Table A-2 Materials and Temperature Ranges (°C) over which Materials Properties Data Were Generated by ANL**

| Material | Tensile Properties | | Creep Properties | |
|---|---|---|---|---|
| | Stress–Strain Curves | Tensile Strengths | Creep Rate | Rupture Time |
| SA 240 Grade Type 316 SS | 700–1100 | 700–1100 | 700–1100 | 700–1100 |
| SA 351 Grade CF8M | 700–1000 | 700–1000 | 700–1000 | 700–1000 |
| SA 516 Grade 70 Carbon steel | 500–800 | 500–800 | 500–800 | 500–800 |
| SA 193 B7 Bolts | 450–650 | 450–650 | 450–650 | 450–650 |
| SA 240 Grade 316 to SA 516 Grade 70 weldment | 700–1000 | 700–1000 | 700–1000 | 700–1000 |
| SA 240 Grade 316 to SA 240 Grade 316 weldment | 700–1000 | 700–1000 | | |
| SA 240 Grade 316 to SA 351 Grade CF8M weldment | | | 700–1000 | 700–1000 |

## A.2 High-Temperature Creep-Rupture Test Data

### Bolt Material (SA 193 B7)

Table A-3 lists all of the bolt creep tests, which were run in duplicate. Because our interest is in station blackout (SBO) severe accidents, which last several hours, tests that did not fail by 100 hours (h) were interrupted. Creep curves at 450, 550, and 650 degrees Celsius (C) (842, 1,022, and 1,202 degrees Fahrenheit (F)) are given in Figures A-1a to A-1c, respectively. Note that, although the tests at 450 and 550 degrees C (842 and 1,022 degrees F) experienced primary creep, those at 650 degrees C (1,202 degrees F) did not.

**Table A-3 Summary of Creep Data for SA 193 B7 Bolt Material**

| Specimen No. | Temperature °C (°F) | Stress ksi (MPa) | Rupture Time (h) | % Elongation | % RA | Minimum Creep Rate (%/h) |
|---|---|---|---|---|---|---|
| B-4 | 450 (842) | 40 (276) | * 100 | - | - | 0.0031 |
| B-5 | 450 (842) | 40 (276) | * 100 | - | - | 0.0026 |
| B-22 | 450 (842) | 30 (207) | * 100 | - | - | 0.0013 |
| B-7 | 450 (842) | 30 (207) | * 100 | - | - | 0.0013 |
| B-8 | 450 (842) | 20 (138) | * 100 | - | - | 0.0007 |
| B-9 | 450 (842) | 20 (138) | * 100 | - | - | 0.0004 |
| B-10 | 550 (1022) | 30 (207) | 57.9 | 49.4 | 78.2 | 0.2923 |
| B-11 | 550 (1022) | 30 (207) | 53.1 | 48.2 | 78.8 | 0.3071 |
| B-12 | 550 (1022) | 20 (138) | * 100 | - | - | 0.0354 |
| B-13 | 550 (1022) | 20 (138) | * 100 | - | - | 0.0377 |
| B-14 | 550 (1022) | 10 (69) | * 100 | - | - | 0.0033 |
| B-15 | 550 (1022) | 10 (69) | * 100 | - | - | 0.0043 |
| B-16 | 650 (1202) | 20 (138) | 0.8 | 73.1 | 89.3 | - |
| B-17 | 650 (1202) | 20 (138) | 0.8 | 56.9 | 87.6 | 27.0500 |
| B-18 | 650 (1202) | 10 (69) | 17.5 | 96.8 | 89.8 | 1.6283 |
| B-19 | 650 (1202) | 10 (69) | 17.7 | 85.8 | 89.1 | 1.6456 |
| B-20 | 650 (1202) | 7.5 (52) | 40.2 | 87.7 | 91.9 | 0.8178 |
| B-21 | 650 (1202) | 7.5 (52) | 45.4 | 91.3 | 88.1 | 0.7560 |
| * Test interrupted | | | | | | |

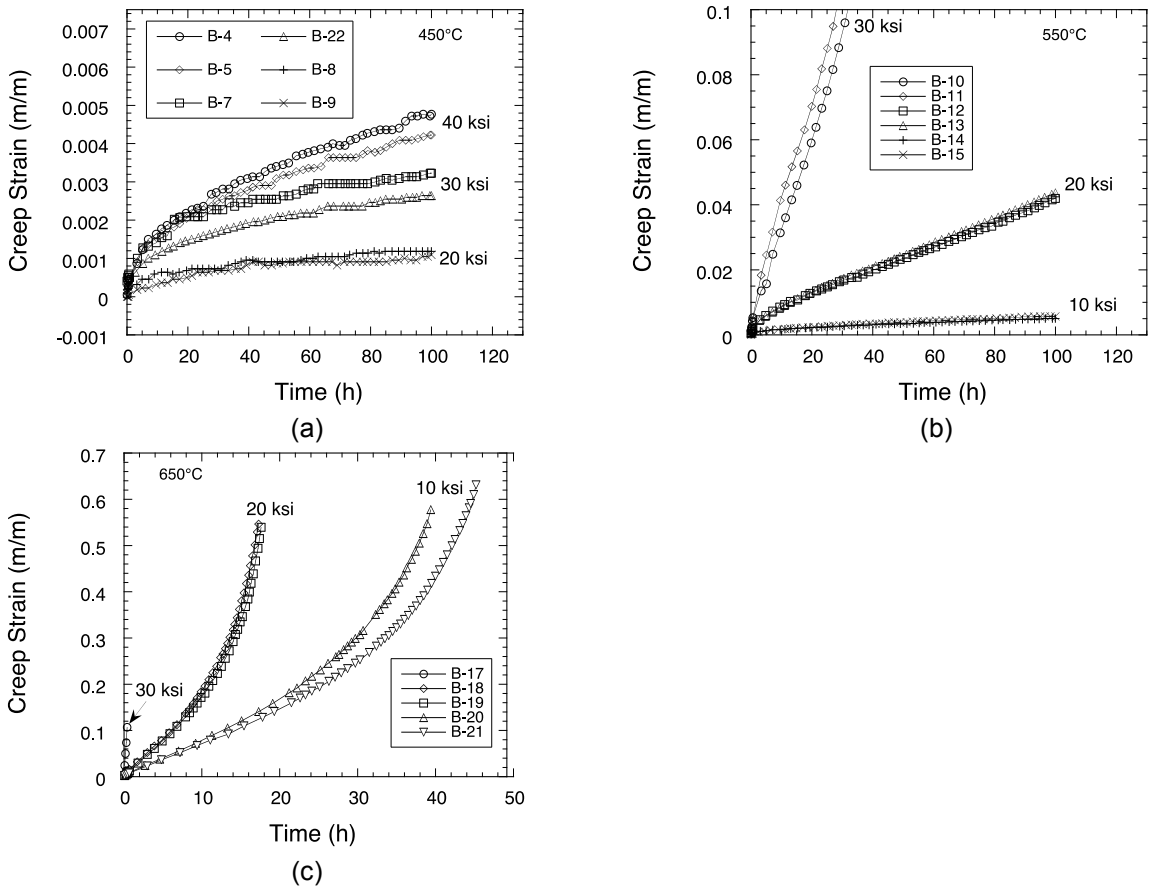


**Figure A-1 Creep curves for SA 193 B7 material at (a) 450 ºC, (b) 550 ºC, (c) 650 ºC**

The built-in equation for the creep strain rate in the finite-element program ABAQUS can be either in the time-hardening form; that is,

$$\dot{\varepsilon}_c = A\sigma^n t^m \tag{0a}$$

or in the strain-hardening form; that is,

$$\dot{\varepsilon}_c = \left(A\sigma^n\left[(m+1)\varepsilon_c\right]^m\right)^{1/(m+1)} \tag{1b}$$

where A, n, and m are functions of temperature, σ is stress, $\varepsilon_c$ is creep strain, $\dot{\varepsilon}_c$ is creep strain rate, and t is time. An integrated version of the creep rate equation is

$$\varepsilon_c = B_0\sigma^n t^{m+1} \tag{0a}$$

where $B_0 = \dfrac{A}{m+1}$. Writing Eq. 2 in an Arrhenius form,

$$\varepsilon_c = B\sigma^n t^{m+1}\exp(-\tfrac{Q}{T}) \tag{2b}$$

where T is absolute temperature, Q is a fitting parameter, and B = B0exp(Q/T). Equation 2b was used to determine the parameters B, m, Q, and n from the creep tests. Table A-4 tabulates the best-fit parameters, with creep strain $\varepsilon_c$ in m/m, stress $\sigma$ in kilopounds per square inch (ksi), time t in h, and absolute temperature T in K. The fitted creep curves are compared with the test curves in Figures A-2 to A-4. Except for a few tests, the fit in the first 2 hours, which is of interest for SBO severe accidents, is reasonable.

**Table A-4 Best-Fit Values of the Parameters B, m, Q, and n of SA 193 B7 As Determined from the Creep Tests**

| T (°C) | B | m | Q | A | N |
|---|---|---|---|---|---|
| 450 | 16800 | -0.501 | 17300 | 3.45E-7 | 1.80 |
| 550 | 16600 | -0.363 | 19700 | 6.5E-7 | 2.60 |
| 650 | 26000 | -0.187 | 18700 | 3.19E-5 | 2.78 |

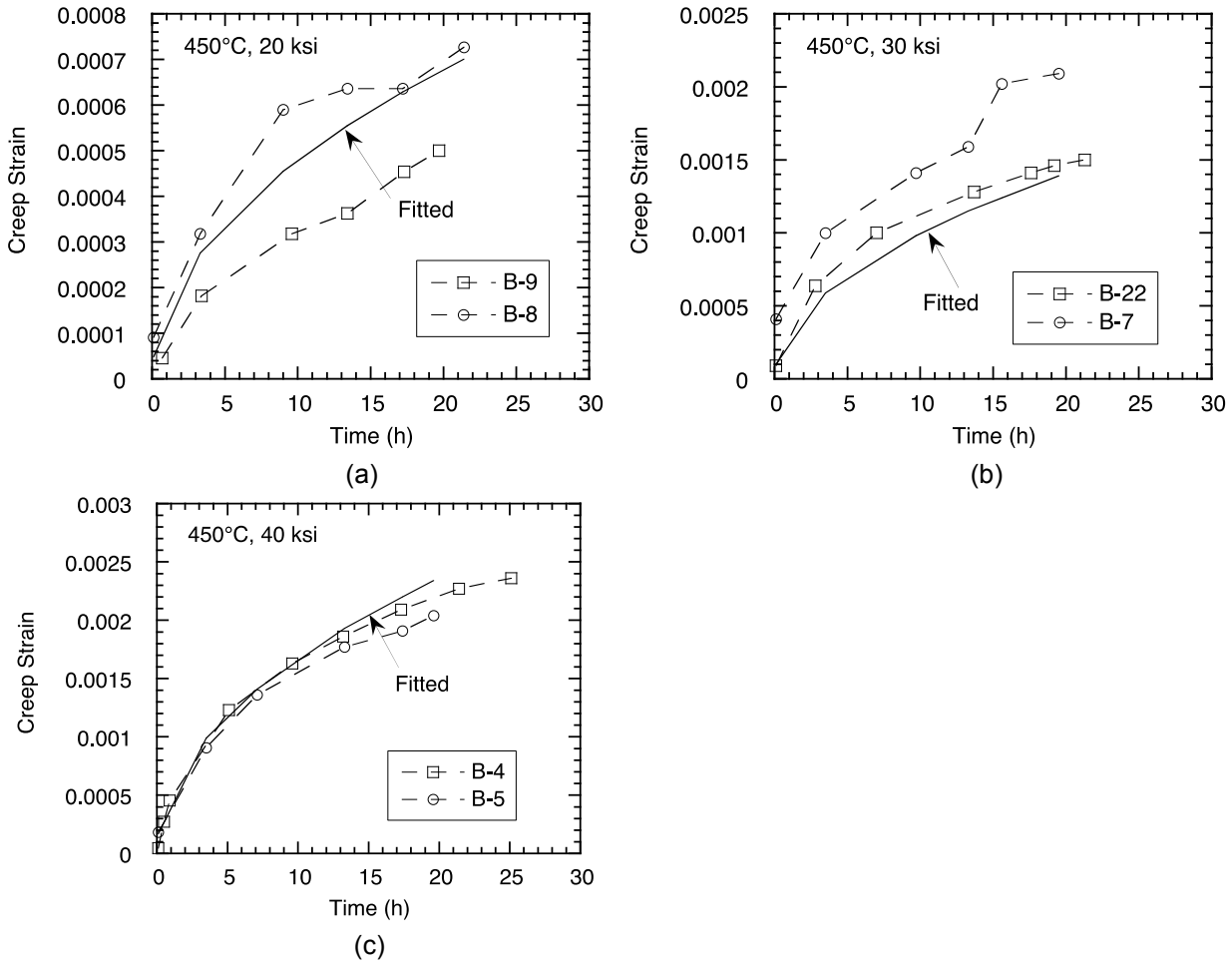


**Figure A-2 Comparison of fitted and test variation of creep strain vs. time for creep tests conducted on SA 193 B7 at 450 degrees C at (a) 20 ksi (138 MPa), (b) 30 ksi (207 MPa), and (c) 40 ksi (278 MPa)**

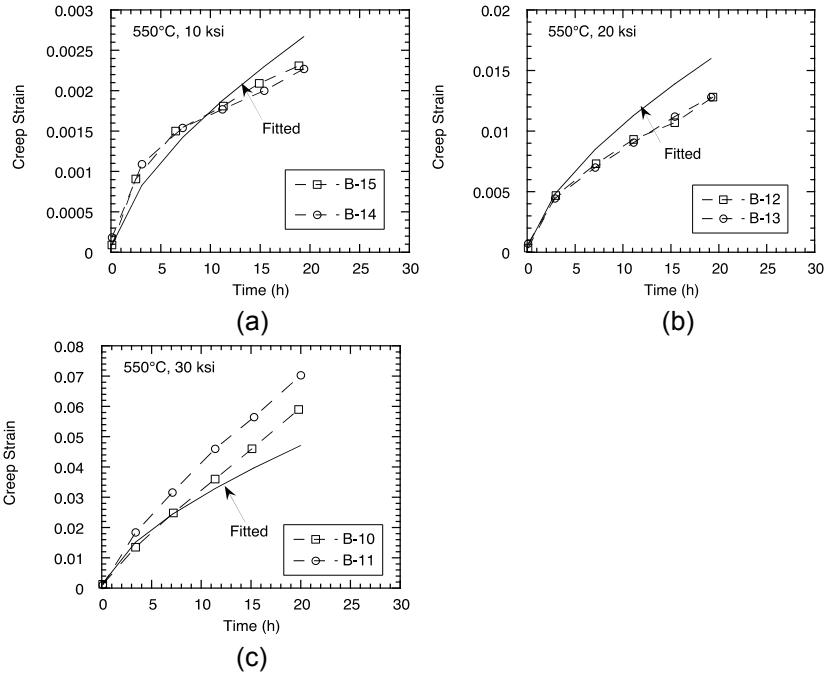


**Figure A-3 Comparison of fitted and test variation of creep strain vs. time for creep tests conducted on SA 193 B7 at 550 degrees C at (a) 10 ksi (69 MPa), (b) 20 ksi (138 MPa), and (c) 30 ksi (207 MPa)**

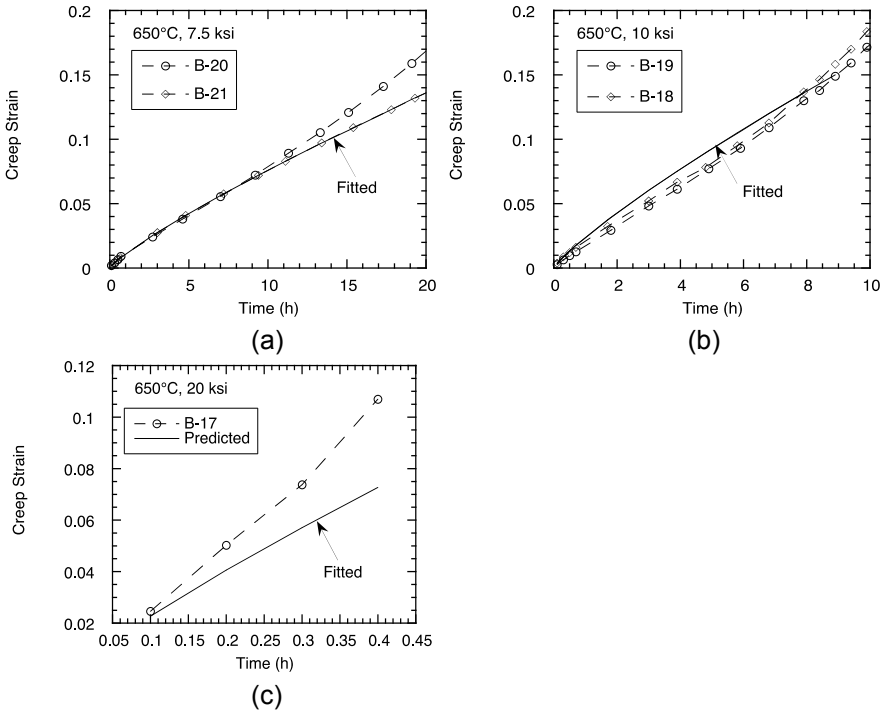


**Figure A-4 Comparison of fitted and test variation of creep strain vs. time for creep tests conducted on SA 193 B7 at 650 degrees C at (a) 7.5 (52 MPa), (b) 10 (69 MPa), and (c) 20 ksi (138 MPa)**

**SA 240 Grade 316 Stainless Steel**

Table A-5 is a summary of all the creep tests, all of which were run in duplicate. Figures A-4 to A-6 plot the representative creep strain vs. time curves at 700, 800, 1,000, and 1,100 degrees C (1,292, 1,472, 1,832, and 2,012 degrees F). In most cases, primary creep is absent and the tests show either a steady-state creep behavior or a steady state followed by tertiary creep behavior. All available U.S. creep rate data were fitted to Eq. 1a, to obtain the parameters A, n, and m at various temperatures, as listed in Table A-6. The fitted creep rates are plotted against the test creep rates in Figure A-7, which shows that the bulk of the creep rate data can be predicted to within a factor of 4.8, and the ANL data fall within the scatter band of the much larger database.

**Table A-5 Summary of Creep Data for SA 240 Grade 316 Stainless Steel**

| Specimen No. | Temperature °C (°F) | Stress ksi (MPa) | Rupture Time (h) | % Elongation | % RA | Minimum Creep Rate (%/h) |
|---|---|---|---|---|---|---|
| O-4 | 700 (1292) | 30 (207) | 7.2 | 49.5 | 80.9 | - |
| O-5 | 700 (1292) | 30 (207) | 7.0 | 51.5 | 81.7 | 2.99 |
| O-10 | 700 (1292) | 28 (193) | 12.3 | 61.2 | 81.2 | 2.40 |
| O-11 | 700 (1292) | 28 (193) | 14.5 | 48.4 | 84.0 | 1.25 |
| O-16 | 700 (1292) | 26 (179) | 31.3 | 51.6 | 76.8 | 0.70 |
| O-17 | 700 (1292) | 26 (179) | 28.6 | 54.1 | 80.9 | 0.73 |
| O-6 | 800 (1472) | 19.0 (131) | 2.4 | 64.7 | 89.0 | - |
| O-7 | 800 (1472) | 19.0 (131) | 2.4 | 61.0 | 88.4 | - |
| O-12 | 800 (1472) | 15.0 (103) | 14.2 | 67.0 | 86.8 | 1.44 |
| O-13 | 800 (1472) | 15.0 (103) | 12.9 | 70.3 | 89.1 | 1.68 |
| O-18 | 800 (1472) | 13.0 (90) | 35.4 | 82.9 | 89.4 | 0.73 |
| O-19 | 800 (1472) | 13.0 (90) | 30.6 | 84.0 | 89.7 | 0.85 |
| O-14 | 1000 (1832) | 4.0 (28) | 11.5 | 75.7 | 88.2 | 0.70 |
| O-15 | 1000 (1832) | 4.0 (28) | 10.3 | 76.6 | 89.8 | 1.11 |
| O-20 | 1100 (2012) | 2.0 (14) | *100 | - | - | 0.079 |
| O-21 | 1100 (2012) | 2.0 (14) | *100 | - | - | 0.079 |
| O-8 | 1100 (2012) | 4.0 (28) | 0.5 | 75.6 | 91.3 | - |
| O-9 | 1100 (2012) | 4.0 (28) | 0.6 | 82.7 | 90.8 | - |
| * Test interrupted | | | | | | |

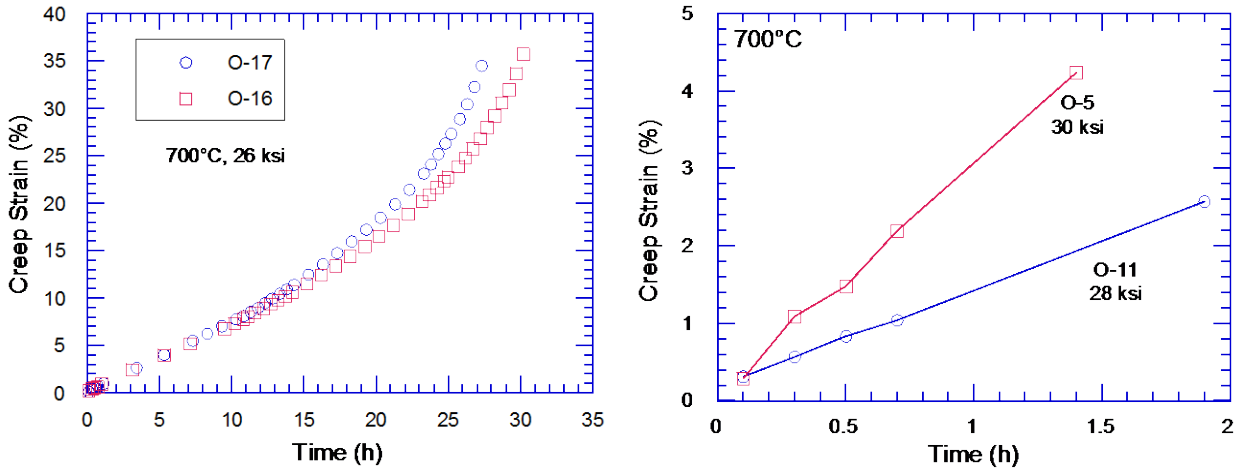


**Figure A-5 Creep strain vs. time curves of SA 240 Grade 316 stainless steel at 700 degrees C (a) 26 ksi (179 MPa) and (b) 28 ksi (193 MPa) and 30 ksi (207 MPa)**

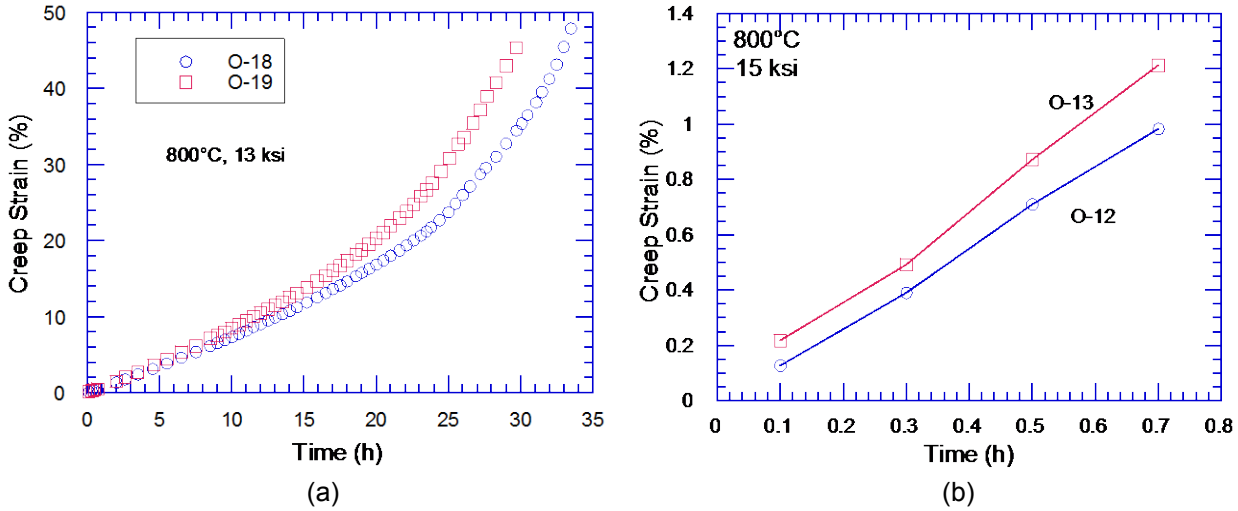


**Figure A-6 Creep strain vs. time curves of SA 240 Grade 316 stainless steel at 800 °C (a) 13 ksi (90 MPa) and (b) 15 ksi (103 MPa)**

**Table A-6 Creep Rate Parameters for Available Data on Type 316 Stainless Steel**
***Mean and ±95% confidence bounds at various temperatures***
***(stress in ksi and creep rate in 1/h)***

| T (°C) | m | N | A (mean) | A(-95%) | A (+95%) |
|---|---|---|---|---|---|
| 350 | 0 | 9.35 | 4.4925E-30 | 9.3594E-31 | 2.1564E-29 |
| 450 | 0 | 9.35 | 1.1269E-24 | 2.3478E-25 | 5.4093E-24 |
| 500 | 0 | 9.35 | 1.6894E-22 | 3.5195E-23 | 8.1090E-22 |
| 550 | 0 | 9.35 | 1.3778E-20 | 2.8703E-21 | 6.6133E-20 |
| 600 | 0 | 9.35 | 6.7869E-19 | 1.4139E-19 | 3.2577E-18 |
| 650 | 0 | 9.35 | 2.1918E-17 | 4.5663E-18 | 1.0521E-16 |
| 675 | 0 | 8.80 | 9.8651E-16 | 2.0552E-16 | 4.7352E-15 |
| 700 | 0 | 7.20 | 2.7813E-13 | 5.7945E-14 | 1.3350E-12 |
| 750 | 0 | 6.52 | 3.9794E-11 | 8.2904E-12 | 1.9101E-10 |
| 800 | 0 | 6.52 | 3.8282E-10 | 7.9755E-11 | 1.8376E-09 |
| 850 | 0 | 6.52 | 3.3115E-09 | 6.8990E-10 | 1.5895E-08 |
| 900 | 0 | 6.52 | 2.3829E-08 | 4.9643E-09 | 1.1438E-07 |
| 1000 | 0 | 6.52 | 7.4218E-07 | 1.5462E-07 | 3.5625E-06 |
| 1100 | 0 | 6.52 | 1.2748E-05 | 2.6558E-06 | 6.1190E-05 |

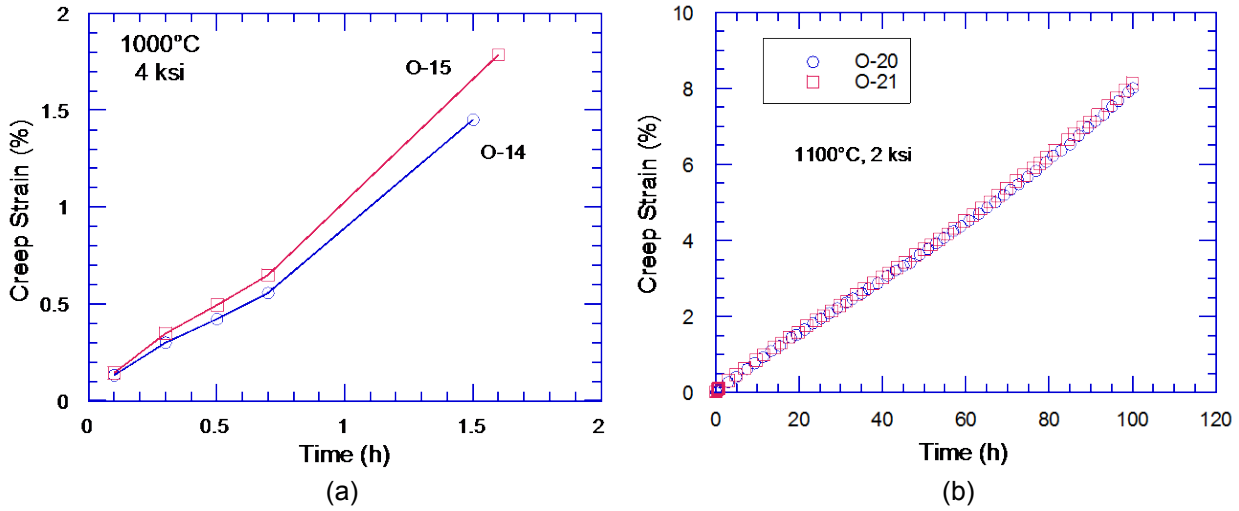


**Figure A-7 Creep strain vs. time curves of SA 240 Grade 316 stainless steel at (a) 1,000 °C, 4 ksi (28 MPa) and (b) 1,100 °C, 2 ksi (14 MPa)**

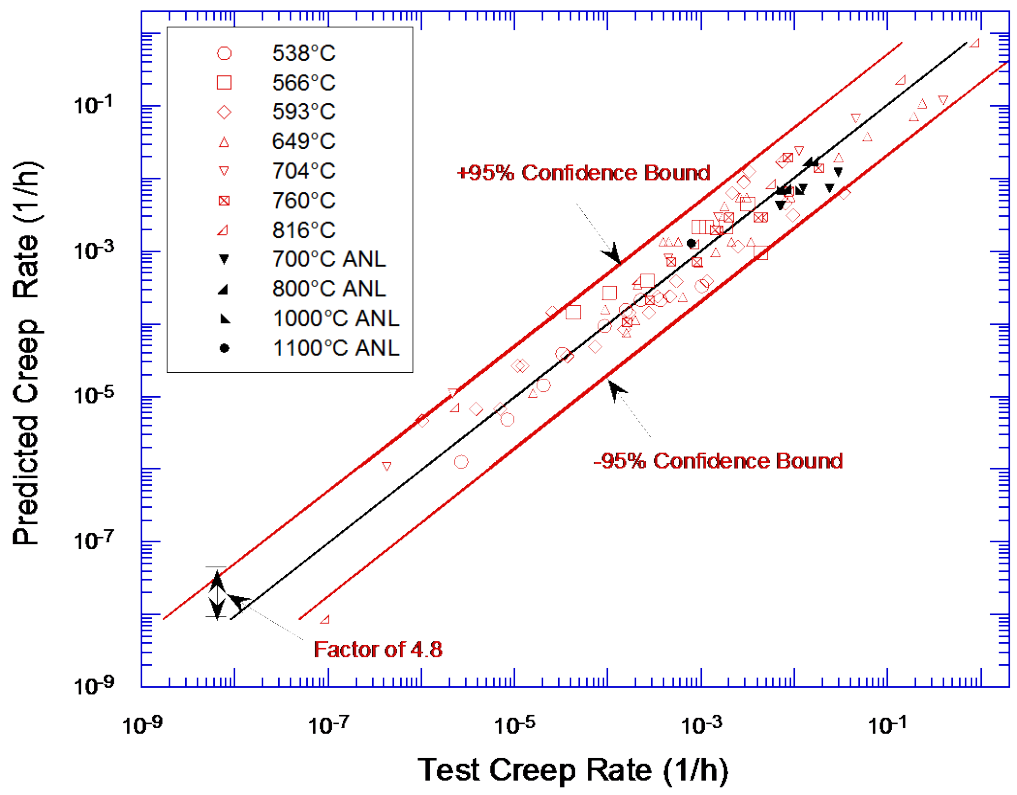


**Figure A-8 Predicted vs. test minimum creep rate of SA 240 Grade 316 stainless steel**

The available time-to-stress-rupture U.S. data for Grade 316 stainless steel were fitted with a Larson-Miller parameter, as shown in Figure A-9. In equation form, the Larson-Miller plot is given by

$$LMP(mean) = \begin{cases} 28085 - 7651.8Log(\sigma) \; for \; \sigma > 25ksi \\ 23940 - 4609.7Log(\sigma) \; for \; \sigma < 25ksi \end{cases} \quad \text{(A0)}$$

and the time to rupture tR in h is given by

$$t_R = 10^{\frac{LMP}{T} - 15.94} \quad \text{(A0)}$$

where T = temperature in K. Figure A-9 also shows the parameter values for ±95-percent confidence limits. The predicted times to rupture are plotted against test rupture times in Figure A-10, which shows that the bulk of the data can be predicted to within a factor of 6.

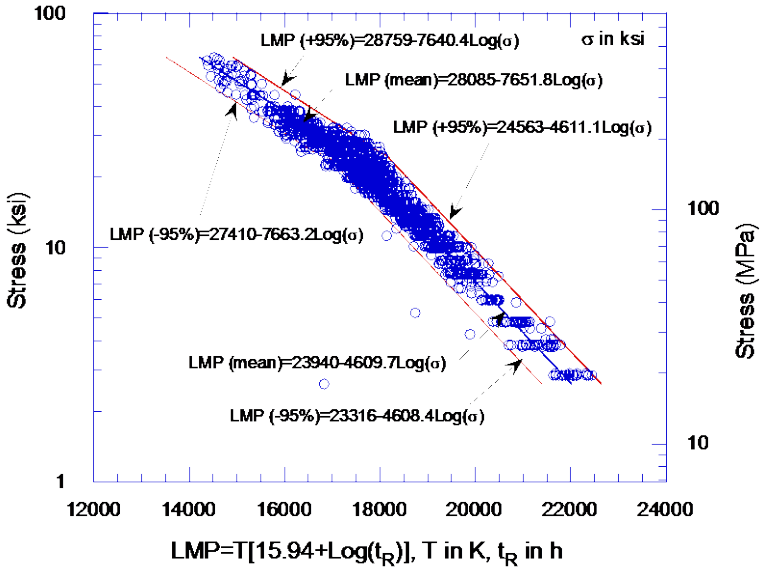


**Figure A-9 Larson-Miller parameter plot for time to stress rupture of SA 240 Grade 316 stainless steel at 538–1,100 °C**

The steady-state creep ductility, defined as the product of the steady-state (or minimum) creep rate and the time to rupture, is plotted as a function of stress and temperature in Figures A-11 to A-14. There is significant scatter in the data but no definite trend as a function of stress. However, the steady-state ductility shows an increase with increasing temperature and leveling off at high temperatures, as shown in Figure A-15.

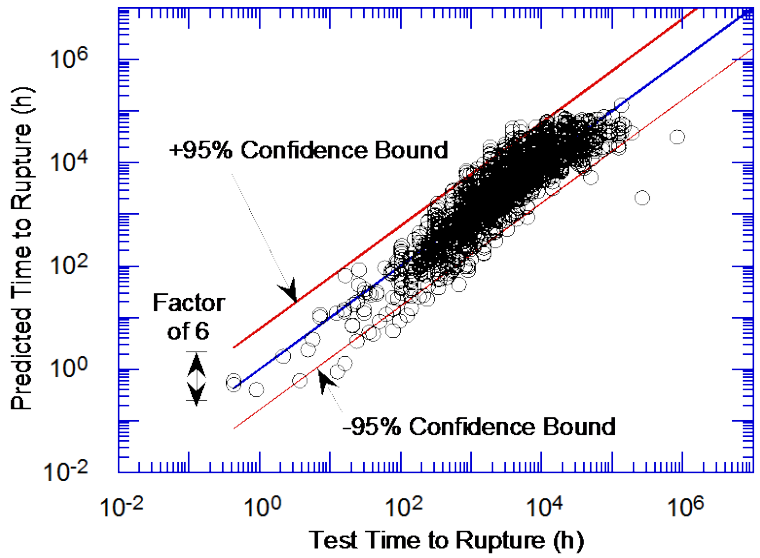


**Figure A-10 Predicted vs. test time to stress rupture of SA 240 Grade 316 stainless steel at 538–1,100 °C**

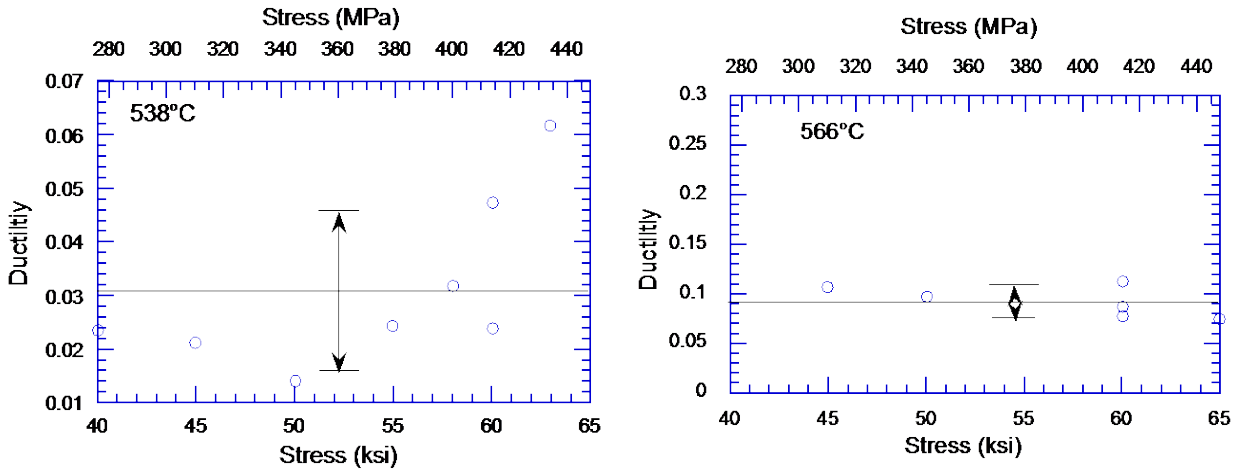


**Figure A-11 Steady-state creep ductility vs. stress of SA 240 Grade 316 stainless steel at (a) 538 °C and (b) 566 °C**

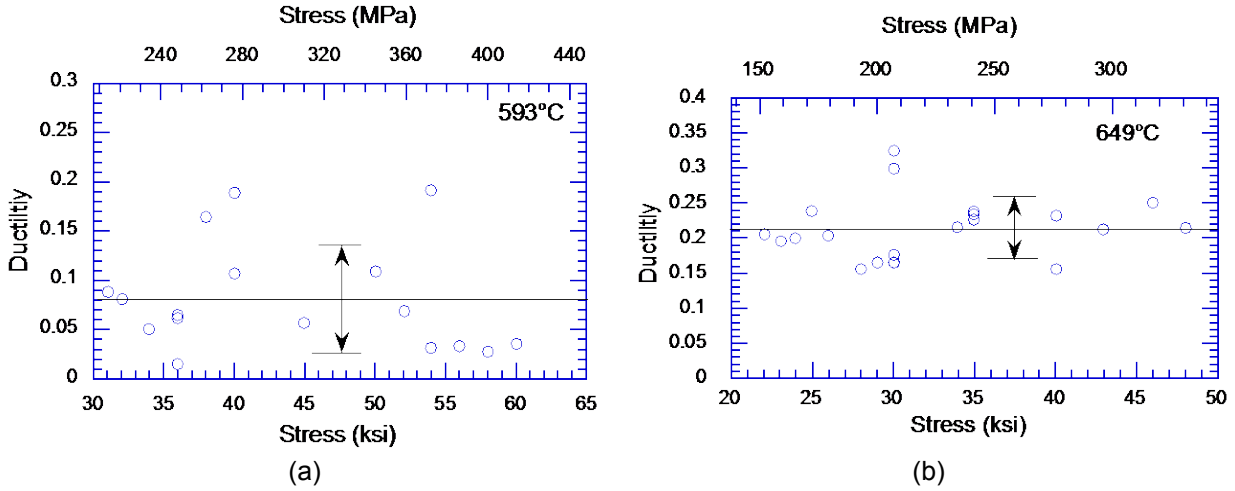


**Figure A-12 Steady-state creep ductility vs. stress of SA 240 Grade 316 stainless steel at (a) 593 °C and (b) 649 °C**

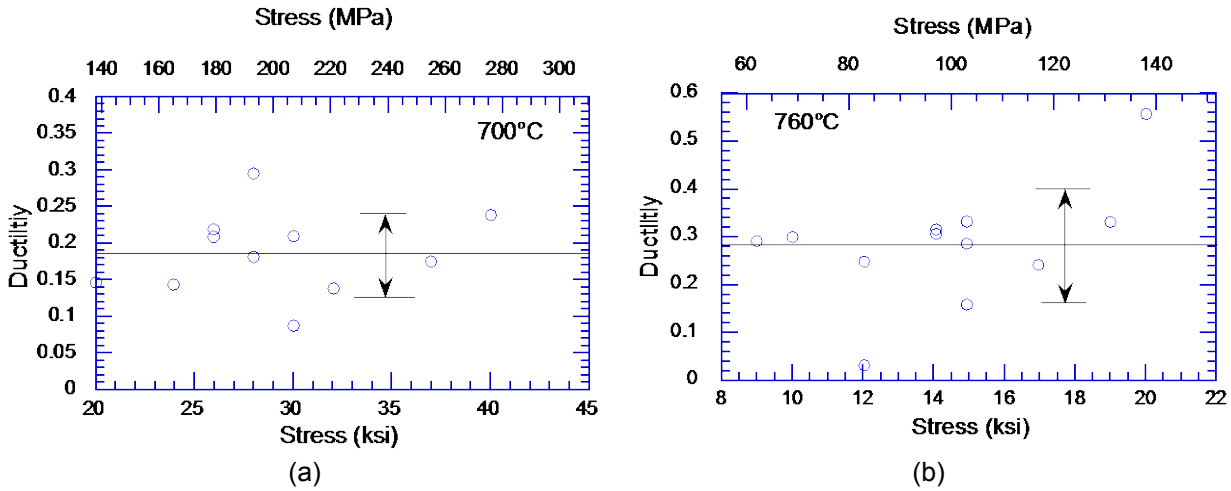


**Figure A-13 Steady-state creep ductility vs. stress of SA 240 Grade 316 stainless steel at (a) 700 °C and (b) 760 °C**

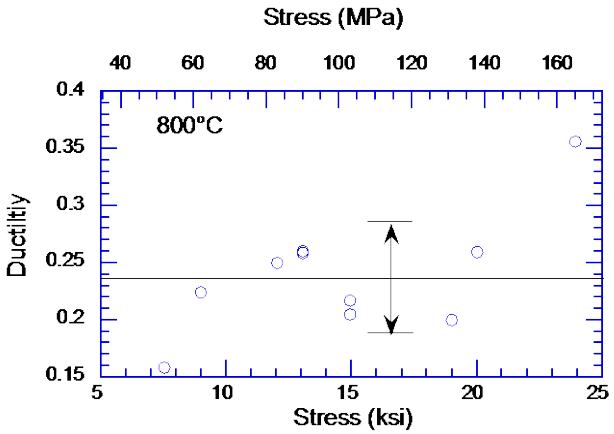


**Figure A-14 Steady-state creep ductility vs. stress of SA 240 Grade 316 stainless steel at 800 °C**

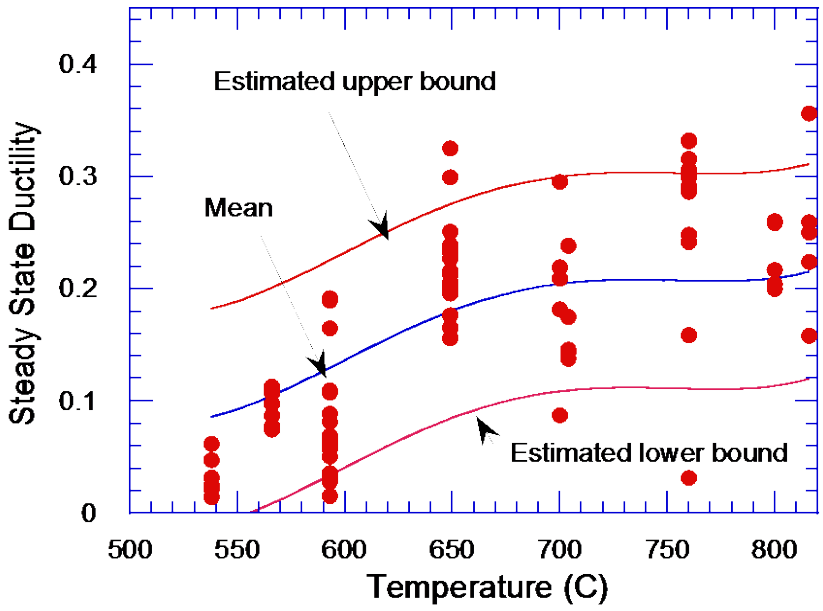


**Figure A-15 Estimated mean, upper, and lower bounds to the steady-state creep ductility of SA 240 Grade 316 stainless steel**

**SA 351 Grade CF8M Cast Stainless Steel**

Table A-7 summarizes the creep tests conducted at ANL. Representative creep strain vs. time curves at 700, 800, and 1,000 degrees C are plotted in Figures A-16 to A-18. In many cases, primary creep is absent, and the tests show either a steady-state creep behavior or a steady state followed by tertiary creep behavior. The available creep database for CF8M cast stainless steel is rather limited. Harada in Japan has reported creep data on CF8M cast stainless steel. The combined creep-rate data were fitted to Eq. 1a to obtain the parameters A, n, and m at various temperatures, as listed in Table A-8. The fitted creep rates are plotted against the test creep rates in Figure A-19a, which shows that the bulk of the creep rate data can be predicted to within a factor of 10.7. The uncertainty is larger than SA 240 Grade 316 stainless steel because of the much more limited database available for SA 351 Grade CF8M cast stainless steel. Note that the ANL data fall within the scatter band of the combined data base.

**Table A-7 Summary of Creep Data for SA 351 Grade CF8M Cast Stainless Steel**

| Specimen No. | Temperature °C (°F) | Stress ksi (MPa) | Rupture Time (h) | % Elongation | % RA | Minimum Creep Rate (%/h) |
|---|---|---|---|---|---|---|
| ATLAS-4 | 700 (1292) | 15 (103) | 60.9 | 8.4 | 24.3 | 7.46E-02 |
| ATLAS-5 | 700 (1292) | 15 (103) | * 100.0 | - | - | 9.04E-02 |
| ATLAS-10 | 700 (1292) | 17 (117) | 8.0 | 5.7 | 18.9 | 1.67E-01 |
| ATLAS-13 | 700 (1292) | 17 (117) | 7.5 | 3.4 | 7.9 | 2.49E-01 |
| ATLAS-14 | 700 (1292) | 16 (110) | 0.5 | 3.5 | 14.3 | - |
| ATLAS-15 | 700 (1292) | 16 (110) | 29.2 | 8.4 | 18.3 | 1.40E-01 |
| ATLAS-6 | 800 (1472) | 14 (97) | 2.1 | 13.5 | 19.7 | 3.88E+00 |
| ATLAS-7 | 800 (1472) | 14 (97) | 1.3 | 10.4 | 30.8 | 4.32E+00 |
| ATLAS-11 | 800 (1472) | 12 (83) | 1.3 | 5.2 | 10.0 | 2.20E+00 |
| ATLAS-16 | 800 (1472) | 12 (83) | 0.7 | 10.0 | 18.3 | - |
| ATLAS-17 | 800 (1472) | 10 (69) | 0.9 | 5.3 | 8.6 | - |
| ATLAS-18 | 800 (1472) | 10 (69) | 7.4 | 12.5 | 23.0 | 8.81E-01 |
| ATLAS-8 | 1000 (1832) | 6 (41) | 0.1 | 13.1 | 29.9 | - |
| ATLAS-9 | 1000 (1832) | 6 (41) | 0.1 | 8.9 | 16.4 | - |
| ATLAS-12 | 1000 (1832) | 3 (21) | 13.3 | 19.1 | 26.9 | 1.19E+00 |
| ATLAS-19 | 1000 (1832) | 3 (21) | 0.9 | 9.1 | 17.0 | 1.96E+00 |
| ATLAS-20 | 1000 (1832) | 2 (14) | * 100.0 | - | - | 9.96E-02 |
| ATLAS-21 | 1000 (1832) | 2 (14) | 14.1 | 5.8 | 12.8 | 2.58E-01 |

* Test interrupted

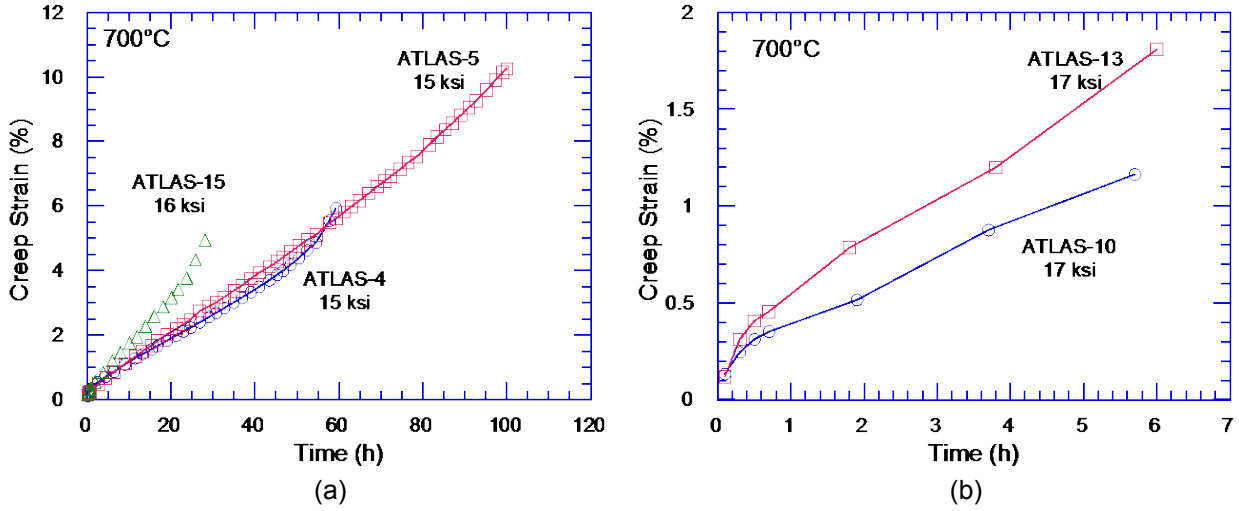


**Figure A-16 Creep strain vs. time curves of SA 351 Grade CF8M cast stainless steel at 700 °C (a) 15–16 ksi (103–110 MPa) and (b) 17 ksi (117 MPa)**

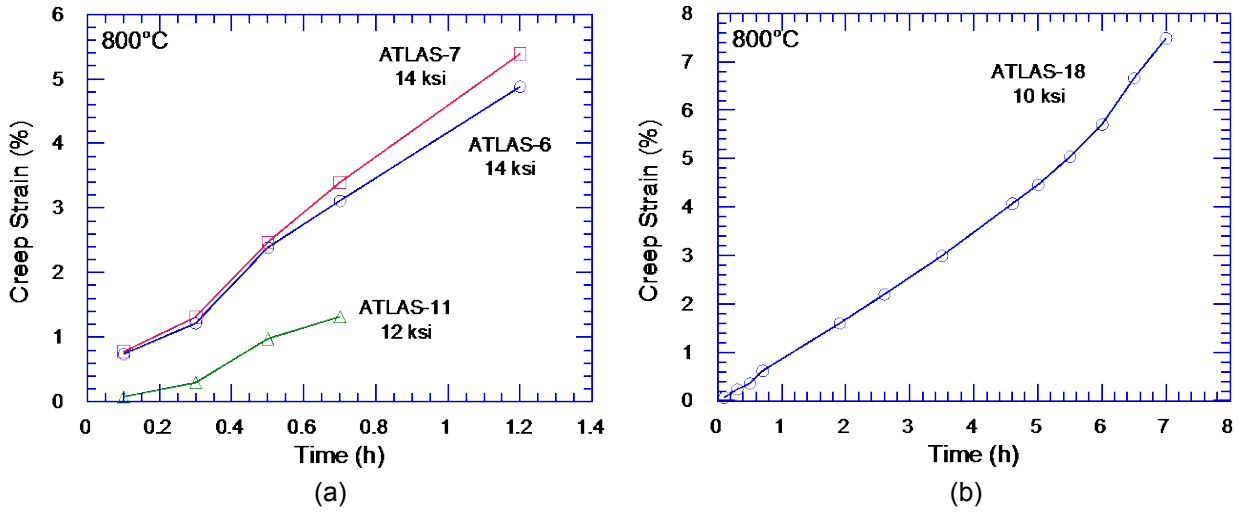


**Figure A-17 Creep strain vs. time curves of SA 351 Grade CF8M cast stainless steel at 800 °C (a) 12 and 14 ksi (83–97 MPa) and (b) 10 ksi (69 MPa)**

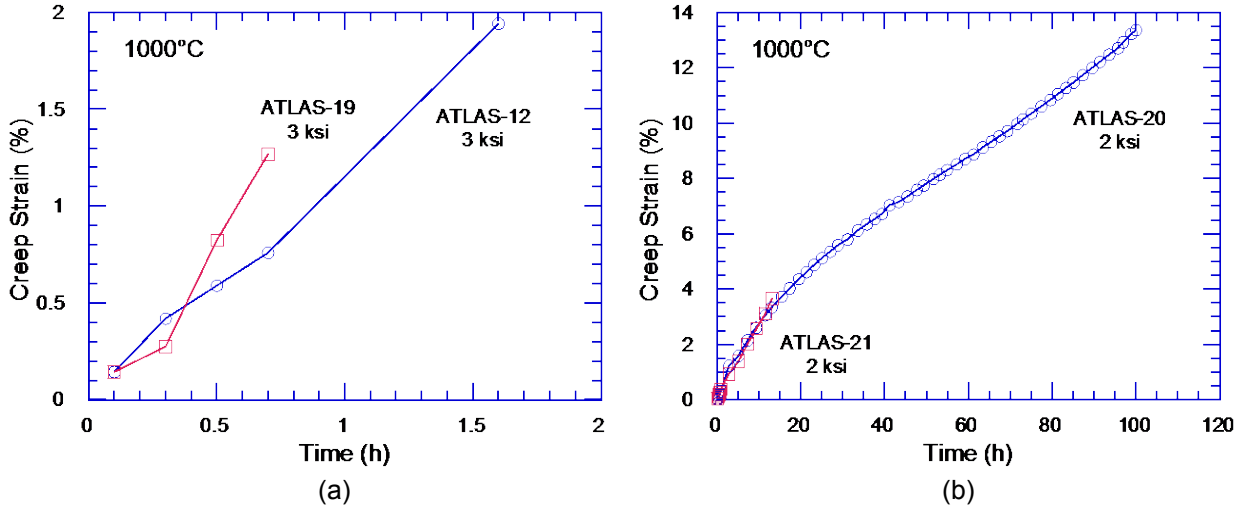


**Figure A-18 Creep strain vs. time curves of SA 351 Grade CF8M cast stainless steel at 1,000 °C (a) 3 ksi (21 MPa) and (b) 2 ksi (14 MPa)**

**Table A-8 Mean and ±95% Confidence Bounds of Creep-Rate Parameters for Combined ANL and Japanese Data on SA 351 Grade CF8M Cast Stainless Steel at Various Temperatures (Stress in ksi and Creep Rate in 1/h)**

| T (°C) | m | n | A (mean) | A (-95%) | A (+95%) |
|---|---|---|---|---|---|
| 350 | 0 | 9.5 | 5.233E-25 | 5.599E-24 | 4.891E-26 |
| 450 | 0 | 9.5 | 5.866E-21 | 6.276E-20 | 5.482E-22 |
| 500 | 0 | 9.5 | 2.513E-19 | 2.689E-18 | 2.349E-20 |
| 550 | 0 | 9.5 | 6.820E-18 | 7.297E-17 | 6.374E-19 |
| 600 | 0 | 9.5 | 1.268E-16 | 1.357E-15 | 1.185E-17 |
| 650 | 0 | 9.5 | 6.919E-16 | 7.403E-15 | 6.466E-17 |
| 700 | 0 | 9.5 | 3.585E-15 | 3.836E-14 | 3.351E-16 |
| 750 | 0 | 8.7 | 2.661E-13 | 2.847E-12 | 2.487E-14 |
| 800 | 0 | 5.0 | 2.003E-08 | 2.143E-07 | 1.872E-09 |
| 850 | 0 | 5.0 | 4.609E-07 | 4.932E-06 | 4.308E-08 |
| 900 | 0 | 5.0 | 3.357E-06 | 3.592E-05 | 3.137E-07 |
| 950 | 0 | 5.0 | 2.281E-05 | 2.441E-04 | 2.132E-06 |
| 1000 | 0 | 5.0 | 1.143E-04 | 1.223E-03 | 1.068E-05 |
| 1050 | 0 | 5.0 | 6.393E-04 | 6.841E-03 | 5.975E-05 |
| 1100 | 0 | 5.0 | 3.156E-03 | 3.376E-02 | 2.949E-04 |

The available time to stress rupture for the combined Japanese and U.S. data for SA 351 Grade CF8M cast stainless steel were fitted with a Larson-Miller parameter, as shown in Figure A-19b. In equation form, the Larson-Miller plot is given by

$$LMP(mean) = 23877 - 5929.4Log(\sigma) \tag{A0}$$

where stress $\sigma$ is in ksi and the time to rupture $t_R$ in h is given by

$$t_R = 10^{\frac{LMP}{T} - 15.98} \tag{A0}$$

where T = temperature in K. Figure A-19b also shows the parameter values for ±95-percent confidence limits. Figure A-20 plots the predicted times to rupture against test rupture times, which shows that the bulk of the combined data can be predicted to within a factor of 4.8.

The steady-state ductility of the ANL CF8M specimens is considerably less than that of the Japanese CF8M heat (Figure A-21a) and also much less than that of the SA 240 Grade 316 stainless steel (Figure A-15). The total elongation of the U.S. CF8M heat is comparable to the steady-state ductility of the Japanese CF8M heat (Figure A-21b).

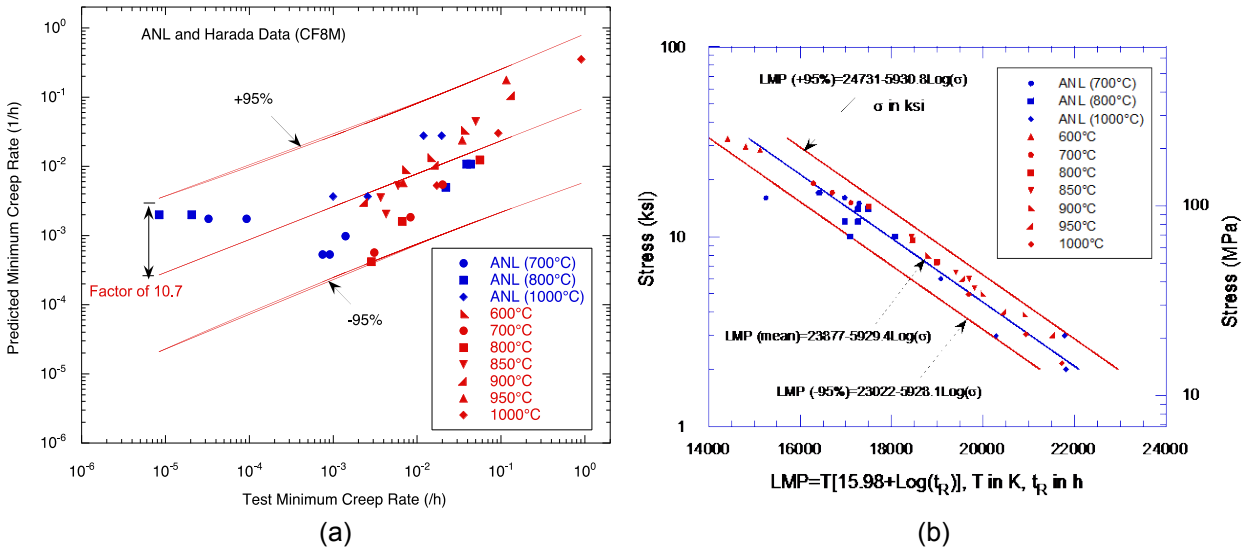


**Figure A-19 Confidence bounds for the prediction of (a) creep rate and (b) Larson-Miller parameter for time to rupture of SA 351 Grade CF8M cast stainless steel based on ANL and Japanese data**

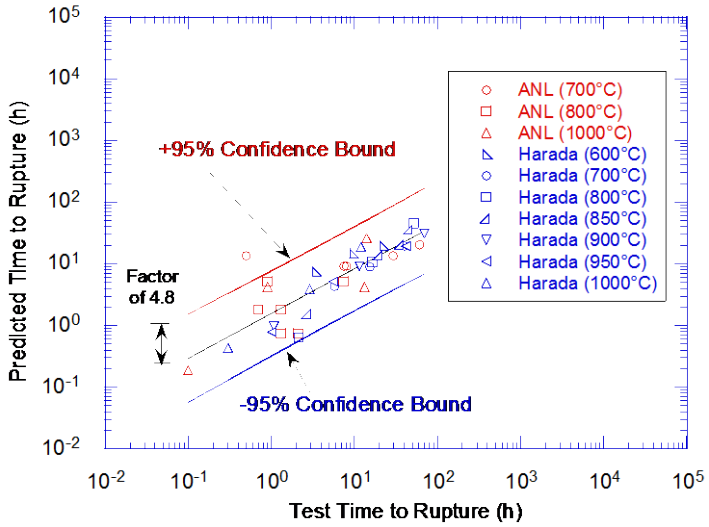


**Figure A-20 Predicted vs. observed time to stress rupture of SA 351 Grade CF8M cast stainless steel**

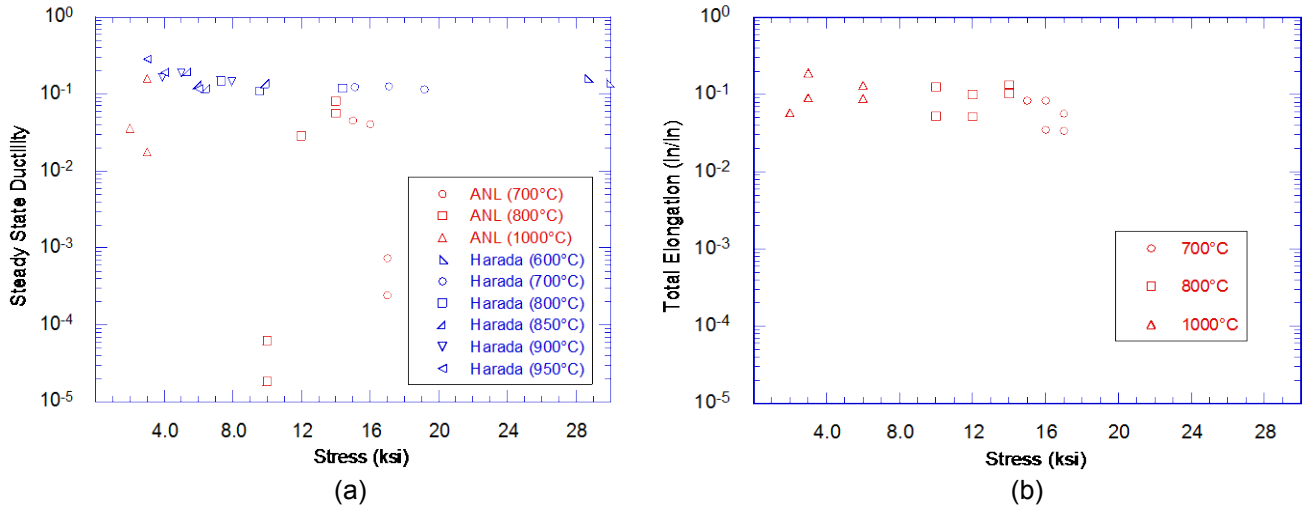


**Figure A-21 Variation of (a) steady-state ductility of U.S. and Japanese CF8M heats and (b) total elongation of U.S. CF8M heat with stress**

**SA 516 Grade 70 Carbon Steel**

Table A-9 summarizes the creep-rupture tests conducted at ANL. The creep curves at 500, 650, and 800 degrees C (932, 1,202, and 1,472 degrees F) are plotted in Figures A-22a to A-22c, respectively. The ANL data for SA 516 Grade 70 were combined with available data for SA 216 Grade WCC from the literature and the combined data fitted to Eq. 1a to obtain the parameters A, n, and m at various temperatures, as listed in Table A-10. Figure A-23a shows that the combined creep-rate data can be predicted to within a factor of 3 by using Eq. 1a and the parameters listed in Table A-10. Although the data sets are limited, both fall within the same scatter band.

The available time to stress rupture for the combined ANL data for SA 516 Grade 70 and literature data on SA 216 Grade WCC carbon steels were fitted with a Larson-Miller parameter, as shown in Figure A-23b. In equation form, the Larson-Miller plot is given by

$$LMP(mean) = 18599 - 4460.6Log(\sigma) \qquad \text{(A0)}$$

where stress σ is in ksi and the time to rupture $t_R$ in h is given by

$$t_R = 10^{\frac{LMP}{T} - 14.25}, \qquad \text{(A0)}$$

where T = temperature in K. Figure A-23b also shows the parameter values for ±95-percent confidence limits. Figure A-24a plots the predicted times to rupture against test rupture times, which shows that the bulk of the combined data can be predicted to within a factor of 4.9. The steady-state creep ductility of SA 216 is 2–5 percent at 500 degrees C (932 degrees F) but increases with temperature to greater than 10 percent at 650 and 800 degrees C (1,202 and 1,472 degrees F) (Figure A-24b).

## Table A-9 Summary of Creep Data for SA 516 Grade 70 Carbon Steel

| Specimen No. | Temperature °C (°F) | Stress ksi (MPa) | Rupture Time (h) | % Elon-gation | % RA | Minimum Creep Rate (%/h) |
|---|---|---|---|---|---|---|
| 6-4 | 500 (932) | 40 (276) | 4.70 | 17.20 | 37.40 | 1.01 |
| 6-5 | 500 (932) | 40 (276) | 5.90 | 21.00 | 42.00 | 0.81 |
| 6-10 | 500 (932) | 38 (262) | 8.70 | 24.90 | 44.00 | 0.49 |
| 6-13 | 500 (932) | 38 (262) | 7.40 | 16.20 | 41.50 | 0.50 |
| 6-14 | 500 (932) | 35 (241) | 15.90 | 22.20 | 44.00 | 0.17 |
| 6-15 | 500 (932) | 35 (241) | 11.10 | 23.50 | 47.00 | 0.18 |
| 6-6 | 650 (1202) | 18.5 (128) | 0.20 | 60.90 | 77.50 | - |
| 6-7 | 650 (1202) | 18.5 (128) | 0.10 | 69.90 | 79.30 | - |
| 6-11 | 650 (1202) | 15.5 (107) | 0.50 | 69.40 | 77.00 | 28.23 |
| 6-16 | 650 (1202) | 14 (97) | 1.60 | 59.50 | 78.00 | 5.36 |
| 6-17 | 650 (1202) | 12 (83) | 3.60 | 65.00 | 77.60 | 3.21 |
| 6-19 | 650 (1202) | 10 (69) | 9.10 | 76.70 | 17.00 | 1.02 |
| 6-8 | 800 (1472) | 9 (62) | 0.20 | 42.80 | 41.50 | - |
| 6-9 | 800 (1472) | 9 (62) | 0.10 | 43.70 | 29.90 | - |
| 6-12 | 800 (1472) | 7 (48) | 0.60 | 45.90 | 16.40 | 36.40 |
| 6-18 | 800 (1472) | 5 (34) | 3.30 | 48.50 | 26.90 | 4.81 |
| 6-20 | 800 (1472) | 5 (34) | 3.10 | 46.20 | - | 5.72 |
| 6-21 | 800 (1472) | 4 (28) | 6.40 | 50.10 | 12.80 | 1.94 |

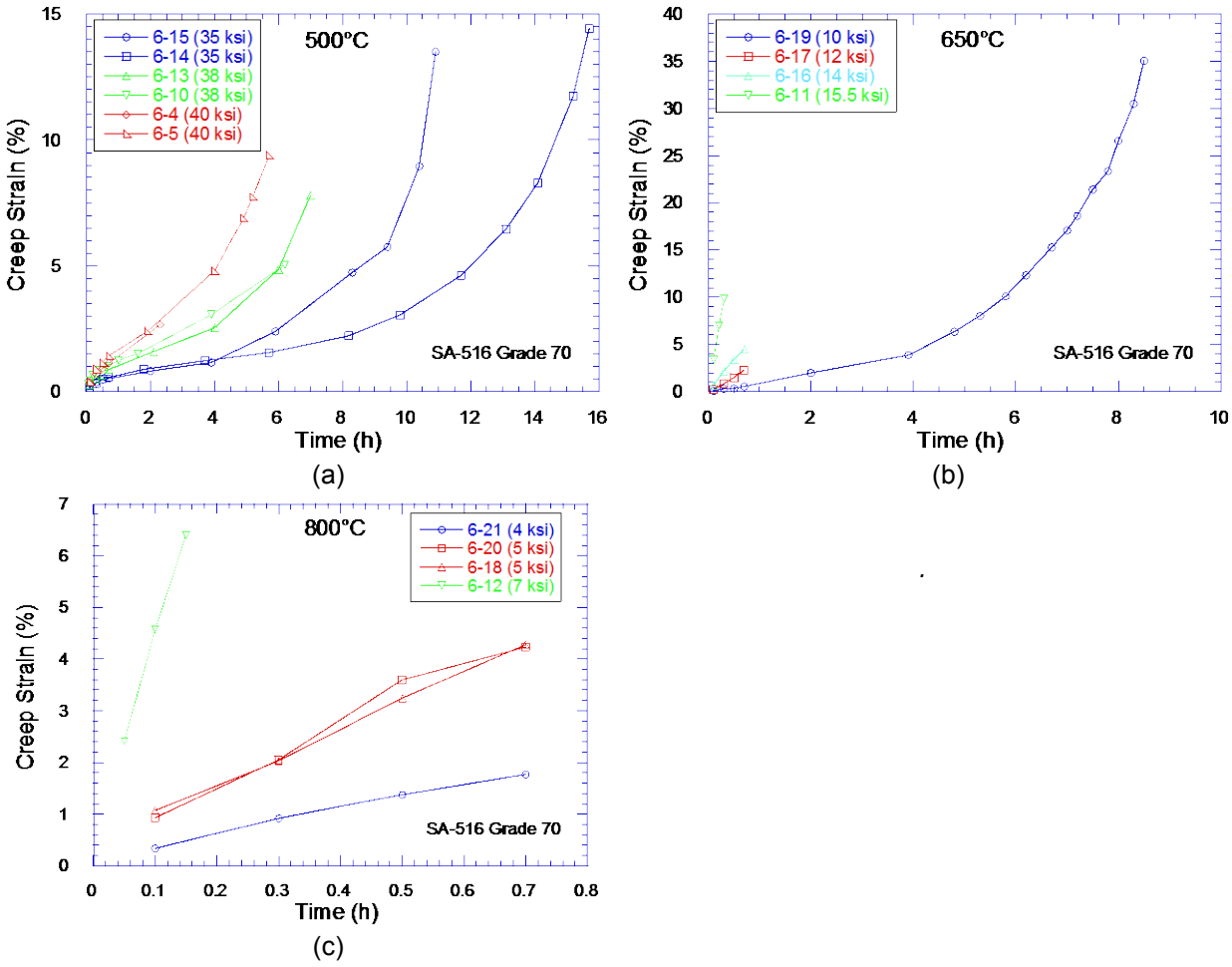


**Figure A-22 Creep curves for SA 516 Grade 70 carbon steel at (a) 500 °C, (b) 650 °C, and (c) 800 °C**

**Table A-10 Creep-Rate Parameters for Combined ANL and Literature Data on SA 216 Grade 70 and SA 216 Grade WCC Carbon Steels**
***Mean and ±95% confidence bounds at various temperatures (stress in ksi and creep rate in 1/h).***

| T (°C) | m | n | A (mean) | A(-95%) | A (+95%) |
|---|---|---|---|---|---|
| 300 | 0 | 5.439 | 4.844E-19 | 1.615E-19 | 1.453E-18 |
| 400 | 0 | 5.439 | 8.654E-15 | 2.885E-15 | 2.596E-14 |
| 500 | 0 | 5.439 | 1.228E-11 | 4.092E-12 | 3.683E-11 |
| 550 | 0 | 5.439 | 2.387E-10 | 7.955E-11 | 7.159E-10 |
| 600 | 0 | 5.439 | 3.303E-09 | 1.101E-09 | 9.907E-09 |
| 650 | 0 | 5.439 | 3.438E-08 | 1.146E-08 | 1.031E-07 |
| 700 | 0 | 5.439 | 2.813E-07 | 9.377E-08 | 8.439E-07 |
| 750 | 0 | 5.439 | 1.874E-06 | 6.248E-07 | 5.623E-06 |
| 800 | 0 | 5.439 | 1.046E-05 | 3.488E-06 | 3.139E-05 |
| 850 | 0 | 5.439 | 5.013E-05 | 1.671E-05 | 1.504E-04 |
| 900 | 0 | 5.439 | 2.101E-04 | 7.004E-05 | 6.304E-04 |
| 950 | 0 | 5.439 | 7.834E-04 | 2.611E-04 | 2.350E-03 |
| 1,000 | 0 | 5.439 | 2.634E-03 | 8.779E-04 | 7.901E-03 |

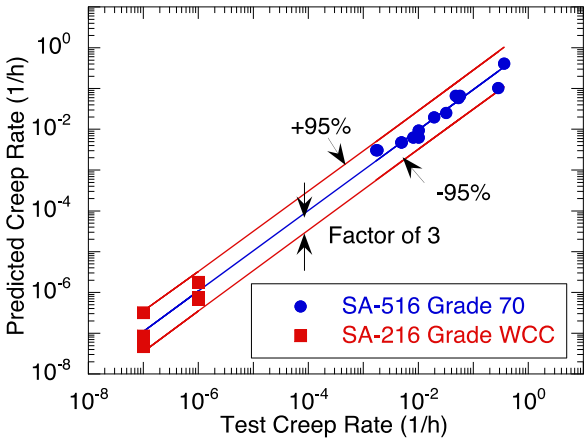


(a)

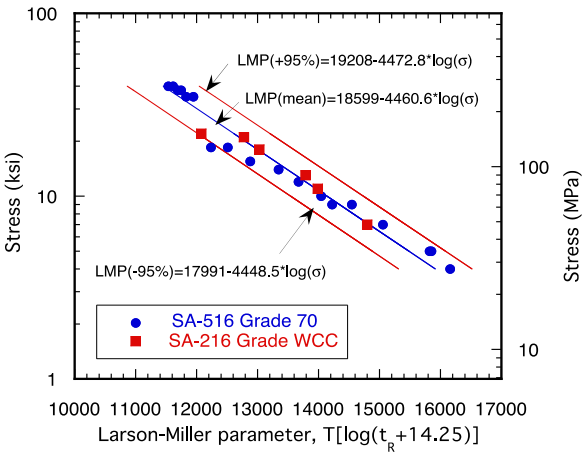


(b)

**Figure A-23(a)** **Predicted vs. observed creep rates**
**Figure A-23(b)** **Larson-Miller plot for time to stress rupture of SA 516 Grade 70 and SA 216 Grade WCC**

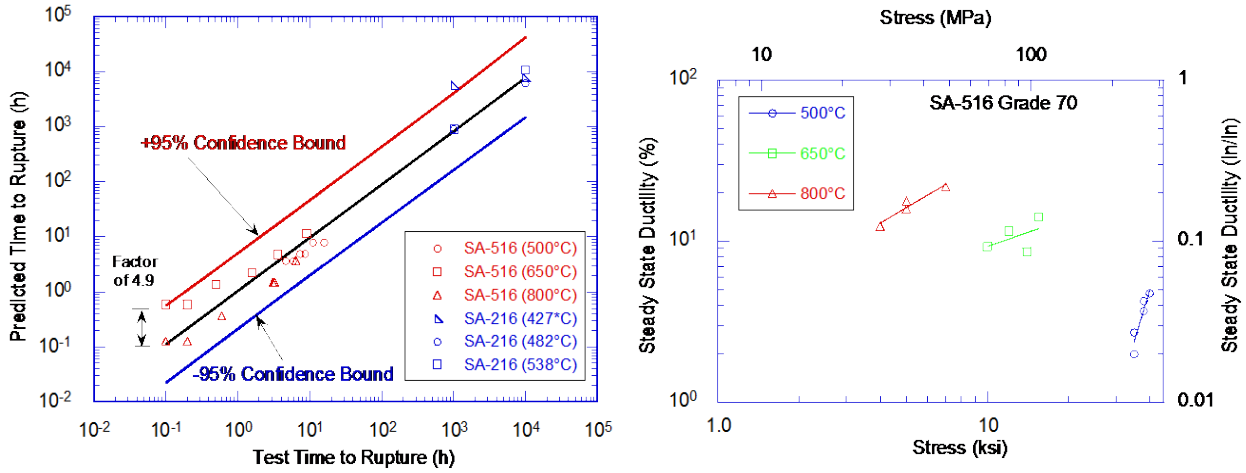


**Figure A-24(a)** **Predicted vs. observed time to stress rupture**
**Figure A-24(b)** **Variation of steady-state ductility with stress and temperature of carbon steels**

### SA 240 Grade 316/SA 516 Grade 70 Weldment

Table A-11 summarizes the creep tests conducted on SA 240 stainless steel/SA 516 carbon steel. Since the strain distribution in the gauge length is nonuniform, the strain and minimum creep-rate data reported in the table represent average values over the entire gauge length, with significantly more strain occurring in the carbon steel than in the stainless steel half. The primary purpose of these tests was to determine the loss of ductility and time to rupture of the weldment relative to the base metals. At 700 degrees C (1,292 degrees F), most of the failure occurred in the weaker SA 516 carbon steel by ductile necking away from the weld. Even in the single specimen (6W-14) in which failure occurred at the weld interface, necking is visible in the carbon steel away from the weld. At 800 degrees C (1,472 degrees F), all of the failure occurred by shear at the SA 516/weld interface at a significantly reduced ductility. At 900 and 1,000 degrees C (1,652 and 1,832 degrees F), failure occurred in the middle of the weld either by shear or flat fracture, and the overall ductility of the specimens was significantly reduced compared to that at 700 degrees C (1,292 degrees F). Necking was not observed in any of the tests conducted at 800–1,000 degrees C (1,472–1,832 degrees F).

## Table A-11 Summary of Creep Data for SA 240 Grade 316 /SA 516 Grade 70 Weldment

| Spec. No. | Temp °C (°F) | Stress ksi (MPa) | Rupture Time (h) | % Elon-gation | % RA | Min. Creep Rate (%/h) | Failure Location |
|---|---|---|---|---|---|---|---|
| 6W-6 | 700 (1292) | 13 (90) | 0.2 | 29.2 | 77.8 | 3.07 | necking of SA 516 |
| 6W-7 | 700 (1292) | 13 (90) | 0.1 | 29.1 | 81.0 | 5.16 | necking of SA 516 |
| 6W-8 | 700 (1292) | 17 (117) | F.O.L. | 24.5 | 65.9 | 1.61 | necking of SA 516 |
| 6W-9 | 700 (1292) | 17 (117) | F.O.L. | 21.8 | 76.3 | 1.28 | necking of SA 516 |
| 6W-14 | 700 (1292) | 10 (69) | 0.6 | 22.4 | 52.6 | 0.36 | shear at weld (SA 516 side) |
| 6W-17 | 700 (1292) | 6 (41) | 9.0 | 29.0 | 69.5 | | necking of SA 516 |
| 6W-10 | 800 (1472) | 8 (55) | 0.2 | 8.3 | 14.3 | | shear at weld (SA 516 side) |
| 6W-11 | 800 (1472) | 8 (55) | 0.2 | 7.2 | 14.4 | | shear at weld (SA 516 side) |
| 6W-12 | 800 (1472) | 10 (69) | F.O.L. | 5.4 | 8.4 | | shear at weld (SA 516 side) |
| 6W-13 | 800 (1472) | 10 (69) | F.O.L. | 7.5 | 12.9 | 1.29 | shear at weld (SA 516 side) |
| 6W-15 | 800 (1472) | 4 (28) | 2.5 | 4.5 | 13.2 | | shear at weld (SA 516 side) |
| 6W-18 | 800 (1472) | 2 (14) | 30.3 | 6.0 | *** | | shear at weld (SA 516 side) |
| 6W-19 | 900 (1472) | 2 (14) | 33.1 | 8.4 | *** | | Flat fracture at weld |
| 6W-20 | 900 (1472) | 1 (7) | 100** | - | | | Flat fracture at weld (middle) |
| 6W-16 | 1000 (1832) | 2 (14) | 7.0 | 8.1 | 14.2 | | Shear at weld (middle) |
| 6W-21 | 1000 (1832) | 1 | 37.2 | 6.0 | 6.6 | | Flat fracture at weld (middle) |

# APPENDIX B

# CONSEQUENTIAL STEAM GENERATOR TUBE RUPTURE CALCULATOR

This study developed software referred to as the consequential steam generator (SG) tube rupture (C-SGTR) calculator to support the work in this report. The calculator is used to estimate failure times and leak sizes of SG tubes with different types of flaws. The software also has built-in models for hot leg (HL) and surge-line (SL) failure caused by the creep-rupture failure mechanism, and it estimates failure times and HL and SL probabilities. The scope of the models currently includes new SG tube materials and the associated property data for both thermally treated Inconel 600 and 690 (600TT and 690TT) tubes.

The Information Systems Laboratories document, ISL-NSAD-TR-10-13, "Technical Basis and Software User Guide for SGTR Probability," issued December 2014 (Ref. B-1), stores the calculator user manual and basis report. The same document also contains the results of a review of the basis report by Argonne National Laboratory.

It is emphasized that the software does not directly calculate a "C-SGTR probability." This probability can be calculated after a case run by using the information from two output files and the probabilities assigned to the set of input flaws. However, the user can observe from the output files whether the HL (or SL) fails before a specified integrated tube leak size (defined as critical leak size in the report) is reached or not.

Section B-1 provides a short discussion of software input-output with an example case. Section B-2 has comments on the uncertainty modeling. Reference B-1 contains more information.

## B.1 Example Case

This software is designed to support the probabilistic risk assessments (PRAs) that address the risk associated with SG tube rupture (SGTR) scenarios; as an initiator, as a consequence of plant transients (design-basis-accident scenarios), and because of core damage sequences (C-SGTR). Plant-specific material properties, plant-specific SG tube flaw data, and scenario-specific thermal-hydraulic (TH) input are required to use this software to support PRA analysis.

An event sequence (scenario) can be defined as the input to the calculator. To define a scenario, the calculator expects five input files:

(7) plant information file
(8) time, temperature, pressure profile of the SG tubes, SL, and HL (TH) file
(9) SG tube flaws file
(10) material properties file (e.g., 600TT or 690TT)
(11) calculation parameters file

The underlying calculations are deterministic. The calculation parameters file is used to apply a probability and to sample the information that comes from the flaw and TH files. This provides probabilistic results. For those characteristics of the scenario that go into the calculations

without uncertainty parameters, no sampling occurs; thus, they do not contribute to the probability calculations.

The software produces the following three output files:

(5) CumulativeLeakAreaFile-XXXX.txt
(12) CSGTRProbabilityFile-XXXX.txt
(13) IntermediateFile-TH-XXXX.txt

This appendix contains an example Table B-1 of some key inputs and outputs, with annotations, and additional example cases are in the later appendices of this report.

The output in Table B-1 allows for the calculation of a "margin," which is defined as the number of minutes between the failure of HL (or SL, whichever occurs first) and the failure of more than one-tube guillotine break equivalent of SG tubes (6 square centimeters ($cm^2$) (0.93 square inch ($in.^2$)) for this example). For example, from Table B-1, a margin M of

$$M = 221 – 235 = -14 \text{ minutes}$$

can be determined. A negative margin is favorable, since tube failures and a fission product release to the atmosphere would be limited or avoided.

Some noteworthy aspects of the software are listed below:

- Axial, circumferential and wear-type SG tube flaws are modeled.
- The software estimates HL and SL failure probabilities. Caution: in this estimation, the effect of SG tube failures on the HL and SL failures is not considered. The software calculates each of the three types of failures, HL, SL, and SG tube, independently.
- Two types of correlations are used to estimate SG tube leakage; one for low-temperature (e.g., much lower than creep-rupture region) but potentially high-pressure cases; the other for temperatures in the creep-rupture range. The threshold temperature for switchover to creep-rupture correlation is a software input: the default is set to 600 degrees Celsius (C) (1,112 degrees Fahrenheit (F)) (ThresholdCreepRupture 600.0, in the calculation parameters file).

The following comments apply to Table B-1:

- Columns A, F–J are input. Columns B–E are output.
- If one tube has a guillotine break, the total leak area would be 6 $cm^2$ (0.93 $in.^2$).
- At 238 minutes into this core damage event, the total expected leak area from multiple partial breaks is 28 $cm^2$ (4.34 $in.^2$), which is equivalent to about 5 guillotine tube breaks.
- At 95-percent confidence level, the total expected leak area from multiple partial breaks is 37 $cm^2$ (5.7 $in.^2$), which is equivalent to about 6 guillotine tube breaks.
- HL fails around 220 minutes.

- SL failure probability is 68 percent at 238 minutes.
- HL and SL failure probabilities are calculated without considering SG tube failures. A substantial failure of SG tubes (greater than 6 $cm^2$ (0.93 $in.^2$) total leakage area) would reduce the reactor coolant system pressure and could delay HL and SL failures.
- This example estimates multiple wear flaws with different sizes and depth.
- The tube material is Alloy 600TT.
- The event is core damage from station blackout with no recovery and early loss of turbine-driven auxiliary feedwater pumps in a PWR.

## B.2 Uncertainty Parameters

The software uses a set of input uncertainty parameters to sample from distributions that apply to various key inputs. Table A-2 of Reference B-1 defines these inputs and their uncertainty parameters. This table is titled “Statistical Parameters in the Calculation: Properties Input File.” If an input parameter is not in this table, then the software does not sample for that parameter but uses the expected value provided.

## B.3 References

B-1. Information Systems Laboratories, “Technical Basis and Software User Guide for SGTR Probability,” ISL-NSAD-TR-10-13, December 2014, Agencywide Documents Access and Management System Accession No. ML15054A495.

**Table B-1 Example Input-Output (Condensed and Processed)**

| A | B | C | D | E | | F | G | H | I | J |
|---|---|---|---|---|---|---|---|---|---|---|
| Time (min) | $A_{mean}$ ($cm^2$) | $A_{0.95}$ (cm sq ) | HL % | Surge Line % | | Surge Line Temp °C | HL Temp °C | Average Hot Tube Temp °C | Average Cold Tube Temp °C | Delta P in psi |
| 210 | 0.027 | 0.18 | 0.000 | 0.000 | | 621 | 713 | 574 | 499 | 15 |
| 210 | 0.027 | 0.18 | 0.000 | 0.000 | | 617 | 715 | 581 | 500 | 15 |
| 211 | 0.030 | 0.18 | 0.000 | 0.000 | | 619 | 722 | 588 | 504 | 15 |
| 212 | 0.034 | 0.18 | 0.002 | 0.000 | | 622 | 730 | 593 | 507 | 15 |
| 213 | 0.037 | 0.19 | 0.013 | 0.000 | | 626 | 738 | 597 | 510 | 15 |
| 214 | 0.039 | 0.20 | 0.041 | 0.000 | | 629 | 746 | 601 | 513 | 15 |
| 215 | 0.039 | 0.20 | 0.104 | 0.000 | | 633 | 755 | 606 | 516 | 15 |
| 216 | 0.039 | 0.20 | 0.267 | 0.000 | | 637 | 764 | 611 | 519 | 15 |
| 217 | 0.039 | 0.20 | 0.511 | 0.000 | | 641 | 772 | 615 | 522 | 15 |
| 218 | 0.039 | 0.20 | 0.795 | 0.000 | | 672 | 786 | 613 | 524 | 15 |
| 219 | 0.039 | 0.20 | 0.884 | 0.000 | | 661 | 791 | 619 | 524 | 15 |
| 219 | 0.039 | 0.20 | 0.945 | 0.000 | | 661 | 797 | 626 | 526 | 15 |
| 220 | 0.039 | 0.20 | 0.987 | 0.000 | | 666 | 809 | 634 | 530 | 15 |
| 221 | 0.039 | 0.20 | 1.000 | 0.000 | | 671 | 822 | 640 | 534 | 15 |
| 222 | 0.039 | 0.20 | 1.000 | 0.000 | | 678 | 836 | 646 | 537 | 15 |
| 223 | 0.039 | 0.20 | 1.000 | 0.000 | | 685 | 854 | 654 | 540 | 15 |
| 224 | 0.039 | 0.20 | 1.000 | 0.000 | | 716 | 868 | 648 | 540 | 15 |
| 224 | 0.039 | 0.20 | 1.000 | 0.000 | | 711 | 879 | 658 | 542 | 15 |
| 225 | 0.039 | 0.20 | 1.000 | 0.000 | | 727 | 925 | 673 | 545 | 15 |
| 225 | 0.039 | 0.20 | 1.000 | 0.000 | | 855 | 1057 | 679 | 545 | 15 |
| 226 | 0.039 | 0.20 | 1.000 | 0.000 | | 826 | 1097 | 710 | 548 | 15 |
| 226 | 0.043 | 0.20 | 1.000 | 0.000 | | 839 | 1137 | 725 | 552 | 15 |
| 227 | 0.051 | 0.68 | 1.000 | 0.000 | | 855 | 1162 | 728 | 556 | 15 |
| 227 | 0.061 | 0.83 | 1.000 | 0.000 | | 916 | 1193 | 719 | 556 | 15 |
| 228 | 0.082 | 0.89 | 1.000 | 0.000 | | 905 | 1,209 | 733 | 558 | 15 |
| 228 | 0.119 | 0.90 | 1.000 | 0.000 | | 908 | 1,233 | 745 | 560 | 15 |
| 229 | 0.186 | 0.91 | 1.000 | 0.002 | | 917 | 1,261 | 756 | 562 | 15 |
| 229 | 0.267 | 0.91 | 1.000 | 0.006 | | 925 | 1,281 | 764 | 564 | 15 |
| 230 | 0.353 | 0.91 | 1.000 | 0.025 | | 954 | 1,304 | 772 | 565 | 15 |
| 230 | 0.423 | 0.91 | 1.000 | 0.067 | | 973 | 1,314 | 766 | 565 | 15 |
| 231 | 0.480 | 0.91 | 1.000 | 0.100 | | 965 | 1,319 | 776 | 566 | 15 |
| 232 | 0.589 | 0.91 | 1.000 | 0.183 | | 969 | 1,332 | 787 | 570 | 15 |
| 233 | 1.080 | 3.55 | 1.000 | 0.312 | | 977 | 1,343 | 797 | 575 | 15 |
| 235 | 3.462 | 7.36 | 1.000 | 0.430 | | 985 | 1,354 | 808 | 580 | 15 |
| 236 | 11.535 | 17.04 | 1.000 | 0.571 | | 994 | 1,368 | 819 | 585 | 15 |
| 238 | 28.206 | 36.86 | 1.000 | 0.681 | | 1002 | 1,374 | 827 | 591 | 15 |

# APPENDIX C

# CONSIDERATIONS FOR PRESSURE-INDUCED CONSEQUENTIAL STEAM GENERATOR TUBE RUPTURE

## C.1 Introduction

Past studies (like NUREG-1570, "Risk Assessment of Severe Accident-Induced Steam Generator Tube Rupture," issued March 1998) discussed two types of potential consequential steam generator (SG) tube rupture (C-SGTR) challenges:

Type-I. temperature-induced C-SGTR (mainly driven by creep rupture at higher temperatures) and

Type-II. pressure-induced C-SGTR (mainly driven by the pressure difference across the SG tube boundary, rather than the temperature).

Later studies, benefiting from the probabilistic risk assessments (PRAs), identified risk-significant core damage sequences, such as unrecovered station blackout, to be Type-I challenges. Thus, the analyses were focused on Type-I C-SGTR challenges with good reason. Note that the Type-I challenges thus analyzed occur after core damage, which is the cause of the high SG tube temperatures. Type-I C-SGTRs do not increase the plant core damage frequency (CDF) but may affect the magnitude and timing of fission product release.

This appendix discusses Type-II C-SGTR challenges. The discussion does not claim to be exhaustive. However, the insights discussed and overall results are applicable in a larger context, since the assumptions used are prudently conservative.

Initiating events challenge and induce a Type-II (pressure-induced) C-SGTR. No core damage exists until additional component failures occur as the event proceeds. In earlier studies, it appeared that the main concern for a Type-II C-SGTR was that it could complicate the original event in progress and might affect the operator response and operator success probability. Type-II C-SGTRs could increase the already calculated plant CDF, if they are added to a PRA model that does not originally consider them.

Potential pressure-induced C-SGTRs, following an initiating event and before core damage, are of interest for some initiating events, including large secondary-side breaks (SSB), spurious opening of one or more secondary relief valves, and anticipated transients without scram (ATWS) scenarios. The initiating events other than ATWS are collectively named L-SSBs. In these initiating events, a pressure spike on the primary side, or a sudden pressure drop on the secondary, or a combination of both could provide high delta pressure (pressure difference) across the SG tube boundary.

In PRA studies, once the reactor coolant system (RCS) pressure reaches 22–22.7 megapascals (MPa) (3,200–3,300 pounds per square in (psi)) (design pressure of the primary side), core damage is postulated (see ATWS event tree modeling in Section C..2.1). Assuming that the operating primary and secondary-side pressure difference is about 6.9 MPa (1,000 psi), the range of interest for an analysis of Type-II C-SGTR PRA scenarios is 6.9–33.7 MPa (1,000–3,300 psi) across the tube boundary.

For a pristine tube (no flaw) made of Alloy 600, the burst pressure varies as a function of tube temperature. It is typically about 65 MPa (9.4 kilopounds per square inch (ksi)) at room temperature and about 58.7 MPa (8.5 ksi) at 500 degrees Celsius (C) (932 degrees Fahrenheit (F)). Therefore, there is generally no concern about the burst probability of a flawless tube due to the various pressure-induced scenarios identified by PRAs. However, the tube failure and burst pressure drops when there are one or more flaws on the tube wall. There are many different degradation mechanisms that could generate flaws. As the degradation mechanism for a type of flaw is better understood, indebted to information generated from the surveillance program in operating reactors, enhancements are identified and implemented to limit the number of flaws generated by that degradation mechanism. In the past, this has resulted in changes in plant operational practices, introduction of new tube materials, and other design modifications implemented to alleviate the identified issues. In fact, many plants have already replaced their SGs with either thermally treated Inconel 690 or Inconel 600, have improved their surveillance program, and have enhanced control of their water chemistry. According to a licensee event report (LER) search, there have been no SG tube leaks in the past 6 years since the 2004 event at Palo Verde (notwithstanding the 2012 SONGS [1] event).

Temperature-induced correlations, which are perfectly adequate for Type-I challenges, are deemed to underestimate the magnitude of the potential failure of a flaw when the SG tubes are subjected to relatively low (e.g., at the order of normal operating) temperatures with high pressure differences across the tube boundary (from the RCS side to the secondary side). At temperatures well below the creep-rupture range, the C-SGTR calculator uses the pressure-induced correlations to accommodate the effect of Type-II challenges. The software switches to thermally induced correlations when a user-specified transition temperature is reached in the scenario of interest. The region of temperature where creep rupture starts to become effective is 600–800 degrees C (1,112–1,472 degrees F). The value of 600 degrees C (1,112 degrees F) is used as the transition between the pressure-induced and the creep-rupture tube failure models. The default user input for the transition temperature is given as 600 degrees C (1,112 degrees F).

## C.2 Events of Interest

Some initiating event categories that are included in both design-basis accident analyses and PRAs are candidates for potentially causing consequential Type-II SG tube failures. These failures may be designated as “leaks” (leak area of less than the equivalent area of a single guillotine tube break). For most of the leak sizes, the RCS inventory can be maintained by the normal capacity of the chemical and volume control system (CVCS). Other larger failures can be designated as leakage from one or more tubes, with a total leak area equal to or greater than the equivalent size of a one-tube guillotine break. Such larger failures will be designated as C-SGTR for the purposes of the discussion in this appendix. For such magnitude of failures (in the small loss-of-coolant-accident range), the flow capacity of the CVCS will not be sufficient and injection from high-pressure safety systems will be needed to maintain the RCS inventory. Also, the leakage will cause a reactor trip, even if the original initiating event had not already tripped the reactor and the turbine.

[1] As identified in the San Onofre Nuclear Generating Station root cause analysis, the cause of the SG degradation was tube-to-tube wear caused by in-plane fluid-elastic instability of the tube u-bends. A design error resulted in the actual SGs having more severe thermal-hydraulic conditions than expected, which contributed, along with other factors, to the rapid SG tube wall degradation.

This appendix discusses the following initiating events that can potentially create pressure differences considerably exceeding normal operating pressure across the SG tube boundaries:

- ATWS
- large SSBs

Several other scenarios could cause pressure differences across SG tubes exceeding normal operating pressure. Station blackout (SBO) scenarios would demand frequent lifting of main steam safety valves (MSSVs), followed by one of them sticking open. Such scenarios are bounded by L-SSB and they have significantly smaller occurrence probabilities.

### C.2.1 ATWS Event

Given the failure of the reactor protection system (RPS) to trip the reactor, the RCS system pressure is questioned to ensure that the reactor vessel is not pressurized to a greater extent than the design pressure. If the RCS pressure exceeds design pressure, core damage is assumed.

The ATWS event tree has the following events arranged in the approximate order in which they would be expected to occur after a failure to scram the reactor, given a transient event. Figure C-1 shows a partial ATWS event tree developed to discuss the Type-II C-SGTR issues. A transient event is used in this example as the initiator; other initiating events of lesser frequency could also be followed by ATWS scenarios.

(1) IE-TRANS

The first top event refers to the initiating event that creates the demand for a reactor trip (in this case, a transient).

(2) RPS

This top event signifies that a transient occurred and the RPS failed to trip the reactor. Credit can be taken for a manual trip in a short time—say, within a minute—but not before the pressure peak has been realized. There are several options for manual trip that can be effective for all ATWS scenarios except those caused by mechanical failures of a sufficient number of rods to inset. There is a high likelihood of success for the operators to perform a manual scram after observing compelling alarms and signals in the main control room.

(3) PR-REL

This top event represents success or failure of the reactor pressure vessel. Success implies that the ATWS event did not increase the RCS pressure above the reactor vessel design pressure boundary. Success also implies that the RCS relief valves opened to relieve RCS pressure.

Success requires that the RCS pressure be limited to less than 22 MPa (3,200 psi). This implies a favorable moderator temperature coefficient. Above this pressure, unpredictable pressure boundary and component failures are assumed to occur. Success also requires three-of-three safety relief valves (SRVs) and two-of-two power-operated relief valves (PORVs) to open and relieve RCS pressure.

Event Tree Nodes 4 and 5 are intended to help calculate the probability of getting a leak or a C-SGTR, given that ATWS pressure relief was successful, but the pressure difference across SG tubes exceeded the normal operational values; namely, it was in the range of ΔP = (6.89–20.6 MPa (1,000–3,300 psi). The upper values of this pressure range could only be reached if the secondary side were also depressurized. That scenario would be highly unlikely, since the heat removal is done through SGs with auxiliary feedwater (AFW) pumps operating. The highest ΔP of interest is, therefore, 15.2 MPa (2,200 psi) unless failure of the AFW pump is also assumed.

The nature of these two event tree nodes is dictated by how the conditional C-SGTR probabilities are calculated for Type-II challenges and how the results are binned. Appendix F provides a detailed discussion of these calculations, and Section C-3 summarizes them.

Section C-3 gives the estimation of some values for these event tree nodes.

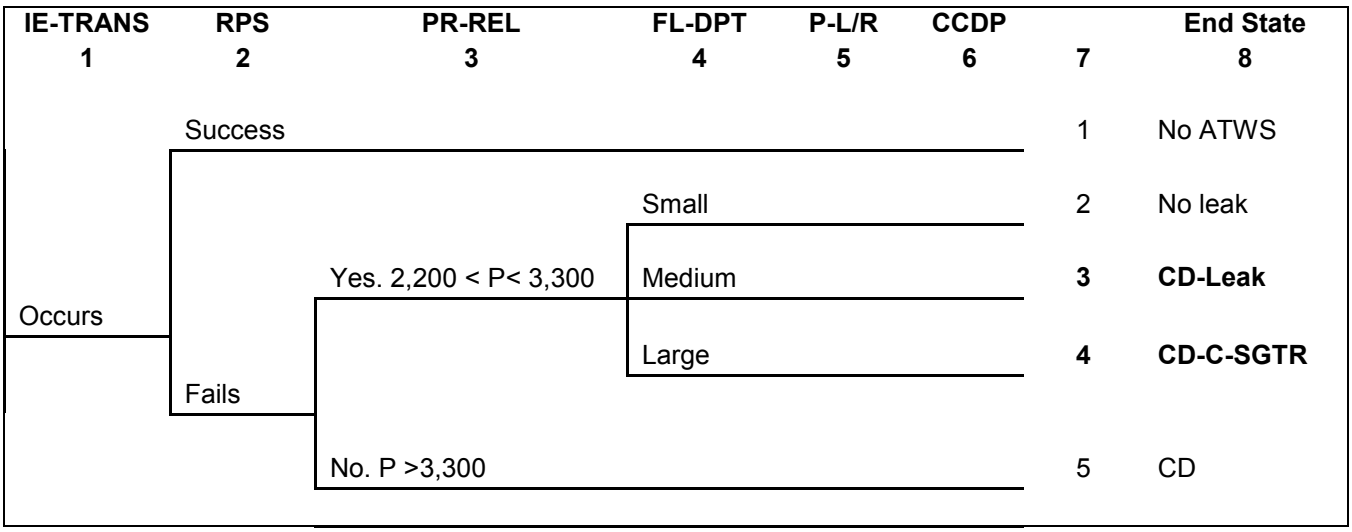


**Figure C-1 ATWS event tree top events to address Type-II C-SGTR**

(4) FL-DPT

This node represents the probability of having a “small,” “medium,” or “large” flaw depth, given that a flaw has originated since the last refueling outage. Any flaws of a depth of 40 percent or less are assumed identified and their tubes plugged, if they occurred before the last outage.

(5) P-L/R

This node represents the probability of leak or C-SGTR, given that a flaw with a depth specified in the FL-DPT node exists. No credit is taken for this event tree node in the current calculations (e.g., set equal to 1.0 when the critical size $A_c$ is reached).

(6) CCDP

This is the conditional core damage probability (CCDP) assigned to the sequence defined so far with Nodes 1 through 5 in the event tree. This CCDP represents the additional failures needed to reach the core damage end state, given that the sequence in question has progressed to the point defined by Nodes 1 through 5.

The event tree Sequences 3 and 4 in column 7 of the figure are the new potential core damage sequences associated with the Type-II C-SGTR challenges. Sequence 4 represents a sequence with a C-SGTR end state, in which an integrated tube break size equivalent to a full guillotine break of one or more tubes is created by the Type-II challenge. The CCDP for this sequence is estimated by crediting manual scram but failing the emergency boration (EB). It is conservatively assumed that the operation of EB cannot be ensured after C-SGTR, so a bounding failure rate of one is assigned for EB. Sequence 3 represents integrated tube break sizes less than the one above, in which CVCS would be able to make up the RCS inventory.

Using the values in Section C-3, Sequences 3 and 4 are quantified (their CDF values are estimated), as shown in Figure C-2.

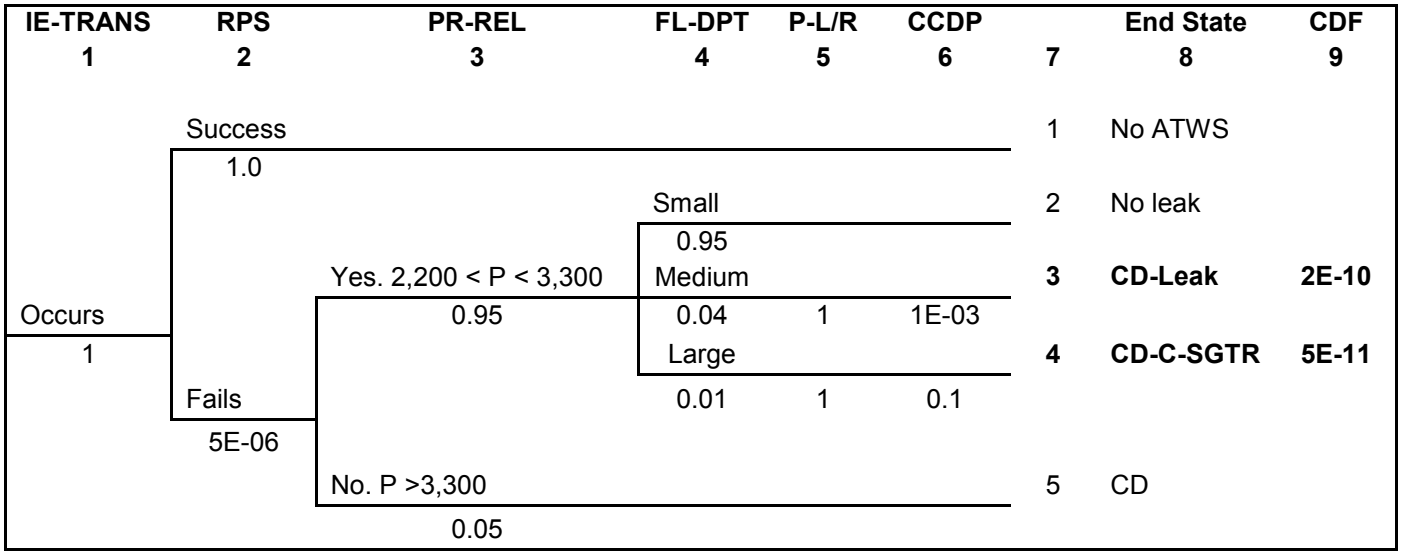


**Figure C-2 ATWS event tree top events to address Type-II C-SGTR—example quantification**

### C.2.2 Large Secondary-Side Break Event

Given an initiating event like a large steamline break (SLB) or stuck-open secondary-side valves, L-SSBs, it is possible for a large delta P across the SG tubes to be generated. This pressure difference can be as high as 15.9 MPa (2,300 psi), assuming that the secondary-side pressure drops to zero at once and the primary pressure is at 15.9 MPa (2,300 psi) initially. The primary pressure is expected to start dropping because of the rapid cooldown.

Note that the size of the SSB, large, that would cause a significant increase in delta P across the SG tubes is not specified. In fact, a cursory examination of main steamline events reported in LERs points out that almost all such events have small steam leaks that do not even cause a reactor trip but eventually may end up with a manual trip.

The L-SSB event tree has the following events arranged in the approximate order in which they would be expected to occur. Figure C-3 shows for a partial L-SSB event tree developed to discuss the Type-II C-SGTR issues.

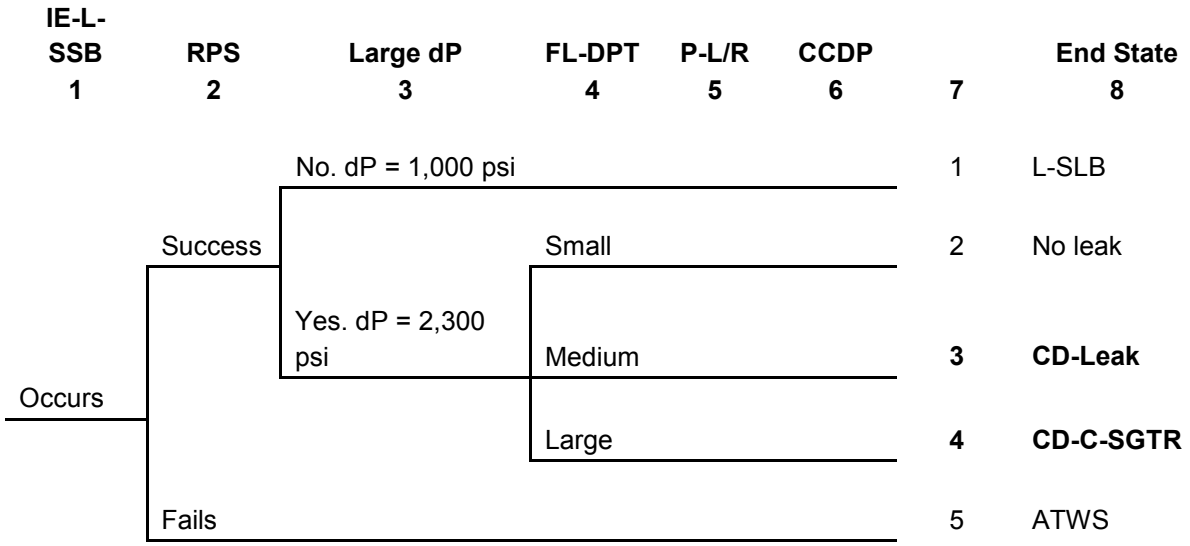


**Figure C-3 L-SSB event tree top events to address Type-II C-SGTR**

(1) IE-L-SSB

The first top event refers to the initiating event of an L-SSB, such as a large SLB or stuck-open secondary-side valves.

(2) RPS

This top event addresses the need for a reactor trip. Failure of RPS would lead to an ATWS event, which was already discussed in the previous section and is not pursued any further here.

(3) LARGE-DP

This top event discusses whether the event across the SG tubes creates a large differential pressure (DP). For the purposes of this appendix, it is postulated that the nature of the event creates a large DP in the range of 6.9–15.9 MPa (1,000–2,300 psi).

Event Tree Nodes 4 and 5 are intended to help calculate the probability of getting a leak or a C-SGTR, given that a Type-II challenge is created.

Section C.3 gives the estimates of some values for these event tree nodes.

(4) FL-DPT

This node represents the probability of getting a “small,” “medium,” or “large” flaw depth, given that a flaw has originated since the last refueling outage. Any flaws with a depth of 40 percent or less are assumed identified and their tubes plugged, if they occurred before the last outage.

(5) P-L/R

This node represents the probability of leak or C-SGTR, given that a flaw with a depth specified in the FL-DPT node exists. No credit is taken for this event tree node in the current calculations (e.g., set equal to 1.0 when the critical size $A_c$ is reached).

(6) CCDP

This is the CCDP assigned to the sequence defined so far with Node 1 through 5 in the event tree. This CCDP represents the additional failures needed to reach a core damage end state, given that the sequence in question has progressed to the point defined by Nodes 1 through 5.

The event tree Sequences 3 and 4 in column 7 of the figure are the new potential core damage sequences associated with the Type-II C-SGTR challenges. Sequence 4 represents a sequence with a C-SGTR end state, in which an integrated tube break size equivalent to a full guillotine break of one or more tubes is created by the Type-II challenge. In such sequences, the CCDP accounts for the following two additional possible failures:

(1) a higher probability for the failure of high-pressure injection, accounting for the possible termination of injection if the operators do not recognize the occurrence of C-SGTR

(2) a higher probability of isolating the affected SG because main steam isolation valves (MSIVs) might have failed to close as indicated by the initiator.

Sequence 3 represents integrated tube break sizes less than the above, in which the CVCS would be able to make up the RCS inventory.

Using the values in Section C.3, Sequences 3 and 4 are quantified (their CDF values are estimated), as shown in Figure C-4.

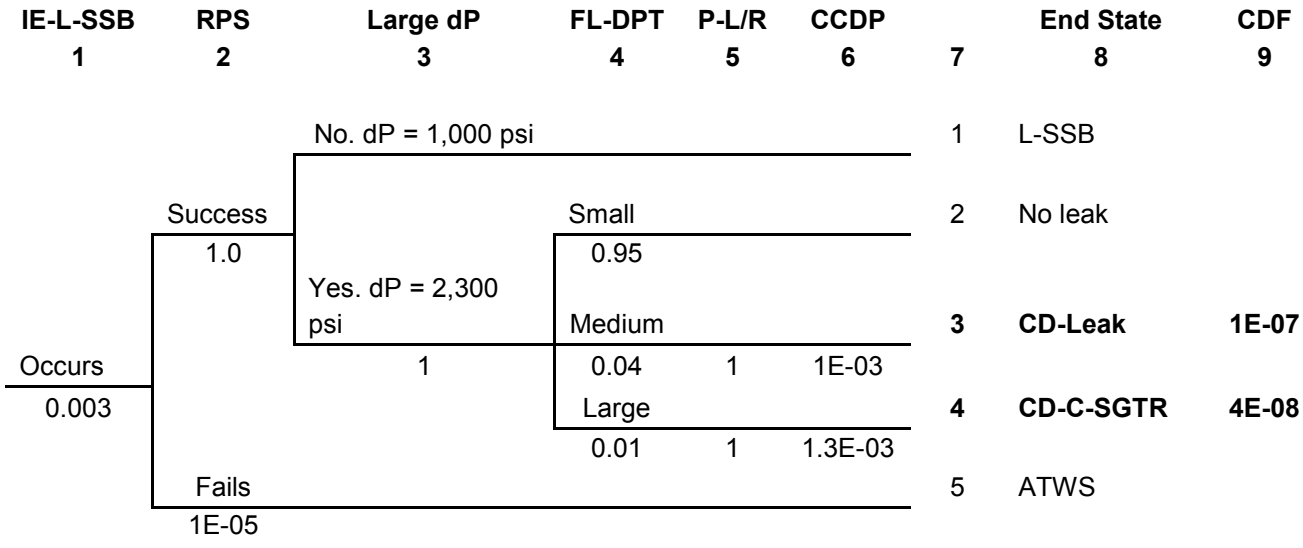


**Figure C-4 L-SSB event tree top events to address Type-II C-SGTR—example quantification**

## C.3 Example for Estimating CDF from Type-II C-SGTR Challenges

The event tree models described in Figures C-1 and C-3 can be quantified to illustrate the model usage and the resulting C-SGTR frequencies. Although these C-SGTR frequencies are for illustration purposes and apply to the cases studied, their values are deemed to be representative of similar plant-specific sequences, as long as the specific plant in question is not an outlier for the event tree nodes considered in the models.

The following data quantify the two event trees mentioned above:

(1) Initiating-event frequency

For the ATWS event, a transient initiating-event frequency of 1 per year is used. The current standardized plant analysis risk (SPAR) model frequency is 0.69 events per year. Other transients have considerably lower frequencies.

For the L-SSB event, a frequency of 0.001 per year is generally used. SPAR models do not have a frequency for such an event. Considering the more than 3,000 plant years of pressurized-water reactor (PWR) experience for U.S. domestic and similar French plants, postulating one such event per 1,000 years of operation is deemed reasonable for this illustration. The location of an SLB could be inside or outside the containment. Breaks inside the containment do not contribute to containment bypass probability, and MSIVs could isolate breakers outside containment. Bounding calculations in Section 7.4 also show that the SLB scenarios followed by pressure-induced C-SGTR have small contributions to both large early release frequency (LERF) and to CDF. Other events, however, such as a spurious opening followed by sticking of MSSVs or SG PORVs could also contribute to a transient with rapid secondary depressurization. It should be noted that the SG PORVs could be isolated by manually closing the block valves, if available. Although the closure of block valves may not occur in time to prevent C-SGTR, it could be credited for isolating the faulted SG after C-SGTR occurred. Considering these other events, a bounding frequency of $3X10^{-3}$/yr from information available in NUREG/CR-6928, “Industry-Average Performance for Components and Initiating Events at U.S. Commercial Nuclear Power Plants,” issued February 2007, is assigned to this class of initiators.

(2) RPS success/failure

The failure of the reactor protection system from all failure mechanisms is assigned a probability of $5X10^{-5}$ per demand. This includes potential credit for the operator action to trip the reactor early on, based on the early symptoms of transient and before the scram signal is initiated. The early symptoms generally include applicable alarms and cues that are observed in the main control room. SPAR model probability for this failure is generally lower than this value.

(3) Failure of RCS pressure relief (thus avoiding high delta P across the SG tube boundary)

For L-SSB, a failure probability of 1 is used, since the nature of the initiating event causes the high delta P.

(4) and (5) Probability of having at least one (large) SG tube subject to C-SGTR or leak.
Probability of C-SGTR or leak, if such a tube is present and high delta occurs

Appendix F discusses the calculation of these probabilities for the example case in Section F-2 for C-SGTR and Section F-3 for SGTR-leak. The highest probability for C-SGTR and SGTR-leak for ATWS or L-SSB scenarios is estimated to be 0.01 and 0.043, respectively. This is the probability estimate based on the example Westinghouse plant at cycle 15 of operation.

(6) Sequence CCDP for C-SGTR (or for SG leak sequence), given high delta P and large flaws

For an ATWS event, a screening CCDP of 0.1 is used, given C-SGTR.

The CCDP value for L-SSB events given C-SGTR is taken as $1.3X10^{-3}$. This value is an order of magnitude higher than those in SPAR models (with SGTR event CCDPs in the range of $10^{-4}$ and $10^{-5}$). This order of magnitude increase in CCDP is postulated to allow for presumed complications in the sequence, potentially increasing operator failure probabilities.

Because an SG-leak sequence is considerably more benign and the CVCS can cope with it, a slightly lower CCDP of $1\ X10^{-3}$ is used.

These values are placed in the event tree model to obtain C-SGTR (and SG leak) sequence frequencies for the events studied. Figures C-2 and C-4 give the quantification results.

These results are deemed to be prudently conservative. Section C.4 gives conclusions about Type-II challenges to the SG tubes based on these illustrative examples.

## C.4 Conclusions

This appendix examines the pressure-induced C-SGTR challenges (Type-II C-SGTR challenges) by referring to specific examples. The examples cover two main Type-II challenge sources:

(6) A sudden pressure spike in the primary side, exemplified by an ATWS event
(7) A sudden pressure drop on the secondary side, exemplified by L-SSBs

By referring to Figure C-2, one concludes that C-SGTR frequencies for ATWS events are not risk significant for the cases studied in this example. This assertion is deemed to be generic for all PWRs, unless a specific plant characteristic is not covered (or bounded) by the assumptions used in the ATWS case of this appendix.

As for the L-SSB event, referring to Figure C-4, one observes that with the prudently conservative assumptions used, the C-SGTR CDF frequency is on the order of $4X10^{-8}$/year. For example, for a PWR with a total CDF of $2X10^{-5}$ per year and a LERF of $1X10^{-6}$, the additional CDF and LERF would add about 2 percent to CDF and 4 percent to LERF. The actual LERF contribution may be even lower if credit is given for severe-accident management guidelines. However, there is also possible core damage contribution from those sequences defined with the end state “core damage-leak.” A simple estimation of CDF of such lesser magnitude SG tube leaks is more dependent on plant-specific modeling and, thus, more elusive.

Further fine tuning to reduce some of the conservativeness may lower this value, but then it could reduce the generic applicability of the conclusions, considering large uncertainties and variations. For example, one obvious possibility of reduction is to recognize that the “length” of a typical flaw is about 1.1 cm, or 0.43 in. (for the 600TT and 690TT flaw distributions discussed in

Appendices B and C). According to the models in the C-SGTR calculator, such a flaw cannot produce more than a leak and cannot reach the critical size of 6 square centimeters (0.93 square inch) assigned to declare a tube failure as a C-SGTR. This could reduce the above CDF for an L-SSB CDF sequence by a factor of 10. But, on the other hand, it would require consideration of multiple smaller tube flaws whose integrated failure area could reach or exceed the critical size. To avoid an explosion of analysis cases and details, further attempts to reduce the above bounding value at this time are not being carried out or recommended.

# APPENDIX D

# UNCERTAINTY AND SENSITIVITY ANALYSIS

The basic tool used to generate steam generator (SG) tube leak area estimates, hot-leg (HL) and surge-line failure probabilities is the consequential steam generator tube rupture (C-SGTR) calculator. The correlations used for these calculations are basically deterministic and would provide nonprobabilistic results unless uncertainty distributions are assigned to certain input parameters. The calculator samples the input parameters for which uncertainty distributions are specified and generates N cases (trials) for each of which it calculates outputs like integrated tube leak area (A), HL and surge-line failure times. These results are then ordered to provide estimates for $A_m$, $A_{95}$, etc. In such estimates, no underlying distribution is assumed. No sampling is done for any parameter for which distributions are not specified.

In addition, a set of sensitivity analyses designed to evaluate the impact of changing the main assumptions or input data in the base case evaluations were performed. The results of these sensitivity analyses could also support development of the Level 2 probabilistic risk assessment (PRA) models. This appendix provides a detailed discussion on the approach, assumptions, case runs, and results of the analyses for both the selected Westinghouse (W) and the Combustion Engineering (CE) plants.

## D.1 Sensitivity Analyses for the Selected W Plant

The following sensitivity analyses were performed for the example W plant. The measure of comparison used for these sensitivity analyses is based on the difference between the time when HL failure is imminent and the time when C-SGTR is expected. The ratio of this time margin over the base time margin is used as a means of qualitatively ranking the impact of sensitivity results.

### D.1.1 Base Case Evaluation and the Uncertainties Calculated

For the purposes of the uncertainty discussion in this appendix, the following base case is used:

- ZION with thermally treated Inconel 600 SG tubes
- Wnewbase; station blackout (SBO) with early failure of turbine-driven auxiliary feed water (TDAFW) pump without recovery of alternating current power, resulting in core damage, is considered. The input file provides the relevant temperatures and pressure for a time window of 300 minutes, starting from the reactor trip and SBO. Figure D-1 summarizes the main parameters of the base case. Note that the secondary side is depressurized.
- A wear-type flaw of 4 centimeters (cm) (1.6 inch (in.)) in length and 40 percent in depth was considered. Such a flaw would require tube plugging when identified at the end of the cycle.
- 2,000 trials were used with the calculator.

- "Critical Area" (Ac) is taken as 6 square centimeters ($cm^2$) (0.93 square inch ($in.^2$)), which is equivalent to a guillotine break of a single tube in this SG. The above flaw is capable of generating an equivalent leak area to the Ac.

- In this sequence, the main driver of the SG tube failure is the creep-rupture failure, induced by the high temperature at the flaw location.

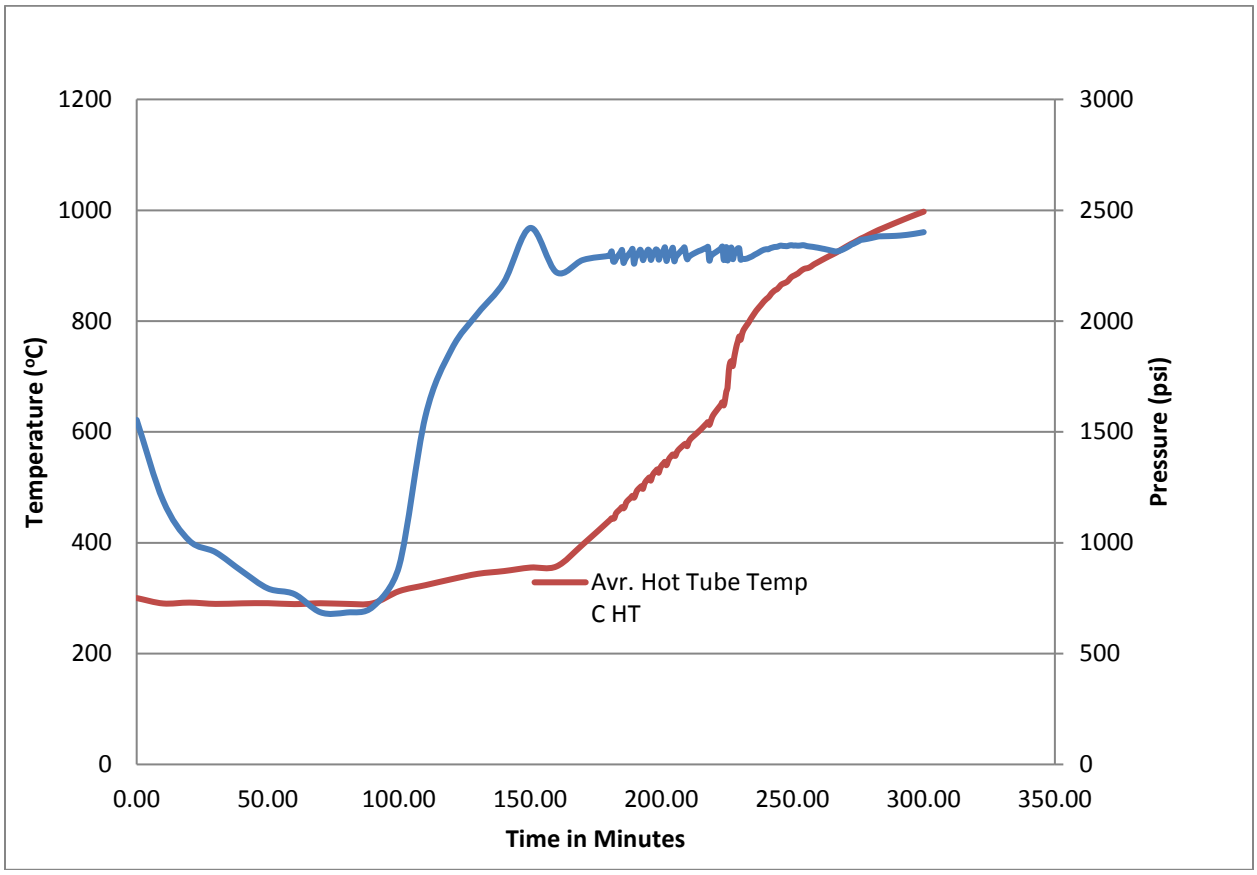


**Figure D-1 Temperature and pressure profile of the base case (at the flaw location)**

This report has already discussed the analyses associated with such a sequence in detail. Here, the focus is mainly on the uncertainty aspects of the results.

When the above case is studied, two types of output of interest are generated:

(8) Estimates of Integrated SG Tube Leak Area (A)

For this output, $A_m$, $A_{05}$, A25, $A_{50}$, $A_{75}$, and $A_{95}$, and $A_{sd}$ (standard deviation) are reported. Figure D-2 shows the output for the percentiles of the leak area distribution. Note that, although the time window of the sequence is 300 minutes, the tube failure develops in a relatively narrow time window of 230–240 minutes into the event. This is the time window shown in the figure. Table D-1 shows the relevant input-output data.

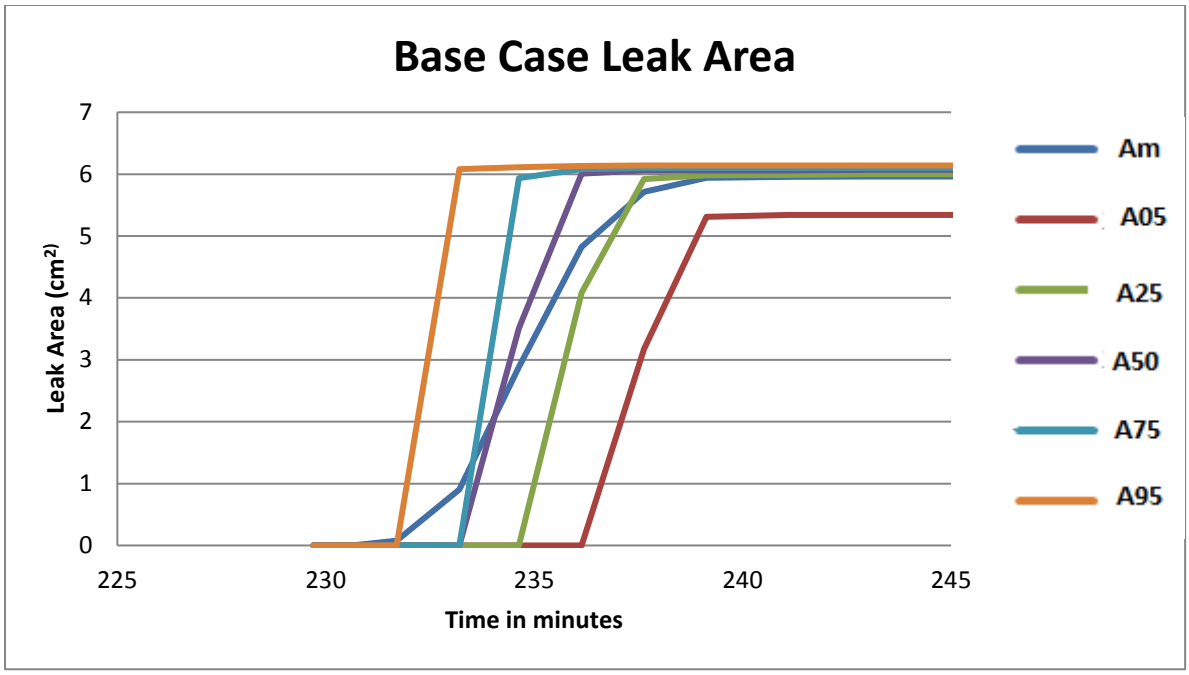


**Figure D-2 Leak area of the base case (4 cm wear flaw with 40 percent depth)**

**Table D-1 Output for the Total Leak Area in the Base Case**

| Time in Minutes | Am in °C | A0.05 | A0.25 | A0.50 | A0.75 | A0.95 | Asd | HL Failure Prob. | Surge Line Failure Prob. | Avr. Hot Tube Temp °C | HL Temp °C | Dt Between HL and Hot Tube |
|---|---|---|---|---|---|---|---|---|---|---|---|---|
| 230 | 0.00 | 0.00 | 0.00 | 0.00 | 0.00 | 0.00 | 0.14 | 1 | 0.02 | 772 | 1304 | 532 |
| 230 | 0.00 | 0.00 | 0.00 | 0.00 | 0.00 | 0.00 | 0.14 | 1 | 0.07 | 766 | 1314 | 548 |
| 231 | 0.01 | 0.00 | 0.00 | 0.00 | 0.00 | 0.00 | 0.16 | 1 | 0.10 | 776 | 1319 | 543 |
| 232 | 0.08 | 0.00 | 0.00 | 0.00 | 0.00 | 0.00 | 0.65 | 1 | 0.19 | 787 | 1332 | 545 |
| 233 | 0.90 | 0.00 | 0.00 | 0.00 | 0.00 | 6.08 | 2.10 | 1 | 0.33 | 797 | 1343 | 546 |
| **235** | **2.88** | 0.00 | 0.00 | 3.51 | 5.94 | 6.11 | 2.71 | 1 | 0.47 | **808** | 1354 | 546 |
| **236** | **4.82** | 0.00 | 4.08 | 6.01 | 6.08 | 6.13 | 1.92 | 1 | 0.59 | **819** | 1368 | 549 |
| **238** | **5.71** | 3.17 | 5.92 | 6.06 | 6.1 | 6.14 | 0.97 | 1 | 0.70 | **827** | 1374 | 547 |
| **239** | **5.94** | 5.31 | 5.98 | 6.06 | 6.1 | 6.14 | 0.37 | 1 | 0.78 | **836** | 1381 | 545 |
| **241** | **5.96** | 5.34 | 6.00 | 6.06 | 6.1 | 6.14 | 0.29 | 1 | 0.86 | **845** | 1385 | 540 |
| 243 | 5.96 | 5.34 | 6.00 | 6.07 | 6.1 | 6.14 | 0.28 | 1 | 0.91 | 855 | 1393 | 538 |
| 245 | 5.96 | 5.34 | 6.00 | 6.07 | 6.1 | 6.14 | 0.29 | 1 | 0.94 | 862 | 1394 | 532 |
| 247 | 5.96 | 5.39 | 6.00 | 6.07 | 6.1 | 6.14 | 0.29 | 1 | 0.95 | 869 | 1391 | 522 |
| 250 | 5.96 | 5.39 | 6.00 | 6.07 | 6.1 | 6.14 | 0.30 | 1 | 0.97 | 879 | 1393 | 514 |
| 252 | 5.96 | 5.39 | 6.00 | 6.07 | 6.1 | 6.14 | 0.30 | 1 | 0.97 | 886 | 1389 | 503 |
| 255 | 5.96 | 5.39 | 6.00 | 6.07 | 6.1 | 6.14 | 0.29 | 1 | 0.98 | 894 | 1388 | 494 |
| 257 | 5.96 | 5.39 | 6.00 | 6.07 | 6.1 | 6.14 | 0.29 | 1 | 0.98 | 898 | 1379 | 481 |
| 260 | 5.96 | 5.39 | 6.00 | 6.07 | 6.1 | 6.14 | 0.29 | 1 | 0.99 | 907 | 1376 | 469 |
| 263 | 5.96 | 5.39 | 6.00 | 6.07 | 6.1 | 6.14 | 0.30 | 1 | 0.99 | 915 | 1375 | 460 |
| 266 | 5.96 | 5.39 | 6.00 | 6.07 | 6.1 | 6.14 | 0.29 | 1 | 0.99 | 922 | 1377 | 455 |
| 270 | 5.96 | 5.39 | 6.00 | 6.07 | 6.1 | 6.14 | 0.29 | 1 | 0.99 | 932 | 1383 | 451 |
| 273 | 5.97 | 5.39 | 6.00 | 6.07 | 6.1 | 6.14 | 0.28 | 1 | 0.99 | 941 | 1388 | 447 |
| 277 | 5.97 | 5.39 | 6.00 | 6.07 | 6.1 | 6.14 | 0.28 | 1 | 0.99 | 950 | 1395 | 445 |
| 280 | 5.97 | 5.39 | 6.00 | 6.07 | 6.1 | 6.14 | 0.29 | 1 | 0.99 | 958 | 1401 | 443 |
| 284 | 5.97 | 5.39 | 6.00 | 6.07 | 6.1 | 6.14 | 0.29 | 1 | 0.99 | 967 | 1405 | 438 |
| 288 | 5.97 | 5.39 | 6.00 | 6.07 | 6.1 | 6.14 | 0.29 | 1 | 1.00 | 975 | 1408 | 433 |
| 292 | 5.97 | 5.39 | 6.00 | 6.07 | 6.1 | 6.14 | 0.29 | 1 | 1.00 | 982 | 1410 | 428 |
| 296 | 5.97 | 5.39 | 6.00 | 6.07 | 6.1 | 6.14 | 0.29 | 1 | 1.00 | 990 | 1412 | 422 |
| 300 | 5.97 | 5.39 | 6.00 | 6.07 | 6.1 | 6.14 | 0.29 | 1 | 1.00 | 997 | 1414 | 417 |

(2) Estimates of HL and Surge-Line Failure Probabilities

The calculator also provides estimates of HL and surge-line failure probabilities as a function of time, without reporting uncertainties. Figure D-3 and Table D-2 show the probabilities for this base case. Also reported are the ratios of the average tube leak area to the critical leak area ($A_m$ / $A_c$).

Because HL failure occurs earlier than surge-line failure in this case, it will be used for further discussions.

The above two sets of estimates of tubes and HL failure are done independently. As long as the leak area is small (less than the critical area), the reactor coolant system (RCS) is deemed to not depressurize sufficiently to affect the temperature and pressures experienced by other parts of the RCS; thus, this independence assumption is valid for this "small" range of integrated SG leaks (from one or more flaws).

One can define a simple measure of comparison between the HL failure time and the tube failure time. This measure is called the Margin in minutes and is defined as:

Margin = {time in minutes of failure of HL when its failure probability reaches 1} –
{time in minutes of integrated SG tube leak area reaches $A_c$: $A_m/A_c$=1}

For this base case, the margin is -18 minutes (221–239 = 18 minutes), as reported in Table D-3. Large, negative margin is considered to be favorable, because it would arrest or reduce SG tube leak area generation or its fission product release. It should be noted that Table D-2 shows that there is a period of about 20 minutes when a nonzero probability of HL is estimated. Therefore, any negative margin value greater than 20 minutes will be indicative of zero probability of C-SGTR.

Figure D-2 also shows that the spread in the time of tube failure is very narrow, although the leak size has a range of 0–6 $cm^2$ (0–0.93 $in.^2$), which reaches $A_c$. The following should be noted:

- No uncertainty distributions are provided for the thermal-hydraulic (TH) input file.
- No uncertainty results are reported for HL and surge-line failures.

Thus, deriving robust uncertainty insights solely based on the calculator should not be expected. Sensitivity analyses on what is deemed as other parameters of significance could be and should be done.

Because the margin as defined above is a simple yet important indicator of avoidance of early and large fission product releases, this appendix offers some sensitivity analyses to determine the uncertainty spread in the margin.

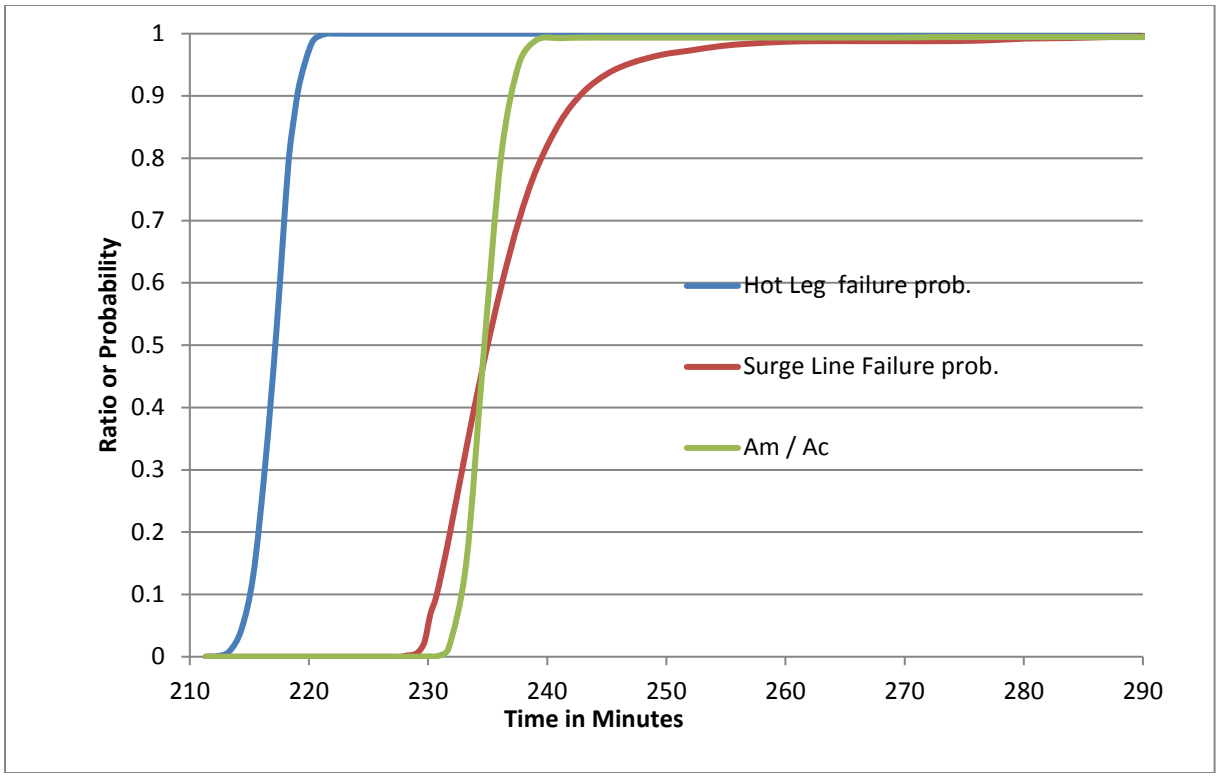


**Figure D-3 Probabilities of HL and surge-line failure**

**Table D-2 Probabilities of HL and Surge Line (Cont.)**

| Time (m) | HL Failure Prob. | Surge-Line Failure Prob. | $A_m$ / $A_c$ |
|---|---|---|---|
| 211 | 0.00 | 0.000 | 0.000 |
| 212 | 0.00 | 0.000 | 0.000 |
| 213 | 0.01 | 0.000 | 0.000 |
| 214 | 0.04 | 0.000 | 0.000 |
| 215 | 0.13 | 0.000 | 0.000 |
| 216 | 0.31 | 0.000 | 0.000 |
| 217 | 0.52 | 0.000 | 0.000 |
| 218 | 0.79 | 0.000 | 0.000 |
| 219 | 0.87 | 0.000 | 0.000 |
| 219 | 0.93 | 0.000 | 0.000 |
| 220 | 0.99 | 0.000 | 0.000 |
| 221 | 1.00 | 0.000 | 0.000 |
| 222 | 1.00 | 0.000 | 0.000 |
| 223 | 1.00 | 0.000 | 0.000 |
| 224 | 1.00 | 0.000 | 0.000 |
| 224 | 1.00 | 0.000 | 0.000 |
| 225 | 1.00 | 0.000 | 0.000 |
| 225 | 1.00 | 0.000 | 0.000 |
| 226 | 1.00 | 0.000 | 0.000 |
| 226 | 1.00 | 0.000 | 0.000 |
| 227 | 1.00 | 0.000 | 0.000 |
| 227 | 1.00 | 0.000 | 0.000 |
| 228 | 1.00 | 0.000 | 0.000 |
| 228 | 1.00 | 0.002 | 0.000 |
| 229 | 1.00 | 0.003 | 0.000 |
| 229 | 1.00 | 0.008 | 0.000 |
| 230 | 1.00 | 0.024 | 0.001 |
| 230 | 1.00 | 0.070 | 0.001 |
| 231 | 1.00 | 0.100 | 0.001 |
| 232 | 1.00 | 0.190 | 0.013 |
| 233 | 1.00 | 0.330 | 0.150 |
| 235 | 1.00 | 0.470 | 0.480 |
| 236 | 1.00 | 0.590 | 0.800 |
| 238 | 1.00 | 0.700 | 0.950 |
| 239 | 1.00 | 0.780 | 0.990 |
| 241 | 1.00 | 0.860 | 0.990 |
| 243 | 1.00 | 0.910 | 0.990 |
| 245 | 1.00 | 0.940 | 0.990 |
| 247 | 1.00 | 0.950 | 0.990 |
| 250 | 1.00 | 0.970 | 0.990 |

**Table D-2 Probabilities of HL and Surge Line (Cont.)**

| Time (m) | HL Failure Prob. | Surge-Line Failure Prob. | $A_m$ / $A_c$ |
|---|---|---|---|
| 252 | 1.00 | 0.970 | 0.990 |
| 255 | 1.00 | 0.980 | 0.990 |
| 257 | 1.00 | 0.980 | 0.990 |
| 260 | 1.00 | 0.990 | 0.990 |
| 263 | 1.00 | 0.990 | 0.990 |
| 266 | 1.00 | 0.990 | 0.990 |
| 270 | 1.00 | 0.990 | 0.990 |
| 273 | 1.00 | 0.990 | 0.990 |
| 277 | 1.00 | 0.990 | 0.990 |
| 280 | 1.00 | 0.990 | 0.990 |
| 284 | 1.00 | 0.990 | 0.990 |
| 288 | 1.00 | 1.000 | 0.990 |
| 292 | 1.00 | 1.000 | 0.990 |
| 296 | 1.00 | 1.000 | 0.990 |
| 300 | 1.00 | 1.000 | 0.990 |

**Table D-3 Calculation of Margin for the Base Case**

| | | Time in Minutes | | |
|---|---|---|---|---|
| | | **NUREG/ CR-6995** | **Calculator** | **Comment** |
| | | | | |
| 1 | Event starts | 000 | 000 | |
| 2 | SG dryout | 100 | | |
| 3 | Evacuation starts | | | 120 |
| 4 | HL fails 13% | | 215 | |
| 5 | First fuel rod clad rupture | 217 | | |
| 6 | HL fails 52% | | 217 | |
| 7 | HL fails 100% | | 221 | |
| 8 | HL 1 fails by creep rupture | 227 | | |
| 9 | SL fails 18% | | 232 | |
| 10 | Hottest tube creep-rupture failure | 233 | | |
| 11 | SL fails 59% | | 236 | |
| 12 | Hot tube fails 6 $cm^2$ (1 tube equivalent) | | 239 | |
| 13 | Hot tube fails xx $cm^2$ (n tube equivalent) | | | |
| 14 | Hot tube fails max 6 $cm^2$ (1 tube equivalent) | | 239 | |
| 15 | SL fails 100% | | 280 | |
| 16 | Evacuation ends for internal events | | | 360 |
| 17 | Evacuation ends for external events | | | 600 |
| | | | | |
| | Margin = HL fails 100%—Hot tube fails 6 $cm^2$ (0.93 $in.^2$) | | **-18** | |
| | | | | |

The definition of margin is based on the crucial TH assumption that a full break of a single SG tube (6 $cm^2$ (0.93 $in.^2$)) would not depressurize the RCS to prevent RCS failure elsewhere.

Hot tube fraction = 1.0 (all flaws are assumed to be on the hot tubes)

NUREG/CR-6995, "SCDAP/RELAP5 Thermal-Hydraulic Evaluations of the Potential for Containment Bypass During Extended Station Blackout Severe Accident Sequences in a Westinghouse Four-Loop PWR" (RELAP 2010)

The following sensitivity calculations are made to seek some insights into these questions:

**Case 1: Sensitivity on delta-T (between HL and hot tube)**

Assume that the delta-T between the HL and hot tube temperatures is only 50 percent as large as the base case. Make a run where, at each time step, the base case delta-T is cut in half by reducing the HL temperature.

**Case 2: Sensitivity to HL thickness (assessing the potential effect of an overlay)**

Although placement of weld overlays at the HL safe-ends may provide a safety enhancement against potential cracks and resulting RCS leaks at those locations, an undesirable side effect may be to delay the expected earlier failure of the HL, thus reducing the margin. To estimate the effect of an overlay on the margin, the HL thickness is increased in this case.

The paragraphs below discuss the results of these cases.

Throughout this report, it is deemed that, in temperature challenges, where core damage has already occurred, the secondary side is depressurized. A small preexisting leak area of 3.22 $cm^2$ (0.5 $in.^2$) is shown in previous TH analyses to be sufficient to depressurize the secondary side. Another sensitivity case run, reported below, questioned: "what would be the effect on the margin if the secondary side is not depressurized?"

**Case 3: Secondary side not depressurized (see Section D.1.4)**

This case is not made to address uncertainty but to illustrate the effect of the secondary side being pressurized on the margin.

Appendix E provides additional sensitivity cases with multiple tube flaws.

### D.1.2 Sensitivity on Temperature Difference between HL and Hot Tube

The TH input file for this case is a modified version of the Wnewbase-short, where the HL temperature at each time step is reduced so that the difference between it and the hot tube temperature is only 50 percent of the difference in the base case.

Table D-4 gives the resulting margin calculation. The margin for this case is -14 minutes, reduced by 4 minutes due to a significant reduction in the delta T. Thus, even if the initial TH analysis is off by a factor of 2 in estimating the temperature difference between the HL and the hot tube, where the flaw is located, the margin is not significantly affected.

**Table D-4 Margin with Smaller Temperature Difference between HL and Hot Tube**

| | | | Time in Minutes | |
|---|---|---|---|---|
| | | NUREG/ CR-6995 | Calculator | Comment |
| | | | | |
| 1 | Event starts | 000 | 000 | |
| 2 | SG dryout | 100 | | |
| 3 | Evacuation starts | | | 120 |
| 4 | HL fails 12% | | 224 | |
| 5 | First fuel rod clad rupture | 217 | | |
| 6 | HL fails 56% | | 225 | |
| 7 | HL fails 100% | | 225 | |
| 8 | HL 1 fails by creep rupture | 227 | | |
| 9 | SL fails 17% | | 232 | |
| 10 | Hottest tube creep-rupture failure | 233 | | |
| 11 | SL fails 57% | | 236 | |
| 12 | Hot tube fails 6 $cm^2$ (1 tube equivalent) | | 239 | |
| 13 | Hot tube fails xx $cm^2$ (n tube equivalent) | | | |
| 14 | Hot tube fails max 6 $cm^2$ (1 tube equivalent) | | 239 | |
| 15 | SL fails 100 % | | 280 | |
| 16 | Evacuation ends for internal events | | | 360 |
| 17 | Evacuation ends for external events | | | 600 |
| | | | | |
| | Margin = HL fails 100%—Hot tube fails 6 $cm^2$ (0.93 $in.^2$) | | **-14** | |
| | | | | |

The definition of margin is based on the crucial TH assumption that a full break of a single SG tube (6 $cm^2$ (0.93 $in.^2$) would not depressurize the RCS to prevent RCS failure elsewhere.

Hot tube fraction = 1.0 (all flaws are assumed to be on the hot tubes)

NUREG/CR-6995 (RELAP 2010)

### D.1.3 Sensitivity to HL Thickness (Potential Effect of an Overlay)

This sensitivity case examines the effect of an increase in HL thickness due to a weld overlay, on the margin. For this purpose, the HL thickness of 6.35 cm in the base case is increased by 50 percent, to 9.5 cm (3.74 in.). This increase is deemed to be a fair representation of what a weld overlay would provide.

Table D-5 gives the resulting margin calculation. The margin for this case is -16 minutes, reduced by 2 minutes because of a significant increase in HL thickness, which is presumed to delay HL failure. Thus, even if the HL contains weld overlay, which increases its thickness by 50 percent, the margin is not significantly affected.

**Table D-5 Margin with Thicker HL**

| | | | Time in Minutes | |
|---|---|---|---|---|
| | | NUREG/ CR-6995 | Calculator | Comment |
| | | | | |
| 1 | Event starts | 000 | 000 | |
| 2 | SG dryout | 100 | | |
| 3 | Evacuation starts | | | 120 |
| 4 | HL fails 18% | | 219 | |
| 5 | First fuel rod clad rupture | 217 | | |
| 6 | HL fails 61% | | 220 | |
| 7 | HL fails 100% | | 223 | |
| 8 | HL 1 fails by creep rupture | 227 | | |
| 9 | SL fails 19% | | 232 | |
| 10 | Hottest tube creep-rupture failure | 233 | | |
| 11 | SL fails 58% | | 236 | |
| 12 | Hot tube fails 6 $cm^2$ (1 tube equivalent) | | 239 | |
| 13 | Hot tube fails xx $cm^2$ (n tube equivalent) | | | |
| 14 | Hot tube fails max 6 $cm^2$ (1 tube equivalent) | | 239 | |
| 15 | SL fails 100 % | | 288 | |
| 16 | Evacuation ends for internal events | | | 360 |
| 17 | Evacuation ends for external events | | | 600 |
| | | | | |
| | Margin = HL fails 100%—Hot tube fails 6 $cm^2$ (0.93 $in.^2$) | | **-16** | |
| | | | | |

The definition of margin is based on the crucial TH assumption that a full break of a single SG tube (6 $cm^2$ (0.93 $in.^2$)) would not depressurize the RCS to prevent RCS failure elsewhere.

Hot tube fraction = 1.0 (all flaws are assumed to be on the hot tubes)

NUREG/CR-6995 (RELAP 2010)

### D.1.4 Secondary Side Not Depressurized

To assess the effect of the secondary side not being depressurized, the TH input file is modified to have the secondary pressure set at 7.6 megapascals (MPa) (1,100 pounds per square inch (psi)), the remaining input values being the same as the base case. Figure D-4 summarizes the main parameters of this case. The TH input file for this case is labeled as TH-wnewbase-short-1100psi.txt.

Table D-6 summarizes the output of the case. The margin is calculated to be 45 minutes. This large margin seems to indicate that the tube is more sensitive than the HL to pressure reduction at the creep-rupture failure temperature range. In fact, as seen in the table below, the HL failure time is not affected, but the tube flaw failure time is considerably delayed.

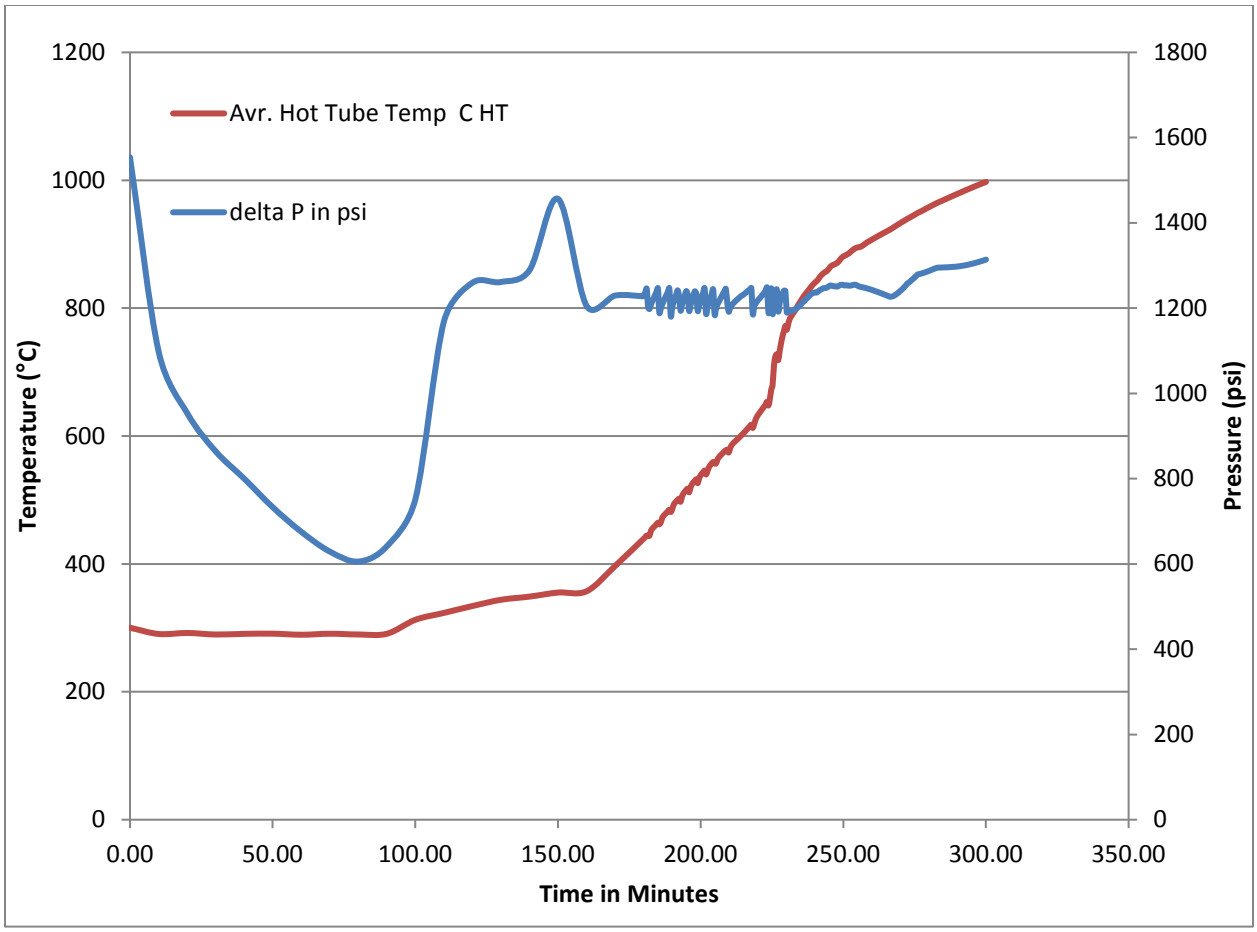


**Figure D-4 Temperature and pressure profile of the case where secondary side is not depressurized**

**Table D-6 Margin with Secondary Side NOT Depressurized (at 1,100 psi)**

| | | | Time in Minutes | |
|---|---|---|---|---|
| | | NUREG/ CR-6995 | Calculator | Comment |
| | | | | |
| 1 | Event starts | 000 | 000 | |
| 2 | SG dryout | 100 | | |
| 3 | Evacuation starts | | | 120 |
| 4 | HL fails 13% | | 215 | |
| 5 | First fuel rod clad rupture | 217 | | |
| 6 | HL fails 55% | | 217 | |
| 7 | HL fails 100% | | 221 | |
| 8 | HL 1 fails by creep rupture | 227 | | |
| 9 | SL fails 16% | | 232 | |
| 10 | Hottest tube creep-rupture failure | 233 | | |
| 11 | SL fails 55% | | 236 | |
| 12 | Hot tube fails 6 $cm^2$ (1 tube equivalent) | | 266 | |
| 13 | Hot tube fails xx $cm^2$ (n tube equivalent) | | | |
| 14 | Hot tube fails max 6 $cm^2$ (1 tube equivalent) | | 266 | |
| 15 | SL fails 100% | | 280 | |
| 16 | Evacuation ends for internal events | | | 360 |
| 17 | Evacuation ends for external events | | | 600 |
| | | | | |
| | Margin = HL fails 100%—Hot tube fails 6 $cm^2$ (0.93 $in.^2$) | | **-45** | |
| | | | | |

The definition of margin is based on the crucial TH assumption that a full break of a single SG tube (6 $cm^2$ (0.93 $in^2$)) would not depressurize the RCS to prevent RCS failure elsewhere.

Hot tube fraction = 1.0 (all flaws are assumed to be on the hot tubes)

NUREG/CR-6995 (RELAP 2010)

The margins are as follows:

| Case Name | Margin | T HL—T Hot Tube |
|---|---|---|
| Base Case | -18 minutes | 221–239 |
| Secondary NOT depressurized | -45 minutes | 221–266 |

### D.1.5 Late Failure of Turbine-Driven AFW Pump

This case study is performed for the W SBO scenario number 153:

**Station Blackout with Failure of TDAFW Pump after Battery Depletion:** The TDAFW pump is initially considered available, but it fails a short time after battery depletion due to loss of direct current (dc).

The study modeled the normal reactor coolant pump seal leakage of 79.5 liters per minute (Lpm) (21 gallons per minute (gpm)) per pump. Operator action to depressurize SGs at 30 minutes by opening at least one SG atmospheric dump valve or SG PORV per SG drops the primary pressure below 4.82 MPa (700 psi). This actuates the accumulator discharge.

Table D-7 shows the input TH parameters taken from the file named 153short-end. Other input files used are as follows:

- ZION- TT600
- Flaw-W4-40.txt

Table D-8 summarizes the results. As shown in this table, the margin is -22 minutes, which is close to the base case margin of -18 minutes. However, both the HL failure and C-SGTR occur much later than in the base case—in about 13 hours into the SBO event. For the base case, this time was 4 hours into the SBO event. The additional 7 hours gained could allow for evacuation, even for the SBOs that may follow seismic or external flooding events.

## Table D-7 T&H Input Parameters for Case 153 (Cont.)

| Time in Min-utes | Primary Pressure (Pa) | Surge-Line Temperature (°C) | HL Temperature (°C) | Hot Tube Temperature (°C) | Cold Tube Temperature (°C) | Secondary Pressure (Pa) | Primary Pressure in psi | Secondary Pressure in psi | Delta P in psi | Avr. Hot Tube Temp °C HT | HL to Tube Hot Side Delta T |
|---|---|---|---|---|---|---|---|---|---|---|---|
| 600 | 11187857 | 317 | 309 | 316 | 316 | 1816161 | 1622 | 263 | 1359 | 316.5 | -7.2 |
| 604 | 11953517 | 321 | 318 | 323 | 323 | 1562022 | 1733 | 226 | 1507 | 323.5 | -5.1 |
| 608 | 12497496 | 320 | 314 | 321 | 321 | 1321353 | 1812 | 192 | 1621 | 320.7 | -6.3 |
| 612 | 13511729 | 320 | 317 | 320 | 320 | 1114784 | 1959 | 162 | 1798 | 320.4 | -3.5 |
| 616 | 14437555 | 320 | 320 | 321 | 321 | 937642 | 2093 | 136 | 1957 | 320.6 | -0.5 |
| 620 | 15378100 | 320 | 324 | 321 | 321 | 787000 | 2230 | 114 | 2116 | 320.8 | 3.0 |
| 624 | 15935722 | 322 | 336 | 331 | 331 | 659257 | 2311 | 96 | 2215 | 330.8 | 5.5 |
| 628 | 16616382 | 333 | 333 | 344 | 344 | 558371 | 2409 | 81 | 2328 | 344.4 | -11.0 |
| 632 | 16439831 | 332 | 334 | 343 | 343 | 465514 | 2384 | 67 | 2316 | 342.6 | -8.9 |
| 636 | 17106500 | 332 | 335 | 342 | 342 | 388108 | 2480 | 56 | 2424 | 341.7 | -6.5 |
| 640 | 17552148 | 332 | 337 | 341 | 341 | 323280 | 2545 | 47 | 2498 | 340.9 | -3.8 |
| 644 | 16971320 | 345 | 342 | 343 | 343 | 268863 | 2461 | 39 | 2422 | 343.1 | -1.4 |
| 648 | 17878938 | 349 | 350 | 353 | 353 | 224552 | 2592 | 33 | 2560 | 353.0 | -3.3 |
| 652 | 16650259 | 351 | 350 | 351 | 351 | 186259 | 2414 | 27 | 2387 | 350.7 | -0.3 |
| 656 | 16952404 | 352 | 352 | 352 | 352 | 157992 | 2458 | 23 | 2435 | 352.1 | -0.5 |
| 660 | 16895284 | 352 | 351 | 352 | 352 | 139242 | 2450 | 20 | 2430 | 351.8 | -0.3 |
| 664 | 17016836 | 352 | 352 | 352 | 352 | 125068 | 2467 | 18 | 2449 | 352.5 | -0.4 |
| 666 | 17627418 | 355 | 353 | 355 | 355 | 119016 | 2556 | 17 | 2539 | 355.2 | -2.7 |
| 667 | 16689429 | 353 | 351 | 352 | 351 | 116987 | 2420 | 17 | 2403 | 351.6 | -0.6 |
| 668 | 16922776 | 352 | 351 | 352 | 352 | 115081 | 2454 | 17 | 2437 | 351.9 | -1.1 |
| 668 | 17383652 | 353 | 352 | 354 | 354 | 113502 | 2521 | 16 | 2504 | 354.1 | -1.9 |
| 669 | 17783698 | 355 | 354 | 356 | 356 | 112031 | 2579 | 16 | 2562 | 356.0 | -2.3 |
| 670 | 16704144 | 357 | 353 | 353 | 351 | 110248 | 2422 | 16 | 2406 | 353.2 | -0.3 |
| 671 | 17124176 | 354 | 356 | 359 | 354 | 109030 | 2483 | 16 | 2467 | 359.3 | -3.5 |
| 672 | 17433450 | 355 | 358 | 360 | 356 | 107944 | 2528 | 16 | 2512 | 360.1 | -1.7 |
| 672 | 17725334 | 356 | 361 | 363 | 358 | 106925 | 2570 | 16 | 2555 | 363.1 | -2.3 |
| 673 | 16603548 | 364 | 359 | 356 | 353 | 105650 | 2408 | 15 | 2392 | 355.7 | 3.0 |
| 674 | 16998104 | 358 | 362 | 64 | 356 | 104833 | 2465 | 15 | 2450 | 363.7 | -1.6 |
| 675 | 17214120 | 354 | 365 | 364 | 359 | 104169 | 2496 | 15 | 2481 | 364.3 | 0.4 |
| 676 | 17420130 | 355 | 367 | 367 | 361 | 103625 | 2526 | 15 | 2511 | 366.9 | 0.0 |
| 676 | 17613248 | 355 | 369 | 370 | 363 | 103102 | 2554 | 15 | 2539 | 369.5 | -0.3 |
| 678 | 16692531 | 368 | 370 | 364 | 360 | 101998 | 2420 | 15 | 2406 | 363.6 | 6.8 |
| 679 | 16964364 | 361 | 374 | 375 | 364 | 101783 | 2460 | 15 | 2445 | 375.0 | -1.4 |
| 680 | 17130560 | 354 | 376 | 375 | 366 | 101655 | 2484 | 15 | 2469 | 375.4 | 1.0 |
| 680 | 17302764 | 354 | 379 | 378 | 368 | 101566 | 2509 | 15 | 2494 | 378.3 | 0.8 |
| 682 | 17598950 | 358 | 384 | 384 | 373 | 101468 | 2552 | 15 | 2537 | 383.5 | 0.7 |
| 683 | 16488133 | 403 | 384 | 381 | 372 | 101305 | 2391 | 15 | 2376 | 380.9 | 3.0 |
| 684 | 16850458 | 372 | 389 | 388 | 373 | 101385 | 2443 | 15 | 2429 | 387.6 | 1.6 |
| 685 | 17014836 | 363 | 392 | 392 | 377 | 101427 | 2467 | 15 | 2452 | 391.9 | 0.5 |

## Table D-7 T&H Input Parameters for Case 153 (Cont.)

| Time in Min-utes | Primary Pressure (Pa) | Surge-Line Temperature (°C) | HL Temperature (°C) | Hot Tube Temperature (°C) | Cold Tube Temperature (°C) | Secondary Pressure (Pa) | Primary Pressure in psi | Secondary Pressure in psi | Delta P in psi | Avr. Hot Tube Temp °C HT | HL to Tube Hot Side Delta T |
|---|---|---|---|---|---|---|---|---|---|---|---|
| 687 | 17269158 | 363 | 398 | 396 | 381 | 101449 | 2504 | 15 | 2489 | 396.0 | 2.2 |
| 688 | 17473758 | 359 | 404 | 401 | 386 | 101438 | 2534 | 15 | 2519 | 401.3 | 2.6 |
| 690 | 17651938 | 358 | 410 | 407 | 390 | 101434 | 2560 | 15 | 2545 | 406.6 | 3.0 |
| 691 | 16515044 | 427 | 410 | 405 | 390 | 101328 | 2395 | 15 | 2380 | 405.1 | 5.3 |
| 692 | 16806486 | 382 | 416 | 408 | 389 | 101380 | 2437 | 15 | 2422 | 408.4 | 7.4 |
| 693 | 16980630 | 370 | 419 | 417 | 394 | 101419 | 2462 | 15 | 2447 | 416.9 | 2.6 |
| 695 | 17173498 | 366 | 426 | 420 | 398 | 101443 | 2490 | 15 | 2475 | 419.7 | 6.3 |
| 696 | 17335400 | 364 | 432 | 425 | 403 | 101437 | 2514 | 15 | 2499 | 424.9 | 7.3 |
| 697 | 17415656 | 356 | 435 | 427 | 405 | 101434 | 2525 | 15 | 2511 | 427.5 | 7.8 |
| 699 | 17610018 | 356 | 441 | 432 | 409 | 101431 | 2553 | 15 | 2539 | 432.0 | 8.6 |
| 700 | 17541364 | 400 | 445 | 437 | 413 | 101424 | 2543 | 15 | 2529 | 436.6 | 8.9 |
| 701 | 16712065 | 392 | 447 | 427 | 408 | 101365 | 2423 | 15 | 2409 | 427.4 | 19.6 |
| 702 | 16932056 | 375 | 451 | 442 | 412 | 101406 | 2455 | 15 | 2440 | 441.9 | 9.2 |
| 703 | 17060404 | 355 | 454 | 444 | 415 | 101422 | 2474 | 15 | 2459 | 444.4 | 10.0 |
| 704 | 17304860 | 355 | 460 | 447 | 419 | 101434 | 2509 | 15 | 2494 | 446.6 | 13.0 |
| 706 | 17532364 | 355 | 466 | 451 | 423 | 101427 | 2542 | 15 | 2527 | 451.3 | 15.0 |
| 707 | 17742650 | 355 | 472 | 456 | 427 | 101421 | 2573 | 15 | 2558 | 455.7 | 16.0 |
| 708 | 16541230 | 419 | 471 | 445 | 423 | 101337 | 2398 | 15 | 2384 | 445.0 | 26.0 |
| 709 | 16814356 | 380 | 476 | 455 | 425 | 101387 | 2438 | 15 | 2423 | 455.0 | 21.0 |
| 710 | 16960858 | 364 | 479 | 463 | 429 | 101407 | 2459 | 15 | 2445 | 462.9 | 17.0 |
| 710 | 17093302 | 354 | 482 | 465 | 431 | 101417 | 2479 | 15 | 2464 | 464.5 | 18.0 |
| 712 | 17346446 | 355 | 488 | 467 | 435 | 101425 | 2515 | 15 | 2501 | 467.3 | 21.0 |
| 714 | 17562786 | 364 | 495 | 471 | 439 | 101418 | 2547 | 15 | 2532 | 471.1 | 24.0 |
| 714 | 17644584 | 373 | 499 | 475 | 441 | 101417 | 2558 | 15 | 2544 | 474.8 | 24.0 |
| 715 | 17722210 | 383 | 503 | 477 | 442 | 101417 | 2570 | 15 | 2555 | 477.4 | 25.0 |
| 716 | 16605336 | 486 | 519 | 473 | 441 | 101350 | 2408 | 15 | 2393 | 473.2 | 45.0 |
| 717 | 16726971 | 427 | 513 | 470 | 439 | 101374 | 2425 | 15 | 2411 | 469.6 | 43.0 |
| 718 | 16866784 | 425 | 515 | 482 | 443 | 101398 | 2446 | 15 | 2431 | 482.4 | 33.0 |
| 719 | 17023420 | 433 | 521 | 488 | 448 | 101412 | 2468 | 15 | 2454 | 487.5 | 33.0 |
| 721 | 17168432 | 441 | 527 | 491 | 451 | 101418 | 2489 | 15 | 2475 | 491.0 | 36.0 |
| 722 | 17309840 | 449 | 534 | 496 | 455 | 101416 | 2510 | 15 | 2495 | 495.6 | 38.0 |
| 724 | 17445408 | 456 | 540 | 500 | 459 | 101413 | 2530 | 15 | 2515 | 500.3 | 40.0 |
| 726 | 17576558 | 463 | 547 | 505 | 462 | 101412 | 2549 | 15 | 2534 | 504.6 | 42.0 |
| 727 | 17677886 | 470 | 553 | 509 | 466 | 101410 | 2563 | 15 | 2549 | 508.8 | 44.0 |
| 729 | 17756554 | 477 | 560 | 513 | 469 | 101408 | 2575 | 15 | 2560 | 513.2 | 47.0 |
| 730 | 17257022 | 495 | 566 | 509 | 467 | 101377 | 2502 | 15 | 2488 | 509.1 | 57.0 |
| 730 | 16494932 | 530 | 573 | 509 | 467 | 101352 | 2392 | 15 | 2377 | 509.3 | 64.0 |
| 731 | 16655850 | 508 | 572 | 514 | 467 | 101380 | 2415 | 15 | 2400 | 513.9 | 59.0 |
| 732 | 16710891 | 508 | 575 | 521 | 471 | 101392 | 2423 | 15 | 2408 | 520.6 | 54.0 |

## Table D-7 T&H Input Parameters for Case 153 (Cont.)

| Time in Min-utes | Primary Pressure (Pa) | Surge-Line Temperature (°C) | HL Temperature (°C) | Hot Tube Temperature (°C) | Cold Tube Temperature (°C) | Secondary Pressure (Pa) | Primary Pressure in psi | Secondary Pressure in psi | Delta P in psi | Avr. Hot Tube Temp °C HT | HL to Tube Hot Side Delta T |
|---|---|---|---|---|---|---|---|---|---|---|---|
| 734 | 16775306 | 513 | 584 | 526 | 476 | 101401 | 2432 | 15 | 2418 | 525.8 | 58.0 |
| 736 | 16790980 | 517 | 590 | 529 | 479 | 101402 | 2435 | 15 | 2420 | 529.4 | 61.0 |
| 737 | 16802604 | 521 | 597 | 534 | 482 | 101400 | 2436 | 15 | 2422 | 533.8 | 63.0 |
| 739 | 16809486 | 525 | 604 | 538 | 485 | 101399 | 2437 | 15 | 2423 | 538.3 | 66.0 |
| 741 | 16821192 | 528 | 611 | 543 | 488 | 101398 | 2439 | 15 | 2424 | 542.8 | 68.0 |
| 742 | 16828688 | 532 | 618 | 547 | 491 | 101398 | 2440 | 15 | 2425 | 547.1 | 71.0 |
| 744 | 16835622 | 535 | 625 | 552 | 494 | 101398 | 2441 | 15 | 2426 | 551.6 | 73.0 |
| 745 | 16837316 | 539 | 632 | 556 | 497 | 101398 | 2441 | 15 | 2427 | 556.1 | 76.0 |
| 747 | 16847754 | 542 | 640 | 561 | 500 | 101398 | 2443 | 15 | 2428 | 560.9 | 79.0 |
| 749 | 16864748 | 546 | 648 | 566 | 503 | 101399 | 2445 | 15 | 2431 | 565.7 | 82.0 |
| 750 | 16878606 | 549 | 655 | 570 | 506 | 101399 | 2447 | 15 | 2433 | 570.2 | 85.0 |
| 752 | 16892486 | 552 | 663 | 575 | 510 | 101399 | 2449 | 15 | 2435 | 574.9 | 89.0 |
| 753 | 16903808 | 556 | 672 | 580 | 513 | 101399 | 2451 | 15 | 2436 | 579.6 | 92.0 |
| 755 | 16916818 | 559 | 680 | 584 | 516 | 101399 | 2453 | 15 | 2438 | 584.4 | 95.0 |
| 757 | 16930512 | 563 | 688 | 589 | 519 | 101399 | 2455 | 15 | 2440 | 589.3 | 99.0 |
| 758 | 16945692 | 566 | 696 | 594 | 522 | 101399 | 2457 | 15 | 2442 | 594.2 | 102.0 |
| 760 | 16961192 | 570 | 705 | 599 | 526 | 101399 | 2459 | 15 | 2445 | 598.9 | 106.0 |
| 761 | 16978144 | 573 | 713 | 604 | 529 | 101399 | 2462 | 15 | 2447 | 603.8 | 109.0 |
| 763 | 16995640 | 577 | 722 | 609 | 532 | 101399 | 2464 | 15 | 2450 | 608.8 | 113.0 |
| 764 | 17013394 | 581 | 731 | 614 | 536 | 101399 | 2467 | 15 | 2452 | 613.8 | 117.0 |
| 766 | 17031428 | 584 | 740 | 619 | 539 | 101399 | 2470 | 15 | 2455 | 618.8 | 121.0 |
| 768 | 17049492 | 588 | 749 | 624 | 542 | 101399 | 2472 | 15 | 2457 | 623.7 | 125.0 |
| 769 | 17068202 | 592 | 758 | 629 | 545 | 101399 | 2475 | 15 | 2460 | 628.9 | 129.0 |
| 771 | 17087730 | 596 | 767 | 634 | 549 | 101399 | 2478 | 15 | 2463 | 634.1 | 133.0 |
| 772 | 17107852 | 600 | 777 | 639 | 552 | 101399 | 2481 | 15 | 2466 | 639.4 | 137.0 |
| 774 | 17129464 | 605 | 787 | 645 | 556 | 101399 | 2484 | 15 | 2469 | 644.8 | 142.0 |
| 776 | 17150636 | 609 | 796 | 650 | 559 | 101399 | 2487 | 15 | 2472 | 650.1 | 146.0 |
| 777 | 17173824 | 614 | 807 | 656 | 562 | 101399 | 2490 | 15 | 2476 | 655.7 | 151.0 |
| 779 | 17198290 | 618 | 818 | 661 | 566 | 101399 | 2494 | 15 | 2479 | 661.4 | 156.0 |
| 780 | 17225090 | 623 | 829 | 667 | 569 | 101399 | 2498 | 15 | 2483 | 667.3 | 161.0 |
| 782 | 17255404 | 629 | 840 | 673 | 573 | 101400 | 2502 | 15 | 2487 | 673.3 | 167.0 |
| 783 | 17289820 | 635 | 853 | 680 | 576 | 101401 | 2507 | 15 | 2492 | 679.5 | 173.0 |
| 785 | 17328194 | 641 | 866 | 686 | 580 | 101402 | 2513 | 15 | 2498 | 686.4 | 180.0 |
| 787 | 17371994 | 648 | 881 | 694 | 584 | 101404 | 2519 | 15 | 2504 | 693.6 | 188.0 |
| 788 | 17424672 | 656 | 898 | 702 | 588 | 101406 | 2527 | 15 | 2512 | 701.6 | 197.0 |
| 789 | 17454806 | 660 | 908 | 706 | 590 | 101408 | 2531 | 15 | 2516 | 705.9 | 202.0 |
| 790 | 17486682 | 665 | 918 | 710 | 592 | 101410 | 2536 | 15 | 2521 | 710.4 | 208.0 |
| 791 | 17523474 | 670 | 929 | 715 | 594 | 101412 | 2541 | 15 | 2526 | 715.2 | 214.0 |
| 791 | 17565386 | 676 | 942 | 720 | 596 | 101415 | 2547 | 15 | 2532 | 720.4 | 221.0 |

## Table D-7 T&H Input Parameters for Case 153 (Cont.)

| Time in Min-utes | Primary Pressure (Pa) | Surge-Line Temperature (°C) | HL Temperature (°C) | Hot Tube Temperature (°C) | Cold Tube Temperature (°C) | Secondary Pressure (Pa) | Primary Pressure in psi | Secondary Pressure in psi | Delta P in psi | Avr. Hot Tube Temp °C HT | HL to Tube Hot Side Delta T |
|---|---|---|---|---|---|---|---|---|---|---|---|
| 792 | 17610286 | 681 | 954 | 726 | 598 | 101418 | 2553 | 15 | 2539 | 725.6 | 229.0 |
| 793 | 17671602 | 689 | 972 | 732 | 601 | 101423 | 2562 | 15 | 2548 | 732.1 | 239.0 |
| 794 | 17295002 | 826 | 1,013 | 739 | 603 | 101419 | 2508 | 15 | 2493 | 738.8 | 274.0 |
| 795 | 16933844 | 804 | 1,077 | 743 | 599 | 101410 | 2455 | 15 | 2441 | 743.2 | 334.0 |
| 795 | 17161326 | 832 | 1,188 | 784 | 608 | 101485 | 2488 | 15 | 2474 | 783.6 | 404.0 |
| 796 | 17240314 | 851 | 1,223 | 788 | 613 | 101523 | 2500 | 15 | 2485 | 788.3 | 435.0 |
| 797 | 17288726 | 864 | 1,245 | 797 | 616 | 101533 | 2507 | 15 | 2492 | 796.8 | 448.0 |
| 798 | 17324848 | 877 | 1,275 | 806 | 618 | 101527 | 2512 | 15 | 2497 | 806.1 | 468.0 |
| 799 | 17355544 | 887 | 1,306 | 816 | 620 | 101509 | 2517 | 15 | 2502 | 816.4 | 489.0 |
| 799 | 17374412 | 898 | 1,341 | 828 | 622 | 101488 | 2519 | 15 | 2505 | 828.4 | 512.0 |
| 800 | 17369112 | 906 | 1,365 | 838 | 623 | 101473 | 2519 | 15 | 2504 | 837.5 | 528.0 |
| 801 | 17362924 | 914 | 1,386 | 846 | 626 | 101461 | 2518 | 15 | 2503 | 845.6 | 541.0 |
| 802 | 17346996 | 921 | 1,401 | 853 | 628 | 101453 | 2515 | 15 | 2501 | 852.5 | 548.0 |
| 803 | 17295070 | 930 | 1,413 | 864 | 632 | 101441 | 2508 | 15 | 2493 | 863.8 | 549.0 |
| 806 | 17222752 | 937 | 1,411 | 875 | 638 | 101419 | 2497 | 15 | 2483 | 875.2 | 536.0 |
| 808 | 17168220 | 941 | 1,409 | 885 | 644 | 101411 | 2489 | 15 | 2475 | 885.4 | 524.0 |
| 811 | 17100416 | 943 | 1,405 | 896 | 651 | 101400 | 2480 | 15 | 2465 | 895.5 | 509.0 |
| 814 | 17033290 | 941 | 1,398 | 904 | 658 | 101394 | 2470 | 15 | 2455 | 903.9 | 494.0 |
| 818 | 17023456 | 943 | 1,387 | 912 | 665 | 101390 | 2468 | 15 | 2454 | 911.8 | 475.0 |
| 822 | 17100190 | 945 | 1,370 | 918 | 673 | 101383 | 2480 | 15 | 2465 | 918.4 | 452.0 |
| 826 | 17211974 | 950 | 1,360 | 926 | 681 | 101380 | 2496 | 15 | 2481 | 925.9 | 434.0 |
| 830 | 17194184 | 945 | 1,350 | 931 | 688 | 101376 | 2493 | 15 | 2478 | 930.6 | 420.0 |
| 833 | 17074150 | 934 | 1,345 | 934 | 694 | 101374 | 2476 | 15 | 2461 | 934.3 | 411.0 |
| 836 | 16953292 | 922 | 1,339 | 937 | 700 | 101373 | 2458 | 15 | 2444 | 937.2 | 402.0 |
| 838 | 16845614 | 911 | 1,334 | 939 | 704 | 101372 | 2443 | 15 | 2428 | 938.8 | 395.0 |
| 841 | 16757801 | 901 | 1,331 | 942 | 710 | 101374 | 2430 | 15 | 2415 | 942.0 | 389.0 |
| 843 | 16804596 | 905 | 1,313 | 941 | 715 | 101371 | 2437 | 15 | 2422 | 941.2 | 372.0 |
| 844 | 16781984 | 901 | 1,300 | 939 | 715 | 101368 | 2433 | 15 | 2419 | 938.8 | 361.0 |
| 845 | 16777074 | 899 | 1,283 | 934 | 716 | 101364 | 2433 | 15 | 2418 | 934.3 | 348.0 |
| 849 | 16719079 | 890 | 1,294 | 940 | 718 | 101364 | 2424 | 15 | 2410 | 940.2 | 354.0 |
| 851 | 16631669 | 880 | 1,299 | 944 | 721 | 101365 | 2412 | 15 | 2397 | 944.3 | 355.0 |
| 853 | 16539559 | 870 | 1,302 | 948 | 725 | 101365 | 2398 | 15 | 2384 | 947.6 | 355.0 |
| 856 | 16444167 | 860 | 1,304 | 950 | 729 | 101365 | 2384 | 15 | 2370 | 949.8 | 354.0 |
| 858 | 16351976 | 850 | 1,303 | 951 | 732 | 101365 | 2371 | 15 | 2356 | 951.3 | 352.0 |
| 860 | 16267959 | 840 | 1,303 | 953 | 735 | 101364 | 2359 | 15 | 2344 | 952.6 | 350.0 |
| 863 | 16149878 | 828 | 1,301 | 953 | 738 | 101364 | 2342 | 15 | 2327 | 953.2 | 348.0 |
| 865 | 16039874 | 817 | 1,300 | 954 | 741 | 101363 | 2326 | 15 | 2311 | 954.2 | 346.0 |
| 868 | 15936266 | 807 | 1,300 | 955 | 743 | 101363 | 2311 | 15 | 2296 | 955.4 | 344.0 |
| 870 | 15829010 | 796 | 1,299 | 957 | 746 | 101363 | 2295 | 15 | 2281 | 956.6 | 342.0 |

## Table D-7 T&H Input Parameters for Case 153 (Cont.)

| Time in Min-utes | Primary Pressure (Pa) | Surge-Line Temperature (°C) | HL Temperature (°C) | Hot Tube Temperature (°C) | Cold Tube Temperature (°C) | Secondary Pressure (Pa) | Primary Pressure in psi | Secondary Pressure in psi | Delta P in psi | Avr. Hot Tube Temp °C HT | HL to Tube Hot Side Delta T |
|---|---|---|---|---|---|---|---|---|---|---|---|
| 872 | 15719427 | 785 | 1,298 | 958 | 749 | 101362 | 2279 | 15 | 2265 | 957.8 | 341.0 |
| 876 | 15764007 | 794 | 1,298 | 963 | 753 | 101363 | 2286 | 15 | 2271 | 963.1 | 335.0 |
| 883 | 15720647 | 783 | 1,307 | 969 | 760 | 101362 | 2279 | 15 | 2265 | 968.7 | 338.0 |
| 885 | 15609858 | 772 | 1,310 | 970 | 762 | 101362 | 2263 | 15 | 2249 | 970.3 | 340.0 |
| 887 | 15493158 | 761 | 1,312 | 972 | 765 | 101362 | 2247 | 15 | 2232 | 971.7 | 340.0 |
| 890 | 15376555 | 750 | 1,313 | 973 | 767 | 101361 | 2230 | 15 | 2215 | 973.0 | 340.0 |
| 891 | 15452803 | 759 | 1,314 | 975 | 769 | 101364 | 2241 | 15 | 2226 | 974.8 | 339.0 |
| 892 | 16746626 | 832 | 1,316 | 994 | 772 | 101383 | 2428 | 15 | 2414 | 994.1 | 321.0 |
| 893 | 16766600 | 1,172 | 1,356 | 997 | 771 | 101351 | 2431 | 15 | 2416 | 997.4 | 359.0 |
| 894 | 17313854 | 1,109 | 1,351 | 981 | 766 | 101360 | 2511 | 15 | 2496 | 981.0 | 370.0 |
| 895 | 17545106 | 1,117 | 1,338 | 968 | 763 | 101358 | 2544 | 15 | 2529 | 968.0 | 370.0 |
| 895 | 17177846 | 1,182 | 1,336 | 963 | 762 | 101351 | 2491 | 15 | 2476 | 963.5 | 372.0 |

**153short-end** Case 153 (late TDAFW pump failure) is shortened by removing some of the earlier time steps not contributing to results

**0.01** Significance factor to reduce time steps (0.0 uses all time steps input)

**1.00** Fraction of “hot” SG tubes (1.00 means all flaws (100 percent) are on the hot tubes)

**Table D-8 Margin for the Case with Failure of TDAFW Pump at 4 Hours**

| | | | Time in Minutes | |
|---|---|---|---|---|
| | | NUREG/ CR-6995 | Calculator | Comment |
| | | | | |
| 1 | Event starts | 000 | 000 | |
| 2 | TDAFW pump fails | 240 | | |
| 3 | Evacuation starts | | | 240 |
| 4 | Evacuation ends for internal events | | | 480 |
| 5 | SGs dryout | 583 | | |
| 6 | Evacuation ends for external events | | | 720 |
| 7 | HL fails 26% | | 768 | |
| 8 | HL fails 49% | | 769 | |
| 9 | HL fails 100% | | **777** | |
| 10 | HL 1 fails by creep rupture | 793 | | |
| 11 | Hot tube fails 6 $cm^2$ (1 tube equivalent) | | **799** | |
| 12 | Hot tube fails max 6 $cm^2$ (1 tube equivalent) | | 799 | |
| 13 | SL fails 33% | | 808 | |
| 14 | SL fails 58% | | 818 | |
| 15 | SL fails 100% | | 893 | |
| | | | | |
| | **Margin** = HL fails 100%—Hot tube fails 6 $cm^2$ (0.93 $in.^2$) | | **-22** | |

The definition of margin is based on the crucial T&H assumption that a full break of a single SG tube (6 $cm^2$ (0.93 $in.^2$)) would not depressurize the RCS to prevent RCS failure elsewhere.

Hot tube fraction = 1.0 (all flaws are assumed to be on the hot tubes)

NUREG/CR-6995 RELAP 2010 Case 153

### D.1.6 Effect of 690TT Material

This sensitivity analysis studies a comparison of both W and CE SG types with 690TT tube material. For this purpose, two cases are defined and are simulated by the calculator:

**Case 1:**

Calvert Cliffs with 690TT tubes; a “large” wear-type flaw 4 cm (1.6 in.) and 40 percent deep. SBO with failure of the turbine-driven pump at the start of the event; loop A with average SG tubes used from the TH analysis.

**Case 2:**

Zion with 690TT tubes; a “large” wear-type flaw 4 cm (1.57 in.) and 40 percent deep. SBO with failure of the turbine-driven pump at the start of the event; Wnewbase case used from the TH analysis.

In terms of the calculator input files used, the case information can be summarized as shown below:

| **Case 1:** | **Case 2:** |
|---|---|
| | |
| TH-CE-A-0-Avr-short | TH-Wnewbase-short |
| W4-40 | W4-40 |
| Calvert Cliffs (TT690) | ZION690 |

Table D-9 summarizes the results. When 690TT material is postulated to be used in a W-type SG, the margin is still favorable for the failure of the HL before the large-flawed SG tube, but it is shortened compared to the same case with 600TT material (Case 3). Case 3 is defined as

| **Case 3:** |
|---|
| |
| TH-Wnewbase-short |
| W4-40 |
| ZION600 |

Table D-9 also shows the Case 3 margin. The result that the Case 3 margin is larger than the Case 2 margin seems to indicate that SG tubes with 690TT material with a “large” flaw will leak earlier than SG tubes with 600TT material with the same “large” flaw (in 233 minutes versus 243 minutes in this case).

**Table D-9 Comparison of 690TT Cases of W vs. CE-Type SGs**

| | | | Time in Minutes | | | |
|---|---|---|---|---|---|---|
| | | NUREG/ CR-6995 | Case 1 Calculator | Case 2 Calculator | Case 3 Calculator | Comment |
| | | | | | | |
| 1 | Event starts | 000 | 000 | | | |
| 2 | TDAFW pump fails | 240 | | | | |
| 3 | Evacuation starts | | | | | 240 |
| 4 | Evacuation ends for internal events | | | | | 480 |
| 5 | SG dryout | 583 | | | | |
| 6 | Evacuation ends for external events | | | | | 720 |
| 7 | HL fails 26% | | | | | |
| 8 | HL fails 49% | | | | | |
| 9 | HL fails 100% | | **357** | **221** | **219** | |
| 10 | HL 1 fails by creep rupture | 793 | | | | |
| 11 | Hot tube fails 6 $cm^2$ (0.93 $in.^2$) (1 tube equivalent) | | **325** | **233** | **243** | Case 1 max. failure area is 4.5 cm-sq. |
| 12 | Hot tube fails max. 6 $cm^2$ (0.93 $in.^2$) (1 tube equivalent) | | | | | |
| 13 | SL fails 33% | | | | | |
| 14 | SL fails 58% | | | | | |
| 15 | SL fails 100% | | | | | |
| | | | | | | |
| | **Margin** = HL fails 100%—Hot tube fails 6 $cm^2$ (0.93 $in.^2$) | | **32** | **-12** | **-24** | |

The definition of margin is based on the crucial TH assumption that a full break of a single SG tube (6 $cm^2$ (0.93 $in.^2$)) would not depressurize the RCS to prevent RCS failure elsewhere.

Hot tube fraction = 1.0 (all flaws are assumed to be on the hot tubes)

NUREG/CR-6995 RELAP 2010 Case 153

### D.1.7 Conclusions

The analyses elsewhere in this report rely on the C-SGTR calculation results. The C-SGTR calculator provides some estimates of uncertainties, especially for the integrated leak areas. However, it does not provide a robust uncertainty estimate for uncertainties in the scenario TH input. For better understanding of the effect of TH uncertainties, sensitivity analyses were performed on a base case (W SBO core-damage sequence with a large flaw subject to temperature challenges). The sensitivity analyses indicate that, for this base case, the margin between the HL failure occurring first and tube failure growing into a large leak is not sensitive to changes to the base values of two major modeling parameters. These two modeling parameters are the HL thickness (to account for the existence of weld overlays) and the temperature difference between the HL and the hot tube.

The margins are as follows:

| Case Name | Margin |
|---|---|
| Base Case | -18 minutes |
| Reduced dT between HL and hot tube | -14 minutes |
| Increased HL thickness | -16 minutes |

The -18-minute base margin is a reliable good margin, which appears to have a tight spread when other major modeling parameters are changed in an unfavorable direction.

Although these conclusions apply to this scenario with these cases, they also provide the following:

- insights about the model stability against some key changes
- some confidence that the margin point estimate is stable

An additional sensitivity analysis was made with the secondary-side pressure set at 6.9 MPa (1,100 psi). The result shows that the margin increases to 45 minutes.

Finally, if the TDAFW pump fails at 4 hours, the HL and C-SGTR failures are pushed further in time to about 13 hours following the SBO.

## D.2 Sensitivity Analyses for the Selected CE Plant

The following sensitivity analyses were performed for the example CE plant. The measure of comparison used for these sensitivity analyses was based on the reevaluation of C-SGTR probability for short-term SBO (*stsbo*) sequences where large early release frequency (LERF) is of concern. In some cases; the C-SGTR probability was only reevaluated for one loop rather than for both loop A and loop B (i.e., the reactor unit). When the sensitivity analysis was limited to one loop, loop B was selected because of its higher contribution to C-SGTR. The difference between the revised C-SGTR probability and the base C-SGTR probability was used to prioritize the effect of the sensitivity results. The changes of less than 25 percent are assigned as low, 25 to 50 percent as moderate, 50 to 100 percent as high, and any increases above 200 percent as significant.

### D.2.1 Stuck-Open Failure of Secondary Relief Valves before SG Dryout

In SBO scenarios, before SG dryout, the secondary-side relief valves (SG power-operated relief valves or main steam safety valves (MSSVs) could be demanded and fail to reclose. This could happen in either or both SGs. Stick-open relief valves initially depressurize and cool the primary below the accumulator discharge setpoint. After accumulator discharge, the SGs will go dry, the primary will repressurize, and the onset of core damage will be reached, although slightly delayed. The probability of C-SGTR is expected to be higher because of a lower secondary-side pressure and delayed HL failure. A bounding analysis of this scenario was evaluated using the MELCOR package. Chapter 3 of this report refers to this scenario to as *stsbo-as* and long-term SBO (*ltsbo*)-*as*.

Figures D-6 through D-9 shows the following graphs for the *stsbo-as* scenario. Figures D-10 through D-13 show the same graphs for *ltsbo-as* scenarios. The specific information presented in each figure for *stsbo-as* and *ltsbo-as* is shown below:

- Figure D-5 shows the primary and secondary pressure
- Figures D-6 and D-10: Overall results for loop A
- Figures D-7 and D-11: Difference of HL temperature and average hot/hottest tube temperature for loop A
- Figures D-8 and D-12: Overall results for loop B
- Figures D-9 and D-13: Difference of HL temperature and average hot/hottest tube temperature for loop B

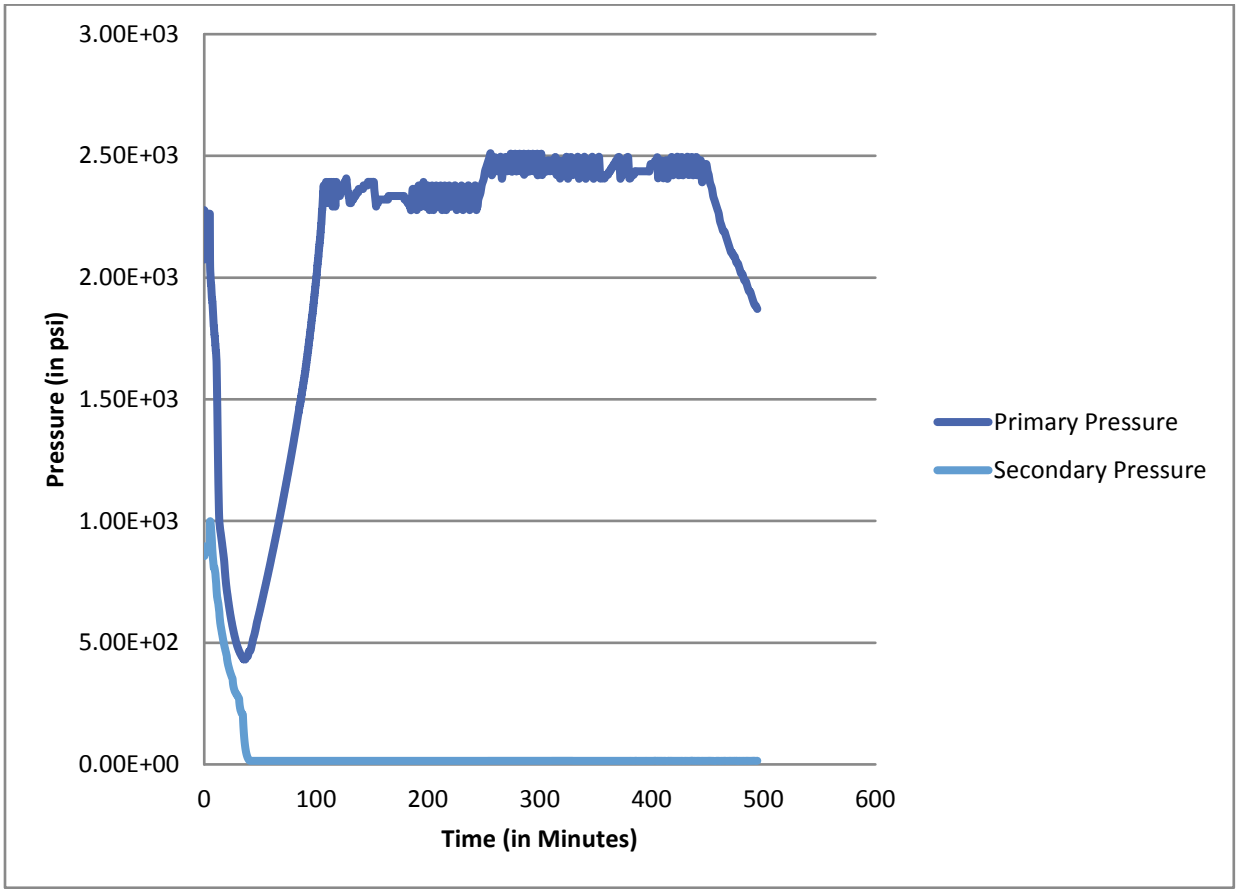


**Figure D-5 SBO with TDAFW pump operating for 0 hours with MSSVs stuck open; Calvert Cliffs**

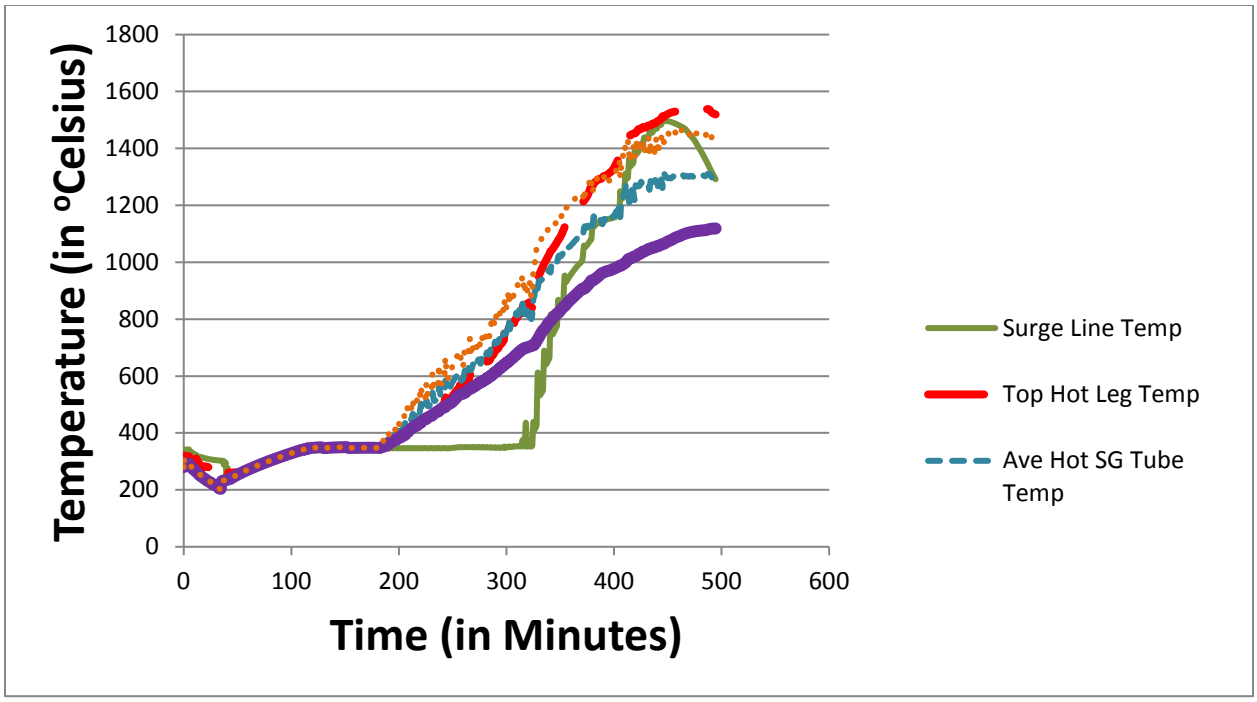


**Figure D-6 SBO with TDAFW pump operating for 0 hours; Calvert Cliffs loop A**

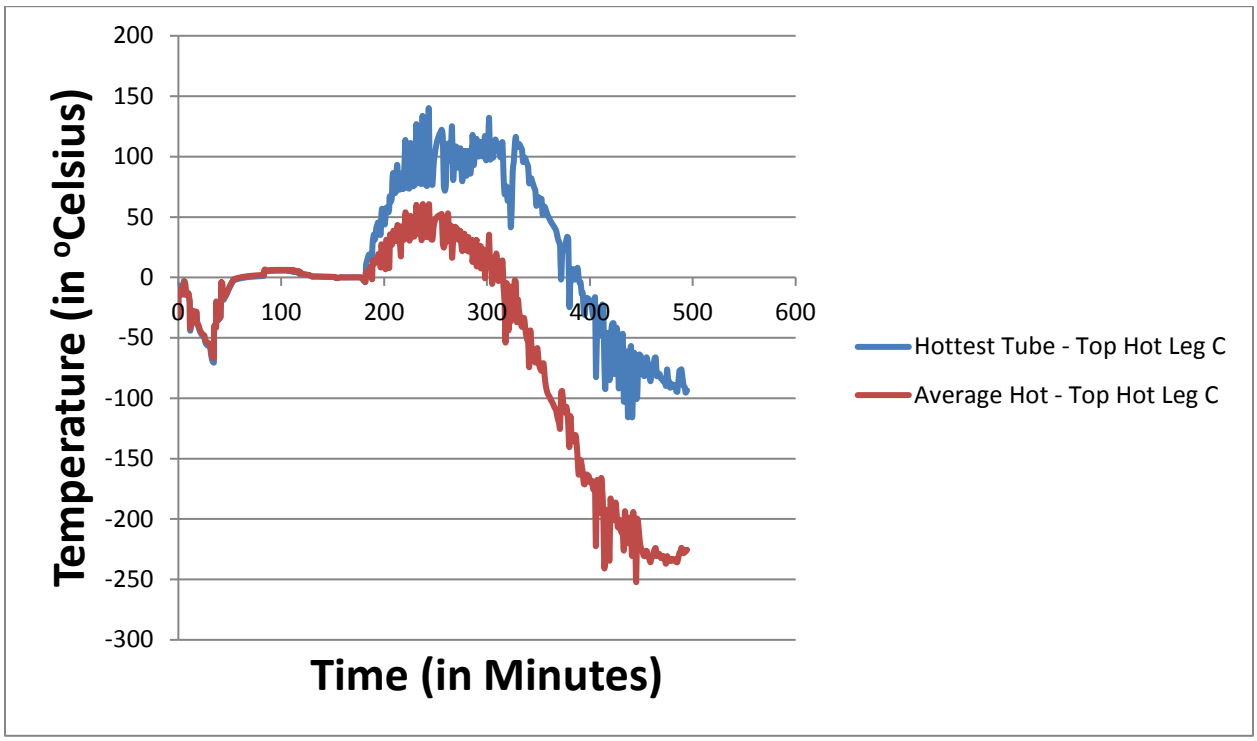


**Figure D-7 Temperature differences in SBO with TDAFW pump operating for 0 hours; Calvert Cliffs loop A**

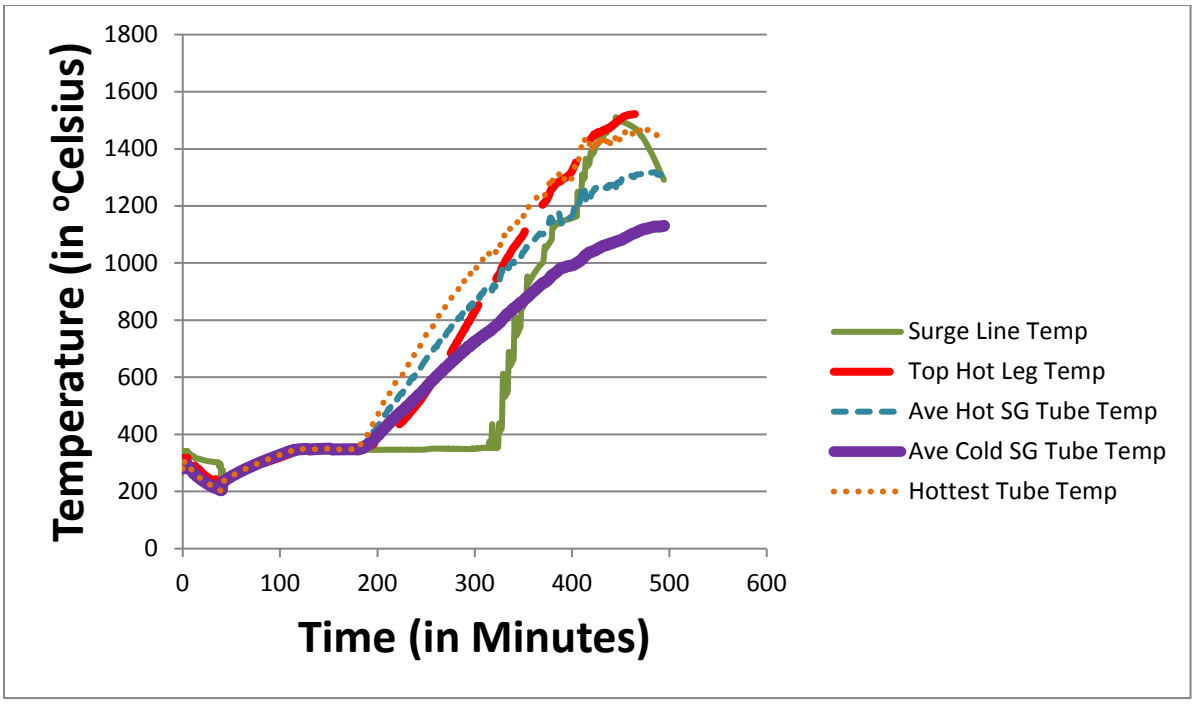


**Figure D-8 SBO with TDAFW pump operating for 0 hours; Calvert Cliffs loop B**

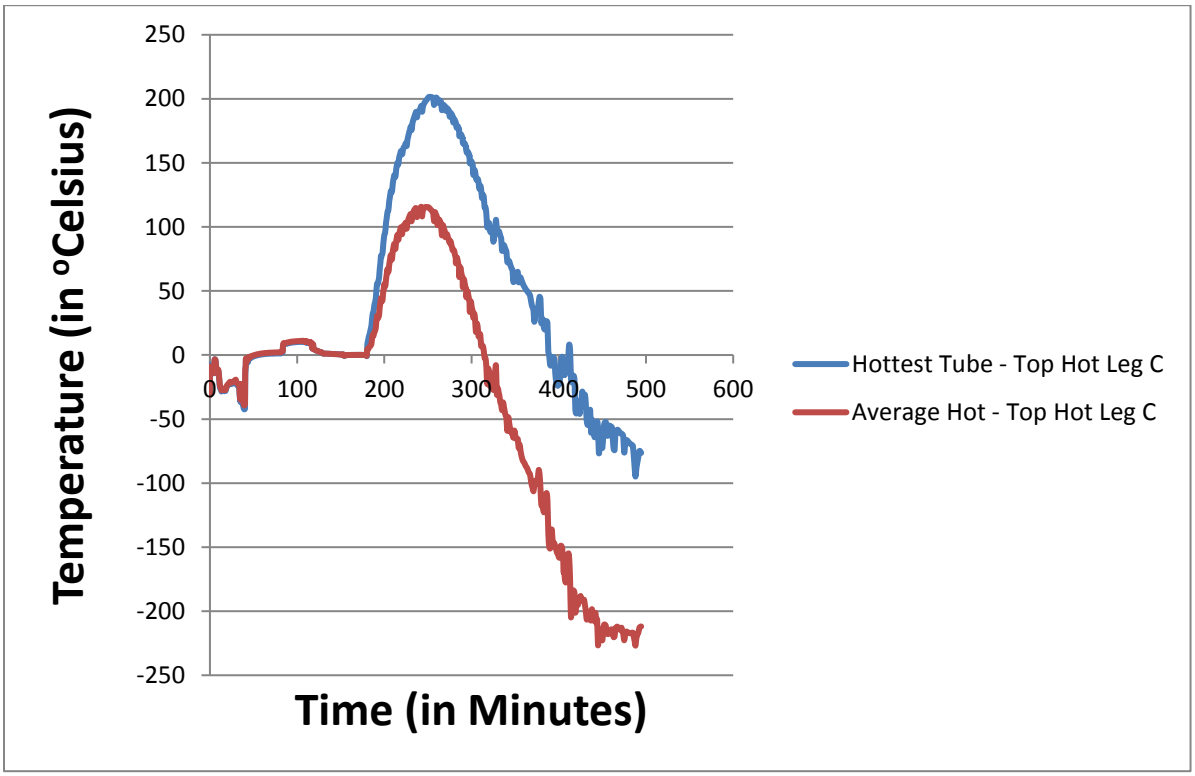


**Figure D-9 Temperature differences in SBO with TDAFW pump operating for 0 hours; Calvert Cliffs loop B**

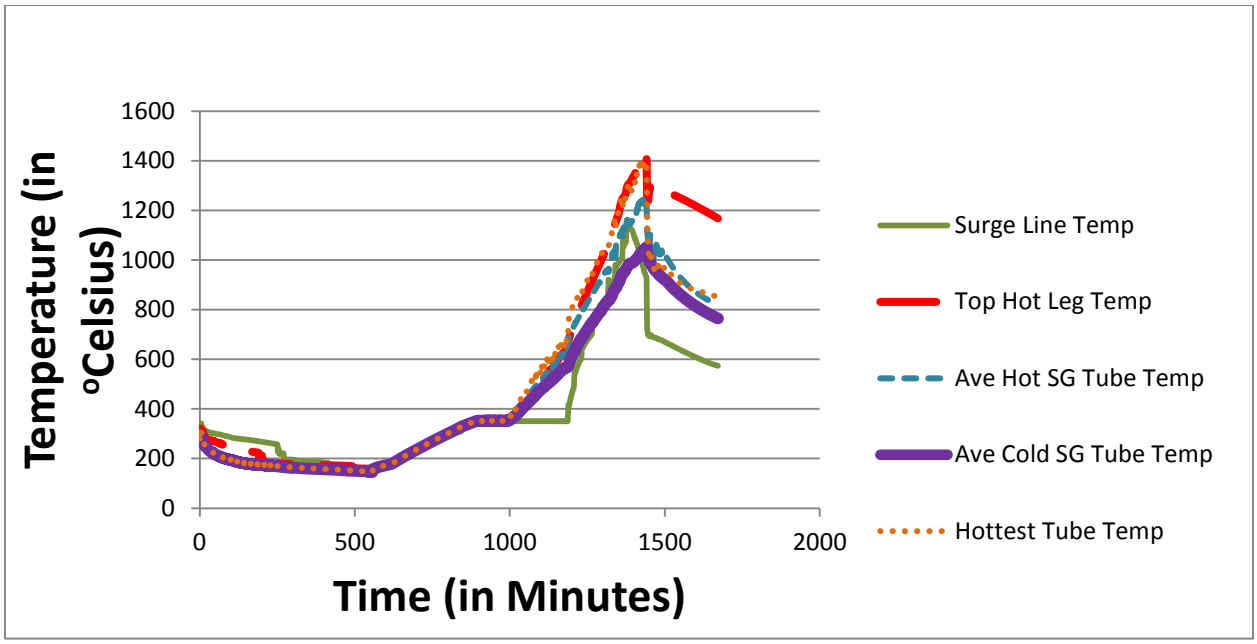


**Figure D-10 SBO with TDAFW pump operating for 4 hours; Calvert Cliffs loop A**

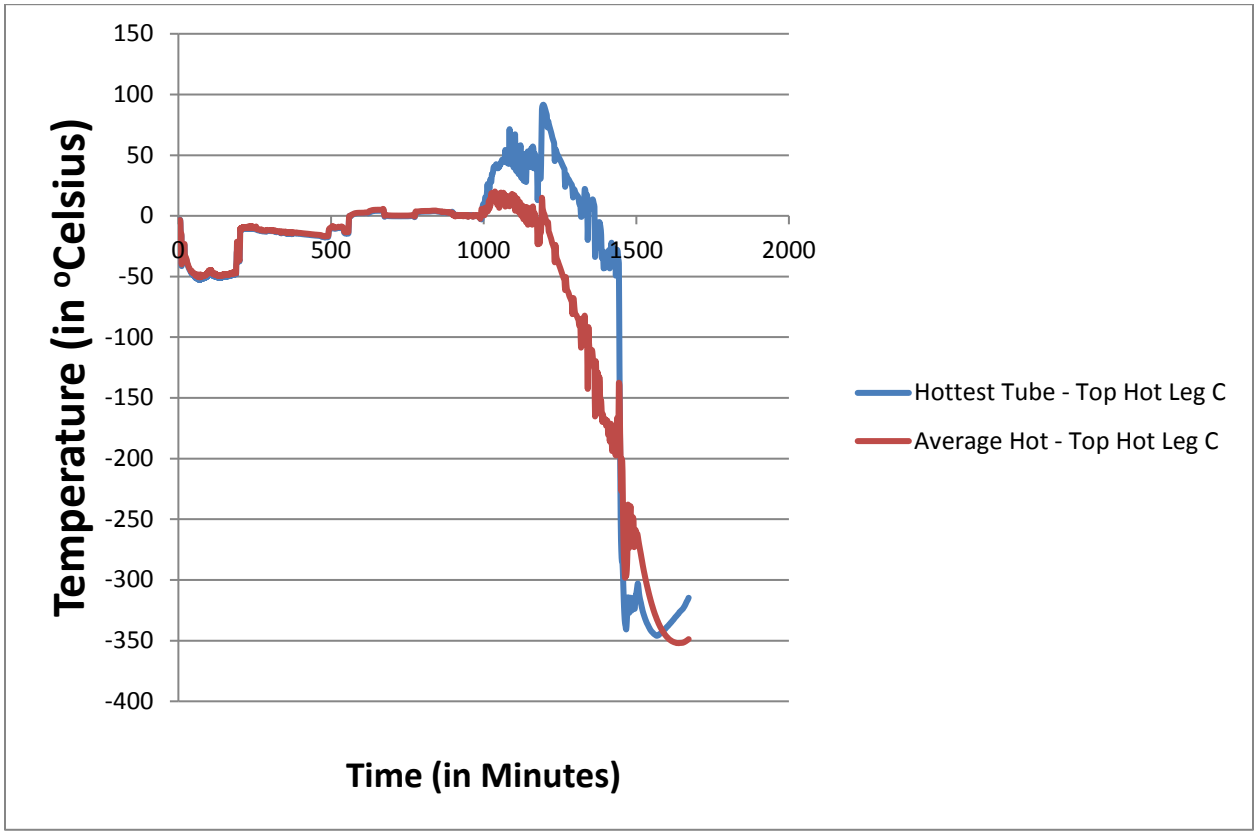


**Figure D-11 Temperature differences in SBO with TDAFW pump operating for 4 hours; Calvert Cliffs loop A**

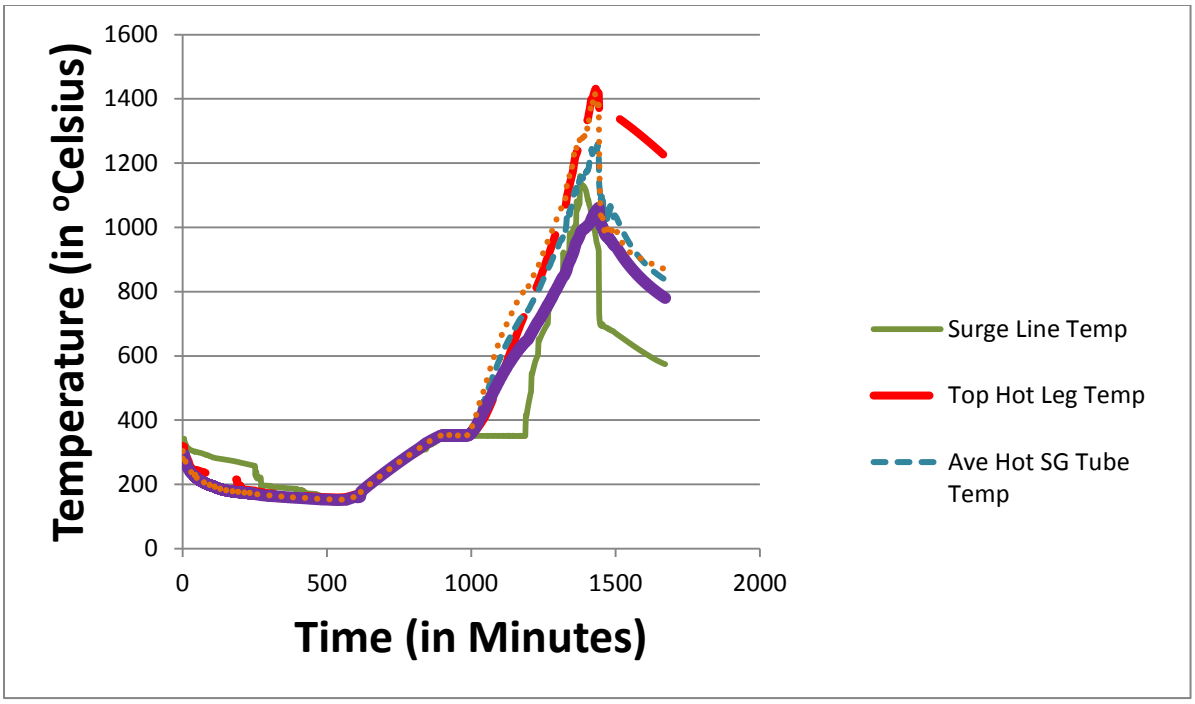


**Figure D-12 SBO with TDAFW pump operating for 4 hours; Calvert Cliffs loop B**

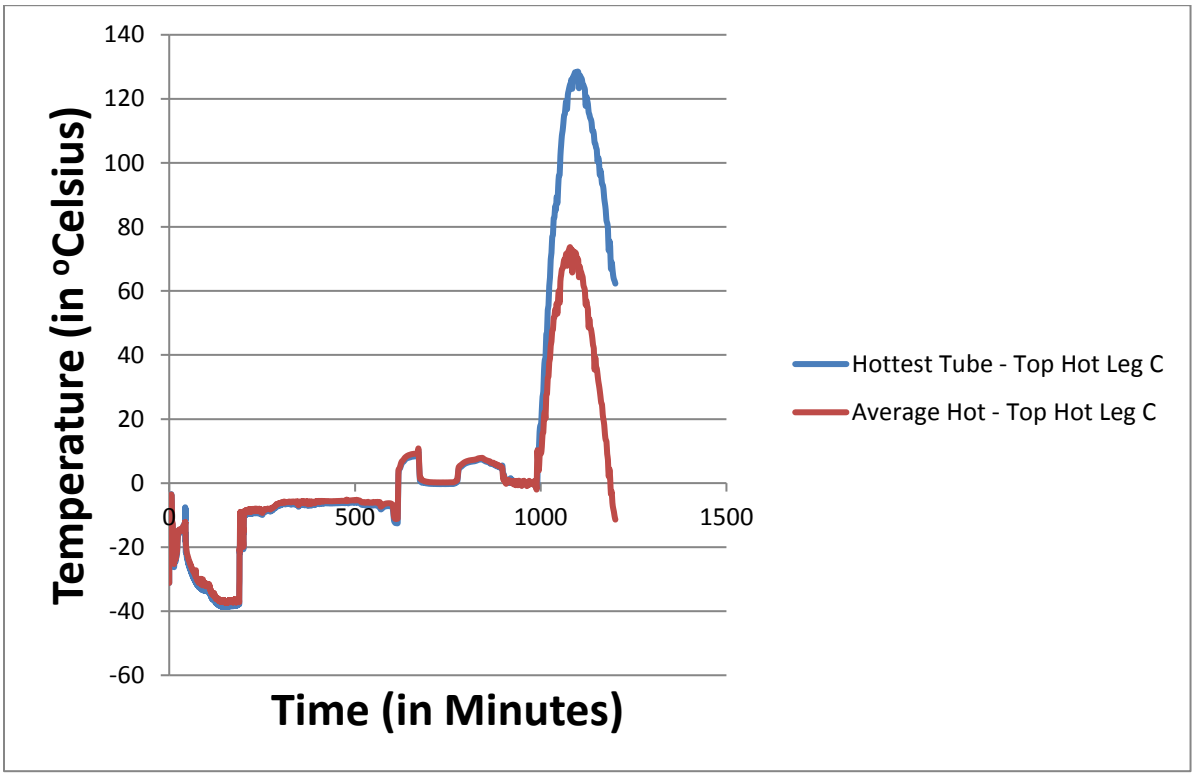


**Figure D-13 Temperature differences in SBO with TDAFW pump operating for 4 hours; Calvert Cliffs loop B**

Separate C-SGTR runs were performed for the average hot and hottest tube for loop A and loop B. The results for average hot and hottest tube for each loop were then combined to estimate the single loop probabilities of C-SGTR. Figures D-14 and D-15 show the results for loops A and B.

As shown in both figures, the curves associated with RCS survival probability are significantly shifted to the right compared to the probability of SG tube rupture (SGTR) with leak areas less than 3 and 6 $cm^2$(0.46 and 0.93 $in.^2$). This indicates that an SGTR that exceeds the critical leak area will occur before the HL failure; therefore, the C-SGTR probability will be very high (close to 1).

Figure D-16 shows a similar graph when the results from loop A and loop B are combined. This figure also shows that the RCS survival probability is on the right side of the graph for SGTR leak probability curves. The results show that the failure of the secondary-side relief valve early during the sequence can have a significant effect on the LERF contribution because of C-SGTR. Table D-10 below shows the results of this reevaluation for *stsbo-as* sequences. As shown in Table D-10, the C-SGTR probability is almost one (0.99) for this scenario.

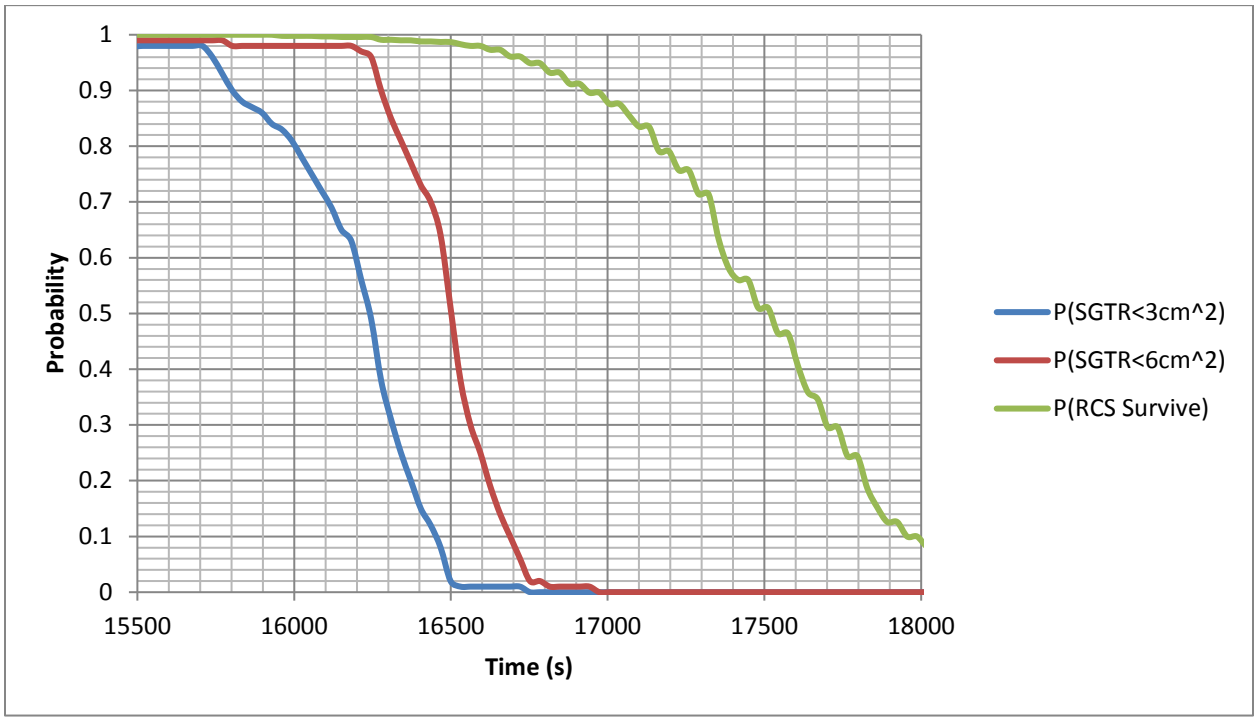


**Figure D-14 Probabilities of SGTR leak rates less than 3 and 6 $cm^2$ vs. HL survival probability for *stsbo-as-a-scf***

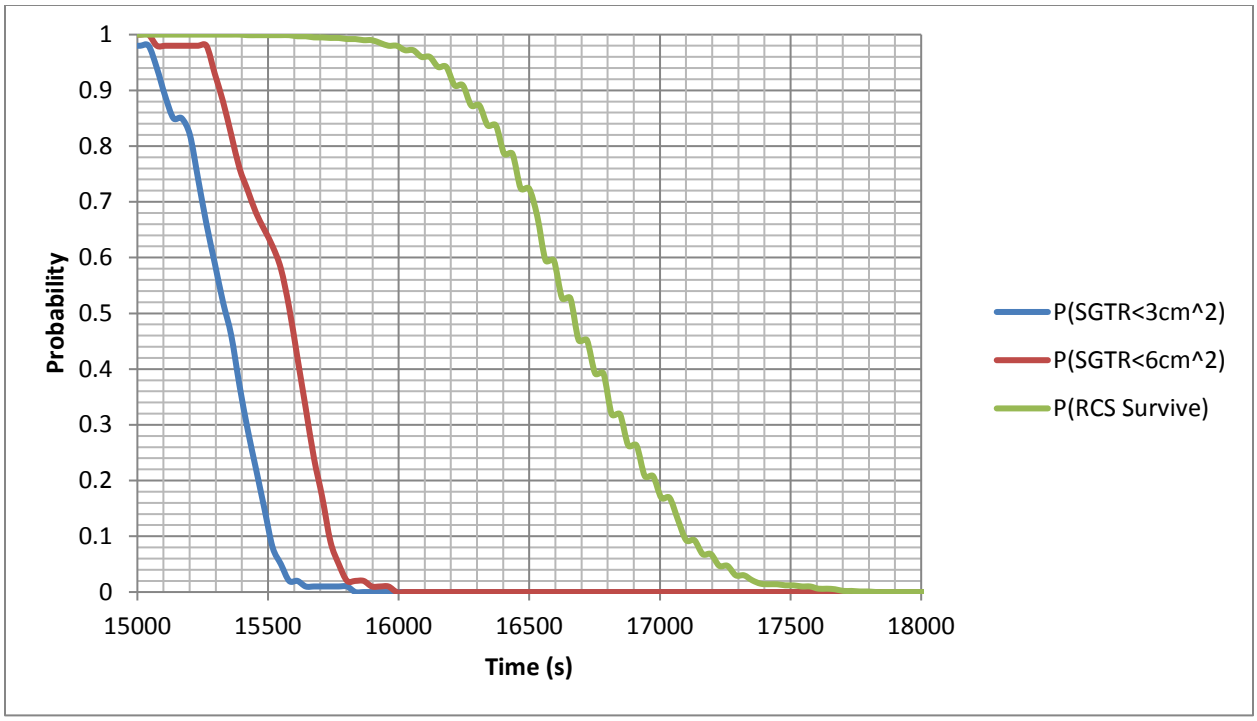


**Figure D-15 Probabilities of SGTR leak rates less than 3 and 6 cm$^2$ vs. HL survival probability for *stsbo-as-b-scf***

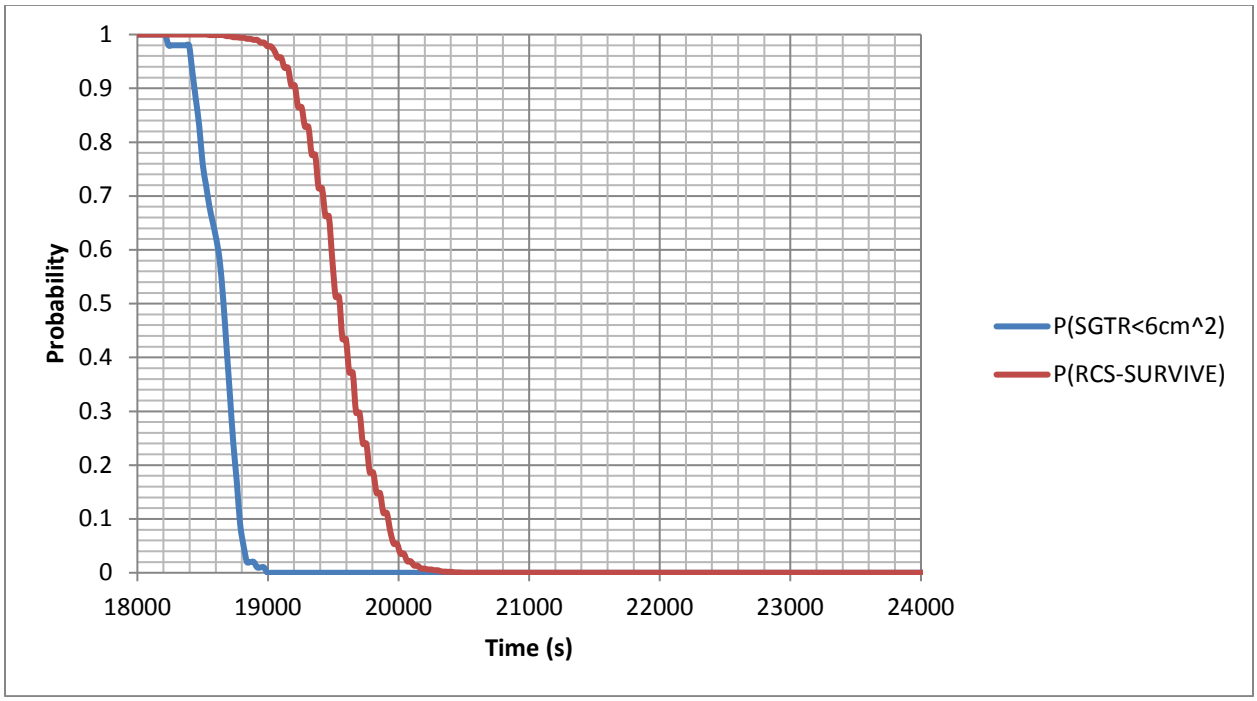


**Figure D-16 Probability of SGTR less than 6 cm$^2$ and probability of RCS survival**

**Table D-10 Sensitivity Results for Early Stick-Open Failures of the Secondary Relief Valves**

| Case runs | Loop B CSGTR > 3 $cm^2$ | Loop A CSGTR > 3 $cm^2$ | CSGTR > 6 $cm^2$ |
|---|---|---|---|
| *Stsbo-a* [base] | 0.45 | 0.217 | 0.2 |
| *Stsbo-as* [stick-open secondary relief valve] | 0.999 | 0.997 | 0.99 |

## Opening of Secondary Relief Valves after SG Dryout

The operators are guided to depressurize the SGs by opening the secondary relief valves in anticipation of using an alternate source of water to refill the SGs as a part of the severe-accident management guidelines. This sensitivity analysis examines the effect of intentionally opening the secondary relief valve after the onset of core damage when the operators fail to refill the SGs. The analysis was performed by setting the secondary-side pressure to $1X10^5$ Pascal after the hot-gas temperature reaches about 640 degrees Celsius (1,184 degrees Fahrenheit) (i.e., at 16,800 seconds for *stsbo-a*). The effects on primary pressure or temperature are not expected to be significant; therefore, no changes were made to these inputs. Figure D-17 shows the results for loop B with and without open secondary relief valves after SG dryout. As can be seen, the graph for the case where the secondary relief valve is open is shifted further to the left, indicating that the likelihood of C-SGTR greater than 3 $cm^2$ (0.46 $in.^2$) is higher than the base case.

Figure D-18 shows the aggregate effect of opening secondary relief valves after SG dryout for both loops. Similar to the previous graph, the SGTR curve associated with open secondary relief valves is shifted to the right, indicating a higher probability of C-SGTR.

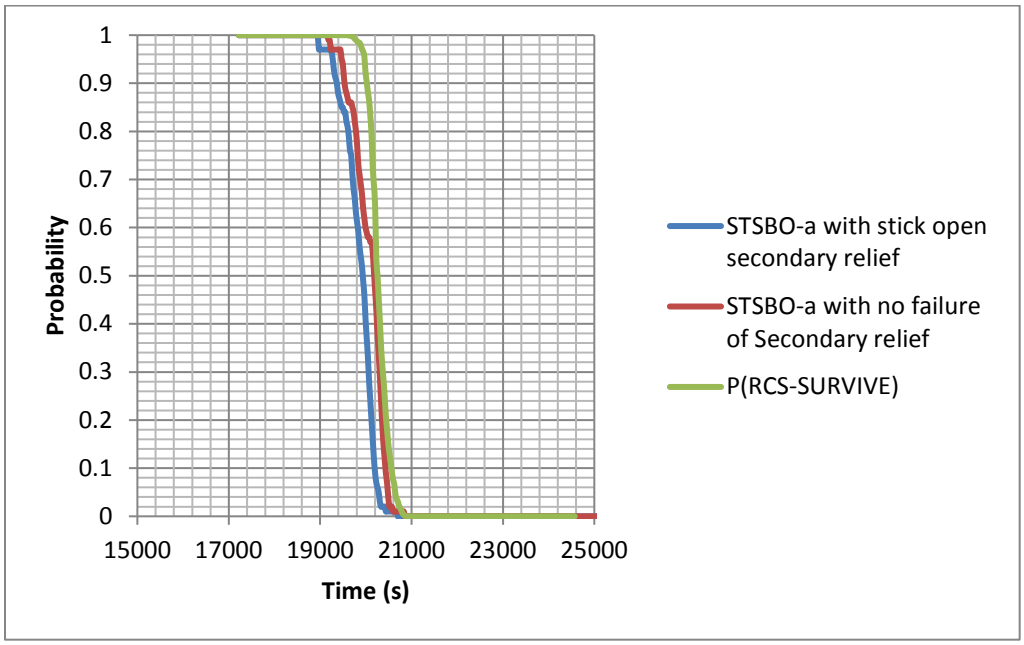


**Figure D-17 Probability of SGTR leak rate less than 3 $cm^2$ for loop B with and without open secondary relief valves after SG dryout**

In summary, the results show that the opening of secondary-side relief valves after SG dryout and the onset of core damage can increase the LERF contribution caused by C-SGTR by about 65 percent (from 0.2 to 0.33) for *stsbo-a* scenarios. Table D-11 shows the results of this reevaluation.

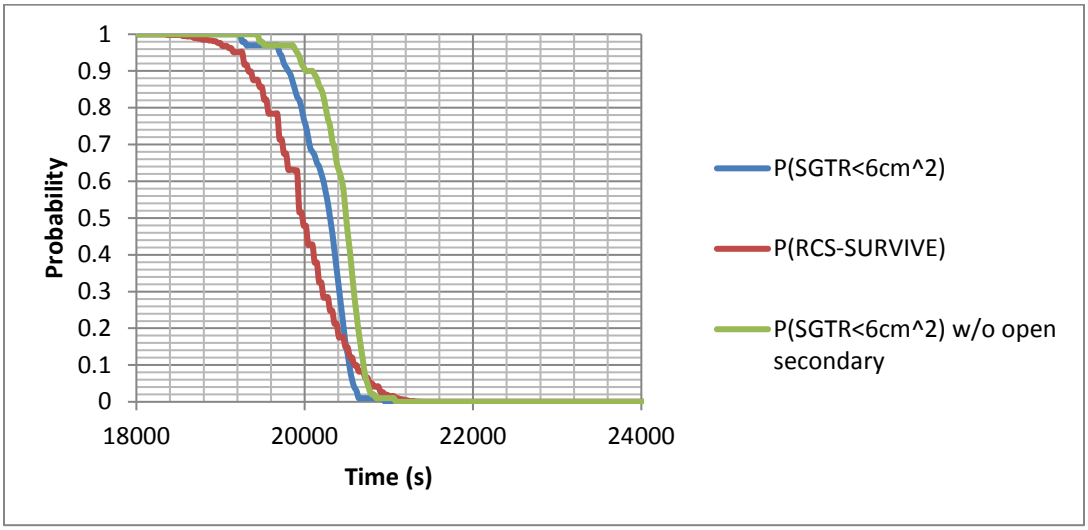


**Figure D-18 Probability of SGTR leak rate less than 6 cm² with and without open secondary relief valves after SG dryout**

**Table D-11 Sensitivity Results for Opening the Secondary Relief Valves after SG Dryout**

| Case runs | Loop B CSGTR > 3 cm² | Loop A CSGTR > 3 cm² | CSGTR > 6 cm² |
|---|---|---|---|
| *Stsbo-a* [base] | 0.450 | 0.217 | 0.200 |
| *Stsbo-a* [secondary relief valve left opened after SG dryout] | 0.591 | 0.262 | 0.330 |

## D.2.2 Critical C-SGTR Leak Area

The critical area equivalent to a guillotine break of one tube (approximately 6 $cm^2$ (0.93 $in.^2$)) was considered to be sufficient to meet the LERF threshold if the secondary-side relief valves are open. Some MELCOR analyses showed that this size of leakage may not pressurize the secondary, such that SG relief valves are demanded. These MELCOR analyses assumed that there is a preexisting secondary leakage area of 3.22 $cm^2$ (0.5 $in.^2$) from the starting point of the sequence. To ensure that the secondary relief valves are demanded and the primary can be depressurized, a larger critical C-SGTR leak area may have to be considered. Figure D-19 shows the probability graph of various leak rates for the *stsbo-a* sequence when considering the expected flaw sample used for this study. The probability of RCS survival is also displayed on the same figure, clearly showing the relative positions of the probability curves for various leak rates to the probability curve of RCS survival.

Figure D-20 shows another way of presenting this information in terms of the probability of C-SGTR. This figure shows how the C-SGTR probability decreases for larger critical leak rates for the *stsbo-a* sequence. It should be emphasized that these curves are only for the expected flaw sample used for this study and shall not be considered generic. Similar graphs, however,

could be generated for different accident sequences and for another set of flaws for each SG using the existing tools and approach.

Using Figure D-20, it can be shown that the probability of C-SGTR is reduced from 0.2 to 0.06 if one assumes a critical C-SGTR leak area of 12 $cm^2$ (1.86 $in.^2$) instead of 6 $cm^2$ (0.93 $in.^2$).

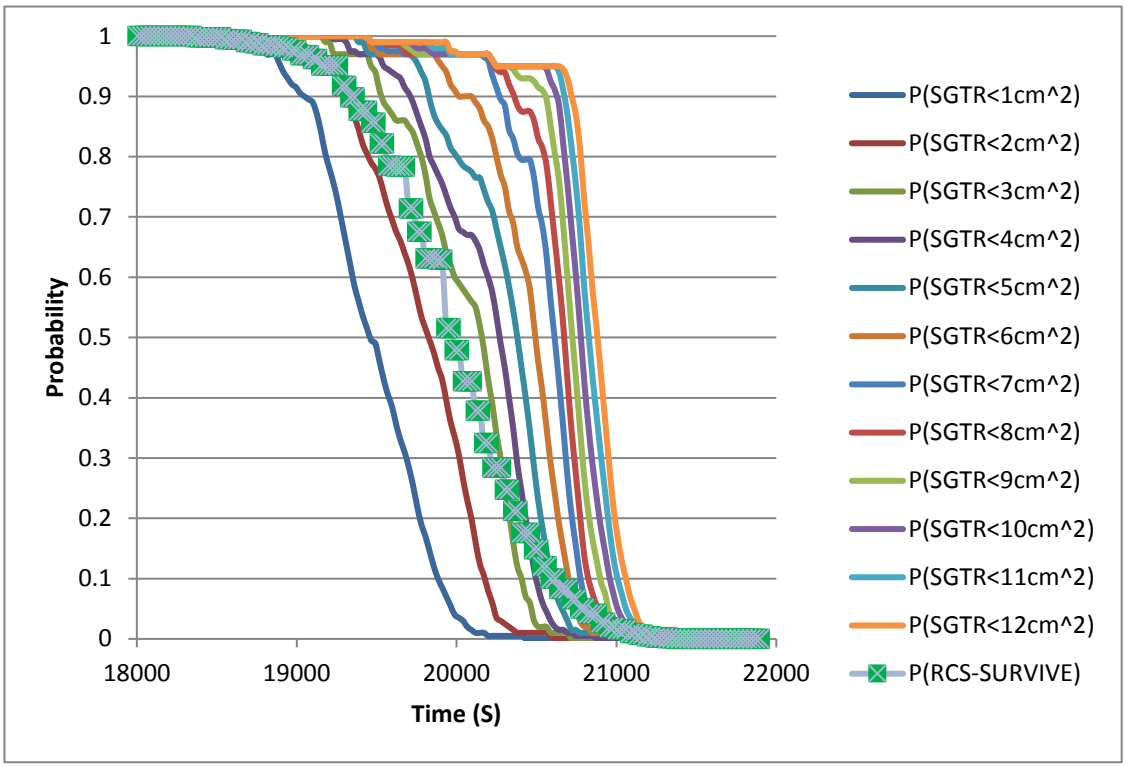


**Figure D-19 Probability of SGTR with leak rates smaller than a specific value and probability of RCS survival as a function of accident time**

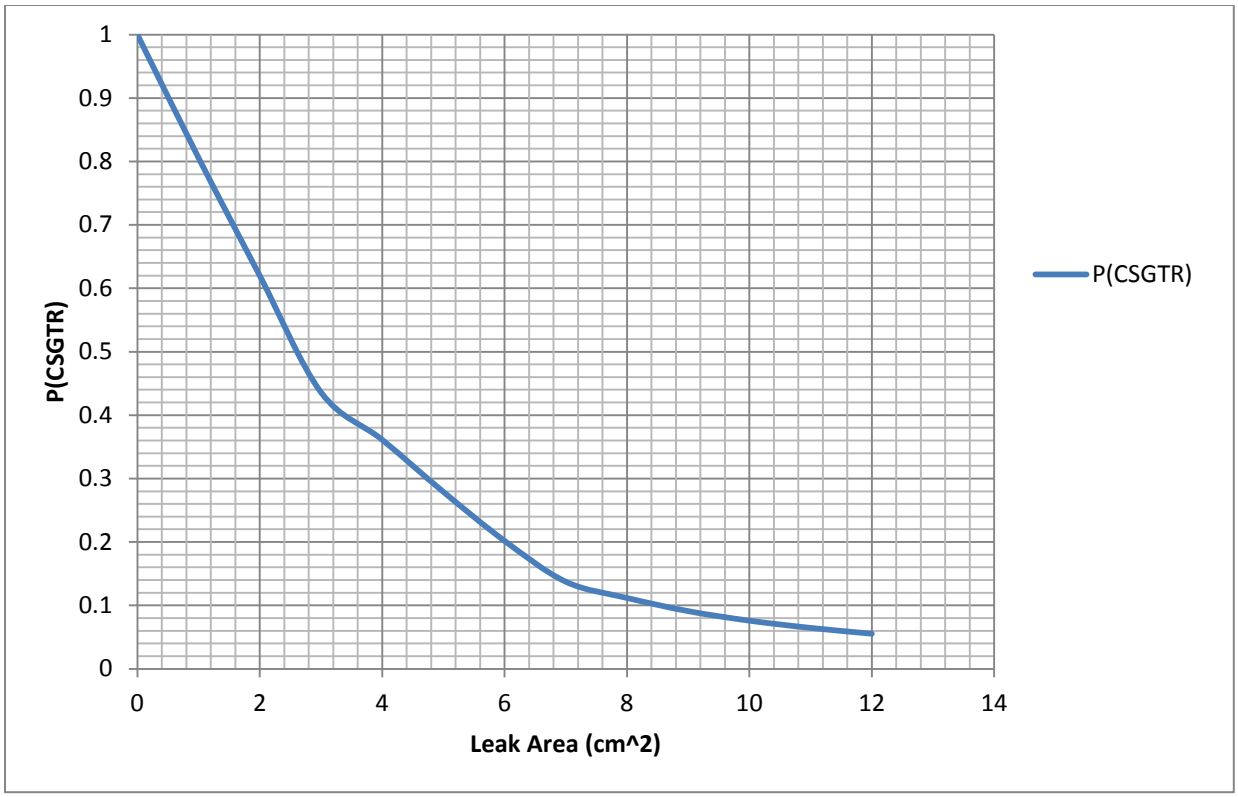


**Figure D-20 Probability of SGTR as a function of critical leak area**

# APPENDIX E

# WESTINGHOUSE STATION BLACKOUT SCENARIO AND SENSITIVITY CASES

This appendix contains additional sensitivity cases for consequential steam generator (SG) tube rupture (C-SGTR) cases in a Westinghouse 4-loop plant with a station blackout (SBO) core damage sequence.

## E.1 Westinghouse SBO Scenario and Sensitivity Cases

The following SBO scenario is considered for the sensitivity cases for temperature-induced C-SGTR events:

| **Scenario Name** | **Scenario Description** (Westinghouse 4-loop NPP–ZION-like) |
|---|---|
| WNEWBASE | SBO at time zero, no turbine-driven auxiliary feedwater (TDAFW) pump, 3.22-$cm^2$ (0.5-$in^2$) leak area in each SG allowing depressurization after dryout. Reactor coolant pump seal leakage of 79.5 liters per minute/pump (21 gallons per minute (gpm)/pump). Ac power is not recovered during this scenario. |

This core damage scenario included the following three cases:

**Case 1** studies the above scenario with thermally treated 600TT material and 1 large SG tube flaw.

**Case 2** studies the above scenario with 600TT material and 10 large SG tube flaws in each of the four SGs.

**Case 3** studies the above scenario with 690TT material and 5 large SG tube flaws in each of the four SGs.

The C-SGTR calculator is used for the calculations. The margin between HL failure time and large SG leak time is estimated. The input files used for the three cases are as follows:

| | **Plant Information File Case** | **TH Scenario File Name** | **Flaw File Name** | **Total # of Flaws in all SGs** |
|---|---|---|---|---|
| Case 1 | ZION600TT | TH-wnewbase-short | Flaw-W3-50 | 1 |
| Case 2 | ZION600TT | TH-wnewbase-short | Flaw-Multi-42 | 42 |
| Case 3 | ZION690TT | TH-wnewbase-short | Flaw-Multi-21-TT690 | 21 |

For comparison with other scenarios, the margin $M_t$ between HL and tube failure is defined as

$M_t$ = Mean time of likely HL failure – mean time of maximum tube flaw failure in terms of minutes

Choosing the mean time of likely HL failure and hot-tube failure is left to the judgment of the analyst.

Figures E-1 and E-2 summarize the relevant scenario parameters.

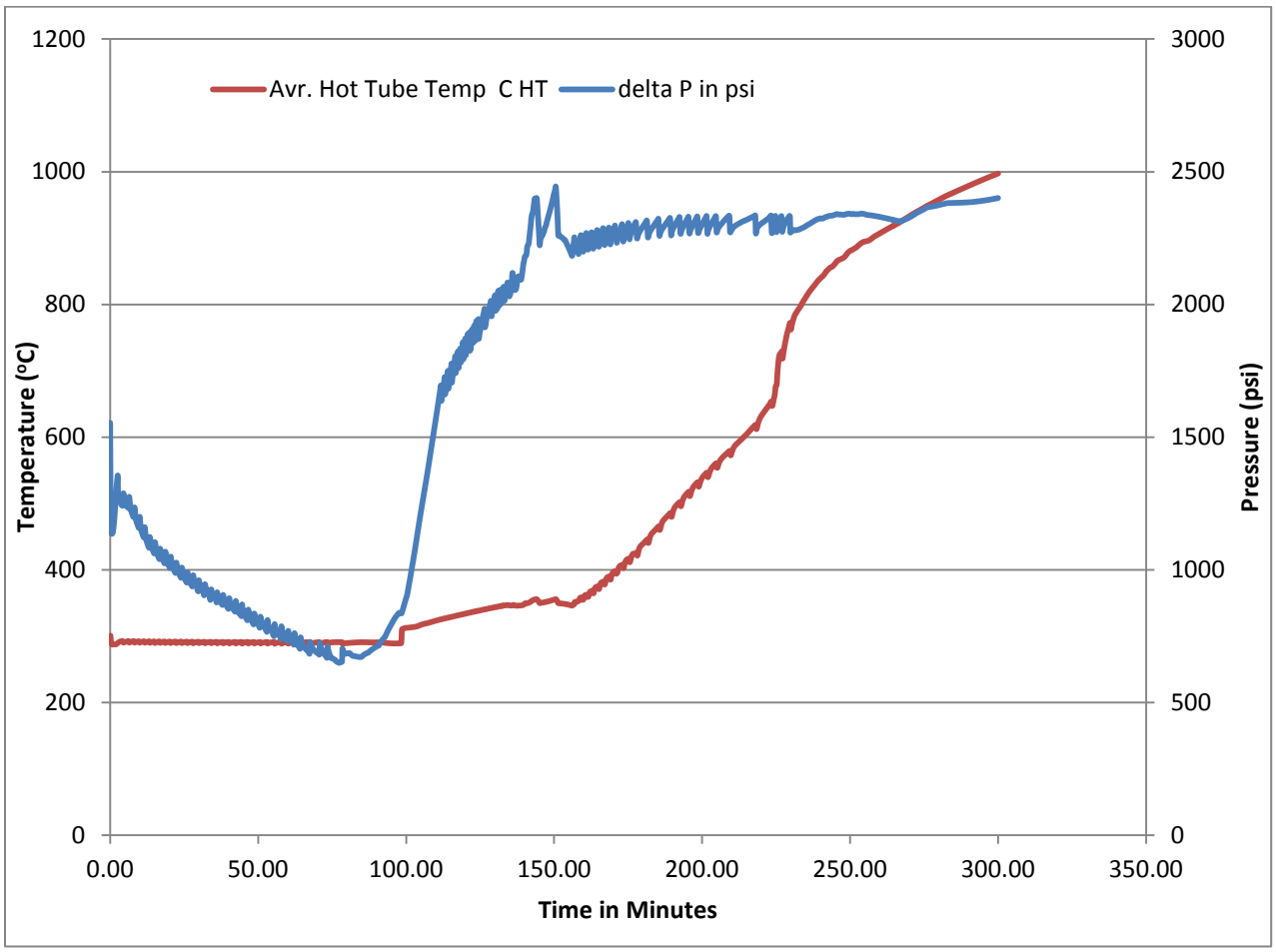


**Figure E-1 WNEWBASE scenario parameters**

Figures E-3 and E-4 summarize the flaw distributions for 600TT and 690TT SG tube materials.

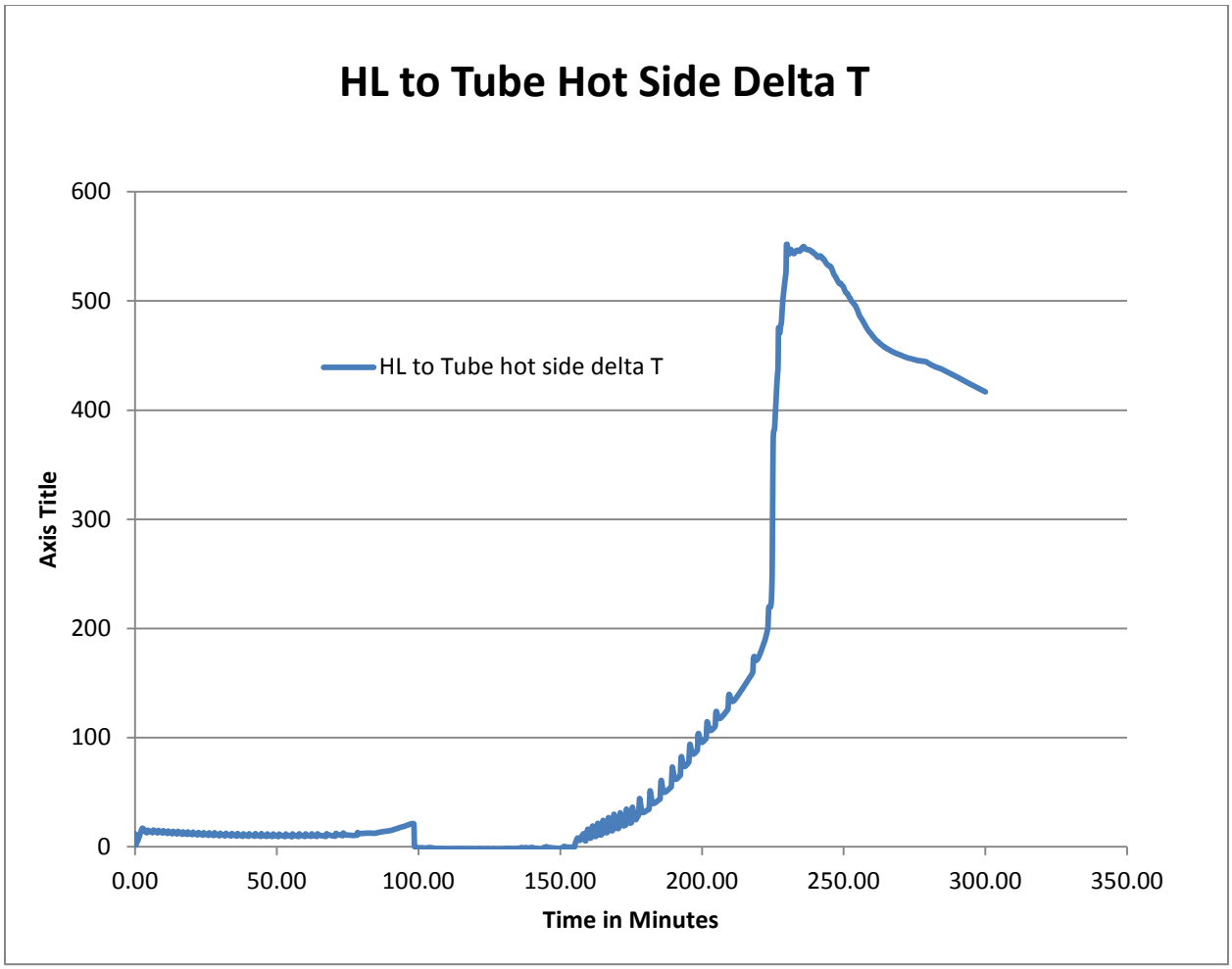


**Figure E-2 Delta T (in degrees Celsius) between HL and hot tube—WNEWBASE**

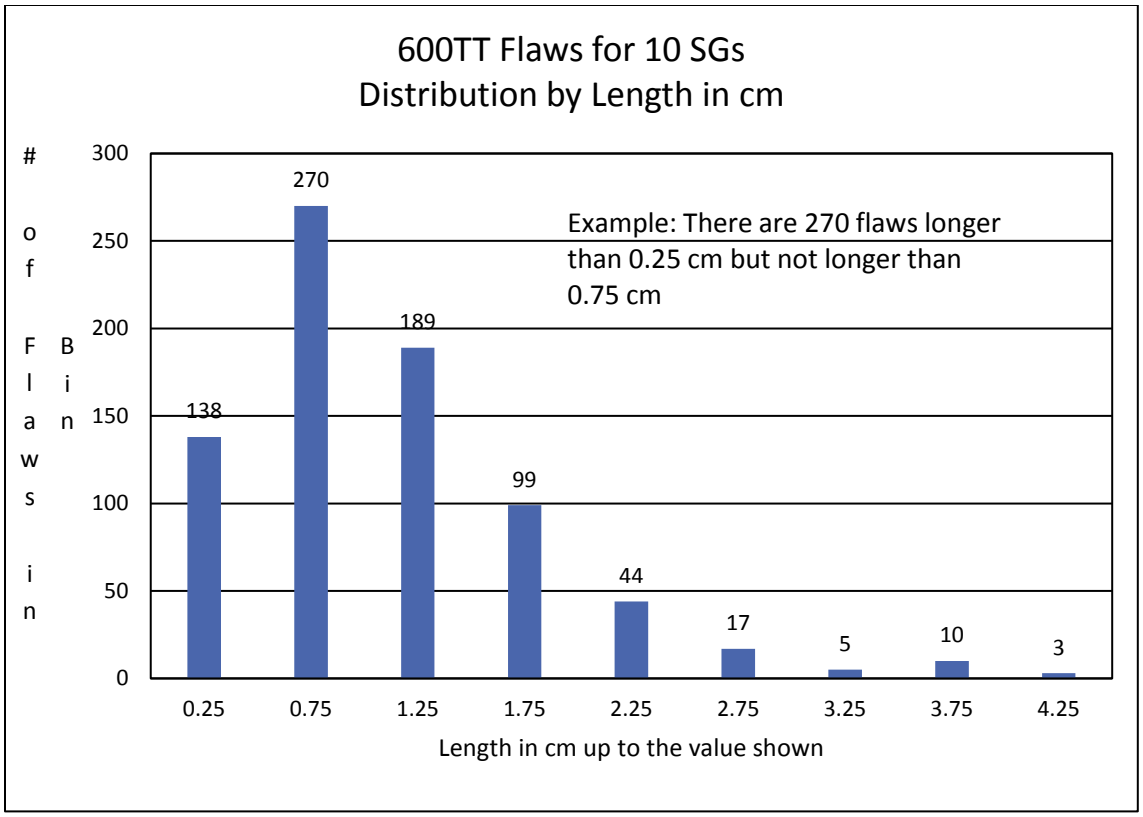


Bin size is ±0.25 centimeter (cm) from the bin center shown above. (For example, bin 0.75 goes from 0.5 to 1.0 cm.)

| Flaw Bin (cm) | # of Flaws |
|---|---|
| 0.25 | 138 |
| 0.75 | 270 |
| 1.25 | 189 |
| 1.75 | 99 |
| 2.25 | 44 |
| 2.75 | 17 |
| 3.25 | 5 |
| 3.75 | 10 |
| 4.25 | 3 |
| | |
| Total = | 775 |

| | | |
|---|---|---|
| Average Size = | 1.1 cm | Average Depth = 13% |
| Largest flaw is 4.46 cm (1.76 in.) in size with a depth of 32%. | | |

**Figure E-3 Histogram for flaw distribution (by size) for 600TT**
***Total of 10 flaw samples for a Zion-like SG with 3,880 600TT tubes after the 15th "cycle"; all flaws are wear type***

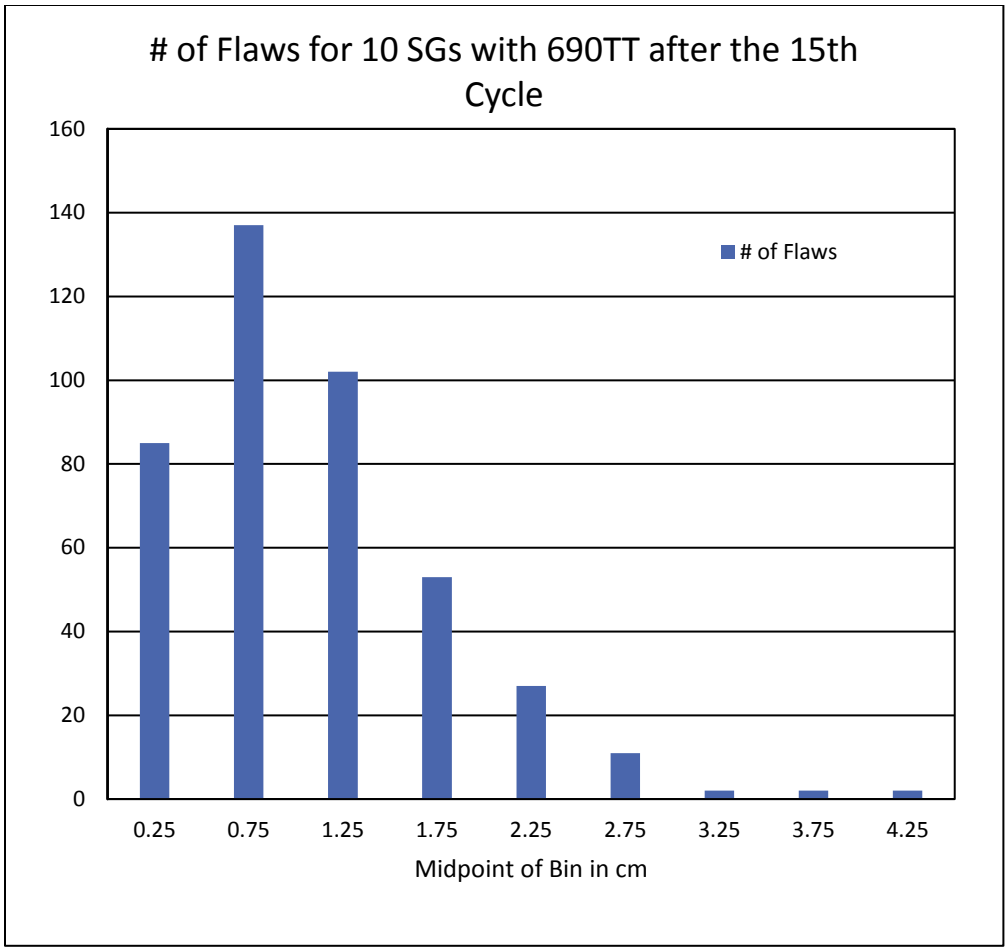


| | |
|---|---|
| Total # of Flaws = | 421 |
| Average Size = | 1.1 cm |
| Average Depth = | 13% |
| Max Length = | 4.4 cm |
| Max Depth = | 47% |

| |
|---|
| Largest flaw is 4.4 cm in size with a depth of 20%. |
| Deepest flaw is 47% with a size of 1.8 cm. |

**Figure E-4 Histogram for flaw distribution (by size) for 690TT**
***Total of 10 flaw samples for a Zion-like SG with 3,880 690TT tubes after the 15th "cycle"; all flaws are wear type***

**Note:** All flaws 40 percent or deeper and generated before K=15 are assumed to be identified and removed by plugging the tubes. Thus, only flaws 40 percent or deeper that are generated in the last cycle would show up in the flaw samples.

## E.2 Case 1: WNEWBASE with 1 Large Flaw and 600TT

The case with 600TT and a single large flaw of W3-50 (wear-type flaw with length 3 cm (1.18 inches (in.)) and depth 50 percent) produced the results shown in Table E-1.

**Table E-1 WNEWBASE Results for Case 1**

| Time in Hours | Time in Seconds | HL Failure Prob. | Surge Line Failure Prob. | $A_{mean}$ $cm^2$ | $A_{75}$ $cm^2$ | $A_{95}$ $cm^2$ |
|---|---|---|---|---|---|---|
| 3.52 | 12656 | 0.00 | 0.00 | 0.00 | 0.00 | 0.00 |
| 3.53 | 12716 | 0.00 | 0.00 | 0.00 | 0.00 | 0.00 |
| 3.55 | 12776 | 0.00 | 0.00 | 0.00 | 0.00 | 0.00 |
| 3.56 | 12830 | 0.02 | 0.00 | 0.00 | 0.00 | 0.00 |
| 3.58 | 12884 | 0.07 | 0.00 | 0.00 | 0.00 | 0.00 |
| 3.59 | 12938 | 0.17 | 0.00 | 0.00 | 0.00 | 0.00 |
| 3.61 | 12992 | 0.33 | 0.00 | 0.00 | 0.00 | 0.00 |
| **3.62** | 13048 | **0.55** | 0.00 | 0.00 | 0.00 | 0.00 |
| 3.63 | 13084 | 0.70 | 0.00 | 0.00 | 0.00 | 0.00 |
| 3.64 | 13090 | 0.72 | 0.00 | 0.00 | 0.00 | 0.00 |
| 3.64 | 13096 | 0.75 | 0.00 | 0.00 | 0.00 | 0.00 |
| 3.64 | 13108 | 0.79 | 0.00 | 0.00 | 0.00 | 0.00 |
| 3.65 | 13132 | 0.86 | 0.00 | 0.00 | 0.00 | 0.00 |
| 3.66 | 13162 | 0.91 | 0.00 | 0.00 | 0.00 | 0.00 |
| 3.67 | 13204 | 0.97 | 0.00 | 0.00 | 0.00 | 0.00 |
| 3.68 | 13246 | 0.99 | 0.00 | 0.00 | 0.00 | 0.00 |
| 3.69 | 13288 | 1.00 | 0.00 | 0.00 | 0.00 | 0.00 |
| 3.70 | 13330 | 1.00 | 0.00 | 0.00 | 0.00 | 0.00 |
| 3.84 | 13812 | 1.00 | 0.19 | 0.01 | 0.00 | 0.00 |
| 3.84 | 13836 | 1.00 | 0.22 | 0.05 | 0.00 | 0.00 |
| 3.85 | 13872 | 1.00 | 0.26 | 0.56 | 1.30 | 2.02 |
| **3.87** | 13938 | 1.00 | 0.32 | **3.23** | 4.47 | 4.93 |
| **3.89** | 14012 | 1.00 | **0.43** | 4.40 | 4.66 | 4.94 |
| 3.91 | 14078 | 1.00 | 0.50 | 4.46 | 4.66 | 4.94 |
| 3.93 | 14150 | 1.00 | 0.59 | 4.46 | 4.67 | 4.94 |
| ….. | | | | | | |
| 4.88 | 17556 | 1.00 | 0.99 | 4.47 | 4.67 | 4.96 |
| 4.94 | 17778 | 1.00 | 0.99 | 4.47 | 4.67 | 4.96 |
| 5.00 | 18000 | 1.00 | 0.99 | 4.47 | 4.67 | 4.96 |

The conclusions are as follows:

- Hot leg fails at 217 minutes.
- Hot tube fails at 232 minutes.
- Surge line fails at 233 minutes.
- Expected value of the maximum SG tube leak area reached is 4.5 $cm^2$ (0.69 $in.^2$).

- Maximum flow area from a single tube is 6.1 $cm^2$ (0.94 $in.^2$).
- Margin is -15 minutes.

Because the maximum leak area of 6 $cm^2$ (0.93 $in.^2$) (critical leak area) is not reached in this case, the margin is defined as follows:

Margin = {time at which HL failure probability exceeds 50%} –
{time at which integrated tube leak probability exceeds 50% of critical leak area}

## E.3 Case 2: WNEWBASE with 42 Flaws and 600TT

A second case is run as follows.

From the 10 flaw samples generated for 600TT, 42 flaws of the largest size and the largest depth are chosen. This corresponds to about 10 large flaws per SG. Other parameters of this case are the same as the one discussed above. All flaws are placed in hot tubes.

Out of the 42 flaws modeled for this case:

Largest flaw is 4.46 cm (1.76 in.) in size with a depth of 32 percent.
Deepest flaw is 40 percent with a size of 0.83 cm (0.32 in.).

The results are summarized in Tables E-2 and E-3.

Max # of tube-equivalent failures = 21 tubes at 250 minutes

Margin = **-15 minutes**

(**Margin** = HL fails 100%—Hot tube fails 6 $cm^2$ (0.93 $in.^2$))

**Table E-2 Summary Output for the Final Scenario with 42 "Large" Flaws**

| | Time in Minutes | | |
|---|---|---|---|
| | **NUREG/CR-6995** | **Calculator** | **Comment** |
| Event starts | 000 | 000 | |
| SG dryout | 100 | | |
| Evacuation starts | | | 120 |
| HL fails 14% | | 215 | |
| First fuel rod clad rupture | 217 | | |
| HL fails 54% | | 217 | |
| HL fails 100% | | **221** | |
| HL 1 fails by creep rupture | 227 | | |
| Surge line fails 16% | | 232 | |
| Hottest tube creep-rupture failure | 233 | | |
| Surge line fails 55% | | 236 | |
| Hot tube fails 6 $cm^2$ (0.93 $in.^2$) (1-tube equivalent) | | **236** | |
| Hot tube fails 22 $cm^2$ (3.41 $in.^2$) (4-tube equivalent) | | 238 | |
| Hot tube fails max 125 $cm^2$ (19.375 $in.^2$)(21-tube equivalent) | | 252 | |
| Surge line fails 100% | | 280 | |
| Evacuation ends for internal events | | | 360 |
| Evacuation ends for external events | | | 600 |
| | | | |
| **Margin** = HL fails 100%—Hot tube fails 6 $cm^2$ (0.93 $in.^2$) | | **-15** | |
| Note: Surge line results are given for completeness only. The surge line correlation and materials assumed may need further examination but are not needed for the purposes of this analysis. | | | |

**Table E-3 WNEWBASE Results for Case 2**

| Time in Hours | Time in Minutes | HL Failure Prob. | Surge Line Failure Prob. | $A_{mean}$ $cm^2$ | $A_{75}$ $cm^2$ | $A_{95}$ $cm^2$ |
|---|---|---|---|---|---|---|
| 3.52 | 211 | 0.00 | 0.00 | 0.00 | 0.00 | 0.00 |
| 3.54 | 212 | 0.00 | 0.00 | 0.00 | 0.00 | 0.00 |
| 3.56 | 213 | 0.01 | 0.00 | 0.00 | 0.00 | 0.00 |
| 3.57 | 214 | 0.04 | 0.00 | 0.00 | 0.00 | 0.00 |
| 3.59 | 215 | 0.14 | 0.00 | 0.00 | 0.00 | 0.00 |
| 3.61 | 216 | 0.31 | 0.00 | 0.00 | 0.00 | 0.00 |
| 3.62 | 217 | 0.54 | 0.00 | 0.00 | 0.00 | 0.00 |
| 3.64 | 218 | 0.78 | 0.00 | 0.00 | 0.00 | 0.00 |
| 3.65 | 219 | 0.87 | 0.00 | 0.00 | 0.00 | 0.00 |
| 3.65 | 219 | 0.94 | 0.00 | 0.00 | 0.00 | 0.00 |
| 3.67 | 220 | 0.99 | 0.00 | 0.00 | 0.00 | 0.00 |
| 3.69 | **221** | **1.00** | 0.00 | 0.00 | 0.00 | 0.00 |
| 3.70 | 222 | 1.00 | 0.00 | 0.00 | 0.00 | 0.00 |
| 3.72 | 223 | 1.00 | 0.00 | 0.00 | 0.00 | 0.00 |
| 3.80 | 228 | 1.00 | 0.00 | 0.00 | 0.00 | 0.00 |
| 3.80 | 228 | 1.00 | 0.00 | 0.00 | 0.00 | 0.00 |
| 3.81 | 229 | 1.00 | 0.00 | 0.00 | 0.00 | 0.00 |
| 3.82 | 229 | 1.00 | 0.01 | 0.00 | 0.00 | 0.00 |
| 3.83 | 230 | 1.00 | 0.03 | 0.00 | 0.00 | 0.00 |
| 3.84 | 230 | 1.00 | 0.08 | 0.00 | 0.00 | 0.00 |
| 3.85 | 231 | 1.00 | 0.10 | 0.00 | 0.00 | 0.00 |
| 3.86 | 232 | 1.00 | 0.16 | 0.00 | 0.00 | 0.00 |
| 3.89 | 233 | 1.00 | 0.28 | 0.01 | 0.00 | 0.00 |
| 3.91 | 235 | 1.00 | 0.41 | 0.46 | 0.61 | 0.89 |
| 3.94 | **236** | 1.00 | 0.55 | **5.40** | 6.40 | 9.90 |
| 3.96 | 238 | 1.00 | 0.67 | 22.00 | 24.00 | 27.00 |
| 3.99 | 239 | 1.00 | 0.76 | 36.00 | 38.00 | 40.00 |
| 4.02 | 241 | 1.00 | 0.85 | 44.00 | 45.00 | 45.00 |
| 4.05 | 243 | 1.00 | 0.89 | 49.00 | 50.00 | 54.00 |
| 4.08 | 245 | 1.00 | 0.91 | 71.00 | 75.00 | 81.00 |
| 4.12 | 247 | 1.00 | 0.93 | 103.00 | 105.00 | 110.00 |
| 4.16 | 250 | 1.00 | 0.95 | 123.00 | 125.00 | 127.00 |
| 4.20 | 252 | 1.00 | 0.96 | 125.00 | 126.00 | 127.00 |
| 4.24 | 255 | 1.00 | 0.97 | 125.00 | 126.00 | 127.00 |
| 4.61 | 277 | 1.00 | 0.98 | 125.00 | 126.00 | 127.00 |
| 4.67 | 280 | 1.00 | 0.99 | 125.00 | 126.00 | 127.00 |
| 5.00 | 300 | 1.00 | 0.99 | 125.00 | 126.00 | 127.00 |

## E.4 Case 3: WNEWBASE with 21 Flaws and 690TT

A third case is run as follows.

From the 10 flaw samples generated for 690TT, 21 flaws of largest size and largest depth are chosen. This corresponds to about 2 large flaws per SG. Other parameters of this case are the same as for the one discussed above.

Out of the 21 flaws modeled for this case:

Largest flaw is 4.4 cm (1.73 in.) in size with a depth of 20 percent.
Deepest flaw is 47 percent with a size of 1.8 cm (0.71 in.).

Table E-4 summarizes the results. The margin is **-7** minutes. Max number of tube-equivalent failures is nine and occurs at 4 hours.

Max # of tube-equivalent failures = 9 tubes at 4 hours

Margin = **-7 minutes**

(**Margin** = HL fails 100%—Hot tube fails 6 $cm^2$ (0.93 $in.^2$))

**Table E-4 WNEWBASE Results for Case 3 with 690TT**

| Time in Hours | Time in Seconds | HL Failure Prob. | Surge Line Failure Prob. | $A_{mean}$ $cm^2$ | $A_{75}$ $cm^2$ | $A_{95}$ $cm^2$ |
|---|---|---|---|---|---|---|
| 3.61 | 216 | 0.35 | 0.00 | 0.01 | 0.02 | 0.02 |
| 3.62 | 217 | 0.54 | 0.00 | 0.02 | 0.02 | 0.03 |
| 3.64 | 218 | 0.79 | 0.00 | 0.04 | 0.05 | 0.06 |
| 3.65 | 219 | 0.88 | 0.00 | 0.05 | 0.06 | 0.07 |
| 3.65 | 219 | 0.93 | 0.00 | 0.07 | 0.08 | 0.09 |
| 3.67 | 220 | 0.98 | 0.00 | 0.11 | 0.12 | 0.13 |
| 3.69 | **221** | **1.00** | 0.00 | 0.17 | 0.18 | 0.20 |
| 3.70 | 222 | 1.00 | 0.00 | 0.24 | 0.25 | 0.28 |
| 3.72 | 223 | 1.00 | 0.00 | 0.33 | 0.35 | 0.39 |
| 3.73 | 224 | 1.00 | 0.00 | 0.40 | 0.42 | 0.47 |
| 3.74 | 224 | 1.00 | 0.00 | 0.46 | 0.49 | 0.54 |
| 3.75 | 225 | 1.00 | 0.00 | 0.56 | 0.60 | 0.66 |
| 3.75 | 225 | 1.00 | 0.00 | 0.69 | 0.73 | 0.80 |
| 3.76 | 226 | 1.00 | 0.00 | 0.97 | 1.03 | 1.13 |
| 3.77 | 226 | 1.00 | 0.00 | 1.60 | 1.70 | 1.80 |
| 3.78 | 227 | 1.00 | 0.00 | 2.40 | 2.50 | 2.80 |
| 3.79 | 227 | 1.00 | 0.00 | 3.20 | 3.40 | 3.70 |
| 3.80 | 228 | 1.00 | 0.00 | 4.10 | 4.30 | 4.70 |
| 3.80 | **228** | 1.00 | 0.00 | **5.50** | 5.80 | 6.30 |
| 3.81 | 229 | 1.00 | 0.00 | 7.50 | 7.90 | 8.50 |
| 3.82 | 229 | 1.00 | 0.01 | 10.10 | 10.60 | 11.30 |
| 3.83 | 230 | 1.00 | 0.02 | 13.20 | 13.80 | 14.90 |
| 3.84 | 230 | 1.00 | 0.07 | 16.30 | 17.10 | 18.00 |
| 3.85 | 231 | 1.00 | 0.11 | 19.30 | 20.00 | 20.80 |
| 3.86 | 232 | 1.00 | 0.18 | 24.70 | 25.40 | 26.60 |
| 3.89 | 233 | 1.00 | 0.32 | 31.10 | 31.80 | 33.00 |
| 3.91 | 235 | 1.00 | 0.44 | 36.80 | 37.50 | 38.70 |
| 3.94 | 236 | 1.00 | 0.60 | 42.80 | 43.60 | 44.70 |
| 3.96 | 238 | 1.00 | 0.70 | 48.10 | 49.00 | 49.90 |
| 3.99 | 239 | 1.00 | 0.80 | 50.50 | 51.10 | 52.00 |
| 4.02 | 241 | 1.00 | 0.90 | 51.70 | 52.20 | 53.00 |
| 4.05 | 243 | 1.00 | 0.90 | 51.80 | 52.30 | 53.00 |
| 4.08 | 245 | 1.00 | 0.90 | 51.80 | 52.30 | 53.00 |

# APPENDIX F

# PRESSURE-INDUCED CONSEQUENTIAL STEAM GENERATOR TUBE RUPTURE—SUPPORTING CALCULATIONS

## F.1 Estimation of C-SGTR for a Flaw Bin

The study selected the loss of a main feedwater anticipated transient without scram (ATWS) event for evaluating the bounding scenario. The analysis used a primary pressure of 22 megapascals (MPa) (3,200 pounds per square inch (psi)), a primary temperature of 370 degrees Celsius (C) (698 degrees Fahrenheit (F)), and a secondary pressure of 6.89 MPa (1,000 psi). The temperature of 370 degrees C (698 degrees F) was selected because it is the saturated temperature of water/steam at 22 MPa (3,200 psi). Table F-1 and Figure F-1 show the thermal-hydraulic (TH) input file for the analysis.

**Table F-1 TH Input File for C-SGTR for Simulating ATWS Scenarios**

| Time (s) | Primary Pressure (pa) | Surge Line Temp (°C) | HL Temp (°C) | Hot SG Tube Temp (°C) | Cold SG Tube Temp (°C) | Secondary Pressure (pa) |
|---|---|---|---|---|---|---|
| 0.0 | 1.56E+7 | 311.21 | 311.21 | 311.21 | 311.21 | 6.10E+6 |
| 2.0 | 2.20E+7 | 370.00 | 370.00 | 370.00 | 370.00 | 6.10E+6 |
| 4.0 | 2.20E+7 | 370.00 | 370.00 | 370.00 | 370.00 | 6.10E+6 |
| 6.0 | 2.20E+7 | 370.00 | 370.00 | 370.00 | 370.00 | 6.10E+6 |
| 8.0 | 2.20E+7 | 370.00 | 370.00 | 370.00 | 370.00 | 6.10E+6 |
| 10.0 | 2.20E+7 | 370.00 | 370.00 | 370.00 | 370.00 | 6.10E+6 |
| 20.0 | 2.20E+7 | 370.00 | 370.00 | 370.00 | 370.00 | 6.10E+6 |
| 30.0 | 2.20E+7 | 370.00 | 370.00 | 370.00 | 370.00 | 6.10E+6 |
| 40.0 | 1.55E+7 | 370.00 | 370.00 | 370.00 | 370.00 | 6.10E+6 |
| 50.0 | 1.55E+7 | 370.00 | 370.00 | 370.00 | 370.00 | 6.10E+6 |
| 60.0 | 1.55E+7 | 370.00 | 370.00 | 370.00 | 370.00 | 6.10E+6 |
| 120.0 | 1.55E+7 | 370.00 | 370.00 | 370.00 | 370.00 | 6.10E+6 |

Similarly, Table F-2 and Figure F-2 show the TH behavior assumed for steamline break (SLB) scenarios.

A set of case runs was performed using the consequential steam generator (SG) tube rupture (C-SGTR) software, the TH files discussed earlier, and a set of flaws representing the expected flaws plus one large flaw. Table F-3 shows an example of a flaw set consisting of the expected flaw set plus one large flaw of 70-percent depth and 3-centimeter (cm) (1.2-inches (in.)) length.

Tables F-4 and F-5 show portions of the two C-SGTR output files (i.e., “intermediate Probability” and “cumulative leak Area” files). Table F-4 shows the flaw failure results for the flaw #126, which corresponds to a large flaw when the SLB TH file is used. The probability of tube failure for a flaw with 70-percent depth and 3-cm (1.2-in.) length is about 0.57 during a severe SLB scenario. It also appears that the upper bound of the leak rate (95 percentile values) is about 4.529, which is approximately equivalent to the guillotine break of one tube in the example

Combustion Engineering (CE) plant. This is further confirmed by examining the Cumulative Leak Area output in Table F-5. Table F-5 also shows that the expected set of flaws do not contribute to C-SGTR during an SLB accident.

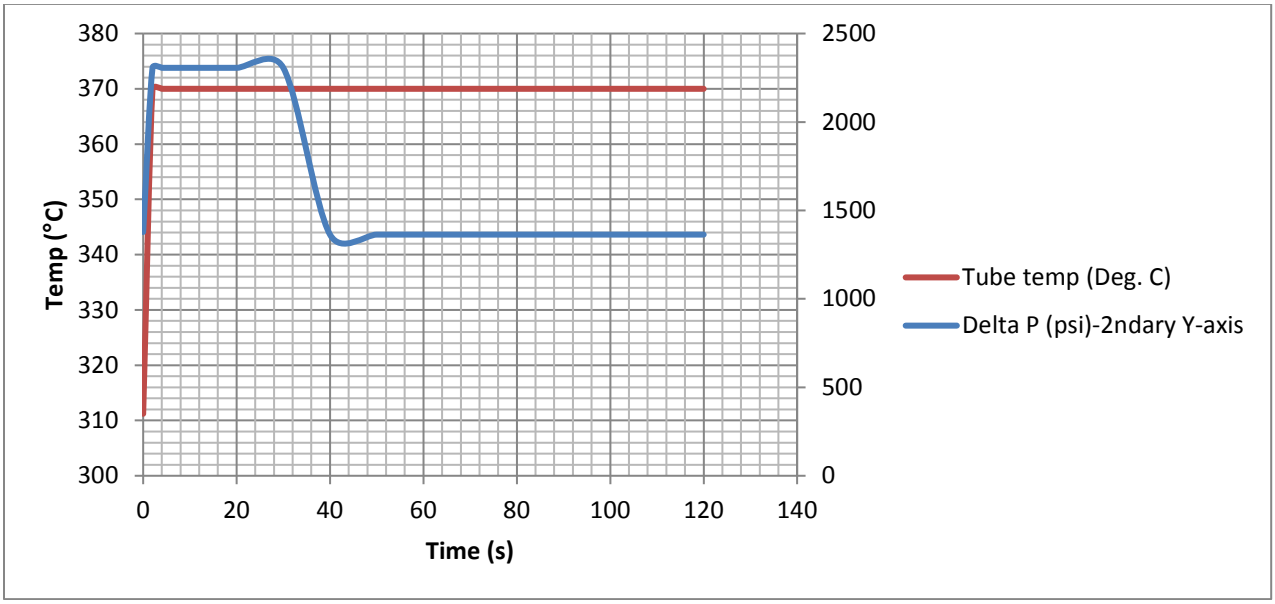


**Figure F-1 Assumed TH behavior for ATWS for C-SGTR analysis**

**Table F-2 TH Input File for C-SGTR for Simulating SLB Scenarios**

| Time (s) | Primary Pressure (pa) | Surge Line Temp (°C) | HL Temp (°C) | Hot SG Tube Temp (°C) | Cold SG Tube Temp (°C) | Secondary Pressure (pa) |
|---|---|---|---|---|---|---|
| 0.0 | 1.56E+7 | 311.21 | 311.21 | 311.21 | 311.21 | 6.10E+6 |
| 2.0 | 1.56E+7 | 300.00 | 300.00 | 300.00 | 300.00 | 9.60E+4 |
| 4.0 | 1.56E+7 | 300.00 | 300.00 | 300.00 | 300.00 | 9.60E+4 |
| 6.0 | 1.56E+7 | 300.00 | 300.00 | 300.00 | 300.00 | 9.60E+4 |
| 8.0 | 1.56E+7 | 300.00 | 300.00 | 300.00 | 300.00 | 9.60E+4 |
| 10.0 | 1.56E+7 | 300.00 | 300.00 | 300.00 | 300.00 | 9.60E+4 |
| 20.0 | 1.56E+7 | 300.00 | 300.00 | 300.00 | 300.00 | 9.60E+4 |
| 30.0 | 1.56E+7 | 300.00 | 300.00 | 300.00 | 300.00 | 9.60E+4 |
| 40.0 | 1.56E+7 | 300.00 | 300.00 | 300.00 | 300.00 | 9.60E+4 |
| 50.0 | 1.56E+7 | 300.00 | 300.00 | 300.00 | 300.00 | 9.60E+4 |
| 60.0 | 1.56E+7 | 300.00 | 300.00 | 300.00 | 300.00 | 9.60E+4 |
| 120.0 | 1.56E+7 | 300.00 | 300.00 | 300.00 | 300.00 | 9.60E+4 |

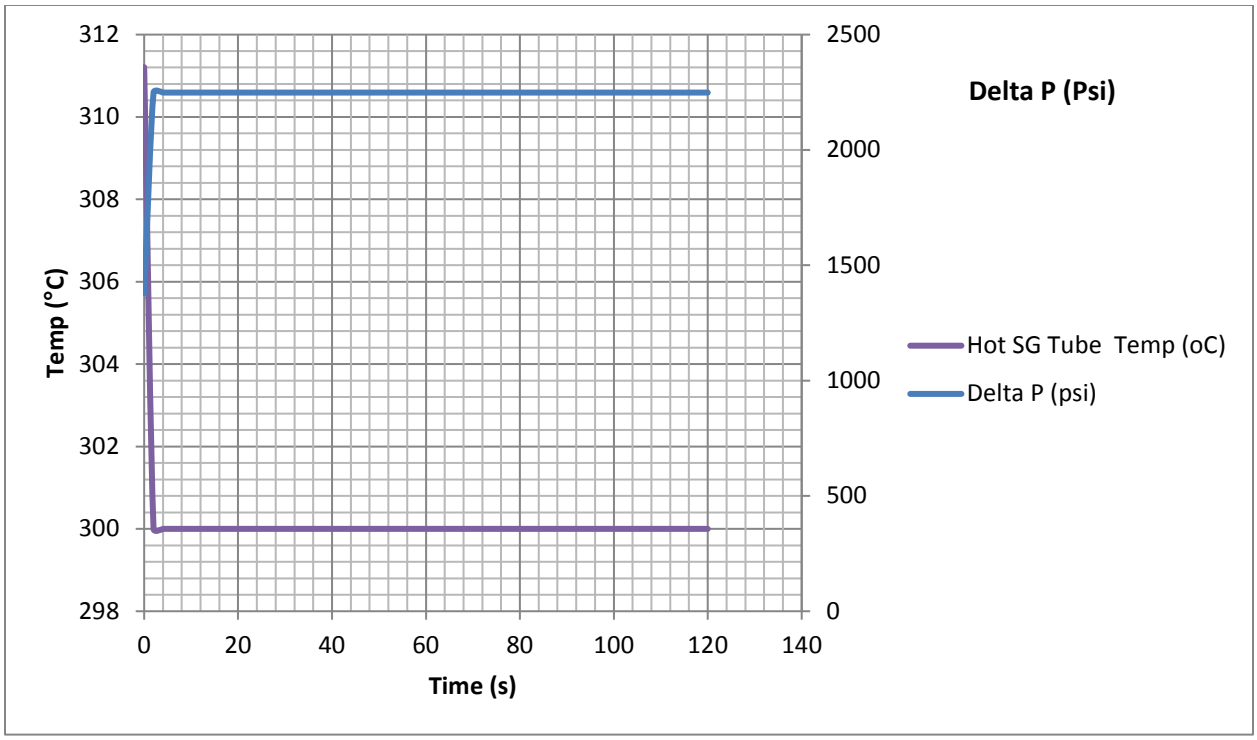


**Figure F-2 Assumed TH behavior for SLB for C-SGTR analysis**

**Table F-3 Example of Expected Flaw Set Plus One Large Flaw of 70-Percent Depth and 3-cm Length for a CE Plant**

| Flaw orientation | Flaw length (cm) | Circ. Angle | Depth | Axial Location (not used) | Flaw type | SD of Error | Mean of Error | Flow reduction factor |
|---|---|---|---|---|---|---|---|---|
| A | 1.5 | 0 | 0.05 | 0 | 2 | 0.03 | 0 | 1 |
| A | 1.5 | 0 | 0.05 | 0 | 2 | 0.03 | 0 | 1 |
| A | 1.5 | 0 | 0.05 | 0 | 2 | 0.03 | 0 | 1 |
| A | 1.5 | 0 | 0.05 | 0 | 2 | 0.03 | 0 | 1 |
| A | 1.5 | 0 | 0.05 | 0 | 2 | 0.03 | 0 | 1 |
| A | 1.5 | 0 | 0.05 | 0 | 2 | 0.03 | 0 | 1 |
| A | 2.5 | 0 | 0.05 | 0 | 2 | 0.03 | 0 | 1 |
| A | 2.5 | 0 | 0.05 | 0 | 2 | 0.03 | 0 | 1 |
| A | 2.5 | 0 | 0.05 | 0 | 2 | 0.03 | 0 | 1 |
| A | 3.5 | 0 | 0.05 | 0 | 2 | 0.03 | 0 | 1 |
| --- | --- | --- | --- | --- | --- | --- | --- | --- |
| --- | --- | --- | --- | --- | --- | --- | --- | --- |
| A | 1.5 | 0 | 0.35 | 0 | 2 | 0.03 | 0 | 1 |
| A | 1.5 | 0 | 0.35 | 0 | 2 | 0.03 | 0 | 1 |
| A | 3.0 | 0 | 0.70 | 0 | 2 | 0.03 | 0 | 1 |

**Table F-4 Results of Intermediate File from C-SGTR for Flaw #126, at 70-Percent Depth and 3-cm Length for a CE Plant and TH File Representing SLB**

| Flaw # | Time (s) | $P_{leak}$ | $P_{burst}$ | $P_{CR}$ (NA) | $Ab_m$ (mean burst area) | $Ab_{0.05}$ (5% burst area) | $Ab_{0.95}$ (95% burst area) | $Al_m$ (mean leak area) | $Al_{0.05}$ (5% leak area) | $Al_{0.95}$ (95% leak area) | $Acr_m$ (mean CR area) | $Acr_{0.05}$ (5% CR area) | $Acr_{0.95}$ (95% CR area) |
|---|---|---|---|---|---|---|---|---|---|---|---|---|---|
| 126 | 0 | 0.000 | 0.000 | 0 | 0.000 | 0 | 0.000 | 0.000 | 0 | 0.000 | 0.000 | 0 | 0 |
| 126 | 2 | 0.569 | 0.569 | 0 | 2.546 | 0 | 4.528 | 2.546 | 0 | 4.528 | 0.000 | 0 | 0 |
| 126 | 4 | 0.569 | 0.569 | 0 | 2.798 | 0 | 4.528 | 2.798 | 0 | 4.528 | 2.546 | 0 | 0 |
| 126 | 6 | 0.569 | 0.569 | 0 | 2.939 | 0 | 4.528 | 2.939 | 0 | 4.528 | 2.798 | 0 | 0 |
| 126 | 8 | 0.569 | 0.569 | 0 | 3.018 | 0 | 4.528 | 3.018 | 0 | 4.528 | 2.939 | 0 | 0 |
| 126 | 10 | 0.569 | 0.569 | 0 | 3.119 | 0 | 4.529 | 3.119 | 0 | 4.529 | 3.018 | 0 | 0 |
| 126 | 20 | 0.569 | 0.569 | 0 | 3.119 | 0 | 4.529 | 3.167 | 0 | 4.529 | 3.119 | 0 | 0 |
| 126 | 30 | 0.569 | 0.569 | 0 | 3.119 | 0 | 4.529 | 3.184 | 0 | 4.529 | 3.119 | 0 | 0 |
| 126 | 40 | 0.569 | 0.569 | 0 | 3.119 | 0 | 4.529 | 3.210 | 0 | 4.529 | 3.119 | 0 | 0 |
| 126 | 50 | 0.569 | 0.569 | 0 | 3.119 | 0 | 4.529 | 3.244 | 0 | 4.529 | 3.119 | 0 | 0 |
| 126 | 60 | 0.569 | 0.569 | 0 | 3.119 | 0 | 4.529 | 3.266 | 0 | 4.529 | 3.119 | 0 | 0 |
| 126 | 120 | 0.569 | 0.569 | 0 | 3.119 | 0 | 4.529 | 3.291 | 0 | 4.529 | 3.119 | 0 | 0 |

**Table F-5 Results of Cumulative Leak Area File from C-SGTR for Expected Flaws Plus One Flaw at 70-Percent Depth and 3-cm Length for a CE Plant and TH File Representing SLB**

| Time | Am | A0.05 | A0.25 | A0.50 | A0.75 | A0.95 | Asd |
|---|---|---|---|---|---|---|---|
| 0 | 0.000 | 0 | 0 | 0.00 | 0.00 | 0.00 | 0.00 |
| 2 | 2.546 | 0 | 0 | 4.41 | 4.49 | 4.53 | 2.213 |
| 4 | 2.798 | 0 | 0 | 4.45 | 4.49 | 4.53 | 2.160 |
| 6 | 2.939 | 0 | 0 | 4.45 | 4.49 | 4.53 | 2.116 |
| 8 | 3.018 | 0 | 0 | 4.45 | 4.49 | 4.53 | 2.087 |
| 10 | 3.119 | 0 | 0 | 4.45 | 4.49 | 4.53 | 2.044 |
| 20 | 3.167 | 0 | 0 | 4.46 | 4.49 | 4.53 | 2.021 |
| 30 | 3.184 | 0 | 0 | 4.46 | 4.49 | 4.53 | 2.013 |
| 40 | 3.210 | 0 | 0 | 4.46 | 4.49 | 4.53 | 1.999 |
| 50 | 3.245 | 0 | 0 | 4.46 | 4.49 | 4.53 | 1.981 |
| 60 | 3.266 | 0 | 0 | 4.46 | 4.49 | 4.53 | 1.969 |
| 120 | 3.291 | 0 | 0 | 4.46 | 4.49 | 4.53 | 1.954 |

Tables F-6 and F-7 summarize the results of these evaluations for the example CE plant for ATWS and SLB scenarios, for Inconel 690, and considering all large flaw bins. The results show that a large flaw with 70-percent depth has about 70-percent chance of failure during ATWS and 57-percent probability of failure during SLB. Furthermore, the results showed that the minimum size of the flaw has to be at least 3 cm (1.2 in.) to create a large enough leak area to be considered as C-SGTR. Limited runs were also performed for the example Westinghouse plant and Inconel 600 tubes for comparison with the CE results. These runs indicated that the probability of the tube failure is slightly lower for the Westinghouse plant because of the differences between the material properties of Inconel 600 and Inconel 690. For example, for a

flaw with 70-percent depth, the tube failure probability for Westinghouse is about 0.46 rather than the 0.57 estimated for the CE plant. The comparison also revealed that the leak area for the Westinghouse plant is slightly larger because of its larger tube diameter.

For example, for a 3-cm (1.2-in.) flaw, the leak area for the example Westinghouse plant was estimated to be about 4.93 square centimeter ($cm^2$) (0.76 square inch ($in.^2$)), compared to the leak area of 4.46 $cm^2$ (0.69 $in.^2$) for the example CE plant.

**Table F-6 Case Results of Pressure-Induced C-SGTR during ATWS**

| Case Run | $A_m$ | $P_l$ | $P_b$ |
|---|---|---|---|
| Expected Flaw Sample | 0.000 | 0.000 | 0.000 |
| Expected Flaw Sample + 1 Flaw with 60% depth and 3-cm length | 0.004 | 0.001 | 0.001 |
| Expected Flaw Sample + 1 Flaw with 70% depth and 3-cm length | 4.400 | 0.676 | 0.676 |
| Expected Flaw Sample + 1 Flaw with 80% depth and 3-cm length | 4.397 | 1.000 | 1.000 |
| Expected Flaw Sample + 1 Flaw with 60% depth and 4-cm length | 0.009 | 0.002 | 0.002 |
| Expected Flaw Sample + 1 Flaw with 70% depth and 4-cm length | 3.659 | 0.687 | 0.687 |
| Expected Flaw Sample + 1 Flaw with 80% depth and 4-cm length | 4.497 | 1.000 | 1.000 |

**Table F-7 Case Results of Pressure-Induced C-SGTR during SLB**

| Case Run | $A_m$ | $P_l$ | $P_b$ |
|---|---|---|---|
| Expected Flaw Sample | 0.00 | 0.00 | 0.00 |
| Expected Flaw Sample + 1 Flaw with 60% depth and 3-cm length | 0.00 | 0.00 | 0.00 |
| Expected F-aw Sample + 1 Flaw with 70% depth and 3-cm length | 3.29 | 0.57 | 0.57 |
| Expected Flaw Sample + 1 Flaw with 80% depth and 3-cm length | 4.40 | 1.00 | 1.00 |
| Expected Flaw Sample + 1 Flaw with 60% depth and 4-cm length | 0.00 | 0.00 | 0.00 |
| Expected Flaw Sample + 1 Flaw with 70% depth and 4-cm length | 4.40 | 0.55 | 0.55 |
| Expected Flaw Sample + 1 Flaw with 80% depth and 4-cm length | 4.40 | 1.00 | 1.00 |

The probability of C-SGTR for the example CE plant bounds the C-SGTR probability for the example Westinghouse plant. Furthermore, the C-SGTR failure probability for ATWS bounds the C-SGTR failure probability for SLB scenarios. Therefore, Tables F-8 and F-9 provide the bounding probability of C-SGTR for both ATWS and SLB scenarios, covering both Westinghouse and CE plants, for each of the flaw bins tabulated in Section 7.1.

Table F-9 shows the probability that the SG tubes fail but without creating sufficient leak rate to be considered as C-SGTR (i.e., called SGTR-Leak). These are caused by flaws with a depth of 70 percent or more but a length of 3 cm (1.18 in.) or less.

**Table F-8 Bounding C-SGTR Probability per a Flaw Bin to be Used for Both SLB and ATWS Scenarios for Westinghouse and CE Plants**

| Depth/ Length | 0 cm to 1 cm | 1 cm to 2 cm | 2 cm to 3 cm | 3 cm to 4 cm | 4 cm to 5 cm | 5 cm to 6 cm |
|---|---|---|---|---|---|---|
| 0.1 to 0.6 | 0 | 0 | 0 | 0 | 0 | 0 |
| 0.6 to 0.7 | 0 | 0 | 0 | 1.0E-03 | 1.0E-03 | 1.0E-03 |
| 0.7 to 0.8 | 0 | 0 | 0 | 5.7E-01 | 5.7E-01 | 5.7E-01 |
| 0.8 to 0.9 | 0 | 0 | 0 | 1.0E+00 | 1.0E+00 | 1.0E+00 |

**Table F-9 Bounding Probability for SGTR—Leak per a Flaw Bin to be Used for Both SLB and ATWS Scenarios for Westinghouse and CE Plants**

| Depth/ Length | 0 cm to 1 cm | 1 cm to 2 cm | 2 cm to 3 cm | 3 cm to 4 cm | 4 cm to 5 cm | 5 cm to 6 cm |
|---|---|---|---|---|---|---|
| 0.1 to 0.6 | 0 | 0 | 0 | 0 | 0 | 0 |
| 0.6 to 0.7 | 0 | 0 | 0 | 0 | 0 | 0 |
| 0.7 to 0.8 | 0.57 | 0.57 | 0.57 | 0 | 0 | 0 |
| 0.8 to 0.9 | 1.00 | 1.00 | 1.00 | 0 | 0 | 0 |

Table F-10 reproduces Table 7-3, which shows, for both Inconel 600 and 690 SG tubes, the probability that a flaw belongs to a flaw bin. Table F-11 shows that the probability of a flaw residing in a flaw bin multiplied by the probability of C-SGTR will yield the probability of C-SGTR per flaw tubes. The bounding probability that a flawed tube results in C-SGTR during ATWS or SLB is estimated to be approximately $2.3X10^{-5}$. Similarly, the bounding probability that a flawed tube fails, not with a sufficient leak area to be considered C-SGTR but considered as an SGTR-Leak, is $1.4X10^{-4}$.

**Table F-10 Probability that a Detected Flaw Belongs to a Bin Size at 15 Effective Full-Power Years**

| Depth/ Length | 0 cm to 1 cm | 1 cm to 2 cm | 2 cm to 3 cm | 3 cm to 4 cm | 4 cm to 5 cm | 5 cm to 6 cm | Total |
|---|---|---|---|---|---|---|---|
| 0 to 0.1 | 2.74E-3 | 4.62E-2 | 2.23E-2 | 5.38E-3 | 1.04E-3 | 1.80E-4 | 7.78E-2 |
| 0.1 to 0.2 | 1.86E-2 | 3.14E-1 | 1.52E-1 | 3.66E-2 | 7.08E-3 | 1.23E-3 | 5.29E-1 |
| 0.2 to 0.3 | 9.59E-3 | 1.62E-1 | 7.81E-2 | 1.89E-2 | 3.64E-3 | 6.31E-4 | 2.73E-1 |
| 0.3 to 0.4 | 3.09E-3 | 5.21E-2 | 2.52E-2 | 6.07E-3 | 1.17E-3 | 2.03E-4 | 8.78E-2 |
| 0.4 to 0.5 | 8.47E-4 | 1.43E-2 | 6.90E-3 | 1.66E-3 | 3.22E-4 | 5.57E-5 | 2.41E-2 |
| 0.5 to 0.6 | 2.14E-4 | 3.61E-3 | 1.74E-3 | 4.21E-4 | 8.13E-5 | 1.41E-5 | 6.08E-3 |
| 0.6 to 0.7 | 5.14E-5 | 8.67E-4 | 4.19E-4 | 1.01E-4 | 1.95E-5 | 3.38E-6 | 1.46E-3 |
| 0.7 to 0.8 | 1.19E-5 | 2.01E-4 | 9.73E-5 | 2.35E-5 | 4.54E-6 | 7.86E-7 | 3.39E-4 |
| 0.8 to 0.9 | 2.71E-6 | 4.57E-5 | 2.21E-5 | 5.32E-6 | 1.03E-6 | 1.78E-7 | 7.70E-5 |
| Total | 3.52E-2 | 5.93E-1 | 2.86E-1 | 6.91E-2 | 1.34E-2 | 2.31E-3 | ~1 |

**Table F-11 C-SGTR Probability for SLB or ATWS Scenarios per Flaw**

| Depth | 0 cm to 1 cm |
|---|---|
| 0.0 to 0.5 | 0 |
| 0.6 to 0.7 | 1.24E-7 |
| 0.7 to 0.8 | 1.64E-5 |
| 0.8 to 0.9 | 6.52E-6 |
| Total | **2.30E-5** |

## F.2 Estimation of Pressure-Induced C-SGTR Probability

For ATWS scenarios, all SGs will be exposed to potentially high reactor coolant system pressure, which could cause C-SGTR. The probability of C-SGTR is estimated by considering the total number of flaws at Cycle 15 for the example Westinghouse and CE plants.

For most SLB scenarios, one or more SGs could be exposed to the pressure environment conducive to the pressure-induced C-SGTR. This would depend on what has led to secondary depressurization and how many main steam isolation valves have closed. A specific SG may be of interest for some scenarios of SLB, rather than all SGs.

The bounding C-SGTR probability for ATWS and SLB, is, therefore, estimated twice; once for one specific SG, and then for all SGs. This is shown below:

**Example Westinghouse Plant at Cycle 15**
Expected number of flaws in each SG = 79
Expected number of flaws in all four SGs = 315
Probability of C-SGTR for the specific SG = $(1-(1-2.3X10^{-5})^{79}) = 2.5\ X10^{-3}$
Probability of C-SGTR for ATWS for any of four SGs = $(1-(1-2.3X10^{-5})^{315}) = 0.01$
**Example CE Plant at Cycle 15**
Expected number of flaws in each SG = 125
Expected number of flaws in both SGs = 253
Probability of C-SGTR for the specific SG = $(1-(1-2.3X10^{-5})^{125}) = 4.0X10^{-3}$
Probability of C-SGTR for ATWS for any of four SGs = $(1-(1-2.3X10^{-5})^{253}) = 8.0X10^{-3}$

Section 7.4 and Appendix C use the above values.

## F.3 Estimation of Pressure-Induced SGTR-Leak Probability

The bounding SGTR-Leak probability for ATWS and SLB is estimated twice; once for one specific SG, and then for all SGs. This is shown below:

**SGTR-Leak Probability for Example Westinghouse Plant at Cycle 15**
Expected number of flaws in each SG = 79
Expected number of flaws in all four SGs = 315
Probability of C-SGTR for the specific SG = $(1-(1-1.4X10^{-4})^{79}) = 1.1X10^{-2}$
Probability of C-SGTR for ATWS for any of four SGs = $(1-(1-1.4X10^{-4})^{315}) = 4.3X10^{-2}$
**SGTR-Leak Probability for Example CE Plant at Cycle 15**
Expected number of flaws in each SG = 125
Expected number of flaws in both SGs = 253
Probability of C-SGTR for the specific SG = $(1-(1-1.4X10^{-4})^{125}) = 1.7X10^{-2}$
Probability of C-SGTR for ATWS for any of four SGs = $(1-(1-1.4X10^{-4})^{253}) = 3.5X10^{-2}$

Appendix C uses the above values.

# APPENDIX G

# ESTIMATING THE ENTRY FREQUENCY FROM LEVEL 1 PROBABILISTIC RISK ASSESSMENT FOR LEVEL 2 PROBABILISTIC RISK ASSESSMENT ANALYSIS

## G.1 Zion Nuclear Power Plant

This study selected the Zion Nuclear Power Plant (ZNPP) for developing the Level 2 probabilistic risk assessment (PRA) models to ensure consistency with the thermal-hydraulic (TH) analyses results. No current PRA or standardized plant analysis risk (SPAR) models are available for ZNPP, and ZNPP units are no longer in operation. The estimates for a prolonged station blackout (SBO) condition, as the entry point for the Level 2 PRA, was, therefore, estimated based on the plant design features and information from vintage ZNPP PRA documents. This appendix discusses the process for developing the Level 2 PRA entry condition for containment bypass resulting from a consequential steam generator (SG) tube rupture (C-SGTR) for ZNPP Unit 1. It considers all potential conditions from internal and external hazards resulting in a prolonged SBO.

### G.1.1 Internal Event

Table G-1 provides the relevant information for ZNPP. The frequency of all scenarios resulting in prolonged SBOs (greater than battery duration of 6 hours) was estimated for internal initiating events excluding internal fires and floods (i.e., from Table 2.2-2 of NUREG/CR-4551, "Evaluation of Severe Accident Risks: Methodology for the Containment, Source Term, Consequence, and Risk Integrations Analyses," issued December 1993). The overall frequency estimated from this process for ZNPP is about $5.23X10^{-6}$ per year.

The reasonableness of the overall frequency of prolonged SBO was examined using the current information on the loss of offsite power (LOOP) from NUREG/CR-6890, "Reevaluation of Station Blackout Risk at Nuclear Power Plants," issued December 2005. This independent examination used both single and dual unit LOOP frequencies, along with the latest common-cause alpha factor model in SPAR.

The frequencies of single- and dual-unit LOOP exceeding 6 hours were estimated as $7.72X10^{-4}$ and $1.64X10^{-3}$. A success criterion for a dual LOOP event was defined as having at least three emergency diesel generators (EDGs) operating. This success criterion could include either of the following:

- at least the three dedicated EDGs operating
- two dedicated EDGs operating in one unit and a swing EDG aligned to the other unit, which will meet all the operational requirements for the service water and the component cooling water (CCW) systems

For single LOOP events, the success criteria were two dedicated EDGs operating or one dedicated EDG in the affected unit plus the operation of the shared EDG.

For a dual unit LOOP, common-cause failures of three out of five EDGs, and for a single LOOP, common-cause failures of three out of three EDGs, will result in an SBO.

**Table G-1 Information from Zion Nuclear Station**

| Systems | System Features |
|---|---|
| Emergency Power System | a. Each unit consists of 3 4160-VAC class 1E buses, each feeding 1 480-VAC class 1E bus and motor control center.<br>b. For the 2 units, there are 5 diesel generators, with 1 being a swing diesel generator shared by both units.<br>c. 3 trains of dc power are supplied from the inverters and 3 unit batteries. The battery duration is 6 hours. |
| Auxiliary Feedwater System | a. Two 50 percent motor-driven pumps and one 100 percent turbine-driven pump.<br>b. Pumps take suction from own unit condensate storage tank (CST) but can be manually cross-tied to the other unit's CST. |
| Service Water (SW) | a. Shared system between both units.<br>b. Consists of 6 pumps and 2 supply headers.<br>c. Cools component cooling heat exchangers, containment fan coolers, diesel generator coolers, auxiliary feedwater pumps.<br>d. 2 out of 6 pumps can supply sufficient flow. |
| Component Cooling Water (CCW) | a. Shared system between both units.<br>b. Consists of 5 pumps, 3 heat exchangers, and 2 surge tanks.<br>c. Cools RHR heat exchangers, reactor coolant pump motors and thermal barriers, RHR pumps, SI pumps, and charging pumps.<br>d. One of 5 pumps can provide sufficient flow. |
| Secondary Relief | a. steam dump valves<br>b. atmospheric dump valves (1 per SG)<br>c. safety relief valves |
| Primary Relief | a. 2 PORVs<br>b. 3 safety relief valves |
| Containment | a. large, dry, prestressed concrete<br>b. 2.6 million cubic foot volume<br>c. 49 psig design pressure |
| Reproduced from NUREG/CR-3300, NUREG/CR-4550, and NUREG/CR-4551 | |

The study obtained a point estimate of the frequency for short SBOs' core damage scenarios (entry point for a Level 2 PRA), for a plant with the same features as ZNPP, including the contribution of extreme weather. This value was about $2.1X10^{-6}$ per year.

The value estimated independently for the frequency of prolonged SBO did not include all the contributors to the SBO events. For example, the mode did not include potential test and maintenance unavailability, human errors in aligning the electrical bus, and common-cause failures (CCFs) of other electrical components such as breakers. The comparison of this limited independent estimation with the PRA results clearly shows that the internal event contribution to the frequency of prolonged SBO as documented in NUREG/CR-4551 is reasonable.

### G.1.2 Seismic Initiating Event

An examination of the Zion probabilistic safety assessment (PSA) (NUREG/CR-3300, "Review and Evaluation of the Zion Probabilistic Safety Study: Plant Analysis," Vol. 1, issued May 1984) indicated that the frequency of loss of total nonrecoverable alternating current (ac) power is about $5.6X10^{-6}$ per year because of seismic events. The two major contributors to a seismic-induced SBO in ZNPP are the following:

(9) LOOP because of a seismic event with a median ground acceleration of 0.3 g

(10) failure of SW pumps caused by a seismic event with median ground acceleration of 0.63 g

The failure of SW pumps will result in an eventual failure of EDGs, because SW supports the operation of EDGs and most of the emergency core cooling system (ECCS) components.

The failure of SW pumps during a seismic event could result for one or more of the following reasons:

- failure of the pumps (the largest contributor)
- failure of all the underground SW piping
- failure of the crib house roofing

Considering the seismicity of the area surrounding ZNPP, NUREG/CR-3300 estimated a total core damage probability of $5.6X10^{-6}$ per reactor year because of an extended SBO beyond the battery duration.

### G.1.3 Fire Initiating Event

The Zion PSA performed a very limited fire analysis, as indicated in NUREG/CR-3300. It basically identified two areas that contributed the most to fire risk: the auxiliary equipment room and the cable-spreading room. The fire in the auxiliary equipment room damaged cabinets to the extent that the operators received incorrect diagnostic information. The loss of diagnostic information also impeded the recovery actions involving auxiliary feedwater (AUX) pumps or high-pressure injection.

The fire in the cable-spreading room damaged the motor-driven AUX pump power cables, the turbine-driven auxiliary feedwater (TDAFW) pump failed randomly, and the operators failed to initiate feed-and-bleed operation for decay heat removal. NUREG/CR-3300 did not agree with the ZNPP assessment of the cable-spreading room. As noted in NUREG/CR-3300, it appears that the ZNPP Unit 1 cable-spreading room contains the following cables:

- power feeds for three CCW pumps and three SW pumps
- power feeds for two charging pumps
- power feeds for two AFW pumps
- control cabling for five fan coolers
- control cabling for at least two containment spray pumps

Docketed information from Commonwealth Edison also indicated that the cable-spreading room contains power cables for the steam supply valves of the TDAFW pump, which is separated by

a minimum distance of 20 feet from the motor-driven AFW pump power cables. Information on the location of safety injection pump cables and the third containment spray pump was not available at the time of evaluation.

Based on this information, it appears that a relatively large fire in the cable-spreading room would have a similar effect as the total loss of ac. However, the TDAFW pump is not expected to be affected, and its operation would not be limited by the battery depletion time similar to other extended SBO scenarios. Because of a lack of detailed cable routing and other fire-related information, NUREG/CR-3300 estimated a core damage probability of $4.0X10^{-5}$ per year. A reanalysis of this scenario was performed with less conservative assumptions and was based on recent data on ignition, detection, and suppression of fires. Furthermore, for this scenario, the operation of the TDAFW pump was assumed to be unaffected by the fire, and it could only fail for reasons independent from the fire scenario. This updated analysis resulted in an estimated core damage probability that was much smaller than the bounding estimate reported in NUREG/CR-3300 ($9.5X10^{-7}$/reactor year (RY)). The assumptions used in this calculation, which is equivalent to the earlier calculation, are as follows:

- cable-spreading room ignition frequency = $1.9X10^{-3}$ per year
- location and severity factor = 0.1
- failure of Halon fire suppression system = 0.05
- failure of TDAFW pump early or late = 0.1

The initiating event frequency for prolonged SBOs, which is required for the entry point to a Level-2 analysis, should exclude the failure of the TDAFW pump. Therefore, the resulting initiating event frequency would be about $9.5X10^{-6}$ per year. It is important to note that the current plants are equipped with additional SBO diesel generators and a set of new FLEX equipment, which can further reduce this frequency.

## G.2 Calvert Cliffs Nuclear Power Plant

Table G-2 provides the relevant plant information for Calvert Cliffs Units 1 and 2 (CCNP). Each CCNP unit is equipped with two TDAFW pumps, and the duration to battery depletion is nominally 2 hours, although they are expected to last 4 hours in the case that was modeled in TH runs.

The SPAR model estimated the scenarios associated with the SBOs with early failures of both TDAFW pumps, reproduced in Table G-3. The early failures of both TDAFW pumps was dominated by the operator's failure to control the flow, causing SG overfill, and failing the TDAFW pumps by carrying water to turbine. The overall frequency estimated from this process is about $1.88X10^{-8}$ and $2.47X10^{-8}$ per year, for Units 1 and 2, respectively. The higher contribution for Unit 2 resulted from the asymmetric dependence on SW. For example, EDG 12 can be supplied with cooling water from the SW system of either Unit 1 or Unit 2.

For losses of offsite power (LOOPs), especially those related to the grid and weather-related causes, there is a high potential that both units experience a LOOP (i.e., a dual LOOP scenario). The following equation provides a rough estimate of the major contributors to the frequency of early core damage in both units from the occurrence of a dual LOOP initiator:

CD due to Dual LOOP = [Frequency of Dual Unit LOOP]* [CCF probability of all Five EDGs]* [Probability the TDAFW fails due to SG overfill in both units]

Substituting the estimates from the SPAR model,

[Frequency of Dual Unit LOOP] = [Frequency of LOOP-GR]+LOOP-WR] = 1.86 $X10^{-2}$ + 4.83$X10^{-3}$
= 2.4$X10^{-2}$,
[CCF probability of all Five EDGs directly from SPAR models] = 2.13$X10^{-5}$, and

[Probability the TDAFW fails due to SG overfill] =
[SPAR model for failure of both TDAFW failure in one Unit due to overfilling = 0.3*0.12 = 0.036]*
[Conditional Probability of failing both TDAFW due to SG overfill in the second Unit = 0.3; estimated] = 1.08$X10^{-2}$

Table G-4 shows the single and dual LOOP core damage frequency (CDF) results for the SBO with the early failures of both TDAFW pumps for internal events.

**Table G-2 Information from Calvert Cliffs Nuclear Station**

| Systems | System Features |
|---|---|
| Emergency Power System | a. Currently there are 5 diesel generators for the 2 units. One of these 5 EDGs is the SBO EDG, which can power any safety related 4-kV bus at either unit. The operation of 1 EDG with success of 1 TDAFW pump per unit is adequate for long-term SG heat removal. The SBO EDG requires operator action to align it to a safety bus and is credited as a recovery action in the PRA models.<br>b. At the time when individual plant evaluation/individual plant evaluation for external events (IPE/IPEEE) was performed, each unit had a dedicated EDG with 1 shared EDG for both units. Therefore, the information contained in IPE/IPEEE should be used as a guide, and they are not directly applicable.<br>c. Each unit has 3 4160-VAC Class 1E buses, each feeding 1 480-VAC Class 1E bus and motor control center.<br>d. 3 trains of dc power are supplied from the inverters and 3 unit batteries. The battery duration is 2 hours, but it is expected to last 4 hours during most scenarios. |
| Auxiliary Feedwater System | Each unit is equipped with 2 turbine-driven pumps (TDAFW) and 1 motor-driven pump (MDAFW). There is a cross-connection to the other unit's MDAFW discharge line. |
| Salt Water System (SW) | There are 2 cross-tied trains, each with 1 pump and 1 heat exchanger. A third pump could also supply either train, if needed. |
| Service Water (SRW) | There are 2 trains, each with a salt water pump, a CCW HX, an SRW HX, and ECCS pump room air cooler. A third pump could be aligned to each train, if needed. |
| Component Cooling Water (CCW) | The CCW pumps do not restart automatically after a LOOP. The operators manually reestablish RCP seal cooling after a LOOP. |
| Secondary Relief | a. 4 turbine bypass valves—TBVs (2 SG)<br>b. atmospheric dump valve (1 per SG)<br>d. main steam safety relief valve (8 per SG) |

| Systems | System Features |
|---|---|
| Primary Relief | a. 2 reverse-seated PORVs (2400 psi);<br>b. the PORVs do not require dc power for once-through cooling (feed and bleed)<br>c. 2 block valves that are powered from the opposite 480 VAC with respect to their PORVs<br>d. 2 spring-loaded safety relief valves (P>2500 psig) |
| Containment | Large, dry |
| Note: The information in this table is reproduced from the CCNP individual plant evaluation (IPE)/IPE for external events (IPEEE). | |

Table G-5 provides similar results for SBO with the failure of TDAFW pumps after battery depletion. The core damage frequencies are estimated by removing the probability of SG overfill and including a probability of about 0.24 for the recovery of power from the EDG or offsite (0.7 for recovery of the EDG in 4 hours and 0.34 for recovery of the offsite power from weather or grid-related causes).

**Table G-3 Core Damage for SBO Scenarios with Early Failure of TDAFW Pumps**

| Calvert Cliffs Unit 1 | | | Calvert Cliffs Unit 2 | | |
|---|---|---|---|---|---|
| **Initiator** | **IE Frequency** | **CDF Contribution** | **Initiator** | **IE Frequency** | **CDF Contribution** |
| LoopGR | 1.86E-2 | 1.02E-8 | LoopGR | 1.86E-2 | 1.43E-8 |
| LoopPC | 2.07E-3 | 2.15E-10 | LoopPC | 2.07E-3 | 3.24E-10 |
| LoopSC | 1.04E-2 | 2.87E-9 | LoopSC | 1.04E-2 | 3.99E-9 |
| LoopWR | 4.83E-3 | 5.48E-9 | LoopWR | 4.83E-3 | 6.14E-9 |
| **Total** | **3.59E-2** | **1.88E-8** | **Total** | **3.59E-2** | **2.47E-8** |

**Table G-4 CDF for the SBO and the Failures of TDAFW Pumps due to Overfill (for Internal Event Initiators Affecting One or Both Units)**

| Affected Unit | CDF Estimates (Per Reactor Year) |
|---|---|
| Unit 1 [only] | 1.3E-8 = [1.88E-8 – 5.5E-9] |
| Unit 2 [only] | 1.9E-8 = [2.47E-8 – 5.5E-9] |
| Both Units | 5.5E-9 |

**Table G-5 CDF for an SBO and the Failures of All TDAFW Pumps after the Battery Depletion (Internal Event Initiators Affecting One or Both Units)**

| Affected Unit | CDF Estimates (Per Reactor Year) |
|---|---|
| Unit 1 [only] | 5.0E-9 = [1.25E-7 – 1.20E-7] |
| Unit 2 [only] | 4.5E-8 = [1.65E-7 – 1.20E-7] |
| Both Units | 1.2E-7 |

### G.2.2 Seismic Initiating Event

An examination of the CCNP IPEEE indicated that the frequency of loss of the total nonrecoverable ac power is about $1.3X10^{-5}$ and $1.5X10^{-5}$ per year due to seismic events for Units 1 and 2. These estimates were found when both units were equipped with only three EDGs, rather than the current configuration of five EDGs. However, the original IPEEE

stated that all EDGs are dependent on SW, and the SW has significantly lower fragility than EDGs. A further examination of the two new EDGs, the SBO EDG, and EDG 1A, revealed that these two EDGs are not dependent on SW for cooling. This is expected to reduce the seismic contribution by a factor of 10. Following the approach used for internal events for the single and dual unit core damage and no recovery credit for ac power after a seismic event, the following results were estimated.

**Table G-6 CDF for the SBO and Failures of TDAFW Pumps due to a Potential Overfill (Seismic Events Affecting One or Both Units)**

| Affected Unit | CDF Estimates (Per Reactor Year) |
|---|---|
| Unit 1 [only] | 3.3E-8 = [4.7E-08 – 1.4E-8] |
| Unit 2 [only] | 5.0E-8 = [5.4E-8 – 1.4E-8] |
| Both Units | 1.4E-8 |

**Table G-7 CDF for SBO and Failures of TDAFW Pumps after the Battery Depletion (Seismic Events Affecting One or Both Units)**

| Affected Unit | CDF Estimates (Per Reactor Year) |
|---|---|
| Unit 1 [only] | Negligible = [1.3E-6 – 1.30E-6] |
| Unit 2 [only] | 2.0E-7 = [1.5E-6 – 1.30E-6] |
| Both Units | 1.30E-6 |

### G.2.3 Fire Initiating Event

The CCNP IPEEE estimates the contributions from internal fire are $7.3X10^{-5}$ and $1.1X10^{-4}$ for Units 1 and 2, respectively. Fires in the control room resulting in its abandonment were the major contributors to the overall fire CDF. This is important because the main control room is shared between the two units, although there are two cable-spreading rooms. Therefore, the majority of the CDF resulting from fires in the control room is considered to affect both units.

Severe fires in control room cabinets are assumed to result in control room evacuation. Once the control room is evacuated, the operators are required to load shed most of the electrical loads, and manually restart these loads. If not restarted, the site would lead to a self-induced SBO. This condition will eventually result in a loss of the 125-volt direct current batteries. Even if the operators successfully reload the buses, a failure of either of the EDGs supporting the fire safe-shutdown trains will eventually result in a loss of two of the four batteries. It will indicate a loss of <something> in the auxiliary shutdown panels, which is the only source of indication for the operators. Therefore, most of the scenarios involving an EDG failure would involve an extended LOOP with initial successful actuation and control of equipment, initially establishing AFW flow but followed by failure of AFW sometime later caused by battery depletion.

The CCNP fire PRA in IPEEE, consistent with the methodology of that time, had several conservative assumptions and used somewhat conservative data. For example, it did not adequately account for fire severity and the plant layout effect on fire ignition frequency. In addition, the analysts considered relatively high heat-release rates, and they did not develop and use scenario-specific propagation and suppression. Conservative assumptions were also made regarding the human error probabilities, specifically for the mitigation of control room fires. Control room fires are significantly affected by the failure of the operator to perform local manual actions and, in some cases, may rely on a self-imposed SBO to avoid spurious actuations.

Subsequent to the submittal of the CCNP IPEEE, several studies were performed to eliminate some of these conservatisms.[1] The results of these studies lowered the CDF contribution of the main control room fire by one unit to $2.45X10^{-5}$ per reactor year. Note that this estimate does not reflect the additional credits for the two added EDGs. The probability of early core damage, before battery depletion, is driven by the human error probabilities. This core damage probability is not generally affected by the added EDGs. The single unit CDF is approximately apportioned (split) to 0.1 and 0.9 for the early and late core damage, which corresponds to the failures of TDAFW pumps before or after battery depletion. As a result, the early CDF of the control room fire would be about $2.4X10^{-6}$ per reactor year. The late core damage (i.e., TDAFW pump failures after the depletion of the batteries, requires the failure of EDGs. This split fraction will then be affected by the addition of two EDGs at Calvert Cliffs. An additional credit of 0.1 is, therefore, assigned to reflect the credit for the added EDGs. For the late core damage affecting both units, this will reduce the fraction of the CDF from 0.9 down to 0.09 (0.1*0.9).

**Table G-8 CDF for SBO and Failures of TDAFW Pumps due to Potential Overfill (Control Room Fire Events Affecting One or Both Units)**

| Affected Unit | CDF Estimates (Per Reactor Year) |
|---|---|
| Unit 1 [only] | Negligible |
| Unit 2 [only] | Negligible |
| Both Units | 2.45E-6 (0.1*2.45E-5) |

**Table G-9 CDF for SBO and Failures of TDAFW Pumps after Battery Depletion (Control Room Fire Events Affecting One or Both Units)**

| Affected Unit | CDF Estimates (Per Reactor Year) |
|---|---|
| Unit 1 [only] | 2.2E-5 = [2.45E-5*0.9] |
| Unit 2 [only] | 2.2E-5 = [2.45E-5*0.9] |
| Both Units | 2.2E-6 = [2.45E-5*0.9*0.1] |

### G.2.4 Contributions from Other Initiating Events

Two initiating events, high wind and internal flood, were considered in estimating the frequencies of the entry points for determining the CSGTR probabilities. The internal flood core damage was estimated at $1.55X10^{-5}$ per reactor year. Most of the flood scenarios resulted in eventual core damage as a result of losing the SW, main feedwater, AFW, and ECCS systems. The failure of the AFW crosstie between the units is needed for core damage if not affected by the flood initiator itself (e.g., if the flood were due to a break in the AFW suction line, which could impede the AFW crosstie). The flood scenarios developed in IPEs are expected to result in core damage that is generally considered late (approximately 12 hours or more after the initiator); therefore, it may not be considered for evaluating containment bypass. The original flood analysis in the IPE also suffered from conservative assumptions and the high flood initiating event frequency. A PRA update of the flood model in 2 January 2000 [2] resulted in an updated

[1] A letter from Charles H. Cruse, Baltimore Gas and Electric Vice President of Nuclear Energy, to U.S. Nuclear Regulatory Commission, May 18, 1999, "Additional Response to Request for Additional Information on Calvert Cliffs Nuclear Power Plant, Unit Nos. 1 and 2, Individual Plant Examination of External Events Submittal (TAC Nos. M83603 and M83604)."

[2] See a presentation by Bruce Mrowca on Calvert Cliffs PRA update, January 2001, titled "Calvert Cliffs PRA, January 22, 2000," Agencywide Documents Access and Management System Accession No. ML010400376.

estimate of $1.6X10^{-6}$ for flood CDF. This value is conservatively used as a single unit CDF contributor due to internal flood for estimating the C-SGTR frequency for scenarios where the AFW system has operated for 4 hours.

The high-wind contribution to the core damage is estimated to be $4.4X10^{-6}$. The main contributors to this estimate were the SBO scenarios. This contribution of CDF is considered to affect both units. The frequency of dual LOOP and early failures of TDAFW pumps was thought to be similar to the internal event CDF [i.e., $4.7X10^{-8}$ per reactor year = $0.0108 \times 4.4X10^{-6}$]. The remaining CDF of $4.3X10^{-6}$ per reactor year was estimated for those scenarios where TDAFW pumps operated early and failed after battery depletion.

# APPENDIX H

# A SCREENING APPROACH BASED ON FLAW DEPTH AND LENGTH

This approach both accounts for the distribution of flaw lengths and depths and considers the possibility of multiple flaws. It evaluates the consequential steam generator (SG) tube rupture (C-SGTR) probability based on the failure of one or more tubes and estimates the contributions of single-tube and multiple-tube failures separately. This approach has less conservatism than Approach 1, and it can be used for progressive screening of probabilistic risk assessment (PRA) scenarios or for evaluating inspection findings where the surveillance data for both depths and lengths are available, especially for large flaws.

This approach considers the contribution of shallower (less than 45-percent deep) and shorter (less than 2-centimeter (cm) (0.79-inch (in.)) flaws to C-SGTR to be negligible and considers the following large flaw bin sizes for this approach:

(11) size bins for length: flaw length from 1.5 to 2.5 cm (0.59 to 0.98 in.), 2.5 to 3.5 cm (0.98 to 1.38 in.), and 3.5 to 4.5 cm (1.38 to 1.77 in.)

(12) size bins for depth: flaw depth from 45 percent to 55 percent, from 55 percent to 65 percent, from 65 percent to 75 percent, from 75 percent to 85 percent, and from 85 percent to 95 percent

The probability that a flaw belongs to each size bin was calculated using following equation.

$$Prob\,[(d1 < flawdepth < d2), (l1 < flawlength < l2)] = Prob\,[Flaw\ large) * Probability[(d1 < flawdepth < d2)|flawlarge] * Pr[(l1 < flawdepth < l2)|flaw\ large]$$

A large flaw here is defined as a flaw large enough to require the tube to be plugged. As discussed earlier, a plugged tube is expected to have a flaw with an average length of 1.3 cm and a depth of 30 percent or more. They account for 0.95 percent of all flawed tubes. The conditional probabilities for a flaw to be in such a flaw bin are estimated from the associated gamma distributions, divided by the probability that a large flaw is observed [1-cumulative gamma (1.3 cm (0.51 in.) and 30 percent; the large flaw thresholds)].

Table H-1 shows the probability that a flaw resides in one of the large-size bins. The size distribution length and depth do not differentiate between Inconel 600 and 690.

**Table H-1 Probability that a Large Wear Flaw in the Last Cycle Has the Specific Length and Depth Ranges**

| Depth Range | 1.5 cm to 2.5 cm | 2.5 cm to 3.5 cm | 3.5 cm to 4.5 cm | Total Probability for Length > 1.5 cm |
|---|---|---|---|---|
| 45%<d<55% | 5.70E-2 | 1.26E-2 | 2.34E-3 | 7.19E-2 |
| 55%<d<65% | 1.36E-2 | 3.01E-3 | 5.59E-4 | 1.71E-2 |
| 65%<d<75% | 3.14E-3 | 6.95E-4 | 1.29E-4 | 3.96E-3 |
| 75%<d<85% | 7.09E-4 | 1.57E-4 | 2.91E-5 | 8.95E-4 |
| 85%<d<95% | 1.57E-4 | 3.48E-5 | 6.47E-6 | 1.99E-4 |
| Total Probability of a flaw is considered large and has a length greater than 2 cm and less than 4.5 cm, and depth between 45% and 95% | | | | 9.41E-2 |

For a wear flaw, the probability of a tube failure is a function of flaw depth only. This is because the current C-SGTR software conservatively models the wear flaw as tube thinning (flaws were assumed to be relatively large). So, the probability of tube failure before the failure of the hot leg (HL) is only a function of the flaw depth. The maximum leak area, however, is a function of the wear length as estimated by C-SGTR software. For a 2-cm (0.78-in.) wear flaw, the maximum area is about 2 square centimeters ($cm^2$) (0.31 square inch ($in.^2$)), for 3-cm (1.18-in.) flaws, it is close to 5 $cm^2$ (0.77 $in.^2$), and for larger flaws, the leak area is limited by twice the cross-sectional area of the tube (approximately 6.08 $cm^2$ (0.94 $in.^2$). There are large uncertainties associated with the estimated leak area as a result of tube failure because of wear flaw. As a bounding approach, it was considered that the failure of at least one large flaw with a length greater than 2 cm (0.78 in.) is required for C-SGTR to occur. The C-SGTR probability estimations in this appendix have considered the following two contributions:

(13) the existence of one tube with a large flaw in any of the plant SGs
(14) the existence of two or more tubes with large flaws

The approach taken here is considered somewhat conservative. For example, the best estimate of the number of tubes resulting in a leak rate equivalent to a guillotine break of one whole tube for a 2-cm (0.78-in.) flaw is about three tubes. However, in this approach, the failure of any one tube is considered sufficient. This conservative approach was adopted to avoid considering several smaller (less than 2-cm (0.78-in.) long) deep flaws as a part of this analysis.

The probabilities of C-SGTR occurring before HL failure for different bin sizes are shown in Table H-2 for Inconel 600 and Table H-3 for Inconel 690. These probabilities are estimated using the C-SGTR calculator for predicting the C-SGTR probability and a thermal-hydraulic (TH) input file for the example plant, which simulates station blackout (SBO) with failure of the turbine-driven auxiliary feedwater (TDAFW) pump at the start of the accident (Case Wnewbase).

The study assumes a tube has failed if it exhibits a leak area of at least 1 $cm^2$ (0.16 $in.^2$). The threshold leak area is conservatively selected to account for the existing large uncertainties associated with the predicted leak area for wear. The results shown in these tables reaffirm that for the wear flaws, the bounding probability of tube failure is only a function of the flaw depth.

**Table H-2 Probability of C-SGTR Occurring before HL Failure for Different Sizes of Flaws in Inconel 600 in Zion Wnewbase Case**

| | | Flaw Depth | | | | | Maximum Leak Area |
|---|---|---|---|---|---|---|---|
| | | 50% | 60% | 70% | 80% | 90% | |
| Flaw Length | 2 cm | ~ 0 | ~ 0.05 | ~0.8 | ~1.0 | NA: May leak during operation | ~2.0 $cm^2$ |
| | 3 cm | ~ 0 | ~ 0.05 | ~0.8 | ~1.0 | NA: May leak during operation | ~5.0 $cm^2$ |
| | 4 cm | ~ 0 | ~ 0.05 | ~0.8 | ~1.0 | NA: May leak during operation | Limited by guillotine break of the tube 6.08 $cm^2$ |

**Table H-3 Probability of C-SGTR Occurring before HL Failure for Different Sizes of Flaws in Inconel 690 in Zion Wnewbase Case**

| Flaw Depth -> Flaw Length↓ | 50% | 60% | 70% | 80% | 90% | Maximum Leak Area |
|---|---|---|---|---|---|---|
| 2 cm | ~ 0 | ~ 0.00 | ~0.75 | ~1.0 | NA: May leak during operation | ~2.0 $cm^2$ |
| 3 cm | ~ 0 | ~ 0.00 | ~0.75 | ~1.0 | NA: May leak during operation | ~5.0 $cm^2$ |
| 4 cm | ~ 0 | ~ 0.00 | ~0.75 | ~1.0 | NA: May leak during operation | Limited by guillotine break of the tube 6.08 $cm^2$ |

The above estimates need to be aggregated through a probability model to produce an estimate of the probability of C-SGTR. To do so, the following terms are defined:

**N:** Number of Flaws

Subscript "**i**": for defining the length bins

Subscript "**j**": for defining the depth bins

**$Q_{i,j}$:** The probability that a large flaw belongs to bin i, j (obtained from Table H-1)

**$\Theta_{i,j}$:** The C-SGTR probability associated with a flaw that belongs to bin i, j (obtained from Table H-2 for 600TT and H-3 for 690TT tubes)

The aggregate probability of C-SGTR (P) is given by the following equation using the variables defined earlier:

$$P = N * \sum_{j} \sum_{i} Q_{i,j} * \theta_{i,j}$$

If $\Theta_{i,j,}$ the C-SGTR probability of a flaw with depth index j and length index i does not depend on index i as it is true for wear flaw (not true for cracks). Then, the above equation is simplified to:

$$P = N * \sum_j \theta_j \sum_i Q_{i,j}$$

For one flaw; with N set to one, the value of P was estimated based on the results in Tables 7.1-9 and 7.1-10 for Inconel 600, and Tables 7.1-9 and 7.1-11 for Inconel 690. These are the values obtained for this single flaw: **$P_{600}$=4.92X10$^{-3}$, and $P_{690}$=4.72X10$^{-3}$.**

As discussed earlier, it is expected that 31 flawed tubes will be generated in Cycle 15 (15 effective full-power years (EFPYs) of operation) for Inconel 600 tubes and 20 flaws for Inconel 690. The probability that one tube fails before HL failure can be estimated using the following equation:

$$Prob\ (1\ tube\ CSGTR) = \sum_{Nl>0} Prob\ (Nl\ tubes\ with\ large\ flaws) * Nl * Prob(tube\ failure)$$

The probability of a two-tube failure can be estimated using the following equation:

$$Prob(2\ tube\ CSGTR) = \sum_{Nl>1} P\,rob\ (Nl\ tube\ with\ large\ flaws) * \binom{Nl}{2} * Prob(tube\ failure) * [1 - Prob(tube\ failure)]^{Nl-2}$$

Similarly, higher numbers of tube failures causing C-SGTR (e.g., 3, 4) can be estimated. Table H-4 shows the results of these calculations for Inconel 600 and 690.

**Table H-4 Probability of Single and Multitube Failure in C-SGTR for Inconel 600/690**

| Tube Materials | C-SGTR: One Tube Failure | C-SGTR: Two-Tube Failure | C-SGTR: More Than Two-Tube Failure |
|---|---|---|---|
| Inconel 600 | 1.31E-2 | 8.24E-5 | Negligible |
| Inconel 690 | 8.90E-3 | 3.85E-5 | Negligible |

The two probabilities of a single tube failure and multiple tube failures are useful in PRA evaluations. For Inconel 600, these values are 0.013 and 8.23X10$^{-5}$; for Inconel 690, the values are 0.0089 and 3.85X10$^{-5}$ for EFPY 15. The probabilities of Inconel 690 are a factor of 1.5 less than Inconel 600. Similar analyses for a limited number of flaw sizes were performed for the SBO scenarios with late failure of TDAFW pumps after battery depletion (Case 153). The preliminary results showed that the probability of single and multiple tube failures is about a factor of 2 higher for Case 153 compared to the Wnewbase case. All analysis results shown in the remainder of this appendix are performed for the Wnewbase case with Inconel 600. The scaling factors—an increase of twofold is used for SBO cases with late failure of TDAFW pumps, and a decrease of one-and-a-half-fold is used for Inconel 690.

The contribution to C-SGTR from a single tube failure can be compared to the estimates obtained from the first approach. The results show that, for Inconel 600, the single tube failure contribution to C-SGTR is about 1.31X10$^{-2}$ from both methods. Similarly, for Inconel 600, the single tube failure contribution to C-SGTR is 8.1X10$^{-3}$ and 8.90X10$^{-3}$ from the first and the second approach, respectively. This provides some confidence that the estimated results are consistent from two different approaches.

# APPENDIX I

# MELTING TEMPERATURES AND STEEL OXIDATION CONSIDERATIONS IN MELCOR MODELING

The melting temperatures for stainless steel and Inconel (1,725 kelvin (K) (1,452 degrees Celsius (C))) originate from the Steam Generator Action Plan (SGAP) analysis. These temperatures are consistent with those listed in the SCDAP/RELAP (1,671–1,727 K (1,398–1,454 degrees C)) and MELCOR (1,700 K (1,426 degrees C)) manuals. The temperatures are also consistent with typical listings of light-water reactor melting temperatures such as those shown in NUREG/CR-6042, "Perspectives on Reactor Safety," issued March 2002 (R-800 course material).

The list shows that the lowest melting temperature for iron is for eutectics with zirconium (Zr) (approximately 940 degrees C (1,724 degrees Fahrenheit (F))) and boron carbide ($B_4C$) eutectics (approximately 1,150 degrees C (2,102 degrees F)). MELCOR models steel reactions with Zr and with $B_4C$.

Severe accident analyses do not typically consider steel oxidation of reactor coolant system (RCS) components. Although the SGAP analysis did not consider the oxidation of RCS components, it did analyze the influence of oxidation on core components. The conclusion was that variations in oxidation of additional metal affect absolute failure timing but do not significantly affect the relative failure timing of different components that are of interest in evaluating whether the containment is bypassed.

MELCOR contains steel oxidation models but they are applied in components in the COR module rather than the HS (heat structure) module used to model the RCS piping.

The analysis below discusses assessing the possible effects of oxidation in the RCS, using the MELCOR steel-$H_2O$ oxidation model. External sources for steel oxidation or steel oxide melting were not sought, since it is expected that the major oxidation mechanisms should have been captured during the study of degradation of steel present in the reactor core.

The steel-$H_2O$ rate constant in MELCOR is calculated using the following equation:

$$K(T) = 2.42 * 10^9 * \exp(-42{,}400/T)$$

The analysis is continued, assuming that the steel-$H_2O$ rate constant listed in MELCOR applies to units of kilogram and square meters.

This was verified in the literature. A paper by the same author as the primary reference in MELCOR (J.F. White)[1] but published 3 years after the MELCOR reference lists the following parabolic rate constant:

$$w^2/t = 2.4 * 10^{12} * \exp(-84{,}300/(RT))$$

[1] See J.T. Bittel, L. H. Sjodahl, and J. F. White, "Oxidation of 304L Stainless Steel by Steam and by Air," Corrosion-NACE, Vol. 25, No. 1, January 1969.

where w is the weight gain (in fact the mass of oxygen added to steel) per unit area in $mg/cm^2$, R is the gas constant in cal/(mole-K), T in K, and t in s.

Applying the universal gas constant of R = 1.987 cal/(mole-K), the equation becomes:

$$w^2/t = 2.4 * 10^{12} * \exp(-42{,}426/T)$$

Because the units of $w^2$ are $mg^2/cm^4$, to convert to rate to $kg^2/m^4$, the constant should be multiplied by $10^{-4}$. This was also the factor used in the conversion of the Urbanic-Heidrich constant for Zr in the MELCOR manual.

The MELCOR manual refers to w as the mass of metal oxidized per unit area, whereas the paper refers to w as the weight gain per unit area. Assuming that the oxidation product is ferrous oxide (FeO), the ratio of weight gain to metal mass oxidized should be the ratio of atomic weights—about 16/56 or 0.29. In parabolic reaction rate, this translates to a factor of about 10, which corresponds to the MELCOR correlation for the stainless steel reaction rate.

Figure I-1 shows the parabolic rate constant for steam-$H_2O$ reaction.

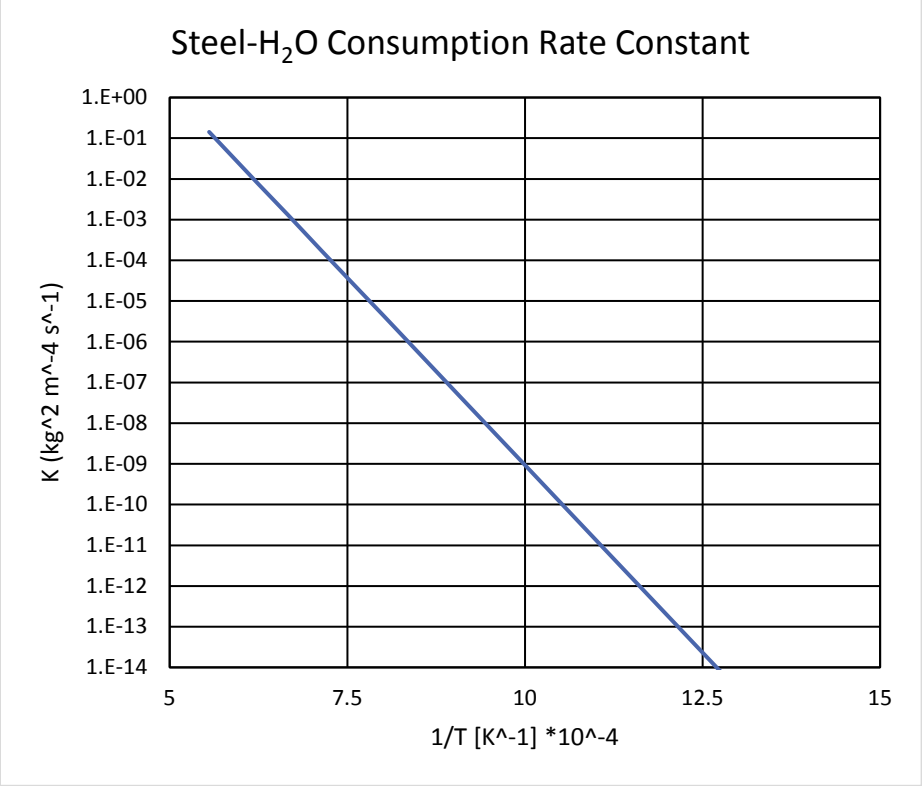


**Figure I-1 The parabolic rate constant for steam-$H_2O$ reaction**

In the C-SGTR analyses, RCS failures typically occur when temperatures are substantially below 1,750 K (1,476 degrees C). The temperatures are rapidly rising, limiting the time at high temperatures. The following plot shows the steel mass loss at a fixed temperature over the course of 1 day for select temperatures below 1,750 K (1,476 degrees C).

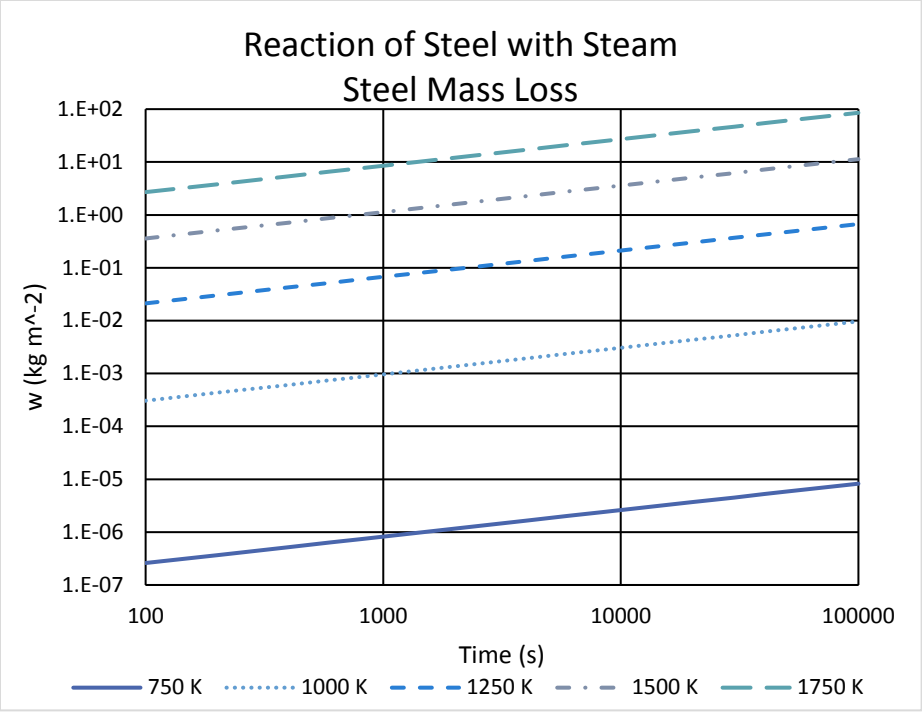


**Figure I-2 Steel mass loss at a fixed temperature**

Figure I-3 shows the corresponding loss of steel thickness, assuming a density of 8,000 kilogram per cubic meter (kg $m^{-3}$).

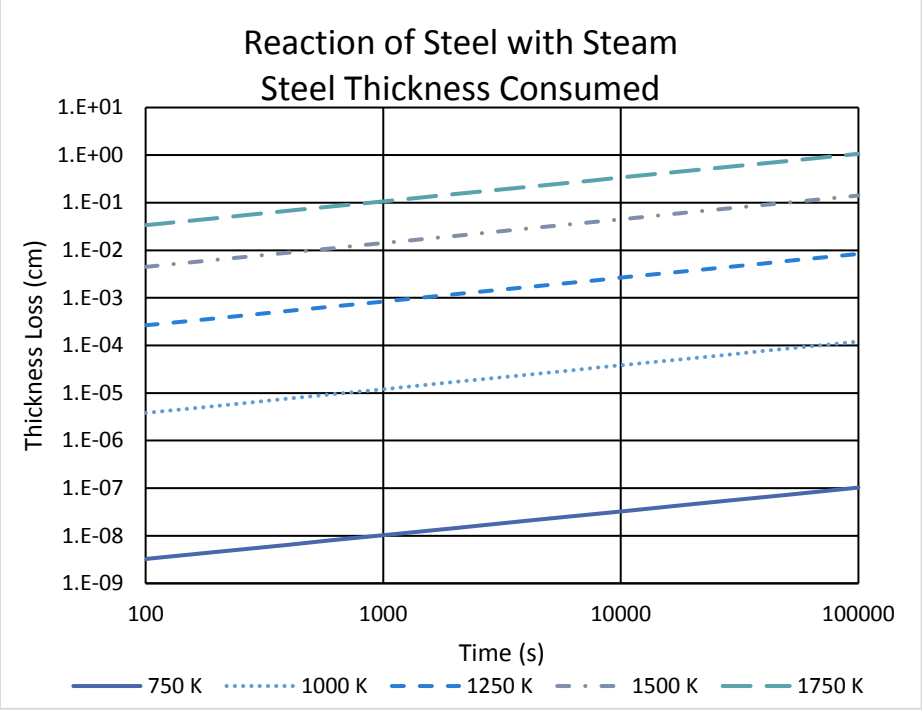


**Figure I-3 Loss of steel thickness**

The steel-$H_2O$ model in the MELCOR reference manual [2] predicts no appreciable oxidation (approximately greater than 1 millimeter (0.04 inch)) except for extended durations (approximately 1 day) at near the melting point. It is assumed that, at these temperatures, failure by creep will occur long before oxidation is significant.

The stainless steel oxidation paper presented steam oxidation for different stainless steels and mild steel with the data points falling in the same general range. It is assumed that the relation is generally applicable to other steels.

The approach to RCS steel oxidation in this report is consistent with how phenomena are handled in severe accident analysis and previous consequential steam generator tube rupture analyses.

Because the existing oxidation model does not predict appreciable oxidation in the absence of the hydrogen affect except at high temperatures, no attempt was made to consider the influence of hydrogen on oxidation, to identify low-melting-point iron oxides, to consider additional heat and hydrogen generation, or to consider the effects of stainless steel foaming, including insulation for the oxidation of RCS components. If additional effects of foaming and other effects are significant, they should probably be considered first for the core, where temperatures are hottest.

[2] "In the MELCOR reference manual" refers to both the use of 9 rather than 8 as the exponent for the reaction rate and the interpretation of the parabolic rate referring to metal mass consumed rather than mass gain (oxide mass gained–metal mass consumed).

# APPENDIX J

# LOOP SEAL CLEARING CONSIDERATIONS

This appendix discusses assumptions related to loop seal clearing. Opinions differ between NUREG/CR-6695, "SCDAP/RELAP5 Thermal-Hydraulic Evaluations of the Potential for Containment Bypass During Extended Station Blackout Severe Accident Sequences in a Westinghouse Four-Loop PWR," issued March 2010, and various sections of this report (e.g., Section 3.7, Section 8.1).

## J.1 TH Analysis-Related Considerations

The assumptions in Section 3.7 build upon NUREG/CR-6995. The issue was not explored fully. Any difference is not expected to be a significant issue for the Combustion Engineering (CE) configuration analyzed in this work. The current scope of the project did not include a thermal-hydraulics (TH) assessment of loop seal clearing for CE. Section 3.7 simply noted that the loop seals did not clear in the simulations that were run.

One of the reasons that this TH analysis was not prioritized is that a high degree of containment bypass was concluded for CE, even in the absence of loop clearing, as a result of the high temperatures to which the steam generator (SG) tubes are exposed. Because the effect of loop seal clearing primarily results from hotter (near core temperature) gases reaching SG tubes, which already occurs in the CE design analyzed even for closed-loop-seal natural circulation, the additional impact of loop seal clearing on the risk for CE is not expected to be significant.

The initial intent to address loop seal clearing for this project was to test the different failure mode hypotheses and to determine whether apparent differences in loop seal behavior were inherent to designs or because of differences in codes or differences in user choices. The plan was to perform a quick related "hand calculation" to ascertain what parameters would be important to both hypothesized failure modes and expected behavior, verify these relevant parameters in the input decks, and then run a series of simulations to test the extent to which the failure modes affected behavior. When the work was initially planned, it included only a general outline for approaching the problem. The text for loop seal clearing in the TH section (Section 3.5) of this report reflects this initial outline. However, the assumptions for loop seal clearing described in the same section do not factor into results, since neither geometry nor system-code models changed. Rather these assumptions factor into how the results are interpreted and to help decide what to look for.

The assumptions for loop seal clearing do not differ appreciably from those in NUREG/CR-6995. One additional factor is considered explicitly: the upper-vessel-to-downcomer leakage. The knowledge of the influence of this leakage is not new. In fact, individuals involved with the Steam Generator Action Plan and NUREG/CR-6695 indicated that core-to-downcomer bypass leakage had also been considered during the development of the system-code inputs. The choice of a small upper-core-to-downcomer leakage area for these Westinghouse analyses resulted in loop seal clearing.

What was planned to be explored further during this study is the expectation that the amount of seal leakage that results in loop seal clearing depends on both the assumed upper-vessel-to-downcomer leakage area and (perhaps to a lesser extent) reactor coolant system (RCS)-to-containment heat transfer.

Additional details of the expected behavior follows:

Upper-loop-seal water can be lost in three different ways:

(14) Flow over to the downcomer or out of the reactor coolant pump (RCP) seal before bubble formation or if the bubble shrinks or water level oscillates (bubble shrinking/not initially forming). In fact, in the absence of upper-vessel-to-downcomer leakage, a bubble should not even form until either the loop-seal water reaches saturation or until the SG side water level drops to the horizontal pipe section of the seal, thereby allowing steam to bubble through. (This seems to be a new consideration for this report.)

(15) Entrainment to the RCP seal once (or if) steam flows through the upper loop seal (lower loop seal must still be intact to maintain differential pressure. This is the primary mechanism for loop seal clearing described in NUREG/CR-6995.

(16) Evaporation/flashing. This is an additional mechanism described in NUREG/CR-6995.

To create sufficient differential pressure across the upper loop seal to cause steam to bubble through it (and thereby remove inventory by the second mechanism listed above) other in-leakage to the upper horizontal part of the cold leg must not be significant. This means that—

- The lower loop seal (downcomer-core) must be intact.
- The upper-vessel-to-downcomer leakage area should not be large relative to the RCP seal leakage area.

If one of the other in-leakage pathways is open, gas driven by the evaporation of any saturated water in the system would take that pathway rather than bubbling through the upper cold-leg loop seal.

The following seven questions for a more detailed treatment of loop seal clearing come to mind for potential future analyses on this subject:

(17) How do the flow resistances across core and SGs in the code input compare with measurements?

(18) How do the Westinghouse and CE flow resistances compare, including the relative flow resistances between SGs and core?

(19) What is the maximum range of pressure drop and pressure drop difference achievable? That is, neglecting any liquid flashing to steam, what would the steam pressure drops across core and SG tubes be for an infinite volume of steam at cold legs if flow is limited by a choked condition at the safety relief valves (parallel channel problem)?

(20) How much does flashing affect behavior—from lower head and from loop seals? How do the elevations of the downcomer skirts in the inputs match expectations?

(21) How do these elevations and those of the loops differ between Westinghouse and CE designs and how would this be expected to affect clearing behavior?

(22) How much condensation is occurring? How does the magnitude compare to that of the Westinghouse calculations?

(23) Are differences primarily because of differing geometry surface areas or because of differing heat transfer coefficients? Do the Westinghouse and CE reactor vessels have differing discharge rates?

## J.2 PRA-Analysis-Related Considerations

The probabilistic risk assessment (PRA) model used in this report postulates that the loop seal issue will occur for both Westinghouse and CE cases in severe accident sequences where a 1,135–1,817 liters per minute/pump (300–480 gallons per minute/pump) leakage exists. These leakage sequences are generally well delineated in PRA studies. Such sequences are assumed to lead to consequential SG tube rupture end state.

# APPENDIX K

# FURTHER DISCUSSION OF STEAM GENERATOR TUBE FLAW DISTRIBUTIONS

This appendix contains a further discussion of steam generator (SG) tube flaw distributions, as already given in Chapter 6 of this report, and their application, as covered in Section 7.1.3. The material in this appendix is based on an Advisory Committee on Reactor Safeguards (ACRS) subcommittee briefing [1] on consequential SG tube rupture (C-SGTR).

## K.1 On Development of Distributions in Chapter 6

The previous work on estimating SG tube flaw distributions was for 600 mill annealed (MA) tube materials (NUREG/CR-6521, "Estimating Probable Flaw Distributions in PWR Steam Generator Tubes," issued 1996 (Gorman Report)) and for cracks only using data that existed before 1995. These (U-tube) SGs have been replaced with those having new SG tube materials (thermally treated Alloy (600TT and 690TT). Use of the information from previous studies could not be justified. The objective is to update the previous study on flaw statistics and provide current statistics sufficient to generate flaw samples for C-SGTR analysis (input to the C-SGTR calculator).

Flaw data for Inconel 600 and 690 (600TT and 690TT) were collected from selected in-service inspection reports available to the U.S. Nuclear Regulatory Commission. Flaw data were manually extracted and compiled into a data base for further analyses. Figures K-1 and K-2 show the empirical data used for the flaw depth and length parameters, before a fitted gamma distribution was imposed. The data were binned against operating time (measured in effective full-power years (EFPYs)) and flaw types. The flaw generation rate per tube as a function of SG service life (measured in EFPYs) is generated for the following:

- Volumetric/Wear Flaw 600TT
- Volumetric/Wear Flaw 690TT
- Axial Cracks 600TT
- Circumferential Cracks 600TT

No crack data were found for 690TT.

[1] See the transcript of the ACRS Meeting of the Subcommittees on Metallurgy & Reactor Fuels and PRA Consequential Steam Generator Tube Rupture (C-SGTR) Subcommittee Briefing, April 7, 2015 (Agencywide Documents Access and Management System Accession No. ML15182A262).

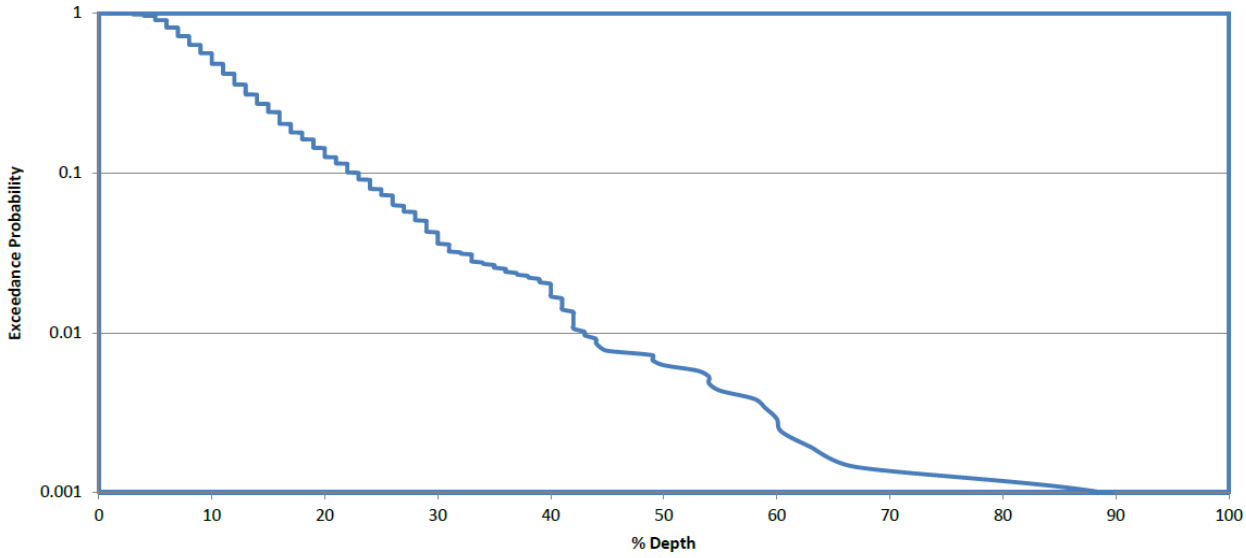


**Figure K-1 Graphical presentation of aggregate flaw data**
***Empirical depth distribution using all flaws in the database***

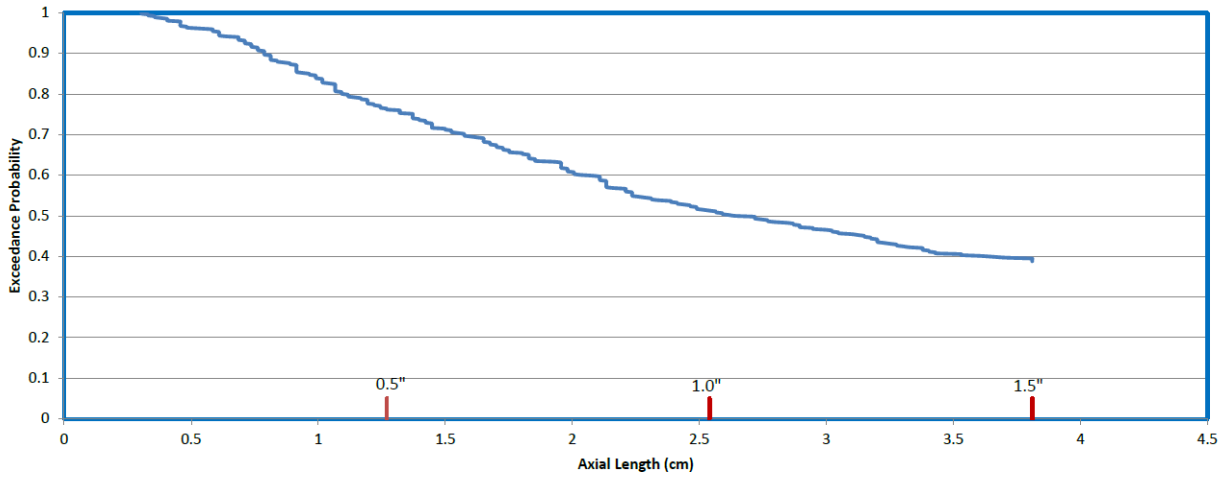


**Figure K-2 Graphical presentation of aggregate flaw data**
***Empirical distribution of axial length of all flaws in the database***

Model Parameters

A flaw model was developed by doing the following:

- linearly increasing rate of volumetric flaws generation as a function of time (i.e., EFPY)
- linearly increasing rate of crack flaws generation as a function of EFPY
- gamma distribution of flaw length
- gamma distribution of flaw depth

The statistical estimation approach included the following:

- regression using Excel routine for estimating the linearly increasing rates
- matching the first two moments for estimating the parameters of gamma distributions

General Findings

The following general findings were made:

- Sufficient statistical results were developed to generate flaw samples for the C-SGTR calculator software.

- New material 600TT/690TT flaw rate generation is about an order of magnitude less than what was reported for MA 600.

- The majority of flaws observed are volumetric rather than cracks.

- The flaw length and depth distribution is somewhat smaller than for MA 600.

The most important flaw parameter that specifies failure resistance of a tube is the flaw depth, as confirmed by the probabilistic risk assessment (PRA) models and the C-SGTR calculator in Chapter 7 of this report. Figure K-3 shows the fitted and empirical cumulative distribution for flaw depth.

The high-end tail of the distribution is affected by the tubes removed because of plugging, because these flaws will not be available for further growth to larger flaws in the next cycle. Section K-2 (also Section 7.1.3) gives the correction for that (shifted distribution) for PRA modeling purposes.

The lower tail of empirical distribution is affected by the error associated with measuring small flaws. With small and shallow flaws, in the relatively small database being used, one plant reported many flaws that were very shallow, at the range of 2-, 3-, and 5-percent depth, where the other plant did not report such small flaws. Knowing that there could be relatively large errors in the identification and size determination of small flaws, the lower tail may not be very accurate, even for the empirical distribution.

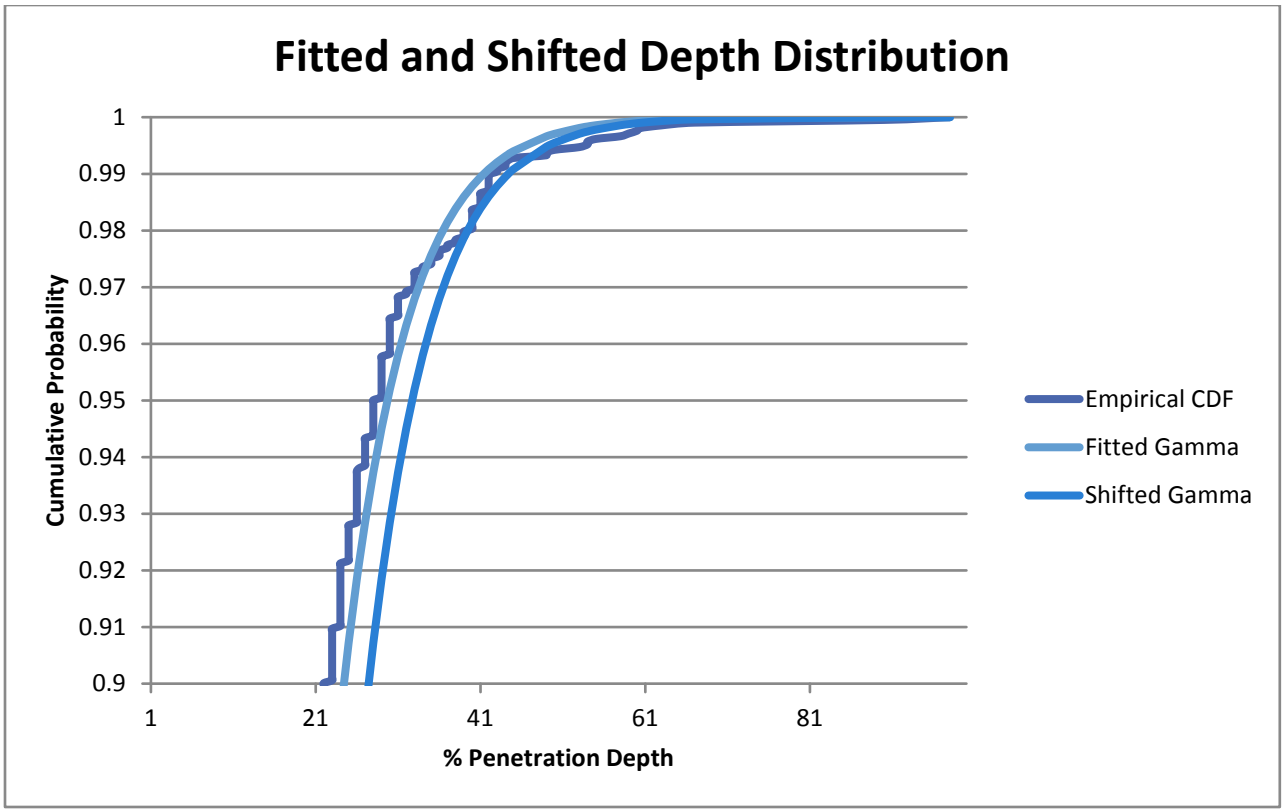


**Figure K-3 Flaw depth distribution**
***Distribution of percentage of flaw depth***

## K.2 he Adjusted (Shifted) Flaw Distributions Used in PRA

As discussed in Section 7.1.3, during PRA analysis, adjustments were made to the original estimated distributions of Chapter 6 for flaw depth and length.

To improve the distribution fit for large flaws, which are more important to C-SGTR, and to compensate for the perceived distortion of flaw size distributions toward the shallower and smaller flaws, the previous distributions were shifted by a small amount of depth and length (adding a scale variable to gamma distribution).

This adjustment also provided much closer estimates of the number of tubes that are plugged in each cycle (better estimate of the number of large and deep flaws at the tails).

For example, for the Westinghouse plant, the large and deep flaws were the major contributor to C-SGTR fraction estimates. Therefore, the PRA needed to model better fits at the tail of distributions of length and depth.

There were also a large number of unreliable small depth and length measurements (i.e., depth less than 10 percent), which skewed the size distributions of depths and lengths toward the lower values, whereas tube plugging criteria removed those larger flaws that could have grown into even larger ones if they had been allowed to remain.

Figure K-4 compares the cumulative probabilities of the empirical, fitted, and shifted flaw distributions for flaw depth. Section 7.1.3 of this report contains additional discussion, figures, and tables.

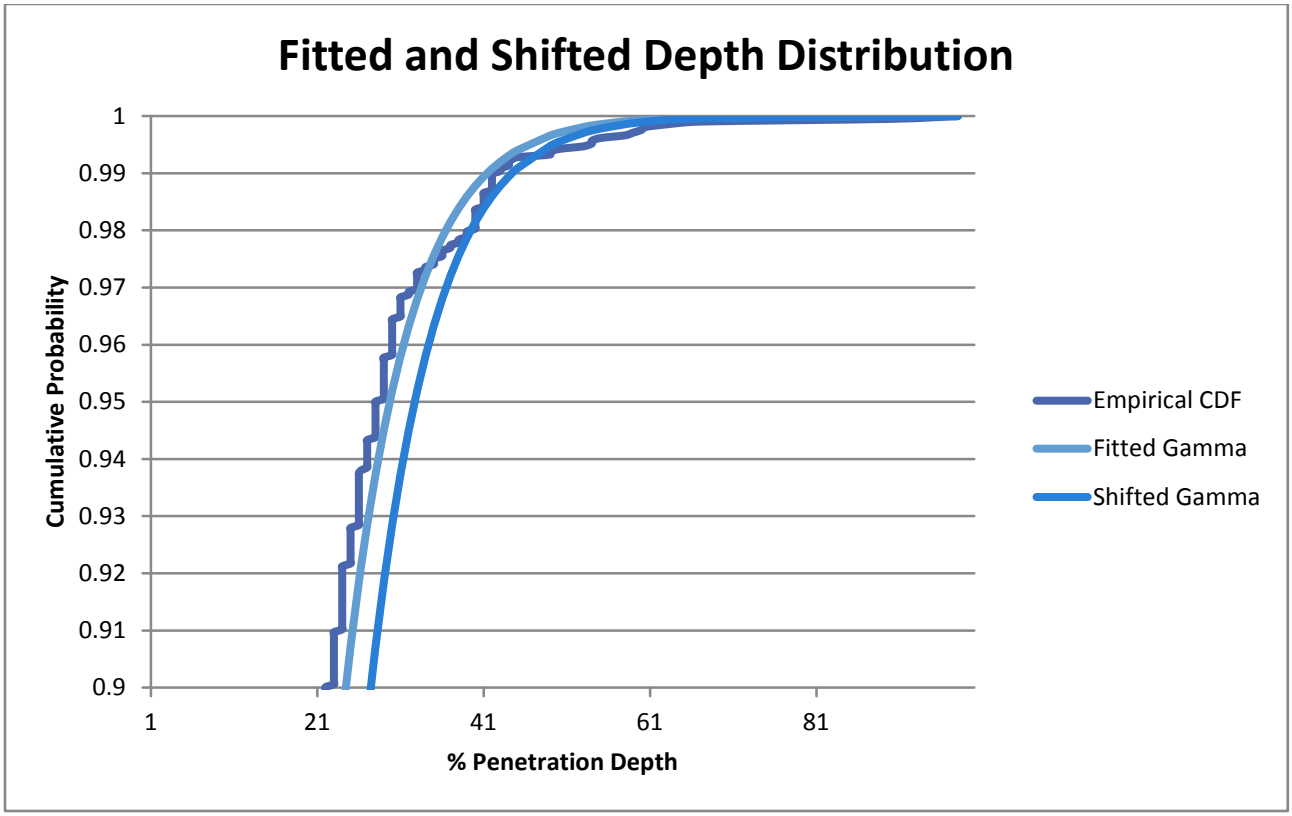


**Figure K-4 Flaw depth distribution (shifted gamma)**
***Fitted and shifted depth distribution***

# APPENDIX L

# A PROCESS TO COMPREHENSIVELY ESTIMATE CONSEQUENTIAL STEAM GENERATOR TUBE RUPTURE CORE DAMAGE FREQUENCY IN A PROBABILISTIC RISK ASSESSMENT MODEL

## L.1 Introduction

This appendix outlines a process to include consequential steam generator (SG) tube rupture (C-SGTR) in a probabilistic risk assessment (PRA) Level 1 model to collect those end states for further modeling in a Level 2 analysis. Section L.2 discusses the PRA Level 1 modeling detail deemed to be sufficient and cost effective to capture the bulk of the potential C-SGTR core damage frequency (CDF) for further modeling in a PRA Level 2 analysis. The validity of this approach was tested by applying it to a PRA model for a 4-loop Westinghouse plant. Section L.3 summarizes the results of this application.

All domestic nuclear power plants already have mature PRA studies that do not necessarily attempt to model C-SGTR in a detailed manner in their event trees. This process is also intended to assess the contribution of those deliberately “unmodeled” potential C-SGTR sequences in an existing PRA study. The example provided in Section L.3 attempts to illustrate such an assessment.

A guidance document containing an expanded version of this process may be produced in the future for use by U.S. Nuclear Regulatory Commission risk analysts.

## L.2 The Process

The objective of this appendix is to outline a process to model C-SGTR in a PRA Level 1 to collect those end states for further consideration in a Level 2 analysis. The process aims to provide PRA Level 1 modeling details sufficient and cost effective enough to capture the bulk of the potential C-SGTR CDF for further treatment in a PRA Level 2 analysis (i.e., to focus effort in collecting C-SGTR CDF from the most likely sources).

The process discussed is for the internal event hazard category during a power operation Level 1 PRA for a pressurized-water reactor; extension to other hazard categories is considered to be straightforward.

An internal events PRA model may have 20-30 event trees leading to numerous accident sequences. It is assumed that, initially, C-SGTR is not modeled, and the objective is to capture C-SGTR candidate sequences for further treatment in the Level 2 model with minimal intrusion into the existing model, yet ensuring the identification of a large fraction of such sequences. For this purpose, two modeling actions may be considered:

(1) Explicitly insert event tree nodes that query sequences to lead to identification of C-SGTR end states (i.e., sequences with C-SGTR occurring before core damage).

(2) Use sequence rules on core damage sequences to mark high primary pressure, dry SG, and low secondary pressure (HDL or H/D/L) sequences and others, if necessary, as

C-SGTR candidates (i.e., sequences with the potential for C-SGTR to occur after core damage).

Both of these approaches are used in this process. Those sequences that may have some C-SGTR potential but are deliberately not modeled are termed unmodeled sequences. As long as the unmodeled sequences are expected to contribute a very small percentage to the total of all C-SGTR sequences, they can be left unmodeled.

The process examines different event trees and accident sequence sets to provide C-SGTR modeling suggestions in five steps. The first two steps are for screening out sequences.

(1) Those event trees and sequences that are already SG tube ruptures (SGTRs)

SGTR event tree already has end states for SGTR; thus, there is no need to model C-SGTR.

(2) Those event trees that cannot cause C-SGTR or have very little potential for C-SGTR

Such event trees and their sequences can be identified and removed from further consideration for C-SGTR. Examples of such event trees are:

- large loss-of-coolant-accident (LOCA) (LLOCA)
- excessive LOCA (vessel failure XLOCA, LOCA beyond emergency core cooling system (ECCS) capacity)
- interfacing systems LOCA (ISLOCA)

Since the primary system is depressurized and stays so in such events, C-SGTR challenges are not expected.

(3) Those event trees where pressure-induced C-SGTR may occur early in the event

Such event trees include anticipated transient without scram (ATWS), secondary-side break (SSB), and consequential secondary side break (CSSB). Whenever possible, an event tree node could be inserted in an early part of such event trees to query for C-SGTR and then the ensuing sequence could be transferred to an SGTR event tree with the appropriate boundary conditions. Figures L-1 and L-2 give suggestions for ATWS and SSB event tree modifications for C-SGTR. Note that these figures introduce a conditional probability of an existing large flaw of 0.01. This value is derived from Appendix C (and, in turn, Appendix F) of this NUREG.

(4) HDL core damage sequences

When the core damage sequences are examined, it is possible to identify those sequences that can clearly be marked as HDL. This can be done either manually or by defining sequence rules. Thus, such sequences can be assigned to the C-SGTR end state (or otherwise tagged) to be modeled in Level 2. The conditional C-SGTR probability for HDL sequences can be calculated

for the plant-specific case; if not, a generic value of 0.02 to 0.03[1] is in order, depending on the type of SGs in question. Use probability of 1 if the primary side loop is cleared.

(5) Indeterminate or faulted SG (FSG) core damage sequences

After Step 4 above, there will be sequences that are indeterminate as to their C-SGTR potential.

Such sequences may arise from the following:

- Auxiliary feedwater (AFW) status is not asked in the sequence definition, which does let the sequence be qualified as HDL or otherwise (indeterminate core damage sequences).

- AFW appears as successful but flow to one or more AFW trains may fail, still meeting the success criteria. If AFW to an SG fails, the operator will isolate that SG by procedures, leading to a dry SG. Similarly, secondary-side leakage (isolation failure, SSB condition) may occur in a fed SG, with other SG loops operating as intended, leading to an FSG that would be isolated. In such scenarios, some level of C-SGTR challenge may exist. The conditional probability of C-SGTR in such SGs can be calculated if the TH properties of such scenarios are known. However, in a typical PRA, such analyses are not readily available. Based on TH expert opinion, the potential for a C-SGTR challenge in such SGs is estimated to be lower or much lower than HDL conditions with no AFW.

This process suggests that the potential C-SGTR that may stem from indeterminate core damage sequences should not be modeled (e.g., they are in the unmodeled C-SGTR category) to avoid extensive modeling. It is deemed that such unmodeled sequences will be a small fraction of the total SG tube rupture frequency captured in Steps 1, 3, and 4.

Two parameters of importance are used in the claim that such sequences are deemed to be a small fraction of the total C-SGTR:[2]

(1) Failure probability of SSB (unisolated leaking loop) in one or more loops, $Q_{fsg} = 0.13$, given that operators isolate an SG because of AFW failure

(2) The conditional probability of C-SGTR = $Q_{csgtr} = 0.01$, given that an indeterminate core damage sequence occurs.

As an approximation, the C-SGTR CDF of unmodeled sequences above can be estimated by multiplying the CDF with the fraction $Q_{fsg}*Q_{csgtr} = 0.0013$. Section L.3 includes an example application.

[1] This range is for SGs with favorable geometry, such as those seen in Westinghouse pressurized-water reactors. For other SGs, values could be used from the main body of this report, or plant-specific calculations, if thermal-hydraulic (TH) analyses are available.

[2] These values are given as expert judgment since they are not supported by publicly available calculations. If plant-specific values are available, they should be used.

Table L-1 summarizes the five steps discussed above.

**Table L-1 Process Summary for Event Trees and CDF Sequences**

| | Category | Treatment |
|---|---|---|
| 1 | Event Tree: SGTR as the initiator | Use IE-SGTR ET; no additional C-SGTR. |
| 2 | Event Trees: LLOCA/XLOCA | No potential for C-SGTR due to depressurization |
| | Event Tree: ISLOCA | No treatment of C-SGTR due to existing bypass |
| 3 | Event Tree: ATWS | If primary pressure relief fails, assume C-SGTR; otherwise, no C-SGTR on basis of very low frequency. |
| | Event Trees: SSB/CSSB | Add new node (SSB-CSGTR) that equates to probability of existence of large flaw depth and route up-branch to the existing (non-C-SGTR) portion of the tree and down-branch to a consequential (subtree) version of the SGTR tree. |
| 4 | CDF Sequences: HDL | Identify and label for Level 2 treatment; to be multiplied by P(C-SGTR), etc. |
| 5 | CDF Sequences: Non-HDL or Indeterminate | Do not model further based on discussion in Step 5 above. |

As a final sanity check, examine the ratio of the following:

(24) (HDL CDF)/(Frequency of indeterminate core damage sequences)

The larger this ratio is, the less significant the unmodeled sequences in Step 5 will be.

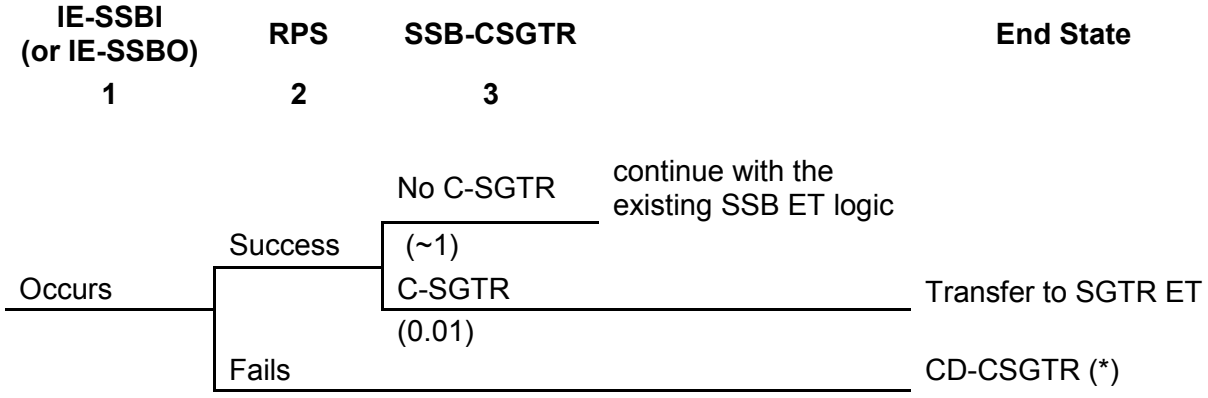


**Figure L-1 Insertion of C-SGTR event tree node in SSB event trees**
***Note: (*) Although this sequence can be transferred to the ATWS event tree for further treatment, it may be more practical to assign it to the core damage end state for further treatment in L2 analysis, since the expected frequency of such a sequence is small.***

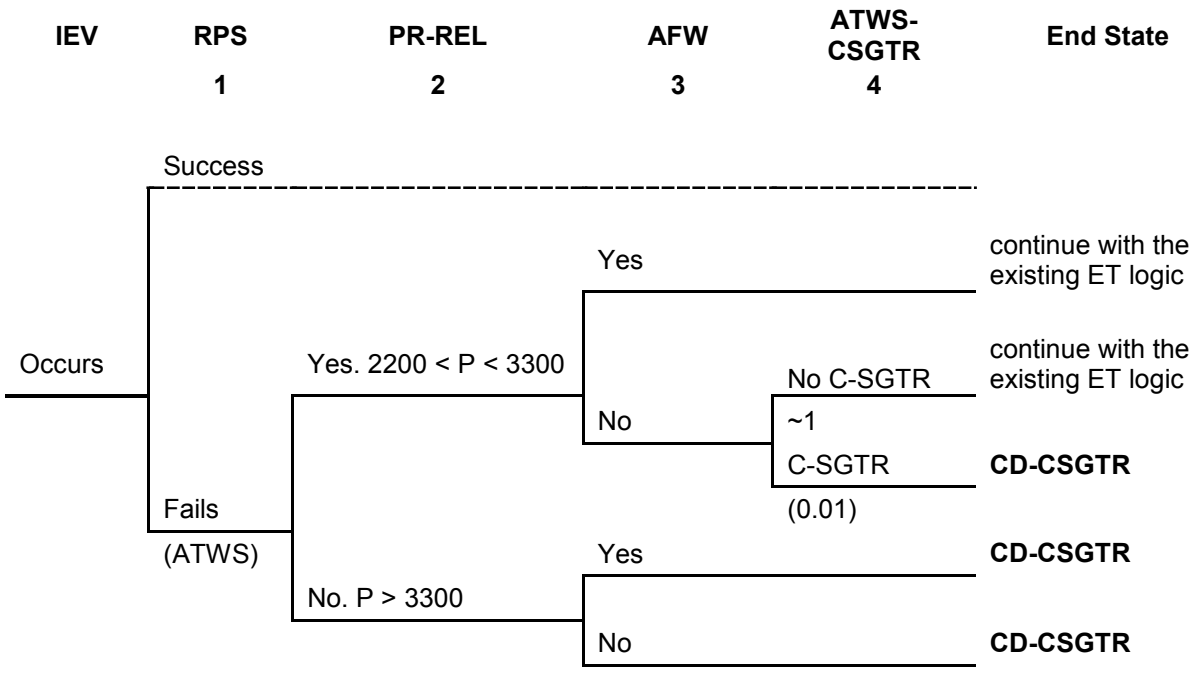


**Figure L-2 Insertion of C-SGTR event tree node in ATWS event tree**
***RPS = Reactor Protection System (trip)***
***PR-REL = Primary system pressure relief***
***P > 3300 = RCS pressure greater than 3,300 psi***

## L.3 Summary of the Results of the Application

The above approach was applied to a 4-loop Westinghouse PRA model that did not originally have C-SGTR explicitly modeled in its Level 1 PRA.

Some changes were made to the base model to capture pressure-induced SGTR (PI-SGTR) CDF sequences. The CDF sequences that are identifiable as HDL are marked by event tree rules to be transferred to the Level 2 model as C-SGTR. Those CDF sequences not captured in the above process, labeled as “unmodeled” sequences that may have some C-SGTR consequence, are then examined for their potential impact. Table L-2 summarizes the results. Based on these results, the following are observed:

- C-SGTR (and IE-SGTR) is a small fraction of CDF (<2 percent).
- C-SGTR potential is dominated by post core damage temperature-induced SGTR (TI-SGTR) (89 percent).
- PI-SGTR is a small contributor to C-SGTR (7 percent) and a very small contributor to CDF (<1 percent).
- Unmodeled C-SGTR sequences in this PRA model would be a small fraction of modeled C-SGTR sequences (3 percent).

The following are important qualifiers on these findings:

- Consistent with the approach outlined in Section L.2, and with the state of practice in C-SGTR modeling, leaks below the critical break area (one double-ended tube break) are not considered.

- These results are for a given version of a PRA model. Any changes made to the model can affect these numbers, although there is no reason to believe that such changes would be significant enough to affect the above findings.

- These estimates (necessarily) project what the Level 2 TI-SGTR frequency will be, based on the H/D/L frequency and the conditional TI-SGTR probability. This capturing does not include any "benefit" that the Level 2 will ultimately estimate with respect to operator actions before HL creep rupture. But again, this is not likely to affect the above findings.

Developing the estimates provided above was a tedious process, because (1) the H/D/L assignment was a manual exercise, and (2) most of the underlying frequencies come from consequential trees and were extracted manually. The former issue can be avoided if event tree rules that identify HDL sequences and label them as such for Level 2 analysis are built into the PRA model as a one-time effort. The latter issue may not apply to some model architecture and software package combinations.

This application to a PRA model illustrates, but does not prove, that the assumptions stated in the modeling approach of Section L.2 for the "unmodeled" sequences are valid. This exercise also demonstrated that this comprehensive, yet limited, intrusion into the PRA Level 1 model to estimate C-SGTR CDF is feasible.

**Table L-2 Summary of C-SGTR Modeling Applied to a Specific PRA Model for a 4-Loop Westinghouse Plant**

| Initiator | Sequence | CDF | C-GTR Multiplier | C-SGTR Frequency | % of C-SGTR |
|---|---|---|---|---|---|
| IE-SGTR | All | 7.6E-8 | 0 | | |
| IE-LLOCA/XLOCA/ISLOCA | All | 2.1E-7 | 0 | | |
| Transients/SLOCA/MLOCA --> ATWS | IE*RPS*/PR-REL*AFW | 6.9E-8 | 0.01 | 6.9E-10 | 0.06% |
| Transients/SLOCA/MLOCA --> ATWS | IE*RPS*PR-REL | 6.2E-8 | 1 | 6.2E-8 | 5.00% |
| IE-SSB --> ATWS | IE-SSBI*RPS | 5.9E-9 | 1 | 5.9E-9 | 0.50% |
| IE-SSB --> ATWS | IE-SSBO*RPS | 3.0E-8 | 1 | 3.0E-8 | 2.40% |
| SSBI/SSBO | IE-SSBI*/RPS*PI-SGTR | 4.5E-10 | 1 | 4.5E-10 | 0.04% |
| SSBI/SSBO | IE-SSBO*/RPS*PI-SGTR | 2.3E-9 | 1 | 2.3E-9 | 0.20% |
| All transients --> consequential SSB | Transient IE*/RPS*…-->CSSB-->PI-SGTR | 2.0E-9 | 1 | 2.0E-9 | 0.16% |
| HDL | No loop clearing | 4.5E-5 | 0.024 | 1.1E-6 | 88.70% |
| HDL | With loop clearing | (*) | 1 | | |
| Non-HDL (b) | Non-HDL with FSG | 2.7E-5 | 0.0013 | 3.5E-8 | 2.90% |
| Non-HDL (a) | Non-HDL with possible AFW failure | (**) | | | |
| | Sum = | 7.3E-5 | | 1.2E-6 | 100% |

The items marked in yellow are not modeled.
(*) No sequences showed up among the dominant CDF sequences; not further examined in this calculation.
(**) Estimated to be a small contributor
(a) and (b) refer to Step 5 in Section L.2 (1).

RPS = Reactor Protection System
PR-REL = Primary System Pressure Relief
SSBI (SSBO) = Secondary Side Break Inside (Outside) Containment
LLOCA (MLOCA, SLOCA) = Large (Medium, Small) LOCA
IE = Initiating Event

NRC FORM 335
(12-2010)
NRCMD 3.7

U.S. NUCLEAR REGULATORY COMMISSION

# BIBLIOGRAPHIC DATA SHEET

*(See instructions on the reverse)*

1. REPORT NUMBER
(Assigned by NRC, Add Vol., Supp., Rev., and Addendum Numbers, if any.)

**NUREG-2195**

2. TITLE AND SUBTITLE

**Consequential SGTR Analysis for Westinghouse and Combustion Engineering Plants with Thermally Treated Alloy 600 and 690 Steam Generator Tubes**

3. DATE REPORT PUBLISHED

| MONTH | YEAR |
|---|---|
| **May** | **2018** |

4. FIN OR GRANT NUMBER


5. AUTHOR(S)

S. Sancaktar, M. Salay, R. Iyengar, A. Azarm, S. Majumdar


6. TYPE OF REPORT

Technical

7. PERIOD COVERED (Inclusive Dates)


8. PERFORMING ORGANIZATION - NAME AND ADDRESS (If NRC, provide Division, Office or Region, U. S. Nuclear Regulatory Commission, and mailing address; if contractor, provide name and mailing address.)

Innovative Engineering and Safety Solutions, LLC, 20817 Spinning Wheel Pl., Germantown, MD 20874

Argonne National Laboratory, 9700 S. Cass Avenue, Argonne, IL 60439


9. SPONSORING ORGANIZATION - NAME AND ADDRESS (If NRC, type "Same as above", if contractor, provide NRC Division, Office or Region, U. S. Nuclear Regulatory Commission, and mailing address.)

Office of Nuclear Regulatory Research
U.S. Nuclear Regulatory Commission
Washington, D.C. 20555-0001

10. SUPPLEMENTARY NOTES


11. ABSTRACT (200 words or less)

This report summarizes consequential steam generator (SG) tube rupture (C-SGTR) analyses recently performed. C-SGTRs are potentially risk significant events because thermally induced SG tube failures caused by hot gases from a damaged reactor core can result in a containment bypass event and a large release of fission products to the environment. The analyses evaluate SGs with thermally treated Alloy 600 and Alloy 690 heat exchange tubes. The methods developed addressed the contribution of thermally induced SGTR during severe accidents and pressure-induced SGTR during a number of design basis accidents. The study developed the methods and the pilot applications so as to establish the framework for performing a more comprehensive probabilistic risk assessment that can address the C-SGTR risk. The main conclusion from this work is that the SG geometry and the fluid flow rates in different SG designs can significantly influence the potential likelihood of C-SGTRs. For SG geometries analyzed in this study, the Combustion Engineering plant design had an increased likelihood of a C-SGTR and a higher potential for a large early release, than the Westinghouse plant design.



12. KEY WORDS/DESCRIPTORS (List words or phrases that will assist researchers in locating the report.)

Steam Generator Tube Rupture, SGTR, Consequential SGTR, C-SGTR, CSGTR, Probabilistic Risk Assessment, PRA, MELCOR


13. AVAILABILITY STATEMENT

unlimited

14. SECURITY CLASSIFICATION

*(This Page)*
unclassified

*(This Report)*
unclassified

15. NUMBER OF PAGES

16. PRICE

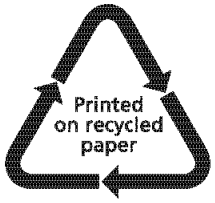


Federal Recycling Program


**UNITED STATES**
**NUCLEAR REGULATORY COMMISSION**
**WASHINGTON, DC 20555-0001**

**OFFICIAL BUSINESS**